Origin and tectonic evolution of the central Serbo-Macedonian Massif

Inauguraldissertation

zur

Erlangung der Würde eines Doktors der Philosophie

vorgelegt der

Philosophisch-Naturwissenschaftlichen Fakultät

der Universität Basel

von

Milorad Antić

aus Belgrad, Serbien

Basel, 2016

Genehmigt von der Philosophisch-Naturwissenschaftlichen Fakultät

auf Antrag von

Prof. Dr. Andreas Wetzel (Fakultätsverantwortlicher, Dissertationsleiter)

Geologie, Departement Umweltwissenschaften, Universität Basel

PD Dr. Alexandre Kounov (Dissertationsleiter)

Geologie, Departement Umweltwissenschaften, Universität Basel

Prof. Dr. Bernhard Fügenschuh (Externer Experte)

Institut für Geologie und Paläontologie, Universität Innsbruck

Basel, 23. 06. 2015

Prof. Dr. Jörg Schibler

(Dekan der Philosophisch-Naturwissenschaftlichen Fakultät)

七転び八起き

“Fall seven times, stand up eight.”

Abstract

The Serbo-Macedonian Massif (SMM) is a composite crystalline belt within the Eastern European Alpine orogen, outcropping from the Aegean Sea in the south, to the Pannonian basin in the north. Farther north, it is correlated with the Supragetic nappe sequences of the South Carpathians. The central part of the massif, located in southeastern Serbia, southwestern Bulgaria and eastern Macedonia, consists of the medium- to high-grade metamorphic Lower Complex, and the low-grade metamorphic Vlasina Unit. Due to sparsity of detailed structural studies, geo- and thermochronological constraints, the geodynamic history of this area was considered enigmatic. In this study, U-Pb LA-ICP-MS analyses of zircons, geochemical analyses of major and trace elements of whole-rock samples, outcrop- and micro-scale investigation of ductile structures as well as ^{40}Ar/^{39}Ar and fission-track thermochronology were applied in order to define the provenance and tectonic evolution of the central SMM.

The new results of U–Pb LA-ICP-MS analyses, coupled with Hf isotopic analyses of magmatic and detrital zircons, and major and trace element concentrations in whole-rock samples suggest that the central SMM and the basement of the adjacent units (i.e. Eastern Veles series and Struma Unit) originated in the central parts of the northern margin of Gondwana. These data provided a basis for a revised tectonic model of the evolution of the SMM from the late Ediacaran to the Early Triassic.

The earliest magmatism in the Lower Complex, Vlasina Unit and the basement of Struma Unit is related to the activity along the late Cadomian magmatic arc (562-522 Ma). A subsequent stage of early Palaeozoic igneous activity is associated with (i) the reactivation of subduction below the Lower Complex and the Eastern Veles series during the Early Ordovician (490-478 Ma), (ii) emplacement of mafic dykes in the Lower Complex due to aborted rifting in the Middle Ordovician (472-456 Ma), and (iii) felsic within-plate magmatism in the early Silurian (439±2 Ma). The third magmatic stage is represented by Carboniferous late- to post-collisional granites (328-304 Ma). These granites intruded the gneisses of the Lower Complex, in which the youngest deformed igneous rocks are of early Silurian age, thus constraining the high-strain deformation and peak metamorphism to the Variscan orogeny. The fourth, Permian-Triassic (255-253 Ma) stage is late- to post-collisional and it is documented by within-plate felsic magmatism, related to the opening of the Mesozoic Tethys.

Three major stages of ductile deformation were revealed based on the investigation of outcrop- and micro-scale ductile structures in the central SMM. The earliest stage of deformation D_1 is related to isoclinal folding, commonly preserved as quartz-feldspar rootless fold hinges up to decimetre-scale. The second deformational stage D_2 is associated with general southeastward tectonic transport and refolding of older structures into recumbent metre- to kilometre-scale tight to isoclinal folds. The deformational stages D_1 and D_2 could not be temporally separated, and probably occurred in close sequence. The age of these two ductile deformational stages was constrained to the Variscan orogeny based on indirect geological evidence (i.e. ca. 408-ca. 328 Ma). During this time the SMM was involved in a transpressional amalgamation of the western and eastern parts of the Galatian super-terrane and subsequent collision with Laurussia. Outcrop-scale evidence of the final stage of ductile deformation D_3 is limited to the spaced and crenulation cleavage, which are probably related to the large-scale folding reported by earlier studies.

Results of the $^{40}Ar/^{39}Ar$ thermochronology revealed three major stages of cooling in the central SMM from the early Carboniferous until the Early Jurassic. Cooling below greenschist facies conditions in the western part of the Vlasina Unit took place in a post-orogenic setting (extensional or transtensional) in the early Permian (ca. 284 Ma). The age of activity along the top-to-the-west shear zone formed within the orthogneiss in the Božica area of the Vlasina Unit was constrained to the Middle Triassic (ca. 246 Ma). This age coincides with widespread extension and magmatism related to the opening of the Mesozoic Tethys. The greenschist facies retrogression in the Lower Complex probably occurred in the Early Jurassic (ca. 195 Ma) and is probably related to thermal processes in the overriding plate above the subducting slab of the Mesozoic Tethys Ocean.

Fission-track analyses on apatites and zircons revealed the existence of three major cooling stages from the late Early Cretaceous to the Oligocene. The first stage represents rapid cooling through zircon and apatite closure temperatures (300–60 °C) during the late Early to early Late Cretaceous (ca. 110–ca. 90 Ma). It is related to a post-orogenic extension following the regional nappe-stacking event in the Early Cretaceous. Middle to late Eocene (ca. 48–ca. 39 Ma) cooling is related to the formation of the Crnook-Osogovo-Lisets extensional dome and its exhumation along low-angle normal faults. The third event is related to the regional cooling following the late Eocene magmatic pulse. During this pulse the area surrounding the Surdulica granodiorite (36±1 Ma) and the slightly younger volcanic bodies (ca. 35 Ma) reached temperatures higher than the apatite closure temperature (110±10 °C) but lower than ca. 250 °C. The geochemistry of the igneous rocks reveals a late- to post-orogenic tectonic setting during magma generation.

Сажетак

Српско-Македонска маса (СММ) представља сложени појас кристаластих стена унутар Алпског орогена источне Европе, који је откривен од Егејског мора на југу, до Панонског басена на северу. Даље ка северу, СММ је изједначена са Супрагетском серијом навлака јужних Карпата. Централни делови масива (југоисточна Србија, југозападна Бугарска и источна Македонија) се састоје од Доњег комплекса окарактерисаног средњим до високим степеном метаморфизма, и Власинке јединице ниског степена метаморфизма. Услед недостатка детаљних структурно-геолошких истраживања, као и гео- и термохронолошких података, геодинамичка историја овог подручја представља непознаницу. У циљу одређивања порекла и тектонске еволуције централне СММ, примењене су анализе изотопа урана-олова добијених ласерским аблирањем циркона, мерених на масеном спектрометру са индукцијски спојеном плазмом (LA-ICP-MS), затим геохемијске анализе главних и елемената у траговима у узорцима целих стена, истраживања дуктилних структура на опсервационом нивоу изданка и микроскопског препарата, као и термохронолошким методама ^{40}Ar/^{39}Ar и трагова фисије.

Нови резултати геохронолошких анализа (U-Pb LA-ICP-MS), заједно са геохемијским анализама изотопа Hf магматских и детриталних циркона, и концентрација главних и елемената у траговима у узорцима целих стена указују на то да централна СММ са кристаластим основама суседних јединица (нпр. Источна Велешка серија и Струмска јединица) потиче од средишњих делова северне маргине Гондване. Ови подаци представљају основу преиспитаног тектонског модела еволуције СММ од горње едијакаре до доњег тријаса.

Најстарија магматска активност у Доњем комплексу, Власинској јединици и кристаластој основи Струмске јединице је повезана са активношћу дуж касног кадомског магматског лука (562-522 Ma). Наредна етапа у виду доњопалеозојског магматизма се везује за наставак субдукције испод Доњег комплекса и Источне Велешке серије током доњег ордовицијума (490-478 Ma), утискивање мафичних дајкова у Доњи комплекс услед прекинутог рифтовања у средњем ордовицијуму (472-456 Ma), и фелзични магматизам унутар плоча у доњем силуру (439±2 Ma). Трећа етапа магматизма је представљена карбонским гранитима насталим у касним фазама колизије или после-колизионом периоду (328-304 Ma). Ови гранити интрудују гнајсеве Доњег комплекса, у коме су најмлађе деформисане магматске стене горњосилурске старости, чиме је старост интезивних дуктилних деформација и метаморфизма ограничена на Варисцијску орогенезу. Пермо-тријаска етапа (255-253 Ma) касно- до после-колизионог и магматизма унутар плоча је повезана са отварањем мезозојског Тетиса.

На основу истраживања дуктилних структура на опсервационом нивоу изданка и микроскопског препарата, у централној СММ издвојене су три главне фазе дуктилних деформација. Најстарија фаза деформације D_1 је представљена изоклиним наборима, најчешће очуваним у виду дециметарских кварц-фелдспатских шарнира без корена. Друга фаза деформација D_2 је повезана са тектонским транспортом усмереном ка југоистоку и пренабирањем старијих структура у полегле метарске до километарске стиснуте до изоклине наборе. Деформационе фазе D_1 и D_2 није било могуће засебно временски одредити и вероватно су се десиле непосредно једна за другом. Старост ових дуктилних деформационих фаза је ограничена на Варисцијску орогенезу (тј. ca. 408-ca. 328 Ma) на основу посредних геолошких доказа. Током овог периода СММ је учествовала у транспресионом спајању западног и источног дела Галатијског супер-терана, а потом и у колизији са Лаурусијом. Показатељи последње фазе дуктилних деформација D_3 су ограничени на раздвојени кливаж опсервиран на величинском нивоу изданка, који је вероватно последица великих отворених набора описаних у ранијим истраживањима.

На основу резултата ^{40}Ar/^{39}Ar термохронологије утврђене су три главне фазе хлађења у централној СММ. Хлађење испод услова фације зелених шкриљаца у западном делу Власинске јединице се одиграло у после-орогеним условима (екстензионим или транстензионим) током доњег перма (ca. 284 Ma). Активности дуж зоне смицања усмерене ка западу формиране у орто-гнајсевима Божице у Власинској јединици је ограничена на средњи тријас (ca. 246 Ma). Ова старост се подудара са распрострањеном екстензијом и магматизмом везаним за отварање мезозојског Тетиса. Ретрогресија до фације зелених шкриљаца у Доњем комплексу се највероватније одвијала током доње јуре (ca. 195 Ma) и могуће је да је повезана са топлотном активношћу у повлатној плочи изнад субдуковане плоче мезозојског Тетиса.

Анализа трагова фисије на апатитима и цирконима открила је постојање три главне фазе хлађења од касне доње креде до олигоцена. Прва фаза представља брзо хлађење кроз температуре затварања система трагова фисије у циркону и апатиту (300-60 ºC) током старије доње и млађе горње креде (ca. 110-ca. 90 Ma). Ова фаза је у вези са после-орогенском екстензијом која прати регионално навлачење из доње креде. Средње- до горњоеоценско хлађење (са, 48-са 39 Ма) је повезано са настанком Црноок-Осогово-Лисецке екстензионе доме и њене ексхумације дуж нормалних раседа благог пада. Трећа фаза је повезана са регионалним хлађењем после горњоеоценске магматске активности. Током овог магматизма подручје око Сурдуличког гранодиорита (36±1 Ма) и нешто млађих вулканских тела (са. 35 Ма) је достигло температуре изнад температура затварања система трагова фисије у апатиту (120 °C) али ниже од са. 250 °C. Геохемијски састав узорака ових магматских стена указује на касне- до после-орогене тектонске услове током настанка магме.

Zusammenfassung

Das Serbo-Mazedonische Massiv (SMM) repräsentiert einen Gürtel aus metamorphen und magmatischen Gesteinen im osteuropäischen alpinen Gebirge, der zwischen der Ägäis im Süden und dem pannonischen Becken im Norden aufgeschlossen ist. Weiter im Norden wird das SMM mit dem Deckenstapel des Supragetikums der Südkarpaten korreliert. Die zentralen Teile des Massivs im südöstlichen Serbien, südwestlichen Bulgarien und östliches Mazedonien bestehen aus einem mittel- bis hoch-gradig metamorphen Unteren Komplex und der niedrig-gradig metamorphen Vlasina Einheit. Aufgrund der bisher spärlichen detaillierten strukturellen Untersuchungen und geo- und thermochronologischen Analysen, ist die geodynamische Geschichte dieses Gebietes nicht genau bekannt. Um die Herkunft und tektonische Entwicklung des zentralen SMM zu definieren wurden in der vorliegenden Arbeit U-Pb LA-ICP-MS Analysen von Zirkon, geochemische Analysen von Haupt- und Spurenelementen von Gesamtgesteinsproben, Aufschluss- und Mikroskala Untersuchungen von duktilen Strukturen sowie ^{40}Ar/^{39}Ar- und Spaltspurthermochronologie durchgeführt.

Die neuen Resultate der U-Pb LA-ICP-MA Analysen in Kombination mit geochemischen Analysen von Hf-Isotopen magmatischer und detritaler Zirkone und die Haupt- und Spurenelementkonzentrationen von Gesamtgesteinsproben legen nahe, dass das zentrale SMM und das Grundgebirge der angrenzenden Einheiten, also die östliche Veles Serien und Struma Einheit, aus den zentralen Teilen des nördlichen Randes von Gondwana stammen. Diese Daten bilden die Basis für ein überarbeitetes tektonisches Model der Evolution des SMM vom späten Ediacarium bis zur Unteren Trias.

Der früheste nachgewiesene Magmatismus im Unteren Komplex, der Vlasina Einheit und dem Basement der Struma Einheit steht in Verbindung mit der Aktivität entlang des spätcadomischen magmatischen Bogens (562-522 Ma). Eine darauffolgende Phase frühpaläozoischer magmatischer Aktivität ist assoziiert mit (1) der Reaktivierung der Subduktion unter den Unteren Komplex und der östlichen Veles Serie im frühen Ordovizium (490-478 Ma), (2) Platznahme mafischer Gänge im Unteren Komplex aufgrund des beendeten Rifting im Mittelordovizium und (3) felsischem Intra-Platten-Magmatismus im frühen Silur (439±2 Ma). Die dritte magmatische Phase wird durch die spät- bis post-kollisionalen Granite im Karbon (328-304 Ma) repräsentiert. Diese Granite intrudierten in Gneise des Unteren Komplex, in welchem die jüngsten deformierten magmatischen Gesteine frühe silurische Alter aufweisen, und legen damit die Grenzen der 'high-strain'-Deformation und 'peak'-Metamorphose der variszischen Orogenese fest. Die permo-triassische Phase (255-253 Ma) des spät- bis post-kollisionalen und felsischen intraplatten Magmatismus steht im Zusammenhang mit der Öffnung der mesozoischen Tethys.

Drei Hauptphasen duktiler Deformation wurden aufgrund der Untersuchung duktiler Strukturen auf Aufschluss- und Mikroskala für das zentrale SMM ausgeschieden. Die erste Deformationsphase D_1 zeigt isoklinale Faltung, die meist durch wurzellose, bis in die Dezimeter-Skala reichende Quarz-Feldspat-Faltenschenkel repräsentiert erhalten geblieben ist. Die zweite Deformationsphase D_2 wird mit allgemeiner Nord-Süd Kompression und erneuter Verfaltung älterer Strukturen in liegende, Meter- bis Kilometer mächtige, spitze bis isoklinale Falten verbunden. Die Deformationsphasen D_1 und D_2 konnten zeitlich nicht zugeordnet werden und traten wahrscheinlich in kurzer Folge auf. Das Alter dieser beiden duktilen Deformationsphasen wurde aufgrund indirekter geologischer Belege auf die variszische Orogenese (d.h. ca. 408 – ca. 328 Ma) festgelegt. Während dieser Zeit wurde das SMM in den transpressiven Zusammenschluss westlicher und östlicher Teile des Galatischen Super-Terrane und die anschießende Kollision mit Laurussia miteinbezogen. In der Grössenordnung von Aufschlüssen sind die Belege für die abschliessende duktile Deformationsphase D_3 auf „spaced cleavage“ und Krenulationsschieferungen begrenzt, welche vermutlich mit der gross-skaligen Faltung, wie sie bei früheren Untersuchungen beschrieben wurde, in Verbindung stehen.

Ergebnisse der ^{40}Ar/^{39}Ar Thermochronologie offenbaren drei Hauptabkühlungsphasen im zentralen SMM vom Perm bis in den Jura. Abkühlung unter Grünschieferfazies-Bedingungen im westlichen Teil der Vlasina Einheit fand post-orogen in einem extensiven oder transtensiven Regime im frühen Perm (ca. 284 Ma) statt. Die Aktivität entlang der Scherzone, welche sich in den Orthogneisen des Božica Gebiets der Vlasina Einheit formte und einen Versatz nach Westen aufweist, konnte auf Mitteltrias (ca. 246 Ma) datiert werden. Dieses Alter stimmt mit der grossflächigen Extension und Magmatismus im Zuge der Öffnung der mesozoischen Tethys überein. Die retrograde grünschiefer-fazielle Überprägung im Unteren Komplex fand wahrscheinlich während des Unteren Juras (ca. 195 Ma) statt und ist vermutlich auf thermische Prozesse in der Platte zurückzuführen, die einen Teil des subduzierten mesozoischen Tethys-Ozean-Bodens überfuhr.

Eine weitere Abkühlung erfolgte in 3 Phasen im Zusammenhang mit der alpinen Orogenese.

Spaltspur-Analysen an Apatiten und Zirkonen belegen drei Hauptabkühlungsphasen von der späten Unter-Kreide bis ins Oligozän. Die erste Phase repräsentiert rasche Abkühlung durch Zirkon und Apatit Schließtemperaturen (300-60 °C) während der späten Unter- bis in die frühe Ober-Kreide (ca. 110-ca. 90 Ma). Diese Phase steht in Bezug zur post-orogenen Extension, welche auf die regionale Deckenstapelung während der Unter-Kreide folgt. Die Abkühlung im mittleren bis späten Eozän (ca. 48-ca. 39 Ma) erfolgte bei der Bildung des Crnook-Osogovo-Lisets-Domes in einem extensiven Spannungsfeld und dessen Exhumation entlang flach einfallender Abschiebungen. Die dritte regionale Abkühlung erfolgte nach dem spät-eozänen magmatischen Puls. Während dieses Pulses erreichte das Gebiet um die Surdulica Granodiorite (36±1 Ma) und die etwas jüngeren vulkanischen Körper (ca. 35 Ma) Temperaturen, die höher als die Apatit-Schliesstemperatur (110±10 °C), aber tiefer als ca. 250 °C lagen. Die Geochemie der magmatischen Gesteine weist auf eine spät- bis post-orogenes tektonische Situation während der Magmen-Entstehung hin.

(Translation by Nicola Kern)

Table of Contents

Chapter 1

Introduction

1 Introduction

1.1 Background

The crystalline basement units within the Alpine orogenic belts are commonly characterised by high structural complexity caused by interaction of multiple deformational and metamorphic events (e.g. Dewey et al., 1973; von Raumer et al., 2003; Schmid et al., 2008). Geological challenges presented by these areas often require long-term studies and multidisciplinary approach in order to fully unravel their evolution. During the last few decades detailed studies of the basement units in the Eastern Mediterranean Alpine orogen such as Tisza, Rhodope and

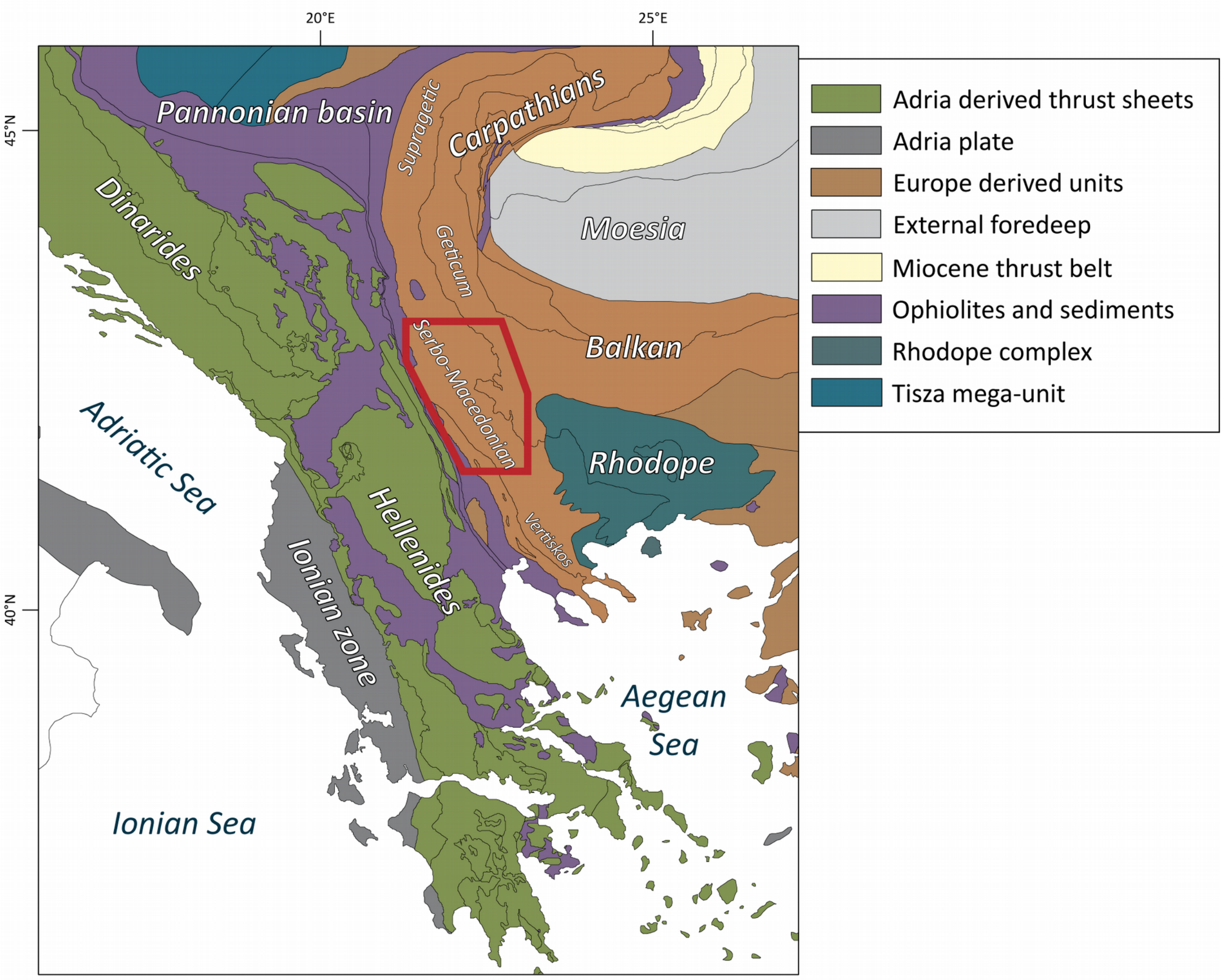

Figure 1-1. Tectonic sketch of the Balkan Peninsula (after Schmid et al., 2008; van Hinsbergen and Schmid, 2012) with the position of the study area (red polygon).

Strandzha/Istranca, have brought significant advances in understanding of the tectonic evolution of these areas, previously considered as ancient microcontinents (“Zwischengebirge” of Kober, 1952) trapped within the Alpine orogen. The Rhodope complex in northeastern Greece and southern Bulgaria represents a perfect example of an intra-Alpine crystalline unit, which was fundamentally misunderstood until the advances in Earth Science in the last decades allowed the reinterpretation of its tectonic evolution revealing the active involvement in the Alpine orogeny (e.g. Burg et al., 1996b; Kaiser-Rohrmeier et al., 2004; Liati, 2005; Bosse et al., 2009; Turpaud and Reischmann, 2010).

The Serbo-Macedonian Massif (SMM) represents a crystalline unit, located between the structurally diverging Dinaride–Hellenide, and the Carpatho-Balkanide chains of the Alpine orogen (Fig. 1-1). Although the southernmost extents of the SMM in Greece and Bulgaria were under a continuous investigation that inevitably yielded a significant amount of pertinent results (e.g. Kilias et al., 1997; Himmerkus et al., 2006, 2009; Zidarov et al., 2007a; Nenova and Zidarov, 2008; Zagorchev, 2008; Meinhold et al., 2010; Zagorchev et al., 2011; Kydonakis et al., 2014, 2015), its central parts in southeastern Serbia, eastern Macedonia and southwestern Bulgaria, lack reliable geo- and thermochronological data, leading to numerous and highly divergent subdivision schemes and tectonic interpretations (e.g. Popović, 1991, 1995; Ricou et al., 1998; Grubić et al., 1999, 2005; Kräutner and Krstić, 2003; Karamata, 2006; Zagorchev and Milovanović, 2006). Despite the existing petrological and geochemical studies of the rocks in the central SMM, the timing of the major metamorphic events which affected the SMM remained rather speculative. The major metamorphism in the SMM was suggested to be of Precambrian (e.g. Balogh et al., 1994; Zagorchev and Milovanović, 2006; Nenova and Zidarov, 2008), Palaeozoic (e.g. Dimitrijević, 1967; Balogh et al., 1994; Zidarov et al., 2007b; Peytcheva et al., 2009; Kounov et al., 2012), Mesozoic (e.g. Milovanović, 1990; Balogh et al., 1994; Zidarov et al., 2003; Himmerkus et al., 2009), or Cenozoic age (e.g. Ricou et al., 1998). Another important question left unanswered was the provenance of the central SMM and its role in the complex interaction of Gondwana- and Laurussia-derived crustal segments presently outcropping along the Balkan Peninsula (Neubauer, 2002; Munteanu and Tatu, 2003; Kalvoda and Bábek, 2010; Kroner and Romer, 2013). Recent studies in the Greek part of the SMM revealed a complex metamorphic and tectonic history since the Cambrian, including intense Alpine overprint suggesting that what was presently referred to as the SMM is not a single tectonic unit (Kilias et al., 1997; Brun and Sokoutis, 2007; Himmerkus et al., 2007). However, the mode and the age of activities along the major tectonic structures in the central parts of the SMM were generally poorly constrained due to lack of relevant sedimentary record and thermochronological data. For example, the western contact of the SMM with the Jurassic ophiolites of the Eastern Vardar zone was previously reported as an east-vergent thrust (Schmid et al., 2008), strike-slip fault (Krstić and Karamata, 1992), west-vergent thrust (Vukanović et al., 1977), or a west-vergent thrust reactivated as a Miocene dextral strike-slip (Kräutner and Krstić, 2003).

Given the importance of its location in the periphery of the Europe-derived Dacia mega-unit at the contact with the ophiolites of Mesozoic Tethys Ocean (Schmid et al., 2008), it is obvious that the reliable reconstruction of provenance, magmatic and deformational history of the central SMM is essential for a correct reconstruction of the tectonic evolution of the Eastern Mediterranean Alpine orogen.

1.2 Geological setting

Although a metamorphic belt outcropping axially along the Balkan Peninsula was reported much earlier (e.g. Boué, 1840; Cvijić, 1902, 1906), its definition as an independent tectonic unit called the Serbo-Macedonian Massif (SMM) occurred only about sixty years ago (Dimitrijević, 1957). The SMM extends from the Aegean Sea to the Southern Carpathians (Fig. 1-1) where it is correlated with the Supragetic nappe sequence (e.g. Săndulescu, 1984; Dimitrijević, 1997; Schmid et al., 2008). The central SMM in Serbia represents an entirely metamorphic belt comprising structurally lower unit (the Lower Complex) and an upper unit (Vlasina Unit), as originally proposed by Dimitrijević (1957). These units are commonly differentiated on the basis of their metamorphic grade, with the Lower Complex predominantly metamorphosed at medium to lower amphibolite facies, and the Vlasina Unit at greenschist facies. The spatial continuations of the Lower Complex and Vlasina Unit in Bulgaria are referred to as the Ograzhden block (Dimitrijević, 1967; Zagorchev, 1984a; Dabovski et al., 2002) and Morava Unit (Zagorchev, 1985; Zagortchev, 1993), respectively. The Vertiskos Unit in Greece is traditionally considered as the continuation of the Lower Complex of the SMM (Kockel et al., 1971; Burg et al., 1995; Himmerkus et al., 2009; Meinhold et al., 2010). Based on the available geological records from the Greek and Bulgarian extents of the SMM, its provenance was previously assigned to the eastern Avalonian (Meinhold et al., 2010) or Cadomian (Stampfli et al., 2002; von Raumer et al., 2003; Balintoni et al., 2010;

Meinhold et al., 2010; Kounov et al., 2012) assemblages of terranes within the Neoproterozoic north-Gondwanan arc.

During the late Early Cretaceous, the Vlasina Unit was thrust to the east onto the Getic units along a system of east- to northeast-vergent thrusts (Fig. 1-2; Petković, 1930; Mihailescu et al., 1967; Petrović, 1969; Zagorchev and Ruseva, 1982; Zagorchev, 1984b; Lilov and Zagorchev, 1993; Kounov et al., 2010). In southwest Bulgaria and northern Greece the contact of the Ograzhden block and the Vertiskos Unit with the Rhodope complex is traced along the Strymon Valley and Kerdillion detachments (Dinter and Royden, 1993; Brun and Sokoutis, 2007; Kounov et al., 2015). The distinction between the SMM and the Rhodope complex was often challenged in the past (Popović, 1991; Ricou et al., 1998; Grubić et al., 1999, 2005), although their differences were firmly established in the Greek and Bulgarian parts of the SMM during the past two decades (Burg, 2012 and references therein). A large number of studies in Bulgaria and Greece have shown that the Rhodope complex was formed during the Alpine orogeny (e.g. Burg et al., 1996a; Kaiser-Rohrmeier et al., 2004; Liati, 2005; Bosse et al., 2009; Turpaud and Reischmann, 2010), whereas the SMM lacks the high-grade Cenozoic overprint (Georgiev et al., 2010; Kounov et al., 2010, 2012).

The SMM is bounded to the west by Mesozoic sediments and Jurassic ophiolites of the Eastern Vardar suture zone (e.g. Karamata, 2006; Schmid et al., 2008; Meinhold et al., 2009; Robertson et al., 2009). In the study area this contact is reported as a strike-slip fault, an east-vergent thrust (Krstić and Karamata, 1992), or a westward thrust which was reactivated as a dextral strike slip fault in the Neogene (Kräutner and Krstić, 2002). South of the Lece andesitic complex, the Lower Complex of the SMM is in tectonic contact with the metamorphic rocks of the Eastern Veles series (Fig. 1-2). The oldest reported, non-metamorphosed, sedimentary rocks that overlie crystalline rocks of the SMM are Middle Triassic (Karamata and Krstić, 1996; Dimitrijević, 1997).

Earlier studies suggest that being previously variably metamorphosed, the Lower Complex and Vlasina Unit have been amalgamated and subsequently accreted to the Moesian platform during the Variscan orogeny (Karamata and Krstić, 1996; Haydoutov and Yanev, 1997). An alternative scenario proposes that the southern extent of the SMM (i.e. Vertiskos Unit) had joined the European craton in the Late Jurassic to Early Cretaceous (Himmerkus et al., 2009). Schmid et al. (2008) suggest that the Eastern Vardar ophiolites are at a structurally higher position in respect to the SMM due to the Late Jurassic obduction and final east-facing nappe stacking in the Late Cretaceous. According to these authors the final suturing in the early Palaeogene, related to the final closure of

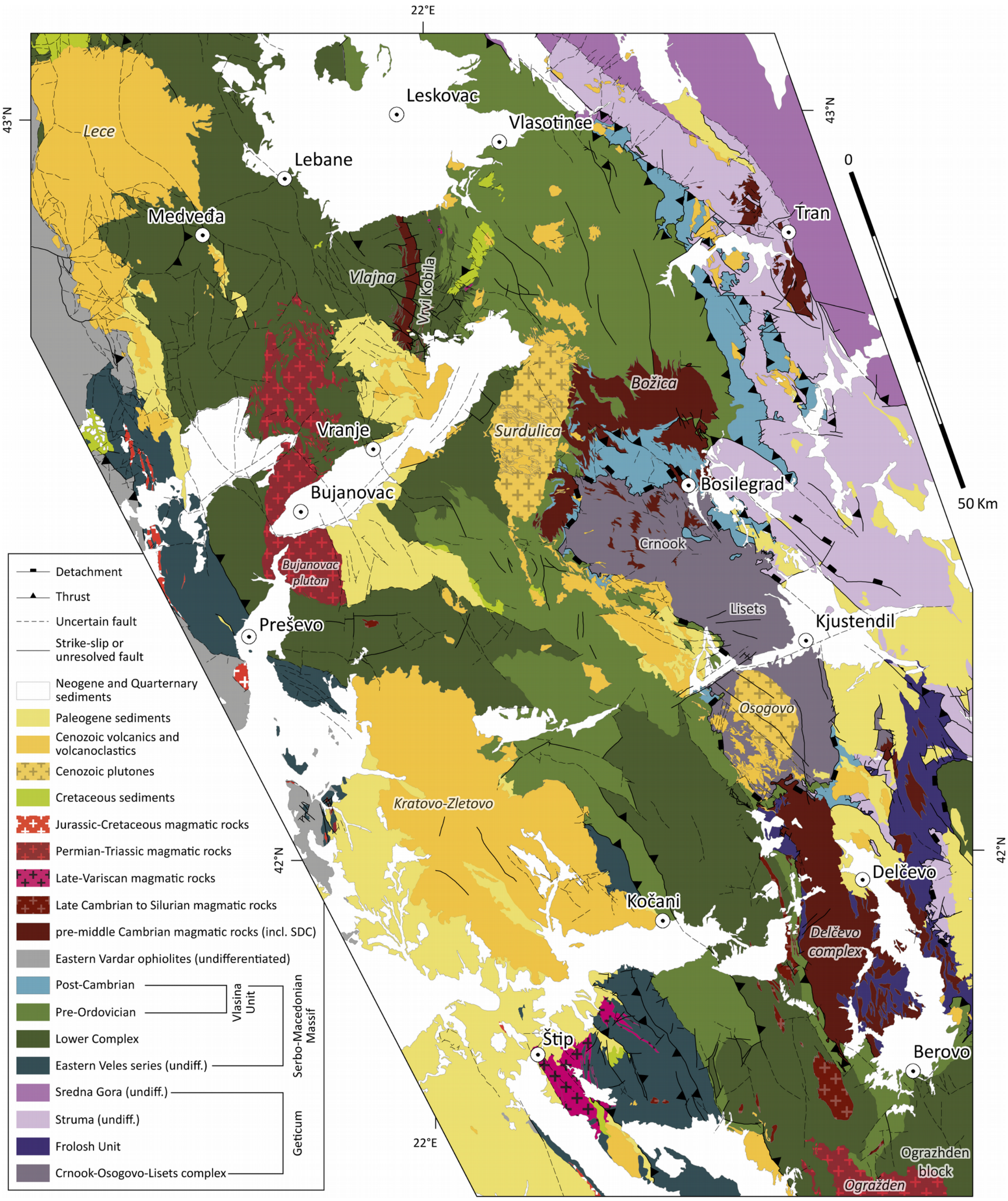

Figure 1-2. Tectonic map of the study area with the position of the analysed samples (after Basic geological maps of SFR Yugoslavia 1:100 0000 and Geological maps of Bulgaria 1:100 000 and 1:50 000). Names in italics represent magmatic bodies.

the remnants of the Vardar Ocean (i.e. the Sava zone) led to the westward thrusting in the Dinarides (Adria-derived). The geology of the units encountered in the study area (Fig. 1-2) is outlined below.

1.2.1 The Lower Complex

The Lower Complex consists mainly of gneisses, micaschists, quartzites with lenses of amphibolites and occasionally marbles and migmatites (Dimitrijević, 1963, 1997). Isolated fragments of serpentinised ultramafic rocks were also reported (Petrović et al., 1973; Vukanović et al., 1973; Nenova and Marinova, 2007; Tarassov et al., 2007). Pelitic and psammitic sediments are usually considered as protoliths of the felsic metamorphic rocks, and tholeiitic within-plate basalts and related tuffs as protoliths of the amphibolites (Milovanović, 1992; Dimitrijević, 1997). The protoliths of the Lower Complex and Vlasina Unit are described as parts of an arc-related volcano-sedimentary series (Dimitrijević, 1967; Krstić and Karamata, 1992; Haydoutov and Yanev, 1997; Kounov et al., 2012). Although the medium- to lower-amphibolite facies metamorphism is characteristic for the Lower Complex (Dimitrijević, 1967; Milovanović, 1990, 1992; Cvetković, 1992), the relicts of an eclogite facies assemblage were also reported as isolated occurrences throughout this unit (Balogh et al., 1994; Vasković and Tasić, 1997; Iancu et al., 1998; Korikovsky et al., 2003; Zidarov et al., 2003; Macheva et al., 2005; Nenova and Zidarov, 2008; Ivanova and Zidarov, 2011; Kydonakis et al., 2015). Age of the high-pressure metamorphism, deduced from overprinting relationships and whole-rock Rb/Sr data, was reported to be of pre- or Cadomian age (ca. 750-550 Ma), with amphibolite facies overprint occurring in the Variscan (Dimitrijević, 1967; Balogh et al., 1994; Medaris Jr. et al., 2003; Zagorchev and Milovanović, 2006; Nenova and Zidarov, 2008). A latest Jurassic and/or Early Cretaceous greenschist facies retrogressive stage was reported in Serbia, Bulgaria and Greece (Milovanović, 1990; Balogh et al., 1994; Kilias et al., 1999; Zidarov et al., 2003).

West of the Vrvi Kobila shear zone, the Lower Complex is intruded by the Vlajna granitoid (Fig. 1-2), which was reported to have been emplaced at 450 Ma (Dimitrijević, 1963). The largest magmatic body intruding the Lower Complex in Serbia is the NNE-SSW elongated Bujanovac S-type granite (Vukanović et al., 1973, 1977; Karamata and Krstić, 1996). Two distinct intrusions form the Bujanovac granitic complex, an older represented by medium-grained foliated granitoids, intruded by younger, fine-grained granites (Dimitrijević, 1958; Vukanović et al., 1977). The ages of these plutons have been reported as 347 Ma (Dimitrijević, 1997), and 234 Ma (Dimitrijević, 1958), respectively.

A group of magmatic bodies, apparently intruding the Vlajna granites, located in the southern part of the Vrvi Kobila shear zone are referred to as Kukavica granites (Fig. 1-2; Vukanović et al., 1973). Both Vlajna and Kukavica granites were deformed together along the Vrvi Kobila shear zone.

The Ogražden pluton intruded into the Lower Complex (i.e. Ograzhden block) gneisses on the southern margin of the study area (Fig. 1-2), consists of biotitic granites and granodiorites. Age of its emplacement is reported as early Palaeozoic (Boev et al., 2002), Early Cretaceous (Rakićević et al., 1973), and most recently as Early Triassic (U-Pb zircon age 252±2 Ma; Georgiev et al., 2012).

1.2.2 Vlasina Unit

The Vlasina Unit represents a Cadomian volcano-sedimentary sequence, similar to the protoliths of the Lower Complex. However, the Vlasina Unit is considered to be dominated by ocean-floor sediments (Pantić et al., 1967; Petrović, 1969) with intercalated basic igneous rocks related to MORB (Popović, 1991), representing an ocean-ward periphery of a magmatic arc (Milovanović et al., 1988), covered by the Lower Ordovician to Lower Carboniferous sedimentary rocks (post-Cambrian in Fig. 1-2; Pavlović, 1962; Babović et al., 1977; Kräutner and Krstić, 2002).

The pre-Ordovician Vlasina is typically represented by chlorite-, biotite-, muscovite-, sericite- and epidote-schists, phyllites and quartzites. Local varieties rich in quartz and albite, or actinolite and stilpnomelane were occasionally reported (Dimitrijević, 1967). Protoliths of these metamorphic rocks are pelitic and to a lesser extent psammitic sediments (Petrović, 1969), together with arc-related tholeiitic basalts and their tuffs (Milovanović et al., 1988). Several small, tectonically imbricated bodies of serpentinites have also been reported (Ilić et al., 1967; Petrović, 1969; Petrović et al., 1973). Intrusions of granites, gabbro and diabase are often deformed and metamorphosed along with the country rock. The age of the pre-Ordovician Vlasina protoliths was determined as "Ripheo-Cambrian" based on the spores recovered at several locations in southeastern Serbia (Pantić et al., 1967; Petrović, 1969). Additionally, lenses of calcschists northeast of Surdulica pluton yielded palynomorphs and fungi of Cambrian age (Vasković and Tasić, 1997 and references therein). Peak metamorphic conditions of 450-500 °C at 3 to 5 kbar (0.3-0.5 GPa) were reported in the pre-Ordovician Vlasina (Milovanović et al., 1988; Vasković, 2002). However, relicts of high-grade metamorphic assemblages have been reported in the vicinity of the Božica magmatic complex and Vranjska Banja area (Fig. 1-2; Petrović, 1969; Vujanović et al., 1974; Babović et al., 1977; Pavlović, 1977; Vasković, 1998; Vasković et al., 2003). This high-grade metamorphism in the Vlasina Unit has been associated with the "Baikalian" (850–650 Ma) and "Caledonian" orogenic events (Karamata and Krstić, 1996), and the age of the greenschist overprint as early Carboniferous (Dimitrijević, 1963; Petrović, 1969; Krstić and Karamata, 1992; Karamata and Krstić, 1996; Graf, 2001), or post-Variscan (Dimitrijević, 1967).

The pre-Ordovician Vlasina is covered by a meta-sedimentary succession reported as Ordovician to lowest Carboniferous in age (Post-Cambrian Vlasina in Fig. 1-2; Pavlović, 1962, 1977; Spassov, 1973; Babović et al., 1977; Lakova, 1997, 2009). These meta-sedimentary rocks crop-out in thrust sheets at the eastern margin of the Vlasina Unit (Fig. 1-2; Petrović, 1969). The originally transgressive contact with the pre-Ordovician Vlasina reported by Pavlović (1962, 1977) northeast of Bosilegrad (Fig. 1-2), is in fact obscured by intensive deformational overprint. The lowermost part of the sedimentary column comprises phyllites, metasandstones, calcschists, quartzite, marble, sericite and chlorite schists (Babović et al., 1977). An inarticulate brachiopod fauna in the "basal quartzites" suggests an Early Ordovician age (Pavlović, 1962). The Ordovician period is represented from base to top by argillo-phylites, spilites, meta-pelites, quartz and sericitic schists with lenses of quartzite and calcschist (Petrović et al., 1973). The Silurian succession continues with graptolitic schists, conspicuous carbonates with Middle Devonian spillites, ending with turbidites of Upper Devonian to lowest Carboniferous age (Petrović, 1969; Petrović et al., 1973; Spassov, 1973; Krstić, 1981; Krstić et al., 2002; Banjac, 2004; Lakova, 2009; Boncheva et al., 2010). These rocks were subjected to predominantly very low-grade metamorphism with only occasional occurrences of greenschist-facies assemblages (Petrović et al., 1973; Spassov, 1973; Babović et al., 1977; Graf, 2001; Krstić et al., 2002).

Karamata and Krstić (1996) regarded Vlasina Unit as a part of the Suprageticum (i.e. highest structural level in the Carpatho-Balkanid orogen), due to the suggested hanging wall position above the thrust zone separating it from the Lower Complex (i.e. Vrvi Kobila shear zone, Fig. 1-2). This contact was reported as a pre-Mesozoic west-vergent thrust (Vukanović et al., 1973; Krstić and Karamata, 1992), or post-Late Cretaceous dextral shear zone (Kräutner and Krstić, 2002).

Additionally, several reports suggest initial stratigraphic contact between these two units which was later tectonically reactivated (Petrović and Karamata, 1965; Petrović, 1969; Dimitrijević, 1997).

A large complex of magmatic rocks east of Surdulica pluton which has been intruded into the sedimentary rocks of the pre-Ordovician Vlasina (Fig. 1-2) is referred to as Božica granitoid in Serbia (Petrović et al., 1973; Babović et al., 1977), and Milevski granite in Bulgaria (e.g. Graf, 2001; Kounov et al., 2012). It comprises partially deformed granites, diorites and gabbros. A late Cadomian age (551±1 Ma) was determined in the Bulgarian part of this magmatic complex (Kounov et al., 2012), whereas an age of 500 Ma was suggested for the Serbian part of Božica (Kräutner and Krstić, 2002).

1.2.3 Geticum

The Geticum represents a large-scale tectonic zone in the Alpine tectonic framework of the Carpatho-Balkan orogen, comprising a number of tectonic units forming southeast-, east- and northeast- vergent nappes (e.g. Struma, Sredna Gora; Fig. 1-2). During the late Early Cretaceous, the Vlasina Unit was thrust to the east onto the Struma and other Getic units along a system of east- to northeast-vergent thrusts (Petković, 1930; Mihailescu et al., 1967; Petrović, 1969; Zagorchev and Ruseva, 1982; Lilov and Zagorchev, 1993; Kounov et al., 2010). The crystalline basement of the Struma Unit consists of variably deformed continent- and ocean-derived rocks of Ediacaran to early Cambrian protolith age (e.g. Kounov et al., 2012), unconformably overlain by a Permian to Lower Cretaceous sedimentary cover (Zagorchev, 1981). The ophiolites (Frolosh Unit) and a magmatic-arc igneous suite, the Struma Diorite Complex (SDC; Stephanov and Dimitrov, 1936; Haydoutov et al., 1994) are tectonically imbricated (Fig. 1-2). Although the present-day contacts between the fragments of ophiolitic ultramafic rocks, gabbros, diabases, basic tuffs and minor clastic metasediments of the Frolosh Unit, and the gabbros, gabbrodiorites, diorites and granites of SDC are mainly tectonic, primary intrusive contacts can be locally observed. The mafic rocks of the Frolosh ophiolites show affinity to MORB (Haydoutov and Pin, 1993; Kounov et al., 2012). The rocks of the Lower Complex (Ograzhden block; Zagorchev, 1984a), situated in the southeast of the study area (Fig. 1-2), are separated from the overlying SDC and Frolosh Unit by the Gabrov Dol detachment east of the study area (Bonev et al., 1995).

The Crnook-Osogovo–Lisets complex (COL; Fig. 1-2), consists of amphibolites, micaschists, muscovite-biotite and amphibole-biotite gneiss (Dimitrova, 1964; Dimitrijević, 1972; Babović et al., 1977). Lenses of ultramafic rocks were also reported (Haydoutov et al., 1994). The magmatic rocks of the SDC and the Crnook-Osogovo-Lisets complex are derived from the same calc-alkaline magma source and represent a magmatic-arc formed during the Ediacaran to early Cambrian (Kounov et al., 2012). The lower amphibolite-facies metamorphism and deformation in the COL complex were associated with late Early Cretaceous compression in the area (Kounov et al., 2010). The contact of the amphibolitic grade micaschists, gneiss and amphibolites of the Crnook dome with the overlying schists of the post-Cambrian Vlasina was previously reported as transgressive or gradual (Pavlović, 1962; Babović et al., 1977). During the middle Eocene–Oligocene extension, the metamorphic rocks of COL were exhumed from below the SDC along a system of low-angle normal faults (Kounov et al., 2004).

1.2.4 Eastern Veles series

South of the Lece volcanic complex (Fig. 1-2), the Lower Complex is in tectonic contact with the metamorphic series of amphibolites, micaschists, gneisses, amphibolites, quartzites and marbles (Fig. 1-2). These rocks are regarded as part of the Veles series (Karajovanović and Hristov, 1976; Vukanović et al., 1977), which is considered as part of the Circum-Rhodope belt (Zagorchev and Milovanović, 2006; Schmid, 2014), or Internal Vardar zone (Dimitrijević and Drakulić, 1958; Dimitrijević, 1997; Robertson et al., 2009). The Veles series is separated in the eastern and the western part by Jurassic ophiolites and Upper Cretaceous sediments (Vukanović et al., 1977; Pavić et al., 1983; Karamata and Krstić, 1996). The Lower Complex in the study area is in direct contact only with the latter (Fig. 1-2). This contact was previously considered as a strike-slip fault (Malešević et al., 1980; Vukanović et al., 1982), an east-vergent thrust (Krstić and Karamata, 1992), or a westward thrust which was reactivated as a dextral strike slip in the Neogene (Kräutner and Krstić, 2002). It has been recently interpreted as a ductile shear zone (Stefan M. Schmid, personal communication, September 2014). The Eastern Veles series comprises Cambrian to Devonian sediments (Pavlović, 1977), initially metamorphosed under amphibolite-facies conditions, preserved only as relicts due to the later intensive greenschist retrogression (Dimitrijević, 1997). The crystalline rocks of the Eastern Veles series are covered by Triassic sediments metamorphosed to greenschist facies, present only in a small area in the northwestern periphery of the unit (Pavić et al., 1983). In contrast, the Western Veles series comprises predominantly Upper Devonian to

Triassic meta-sedimentary rocks (Pavić et al., 1983; Grubić and Ercegovac, 2002), and low-grade igneous rocks related to a Carboniferous magmatic arc (Karamata, 2006). Most of the previous authors agree that the crystalline rocks of the Eastern Veles series (excluding the Triassic cover) were originally a part of the Lower Complex of the SMM which have subsequently suffered intensive Alpine overprint, less pronounced in the rest of the Lower Complex (Brković et al., 1980; Dolić et al., 1981; Karamata and Krstić, 1996; Dimitrijević, 1997). Another distinctive feature of the Eastern Veles series compared to the SMM is the higher occurrence of marbles (Dimitrijević, 1997).

The voluminous Štip magmatic complex represents a heterogeneous magmatic body comprising granites, monzonites and granodiorites, which intruded the Eastern Veles series near the town of Štip (Fig. 1-2). They contain xenoliths of serpentinite and amphibolite schists, which were considered as Jurassic by Rakićević et al. (1976), and Palaeozoic by Karajovanović and Hadži-Mitrova (1982). The upper age limit for the emplacement of the Štip complex is constrained by the Albian-Cenomanian (i.e. 113-94 Ma) sediments covering the southeastern periphery of the pluton. Rb-Sr dating of biotite from the Štip complex yielded an age of 161±3 Ma which was interpreted as the age of its emplacement (Šoptrajanova, 1967), or as a metamorphic overprint (Spray et al., 1984).

1.2.5 Sedimentary cover

Although a minor extent of Triassic sediments was reported north of the study area, within the study area the oldest undeformed and non-metamorphosed rocks are the Santonian to Lower Maastrichtian sediments (86–70 Ma, Fig. 1-2). These Late Cretaceous basins were formed in a relatively shallow environment, filled with predominantly terrigenous clastics with subordinate marls and limestones (Petrović et al., 1973). Palaeogene sediments are represented by terrigenous to carbonate continental deposits of the middle Eocene (Petrović et al., 1973; Vukanović et al., 1973; Anđelković and Anđelković, 1995), turbidites of the Upper Eocene (Vukanović et al., 1977; Dimitrijević and Dimitrijević, 1987), and marine to limnic sediments of the Oligocene (Vukanović et al., 1973, 1977). These deposits were most probably deposited in the extensional half-grabens formed in the hanging wall position of the low-angle normal faults. Palaeogene sediments are often intercalated with various pyroclastic rocks or intruded by small dacitic or andesitic bodies and dykes, that also intruded into the basement. The largest magmatic body in the area is the Surdulica granodiorite (Fig. 1-2), previously reported to be emplaced at 30–25 Ma (Rb-Sr; Deleon, 1969), or 34–28 Ma (K-Ar; Simić, 1997). The most prominent occurrence of Oligocene volcanism is the Lece andesitic complex (Vukanović et al., 1973) with a formation age of 32-28 Ma as determined by K-Ar method (Pamić and Balen, 2001).

The Neogene sediments in the area are represented by middle Miocene clastic deposits and fresh-water marls, which have been continually deposited also during the Pliocene (Vukanović et al., 1973, 1977). These sediments are intercalated with dacitic and andesitic volcanoclastic rocks (Vukanović et al., 1977).

1.3 Objectives

An overarching goal of this study is to define the origin and tectonic evolution of the central SMM. Although an overview of petrological and geochemical properties of the rocks exposed in this area was already available, their provenance, relationships, deformational evolution and timing of exhumation needed thorough reinterpretation in context of contemporary tectonic paradigms.

The ages of emplacement of variously deformed magmatic rocks were determined by analyses of U-Pb isotopic ages obtained by LA-ICP-MS measurements. Geochronological data obtained by this method was supplemented by analyses of Hf isotopes in the previously dated zircon domains, in order to examine possible sources of magma generated during distinct phases of magmatic activity. Geotectonic settings during these magmatic phases were investigated further by geochemical analyses of main- and trace-element concentrations of whole-rock samples of magmatic rocks. Furthermore, U-Pb ages from inherited cores, xenocrysts and detrital zircons gave insights into the provenance of sedimentary rocks and the possible basement of magmatic rocks in the central SMM and adjacent crystalline units. Detailed description of the samples, analytical procedures, their results and the resulting tectonic model are presented in Chapter 2.

The history of ductile deformation in the central SMM was often neglected or misinterpreted in the previous large-scale tectonic reconstructions. Despite the overall poor condition of exposures, the outrcop- and micro-scale structural evidence was examined in order to define the different stages of ductile deformation and their relative succession. Contacts between the different units constituting the central SMM were previously reported with high ambiguity and needed thorough substantiation. Medium-temperature cooling ages were investigated using the $^{40}Ar/^{39}Ar$ thermochronology in order to constrain the timing of deformational and metamorphic events. The $^{40}Ar/^{39}Ar$ method was applied on hornblende, muscovite and biotite minerals in order to constrain the thermal evolution of rocks in the central SMM at temperatures ranging from 545 to 325 °C. Detailed structural analyses, interpretation of $^{40}Ar/^{39}Ar$ cooling ages and the resulting reconstruction are presented in Chapter 3.

The timing and mode of exhumation of metamorphic rocks in the study area was investigated using the fission-track analyses on zircon and apatite. Given the effective detection range of this method for geological processes taking place between 300 and 60 °C, the ages of tectonic activity along the major structures could be constrained, along with examination of the low-temperature evolution of the central SMM and the neighbouring basement units. Additionally, U–Pb dating of zircons from the Palaeogene igneous rocks was used to determine the exact age of their emplacement, while the results of the fission-track analyses from these rocks contribute to determining the influence of this magmatism on the regional thermal gradient. The Palaeogene magmatic activity and the low-temperature evolution of the study area are presented in Chapter 4.

References

Anđelković, M., Anđelković, J., 1995. Značaj Ilirske faze za geološki razvoj Moravida. Geološki anali Balkanskoga poluostrva 59, 1–11.

Babović, M., Roglić, Č., Avramović, V., Marić, S., 1977. Tumač za list Trgovište sa Radomirom, Osnovna Geološka Karta 1:100000. Savezni Geološki Zavod, Belgrade.

Balintoni, I., Balica, C., Seghedi, A., Ducea, M.N., 2010. Avalonian and Cadomian terranes in North Dobrogea, Romania. Precambrian Research 182, 217–229.

Balogh, K., Svingor, É., Cvetković, V., 1994. Ages and intensities of metamorphic processes in the Batočina area, Serbo-Macedonian massif. Acta Mineralogica-Petrographica XXXV, 81–94.

Banjac, N., 2004. Stratigrafija Srbije i Crne Gore. Rudarsko-geološki fakultet, Belgrade.

Boev, B., Lepitkova, S., Petrov, G., 2002. Granitoid formations in the Republic of Macedonia, in: Proceedings of XVII Congress of CBGA. Presented at the XVII Congress of CBGA, VEDA, Bratislava, pp. 1–22.

Boncheva, I., Lakova, I., Sachanski, V., Koenigshof, P., 2010. Devonian stratigraphy, correlations and basin development in the Balkan Terrane, western Bulgaria. The Rheic Ocean: Palaeozoic Evolution from Gondwana and Laurussia to Pangaea 17, 573–582.

Bonev, K., Ivanov, Z., Ricou, L.-E., 1995. Dénudation tectonique au toit du noyau métamorphique Rhodopien-macédonien: La faille normale ductile de Gabrov Dol (Bulgarie). Bulletin de la Société Géologique de France 166, 47–55.

Bosse, V., Boulvais, P., Gautier, P., Tiepolo, M., Ruffet, G., Devidal, J.L., Cherneva, Z., Gerdjikov, I., Paquette, J.L., 2009. Fluid-induced disturbance of the monazite Th–Pb chronometer: In situ dating and element mapping in pegmatites from the Rhodope (Greece, Bulgaria). Chemical Geology 261, 286–302.

Boué, A., 1840. La Turquie d'Europe. Bertrand, Paris.

Brković, T., Radovanović, Z., Pavlović, Z., 1980. Tumač za list Kragujevac, Osnovna Geološka Karta 1:100000. Savezni Geološki Zavod, Belgrade.

Brun, J.-P., Sokoutis, D., 2007. Kinematics of the Southern Rhodope Core Complex (North Greece). International Journal of Earth Sciences 96, 1079–1099.

Burg, J.-P., 2012. Rhodope: From Mesozoic convergence to Cenozoic extension. Review of petro-structural data in the geochronological frame. Journal of the Virtual Explorer, The Geology of Greece 42.

Burg, J.-P., Godfriaux, I., Ricou, L.-E., 1995. Extension of the Mesozoic Rhodope thrust units in the Vertiskos-Kerdilion Massifs (Northern Greece). Comptes Rendus de l'Académie des Sciences Paris, Sciences de la Terre et des Planetes 320, 889–896.

Burg, J.-P., Ricou, L.-E., Ivano, Z., Godfriaux, I., Dimov, D., Klain, L., 1996a. Syn-metamorphic nappe complex in the Rhodope Massif. Structure and kinematics. Terra Nova 8, 6–15.

Burg, J.-P., Ricou, L.-E., Klain, L., Ivanov, Z., Dimov, D., 1996b. Crustal-Scale Thrust Complex in the Rhodope Massif, in: Nairn, A.M., Ricou, L.-E., Vrielynck, B., Dercourt, J. (Eds.), The Tethys Ocean, The Ocean Basins and Margins. Plenum Press, New York, pp. 125–149.

Cvetković, V., 1992. Petrology of the metamorphic rocks from the northern parts of the Serbo-macedonian massif in the Batočina area (Magistar thesis). Faculty of Mining and Geology, Belgrade.

Cvijić, J., 1902. Struktura i podela planina Balkanskog poluostrva. Glas Srpske kraljevske akademije 63, 1–71.

Cvijić, J., 1906. Osnove za geografiju i geologiju Makedonije i Stare Srbije. Srpska Kraljevska Akadmija, Belgrade.

Dabovski, C., Boyanov, I., Khrischev, K., Nikolov, T., Sapunov, I., Yanev, Y., Zagorchev, I.S., 2002. Structure and Alpine evolution of Bulgaria. Geologica Balcanica 32, 9–15.

Deleon, G., 1969. Pregled rezultata određivanja apsolutne geološke starosti granitoidnih stena u Jugoslaviji. Radovi Instituta za geološko-rudarska istraživanja i ispitivanja nuklearnih i drugih mineralnih sirovina 6, 165–180.

Dewey, J.F., Pitman, W.C., Ryan, W.B.F., Bonnin, J., 1973. Plate Tectonics and the Evolution of the Alpine System. Geological Society of America Bulletin 84, 3137–3180.

Dimitrijević, M.D., 1957. Struktura kristalastih terena između Slišana i Preševa, in: Referati, predavanja, diskusije. Presented at the II kongres geologa FNRJ, Savez geoloških društava Jugoslavije, Sarajevo.

Dimitrijević, M.D., 1958. Geološki sastav i struktura bujanovačkog granitskog masiva. Rasprave zavoda za geološka i geofizička ispitivanja narodne republike Srbije 3.

Dimitrijević, M.D., 1963. Sur l'âge du métamorphisme et des plissements dans la masse Serbo-macédonienne, in: Bulletin. Presented at the VIe Congrès de l'Association géologique carpatho-balkanique, Instytut Geologiczny, Warszawa, pp. 339–347.

Dimitrijević, M.D., 1967. Some Problems of Crystalline Schists in the Serbo-Macedonian Massif, in: Reports. Presented at the VIII Congress of CBGA, Serbian Geological Society, Belgrade, pp. 59–67.

Dimitrijević, M.D., 1972. Variscijski metamorfizam u aksijalnom delu Balkanskog poluostrva (mogućnosti nove genetske interpretacije). Zapisnici Srpskog geološkog društva za 1971. godinu, 115–124.

Dimitrijević, M.D., 1997. Geology of Yugoslavia. Geological Institute GEMINI, Belgrade.

Dimitrijević, M.D., Drakulić, N., 1958. Kristalasti škriljci Jablanice. Zbornik radova Rudarsko-geološkog fakulteta 6.

Dimitrijević, M.N., Dimitrijević, M.D., 1987. The Turbiditic Basins of Serbia, Serbian Academy of Science and Arts, Monographs. Serbian Academy of Science and Arts, Belgrade.

Dimitrova, E., 1964. Petrologie des kristallinen Sockels des Osogovo Gebirges. Bulgarian Academy of Sciences Bulletin of the Geological Institute, Stratigr Lithol 13, 99–110.

Dinter, D.A., Royden, L., 1993. Late Cenozoic extension in northeastern Greece: Strymon Valley detachment system and Rhodope metamorphic core complex. Geology 21, 45.

Dolić, D., Kalenić, M., Marković, B., Dimitrijević, M., Radoičić, R., Lončarević, Č., 1981. Tumač za list Paraćin, Osnovna Geološka Karta 1:100000. Savezni Geološki Zavod, Belgrade.

Georgiev, N., Pleuger, J., Froitzheim, N., Sarov, S., Jahn-Awe, S., Nagel, T.J., 2010. Separate Eocene–Early Oligocene and Miocene stages of extension and core complex formation in the Western Rhodopes, Mesta Basin, and Pirin Mountains (Bulgaria). Tectonophysics 487, 59–84.

Georgiev, S., Peytcheva, I., Stefanova, E., von Quadt, A., Marchev, P., Grozdev, V., Serafimovski, T., 2012. Geochemistry and geochronology of Ilovitsa magmatic rocks, SE FYR Macedonia, in: Abstracts Book. Presented at the International Earth Science Colloquium on the Aegean Region, IESCA-2012, Izmir, p. 94.

Graf, J., 2001. Alpine tectonics in Western Bulgaria: Cretaceous compression of the Kraishte region and Cenozoic exhumation of the crystalline Osogovo–Lisets Complex (PhD). ETH Zürich, Zürich.

Grubić, A., Đoković, I., Marović, M., Branković, M., 1999. Srpsko-Makedonska masa ne postoji. Vesnik, Geologija, hidrogeologija i inženjerska geologija 49, 1–14.

Grubić, A., Đoković, I., Marović, M., Branković, M., 2005. Problem tektonskog položaja kristalina

Srpsko-Makedonske mase. Zapisnici Srpskog geološkog društva za 1998, 1999, 2000, 2001, 2002 i 2003. godinu, 35–39.

Grubić, A., Ercegovac, M., 2002. Age of the Veles “Schistes Lustres” Formation from the Vardar Ocean, in: Proceedings of XVII Congress of CBGA. Presented at the XVII Congress of CBGA, VEDA, Bratislava, pp. 66–68.

Haydoutov, I., Kolcheva, K., Daieva, L., 1994. The Struma diorite fm from Vlahina block, SW Bulgaria. Review of the Bulgarian Geological Society 55, 9–35.

Haydoutov, I., Pin, C., 1993. Geochemical and Nd isotope characteristics of pre-variscan ophiolites and meta-igneous rocks from the Struma Diorite Formation in SW Bulgaria. Geologica Balcanica 23, 51–59.

Haydoutov, I., Yanev, S., 1997. The Protomoesian microcontinent of the Balkan Peninsula — a peri-Gondwanaland piece. Tectonophysics 272, 303–313.

Himmerkus, F., Anders, B., Reischmann, T., Kostopoulos, D., 2007. Gondwana-derived terranes in the northern Hellenides. Geological Society of America Memoirs 200, 379–390.

Himmerkus, F., Reischmann, T., Kostopoulos, D., 2006. Late Proterozoic and Silurian basement units within the Serbo-Macedonian Massif, northern Greece: the significance of terrane accretion in the Hellenides. Geological Society, London, Special Publications 260, 35–50.

Himmerkus, F., Reischmann, T., Kostopoulos, D., 2009. Serbo-Macedonian revisited: A Silurian basement terrane from northern Gondwana in the Internal Hellenides, Greece. Tectonophysics 473, 20–35.

Iancu, V., Màruntiu, M., Johan, V., Ledru, P., 1998. High-grade metamorphic rocks in the pre-Alpine nappe stack of the Getic-Supragetic basement (Median Dacides, South Carpathians, Romania). Mineralogy and Petrology 63, 173–198.

Ilić, M., Karamata, S., Knežević-Đorđević, V., 1967. Serpentinites and Ultramafic Rocks of East Serbia, in: Reports. Presented at the VIII Congress of CBGA, Serbian Geological Society, Belgrade, pp. 91–105.

Ivanova, P., Zidarov, N., 2011. Metamorphic evolution of spinel clinopyroxenites with clinopyroxene megacrysts from Ograzhden Mountain, SW Bulgaria, in: Proceedings. Presented at the National Conference with international participation Geosciences 2011, Bulgarian Geological Society, Sofia, pp. 61–62.

Kaiser-Rohrmeier, M., Handler, R., von Quadt, A., Heinrich, C., 2004. Hydrothermal Pb–Zn ore formation in the Central Rhodopian Dome, south Bulgaria: Review and new time constraints from Ar–Ar geochronology. Swiss Bulletin of Mineralogy and Petrology 84, 37–58.

Kalvoda, J., Bábek, O., 2010. The Margins of Laurussia in Central and Southeast Europe and Southwest Asia. Gondwana Research 17, 526–545.

Karajovanović, M., Hadži-Mitrova, S., 1982. Tolkuvač za listot Titov Veles, Osnovna Geološka Karta 1:100000. Savezni Geološki Zavod, Belgrade.

Karajovanović, M., Hristov, S., 1976. Tolkuvač za listot Kumanovo, Osnovna Geološka Karta 1:100000. Savezni Geološki Zavod, Belgrade.

Karamata, S., 2006. The geological development of the Balkan Peninsula related to the approach, collision and compression of Gondwanan and Eurasian units. Geological Society, London, Special Publications 260, 155–178.

Karamata, S., Krstić, B., 1996. Terranes of Serbia and Neighbouring Areas, in: Knežević-Đorđević, V., Krstić, B. (Eds.), Terranes of Serbia. Faculty of Mining and Geology, University of Belgrade, Belgrade, pp. 25–40.

Kilias, A., Falalakis, G., Mountrakis, D., 1997. Alpine tectonometamorphic history of the Serbomacedonian metamorphic rocks: implication for the tertiary unroofing of the Serbomacedonian-Rhodope metamorphic complexes (Makedonia, Greece). Ορυκτός

Πλούτος 105, 32–50.

Kilias, A., Falalakis, G., Mountrakis, D., 1999. Cretaceous–Tertiary structures and kinematics of the Serbomacedonian metamorphic rocks and their relation to the exhumation of the Hellenic hinterland (Macedonia, Greece). International Journal of Earth Sciences 88, 513–531.

Kober, L., 1952. Leitlinen der Tektonik Jugoslawiens, Posebna izdanja Srpske akademije nauka. Naučna knjiga, Beograd.

Kockel, F., Mollat, H., Walther, H.W., 1971. Geologie der Serbo-Mazedonischen Massivs und seines mesozoischen Rahmens (Nordgriechenland). Geologisches Jahrbuch 89, 529–551.

Korikovsky, S., Karamata, S., Milovanović, D., 2003. Retrograted kyanite eclogites and eclogittized gabbro-norites of the Serbo-macedonian unit, Central Serbia , reaction textures and geothermobarometry, in: Zbornik Abstraktov. Presented at the Konferencia venovanej Prof. rNDr. Dušanovi Hovorkovi, DrSc. k životnému jubileu, Bratislava, pp. 13–14.

Kounov, A., Burg, J.-P., Bernoulli, D., Seward, D., Ivanov, Z., Dimov, D., Gerdjikov, I., 2011. Paleostress analysis of Cenozoic faulting in the Kraishte area, SW Bulgaria. Journal of Structural Geology 33, 859–874.

Kounov, A., Graf, J., von Quadt, A., Bernoulli, D., Burg, J.-P., Seward, D., Ivanov, Z., Fanning, M., 2012. Evidence for a “Cadomian” ophiolite and magmatic-arc complex in SW Bulgaria. Precambrian Research 212–213, 275–295.

Kounov, A., Seward, D., Bernoulli, D., Burg, J.-P., Ivanov, Z., 2004. Thermotectonic evolution of an extensional dome: the Cenozoic Osogovo-Lisets core complex (Kraishte zone, western Bulgaria). International Journal of Earth Sciences 93, 1008–1024.

Kounov, A., Seward, D., Burg, J.-P., Bernoulli, D., Ivanov, Z., Handler, R., 2010. Geochronological and structural constraints on the Cretaceous thermotectonic evolution of the Kraishte zone, western Bulgaria. Tectonics 29, TC2002.

Kounov, A., Wüthrich, E., Seward, D., Burg, J.-P., Stockli, D., 2015. Low-temperature constraints on the Cenozoic thermal evolution of the Southern Rhodope Core Complex (Northern Greece). International Journal of Earth Sciences 104, 1–16.

Kräutner, H.G., Krstić, B., 2002. Alpine and pre-Alpine structural units within the southern Carpathians and eastern Balkanides, in: Proceedings of XVII Congress of CBGA. Presented at the XVII Congress of CBGA, VEDA, Bratislava.

Kräutner, H.G., Krstić, B., 2003. Geological map of the Carpatho-Balkanides between Mehadia, Oravița , Niš and Sofia.

Kroner, U., Romer, R.L., 2013. Two plates — Many subduction zones: The Variscan orogeny reconsidered. Gondwana Research 24, 298–329.

Krstić, B., 1981. Niški kaledonsko-hercinski geosinklinalni pojas u istočnoj Srbiji. Zapisnici Srpskog geološkog društva za 1980. godinu, 99–103.

Krstić, B., Maslarević, L., Ercegovac, M., Đajić, S., 2002. Devonian of the Serbian Carpatho-Balkanides, in: Proceedings of XVII Congress of CBGA. Presented at the XVII Congress of CBGA, VEDA, Bratislava.

Krstić, N., Karamata, S., 1992. Terani u Karpato-Balkanidima istočne Srbije. Zapisnici Srpskog geološkog društva jubilarna knjiga (1891-1991), 57–69.

Kydonakis, K., Gallagher, K., Brun, J.-P., Jolivet, M., Gueydan, F., Kostopoulos, D., 2014. Upper Cretaceous exhumation of the western Rhodope Metamorphic Province (Chalkidiki Peninsula, northern Greece). Tectonics 33, 2014TC003572.

Kydonakis, K., Moulas, E., Chatzitheodoridis, E., Brun, J.-P., Kostopoulos, D., 2015. First-report on Mesozoic eclogite-facies metamorphism preceding Barrovian overprint from the western Rhodope (Chalkidiki, northern Greece). Lithos 220–223, 147–163.

Lakova, I., 1997. Additional palynological data on the age of the Razhcha Formation, Osogovo

Mts., West Bulgaria. Geologica Balcanica 27, 36.

Lakova, I., 2009. Acritarch evidence on Silurian age of the low-grade metamorphic Palaeozoic rocks in the Kraishte area (Morava Unit). Review of the Bulgarian Geological Society 70, 23–30.

Liati, A., 2005. Identification of repeated Alpine (ultra) high-pressure metamorphic events by U–Pb SHRIMP geochronology and REE geochemistry of zircon: the Rhodope zone of Northern Greece. Contributions to Mineralogy and Petrology 150, 608–630.

Lilov, P., Zagorchev, I.S., 1993. K-Ar data for the deformation and low-grade metamorphism in Permian and Triassic red beds in SW Bulgaria. Geologica Balcanica 23, 46.

Macheva, L., Titorenkova, R., Zidarov, N., 2005. Kyanite-staurolite-garnet orthoschists (Annual No. 11).

Malešević, M., Vukanović, M., Obradinović, Z., Dimitrijević, M., Brković, T., Stefanović, M., Stanisavljević, R., Jovanović, O., Trifunović, S., Karajičić, L., Jovanović, M., Pavlović, Z., 1980. Tumač za list Kuršumlija, Osnovna Geološka Karta 1:100000. Savezni Geološki Zavod, Belgrade.

Medaris Jr., G., Ducea, M., Ghent, E., Iancu, V., 2003. Conditions and timing of high-pressure Variscan metamorphism in the South Carpathians, Romania. Lithos 70, 141–161.

Meinhold, G., Kostopoulos, D., Frei, D., Himmerkus, F., Reischmann, T., 2010. U–Pb LA-SF-ICP-MS zircon geochronology of the Serbo-Macedonian Massif, Greece: palaeotectonic constraints for Gondwana-derived terranes in the Eastern Mediterranean. International Journal of Earth Sciences 99, 813–832.

Meinhold, G., Kostopoulos, D., Reischmann, T., Frei, D., BouDagher-Fadel, M.K., 2009. Geochemistry, provenance and stratigraphic age of metasedimentary rocks from the eastern Vardar suture zone, northern Greece. Palaeogeography, Palaeoclimatology, Palaeoecology 277, 199–225.

Mihailescu, N., Dimitrijević, M.D., Dimitrijević, M.N., 1967. Les fossiles dans le flysch, in: Reports. Presented at the VIII Congress of CBGA, Serbian Geological Society, Belgrade, pp. 371–378.

Milovanović, D., 1990. Petrologija gnajseva Srpsko-makedonske mase u području između Tulara i Lebana, in: Proceedings of the XII Congress of the Geologists of Yugoslavia. Presented at the XII Kongres na geolozi na Jugoslavija, Prosveta, Ohrid, pp. 310–321.

Milovanović, D., 1992. Amfibolske stene u području između Medveđe i Lebana. Geološki anali Balkanskoga poluostrva 56, 253–268.

Milovanović, D., Milovanović, M., Oberhänsli, R., 1988. Petrology of green-rocks of the Vlasina complex in the Manastiriška river area (Vlasotince). Vesnik, Geologija 44, 101–128.

Munteanu, M., Tatu, M., 2003. The East-Carpathian Crystalline-Mesozoic Zone (Romania): Paleozoic Amalgamation of Gondwana- and East European Craton-derived Terranes. Gondwana Research 6, 185–196.

Nenova, P., Marinova, I., 2007. New data on serpentinized ultramafic body near Kamena village, Belasitsa Mountain, Serbo-Macedonian Massif, SW Bulgaria (Annual No. 13).

Nenova, P., Zidarov, N., 2008. Eclogites from Maleshevska Mountain, SW Bulgaria (Annual No. 14).

Neubauer, F., 2002. Evolution of late Neoproterozoic to early Paleozoic tectonic elements in Central and Southeast European Alpine mountain belts: review and synthesis. Tectonophysics 352, 87–103.

Pamić, J., Balen, D., 2001. Tertiary magmatism of the Dinarides and the adjoining South Pannonian Basin. Acta vulcanologica 13, 9–24.

Pantić, N., Dimitrijević, M.D., Hercegovac, M., 1967. Mikrofloristički podaci o starosti Vlasinskog kompleksa. Zapisnici Srpskog geološkog društva.

Pavić, A., Menković, L., Košćal, M., 1983. Tumač za list Uroševac, Osnovna Geološka Karta 1:100000. Savezni Geološki Zavod, Belgrade.

Pavlović, P., 1962. O nekim ordovicijskim inartikulatnim brahiopodima u metamorfnim stenama kod Bosiljgrada (Jugoistočna Srbija) i o značaju ovog nalaska. Geološki anali Balkanskoga poluostrva 39, 99–112.

Pavlović, P., 1977. O “Gornjem (Vlasinskom) kompleksu” i podeli metamorfnih stena Srpsko-Makedonskog metamorfnog terena. Zapisnici Srpskog geološkog društva za 1975. i 1976. godinu, 123–132.

Petković, V., 1930. O tektonskom sklopu istočne Srbije. Glas Srpske kraljevske akademije, drugi razred 140, 151–188.

Petrović, B., Dimitrijević, M.D., Karamata, S., 1973. Tumač za list Vlasotince, Osnovna Geološka Karta 1:100000. Savezni Geološki Zavod, Belgrade.

Petrović, B., S., 1969. The Structure of the Vlasina Crystalline Complex in the Broad Area of Crna Trava. Belgrade.

Petrović, B., S., Karamata, S., 1965. Metaklastiti - baza gornjeg kompleksa kristalastih škriljaca SMM, in: Proceedings. Presented at the 7th Congress of the Geologists of Yugoslavia, Zagreb.

Peytcheva, I., von Quadt, A., Tarassov, M., Zidarov, N., Tarassova, E., Andreichev, V., 2009. Timing of Igralishte pluton in Ograzhden Mountain, SW Bulgaria: implications for the tectono-magmatic evolution of the region. Geologica Balcanica 38, 5–14.

Popović, R., 1991. Srpsko-Makedonska masa ili Pelagonsko-Rodopski i Moravski masiv. Radovi Geoinstituta 25, 7–20.

Popović, R., 1995. Srpsko-Makedonska masa: da ili ne? Zapisnici Srpskog geološkog društva za 1990. i 1991. godinu, 59–61.

Rakićević, T., Dumurdžanov, N., Petkovski, P., 1976. Tolkuvač za listot Štip, Osnovna Geološka Karta 1:100000. Savezni Geološki Zavod, Belgrade.

Rakićević, T., Kovačević, M., Radović, N., Pendžerkovski, J., 1973. Tolkuvač za listot Strumica, Osnovna Geološka Karta 1:100000. Savezni Geološki Zavod, Belgrade.

Ricou, L.-E., Burg, J.-P., Godfriaux, I., Ivanov, Z., 1998. Rhodope and Vardar: the metamorphic and the olistostromic paired belts related to the Cretaceous subduction under Europe. Geodinamica Acta 11, 285–309.

Robertson, A., Karamata, S., Šarić, K., 2009. Overview of ophiolites and related units in the Late Palaeozoic–Early Cenozoic magmatic and tectonic development of Tethys in the northern part of the Balkan region. Lithos 108, 1–36.

Săndulescu, M., 1984. Geotectonica Romaniei. Editura Tehnică, Bucharest.

Schmid, S.M., 2014. A compilation of tectonic units of the Alpine collision zone between Alps and Western Turkey.

Schmid, S.M., Bernoulli, D., Fügenschuh, B., Matenco, L., Schefer, S., Schuster, R., Tischler, M., Ustaszewski, K., 2008. The Alpine-Carpathian-Dinaridic orogenic system: correlation and evolution of tectonic units. Swiss Journal of Geosciences 101, 139–183.

Simić, M., 1997. Geohronološka starost tercijarnih granitoida Surdulice (JI Srbija). Geološki anali Balkanskoga poluostrva 61, 63–82.

Šoptrajanova, G., 1967. Petrološke i geohronološke karakteristike nekih granitoida Makedonije. University of Belgrade, Belgrade.

Spassov, C., 1973. Stratigraphie des Devons in Sudwest-Bulgarien. Bulletin of the Geological Institute, Stratigraphy and Lithology 22, 5–38.

Spray, J.G., Bébien, J., Rex, D.C., Roddick, J.C., 1984. Age constraints on the igneous and metamorphic evolution of the Hellenic-Dinaric ophiolites. Geological Society, London, Special Publications 17, 619–627.

Stampfli, G.M., von Raumer, J.F., Borel, G.D., 2002. Paleozoic evolution of pre-Variscan terranes: From Gondwana to the Variscan collision. Geological Society of America Special Papers 364, 263–280.

Stephanov, A., Dimitrov, Z., 1936. Geologische Untersuchungen im Kustendiler Gebiet. Review of the Bulgarian Geological Society 8, 1–28.

Tarassov, M., Tarassova, E., von Quadt, A., 2007. Electron microprobe dating of allanite from the Skrat granitoids (Annual No. 13).

Turpaud, P., Reischmann, T., 2010. Characterisation of igneous terranes by zircon dating: implications for UHP occurrences and suture identification in the Central Rhodope, northern Greece. International Journal of Earth Sciences 99, 567–591.

Van Hinsbergen, D.J.J., Schmid, S.M., 2012. Map view restoration of Aegean–West Anatolian accretion and extension since the Eocene. Tectonics 31, TC5005.

Vasković, N., 1998. P-T condition of the mica schists from the Vranjska Banja Series, in: Proceedings of the XIII Congress of the Geologists of Yugoslavia. Presented at the XIII Congress of the Geologists of Yugoslavia, Herceg Novi, pp. 41–59.

Vasković, N., 2002. Petrology and P-T condition of white mica-chlorite schists from Vlasina series - Surdulica, SE Serbia. Geološki anali Balkanskoga poluostrva 199–220.

Vasković, N., Matović, V., Srećković-Batoćanin, D., 2003. Petrology of Garnet-amphibolite with White Mica from Vranjska Banja Series (Serbian-Macedonian Massif, SE Serbia). Studia Universitatis Babeş-Bolyai, Studia Geologia 128–133.

Vasković, N., Tasić, Z., 1997. Geologija granodioritskog masiva Surdulice, Geološka karta SRJ 1:50.000. Savezno ministarstvo za privredu SRJ, Belgrade.

Von Raumer, J.F., Stampfli, G.M., Bussy, F., 2003. Gondwana-derived microcontinents — the constituents of the Variscan and Alpine collisional orogens. Tectonophysics 365, 7–22.

Vujanović, V., Cvetić, S., Teofilović, M., 1974. Poreklo gnajseva Srbije i Makedonije. Zapisnici Srpskog geološkog društva za 1973. godinu, 266–270.

Vukanović, M., Dimitrijević, M.D., Dimitrijević, M., Karajičić, L., Rakić, M.., 1977. Tumač za list Vranje, Osnovna Geološka Karta 1:100000. Savezni Geološki Zavod, Belgrade.

Vukanović, M., Dimitrijević, M., Dimitrijević, M.D., Karajičić, L., Rajčević, D., Pejčić, M., 1982. Tumač za list Podujevo, Osnovna Geološka Karta 1:100000. Savezni Geološki Zavod, Belgrade.

Vukanović, M., Karajičić, L., Dimitrijević, M.D., Možina, A., Gagić, N., Jevremović, M., 1973. Tumač za list Leskovac, Osnovna Geološka Karta 1:100000. Savezni Geološki Zavod, Belgrade.

Zagorchev, I.S., 1981. Early Alpine deformations in the red beds within the Poletinci-Skrino fault zone. 2. Structure and deformations in the northern parts of the Vlahina block. Geologica Balcanica 11, 101–126.

Zagorchev, I.S., 1984a. Pre-Alpine structure of South-west Bulgaria, in: Zagorchev, I.S., Mankov, S., Bozkov, I. (Eds.), Problems of the Geology of Southwestern Bulgaria. Tehnika, Sofia, pp. 9–20.

Zagorchev, I.S., 1984b. The role of overthrusts in the Alpine structure of Krajistides. Geologica Balcanica 14, 37–64.

Zagorchev, I.S., 1985. Deformation during the first stage of the Alpine Orogeny in the Skrino-Poletintsi faulted zone; IV Shipochan Anticline. Review of the Bulgarian Geological Society 46, 287–298.

Zagorchev, I.S., 2008. Amphibolite-facies metamorphic complexes in Bulgaria and Precambrian geodynamics: controversies and “state of the art.” Geologica Balcanica 37, 33–46.

Zagorchev, I.S., Balica, C., Balintoni, I., Kozhoukharova, E., Dimitrescu, R., Sâbâu, G., Negulescu, E., 2011. New Isotopic Data on the Metamorphic Rocks in SW Bulgaria, in: Proceedings of the 3rd International Symposium on the Geology of the Black Sea Region. Presented at the 3rd International Symposium on the Geology of the Black Sea Region, GeoEcoMar, Bucharest, pp. 223–225.

Zagorchev, I.S., Milovanović, D., 2006. Deformations and Metamorphism in the Eastern Parts of the Serbo-Macedonian Massif, in: Proceedings. Presented at the XVIII Congress of CBGA, Serbian Geological Society, Belgrade, pp. 670–673.

Zagorchev, I.S., Ruseva, M., 1982. Nappe structure of the southern parts of Osogovo Mts and the Pijanec region (SW Bulgaria). Geologica Balcanica 12, 35–57.

Zagortchev, I.S., 1993. Alpine evolution of the pre-Alpine amphibolite-facies basement in South Bulgaria. Mitteilungen der Österreichischen Geologischen Gesellschaft 86, 9–21.

Zidarov, N., Peytcheva, I., von Quadt, A., Andreichev, V., Macheva, L., Titorenkova, R., 2003. Mineral-petrological, geochemical and isotope studies of geological units in Serbo-Macedonian Massif, SW Bulgaria (Annual No. 9).

Zidarov, N., Peytcheva, I., von Quadt, A., Macheva, L., Nenova, P., 2007a. Distinction of crustal terranes in Ograzhden and Belassitsa Mountains, Serbo-Macedonian Massif (SW Bulgaria), based on U-Pb conventional and LA-ICP-MS dating of zircons (Annual No. 13).

Zidarov, N., Tarassova, E., Peytcheva, I., von Quadt, A., Andreichev, V., Titorenkova, R., 2007b. Petrology, geochemistry and age dating of Skrut granitoids – new evidence for Early Triassic magmatism in Belasitsa Mountain (SW Bulgaria). Geologica Balcanica 36, 17–29.

Chapter 2

Pre-Alpine evolution of a segment of the North-Gondwanan margin: Geochronological and geochemical evidence from the central Serbo-Macedonian Massif

Milorad Antić[a], Irena Peytcheva[bc], Albrecht von Quadt[c], Alexandre Kounov[a], Branislav Trivić[d], Todor Serafimovski[e], Goran Tasev[e], Ianko Gerdjikov[f], Andreas Wetzel[a]

[a]Institute for Geology and Palaeontology, Basel University, 4056 Basel, Switzerland;

[b]Geological Institute, Bulgarian Academy of Sciences, 1113 Sofia, Bulgaria

[c]Institute of Geochemistry and Petrology, ETH-Zürich, 8092 Zürich, Switzerland

[d]Faculty of Mining and Geology, University of Belgrade, 11000 Belgrade, Serbia

[e]Faculty of Natural and Technical Sciences, University "Goce Delčev", 2000 Štip, Republic of Macedonia

[f]Faculty of Geology and Geography, University "St. Kl. Ohridski", 1504 Sofia, Bulgaria

This chapter has been published in: Gondwana Research 36, 523–544.
doi:10.1016/j.gr.2015.07.020.

Abstract

The Serbo-Macedonian Massif (SMM) represents a composite crystalline belt within the Eastern European Alpine orogen, outcropping from the Pannonian basin in the north, to the Aegean Sea in the south. The central parts of the massif (i.e. southeastern Serbia, southwestern Bulgaria, eastern Macedonia) consist of the medium- to high-grade Lower Complex, and the low-grade Vlasina Unit. New results of U–Pb LA-ICP-MS analyses, coupled with geochemical analyses of Hf isotopes on magmatic and detrital zircons, and main and trace element concentrations in whole-rock samples suggest that the central SMM and the basement of the adjacent units (i.e. Eastern Veles series and Struma Unit) originated in the central parts of the northern margin of Gondwana. These data provided a basis for a revised tectonic model of the evolution of the SMM from the late Ediacaran to the Early Triassic.

The earliest magmatism in the Lower Complex, Vlasina Unit and the basement of Struma Unit is related to the activity along the late Cadomian magmatic arc (562-522 Ma). Subsequent stage of early Palaeozoic igneous activity is associated with the reactivation of subduction below the Lower Complex and the Eastern Veles series during the Early Ordovician (490-478 Ma), emplacement of mafic dykes in the Lower Complex due to aborted rifting in the Middle Ordovician (472-456 Ma), and felsic within-plate magmatism in the early Silurian (439±2 Ma). The third magmatic stage is represented by Carboniferous late to post-collisional granites (328-304 Ma). These granites intrude the gneisses of the Lower Complex, in which the youngest deformed igneous rocks are of early Silurian age, thus constraining the high-strain deformation and peak metamorphism to the Variscan orogeny. The Permian-Triassic (255-253 Ma) stage of late- to post-collisional and within-plate felsic magmatism is related to the opening of the Mesozoic Tethys.

2.1 Introduction

The Alpine orogen is probably the best studied orogenic belt and yet there are several parts where the geological history is still very poorly resolved. These inadequately studied areas hinder the accuracy of global tectonic models, especially those concerning the pre-Alpine evolution. Prime example of such areas are the crystalline basement units of southeastern Europe, which were often omitted from the large-scale tectonic models. However, the last twenty years brought significant amount of knowledge concerning the palaeogeographic position and tectonic evolution of a number of crystalline units previously considered to be ancient microcontinents trapped within the Eastern European Alpine orogenic belt (e.g. Tisza, Rhodope; Kober, 1921). These recent studies revealed that such terranes represent complex collages of reworked continental (and locally oceanic) crust and sediments actively involved in several phases of Alpine deformation and metamorphism (e.g. Ivanov, 1988; Burg et al., 1990, 1996; Liati and Gebauer, 1999; Burg, 2012). Among these terranes, the tectonic position and evolution of the Serbo-Macedonian Massif (SMM) outcropping in Serbia, southwest Bulgaria, Macedonia, and northern Greece, remains enigmatic (Fig. 2-1). It becomes crucial for valid reconstruction of the long and complex interaction of Gondwana- and Laurussia-derived crustal segments presently outcropping along the Balkan

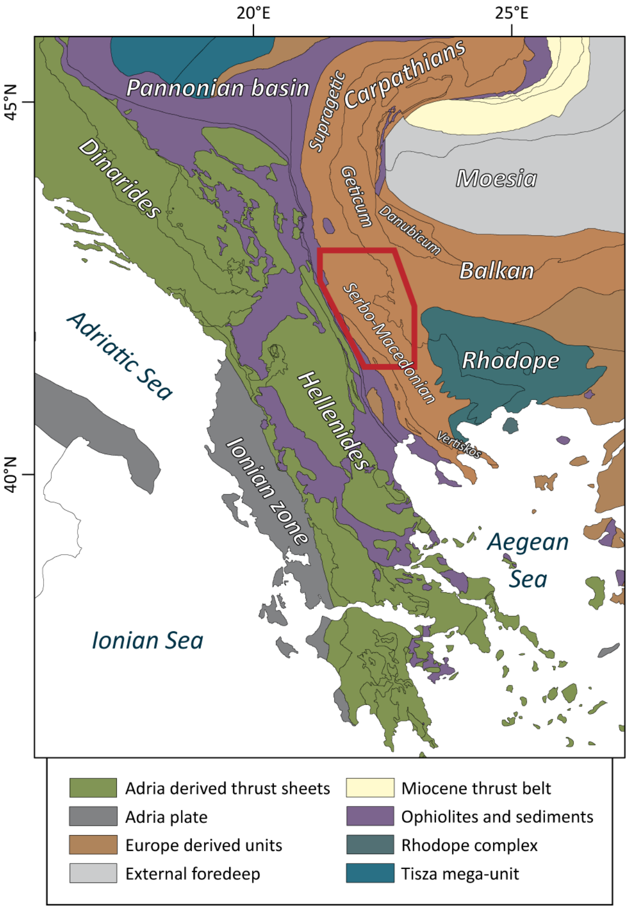

Peninsula (e.g. Munteanu and Tatu, 2003; Himmerkus et al., 2009a; Kalvoda and Bábek, 2010; Meinhold et al., 2010; Kroner and Romer, 2013), to resolve the enigma concerning the provenance and geological history of the Serbo-Macedonian Massif. Recent studies in the Greek part of the SMM reveal a complex metamorphic and tectonic history since the Cambrian, including intense Alpine overprint suggesting that what we today refer to as the Serbo-Macedonian Massif is not a single tectonic unit (e.g. Kilias et al., 1997; Brun and Sokoutis, 2007; Himmerkus et al., 2007).

In order to provide a basis for reliable reconstruction of the early tectonic history of crystalline units in southeastern Europe, this article presents evidence for the origin and evolution of the SMM obtained through analyses of U–Pb isotopic ages of magmatic and detrital zircons coupled with Hf isotope analysis of the dated zircons and whole-rock geochemical analysis of major and trace elements. The analyses were performed on a wide range of rock types in all units constituting the SMM in southeastern Serbia, southwestern Bulgaria and eastern Macedonia, with additional samples from the adjacent tectonic domains occasionally reported as parts of the SMM (Brković et al., 1980; Dolić et al., 1981; Karamata and Krstić, 1996; Dimitrijević, 1997). The results of the geochronological and geochemical analyses allow correlation with similar units of the Eastern Mediterranean Alpine orogen. These data are used to propose a model of tectonic evolution of the study area and adjacent domains since the late Neoproterozoic until the earliest Mesozoic. This dataset will serve as a sound basis for further research including more detailed sedimentary provenance analyses and geochemical correlations in the wider region, which could correct the deficiencies in the palaeogeographic reconstructions and tectonic models concerning the early evolution of tectonic units presently located in the Eastern Mediterranean Alpine orogen.

2.2 Geological setting

The Serbo-Macedonian Massif extends from the Aegean Sea to the Southern Carpathians

(Fig. 2-1) where it is correlated with the Supragetic nappe sequence (Dimitrijević, 1997; Iancu et al., 2005). It should be noted that although our study concerns only the pre-Alpine evolution of the SMM, the names of the tectonic units discussed below refer to the Alpine orogen so that results presented here could be correlated with the previously published tectonic frameworks of southeastern Europe. The SMM in Serbia and Macedonia represents an entirely metamorphic belt comprising a structurally lower unit (the Lower Complex) and an upper unit (Vlasina Unit), as originally proposed by Dimitrijević (1957). These units are commonly differentiated on the basis of their metamorphic grade, with the Lower Complex predominantly metamorphosed at medium to lower amphibolite facies, and the Vlasina Unit at greenschist facies. The boundary of these two units is usually reported as tectonic, i.e. the Vrvi Kobila shear zone (Fig. 2-2). This contact was previously described as a pre-Mesozoic west-vergent brittle thrust of Vlasina Unit over the Lower Complex (Vukanović et al., 1973; Krstić and Karamata, 1992), or a post-Late Cretaceous dextral shear zone (Kräutner and Krstić, 2002). The continuations of the Lower Complex and Vlasina Unit in Bulgaria are referred to as the Ograzhden block (Dimitrijević, 1967; Zagorchev, 1984a; Dabovski et al., 2002) and Morava Unit (Zagorchev, 1985; Zagortchev, 1993), respectively. The Vertiskos Unit in Greece is traditionally considered as the continuation of the Lower Complex of the SMM (Kockel et al., 1971; Burg et al., 1995; Himmerkus et al., 2009a; Meinhold et al., 2010; Burg, 2012). Based on the available geological records from the Greek and Bulgarian extents of the SMM, its provenance was previously assigned to the eastern Avalonian (Meinhold et al., 2010) or Cadomian (Stampfli et al., 2002; von Raumer et al., 2003; Balintoni et al., 2010b; Meinhold et al., 2010; Kounov et al., 2012) assemblages of terranes within the Neoproterozoic north-Gondwanan arc.

During the late Early Cretaceous, the Vlasina Unit was thrust to the east onto the Getic units along a system of east- to northeast-vergent thrusts (Petković, 1930; Mihailescu et al., 1967;

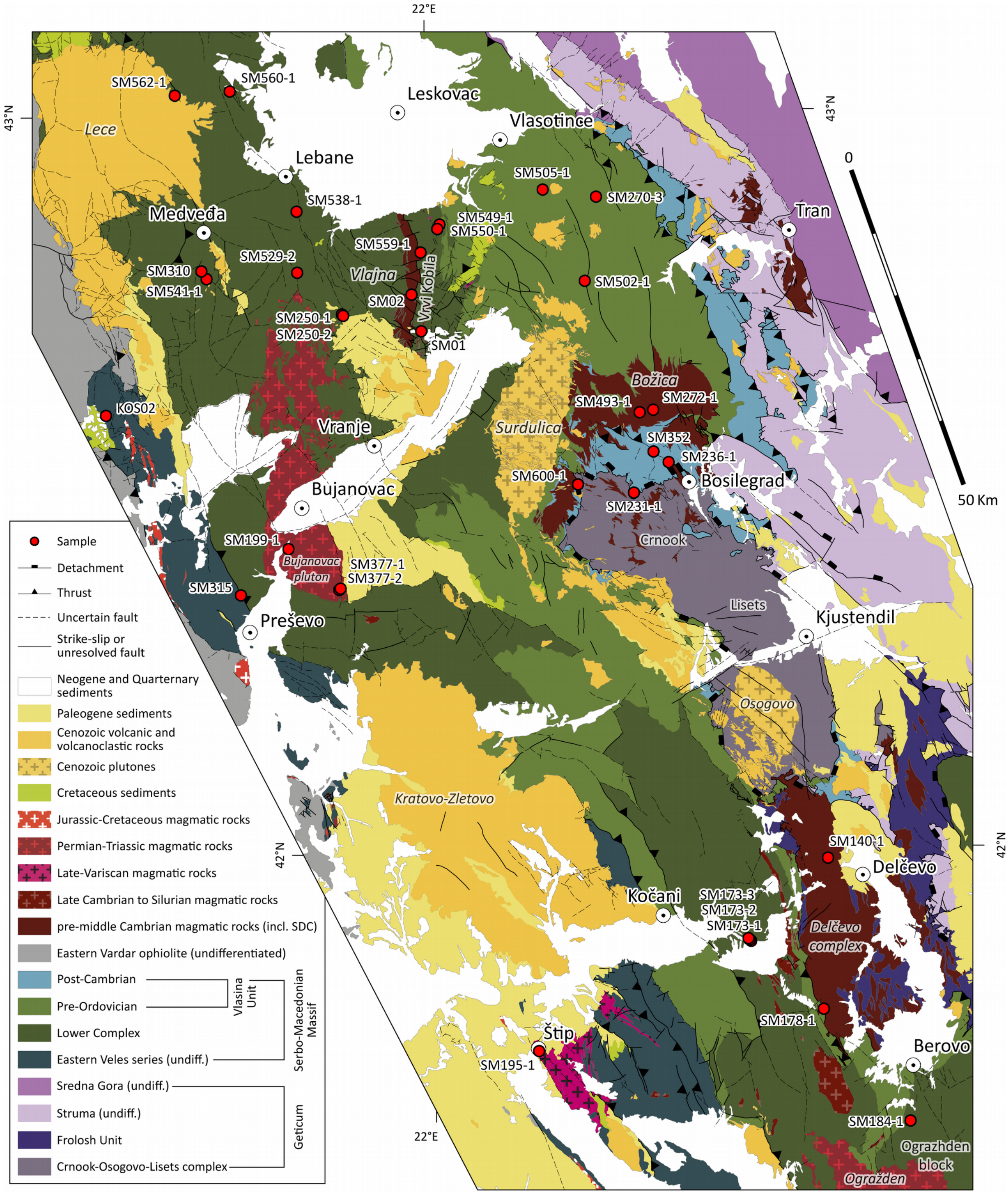

Figure 2-2. Tectonic map of the study area with the position of the analysed samples (after Basic geological maps of SFR Yugoslavia 1:100 0000 and Geological maps of Bulgaria 1:100 000 and 1:50 000). Names in italic represent magmatic bodies.

Petrović, 1969; Zagorchev and Ruseva, 1982; Zagorchev, 1984b; Lilov and Zagorchev, 1993; Kounov et al., 2010). In southwestern Bulgaria and northern Greece the contact of the Ograzhden block and the Vertiskos Unit with the Rhodope complex is traced along the Strymon Valley and Kerdillion detachments (Dinter and Royden, 1993; Brun and Sokoutis, 2007; Kounov et al., 2015). The distinction between the SMM and the Rhodope complex was often challenged in the past (Popović, 1991; Ricou et al., 1998; Grubić et al., 1999, 2005), although their differences were firmly established in the Greek and Bulgarian parts of the SMM during the past two decades (Burg, 2012 and references therein). A large number of studies in Bulgaria and Greece have shown that the Rhodope complex was formed during the Alpine orogeny (e.g. Burg et al., 1996; Kaiser-Rohrmeier et al., 2004; Liati, 2005; Bosse et al., 2009; Turpaud and Reischmann, 2010), whereas the SMM lacks the high-grade Cenozoic overprint (Georgiev et al., 2010; Kounov et al., 2010, 2012).

The SMM is bounded to the west by Mesozoic sediments and Jurassic ophiolites of the Eastern Vardar suture zone (e.g. Karamata, 2006; Schmid et al., 2008; Meinhold et al., 2009; Robertson et al., 2009). In the study area this contact is reported as a strike-slip fault, an east-vergent thrust (Krstić and Karamata, 1992), or a westward thrust which was partially reactivated as a dextral strike slip fault in the Neogene (Kräutner and Krstić, 2002). South of the Lece andesitic complex, the Lower Complex of the SMM is in tectonic contact with the metamorphic rocks of the Eastern Veles series (Fig. 2-2). The oldest reported, non-metamorphosed, sedimentary rocks that overlie crystalline rocks of the SMM are Middle Triassic (Karamata and Krstić, 1996; Dimitrijević, 1997).

Earlier studies suggest that being previously variably metamorphosed, the Lower Complex and Vlasina Unit have been amalgamated and subsequently accreted to the Moesian platform during the Variscan orogeny (Karamata and Krstić, 1996; Haydoutov and Yanev, 1997). An alternative scenario proposes that the southern extent of the SMM (i.e. Vertiskos Unit) had joined the European craton in the Late Jurassic to Early Cretaceous (Himmerkus et al., 2009a). Schmid et al. (2008) suggest that the Eastern Vardar ophiolites are at a structurally higher position in respect to the SMM due to the Late Jurassic obduction and final east-facing nappe stacking in the Late Cretaceous. According to these authors the final suturing in the early Palaeogene, related to the final closure of the remnants of the Vardar Ocean (i.e. the Sava zone), led to the westward thrusting in the Dinarides (Adria-derived).

2.2.1 The Lower Complex

The Lower Complex consists mainly of gneisses, micaschists, quartzites with lenses of amphibolites and occasionally marbles and migmatites (Dimitrijević, 1963, 1997). Isolated fragments of serpentinised ultramafic rocks were also reported (Petrović et al., 1973; Vukanović et al., 1973; Nenova and Marinova, 2007; Tarassov et al., 2007). Pelitic and psammitic sediments are usually considered as protoliths of the felsic metamorphic rocks, and tholeiitic within-plate basalts and related tuffs as protoliths of the amphibolites (Milovanović, 1992; Dimitrijević, 1997). The protoliths of the Lower Complex and Vlasina Unit are described as parts of an arc-related volcano-sedimentary series (Dimitrijević, 1967; Krstić and Karamata, 1992; Haydoutov and Yanev, 1997; Kounov et al., 2012). Although a medium amphibolitic facies metamorphism was suggested for the Lower Complex and the Ograzhden block (Milovanović, 1990; Cvetković et al., 1995; Zidarov et al., 2003a; Nenova and Zidarov, 2008; Erić et al., 2009), relict kyanite and boudins of eclogites were also reported (Balogh et al., 1994; Fed'kin et al., 1996; Vasković and Tasić, 1997; Iancu et al., 1998; Korikovsky et al., 2003; Nenova and Zidarov, 2008). This high pressure event was related to the late Neoproterozoic or Early Palaeozoic (Balogh et al., 1994; Zagorchev and Milovanović, 2006; Nenova and Zidarov, 2008), while the amphibolite facies overprint is assigned to the Variscan orogeny (Dimitrijević, 1967; Medaris Jr. et al., 2003; Nenova and Zidarov, 2008). A latest Jurassic and/or Early Cretaceous greenschist facies retrogressive stage was reported in Serbia, Bulgaria and Greece (Milovanović, 1990; Balogh et al., 1994; Kilias et al., 1999; Zidarov et al., 2003a).

West of the Vrvi Kobila shear zone, the Lower Complex is intruded by the Vlajna granitoid (Fig. 2-2), which was reported to have been emplaced at 450 Ma (Dimitrijević, 1963). The largest magmatic body intruding the Lower Complex in Serbia is the north to northeast-south to southwest elongated Bujanovac S-type granite (Vukanović et al., 1973, 1977; Karamata and Krstić, 1996). Two distinct intrusions form the Bujanovac granitic complex, an older represented by medium-grained foliated granitoids, intruded by younger, fine-grained granites (Dimitrijević, 1958; Vukanović et al., 1977). The ages of these plutons have been reported as 347 Ma (Dimitrijević, 1997), and 234 Ma (Dimitrijević, 1958), respectively.

A group of magmatic bodies, apparently intruding the Vlajna granites, located in the southern part of the Vrvi Kobila shear zone are referred to as Kukavica granites (Fig. 2-2). Both Vlajna and Kukavica granites were deformed together along the Vrvi Kobila shear zone.

The Ogražden pluton intruded into the Lower Complex (i.e. Ograzhden block) gneisses on the southern margin of the study area (Fig. 2-2), consists of biotitic granites and granodiorites. Age of its emplacement is reported as early Palaeozoic (Boev et al., 2002), Early Cretaceous (Rakićević et al., 1973), and most recently as Early Triassic (252±2 Ma; Georgiev et al., 2012).

2.2.2 Vlasina Unit

Karamata and Krstić (1996) regarded Vlasina Unit as a part of the Suprageticum (i.e. highest structural unit in the Carpatho-Balkanide orogen), due to the suggested hanging wall position in the thrust over the Lower Complex (i.e. Vrvi Kobila shear zone, Fig. 2-2). Additionally, several reports suggest that these units originally shared a stratigraphic contact, which was later tectonically reactivated (Petrović and Karamata, 1965; Dimitrijević, 1997).

The Vlasina Unit consists of the pre-Ordovician greenschist-facies basement rocks, overlain by a low-grade post-Cambrian sedimentary sequence (Kräutner and Krstić, 2002). Both parts show a similar style of deformation and metamorphism exhibiting a consistent gradient throughout the area. The apparent abrupt changes in the metamorphic grade observed at certain localities could be explained by subsequent telescoping due to brittle thrusting.

Although regarded as a volcano-sedimentary complex similarly as the Lower Complex, the rocks of the pre-Ordovician Vlasina are dominated by ocean-floor sediments and contain basic magmatic rocks related to MORB (Popović, 1991), representing an ocean-ward periphery of a magmatic arc (Milovanović et al., 1988). The Pre-Ordovician Vlasina is represented by chlorite, biotite, muscovite, sericite and epidote schists. Local varieties rich in quartz and albite, or actinolite and stilpnomelane were occasionally reported (Dimitrijević, 1967). Phyllites and quartzites are also common. Protoliths of these metamorphic rocks are pelitic and to a lesser extent psammitic sediments (Petrović, 1969), together with arc-related tholeiitic basalts and their tuffs (Milovanović et al., 1988). Several small, tectonically imbricated bodies of serpentinites have been reported (Ilić et al., 1967; Petrović, 1969; Petrović et al., 1973). Intrusions of granites, gabbro and diabase are often deformed and metamorphosed along with the country rock. The age of the pre-Ordovician Vlasina protoliths was determined as “Ripheo-Cambrian” based on the spores recovered at several locations in southeastern Serbia (Pantić et al., 1967; Petrović, 1969). Additionally, lenses of calcschists northeast of Surdulica pluton yielded palynomorphs and fungi of Cambrian age (Vasković and Tasić, 1997 and references therein).

At the type locality of Vlasina Unit (northeast of Surdulica pluton near sampling location of SM502-1, Fig. 2-2) the peak metamorphic conditions reached greenschist facies (Milovanović et al., 1988; Vasković, 2002). However, relict amphibolite and transitional amphibolite-greenschist facies assemblages were reported in the Vrvi Kobila area (Petrović, 1969), vicinity of the Božica magmatic complex (Babović et al., 1977; Krstić and Karamata, 1992), north of the Surdulica pluton (Pavlović, 1977) and east of Vranje (Babović et al., 1977; Vasković, 1998; Vasković et al., 2003). This higher grade metamorphism in the Vlasina Unit has been associated with the "Baikalian" (850–650 Ma) and "Caledonian" orogenic events (Karamata and Krstić, 1996), and the age of the greenschist overprint as early Carboniferous (Dimitrijević, 1963; Petrović, 1969; Krstić and Karamata, 1992; Karamata and Krstić, 1996; Graf, 2001), or post-Variscan (Dimitrijević, 1967).

The pre-Ordovician Vlasina is covered by a meta-sedimentary succession reported as Ordovician to lowest Carboniferous in age (Spassov, 1973; Babović et al., 1977; Pavlović, 1977; Lakova, 1997). These meta-sedimentary rocks crop out along the eastern margin of the Vlasina Unit, often separated from the pre-Ordovician Vlasina by east-vergent thrusts (Petrović, 1969; Fig. 2-2). The originally transgressive contact with the pre-Ordovician Vlasina reported by Pavlović (1962, 1977) northeast of Bosilegrad, is in fact obscured by intensive deformational overprint. The lowermost part of the sedimentary column comprises phyllites, metasandstones, calcschists, quartzite, marble, sericite and chlorite schists (Babović et al., 1977). Inarticulate brachiopod fauna in the "basal quartzites" suggests an Early Ordovician age (Pavlović, 1962). The Ordovician period is represented upward by argillo-phylites, spilites, meta-pelites, quartz and sericitic schists with lenses of quartzite and calcschist (Petrović et al., 1973). The Silurian succession continues with graptolitic schists, conspicuous carbonates with Middle Devonian spillites, ending with turbidites of Upper Devonian to lowest Carboniferous age (Petrović, 1969; Petrović et al., 1973; Spassov, 1973; Krstić, 1981; Krstić et al., 2002; Banjac, 2004; Lakova, 2009; Boncheva et al., 2010).

A large complex of magmatic rocks located east of Surdulica (Fig. 2-2), which was intruded into the pre-Ordovician Vlasina is referred to as Božica granitoid in Serbia (Petrović et al., 1973; Babović et al., 1977), and Milevski granite in Bulgaria (e.g. Graf, 2001; Kounov et al., 2012). It comprises partially deformed granites, diorites and gabbros. A late Cadomian age (551±1 Ma) was determined in the Bulgarian part of this magmatic complex (Kounov et al., 2012), whereas an age of 500 Ma was suggested for the Serbian part of Božica (Kräutner and Krstić, 2002).

2.2.3 Geticum

The Geticum represents a large-scale tectonic zone in the Alpine tectonic framework of the Carpatho-Balkan orogen, comprising a number of tectonic units forming southeast-, east- and northeast vergent nappes (e.g. Struma, Sredna Gora). The crystalline basement of the Struma Unit consists of variably deformed continent- and ocean-derived rocks of Ediacaran to early Cambrian protolith age (e.g. Kounov et al., 2012), unconformably overlain by a Permian to Lower Cretaceous sedimentary cover (Zagorchev, 1981). The ophiolites (Frolosh Unit) and a magmatic-arc igneous suite, the Struma Diorite Complex (SDC; Stephanov and Dimitrov, 1936; Haydoutov et al., 1994) are tectonically imbricated (Fig. 2-2). Although the present-day contacts between the fragments of ophiolitic ultramafic rocks, gabbros, diabases, basic tuffs and minor clastic metasedimentary rocks of the Frolosh Unit, and the gabbros, gabbrodiorites, diorites and granites of SDC are mainly tectonic, primary intrusive contacts can be locally observed. The mafic rocks of the Frolosh ophiolites show affinity to MORB (Haydoutov and Pin, 1993; Kounov et al., 2012). The rocks of the Lower Complex (Ograzhden block; Zagorchev, 1984a), situated in the southeast of the study area (Fig. 2-2), are separated from the overlying SDC and Frolosh Unit by the Gabrov Dol detachment east of the study area (Bonev et al., 1995).

The Crnook–Osogovo–Lisets complex (COL; Fig. 2-2), consists of amphibolites, micaschists, muscovite-biotite and amphibole-biotite gneisses (Dimitrova, 1964). Lenses of ultramafic rocks were also reported (Haydoutov et al., 1994). The magmatic rocks of the SDC and the Crnook–Osogovo–Lisets complex are derived from the same calc-alkaline magma source and represent a magmatic-arc formed during the Ediacaran to early Cambrian (Kounov et al., 2012).

The lower amphibolite-facies metamorphism and deformation in the COL complex were associated with late Early Cretaceous compression in the area (Kounov et al., 2010). The COL metamorphic rocks were exhumed from below the SDC during the middle Eocene–Oligocene extension (Chapter 4; Kounov et al., 2004, 2010).

2.2.4 Eastern Veles series

South of the Lece volcanic complex (Fig. 2-2), the Lower Complex is in tectonic contact with the metamorphic series of amphibolites, micaschists, gneisses, quartzites and marbles (Fig. 2-2). These rocks are regarded as part of the Veles series (Karajovanović and Hristov, 1976; Vukanović et al., 1977), which is considered as part of the Circum-Rhodope belt (definitions provided in Zagorchev and Milovanović, 2006; Kounov et al., 2011; Schmid, 2014), or internal Vardar zone (Dimitrijević and Drakulić, 1958; Dimitrijević, 1997; Robertson et al., 2009). The Veles series is separated in the eastern and the western part by Jurassic ophiolites and Upper Cretaceous sediments (Vukanović et al., 1977; Pavić et al., 1983; Karamata and Krstić, 1996). The Lower Complex in the study area is in direct contact only with the latter (Fig. 2-2). The Eastern Veles series comprises Cambrian to Devonian sediments (Pavlović, 1977), initially metamorphosed under amphibolite facies conditions, preserved only as relicts due to intensive greenschist retrogression (Dimitrijević, 1997). The crystalline rocks of the Eastern Veles series are covered by Triassic sediments metamorphosed to greenschist facies, present only in a small area in the northwestern periphery of the unit (Pavić et al., 1983). In contrast, the Western Veles series comprises predominantly Upper Devonian to Triassic meta-sedimentary rocks (Pavić et al., 1983; Grubić and Ercegovac, 2002), and low-grade igneous rocks related to a Carboniferous magmatic arc (Karamata, 2006). Most previous authors agree that the crystalline rocks of the Eastern Veles series (excluding the Triassic cover) were originally a part of the Lower Complex which have subsequently suffered intensive Alpine overprint, less pronounced in the rest of the Lower Complex (Brković et al., 1980; Dolić et al., 1981; Karamata and Krstić, 1996; Dimitrijević, 1997). Another distinctive feature of the Eastern Veles series compared to the Lower Complex of the SMM is the higher occurrence of marble (Dimitrijević, 1997).

The voluminous Štip magmatic complex represents a heterogeneous magmatic body comprising granites, monzonites and granodiorites, which intruded the Eastern Veles series near the town of Štip (Fig. 2-2). They contain xenoliths of serpentinite and amphibolite schists, which were considered as Jurassic by Rakićević et al. (1976), and Palaeozoic by Karajovanović and Hadži-Mitrova (1982). The upper limit on the age of emplacement of the Štip complex is constrained by the Albian-Cenomanian (i.e. 113-94 Ma) sediments covering the southeastern periphery of the pluton. Rb-Sr dating of biotite from the Štip complex yielded an age of 161±3 Ma which was interpreted as the age of its emplacement (Šoptrajanova, 1967), or as a metamorphic overprint (Spray et al., 1984).

2.3 Samples and analytical methods

Sample descriptions with locations are presented in Table 2-1. Twenty two samples were taken from the Lower Complex, eight from the Vlasina Unit, three from the Eastern Veles series, and two samples were taken from the COL complex. Major element analyses on whole-rock samples were performed using the X-ray fluorescence (XRF) method, whereas the trace element and REE measurements were carried out with Laser Ablation Inductively Coupled Plasma-Mass Spectrometry (LA-ICP-MS) at ETH Zürich. All diagrams representing results of geochemical analyses were plotted using GCDkit software (Janoušek et al., 2006). The results of the chemical analyses are presented in Appendix 2-1. Whole rock samples were mechanically fragmented (jaw crusher, milling) and sieved through a 450 µm sieve. A heavy-minerals concentrates were obtained by gravity separation (Wilfley table). Zircon concentrates were recovered by conventional heavy liquid (methylene iodide 3.3 g·cm^{-3}) and magnetic susceptibility (Frantz isodynamic separator) separation methods. Extracted zircon grains were hand-picked and mounted in epoxy resin. The polished mounts were photographed, and SEM cathodoluminescence (CL) and backscatter electron images were taken in order to analyse the internal structure of the grains prior to the LA-ICP-MS analyses. Instrument parameters used during the course of this study are presented in detail in Appendix 2-2. First round of data acquisition was performed at Department of Earth Science, ETH Zürich in 2010 using an Elan 6100 ICP-MS (PerkinElmer, Norwalk, CT, USA) coupled to an 193 nm ArF-Excimer laser ablation system similar to a Geolas system (Coherent, USA). The laser was operated at 10 Hz, spot size was 40 μm and a fluence of 4.0 J·cm^{-2} was used. Data obtained by this set-up are designated with an "o" as a prefix to the spot name. The second round of measurements were made in 2012 (ETH Zürich), using an Element-XR SF-ICP-MS (Thermo Fisher, Bremen, Germany) coupled with an 193 nm Excimer laser (Resonetics Resolution S155-LR) that was operated at 5 Hz and a fluence of 2.0 J·cm^{-2} . The spot size of 30 μm was used to obtain the data in this round of measurements. All experiments were performed using helium as carrier gas. The carrier gas was mixed with argon as make-up gas before entering the ICP (Appendix 2-2).

Appendix 2-3 contains detailed descriptions of samples and obtained U–Pb ages, a comprehensive table with results of the U, Th and Pb isotopic measurements is presented in Appendix 2-4, while the CL images of analysed zircon grains are provided in Appendix 2-5. Unless stated otherwise, concordia diagrams and density distribution plots were produced using the programs Isoplot (v3.71.09.05.23nx, Ludwig, 2012) and DensityPlotter (v.6.1; Vermeesch, 2012), respectively. Unless explicitly stated, uncertainties in the calculated weighted mean ages are reported at 95% confidence limit. Results referred to as concordant are within 95–105% tolerance defined by 100·((^{206}Pb/^{238}U age)·(^{207}Pb/^{235}U age)$^{-1}$). Weighted average plots do not include discordant

Table 2-1. Sample descriptions and locations.

Sample	Rock type	Gauß-Krüger[1]		DMS[2]		Locality	Analyses[3]
		x	y	x	y		
Lower Complex							
SM01	Mylonite	7581020	4729839	21°59'3.29"E	42°42'12.496"N	Ovča Strana	3
SM02	Granodiorite	7579581	4735334	21°58'1.844"E	42°45'8.702"N	Kukavica	3
SM173-1	Amp-schist	7630610	4638229	22°34'25.481"E	41°52'36.782"N	Vinica	3
SM173-2	Two-mica gneiss	7630610	4638229	22°34'25.481"E	41°52'36.782"N	Vinica	1
SM173-3	Leucocratic dyke	7630610	4638229	22°34'25.481"E	41°52'36.782"N	Vinica	3
SM184-1	Two-mica gneiss	7654525	4611248	22°50'58.068"E	41°37'27.378"N	Maleševski Mts.	3
SM199-1	Granite	7561075	4697110	21°43'40.285"E	42°24'12.474"N	Borovac	3
SM250-1	Amphibolite	7569098	4732307	21°50'12.623"E	42°43'32.618"N	Golemo Selo	3
SM250-2	Paragneiss	7569098	4732307	21°50'12.623"E	42°43'32.618"N	Golemo Selo	2
SM310	Paragneiss	7548389	4738347	21°35'6.753"E	42°47'1.236"N	Sijarinska Banja	2
SM377-1	Weakly deformed granite	7568705	4690941	21°50'2.944"E	42°21'33.452"N	Spančevac	3
SM377-2	Deformed Qz-monzonite	7568705	4690941	21°50'2.944"E	42°21'33.452"N	Spančevac	3
SM529-2	Amphibolite	7562402	4738588	21°45'40.644"E	42°47'11.034"N	Šumanska Reka	1
SM538-1	Metagabbro	7562291	4747753	21°44'26.448"E	42°51'40.215"N	Popovce	1
SM541-1	Amphibolite	7548798	4737626	21°35'30.155"E	42°46'39.822"N	Sijarina	1
SM549-1	Metagabbro	7583799	4745848	22°1'23.325"E	42°51'2.239"N	Mala Oraovica	1
SM550-1	Granite	7583796	4745423	22°1'23.855"E	42°50'40.234"N	Slatinska Reka	2
SM559-1	Granite	7580913	4741665	21°59'22.368"E	42°48'53.175"N	Muratovica	1
SM560-1	Metagranite	7552276	4765813	21°38'8.152"E	43°1'51.78"N	Brestovac	1
SM562-1	Amphibolite	7543986	4765206	21°31'53.954"E	43°1'25.933"N	Dobra Voda	1
Vlasina Unit							
SM178-1	Ep-Chl-Amp schists	7641503	4628070	22°41'53.009"E	41°46'45.925"N	Mitrašinci	1
SM270-3	Diabase	7607295	4750047	22°18'49.385"E	42°53'13.117"N	Dobro Polje	1
SM272-1	Granite	7615854	4718033	22°24'17.378"E	42°35'33.171"N	Božica	3
SM352	Gabbro	7615948	4711742	22°24'33.416"E	42°32'21.373"N	Donja Lisina	3
SM493-1	Diorite	7613838	4717645	22°22'50.226"E	42°35'17.209"N	Toplodolska Reka	1
SM502-1	Komatiite	7605584	4737380	22°16'50.478"E	42°46'3.893"N	Veljkovci	1
SM505-1	Ab-gneiss	7599255	4751127	22°12'23.016"E	42°53'35.606"N	Gornja Lopušnja	1
SM600-1	Metagranite	7604563	4706769	22°15'19.318"E	42°29'29.268"N	Gornja Ljubata	2
Eastern Veles series							
KOS02	Micaschist	7533668	4717085	21°24'33.357"E	42°35'43.487"N	Izvor	2
SM195-1	Bt-granite	7598733	4621701	22°11'0.429"E	41°43'44.482"N	Štip	3
SM315	Orthogneiss	7553957	4690113	21°38'54.581"E	42°21'1.032"N	Bukovac	3
Basement of Struma Unit							
SM140-1	Granite	7642147	4650734	22°42'42.195"E	41°58'59.254"N	Delčevo	3
SM231-1	Gabbro	7612988	4705575	22°22'19.907"E	42°28'56.439"N	Donja Ljubata	1
SM236-1	Monzonite	7618183	4710189	22°26'17.931"E	42°31'25.908"N	Bosilegrad	3

[1] Gauß-Krüger coordinate system is used in SFR-Yugoslavian Basic Geological 1:100000 maps.
[2] Coordinates given in degree-minute-second (DMS) format.
[3] Explanation of values: 1 – geochemical analysis only; 2 – U-Pb age determination only; and 3 – geochemical analysis and U–Pb age determination.

measurements. Since annealing and chemical leaching were not performed on the analysed zircon grains, the results obtained on partially metamict domains might yield concordant ages that can be possibly younger than the real age due to partial radiogenic lead loss. In cases where a group of age results forms a continuous array lacking "plateau" or evident clustering related to specific growth domains, the weighted average of the array is reported as the most correct result. Discordant measurements and results from spots located in the "mixed zones" within the zircon grain (e.g. on the interface of core and rim), were omitted from the interpretation and the plots. However, discordant results are plotted on concordia diagrams in Appendix 2-3.

2.4 Results

2.4.1 Geochemistry

2.4.1.1 The Lower Complex

Major oxide analysis of eleven sampled felsic magmatic rocks and gneisses from the Lower Complex (Appendix 2-1) indicates predominant calc-alkaline granitic composition (Fig. 2-3a), with a subordinate intermediate composition of the Vlajna granitoid (SM02; Fig. 2-2), deformed Bujanovac Qz-monzonite (SM377-2) and Vinica gneiss (SM173-2 in Fig. 2-3a). Amphibolites from the Vinica area east of Kočani (SM173-1; Fig. 2-2) and Dobra Voda locality east of Lece (SM562-1; Fig. 2-2) are presented in this section as they are classified as intermediate magmatic rocks (i.e. gabbro diorites in Fig. 2-3a). These three samples represent the tholeiitic type of rocks in this group (Fig. 2-3b).

The majority of granitic rocks from the Lower Complex plot within the volcanic-arc granites field (Fig. 2-4). The sample SM02 from the southern part of the Vlajna granitoid and a leucocratic dyke from Vinica area (SM173-3, east of Kočani, Fig. 2-2) are slightly enriched in Y and Nb compared to the remaining arc-related rocks of the Lower Complex. This Y enrichment coupled with their peraluminous signature (Fig. 2-5) reveals involvement of crustal material in their magmatic source. The peraluminous Kukavica granite in the Vrvi Kobila area (SM01, Figs. 2-4 and 2-6) plots closer to the field of syn-collisional granites probably due to enrichment in Rb. High contents of Ta in fine-grained granites from the periphery of Bujanovac pluton (SM377-1) and Maleševski Mts. orthogneiss (SM184-1) suggest within-plate setting for these rocks (Fig. 2-6a).

Most of the analysed acidic and intermediate rocks from the Lower Complex show enrichment in light rare earth elements (LREE) (Fig. 2-7a left). The samples from the Bujanovac magmatic complex (SM199-1, SM377-1 and SM377-2) as well as central Vlajna granite (SM559-1), Kukavica granite (SM01) and gneiss sample SM184-1 show slight depletion in heavy rare earth elements (HREE). The distinct negative Eu anomalies detected in the Vinica leucocratic dyke (SM173-3), the Kukavica (SM01), central Bujanovac (SM199-1) and central Vlajna (SM559-1) granites, as well as Maleševski Mts. orthogneiss (SM184-1) could be attributed to crystal fractionation of plagioclase.

Trace element diagram, normalised to primitive mantle (Hofmann, 1988), reveals general affinity to magmatic arc environment of most of the analysed samples (grey field in Fig. 2-7a right). This is inferred from their enrichment in incompatible elements (i.e. Rb, Ba, Th and U) and relative depletion of Nb and Ta. The exceptions include samples SM02, SM562-1 and SM559-1 that display depletion in Sr or higher concentration of HREE indicative of their affinity to within-plate setting. Furthermore, the coarse-grained Bujanovac Qz-monzonite (SM377-2) is relatively enriched in Ba, Nb, Ta, Hf and Zr supporting within-plate origin despite slightly elevated Sr and lower HREE concentrations (Fig. 2-7a right).

Amphibolites and meta-gabbros from the Lower Complex (Appendix 2-1), chemically

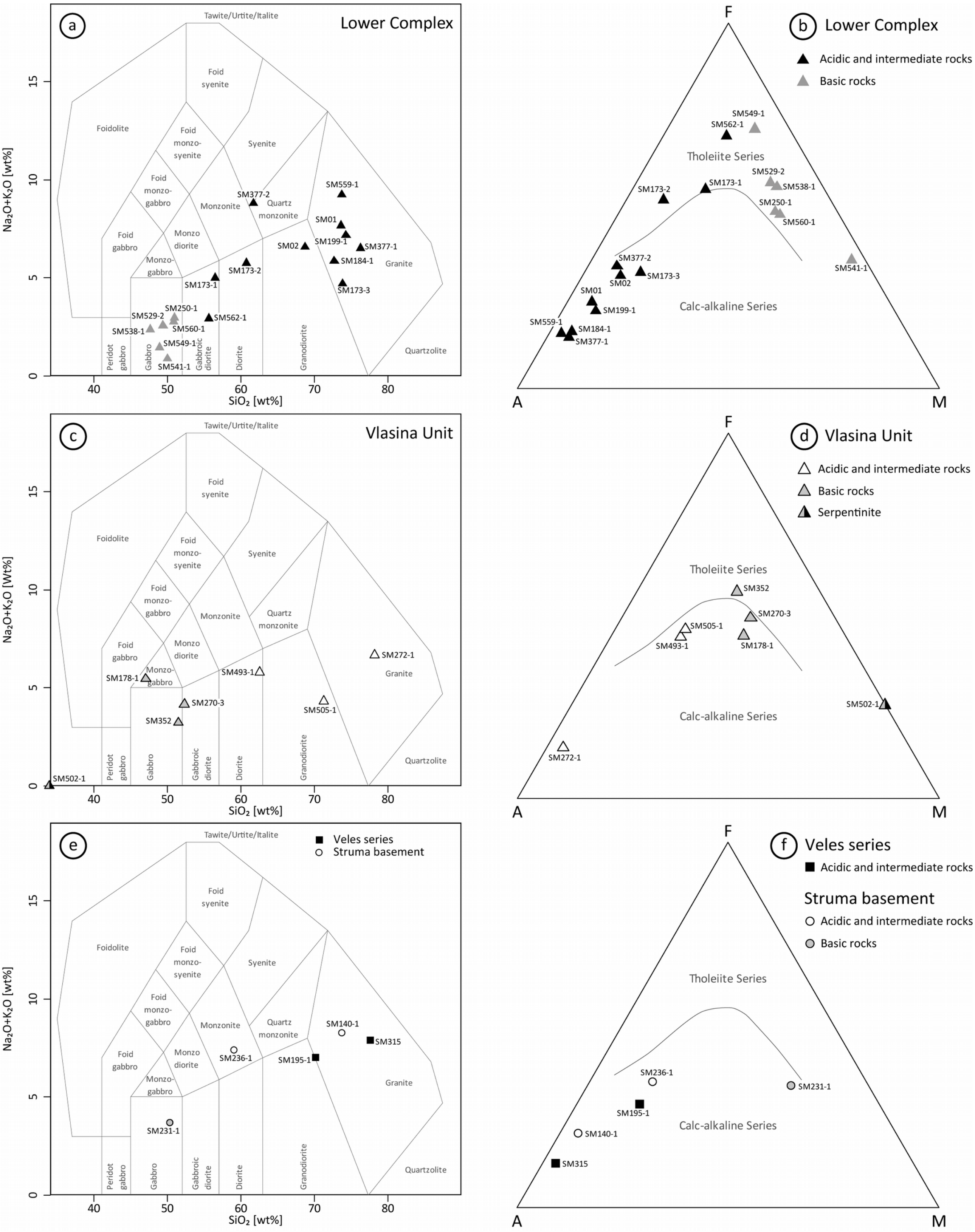

Figure 2-3. (a), (c) and (e) Total alkali versus silica classification plots (Middlemost, 1985); (b), (d) and (f) AFM discrimination plots (Irvine and Baragar, 1971) of all analysed samples.

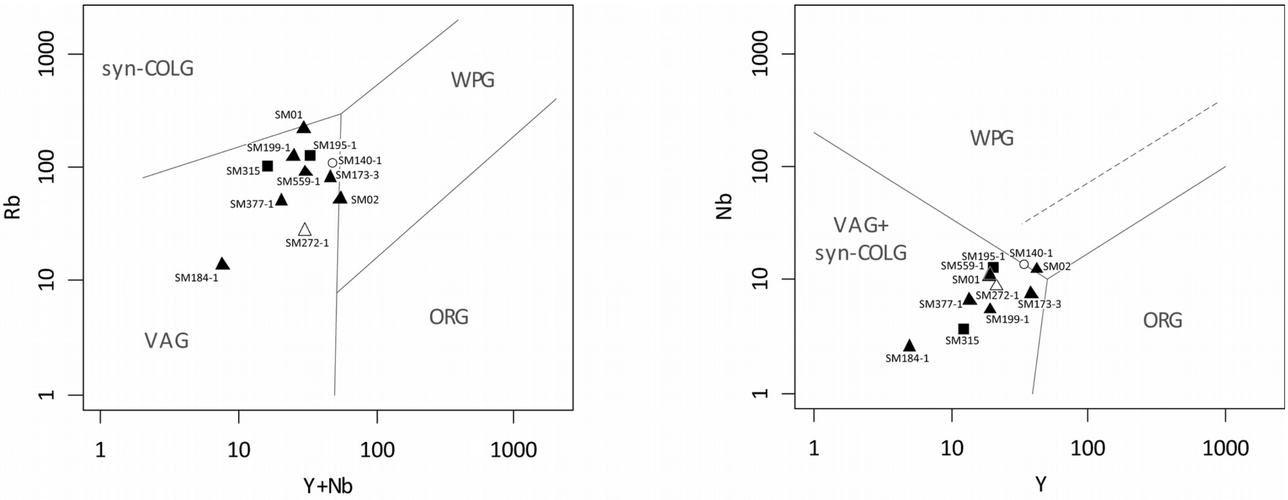

Figure 2-4. Tectonomagmatic discrimination diagrams for granites (Pearce et al., 1984). Symbols as in Fig. 2-3. Abbreviations: Syn-COLG – syn-collisional granites, WPG – within-plate granites, ORG – ocean ridge granites, VAG – volcanic-arc granites.

equivalent to gabbros (Fig. 2-3a), are associated with tholeiitic series (Fig. 2-3b). Most of the analysed samples are designated as enriched MORB or within-plate tholeiites (Fig. 2-6b) except Sijarina amphibolites (SM541-1) that plot as within-plate alkali-basalt, and Slatina meta-gabbro (SM549-1) pertaining to the continental-arc environment. Most of the sampled basic rocks from the Lower Complex display a relatively enriched pattern in REE with slight downward sloping towards HREE (Fig. 2-7b left). Exceptions are Sijarina amphibolites (SM541-1, south of Medveđa, Fig. 2-2) with more pronounced depletion of HREE, and Gornji Brestovac meta-gabbro (SM560-1, north to northeast of Lebane, Fig. 2-2) that shows excess of LREE and notable negative Eu anomaly. Enrichment in Sr and lack of negative Eu anomaly observed for most of the samples (Fig. 2-7b right), coupled with elevated concentration of Ca (Appendix 2-1) is explained by the high content of

Figure 2-5. A/CNK vs. A/NK classification plot (Shand, 1943) for granitic rocks; area stippled with dots is related to S- type granites; area stippled with plus symbols denominates I-type granites. Symbols as in Fig. 2-3.

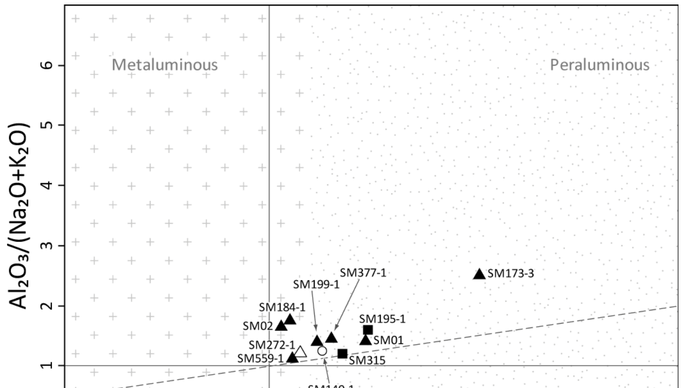

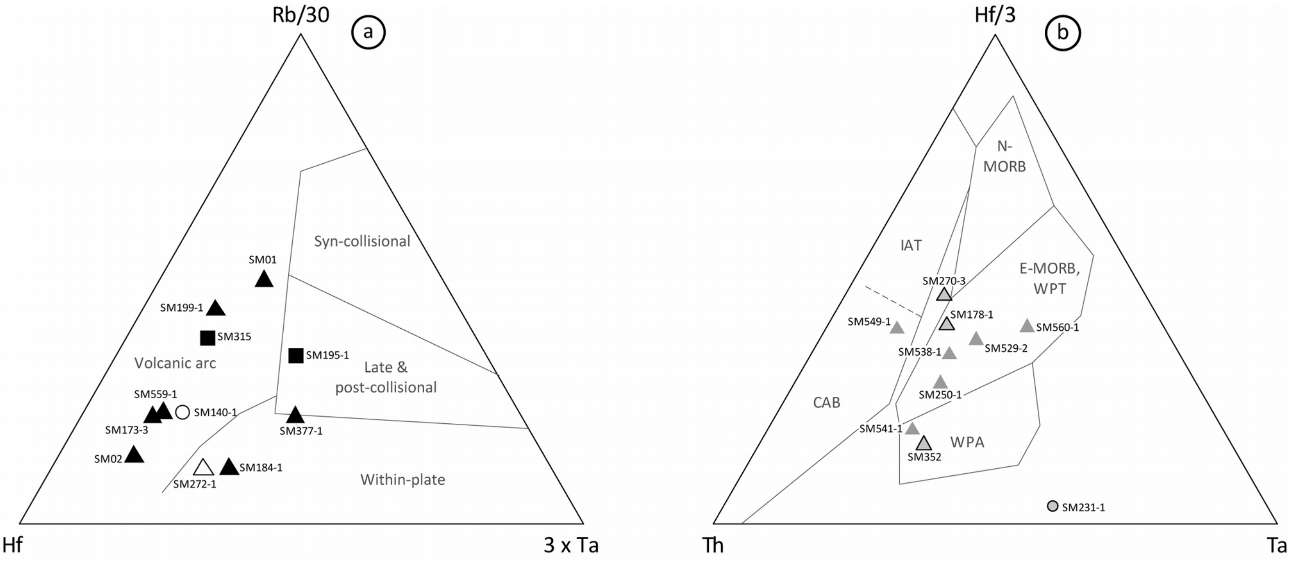

Figure 2-6. (a) Ternary geotectonic discrimination diagram for granites (Harris et al., 1986); (b) Tectonomagmatic classification diagram for basic rocks (Wood et al., 1979). Symbols as in Fig. 2-3. Abbreviations: CAB – continental-arc basalts, IAT – island-arc tholeiits, N-MORB – normal mid-ocean ridge basalts, E-MORB – enriched mid-ocean ridge basalts, WPT – within-plate tholeiits, WPA – within-plate alkaline magma.

clinopyroxene and/or plagioclase. Exceptions are again Sijarina amphibolites (SM541-1) and Gornji Brestovac meta-gabbro (SM560-1) showing slightly lower Sr concentrations. The negative anomalies of Nb and Ta (Fig. 2-7b right), and its position on the discrimination diagram in Figure 2-6b, suggest a continental-arc environment for the Slatina metagabbro (SM549-1).

2.1.1.1 Vlasina Unit

Acidic and intermediate rocks from Vlasina Unit include a granite (SM272-1), and a diorite (SM493-1) from the Božica magmatic complex, and an albitic gneiss (SM505-1) chemically equivalent to granodiorite (Fig. 2-3c). All samples from this group are associated with calc-alkaline series (Fig. 2-3d). Although granite from the Božica complex (SM272-1) shows magmatic-arc signature on the classification diagrams of Pearce et al. (1984)(Fig. 2-4), it plots in the field of within-plate granites on the discrimination diagram of Harris et al. (1986)(Fig. 2-6a), due to higher Ta content.

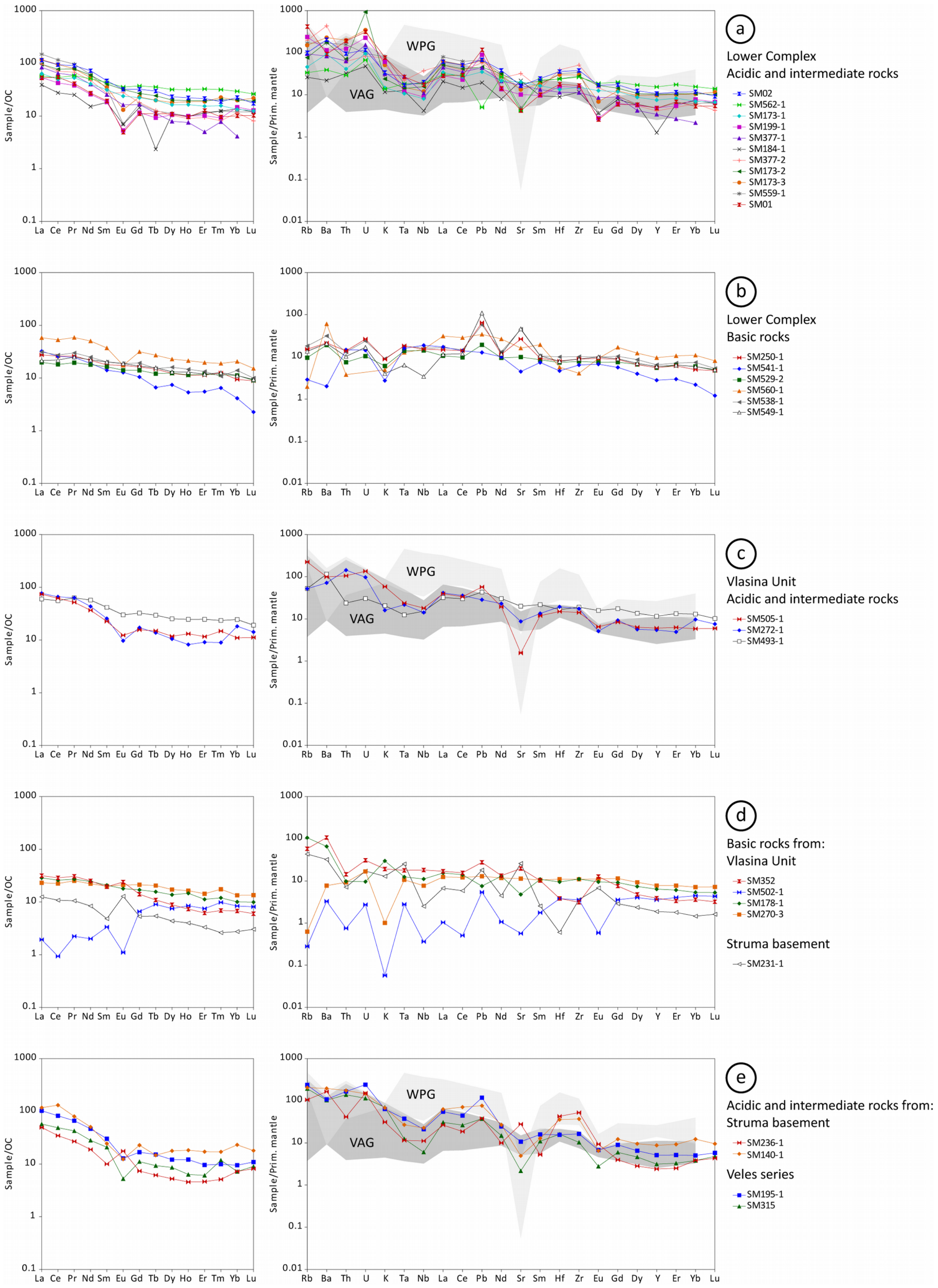
Sample/OC
Sample/Prim. mantle
1000
100
10
1
0.1
0.01
La Ce Pr Nd Sm Eu Gd Tb Dy Ho Er Tm Yb Lu
Rb Ba Th U K Ta Nb La Ce Pb Nd Sr Sm Hf Zr Eu Gd Dy Y Er Yb Lu
WPG
VAG
a
Lower Complex
Acidic and intermediate rocks
SM02
SM562-1
SM173-1
SM199-1
SM377-1
SM184-1
SM377-2
SM173-2
SM173-3
SM559-1
SM01
b
Lower Complex
Basic rocks
SM250-1
SM541-1
SM529-2
SM560-1
SM538-1
SM549-1
c
Vlasina Unit
Acidic and intermediate rocks
SM505-1
SM272-1
SM493-1
d
Basic rocks from:
Vlasina Unit
SM352
SM502-1
SM178-1
SM270-3
Struma basement
SM231-1
e
Acidic and intermediate rocks from:
Struma basement
SM236-1
SM140-1
Veles series
SM195-1
SM315

Granites and gneisses from the Vlasina Unit exhibit elevated LREE concentrations with relatively flat HREE pattern and a negative Eu anomaly typical for continental crustal rocks and volcanic-arc granites (VAG) with lack or negligible garnet and zircon fractionation. The Eu anomaly is less pronounced and HREE content is slightly higher in the case of diorite from the Božica complex (SM493-1, Fig. 2-7c left). It also lacks the pronounced negative Sr anomaly observed in other samples of this group (Fig. 2-7c right). Both samples from Božica magmatic complex display somewhat lower Rb and K content with elevated Ba concentrations. Similar signature is previously reported for monzogranites and granites in this complex (Vasković and Tasić, 1997).

The basic rocks from the Vlasina Unit are represented by the Lisina gabbro (SM352), deformed monzo-gabro (SM178-1) and a diabase (SM270-3) chemically equivalent to gabbro-diorite (Fig. 2-3c). The latter two are representing calc-alkaline differentiation series, while the Lisina gabbro (SM352) plots within the tholeiitic series field (Fig. 2-3d). Based on the classification diagram of Wood (1980), the protoliths of samples SM178-1 and SM270-3 originated from MORB (Fig. 2-6b), whereas Lisina gabbro (SM352) plots in the field representing within-plate setting.

Similarly to the basic samples of the Lower Complex, basic rocks of the Vlasina Unit also show almost flat REE pattern, with slight depletion in HREE (Fig. 2-7d left). However, more prominent depletion of HREE is observed for Lisina gabbro (SM352). Content of incompatible alkalis and alkaline earth metals varies strongly, ranging from enriched in SM352 to relatively depleted in diabases SM270-3 (Fig. 2-7d right).

A single sample of serpentinite (SM502-1) was taken from the Vlasina Unit north of

Figure 2-7. Trace element pattern plots normalised for chondritic (Nakamura, 1974) and primitive mantle concentrations (Hofmann, 1988). Shaded areas WPG and VAG represent envelope concentrations of within-plate and volcanic-arc granites, respectively (Pearce et al., 1984). OC stands for ordinary chondrite. In (e) and (d) basement of Struma Unit includes samples from both the COL complex and the SDC.

Surdulica granodiorite. It shows high Mg and very low Si content (Appendix 2-1) and its protolith is equivalent to komatiite according to the geochemical classification of Jensen (1976; Appendix 2-6). This sample displays depleted and disturbed LREE pattern with pronounced negative Eu anomaly and slightly enriched HREE contents (Fig. 2-7d left). Contaminated source of the protolith is suggested from the elevated contents of Ba, Ta, Hf and Zr.

2.4.1.2 Eastern Veles series

The metagranite from the Bukovac locality southwest of Bujanovac (SM315) and granite from the Štip magmatic complex (SM195-1) from the Eastern Veles series belong to the calc-alkaline series (Fig. 2-3e and f). Although the respective content of Y, Nb and Rb designate these rocks as magmatic-arc granites (Fig. 2-4), their peraluminous signatures suggest significant crustal input (Fig. 2-5). Furthermore, based on the Hf–Rb/30–3·Ta systematics of Harris et al. (1986), granite from the Štip complex shows post-collisional signature (Fig. 2-6a).

Both samples show enrichment in LREE, pronounced negative Eu anomalies and relatively flat HREE patterns, with an exception of a Tm spike for sample SM315 (Fig. 2-7e left). Accordingly, similar pattern typical for volcanic-arc granites can be observed on P-MORB normalised diagram, with more pronounced negative anomalies in Nb, Ta, Sr and Eu in case of SM315 (Fig. 2-7e right).

2.4.1.3 Basement of the Struma Unit

The analysed Delčevo granite (SM140-1) belongs to the Struma Diorite Complex (SDC), while the Bosilegrad monzonite (SM236-1), and a single basic sample (SM231-1) consistent with gabbroic rocks (Fig. 2-3e), were taken from the COL complex. All of the COL complex samples are associated with calc-alkaline differentiation series (Fig. 2-3f). Delčevo granite (SM140-1) shows signature typical for magmatic-arc granites (Fig. 2-6a), however a high affinity to within-plate setting is also suggested by its position on the Nb/Y diagram and by its peraluminous signature (Fig. 2-4 and 5, respectively). On a geotectonic discrimination plot for basic rocks, COL complex gabbro (SM231-1) plots well outside the within-plate area due to its anomalously high Ta and Hf content (Fig. 2-6b).

Sample SM140-1 shows an REE pattern with elevated content of LREE followed by slightly negative Eu anomaly and a relatively flat HREE pattern except for the slight enrichment of Yb and Tm (Fig. 2-7e left). Bosilegrad monzonite (SM236-1) is generally more depleted than the other two samples and displays a positive Eu anomaly and an enrichment in heaviest REE. All three samples exhibit prominent enrichment in Rb, Ba, K, Hf and Zr and a depletion of Ta and Nb, owing to their magmatic-arc origin (Fig. 2-7e right). Bosilegrad monzonite (SM236-1) displays an elevated Sr content, in which Delčevo granite (SM140-1) is considerably depleted most probably due to lower plagioclase content. Gabbroic sample (SM231-1) shows overall depleted REE pattern, with somewhat higher content of LREE, prominent positive Eu anomaly and gently sloping HREE sequence (Fig. 2-7d left). Additionally, Rb, Ba, Ta and Zr contents are quite elevated with significant loss in Nb and Hf (Fig. 2-7d right). Elevated concentrations of Sr and Eu could be explained by increased contents of clinopyroxene and plagioclase.

2.4.2 Geochronology

In this section only the emplacement ages of the magmatic, and maximum ages of deposition of the para-metamorphic rocks will be presented. For extensive sample descriptions and discussion of measurements see Appendix 2-3. Interpretation of the detrital and inherited zircon ages is given in Section 2.5.5.

2.4.2.1 The Lower Complex

Ten samples of magmatic rocks and two para-metamorphic rocks were taken for age determination in the Lower Complex (Table 2-1 and Fig. 2-8). The oldest magmatic body in the Lower Complex is the Vlajna granitoid with an age of 558±6 Ma (SM02, Section 2-3-1.1. in Appendix 2-3). Forty age measurements of detrital zircons from the para-metamorphic rocks in Golemo Selo (SM250-2, Section 2-3-1.2.2. in Appendix 2-3) and Sijarinska Banja (SM310, Section 2-3-1.4.2. in Appendix 2-3) constrain the maximum depositional age close to the emplacement age of Vlajna granitoid (569±9 Ma and 562±6 Ma, respectively). Reactivation of the magmatic activity in the Lower Complex occurred at 490±7 Ma with the emplacement of the leucocratic dykes in Vinica area (SM173-3, Fig. 2-8, Section 2-3-1.3.2. in Appendix 2-3), and a group of small leucocratic bodies in Vrvi Kobila area at 478±3 Ma (i.e. Kukavica granites; SM01; Fig. 2-8, Section 2-3-1.6.1. in Appendix 2-3). Orthogneiss in the Maleševski Mts. of the Ograzhden block intruded at 472±4 Ma (SM184-1, Fig. 2-8, Section 2-3-1.4.1. in Appendix 2-3). Emplacement ages of amphibolites in Golemo Selo (SM250-1, Section 2-3-1.2.1. in Appendix 2-3), and Vinica area (SM173-1, Section 2-3-1.3.1. in Appendix 2-3), were determined at 462±6 Ma and 456±2 Ma, respectively. Zircons from the deformed coarse-grained Qz monzonite in the southwestern periphery of the Bujanovac pluton gave an emplacement age of 439±2 Ma (SM377-2, Section 2-3-1.5.3. in Appendix 2-3). Late Variscan magmatic activity in the Lower Complex is represented by rather small, undeformed Slatinska Reka granite intruded at 328±5 Ma (SM550-1, Section 2-3-1.6.2. in Appendix 2-3). Two samples from the fine-grained Bujanovac pluton represent the youngest magmatic activity revealed in the Lower Complex with emplacement age of 253±2 Ma in the central part (SM199-1, Section 2-3-1.5.1. in Appendix 2-3), and 255±3 Ma in the southwestern periphery of the pluton (SM377-1, Section 2-3-1.5.1.2. in Appendix 2-3).

Most of the single grain U–Pb ages in the Lower Complex are Late Ordovician, but the

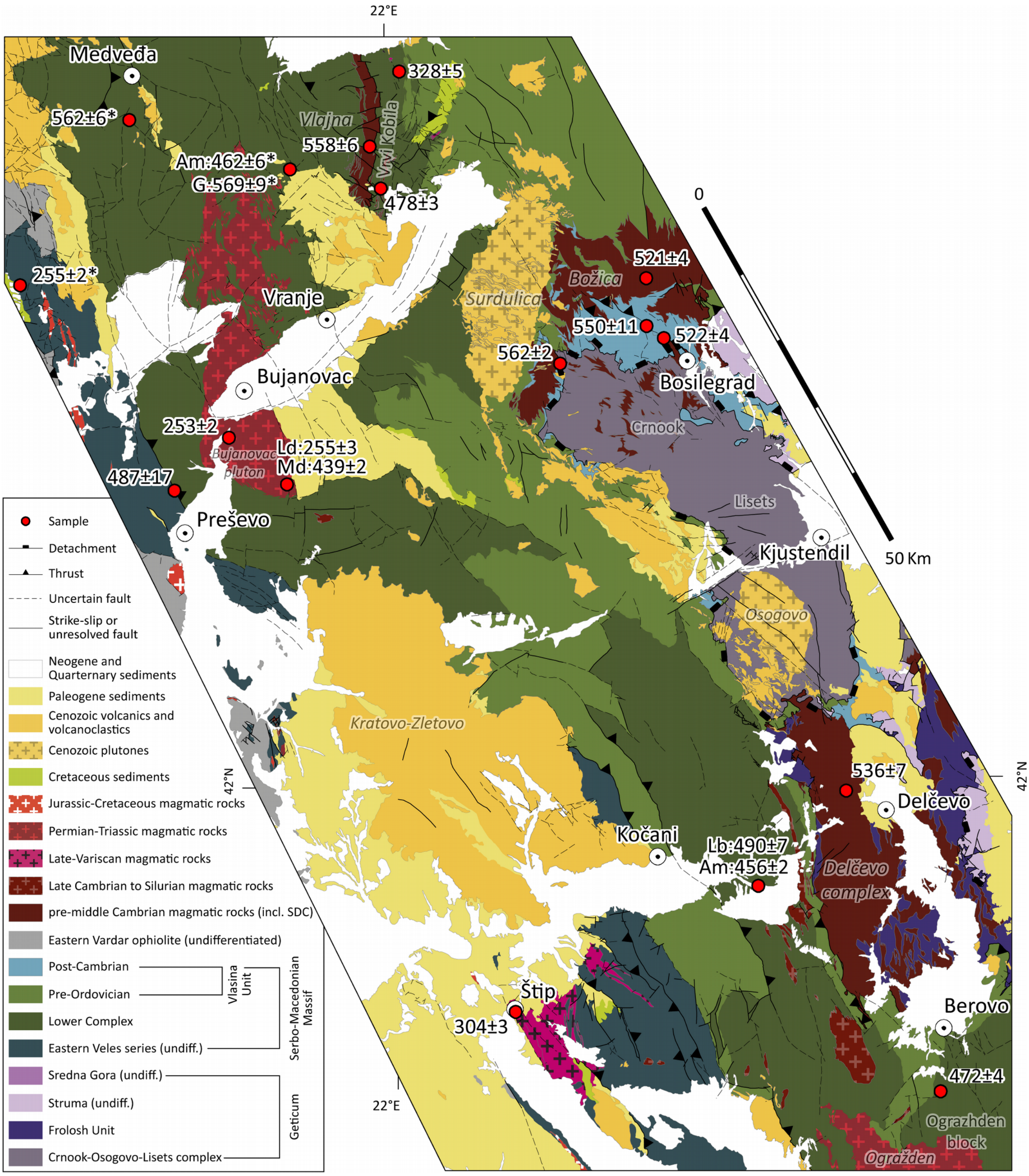

Figure 2-8. Tectonic map of the study area with the 206Pb/238U age results including 2σ errors. Ages reported with an asterisk (*) were determined based on detrital or xenocrystic zircon content. Abbreviations: Am – amphibolite, G – gneiss, Lb – leucocratic dykes, Md – more deformed, Ld – less deformed.

duration of magmatic activity lasted from late Cambrian to earliest Silurian (Fig. 2-9). Late Neoproterozoic, late early Carboniferous and Permian-Triassic zircon ages are also present.

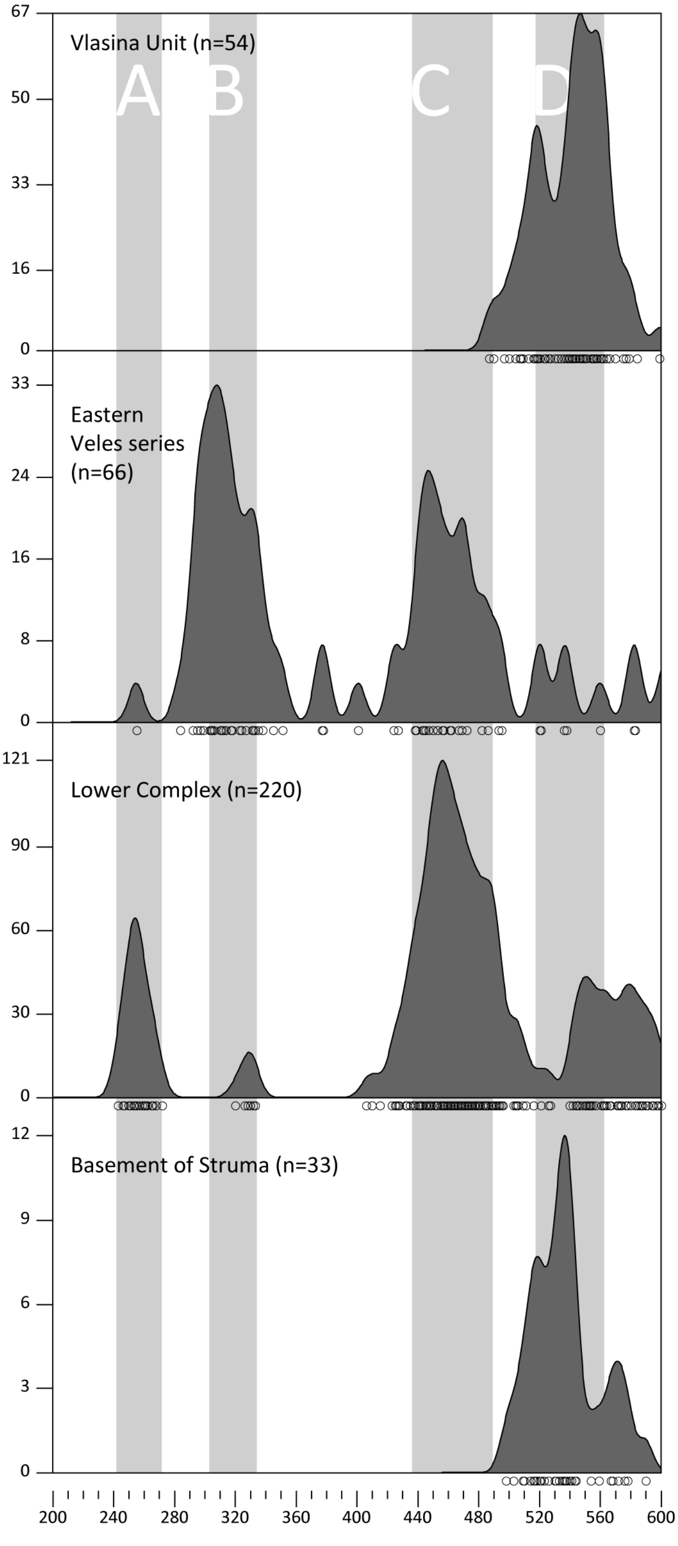

Figure 2-9. Kernel density estimates of $^{206}Pb/^{238}U$ age results between 200 and 600 Ma, related to tectonic units. Age results considered include both the measurements from detrital and magmatic zircons. Letters A, B, C, and D correspond to different magmatic stages.

2.1.1.2 Vlasina Unit

Only three samples from Vlasina Unit yielded zircon grains of sufficient size and quantity for LA-ICP-MS U–Pb measurements. The age results derived from these measurements show that magmatic activity in Vlasina Unit lasted from late Neoproterozoic until early Cambrian (Fig. 2-9). The Doganica metagranite is the oldest magmatic body in the Vlasina Unit with an emplacement age of 562±2 Ma (SM600-1, Fig. 2-8, Section 2-3-2.1. in Appendix 2-3). The slightly younger Lisina gabbro was emplaced at 550±11 Ma (SM3352, Section 2-3-2.3. in Appendix 2-3). Finally, a granitoid within the Božica magmatic complex was emplaced at 521±4 Ma (SM272-1, Section 2-3-2.2. in Appendix 2-3).

2.4.2.2 Eastern Veles series

Crystallisation ages of zircon domains from the rocks of the Eastern Veles series resemble those obtained from the Lower

Complex (Fig. 2-9). The earliest magmatic activity is represented by the Bukovac leuco-granite with an emplacement age of 487±17 Ma (SM315, Fig. 2-8, Section 2-3-3.1. in Appendix 2-3). A sample of biotite-rich granites from the Štip magmatic complex has a weighted average of the youngest group of age-results of 304±3 Ma (SM195-1, Fig. 2-8, Section 2-3-3.3. in Appendix 2-3). Seventeen age-measurements of detrital zircons from the Novo Brdo schists allowed only tentative constraints on the maximum deposition age of its sedimentary protolith at 255±2 Ma (KOS02, Fig. 2-8, Section 2-3-3.2. in Appendix 2-3).

2.4.2.3 Basement of the Struma Unit

Similarly to Vlasina Unit, the magmatic record in the COL complex and SDC in the basement of the Struma Unit reveal igneous activity lasting from the late Neoproterozoic to the early Cambrian (Fig. 2-9). The granites from the Delčevo magmatic complex (part of SDC) were emplaced at 536±7 Ma (SM140-1, Fig. 2-8, Section 2-3-4.2. in Appendix 2-3). A slightly younger age of 522±4 Ma was determined for the Bosilegrad monzonite in the COL complex (SM236-1, Fig. 2-8, Section 2-3-4.1. in Appendix 2-3).

2.4.3 Lu-Hf isotopic composition

Deviation of the Hf isotopic composition of zircon grains from the chondritic uniform reservoir (CHUR) reported in age-corrected epsilon units is a widely used parameter for description of the magma sources from which the zircons have crystallised, thus providing an estimate of the significance of juvenile depleted mantle (DM) or reworked old crust during the formation of the melt (e.g. Amelin et al., 1999; Kinny and Maas, 2003). In our study a total of 112 zircon spots were measured for their Lu-Hf isotopic composition (Appendix 2-7 and Fig. 2-10a). Details concerning the calculation of εHf values and DM model ages are provided in Appendix 2-7.

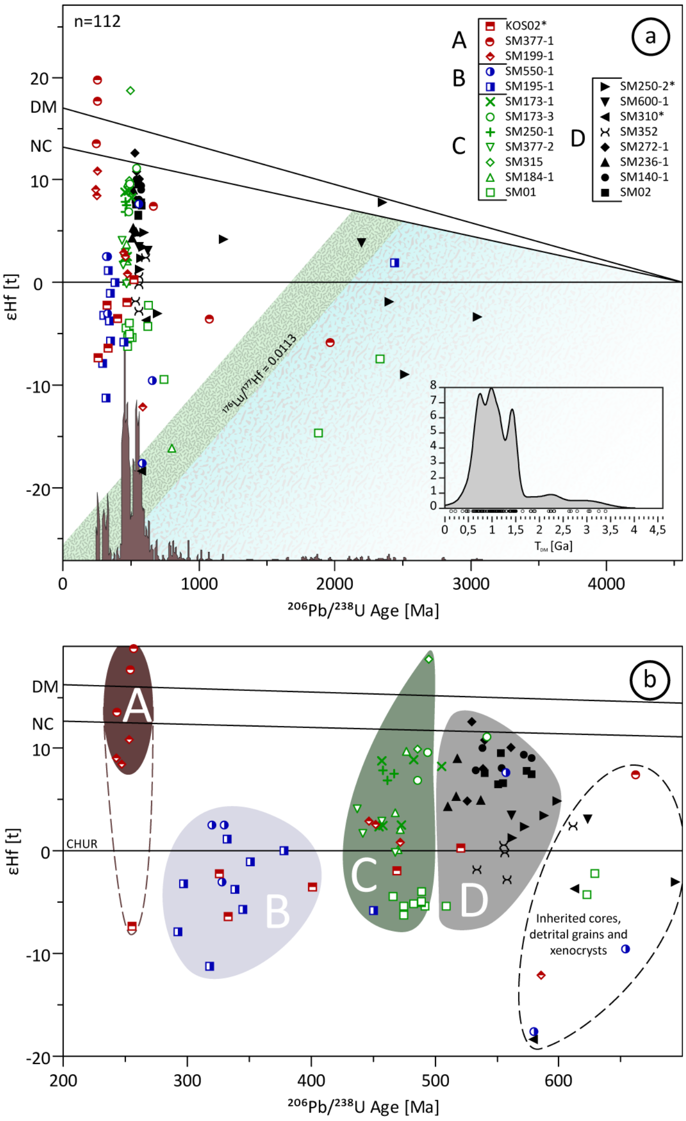

Figure 2-10. (a) Hf isotope evolution diagram of all analysed zircons. Samples with detrital zircons are marked with an asterisk. Evolution curves for the new crust (NC) and depleted mantle (DM) after Dhuime et al. (2011). CHUR stands for chondritic uniform reservoir. Crustal evolution trend (^{176}Lu/^{177}Hf=0.0113) after Linnemann et al. (2014). Stippled fields represent Siderian-Rhyacian and Archean crustal trends (from left to right, respectively). Probability density plot at the bottom of the diagram was produced by AgeDisplay (Sircombe, 2004), and represents all age results. Inset contains Kernel density estimate of DM model ages produced by DensityPlotter (v 6.1; Vermeesch, 2012). See text and Appendix 2-7 for details. (b) Magnified area between 200 and 700 Ma from (a).

The vast majority of the analysed spots (101 of total 112) are related to a group of zircons that crystallised from the Neoproterozoic to the earliest Triassic (Fig. 2-10a). Four groups of results younger than 1 Ga are defined based on U-Pb ages of the analysed zircon domains (Fig. 2-10b). Group D comprises measurements made on Ediacaran to early Cambrian zircon domains, which show a range of εHf values between +12.6 and -2.8 (Fig. 2-10b). Zircon grains from Vlajna granite (SM02), Bosilegrad monzonite (SM236-1), and granites from Božica (SM272-1), and Delčevo (SM140-1) magmatic complexes show more positive values (+12.6 to +4.2) indicating predominantly juvenile magma source, while the εHf values between +3.7 and -2.8 of zircons from Doganica granite (SM600-1) and Lisina gabbro (SM352) suggest higher presence of crustal material. Zircons with ages corresponding to this age-group are found as detrital grains in Novo Brdo schists (KOS02) and as xenocrysts in Slatinska Reka granite (SM550-1), Kukavica granite (SM01), and amphibolites (SM173-1) and leucocratic dykes in Vinica area (SM173-3). Group C contains measurements made on zircons that crystallised between the late Cambrian and the early Silurian (Fig. 2-10b). The εHf values of these zircon domains range between +18.7 and -6.2. Zircons from Kukavica granite (SM01), coarse-grained Bujanovac Qz-monzonite (SM377-2), Maleševski Mts. orthogneiss (SM184-1) represent part of the group C with lower εHf values (+4.3 to -6.2) indicating mixed juvenile and continental crust signature of the melt. Zircons of similar age and range of εHf values occur as detrital grains in Novo Brdo schists (KOS02) and as xenocrysts in fine-grained Bujanovac granite (SM199-1), granite from the Štip complex (SM195-1) and amphibolites from Vinica area (SM173-1). Formation of new crust associated with age-group C is documented by zircons with εHf values between +18.7 and +6.9, from amphibolites and leucocratic dykes in Vinica area (SM173-1 and SM173-3, respectively), and Bukovac leuco-granite (SM315). Xenocrysts from the Golemo Selo amphibolite (SM250-1) and Maleševski Mts. orthogneiss (SM184-1) yielded similarly high εHf values. Group B is composed of zircon domains crystallised in Devonian and Carboniferous (Fig. 2-10b). Low to negative εHf values of these zircons (+2.6 to -11.2) suggest crystallisation in magma predominantly related to reworking of older continental crust. Group B includes zircons of similar age and εHf values from the granite in the Štip magmatic complex (SM195-1), Slatinska Reka granites (SM550-1), and zircon domains from the Novo Brdo schists (KOS02). Zircons from fine-grained Bujanovac granite (SM199-1 and SM377-1) constitute the youngest group A (Fig. 2-10b), with crystallisation ages ranging from the late Permian to the Early Triassic. High εHf values of these zircon domains +19.7 and +8.5 suggests crystallisation from a juvenile magma source. Permian-Triassic age of the youngest detrital grain of Novo Brdo schists (KOS02) fits within the group A. However, its εHf value of -7.3 is in contrast to very high values of zircons from the Bujanovac granite, indicating a source area exotic to the SMM. The presence of late Neoproterozoic inherited zircon cores, detrital grains and xenocrysts with εHf values between +7.5 and -18.3 (580–694 Ma; Fig. 2-10b), suggests that the hypothetical basement of the magmatic and sedimentary rocks of the SMM, originated as a mixture of reworked crust and DM-derived magmas, comparable to the Neoproterozoic arc at the northern margin of Gondwana (e.g. Linnemann et al., 2007).

The negative εHf value (-3.3) and the resulting DM model age (T_{DM}) of 3.4 Ga of the single oldest inherited core (Fig. 2-10a and Appendix 2-7; SM250-2-o19; 3049 Ma) suggest that this initially detrital grain could be derived from a reworked Archean crust. Range of εHf values of Siderian-Rhyacian zircon domains (2.4–2.2 Ga; Fig. 2-10a) reveal that the early Palaeoproterozoic crust comprised both reworked Archean crust and DM sources. The DM model ages of the two spots with the lowest epsilon values correspond to the crustal evolution trend for the Siderian-Rhyacian juvenile crust (ca. 2.2 Ga). However these T_{DM} could also result from mixing of minor quantities of juvenile material at 580 Ma with large volumes of partial melts of an Archean crust. Four late Neoproterozoic to late Mesoproterozoic (from 586 to 1075 Ma; Appendix 2-7 and Fig. 2-10a) cores from magmatic zircons with negative epsilon values between -3.56 and -12, are aligned along a line subparallel to the crustal evolution trend (Fig. 2-10a). Their DM model ages (between 1.81 and 1.9 Ga) would suggest existence of an Orosirian juvenile crust, although they could also be related to reworking of an older crustal segment at, or prior to 1075 Ma. A group of 17 Cryogenian to Triassic zircons (694–255 Ma) with negative epsilon values and a single εHf -positive Stenian grain (1177 Ma) are roughly aligned along a linear trend with T_{DM} between 1.3 and 1.5 Ga (Fig. 2-10a and Appendix 2-7). Although similar DM model ages were determined for the Neoproterozoic granites of the Menderes Massif (Zlatkin et al., 2013), their parent-magma is suggested to represent a mixture of sources with different isotopic compositions.

2.5 Discussion

The results of our research suggest the existence of four major stages of magmatic activity within the Serbo-Macedonian Massif and the adjacent basement units (Figs. 2-8 and 2-9): i) Ediacaran to mid-Cambrian (late Cadomian; 562-521 Ma), ii) late Cambrian to early Silurian (490-439 Ma), ii) Carboniferous (late Variscan; 328-304 Ma), and iii) late Permian to Early Triassic (Permian-Triassic; 255-253 Ma).

2.5.1 Late Cadomian magmatic stage (Ediacaran to mid-Cambrian, 562-521 Ma)

Magmatic bodies emplaced during the Ediacaran to mid-Cambrian stage are present in all studied tectonic units (phase D in Fig. 2-9). This phase could be separated in two substages (562-550 Ma and 536-521 Ma) separated by a short period of quiescence. This magmatic phase could correspond to the Cadomian orogeny which is generally manifested by a series of tectonic events which took place along the northern margin of Gondwana from ca. 750 to 540 Ma (Nance et al., 2002; Murphy et al., 2004; Linnemann et al., 2007).

The older episode is represented by the emplacement of the Vlajna granite (SM02; 558±6 Ma) in the Lower Complex, and Doganica metagranites (SM600-1; 562±2 Ma) and Lisina gabbro (SM352; 550±11 Ma) in the Vlasina Unit. Geochemical signatures of Vlajna granite and Lisina gabbro indicate formation in convergent setting and contamination with crustal material (Figs. 2-4, 2-6b, and 2-7a and 2-d).

The continuation of the magmatic activity in the early Cambrian includes intrusion of peraluminous Delčevo granite (SM140-1; 536±7 Ma) of the Struma Diorite Complex into the ophiolites of Frolosh Unit, the Božica complex (SM272-1; 521±4 Ma) into the Vlasina Unit, and the Bosilegrad monzonite (SM236-1; 522±4 Ma) into the COL complex. The geochemical signatures of samples from the Božica magmatic complex and the magmatic rocks of the COL complex are consistent with mainly magmatic-arc setting (Figs. 2-4, 2-6a, 2-7c and e).

Magmatic rocks of similar age have been reported in the basement of Struma Unit in Bulgaria (Zagorchev et al., 2011a; Kounov et al., 2012), in the magmatic basement of the Pirgadikia Unit in the Internal Hellenides (Himmerkus et al., 2007, 2009a), and in the Neoproterozoic basement of the Sebeş–Lotru Unit in the southeastern Carpathian mountains (Balintoni et al., 2010a; Balintoni and Balica, 2013a). Additionally, coeval Ediacaran to early Cambrian I-type arc-related magmatism was determined in the İstanbul (Chen et al., 2002; Ustaömer et al., 2005) and Istranca (Yilmaz Şahin et al., 2014) terranes of the Western Pontides.

2.5.2 Late Cambrian to early Silurian magmatic stage (490-439 Ma)

An apparent 30 Ma of quiescence are followed by a long period of recurrent magmatic activity throughout the Lower Complex and the Eastern Veles series dominated by peraluminous granites and mafic intrusions (phase C in Fig. 2-9). Three pulses could be distinguished within this stage. The oldest pulse is represented by leucocratic dykes from the Vinica area of the Lower Complex (SM173-3; 490±7 Ma), Bukovac leucocratic metagranite from the eastern margin of the Eastern Veles series (SM315; 487±17 Ma), and Kukavica granites (SM01; 478±3). All these igneous rocks are peraluminous and have prevalent magmatic-arc signature (Figs. 2-4, 2-5, 2-6a, 2-7a and e), with the Kukavica granites showing substantial enrichment in crustal material (Fig. 2-10). Similar age of emplacement was obtained for the Lower Complex orthogneiss in Maleševski Mts. at the southeastern margin of the study area (SM184-1; 472±4 Ma). Although they share a dominant magmatic-arc geochemical signature, this orthogneiss exhibits a clear I-type signature and within-plate affinity (Figs. 2-5 and 2-6a). Meta-granites from the Bulgarian part of the same mountain range yielded Late Ordovician to early Silurian ages (476-433 Ma) and nearly identical geochemical signature (Zidarov et al., 2003a, 2003b; Macheva et al., 2006; Zagorchev et al., 2011a; Kounov et al., 2012). The Bretila and Cumpăna units of the Carpathian Mts. in Romania comprise arc-related magmatic rocks within the same age range (Balintoni et al., 2010a; Balintoni and Balica, 2013b). Slightly younger age (443-426 Ma) and magmatic-arc origin was determined for the peraluminous granites and orthogneisses of the Vertiskos unit in Greece (Himmerkus et al., 2007, 2009a; Meinhold et al., 2010).

The second magmatic pulse is marked by mafic intrusions in the Lower Complex. Zircon xenocrysts from an amphibolite near Golemo Selo in the Lower Complex yielded Middle Ordovician ages (SM250-1; ca. 462 Ma). These amphibolites represent dykes of within-plate tholeiitic basalts most probably intruded during an early episode of continental rifting, and later deformed together with the sedimentary host rocks. Compatibility in trace-element concentrations with undated amphibolites and meta-gabbros elsewhere along the Lower Complex (Fig. 2-7), together with rocks of similar chemistry north of the study area (Cvetković, 1992; Karamata and Krstić, 1996), suggest a regional importance of this rifting event. Nearly coeval age of emplacement was determined for amphibolites in the Vinica area of the Lower Complex (SM173-1; 456±2 Ma), however their trace element content points to arc-related setting. Higher concentrations of large-ion lithophile elements (LILE) and LREE concentrations (Fig. 2-7) and wider range of (positive) εHf values (Fig. 2-10b) suggest higher amount of crustal material involved in the formation of the Vinica amphibolite compared to the other analysed mafic bodies from the Lower Complex.

The final magmatic pulse during the stage C (Fig. 2-9) took place in the earliest Silurian when the medium to coarse-grained Bujanovac Qz-monzonite was intruded in the Lower Complex (SM377-2; 439±2 Ma). High content of elongated zircons (Pupin, 1980), low positive εHf values (0 to +4.3, Appendix 2-7 and Fig. 2-10b), and slightly elevated Eu content (Fig. 2-7a), suggest that these rocks were formed by primary mantle-derived magma that was significantly contaminated by crustal material or by partial melting of the arc-related crust.

2.5.3 Late Variscan magmatic phase (Carboniferous; 328-304 Ma)

Although only two magmatic bodies yielded Carboniferous ages in the study area, their emplacement diverges both temporally and in terms of geochemical signature (phase B in Fig. 2-9). The undeformed Slatinska Reka granite (SM550-1; 328±5 Ma) intruded the gneisses of the Lower Complex, providing the upper age-limit of the high-strain event(s) that affected the host rocks (Fig. 2-11a). Given the early Silurian age of the youngest dated highly deformed igneous rocks in the SMM (deformed Kukavica granite, SM01; 478±3 Ma), the high strain deformation and peak metamorphism is most probably related to the Variscan orogeny. The nearest magmatic rocks of similar age (334±1 Ma) are the undeformed post-collisional I-type granitoids in the Tran region in Bulgaria (Peytcheva et al., 2009a; Dyulgerov et al., 2010).

The undeformed granite of the Štip magmatic complex in the Eastern Veles series was emplaced during the late Carboniferous (SM195-1; 304±3 Ma). Previously reported

Figure 2-11. (a) Slatinska Reka valley (22°1'30.716"E, 42°50'53.365"N). Contact of the Lower Complex gneiss (G) with undeformed Slatinska Reka granite (Γ). Dashed white line indicates the trace of foliation (S_f) in the gneiss. Coin diameter 26 mm; (b) Spančevac locality (21°50'2.569"E, 42°21'33.025"N). Weakly deformed Bujanovac granite (Γ”) intruding the penetratively deformed coarse-grained Qz-monzonite (Γ') of the Lower Complex. Dashed white lines indicate the trace of foliation (S_f) in the coarse grained Qz-monzonite.

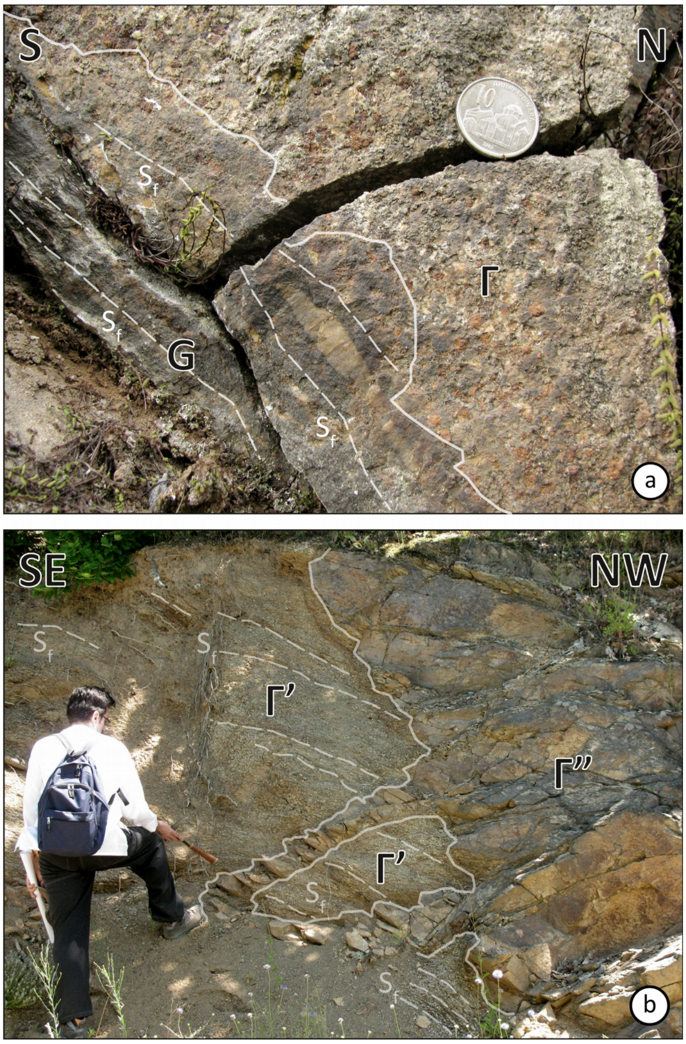

Callovian-Oxforidan Rb-Sr age of biotite (Šoptrajanova, 1967) is most probably related to thermal overprint (Spray et al., 1984), or to a much younger magmatic body that was intruded in the Carboniferous pluton. Large number of inherited zircons, peraluminous character of the granite (Fig. 2-5), and a wide range of low εHf values (-11.2 to +2, Fig. 2-10) suggest that the magmatic-arc geochemical signature (Fig. 2-4) is probably an artefact of the arc-related volcano-sedimentary basement, that was partially melted during the generation of the source magma of the Carboniferous granite in the Štip magmatic complex. The geochemical affinity to late- or post-collisional setting (Fig. 2-6a), most probably represents the correct geotectonic setting of this granite. Similar ages were obtained from granitoids in the Balkan terrane (Carrigan et al., 2005), and Danubian and Getic nappes of the Carpatho-Balkanides (Duchesne et al., 2008; Vasković et al., 2012).

2.5.4 Late Permian to Early Triassic magmatic phase (255-253 Ma).

The fine-grained Bujanovac granite (SM377-1 and SM199-1) was emplaced within the deformed medium- to coarse-grained Silurian Bujanovac Qz-monzonite (SM377-2, Fig. 2-11b) and the gneisses of the Lower Complex at the end of Permian and beginning of Triassic (SM377-1: 255±3, and SM199-1: 253±2 Ma). Magmatic-arc geochemical signature of the central part of the fine-grained Bujanovac pluton (SM199-1; Figs. 2-4, 2-6a and 2-7a) could be related to the extensive contamination by reworked lower crustal material of arc-related origin, rather than geotectonic setting during the magma generation. This interpretation is supported by an abundance of inherited zircons of Early Palaeozoic and Cadomian age and a peraluminous signature of the Bujanovac granite (Figs. 2-5 and 2-12). Within-plate affinity interpreted for the sample from the southern periphery of the pluton (SM377-1) is presumed to be more representative for the Permian-Triassic Bujanovac pluton (Fig. 2-6a). Furthermore, positive εHf values (+8.5 to +19.7) are associated with the significant influence of the depleted mantle on the source of late Bujanovac granites (Fig. 2-10a and b). Such contamination with juvenile material could be caused by mafic intrusions in the severely attenuated continental crust during the rifting stage leading to the opening of the Mesozoic Tethys (Karamata and Krstić, 1996; Karamata, 2006).

Intrusions of similar age have been reported in other parts of the SMM, such as rift-related Arnea and Kerkini A-type granites in Vertiskos (Christofides et al., 1999, 2007; Himmerkus et al., 2009b), and Igralishte, Skrat (Skrut) and Ogražden granites in the Ograzhden block (Zidarov et al.,

Figure 2-12. Zircon-age content of notable occurrences in the pre-Mesozoic basement in southeastern Europe and the samples from this study. These are delimited by synoptic density distribution of results from this study produced by AgeDisplay (Sircombe, 2004). Presented data includes magmatic, metamorphic and detrital zircons including 2σ errors. Right side of the diagram displays data until 600 Ma. Dot-stippled fields denote samples of sedimentary origin. Sources: [1]Chen et al. (2002); [2]Ustaömer et al. (2011); [3]Ustaömer et al. (2005); [4]Meinhold et al. (2010); [5]Includes: Himmerkus et al. (2006), Himmerkus et al. (2009a), Christofides et al. (2007) and Himmerkus et al. (2009b); [6]Zagorchev et al. (2011b); [7]Kounov et al. (2012); [8]Includes: Zidarov et al. (2003a), Zidarov et al. (2003b), Zidarov et al. (2004), Peytcheva et al. (2005); Macheva et al. (2006), Zidarov et al. (2007), Peytcheva et al. (2009b), Haydoutov et al. (2010) and Zagorchev et al. (2011a); [9]Balintoni et al. (2010a); [10]Balintoni and Balica (2013b); [11]Includes: Carrigan et al. (2005) and Carrigan et al. (2006).

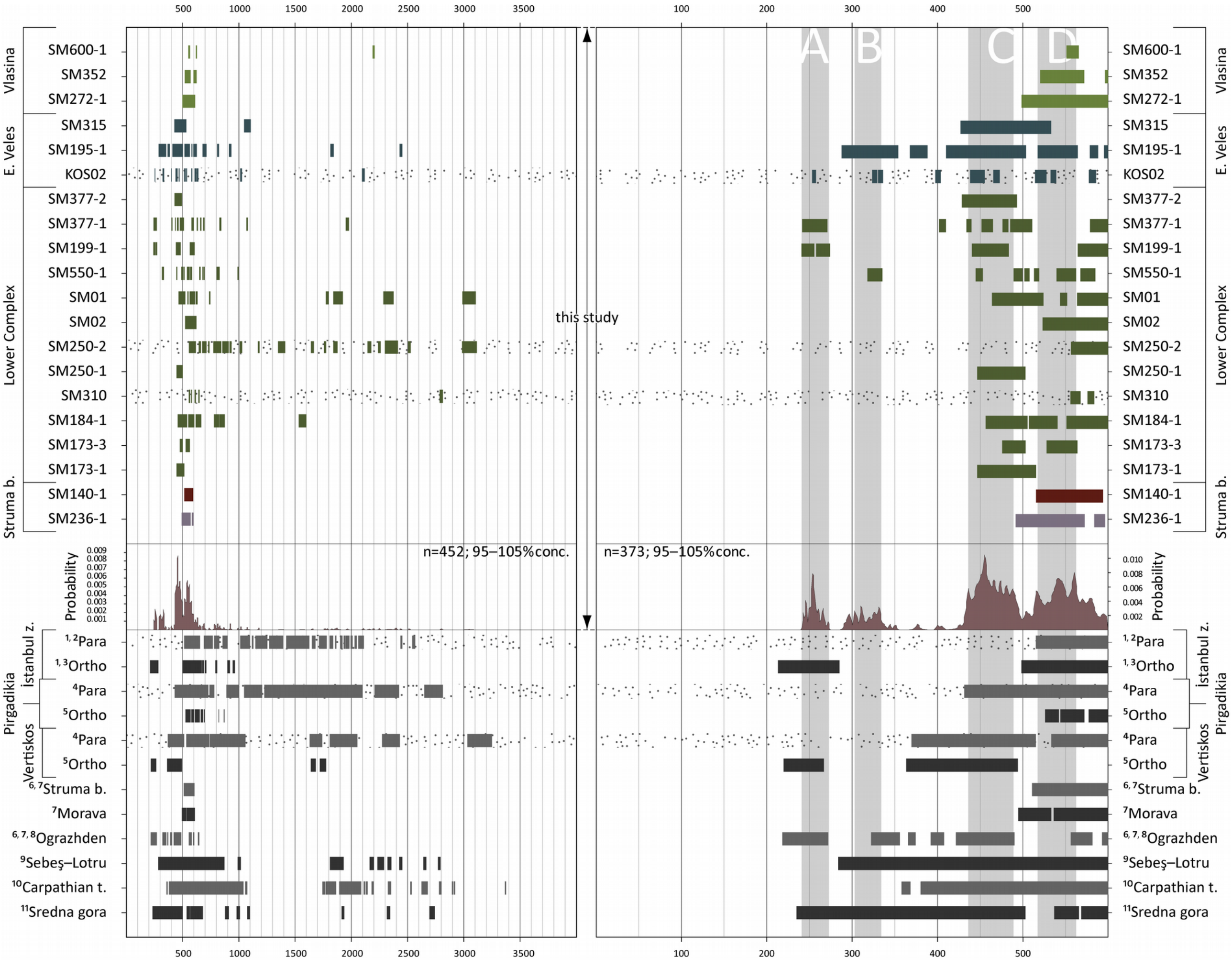

2004, 2007; Peytcheva et al., 2005, 2009b; Georgiev et al., 2012).

2.5.5 Detrital and inheritance record and implications on the provenance of the SMM

Age results of the detrital zircons from the para-metamorphic samples allowed determination of relative depositional age of the sedimentary protoliths. The maximum depositional age of the sedimentary protoliths of the paragneisses within the volcano-sedimentary Lower Complex could be constrained as late-Cadomian from the youngest detrital zircons obtained from the Sijarinska Banja and Golemo Selo paragneiss (SM310; 562±6 and SM250-2; 569±9 Ma, respectively). Although much younger (Meinhold et al., 2010), the sedimentary cover of the Pirgadikia Unit of the internal Hellenides shares much of its Precambrian detrital record with Golemo Selo paragneiss of the SMM (Fig. 2-12).

The age of the Vlasina volcano-sedimentary successions could not be determined directly since meta-sedimentary rock samples collected for this purpose did not yield sufficient number of zircon grains of appropriate size for an LA-ICP-MS analysis. However, the early Cambrian age of emplacement of a granite in the Božica magmatic complex constrains the youngest age of Vlasina Unit, since the xenoliths found within the Božica complex in Bulgaria are suspected to be derived from the pre-Ordovician Vlasina (Graf, 2001). Additionally, the Cadomian ages of Doganica and Lisina magmatic bodies demand a reassessment of the originally proposed intrusive relationship with the Lower Ordovician meta-sediments (Babović et al., 1977; Pavlović, 1977), as they clearly represent inliers within this para-metamorphic succession.

Although based on scarce zircon content (Appendices 2-3 and 2-4), the maximum depositional age of the Novo Brdo schists from the sedimentary cover in the northwestern periphery of the Eastern Veles series was tentatively constrained by the youngest result of 255±2 Ma obtained on a zircon fragment with oscillatory zoning (Appendix 2-3). This detrital age is in agreement with the Triassic age proposed by Pavić et al. (1983), based on the fossil record.

The range of ages of detrital grains, inherited cores and xenocrysts from samples of sedimentary and magmatic origin in the central SMM provides some information on the initial palaeogeographic position of the basement. Late Ediacaran (562–550 Ma) igneous rocks were determined in the Lower Complex, Vlasina Unit and the basement of the Struma Unit, with Cadomian (ca. 700–ca. 540 Ma) magmatic zircons as preponderant inherited population in these units and the Eastern Veles series (Figs. 2-9 and 2-12). This prominent population of U–Pb zircon ages coupled with geochemical results, suggests that the basement of the SMM was most probably involved in the Cadomian orogeny as a segment within the active continental margin of north Gondwana (Nance et al., 2002; Neubauer, 2002; Murphy et al., 2004; Stampfli et al., 2013). In this context, the presence of Early Cryogenian to Tonian zircons (677 to 994 Ma, Fig. 2-12), could be related to the Cadomian part of the arc (Linnemann et al., 2007, 2014; Zulauf et al., 2007; Avigad et al., 2012; Pereira et al., 2012a, 2012b), or as detrital input related to the amalgamation of the South-China craton (Cawood et al., 2013; Zhang et al., 2013). The Avalonian provinces are virtually devoid of this age signature since this arc accreted to Gondwanan active margin at ca. 665-650 Ma (Nance et al., 2008). Additional proof excluding Avalonian provenance is the general scarcity of magmatic zircons of Mesoproterozoic age (ca. 1600–1000 Ma). Presence of Mesoproterozoic zircons is commonly related to the orogenic magmatism affecting Laurentia, Baltica or Amazonia (Nance and Murphy, 1996). Thus they are absent from the South China (Zhang and Zheng, 2013) and West African cratons (Nance and Murphy, 1994; Friedl et al., 2000). However, minor population of late Mesoproterozoic zircons determined in samples from the central SMM (Fig. 2-9 and 12) does not necessarily imply Avalonian provenance, as similar ages were reported for volcanic rocks of the western Yangtze block (South-China craton; Zhang and Zheng, 2013, and references therein), from the Arabian-Nubian Shield and its cover sequence (e.g. Dixon, 1981;

Avigad et al., 2003; Be’eri-Shlevin et al., 2012), and from Neoproterozoic and Palaeozoic siliciclastic sediments of southern Libya (Meinhold et al., 2011). Minor presence of this population throughout the Cadomian domain (Linnemann et al., 2007, 2014; Pereira et al., 2012a), including Minoan terranes (Zulauf et al., 2007; Zlatkin et al., 2013), was traditionally attributed to distant dispersion by large river systems (Zeh et al., 2001), and recently to a super-fan system shedding detritus with ca, 1.0 Ga-old zircons from the Transgondwanan supermountain towards the Gondwana margin (Meinhold et al., 2013). Minor quantities of 1.6–2 and 2.1–2.5 Ga zircon ages determined in this study (Fig. 2-12), could potentially be attributed to sources from Arabian-Nubian shield (e.g. Stacey and Hedge, 1984; Ali et al., 2009), West African (Nance and Murphy, 1994), and/or South-China craton (Zhang and Zheng, 2013). In conclusion, the basement of the SMM was most probably located in eastern parts of the north Gondwana margin in late Neoproterozoic, i.e. northeast of Saharan metacraton and southwest of South-China craton.

2.5.6 Tectonic evolution

From late Ediacaran to mid-Cambrian (562–522 Ma), the SMM together with the basement of the Struma Unit represented a part of an Andean-type continental magmatic arc situated along the northern margin of Gondwana (Fig. 2-13a). Based on U–Pb zircon age record, similar late Neoproterozic position could also be suggested for the Pirgadikia micro-terrane of the Internal Hellenides, Lotru unit of the Carpathians and the İstanbul zone of the western Pontides (Fig. 2-12). Although xenocryst ages, Lu/Hf trends and DM model ages of zircons from the magmatic rocks in the SMM suggest reworking of an older continental basement in which they were intruded (Fig. 2-10), these continental basement rocks were not recognised in the study area. However, such rocks were reported in the neighbouring Tran region in the Struma Unit (Kounov et al., 2012), in basement from the Pelagonian zone (Anders et al., 2006; Schenker et al., 2014; Zlatkin et al., 2014),

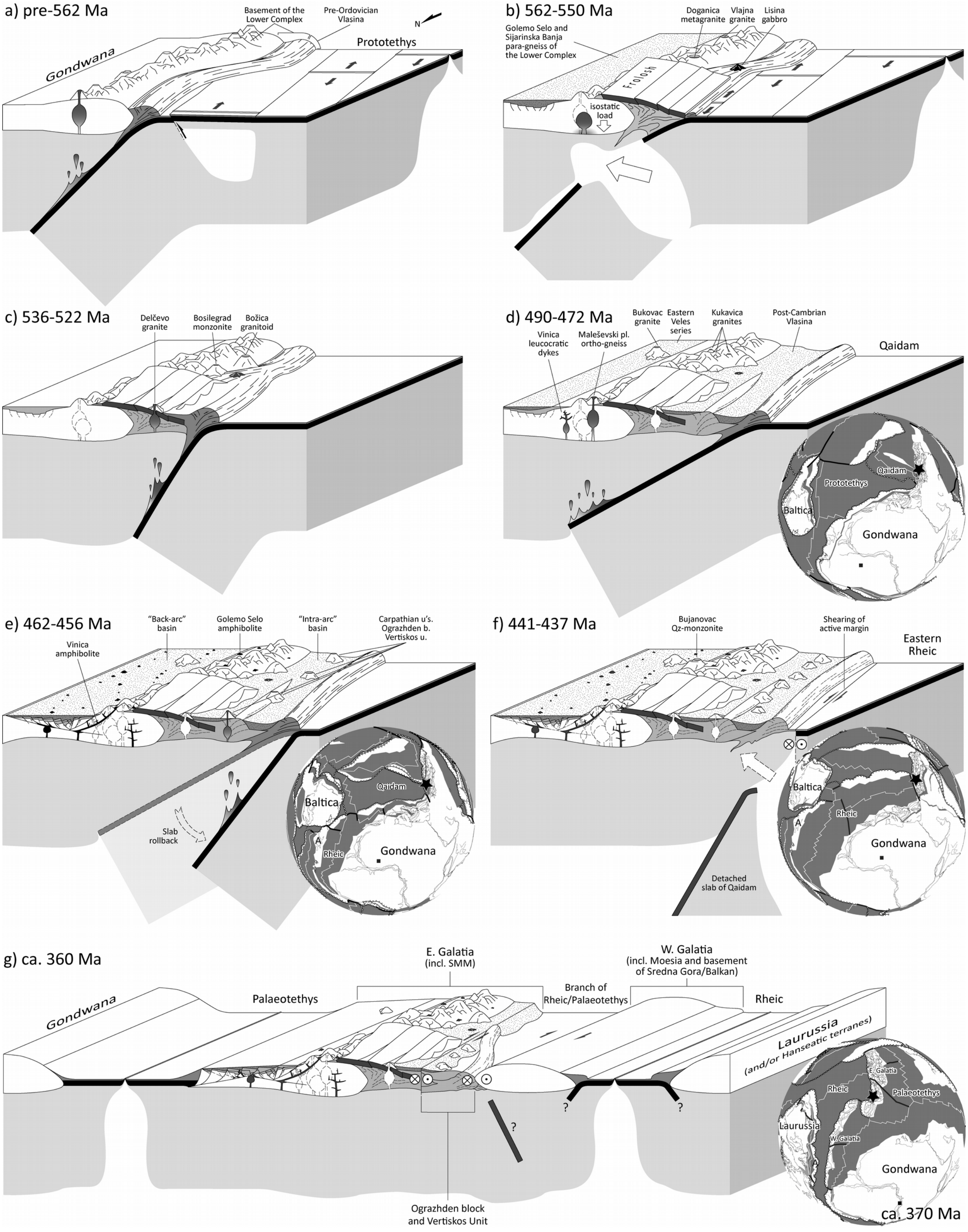
a) pre-562 Ma
Basement of the Lower Complex
Pre-Ordovician Vlasina
N
Prototethys
Gondwana
b) 562-550 Ma
Golemo Selo and Sijarinska Banja para-gneiss of the Lower Complex
Doganica metagranite
Vlajna granite
Lisina gabbro
Frolosh
isostatic load
c) 536-522 Ma
Delčevo granite
Bosilegrad monzonite
Božica granitoid
d) 490-472 Ma
Vinica leucocratic dykes
Bukovac granite
Eastern Veles series
Maleševski pl. ortho-gneiss
Kukavica granites
Post-Cambrian Vlasina
Qaidam
Qaidam
Prototethys
Baltica
Gondwana
e) 462-456 Ma
Vinica amphibolite
"Back-arc" basin
Golemo Selo amphibolite
"Intra-arc" basin
Carpathian u's. Ograzhden b. Vertiskos u.
Slab rollback
Baltica
Qaidam
A
Rheic
Gondwana
f) 441-437 Ma
Bujanovac Qz-monzonite
Shearing of active margin
Eastern Rheic
Baltica
A
Rheic
Gondwana
Detached slab of Qaidam
g) ca. 360 Ma
Gondwana
Palaeotethys
E. Galatia (incl. SMM)
Branch of Rheic/Palaeotethys
W. Galatia (incl. Moesia and basement of Sredna Gora/Balkan)
Rheic
Laurussia (and/or Hanseatic terranes)
?
?
?
Ograzhden block and Vertiskos Unit
Rheic
E. Galatia
Palaeotethys
Laurussia
W. Galatia
A
Gondwana
ca. 370 Ma

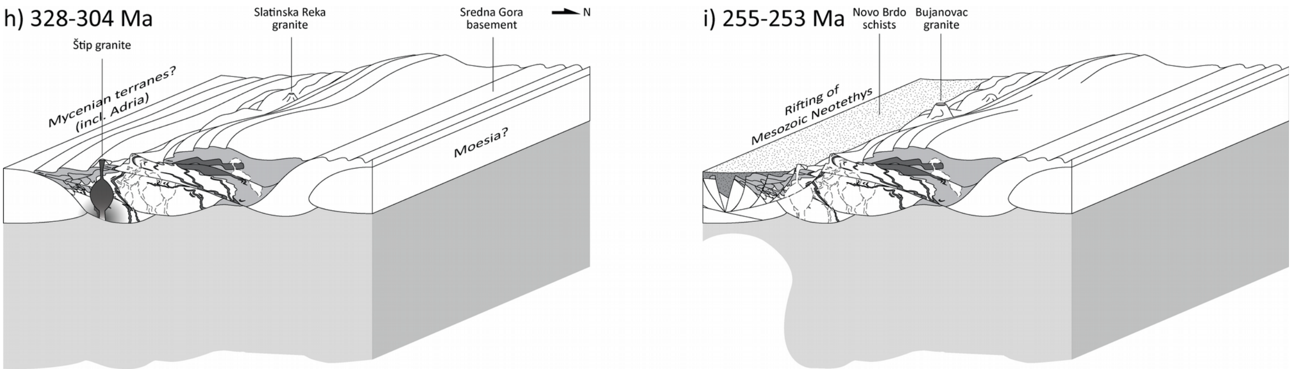

Figure 2-13. Unscaled sketches of the inferred tectonic evolution of the study area since the Cadomian until the earliest Mesozoic. Dot-stippled areas represent basins with ongoing sedimentation (both clastic and biochemical), and black units designate emplacement of mafic and ultramafic rocks. In (d), (e), (f), and (g), the location of the SMM is designated by a black star on the global reconstruction of Stampfli et al. (2013), where black square represents the South Pole, white line a spreading centre, thick black line a wrenching zone, and notched black line an active margin. See text for details.

and the İstanbul (Ustaömer et al., 2005) and the Sakarya zones (Aysal et al., 2012) in northwestern Turkey. This hypothetical continental basement was adjacent to an Ediacaran accretionary wedge or a fore-arc basin dominated by terrigenous sediments, presently a part of the Lower Complex (Dimitrijević, 1967; Krstić and Karamata, 1992), whereas the pre-Ordovician Vlasina Unit would correspond to an external part of the wedge dominated by sediments scraped off the ocean bottom (Fig. 2-13a; Milovanović et al. 1988; Popović 1991 and references therein). Both the terrigenous and ocean-floor-dominated parts were subsequently intruded by magmatic rocks of the late Cadomian arc. This magmatic arc was most probably related to the oblique subduction of the Prototethys (Fig. 2-13a), with dextral transform boundary already terminating subduction in the western (i.e. Avalonian) section of the belt (Nance et al., 2002, 2010). Given the proximity of the trench and the oblique direction of the subduction, a minor intra-oceanic thrusting might have been initiated, which potentially led to a partial obduction of small oceanic fragments represented by the ophiolites of Frolosh Unit, on a still active continental magmatic arc (Fig. 2-13b). A “gap” in the subducting slab due to the missing obducted segment would result in incursion of depleted mantle into the mantle wedge. Increased heat flow would promote partial melting at the base of the arc resulting in the formation of granites and gabbros with zircons crystallised in a juvenile melt contaminated with crustal material (Figs. 2-10b and 2-13b; Lisina gabbro, Vlajna and Doganica granites). Units with similar age of magmatic-arc activity and basement provenance, as Sebeş–Lotru in the Carpathians or Pirgadikia Unit in the internal Hellenides are devoid of ophiolitic segments and mixed magmatic sources, suggesting minor size and local importance of this obduction. Increased load on the margin of the magmatic arc could cause slight subsidence of the entire arc facilitating deposition in a retro-arc basin, currently represented by para-metamorphic series of the Lower Complex (Fig. 2-13b). The continuation of the subduction of the Prototethys in the early Cambrian reinitialised continental arc magmatism in Vlasina Unit (granite from the Božica magmatic complex), and the basement of Struma Unit (i.e. COL complex including Bosilegrad monzonite, and SDC including Delčevo granite; Fig. 2-13c). Termination of the subduction and transition to sheared continental margin via dextral wrenching reported for Avalonia between 605 and 545 Ma (Nance et al., 2002), and central Cadomia at ca. 540 Ma (Linnemann et al., 2007), potentially took place in the studied region after 521 Ma. Alternatively, termination of activity along this margin occurred by a southward-migrating intra-oceanic subduction zone (Stampfli et al., 2013).

Following the period of magmatic quiescence, predominantly peraluminous, leucocratic granitic magmatism indicates a reactivation of the North-Gondwanan active margin (i.e. Vinica dyke, Kukavica and Bukovac granites, and Maleševski Mts. orthogneiss Fig. 2-13d). This felsic magmatism is probably caused by the subduction of the Qaidam back-arc ocean or the remaining Protothetyan domain (Stampfli et al., 2013). Lower Ordovician sediments were deposited in the Vlasina Unit (i.e. post-Cambrian Vlasina), and in the Veles series (Pavlović, 1962; Karamata and Krstić, 1996). The former could represent a fore-arc basin, while the sediments of the latter were most probably deposited in the retro-arc or an incipient back-arc basin (Fig. 2-13d).

Widespread within-plate mafic magmatism occurred in the SMM in late Middle Ordovician

(456-462 Ma; Vinica and Golemo Selo amphibolites; Fig. 2-13d). Most of these tholeiitic dykes were intruded in the Lower Complex, whereas the variety of geochemical signatures of the mafic magmatic rocks in the Vlasina Unit suggests that they represent a collection of various sources, probably amalgamated during the earlier, subduction-related accretion of this unit. The basaltic magmatism from the Lower Complex could possibly be attributed to the rifting of a back arc basin (Fig. 2-13e), although felsic igneous rocks of this age are absent in the study area, and marine sedimentation, including carbonates, continued uninterrupted on both flanks of the SMM (Pavlović, 1977; Karamata and Krstić, 1996; Banjac, 2004). Remnants of these sediments are presently part of the Eastern Veles series and Vlasina Unit. Arc-related magmatism was reported southeast of the study area (in present coordinates; i.e. Ograzhden block), from Middle Ordovician to early Silurian (Macheva et al., 2006; Zagorchev et al., 2011a; Kounov et al., 2012). Similar magmatic-arc activity was determined in the Cumpăna Unit (Balintoni et al., 2010a), and the Carpathian-type units in Romania (Balintoni and Balica, 2013b), as well as the Vertiskos Unit in Greece (Himmerkus et al., 2009a; Meinhold et al., 2010). Since the host rocks of these magmatic bodies are upper Cambrian to Lower Ordovician sediments, we suggest oceanward migration of the magmatic arc due to slab rollback, with continuing passive-margin deposition in thus formed "intra-arc basin" (i.e. post-Cambrian Vlasina; Fig. 2-13e).

Subduction was terminated in the early Silurian by dextral shearing of the subducting slab, related to an oblique opening of the Rheic Ocean (Fig. 2-13f; Stampfli et al., 2013). Within-plate peraluminous Bujanovac Qz-monzonite is possibly a result of the partial melting of the continental crust due to high thermal gradient resulting from the penetration of the astenospheric material into the mantle wedge following the detachment of the sheared slab (Fig. 2-13f, 439±2 Ma). Magmatism in the Vertiskos Unit in Greece (Himmerkus et al., 2009a; Meinhold et al., 2010), and Ograzhden block in Bulgaria (Zagorchev et al., 2011a), that lasted until 426 and 433 Ma respectively, shows a predominant magmatic-arc affinity. Since the magma sources in these two areas were found to be heavily contaminated with crustal material, there is a distinct possibility that this magmatism was also caused by the process proposed for the formation of the Bujanovac Qz-monzonite.

During the subsequent period of magmatic quiescence, the SMM had presumably drifted westwards across the Rheic Ocean towards Laurussia, as an eastern part of the ribbon-like Galatian super-terrane (Karamata, 2006; Stampfli et al., 2013). Meanwhile, Eastern Galatia had collided with its western counterpart generating dextral wrenching of constituent units and opening of pull-apart basins (Fig. 2-13g; Stampfli et al., 2013). This event resulted in eastward movement of Ograzhden block and Vertiskos Unit, and concomitant deposition of Upper Devonian turbidites with evidence of mafic volcanism along the eastern part of the Vlasina Unit (Spassov, 1973; Zagorčev and Bončeva, 1988; Krstić et al., 2002). This depositional setting persisted until the lower Carboniferous when the final amalgamation/juxtaposition of the SMM to the Western Galatia (including Moesia and possibly also basement of Balkan and Sredna Gora units), most probably took place (Haydoutov and Yanev, 1997; Banjac, 2004 and references therein; Karamata, 2006; Gerdjikov et al., 2010). Subduction direction of the branch of Rheic or Palaeotethys ocean that was located between the two parts of the Galatian super-terrane is still uncertain (e.g. Iancu et al., 2006; Plissart, 2012). Sustained collision of segments of the Galatian super-terrane and the margin of Laurussia had probably caused top-to-the-west thrusting along the SMM (in present orientation), separating it into distinct structural levels (Fig. 2-13h). An overall crustal thickening would have promoted metamorphism, varying according to depth at which each of these segments was buried. Ultimately, this tectonic overburden could lead to the partial melting of the lower crust, possibly resulting in emplacement of the minor granitic bodies in Vrvi Kobila area (i.e. Slatinska Reka granite, 328±5 Ma), and a late peraluminous granite within the Štip magmatic complex in the Eastern Veles series (304±3 Ma, Fig. 2-13h). Similar magmatism was not found in the rest of the

SMM, but was reported further east in the basement of Sredna Gora and Balkan units (Carrigan et al., 2005), and the central Rhodope complex (Peytcheva et al., 2004). The southern boundary of the SMM in late Carboniferous was either an active northward subduction zone of Palaeotethys (Zulauf et al., 2015), or it was occupied by the Mycenian terranes which were also part of the Eastern Galatia, juxtaposed to the SMM by dextral wrenching (Stampfli et al., 2013; Fig. 2-13h).

The final magmatic episode along the SMM is represented by the emplacement of the late Permian–Early Triassic peraluminous Bujanovac granites (SM199-1 and SM377-1, ca. 255 Ma, Fig. 2-13i). Similar igneous activity reported elsewhere along the European continental margin was related to the closure of the remaining Palaeotethyan domains and the following extension which consequently led to the opening of the Mesozoic Tethys (Robertson and Karamata, 1994; Karamata and Krstić, 1996; Pe-Piper, 1998; Stampfli et al., 2002; Karamata, 2006; Himmerkus et al., 2009b; Burg, 2012).

2.6 Conclusions

In the present study, the geochemical analysis, Hf isotope measurements, and U–Pb LA-ICP-MS zircon dating of igneous and sedimentary rocks from the Serbo-Macedonian Massif and the basement of the adjacent units have allowed the following conclusions to be made:

- During the Cadomian orogenic cycle the Lower Complex of the SMM was part of a continental magmatic arc developed along the northern margin of Gondwana. The complex could be correlated with the Lotru and Pirgadikia units of the Carpathians and the Internal Hellenides, respectively. Based on inherited and detrital zircon data, its late Neoproterozoic position in the eastern part of the northern margin of Gondwana is tentatively proposed (i.e. northeast of Saharan metacraton and southwest of South-China craton).
- The volcano-sedimentary pre-Ordovician Vlasina Unit most probably represents part of a late

Neoproterozoic accretionary wedge dominated by ocean-floor sediments. During this time the Lower Complex was most probably a more internal part of the same volcano-sedimentary succession or a fore-arc basin.

- The magmatic-arc activity in the study area was detected in the Ediacaran to the mid-Cambrian in the Lower Complex, Vlasina Unit and the basement of Struma Unit. These units together with the Eastern Veles series, experienced renewal of arc-related magmatism in the late Cambrian to Early Ordovician, while mafic magmatism related to rifting occurred in the Lower Complex during Middle to Late Ordovician. Minor pulse of within-plate felsic magmatism in the Lower Complex took place in the early Silurian.
- The age of the high-strain deformation and peak metamorphism in the SMM was constrained to the Variscan orogeny by the presence of highly deformed early Silurian meta-granites and undeformed late Carboniferous granites intruding the gneisses of the Lower Complex.
- The Variscan collisional tectonics led to the differential burial of constituents of the SMM (i.e. Lower Complex, Vlasina Unit, basement of Struma Unit, and Eastern Veles series), resulting in different metamorphic grades of these domains with a common late Neoproterozoic–early Palaeozoic history. Additionally, this complex Variscan framework was subsequently severely disrupted by the Alpine events.
- During the Permian-Triassic the entire SMM experienced widespread crustal extension and emplacement of within-plate granites, most probably related to the rifting of the Mesozoic Neotethys.

References

Ali, B.H., Wilde, S.A., Gabr, M.M.A., 2009. Granitoid evolution in Sinai, Egypt, based on precise SHRIMP U–Pb zircon geochronology. Gondwana Research 15, 38–48.

Amelin, Y., Lee, D.-C., Halliday, A.N., Pidgeon, R.T., 1999. Nature of the Earth's earliest crust from hafnium isotopes in single detrital zircons. Nature 399, 252–255.

Anders, B., Reischmann, T., Kostopoulos, D., Poller, U., 2006. The oldest rocks of Greece: first evidence for a Precambrian terrane within the Pelagonian Zone. Geological Magazine 143, 41–58.

Avigad, D., Gerdes, A., Morag, N., Bechstädt, T., 2012. Coupled U–Pb–Hf of detrital zircons of Cambrian sandstones from Morocco and Sardinia: Implications for provenance and Precambrian crustal evolution of North Africa. Gondwana Research 21, 690–703.

Avigad, D., Kolodner, K., McWilliams, M., Persing, H., Weissbrod, T., 2003. Origin of northern Gondwana Cambrian sandstone revealed by detrital zircon SHRIMP dating. Geology 31, 227–230.

Aysal, N., Öngen, S., Peytcheva, I., Keskin, M., 2012. Origin and evolution of the Havran Unit, Western Sakarya basement (NW Turkey): new LA-ICP-MS U-Pb dating of the metasedimentary-metagranitic rocks and possible affiliation to Avalonian microcontinent. Geodinamica Acta 25, 226–247.

Babović, M., Roglić, Č., Avramović, V., Marić, S., 1977. Tumač za list Trgovište sa Radomirom, Osnovna Geološka Karta 1:100000. Savezni Geološki Zavod, Belgrade.

Balintoni, I., Balica, C., 2013a. Avalonian, Ganderian and East Cadomian terranes in South Carpathians, Romania, and Pan-African events recorded in their basement. Mineralogy and Petrology 107, 709–725.

Balintoni, I., Balica, C., 2013b. Carpathian peri-Gondwanan terranes in the East Carpathians (Romania): A testimony of an Ordovician, North-African orogeny. Gondwana Research 23, 1053–1070.

Balintoni, I., Balica, C., Ducea, M.N., Hann, H.P., Şabliovschi, V., 2010a. The anatomy of a Gondwanan terrane: The Neoproterozoic–Ordovician basement of the pre-Alpine Sebeş–Lotru composite terrane (South Carpathians, Romania). Gondwana Research 17, 561–572.

Balintoni, I., Balica, C., Seghedi, A., Ducea, M.N., 2010b. Avalonian and Cadomian terranes in North Dobrogea, Romania. Precambrian Research 182, 217–229.

Balogh, K., Svingor, É., Cvetković, V., 1994. Ages and intensities of metamorphic processes in the Batočina area, Serbo-Macedonian massif. Acta Mineralogica-Petrographica XXXV, 81–94.

Banjac, N., 2004. Stratigrafija Srbije i Crne Gore. Rudarsko-geološki fakultet, Belgrade.

Be'eri-Shlevin, Y., Eyal, M., Eyal, Y., Whitehouse, M.J., Litvinovsky, B., 2012. The Sa'al volcano-sedimentary complex (Sinai, Egypt): A latest Mesoproterozoic volcanic arc in the northern Arabian Nubian Shield. Geology 40, 403–406.

Boev, B., Lepitkova, S., Petrov, G., 2002. Granitoid formations in the Republic of Macedonia, in: Proceedings of XVII Congress of CBGA. Presented at the XVII Congress of CBGA, VEDA, Bratislava, pp. 1–22.

Boncheva, I., Lakova, I., Sachanski, V., Koenigshof, P., 2010. Devonian stratigraphy, correlations and basin development in the Balkan Terrane, western Bulgaria. The Rheic Ocean: Palaeozoic Evolution from Gondwana and Laurussia to Pangaea 17, 573–582.

Bonev, K., Ivanov, Z., Ricou, L.-E., 1995. Dénudation tectonique au toit du noyau métamorphique

Rhodopien-macédonien: La faille normale ductile de Gabrov Dol (Bulgarie). Bulletin de la Société Géologique de France 166, 47–55.

Bosse, V., Boulvais, P., Gautier, P., Tiepolo, M., Ruffet, G., Devidal, J.L., Cherneva, Z., Gerdjikov, I., Paquette, J.L., 2009. Fluid-induced disturbance of the monazite Th–Pb chronometer: In situ dating and element mapping in pegmatites from the Rhodope (Greece, Bulgaria). Chemical Geology 261, 286–302.

Brković, T., Radovanović, Z., Pavlović, Z., 1980. Tumač za list Kragujevac, Osnovna Geološka Karta 1:100000. Savezni Geološki Zavod, Belgrade.

Brun, J.-P., Sokoutis, D., 2007. Kinematics of the Southern Rhodope Core Complex (North Greece). International Journal of Earth Sciences 96, 1079–1099.

Burg, J.-P., 2012. Rhodope: From Mesozoic convergence to Cenozoic extension. Review of petro-structural data in the geochronological frame. Journal of the Virtual Explorer, The Geology of Greece 42.

Burg, J.-P., Godfriaux, I., Ricou, L.-E., 1995. Extension of the Mesozoic Rhodope thrust units in the Vertiskos-Kerdilion Massifs (Northern Greece). Comptes Rendus de l'Académie des Sciences Paris, Sciences de la Terre et des Planetes 320, 889–896.

Burg, J.-P., Ivanov, Z., Ricou, L.-E., Dimor, D., Klain, L., 1990. Implications of shear-sense criteria for the tectonic evolution of the Central Rhodope massif, southern Bulgaria. Geology 18, 451–454.

Burg, J.-P., Ricou, L.-E., Ivano, Z., Godfriaux, I., Dimov, D., Klain, L., 1996. Syn-metamorphic nappe complex in the Rhodope Massif. Structure and kinematics. Terra Nova 8, 6–15.

Carrigan, C.W., Mukasa, S.B., Haydoutov, I., Kolcheva, K., 2005. Age of Variscan magmatism from the Balkan sector of the orogen, central Bulgaria. Lithos 82, 125–147.

Carrigan, C.W., Mukasa, S.B., Haydoutov, I., Kolcheva, K., 2006. Neoproterozoic magmatism and Carboniferous high-grade metamorphism in the Sredna Gora Zone, Bulgaria: An extension of the Gondwana-derived Avalonian-Cadomian belt? Precambrian Research 147, 404–416.

Cawood, P.A., Wang, Y., Xu, Y., Zhao, G., 2013. Locating South China in Rodinia and Gondwana: A fragment of greater India lithosphere? Geology 41, 903–906.

Chen, F., Siebel, W., Satir, M., Terzioğlu, M., Saka, K., 2002. Geochronology of the Karadere basement (NW Turkey) and implications for the geological evolution of the Istanbul zone. International Journal of Earth Sciences 91, 469–481.

Christofides, G., Koroneos, A., Liati, A., Král, J., 2007. The A-type Kerkini granitic complex in north Greece: geocrhonology and geodynamic implications, in: Proceedings. Presented at the 11th International conference of the Geological Society of Greece, Geological Society of Greece, Athens, pp. 700–711.

Christofides, G., Koroneos, A., Pe-Piper, G., Katirtzoglou, K., Chatzikirkou, A., 1999. Pre-Tertiary A-Type magmatism in the Serbomacedonian massif (N. Greece) : Kerkini granitic complex. Bulletin of the Geological Society of Greece 33, 131–148.

Cvetković, V., 1992. Petrology of the metamorphic rocks from the northern parts of the Serbo-macedonian massif in the Batočina area (Magistar thesis). Faculty of Mining and Geology, Belgrade.

Cvetković, V., Karamata, S., Balogh, K., Fed'kin, V., Milovanović, D., 1995. Petrology of medium-grade gneisses from the Batočina area (Serbo-Macedonian massif, Yugoslavia), in: Proceedings. Presented at the XV Congress of the CBGA, Geological Society of Greece, Athens, Greece, pp. 591–595.

Dabovski, C., Boyanov, I., Khrischev, K., Nikolov, T., Sapunov, I., Yanev, Y., Zagorchev, I.S., 2002. Structure and Alpine evolution of Bulgaria. Geologica Balcanica 32, 9–15.

Dhuime, B., Hawkesworth, C., Cawood, P., 2011. When Continents Formed. Science 331, 154–155.

Dimitrijević, M.D., 1957. Struktura kristalastih terena između Slišana i Preševa, in: Referati, predavanja, diskusije. Presented at the II kongres geologa FNRJ, Savez geoloških društava Jugoslavije, Sarajevo.

Dimitrijević, M.D., 1958. Geološki sastav i struktura bujanovačkog granitskog masiva. Rasprave zavoda za geološka i geofizička ispitivanja narodne republike Srbije 3.

Dimitrijević, M.D., 1963. Sur l'âge du métamorphisme et des plissements dans la masse Serbo-macédonienne, in: Bulletin. Presented at the VIe Congrès de l'Association géologique carpatho-balkanique, Instytut Geologiczny, Warszawa, pp. 339–347.

Dimitrijević, M.D., 1967. Some Problems of Crystalline Schists in the Serbo-Macedonian Massif, in: Reports. Presented at the VIII Congress of CBGA, Serbian Geological Society, Belgrade, pp. 59–67.

Dimitrijević, M.D., 1997. Geology of Yugoslavia. Geological Institute GEMINI, Belgrade.

Dimitrijević, M.D., Drakulić, N., 1958. Kristalasti škriljci Jablanice. Zbornik radova Rudarsko-geološkog fakulteta 6.

Dimitrova, E., 1964. Petrologie des kristallinen Sockels des Osogovo Gebirges. Bulgarian Academy of Sciences Bulletin of the Geological Institute, Stratigr Lithol 13, 99–110.

Dinter, D.A., Royden, L., 1993. Late Cenozoic extension in northeastern Greece: Strymon Valley detachment system and Rhodope metamorphic core complex. Geology 21, 45.

Dixon, T.H., 1981. Age and Chemical Characteristics of some Pre-Pan-African rocks in the Egyptian Shield. Precambrian Research 14, 119–133.

Dolić, D., Kalenić, M., Marković, B., Dimitrijević, M., Radoičić, R., Lončarević, Č., 1981. Tumač za list Paraćin, Osnovna Geološka Karta 1:100000. Savezni Geološki Zavod, Belgrade.

Duchesne, J.-C., Liègeois, J.-P., Iancu, V., Berza, T., Matukov, D.I., Tatu, M., Sergeev, S.A., 2008. Post-collisional melting of crustal sources: constraints from geochronology, petrology and Sr, Nd isotope geochemistry of the Variscan Sichevita and Poniasca granitoid plutons (South Carpathians, Romania). International Journal of Earth Sciences 97, 705–723.

Dyulgerov, M., Peytcheva, I., Nedyalkov, R., von Quadt, A., 2010. Characteristic of Variscan granitoid magmatism in Tran region, Bulgaria. Review of the Bulgarian Geological Society 71, 69–82.

Erić, S., Logar, M., Milovanović, D., Babič, D., Adnađević, B., 2009. Ti-in-biotite geothermometry in non-graphitic, peraluminous metapelites from Crni vrh and Resavski humovi (Central Serbia). Geologica Carpathica 60, 3–14.

Fed'kin, V., Karamata, S., Cvetković, V., Balogh, K., 1996. Two stories of metamorphism presented by amphibolites from two different terranes of Serbia, in: Knežević-Đorđević, V., Krstić, B. (Eds.), Terranes of Serbia. Faculty of Mining and Geology, University of Belgrade, Belgrade, pp. 145–150.

Friedl, G., Finger, F., McNaughton, N.J., Fletcher, I.R., 2000. Deducing the ancestry of terranes: SHRIMP evidence for South America–derived Gondwana fragments in central Europe. Geology 28, 1035.

Georgiev, N., Pleuger, J., Froitzheim, N., Sarov, S., Jahn-Awe, S., Nagel, T.J., 2010. Separate Eocene–Early Oligocene and Miocene stages of extension and core complex formation in the Western Rhodopes, Mesta Basin, and Pirin Mountains (Bulgaria). Tectonophysics 487, 59–84.

Georgiev, S., Peytcheva, I., Stefanova, E., von Quadt, A., Marchev, P., Grozdev, V., Serafimovski, T., 2012. Geochemistry and geochronology of Ilovitsa magmatic rocks, SE FYR Macedonia, in: Abstracts Book. Presented at the International Earth Science Colloquium on the Aegean Region, IESCA-2012, Izmir, p. 94.

Gerdjikov, I., Lazarova, A., Balkanska, E., Bonev, K., Vangelov, D., Dimov, D., Kounov, A., 2010.

A New Model For the Pre-Permian Basemen of the Central Stara Planina Mountain. Comptes Rendus de l'Académie bulgare des Sciences, Geologie 63, 1169–1176.

Graf, J., 2001. Alpine tectonics in Western Bulgaria: Cretaceous compression of the Kraishte region and Cenozoic exhumation of the crystalline Osogovo–Lisets Complex (PhD). ETH Zürich, Zürich.

Grubić, A., Đoković, I., Marović, M., Branković, M., 1999. Srpsko-Makedonska masa ne postoji. Vesnik, Geologija, hidrogeologija i inženjerska geologija 49, 1–14.

Grubić, A., Đoković, I., Marović, M., Branković, M., 2005. Problem tektonskog položaja kristalina Srpsko-Makedonske mase. Zapisnici Srpskog geološkog društva za 1998, 1999, 2000, 2001, 2002 i 2003. godinu, 35–39.

Grubić, A., Ercegovac, M., 2002. Age of the Veles "Schistes Lustres" Formation from the Vardar Ocean, in: Proceedings of XVII Congress of CBGA. Presented at the XVII Congress of CBGA, VEDA, Bratislava, pp. 66–68.

Harris, N.B.W., Pearce, J.A., Tindle, A.G., 1986. Geochemical characteristics of collision-zone magmatism. Geological Society, London, Special Publications 19, 67–81.

Haydoutov, I., Kolcheva, K., Daieva, L., 1994. The Struma diorite fm from Vlahina block, SW Bulgaria. Review of the Bulgarian Geological Society 55, 9–35.

Haydoutov, I., Pin, C., 1993. Geochemical and Nd isotope characteristics of pre-variscan ophiolites and meta-igneous rocks from the Struma Diorite Formation in SW Bulgaria. Geologica Balcanica 23, 51–59.

Haydoutov, I., Pristavova, S., Daieva, L.-A., 2010. Some Features of the Neoproterozoic - Cambrian Geodynamics in Southeastern Europe. Proceeding of the Bulgarian Academy of Sciences 63, 1597–1608.

Haydoutov, I., Yanev, S., 1997. The Protomoesian microcontinent of the Balkan Peninsula — a peri-Gondwanaland piece. Tectonophysics 272, 303–313.

Himmerkus, F., Anders, B., Reischmann, T., Kostopoulos, D., 2007. Gondwana-derived terranes in the northern Hellenides. Geological Society of America Memoirs 200, 379–390.

Himmerkus, F., Reischmann, T., Kostopoulos, D., 2006. Late Proterozoic and Silurian basement units within the Serbo-Macedonian Massif, northern Greece: the significance of terrane accretion in the Hellenides. Geological Society, London, Special Publications 260, 35–50.

Himmerkus, F., Reischmann, T., Kostopoulos, D., 2009a. Serbo-Macedonian revisited: A Silurian basement terrane from northern Gondwana in the Internal Hellenides, Greece. Tectonophysics 473, 20–35.

Himmerkus, F., Reischmann, T., Kostopoulos, D., 2009b. Triassic rift-related meta-granites in the Internal Hellenides, Greece. Geological Magazine 146, 252.

Hofmann, A.W., 1988. Chemical differentiation of the Earth: the relationship between mantle, continental crust, and oceanic crust. Earth and Planetary Science Letters 90, 297–314.

Iancu, V., Berza, T., Seghedi, A., Gheuca, I., Hann, H.-P., 2005. Alpine polyphase tectono-metamorphic evolution of the South Carpathians: A new overview. Tectonophysics 410, 337–365.

Iancu, V., Berza, T., Seghedi, A., Marunțiu, M., 2006. Palaeozoic rock assemblages incorporated in the South Carpathian Alpine thrust belt (Romania and Serbia): A review. Geologica Belgica 8, 48–86.

Iancu, V., Màruntiu, M., Johan, V., Ledru, P., 1998. High-grade metamorphic rocks in the pre-Alpine nappe stack of the Getic-Supragetic basement (Median Dacides, South Carpathians, Romania). Mineralogy and Petrology 63, 173–198.

Ilić, M., Karamata, S., Knežević-Đorđević, V., 1967. Serpentinites and Ultramafic Rocks of East Serbia, in: Reports. Presented at the VIII Congress of CBGA, Serbian Geological Society, Belgrade, pp. 91–105.

Irvine, T.N., Baragar, W.R.A., 1971. A Guide to the Chemical Classification of the Common Volcanic Rocks. Canadian Journal of Earth Sciences 8, 523–548.

Ivanov, Z., 1988. Aperçu général sur l'évolution géologique et structurale du massif des Rhodopes dans le cadre des Balkanides. Bulletin de la Société Géologique de France 4, 227–240.

Janoušek, V., Farrow, C.M., Erban, V., 2006. Interpretation of Whole-rock Geochemical Data in Igneous Geochemistry: Introducing Geochemical Data Toolkit (GCDkit). Journal of Petrology 47, 1255–1259.

Jensen, L.S., 1976. A new cation plot for classifying subalkalic volcanic rocks. Ontario Division of Mines Miscellaneous papers 66.

Kaiser-Rohrmeier, M., Handler, R., von Quadt, A., Heinrich, C., 2004. Hydrothermal Pb–Zn ore formation in the Central Rhodopian Dome, south Bulgaria: Review and new time constraints from Ar–Ar geochronology. Swiss Bulletin of Mineralogy and Petrology 84, 37–58.

Kalvoda, J., Bábek, O., 2010. The Margins of Laurussia in Central and Southeast Europe and Southwest Asia. Gondwana Research 17, 526–545.

Karajovanović, M., Hadži-Mitrova, S., 1982. Tolkuvač za listot Titov Veles, Osnovna Geološka Karta 1:100000. Savezni Geološki Zavod, Belgrade.

Karajovanović, M., Hristov, S., 1976. Tolkuvač za listot Kumanovo, Osnovna Geološka Karta 1:100000. Savezni Geološki Zavod, Belgrade.

Karamata, S., 2006. The geological development of the Balkan Peninsula related to the approach, collision and compression of Gondwanan and Eurasian units. Geological Society, London, Special Publications 260, 155–178.

Karamata, S., Krstić, B., 1996. Terranes of Serbia and Neighbouring Areas, in: Knežević-Đorđević, V., Krstić, B. (Eds.), Terranes of Serbia. Faculty of Mining and Geology, University of Belgrade, Belgrade, pp. 25–40.

Kilias, A., Falalakis, G., Mountrakis, D., 1997. Alpine tectonometamorphic history of the Serbomacedonian metamorphic rocks: implication for the tertiary unroofing of the Serbomacedonian-Rhodope metamorphic complexes (Makedonia, Greece). Ορυκτός Πλούτος 105, 32–50.

Kilias, A., Falalakis, G., Mountrakis, D., 1999. Cretaceous–Tertiary structures and kinematics of the Serbomacedonian metamorphic rocks and their relation to the exhumation of the Hellenic hinterland (Macedonia, Greece). International Journal of Earth Sciences 88, 513–531.

Kinny, P.D., Maas, R., 2003. Lu–Hf and Sm–Nd isotope systems in zircon. Reviews in Mineralogy & Geochemistry 53, 327–341.

Kober, L., 1921. Der Bau der Erde. Gebrüder Borntraeger, Berlin.

Kockel, F., Mollat, H., Walther, H.W., 1971. Geologie der Serbo-Mazedonischen Massivs und seines mesozoischen Rahmens (Nordgriechenland). Geologisches Jahrbuch 89, 529–551.

Korikovsky, S., Karamata, S., Milovanović, D., 2003. Retrograted kyanite eclogites and eclogittized gabbro-norites of the Serbo-macedonian unit, Central Serbia , reaction textures and geothermobarometry, in: Zbornik Abstraktov. Presented at the Konferencia venovanej Prof. rNDr. Dušanovi Hovorkovi, DrSc. k životnému jubileu, Bratislava, pp. 13–14.

Kounov, A., Burg, J.-P., Bernoulli, D., Seward, D., Ivanov, Z., Dimov, D., Gerdjikov, I., 2011. Paleostress analysis of Cenozoic faulting in the Kraishte area, SW Bulgaria. Journal of Structural Geology 33, 859–874.

Kounov, A., Graf, J., von Quadt, A., Bernoulli, D., Burg, J.-P., Seward, D., Ivanov, Z., Fanning, M., 2012. Evidence for a "Cadomian" ophiolite and magmatic-arc complex in SW Bulgaria. Precambrian Research 212–213, 275–295.

Kounov, A., Seward, D., Bernoulli, D., Burg, J.-P., Ivanov, Z., 2004. Thermotectonic evolution of an extensional dome: the Cenozoic Osogovo-Lisets core complex (Kraishte zone, western Bulgaria). International Journal of Earth Sciences 93, 1008–1024.

Kounov, A., Seward, D., Burg, J.-P., Bernoulli, D., Ivanov, Z., Handler, R., 2010. Geochronological and structural constraints on the Cretaceous thermotectonic evolution of the Kraishte zone, western Bulgaria. Tectonics 29, TC2002.

Kounov, A., Wüthrich, E., Seward, D., Burg, J.-P., Stockli, D., 2015. Low-temperature constraints on the Cenozoic thermal evolution of the Southern Rhodope Core Complex (Northern Greece). International Journal of Earth Sciences 104, 1–16.

Kräutner, H.G., Krstić, B., 2002. Alpine and pre-Alpine structural units within the southern Carpathians and eastern Balkanides, in: Proceedings of XVII Congress of CBGA. Presented at the XVII Congress of CBGA, VEDA, Bratislava.

Kroner, U., Romer, R.L., 2013. Two plates — Many subduction zones: The Variscan orogeny reconsidered. Gondwana Research 24, 298–329.

Krstić, B., 1981. Niški kaledonsko-hercinski geosinklinalni pojas u istočnoj Srbiji. Zapisnici Srpskog geološkog društva za 1980. godinu, 99–103.

Krstić, B., Maslarević, L., Ercegovac, M., Đajić, S., 2002. Devonian of the Serbian Carpatho-Balkanides, in: Proceedings of XVII Congress of CBGA. Presented at the XVII Congress of CBGA, VEDA, Bratislava.

Krstić, N., Karamata, S., 1992. Terani u Karpato-Balkanidima istočne Srbije. Zapisnici Srpskog geološkog društva jubilarna knjiga (1891-1991), 57–69.

Lakova, I., 1997. Additional palynological data on the age of the Razhcha Formation, Osogovo Mts., West Bulgaria. Geologica Balcanica 27, 36.

Lakova, I., 2009. Acritarch evidence on Silurian age of the low-grade metamorphic Palaeozoic rocks in the Kraishte area (Morava Unit). Review of the Bulgarian Geological Society 70, 23–30.

Liati, A., 2005. Identification of repeated Alpine (ultra) high-pressure metamorphic events by U–Pb SHRIMP geochronology and REE geochemistry of zircon: the Rhodope zone of Northern Greece. Contributions to Mineralogy and Petrology 150, 608–630.

Liati, A., Gebauer, D., 1999. Constraining the prograde and retrograde P-T-t path of Eocene HP rocks by SHRIMP dating of different zircon domains: inferred rates of heating, burial, cooling and exhumation for central Rhodope, northern Greece. Contributions to Mineralogy and Petrology 135, 340–354.

Lilov, P., Zagorchev, I.S., 1993. K-Ar data for the deformation and low-grade metamorphism in Permian and Triassic red beds in SW Bulgaria. Geologica Balcanica 23, 46.

Linnemann, U., Gerdes, A., Drost, K., Buschmann, B., 2007. The continuum between Cadomian orogenesis and opening of the Rheic Ocean: Constraints from LA-ICP-MS U-Pb zircon dating and analysis of plate-tectonic setting (Saxo-Thuringian zone, northeastern Bohemian Massif, Germany). Geological Society of America Special Papers 423, 61–96.

Linnemann, U., Gerdes, A., Hofmann, M., Marko, L., 2014. The Cadomian Orogen: Neoproterozoic to Early Cambrian crustal growth and orogenic zoning along the periphery of the West African Craton—Constraints from U–Pb zircon ages and Hf isotopes (Schwarzburg Antiform, Germany). Precambrian Research 244, 236-278

Ludwig, K.R., 2012. Isoplot 3.75: A Geochronological Toolkit for Microsoft Excel, Berkeley Geochronology Center Special Publication. Berkeley Geochronological Center, Berkeley.

Macheva, L., Peytcheva, I., von Quadt, A., Zidarov, N., Tarassova, E., 2006. Petrological, geochemical and isotope features of Lozen metagranite, Belasitza Mountain – evidence for widespread distribution of Ordovician metagranitoids in the Serbo-Macedonian Massif, SW Bulgaria, in: Proceedings. Presented at the National conference “Geosciences 2006” with international participation, Bulgarian Geological Society, Sofia.

Medaris Jr., G., Ducea, M., Ghent, E., Iancu, V., 2003. Conditions and timing of high-pressure Variscan metamorphism in the South Carpathians, Romania. Lithos 70, 141–161.

Meinhold, G., Kostopoulos, D., Frei, D., Himmerkus, F., Reischmann, T., 2010. U–Pb LA-SF-ICP-MS zircon geochronology of the Serbo-Macedonian Massif, Greece: palaeotectonic constraints for Gondwana-derived terranes in the Eastern Mediterranean. International Journal of Earth Sciences 99, 813–832.

Meinhold, G., Kostopoulos, D., Reischmann, T., Frei, D., BouDagher-Fadel, M.K., 2009. Geochemistry, provenance and stratigraphic age of metasedimentary rocks from the eastern Vardar suture zone, northern Greece. Palaeogeography, Palaeoclimatology, Palaeoecology 277, 199–225.

Meinhold, G., Morton, A.C., Avigad, D., 2013. New insights into peri-Gondwana paleogeography and the Gondwana super-fan system from detrital zircon U–Pb ages. Gondwana Research 23, 661–665.

Meinhold, G., Morton, A.C., Fanning, C.M., Frei, D., Howard, J.P., Phillips, R.J., Strogen, D., Whitham, A.G., 2011. Evidence from detrital zircons for recycling of Mesoproterozoic and Neoproterozoic crust recorded in Paleozoic and Mesozoic sandstones of southern Libya. Earth and Planetary Science Letters 312, 164–175.

Middlemost, E.A.K., 1985. Magmas and magmatic rocks: an introduction to igneous petrology. Longman, London; New York.

Mihailescu, N., Dimitrijević, M.D., Dimitrijević, M.N., 1967. Les fossiles dans le flysch, in: Reports. Presented at the VIII Congress of CBGA, Serbian Geological Society, Belgrade, pp. 371–378.

Milovanović, D., 1990. Petrologija gnajseva Srpsko-makedonske mase u području između Tulara i Lebana, in: Proceedings of the XII Congress of the Geologists of Yugoslavia. Presented at the XII Kongres na geolozi na Jugoslavija, Prosveta, Ohrid, pp. 310–321.

Milovanović, D., 1992. Amfibolske stene u području između Medveđe i Lebana. Geološki anali Balkanskoga poluostrva 56, 253–268.

Milovanović, D., Milovanović, M., Oberhänsli, R., 1988. Petrology of green-rocks of the Vlasina complex in the Manastiriška river area (Vlasotince). Vesnik, Geologija 44, 101–128.

Munteanu, M., Tatu, M., 2003. The East-Carpathian Crystalline-Mesozoic Zone (Romania): Paleozoic Amalgamation of Gondwana- and East European Craton-derived Terranes. Gondwana Research 6, 185–196.

Murphy, J.B., Pisarevsky, S.A., Nance, R.D., Keppie, J.D., 2004. Neoproterozoic--Early Paleozoic evolution of peri-Gondwanan terranes: implications for Laurentia-Gondwana connections. International Journal of Earth Sciences 93, 659–682.

Nakamura, N., 1974. Determination of REE, Ba, Fe, Mg, Na and K in carbonaceous and ordinary chondrites. Geochimica et Cosmochimica Acta 38, 757–775.

Nance, R.D., Gutiérrez-Alonso, G., Keppie, J.D., Linnemann, U., Murphy, J.B., Quesada, C., Strachan, R.A., Woodcock, N.H., 2010. Evolution of the Rheic Ocean. Gondwana Research 17, 194–222.

Nance, R.D., Murphy, J.B., 1994. Contrasting basement isotopic signatures and the palinspastic restoration of peripheral orogens: Example from the Neoproterozoic Avalonian-Cadomian belt. Geology 22, 617.

Nance, R.D., Murphy, J.B., 1996. Basement isotopic signatures and Neoproterozoic paleogeography of Avalonian-Cadomian and related terranes in the Circum-North Atlantic. Geological Society of America Special Papers 304, 333–346.

Nance, R.D., Murphy, J.B., Keppie, J.D., 2002. A Cordilleran model for the evolution of Avalonia.

Tectonophysics 352, 11–31.

Nance, R.D., Murphy, J.B., Strachan, R.A., Keppie, J.D., Gutiérrez-Alonso, G., Fernández-Suárez, J., Quesada, C., Linnemann, U., D'lemos, R., Pisarevsky, S.A., 2008. Neoproterozoic-early Palaeozoic tectonostratigraphy and palaeogeography of the peri-Gondwanan terranes: Amazonian v. West African connections. Geological Society, London, Special Publications 297, 345–383.

Nenova, P., Marinova, I., 2007. New data on serpentinized ultramafic body near Kamena village, Belasitsa Mountain, Serbo-Macedonian Massif, SW Bulgaria. Annual report No. 13 of the Central Laboratory of Mineralogy and Crystallography "Acad. Ivan Kostov," Sofia.

Nenova, P., Zidarov, N., 2008. Eclogites from Maleshevska Mountain, SW Bulgaria. Annual report No. 14 of the Central Laboratory of Mineralogy and Crystallography "Acad. Ivan Kostov," Sofia.

Neubauer, F., 2002. Evolution of late Neoproterozoic to early Paleozoic tectonic elements in Central and Southeast European Alpine mountain belts: review and synthesis. Tectonophysics 352, 87–103.

Pantić, N., Dimitrijević, M.D., Hercegovac, M., 1967. Mikrofloristički podaci o starosti Vlasinskog kompleksa. Zapisnici Srpskog geološkog društva za 1966. godinu.

Pavić, A., Menković, L., Koščal, M., 1983. Tumač za list Uroševac, Osnovna Geološka Karta 1:100000. Savezni Geološki Zavod, Belgrade.

Pavlović, P., 1962. O nekim ordovicijskim inartikulatnim brahiopodima u metamorfnim stenama kod Bosiljgrada (Jugoistočna Srbija) i o značaju ovog nalaska. Geološki anali Balkanskoga poluostrva 39, 99–112.

Pavlović, P., 1977. O "Gornjem (Vlasinskom) kompleksu" i podeli metamorfnih stena Srpsko-Makedonskog metamorfnog terena. Zapisnici Srpskog geološkog društva za 1975. i 1976. godinu, 123–132.

Pearce, J.A., Harris, N.B.W., Tindle, A.G., 1984. Trace Element Discrimination Diagrams for the Tectonic Interpretation of Granitic Rocks. Journal of Petrology 25, 956–983.

Pe-Piper, G., 1998. The nature of Triassic extension-related magmatism in Greece; evidence from Nd and Pb isotope geochemistry. Geological Magazine 135, 331–348.

Pereira, M.F., Linnemann, U., Hofmann, M., Chichorro, M., Solá, A.R., Medina, J., Silva, J.B., 2012a. The provenance of Late Ediacaran and Early Ordovician siliciclastic rocks in the Southwest Central Iberian Zone: Constraints from detrital zircon data on northern Gondwana margin evolution during the late Neoproterozoic. Precambrian Research 192–195, 166–189.

Pereira, M.F., Solá, A.R., Chichorro, M., Lopes, L., Gerdes, A., Silva, J.B., 2012b. North-Gondwana assembly, break-up and paleogeography: U–Pb isotope evidence from detrital and igneous zircons of Ediacaran and Cambrian rocks of SW Iberia. Gondwana Research 22, 866–881.

Petković, V., 1930. O tektonskom sklopu istočne Srbije. Glas Srpske kraljevske akademije, drugi razred 140, 151–188.

Petrović, B., Dimitrijević, M.D., Karamata, S., 1973. Tumač za list Vlasotince, Osnovna Geološka Karta 1:100000. Savezni Geološki Zavod, Belgrade.

Petrović, B., S., 1969. The Structure of the Vlasina Crystalline Complex in the Broad Area of Crna Trava. Belgrade.

Petrović, B., S., Karamata, S., 1965. Metaklastiti - baza gornjeg kompleksa kristalastih škriljaca SMM, in: Proceedings. Presented at the 7th Congress of the Geologists of Yugoslavia, Zagreb.

Peytcheva, I., von Quadt, A., Dyulgerov, M., Nedyalkov, R., 2009a. Au-Ag±W Mineralization

Related to the Collisional Granitoids of the Composite Lutzkan Magmatic Complex, Bulgaria. Geochimica et Cosmochimica Acta 73, 1023.

Peytcheva, I., von Quadt, A., Ovtcharova, M., Handler, R., Neubauer, F., Salnikova, E., Kostitsyn, Y., Sarov, S., Kolcheva, K., 2004. Metagranitoids from the eastern part of the Central Rhodopean Dome (Bulgaria): U–Pb, Rb–Sr and 40Ar/39Ar timing of emplacement and exhumation and isotope-geochemical features. Mineralogy and Petrology 82, 1–31.

Peytcheva, I., von Quadt, A., Tarassov, M., Zidarov, N., Tarassova, E., Andreichev, V., 2009b. Timing of Igralishte pluton in Ograzhden Mountain, SW Bulgaria: implications for the tectono-magmatic evolution of the region. Geologica Balcanica 38, 5–14.

Peytcheva, I., von Quadt, A., Titorenkova, R., Zidarov, N., Tarassova, E., 2005. Skrut Granitoids from Belassitsa Mountain, SW Bulgaria: Constraints from isotope geochronological and geochemical zircon data, in: Proceedings. Presented at the Bulgarian Geological Society 80th Anniversary, Bulgarian Geological Society, Sofia, pp. 205–208.

Plissart, G., 2012. La chaîne varisque dans les Carpates Méridionales et les Balkans Occidentaux: études pétrostructurales des massifs d'Almăj (Roumanie), de Deli Jovan (Serbie) et de la Stara Planina Occidentale (Bulgarie) (PhD). Université Libre de Bruxelles & Université de La Nantes, Brussels.

Popović, R., 1991. Srpsko-Makedonska masa ili Pelagonsko-Rodopski i Moravski masiv. Radovi Geoinstituta 25, 7–20.

Pupin, J.P., 1980. Zircon and granite petrology. Contributions to Mineralogy & Petrology 73, 207–220.

Rakićević, T., Dumurdžanov, N., Petkovski, P., 1976. Tolkuvač za listot Štip, Osnovna Geološka Karta 1:100000. Savezni Geološki Zavod, Belgrade.

Rakićević, T., Kovačević, M., Radović, N., Pendžerkovski, J., 1973. Tolkuvač za listot Strumica, Osnovna Geološka Karta 1:100000. Savezni Geološki Zavod, Belgrade.

Ricou, L.-E., Burg, J.-P., Godfriaux, I., Ivanov, Z., 1998. Rhodope and Vardar: the metamorphic and the olistostromic paired belts related to the Cretaceous subduction under Europe. Geodinamica Acta 11, 285–309.

Robertson, A.H.F., Karamata, S., 1994. The role of subduction-accretion processes in the tectonic evolution of the Mesozoic Tethys in Serbia. Tectonophysics 234, 73–94.

Robertson, A., Karamata, S., Šarić, K., 2009. Overview of ophiolites and related units in the Late Palaeozoic–Early Cenozoic magmatic and tectonic development of Tethys in the northern part of the Balkan region. Lithos 108, 1–36.

Schenker, F.L., Burg, J.-P., Kostopoulos, D., Moulas, E., Larionov, A., von Quadt, A., 2014. From Mesoproterozoic magmatism to collisional Cretaceous anatexis: Tectono-magmatic history of the Pelagonian Zone, Greece. Tectonics 2014TC003563.

Schmid, S.M., 2014. A compilation of tectonic units of the Alpine collision zone between Alps and Western Turkey. Presented at the XX Congress of CBGA. Tirana.

Schmid, S.M., Bernoulli, D., Fügenschuh, B., Matenco, L., Schefer, S., Schuster, R., Tischler, M., Ustaszewski, K., 2008. The Alpine-Carpathian-Dinaridic orogenic system: correlation and evolution of tectonic units. Swiss Journal of Geosciences 101, 139–183.

Shand, S.J., 1943. Eruptive rocks: Their genesis, composition, and classification, with a chapter on meteorites. J. Wiley & sons, Incorporated.

Sircombe, K.N., 2004. AgeDisplay: an EXCEL workbook to evaluate and display univariate geochronological data using binned frequency histograms and probability density distributions. Computers & Geosciences 30, 21–31.

Šoptrajanova, G., 1967. Petrološke i geohronološke karakteristike nekih granitoida Makedonije. University of Belgrade, Belgrade.

Spassov, C., 1973. Stratigraphie des Devons in Sudwest-Bulgarien. Bulletin of the Geological Institute, Stratigraphy and Lithology 22, 5–38.

Spray, J.G., Bébien, J., Rex, D.C., Roddick, J.C., 1984. Age constraints on the igneous and metamorphic evolution of the Hellenic-Dinaric ophiolites. Geological Society, London, Special Publications 17, 619–627.

Stacey, J.S., Hedge, C.E., 1984. Geochronologic and isotopic evidence for early Proterozoic crust in the eastern Arabian Shield. Geology 12, 310–313.

Stampfli, G.M., Hochard, C., Vérard, C., Wilhem, C., von Raumer, J.F., 2013. The formation of Pangea. Tectonophysics 593, 1–19.

Stampfli, G.M., von Raumer, J.F., Borel, G.D., 2002. Paleozoic evolution of pre-Variscan terranes: From Gondwana to the Variscan collision. Geological Society of America Special Papers 364, 263–280.

Stephanov, A., Dimitrov, Z., 1936. Geologische Untersuchungen im Kustendiler Gebiet. Review of the Bulgarian Geological Society 8, 1–28.

Tarassov, M., Tarassova, E., von Quadt, A., 2007. Electron microprobe dating of allanite from the Skrat granitoids (Annual No. 13).

Turpaud, P., Reischmann, T., 2010. Characterisation of igneous terranes by zircon dating: implications for UHP occurrences and suture identification in the Central Rhodope, northern Greece. International Journal of Earth Sciences 99, 567–591.

Ustaömer, P.A., Mundil, R., Renne, P.R., 2005. U/Pb and Pb/Pb zircon ages for arc-related intrusions of the Bolu Massif (W Pontides, NW Turkey): evidence for Late Precambrian (Cadomian) age. Terra Nova 17, 215–223.

Ustaömer, P.A., Ustaömer, T., Gerdes, A., Zulauf, G., 2011. Detrital zircon ages from a Lower Ordovician quartzite of the İstanbul exotic terrane (NW Turkey): evidence for Amazonian affinity. International Journal of Earth Sciences 100, 23–41.

Van Hinsbergen, D.J.J., Schmid, S.M., 2012. Map view restoration of Aegean–West Anatolian accretion and extension since the Eocene. Tectonics 31, TC5005.

Vasković, N., 1998. P-T condition of the mica schists from the Vranjska Banja Series, in: Proceedings of the XIII Congress of the Geologists of Yugoslavia, Herceg Novi, pp. 41–59.

Vasković, N., 2002. Petrology and P-T condition of white mica-chlorite schists from Vlasina series - Surdulica, SE Serbia. Geološki anali Balkanskoga poluostrva 199–220.

Vasković, N., Belousova, E.A., O'Reilly, S.Y., Griffin, W.L., Srećković-Batoćanin, D., Christofides, G., Koroneos, A., 2012. New U-Pb dating and Hf-isotope composition of the Gornjane granitoids (South Carpathians, East Serbia), in: Acta Mineralogica-Petrographica. Presented at the MSCC+CEMC 2012, Department of Mineralogy, Geochemistry and Petrology, University of Szeged, Miskolc, p. 146.

Vasković, N., Matović, V., Srećković-Batoćanin, D., 2003. Petrology of Garnet-amphibolite with White Mica from Vranjska Banja Series (Serbian-Macedonian Massif, SE Serbia). Studia Universitatis Babeş-Bolyai, Studia Geologia 128–133.

Vasković, N., Tasić, Z., 1997. Geologija granodioritskog masiva Surdulice, Geološka karta SRJ 1:50.000. Savezno ministarstvo za privredu SRJ, Belgrade.

Vermeesch, P., 2012. On the visualisation of detrital age distributions. Chemical Geology 312–313, 190–194.

Von Raumer, J.F., Stampfli, G.M., Bussy, F., 2003. Gondwana-derived microcontinents — the constituents of the Variscan and Alpine collisional orogens. Tectonophysics 365, 7–22.

Vukanović, M., Dimitrijević, M.D., Dimitrijević, M., Karajičić, L., Rakić, M.., 1977. Tumač za list Vranje, Osnovna Geološka Karta 1:100000. Savezni Geološki Zavod, Belgrade.

Vukanović, M., Karajičić, L., Dimitrijević, M.D., Možina, A., Gagić, N., Jevremović, M., 1973.

Tumač za list Leskovac, Osnovna Geološka Karta 1:100000. Savezni Geološki Zavod, Belgrade.

Wood, D.A., 1980. The application of a ThHfTa diagram to problems of tectonomagmatic classification and to establishing the nature of crustal contamination of basaltic lavas of the British Tertiary Volcanic Province. Earth and Planetary Science Letters 11–30.

Wood, D.A., Joron, J.-L., Treuil, M., 1979. A re-appraisal of the use of trace elements to classify and discriminate between magma series erupted in different tectonic settings. Earth and Planetary Science Letters 45, 326–336.

Yilmaz Şahin, S., Aysal, N., Güngör, Y., Peytcheva, I., Neubauer, F., 2014. Geochemistry and U–Pb zircon geochronology of metagranites in Istranca (Strandja) Zone, NW Pontides, Turkey: Implications for the geodynamic evolution of Cadomian orogeny. Gondwana Research 26, 755–771.

Zagorčev, I.S., Bončeva, I., 1988. Indications of Devonian basic volcanism in Southwest Bulgaria. Geologica Balcanica 18, 55–63.

Zagorchev, I.S., 1981. Early Alpine deformations in the red beds within the Poletinci-Skrino fault zone. 2. Structure and deformations in the northern parts of the Vlahina block. Geologica Balcanica 11, 101–126.

Zagorchev, I.S., 1984a. Pre-Alpine structure of South-west Bulgaria, in: Zagorchev, I.S., Mankov, S., Bozkov, I. (Eds.), Problems of the Geology of Southwestern Bulgaria. Tehnika, Sofia, pp. 9–20.

Zagorchev, I.S., 1984b. The role of overthrusts in the Alpine structure of Krajistides. Geologica Balcanica 14, 37–64.

Zagorchev, I.S., 1985. Deformation during the first stage of the Alpine Orogeny in the Skrino-Poletintsi faulted zone; IV Shipochan Anticline. Review of the Bulgarian Geological Society 46, 287–298.

Zagorchev, I.S., Balica, C., Balintoni, I., Kozhoukharova, E., Dimitrescu, R., Sâbâu, G., Negulescu, E., 2011a. New Isotopic Data on the Metamorphic Rocks in SW Bulgaria, in: Proceedings of the 3rd International Symposium on the Geology of the Black Sea Region, GeoEcoMar, Bucharest, pp. 223–225.

Zagorchev, I.S., Balica, C., Balintoni, I., Kozhoukharova, E., Sâbâu, G., Dimitrescu, R., Negulescu, E., 2011b. New isotopic data on the Cadomian age of the Frolosh metamorphic complex and the Struma diorite complex, in: Proceedings. Presented at the National Conference with international participation Geosciences 2011, Bulgarian Geological Society, Sofia.

Zagorchev, I.S., Milovanović, D., 2006. Deformations and Metamorphism in the Eastern Parts of the Serbo-Macedonian Massif, in: Proceedings. Presented at the XVIII Congress of CBGA, Serbian Geological Society, Belgrade, pp. 670–673.

Zagorchev, I.S., Ruseva, M., 1982. Nappe structure of the southern parts of Osogovo Mts and the Pijanec region (SW Bulgaria). Geologica Balcanica 12, 35–57.

Zagortchev, I.S., 1993. Alpine evolution of the pre-Alpine amphibolite-facies basement in South Bulgaria. Mitteilungen der Österreichischen Geologischen Gesellschaft 86, 9–21.

Zeh, A., Brätz, H., Millar, I.L., Williams, I.S., 2001. A combined zircon SHRIMP and Sm–Nd isotope study of high-grade paragneisses from the Mid-German Crystalline Rise: evidence for northern Gondwanan and Grenvillian provenance. Journal of the Geological Society 158, 983–994.

Zhang, G., Guo, A., Wang, Y., Li, S., Dong, Y., Liu, S., He, D., Cheng, S., Lu, R., Yao, A., 2013. Tectonics of South China continent and its implications. Science China Earth Sciences 56, 1804–1828.

Zhang, S.-B., Zheng, Y.-F., 2013. Formation and evolution of Precambrian continental lithosphere in South China. Gondwana Research 23, 1241–1260.

Zidarov, N., Peytcheva, I., von Quadt, A., Andreichev, V., Macheva, L., Titorenkova, R., 2003a. Mineral-petrological, geochemical and isotope studies of geological units in Serbo-Macedonian Massif, SW Bulgaria. Annual report No. 9 of the Central Laboratory of Mineralogy and Crystallography "Acad. Ivan Kostov," Sofia.

Zidarov, N., Peytcheva, I., von Quadt, A., Andreichev, V., Macheva, L., Titorenkova, R., 2003b. Timing and Magma Sources of Metagranites from the Serbo-Macedonian Massif (Ograzhden and Maleshavska Mountains, SW Bulgaria): Constraints from UPb and Hf-Zircon and Sr Whole Rock Isotope Studies, in: Proceedings. Presented at the Bulgarian Geological Society Annual Scientific Conference "Geology 2003," Bulgarian Geological Society, Sofia, pp. 89–91.

Zidarov, N., Peytcheva, I., von Quadt, A., Tarassova, E., Andreichev, V., 2004. Timing and Magma Sources of Igralishte Pluton (SW Bulgaria): Preliminary Isotope-Geochronological and Geochemical Data, in: Proceedings. Presented at the Bulgarian Geological Society Annual Scientific Conference "Geology 2004," Bulgarian Geological Society, Sofia.

Zidarov, N., Tarassova, E., Peytcheva, I., von Quadt, A., Andreichev, V., Titorenkova, R., 2007. Petrology, geochemistry and age dating of Skrut granitoids – new evidence for Early Triassic magmatism in Belasitsa Mountain (SW Bulgaria). Geologica Balcanica 36, 17–29.

Zlatkin, O., Avigad, D., Gerdes, A., 2013. Evolution and provenance of Neoproterozoic basement and Lower Paleozoic siliciclastic cover of the Menderes Massif (western Taurides): Coupled U–Pb–Hf zircon isotope geochemistry. Gondwana Research 23, 682–700.

Zlatkin, O., Avigad, D., Gerdes, A., 2014. Peri-Amazonian provenance of the Proto-Pelagonian basement (Greece), from zircon U–Pb geochronology and Lu–Hf isotopic geochemistry. Lithos 184–187, 379–392.

Zulauf, G., Dörr, W., Fisher-Spurlock, S.C., Gerdes, A., Chatzaras, V., Xypolias, P., 2015. Closure of the Paleotethys in the External Hellenides: Constraints from U–Pb ages of magmatic and detrital zircons (Crete). Gondwana Research 28, 642–667.

Zulauf, G., Romano, S.S., Dörr, W., Fiala, J., 2007. Crete and the Minoan terranes: Age constraints from U-Pb dating of detrital zircons. Geological Society of America Special Papers 423, 401–411.

Appendices to
Chapter 2: Pre-Alpine evolution of a segment of the North-Gondwanan margin: Geochronological and geochemical evidence from the central Serbo-Macedonian Massif

Milorad Antić[a]*, Irena Peytcheva[bc], Albrecht von Quadt[c], Alexandre Kounov[a], Branislav Trivić[d], Todor Serafimovski[e], Goran Tasev[e], Ianko Gerdjikov[f], Andreas Wetzel[a]

[a]Institute for Geology and Palaeontology, Basel University, 4056 Basel, Switzerland;
[b]Geological Institute, Bulgarian Academy of Sciences, 1113 Sofia, Bulgaria
[c]Institute of Geochemistry and Petrology, ETH-Zürich, 8092 Zürich, Switzerland
[d]Faculty of Mining and Geology, University of Belgrade, 11000 Belgrade, Serbia
[e]Faculty of Natural and Technical Sciences, University "Goce Delčev", 2000 Štip, Republic of Macedonia
[f]Faculty of Geology and Geography, University "St. Kl. Ohridski", 1504 Sofia, Bulgaria

Contents

Appendix 2-1

Results of the main and trace elements measurements

Appendix 2-1 Results of the main and trace elements measurements

sample	SM01	SM02	SM140-1	SM173-1	SM173-2	SM173-3
unit	LC	LC	SDC	LC	LC	LC
location	Ovča Strana	Kukavica	Delčevo	Vinica	Vinica	Vinica
rock type	Mylonite	Granodiorite	Granite	Amp schist	Two-mica gneiss	Leucocratic dyke
SiO_2	72,3	67,5	73	55,3	59,6	71,9
TiO_2	0,354	0,608	0,342	1,23	1,21	0,238
Al_2O_3	13,6	15,6	13,9	17,1	14,8	14,4
Fe_2O_3 (total)	2,82	3,68	2,44	10,6	8,19	2,96
MnO	0,034	0,084	0,047	0,135	0,123	0,04
MgO	0,618	0,959	0,465	3,02	1,25	1,11
CaO	0,735	3,15	0,625	5,42	5,58	2,07
Na_2O	2,77	4,37	3,99	3,98	4,17	1,42
K_2O	4,77	2,11	4,21	0,913	1,48	3,17
P_2O_5	0,135	0,203	0,089	0,217	1,7	0,047
LOI	1,15	1,27	1,14	1,82	0,99	2,13
Total	99,3	99,6	100	99,7	99,1	99,5
Ba	564	1228	1186	564	1067	1379
Rb	223	53,6	110	24,6	41	80,5
Sr	76,7	297	89,8	370	334	243
Zr	161	368	359	147	269	286
Nb	10,7	12,4	14	4,99	9,69	7,48
Ni	n/a	n/a	n/a	4,64	4,74	1,15
Co	4,21	4,97	2,83	28,2	9,03	2,35
Zn	37,3	50,6	23,7	85,1	59,2	38,2
Cr	25,6	18,1	9,47	17,5	n/a	n/a
La	17,3	37,5	38,6	20,9	31,4	38,4
Ce	47,1	81,1	113	42,9	66,5	81,9
Pr	4,59	10,1	8,95	5,92	8,78	8,85
Nd	17	45,5	31,9	25,6	37,5	33,5
Sm	3,93	9,44	4,96	6,35	8,21	7,16
Eu	0,379	2,47	0,951	1,83	2,44	1,01
Gd	3,04	8,88	6,29	6,13	7,39	6,34
Tb	0,522	1,39	0,69	0,931	1,14	0,935
Dy	3,73	7,96	6,1	5,59	6,89	6,18
Ho	0,669	1,55	1,28	1,15	1,37	1,3
Er	2,85	4,82	3,86	3,46	4,37	4,24
Tm	0,288	0,562	0,511	0,47	0,61	0,673
Yb	2,22	4,92	5,09	2,93	4,43	4,37
Lu	0,348	0,588	0,609	0,425	0,647	0,738
Y	19	42,3	34,5	29,7	40,4	38,7
Cs	8,94	2,2	6,75	0,911	2,36	2,3
Ta	0,933	0,594	0,943	0,377	0,497	0,528
Hf	4,76	9,55	9,55	3,6	6,47	8,05
Be	3,75	4,02	3,27	1,74	1,92	2,68
Sc	6,23	13	6,39	24,4	19,6	7,93
V	35,2	41,2	15,8	155	103	25,5
Cu	3,11	2,75	3	13,9	1,05	3,07
Ga	16,4	18,8	17,7	19,1	17,1	17,6
As	n/a	n/a	1,74	0,988	8,52	1,12
Mo	0,813	0,682	0,624	1,67	0,666	n/a
Sn	4,38	1,62	1,41	2,25	1,92	3,87
Sb	n/a	n/a	n/a	0,512	0,951	n/a
W	3	0,394	0,868	0,229	0,947	0,945
Tl	0,625	0,187	0,572	0,075	0,194	0,352
Pb	20,5	11,8	13,4	6,14	7,92	11,2
Bi	0,136	n/a	n/a	n/a	0,09	0,164
Th	15,4	7,74	14,2	3,35	5,73	16,1
U	6,31	2,37	2,99	1,94	18,8	7

Appendix 2-1 Results of the main and trace elements measurements

sample	SM178-1	SM184-1	SM195-1	SM199-1	SM231-1	SM236-1
unit	Vlasina	LC	Veles	LC	LC	COL
location	Mitrašinci	Maleševski Mts.	Štip	Borovac	Donja Ljubata	Bosilegrad
rock type	Ep Chl Amp schists	Two-mica gneiss	Bt granite	Granite	Gabbro	Monzonite
SiO_2	42,7	72,3	69,1	73,8	47,8	57,4
TiO_2	1,69	0,185	0,495	0,291	0,664	0,848
Al_2O_3	17	16,1	14,6	13,4	18,2	19,6
Fe_2O_3 (total)	10,2	1,28	3,84	2,38	7,18	5,44
MnO	0,232	0,018	0,07	0,04	0,104	0,094
MgO	6,47	0,37	1,82	0,798	9,29	2,09
CaO	7,34	3,35	1,44	1,32	8,27	4,22
Na_2O	3,11	5,11	2,95	3,35	2,71	5,27
K_2O	1,85	0,728	3,95	3,78	0,8	1,93
P_2O_5	0,212	0,076	0,177	0,197	0,067	0,344
LOI	8,51	0,807	1,31	0,825	4,96	3,02
Total	99,4	100	99,7	100	100	100
Ba	398	133	650	694	195	997
Rb	56,6	14	127	127	23,1	56,5
Sr	86,8	395	195	186	472	508
Zr	108	113	159	147	34,9	508
Nb	6,85	2,58	13	5,46	1,54	6,89
Ni	46,9	n/a	9,93	n/a	42,7	4,07
Co	32,3	5,8	8,23	5,21	32,4	12,4
Zn	39,7	17,5	54,6	19,9	37,1	51,3
Cr	227	18,6	24,6	24,4	118	9,89
La	9,46	12,8	33,7	17,6	4,12	16,3
Ce	22,5	23,7	71,1	36,7	9,37	29,9
Pr	3,04	2,82	7,43	4,27	1,18	3,02
Nd	15,5	9,51	29,3	16,2	5,29	11,9
Sm	4,23	3,68	6,14	3,73	0,98	2,03
Eu	1,38	0,533	0,985	0,407	0,99	1,36
Gd	4,69	3,99	4,63	3,19	1,47	2,03
Tb	0,735	0,11	0,712	0,434	0,255	0,289
Dy	4,71	3,7	4,16	3,6	1,5	1,8
Ho	1,02	0,688	0,851	0,699	0,28	0,319
Er	2,53	2,52	2,15	2,28	0,746	1,04
Tm	0,36	0,371	0,297	0,275	0,079	0,153
Yb	2,21	2,99	2,09	3,23	0,604	1,59
Lu	0,337	0,406	0,37	0,434	0,103	0,276
Y	25,1	5	20,2	19,4	7,38	9,49
Cs	0,708	0,441	4,27	3,58	2,82	1,98
Ta	0,437	0,445	1,32	0,422	0,888	0,404
Hf	2,53	2,4	4,18	4,21	0,161	11,5
Be	2,17	2,06	4,27	n/a	n/a	2,14
Sc	32,4	2,26	9,68	5,81	14,5	6,27
V	257	37,9	61,2	30,8	89,3	51,2
Cu	73	9,83	12,3	11,7	3,95	33,6
Ga	20,8	15,5	18,3	12,6	11,5	18,5
As	2,23	n/a	3,82	n/a	6,56	1,22
Mo	0,993	1,02	1,17	0,945	0,857	0,46
Sn	1,21	3,84	3,94	1,78	2,67	n/a
Sb	0,344	n/a	n/a	n/a	0,22	n/a
W	1,15	0,726	2,5	n/a	0,501	0,62
Tl	0,196	0,456	0,469	0,51	0,152	0,805
Pb	1,32	3,42	20,7	15,7	3,16	6,66
Bi	n/a	n/a	0,144	n/a	0,116	0,107
Th	0,796	2,62	13,5	10,1	0,578	3,36
U	0,195	0,968	4,9	4,58	0,347	3,08

Appendix 2-1 Results of the main and trace elements measurements

sample	SM250-1	SM250-2	SM270-3	SM272-1	SM315	SM352
unit	LC	LC	Vlasina	Vlasina	Veles	Vlasina
location	Golemo Selo	Golemo Selo	Dobro Polje	Božica	Bukovac	Lisina
rock type	Amphibolite	Para-gneiss	Diabase	Granite	Ortho-gneiss	Gabbro
SiO_2	50,4	72,6	51,4	77,4	75,5	47,5
TiO_2	1,53	0,618	1,56	0,206	0,176	2,98
Al_2O_3	13,8	12,1	14,1	12,4	12,3	15,3
Fe_2O_3 (total)	10,8	4,21	11,2	1,24	1,21	9,56
MnO	0,171	0,049	0,179	0,046	0,007	0,169
MgO	7,42	1,73	6,26	0,308	0,281	3,59
CaO	11,6	1,58	9,33	0,681	0,124	10,1
Na_2O	2,4	3,04	4,03	5,62	3,36	1,8
K_2O	0,547	1,92	0,063	0,996	4,34	1,19
P_2O_5	0,165	0,141	0,154	0,05	0,013	0,17
LOI	1,16	0,886	1,99	0,643	0,773	7,35
Total	100	98,9	100	99,6	98,1	99,7
Ba	130	616	46,9	433	624	646
Rb	8,15	63,2	0,334	27,8	104	31
Sr	481	209	206	159	39,6	358
Zr	86,6	221	106	169	100	30,3
Nb	9,42	12,8	4,75	8,77	3,73	11,2
Ni	89,1	6,94	26,4	n/a	n/a	12
Co	41,3	7,1	37,1	1,17	0,366	21,7
Zn	78,9	31,3	67,2	17,1	5,32	104
Cr	255	85,6	129	12,6	14	n/a
La	9,01	14,4	7,62	25,3	18,9	10,4
Ce	22,5	31,4	19,4	57,1	42,2	24,9
Pr	2,92	3,44	2,83	7,08	4,76	3,44
Nd	13,6	12,5	14	27,3	17,7	15,9
Sm	3,6	2,79	4,07	5,19	4,23	3,95
Eu	1,34	0,842	1,62	0,745	0,405	1,84
Gd	4,47	2,86	5,86	4,74	3,06	3,88
Tb	0,691	0,417	0,964	0,645	0,438	0,514
Dy	4,19	2,97	5,91	3,59	2,95	3,04
Ho	0,789	0,73	1,15	0,574	0,443	0,514
Er	2,54	2,38	3,22	2,05	1,37	1,4
Tm	0,374	0,325	0,524	0,268	0,354	0,207
Yb	2,06	2,08	2,95	4,01	1,58	1,49
Lu	0,3	0,322	0,458	0,481	0,305	0,204
Y	22	17,6	30,4	21,5	12,4	15,3
Cs	0,701	2,24	0,172	0,576	1,51	2,17
Ta	0,642	0,785	0,373	0,76	0,437	0,625
Hf	2,13	5,47	2,95	5,18	4,31	1,03
Be	1,9	2,32	1,1	2,57	7,64	1,66
Sc	36,8	12	44	2,39	3,68	33
V	296	84	303	7,64	11,3	120
Cu	29,2	34	17,1	2,22	1,12	1,41
Ga	16,8	13,7	16,4	13,8	11	18,7
As	2,73	2,44	9,05	n/a	n/a	3,12
Mo	1,33	0,814	0,303	1,09	0,705	0,721
Sn	2,21	n/a	1,03	n/a	1,91	n/a
Sb	n/a	n/a	0,517	n/a	n/a	0,325
W	2,08	1,46	0,309	n/a	2,15	1,28
Tl	n/a	0,089	n/a	0,42	0,323	0,474
Pb	11,4	13,1	2,25	4,98	6,55	4,82
Bi	0,326	n/a	0,068	n/a	n/a	n/a
Th	1,13	10,2	0,752	11,7	11,3	1,17
U	0,537	2	0,34	1,97	2,32	0,627

sample	SM377-1	SM377-2	SM493-1	SM502-1	SM505-1	SM529-2
unit	LC	LC	Vlasina	Vlasina	Vlasina	LC
location	Spančevac	Spančevac	Toplodolska Reka	Veljkovci	Gornja Lopušnja	Šumanska Reka
rock type	w.d. granite	Metagranite	Diorite	Komatiite	Ab gneiss	Amphibolite
SiO_2	75,8	60,1	61,7	30	69,3	49
TiO_2	0,146	0,563	0,871	0,987	0,62	1,64
Al_2O_3	13,9	19,1	15,6	16,7	15	13,8
Fe_2O_3 (total)	1,25	5,37	7,17	11,2	5,85	13,7
MnO	0,028	0,113	0,216	0,098	0,076	0,217
MgO	0,421	0,985	2,4	29,3	1,9	6,93
CaO	1,37	2,4	4,87	0,127	0,167	11,3
Na_2O	4,53	3,95	4,44	0	0,575	2,18
K_2O	1,95	4,64	1,28	0,004	3,63	0,379
P_2O_5	0,054	0,24	0,166	0,06	0,12	0,149
LOI	0,831	2,42	1,46	11,6	2,98	0,764
Total	100	99,9	100	100	100	100
Ba	503	2612	696	20	599	115
Rb	50,1	105	28,1	0,15	120	5,13
Sr	307	584	363	10,3	28,2	180
Zr	110	494	184	34,4	138	76,2
Nb	6,73	23	9,39	0,224	11,1	8,77
Ni	n/a	n/a	n/a	549	23	42,8
Co	2,38	6,12	12,9	69,4	11,6	35,7
Zn	43,1	48,2	72,7	48	60,5	69,3
Cr	n/a	13,2	14,1	756	41	133
La	27,5	31,5	19,7	0,635	24,3	6,5
Ce	56	61	48,2	0,808	53,4	15,6
Pr	6,59	7,59	7,07	0,25	5,81	2,18
Nd	25,3	29,8	36,1	1,27	23,1	11,3
Sm	5,15	5,45	8,45	0,681	4,59	3,31
Eu	1,25	2,14	2,3	0,085	0,947	1,08
Gd	4,57	4,97	8,96	1,83	4,29	3,85
Tb	0,529	0,6	1,39	0,423	0,701	0,568
Dy	2,71	3,53	8,67	2,57	4,04	4,24
Ho	0,527	0,624	1,73	0,594	0,918	0,801
Er	1,12	2,11	5,56	1,69	2,61	2,65
Tm	0,233	0,243	0,705	0,295	0,442	0,344
Yb	0,903	2,55	5,39	1,84	2,42	2,46
Lu	n/a	0,273	0,648	0,275	0,379	0,307
Y	13,6	16,4	45,6	14	23,8	21,8
Cs	1,58	7,83	1,07	0,083	5,76	0,122
Ta	0,976	0,777	0,437	0,098	0,833	0,487
Hf	3,09	10,5	4,45	1,01	4,02	1,97
Be	7,85	n/a	n/a	n/a	5,13	3,31
Sc	4,14	14,5	22,6	36,8	15	33,7
V	14,4	45,1	142	206	90,6	286
Cu	n/a	7,81	8,67	5,5	27,7	55,1
Ga	24,9	18,7	17,9	9,6	16,6	12,2
As	n/a	1,92	2,34	4,17	1,59	0,993
Mo	n/a	0,769	n/a	n/a	n/a	0,881
Sn	n/a	n/a	n/a	n/a	2,14	1,3
Sb	n/a	n/a	n/a	1,17	0,934	0,08
W	n/a	n/a	0,403	0,511	1,17	0,442
Tl	0,244	0,478	0,23	n/a	0,827	0,135
Pb	7,69	10,1	7,6	0,948	10	3,38
Bi	n/a	0,078	0,121	n/a	0,149	0,04
Th	5,15	5	1,93	0,061	8,58	0,608
U	3,11	1,69	0,614	0,055	2,74	0,211

Appendix 2-1 Results of the main and trace elements measurements

sample	SM538-1	SM541-1	SM549-1	SM559-1	SM560-1	SM562-1
unit	LC	LC	LC	LC	LC	LC
location	Popovce	Sijarina	Mala Oraovica	Muratovica	Brestovac	Dobra Voda
rock type	Metagabbro	Amphibolite	Metagabbro	Granite	Metagabbro	Amphibolite
SiO_2	46,5	49,5	48,2	73,4	50,5	54,8
TiO_2	1,82	1,02	2,08	0,276	1,31	2,62
Al_2O_3	15,9	8,02	14,3	14	15,7	13,2
Fe_2O_3 (total)	13	10,6	14,1	1,92	10,5	14,1
MnO	0,189	0,184	0,209	0,017	0,171	0,26
MgO	7,16	16,7	3,72	0,306	7,62	2,75
CaO	10,6	12,2	14,3	0,44	10,6	7,47
Na_2O	1,76	0,698	1,19	4,44	2,45	2,04
K_2O	0,563	0,17	0,25	4,81	0,307	0,859
P_2O_5	0,144	0,105	0,174	0,067	0,199	0,407
LOI	2,42	0,97	1,87	0,656	0,978	1,57
Total	100	100	100	100	100	100
Ba	190	12,2	126	1020	367	237
Rb	9,71	1,55	7,26	91,2	1,05	18
Sr	821	81,5	845	88,8	294	77,5
Zr	98,4	62,5	86,7	330	39,6	256
Nb	9,85	11,6	2,12	11,3	9,32	11,6
Ni	55,2	472	16,3	n/a	9,8	n/a
Co	46,4	64,6	43,8	1,6	33,8	18,9
Zn	72,9	67,3	49,8	15,2	58,7	103
Cr	262	1353	21,9	20,9	293	21,2
La	10,2	10,6	7,08	48,9	19,1	18,6
Ce	23,6	22,3	19	99,8	45,8	46,2
Pr	3,35	2,75	2,8	10,8	6,57	6,53
Nd	15,7	11,9	13,9	38,2	31,7	32,1
Sm	4,08	2,85	4,11	6,77	7,53	8,76
Eu	1,45	0,98	1,46	0,542	1,34	2,73
Gd	5,31	2,89	4,63	4,66	8,67	10,3
Tb	0,707	0,31	0,738	0,58	1,27	1,66
Dy	5,48	2,54	4,49	3,84	7,82	10,9
Ho	1,02	0,373	0,902	0,692	1,49	2,21
Er	2,98	1,24	2,67	2,64	4,42	7,3
Tm	0,324	0,194	0,378	0,371	0,566	0,947
Yb	3,06	0,907	2,45	2,61	4,53	6,46
Lu	0,338	0,077	0,317	0,406	0,514	0,886
Y	25,6	11	23,3	19,2	37,8	61
Cs	0,548	1,09	1,05	2,5	0,417	0,586
Ta	0,635	0,56	0,224	0,639	0,449	0,642
Hf	2,67	1,25	2,11	8,5	1,52	6,33
Be	n/a	4,15	3,34	6,7	n/a	2,93
Sc	43,6	37,1	39,9	5,2	43,4	36,4
V	333	172	544	18,7	262	329
Cu	111	13,1	44,4	2,52	17,4	18,8
Ga	17,2	10,9	23,1	21,1	15,3	21,3
As	1,92	3,76	4,27	n/a	3,53	3,14
Mo	n/a	0,498	0,798	1,71	1,06	1,03
Sn	n/a	2,57	n/a	1,52	n/a	2,1
Sb	n/a	n/a	0,814	0,27	n/a	1,09
W	n/a	1,05	0,953	0,733	0,459	1,72
Tl	n/a	n/a	n/a	0,247	n/a	0,201
Pb	10	2,23	19,2	11,6	5,99	0,884
Bi	0,309	0,318	0,122	n/a	n/a	0,129
Th	1,06	1,2	0,837	12,7	0,308	2,37
U	0,482	0,293	0,341	1,94	n/a	1,36

Major element oxides in wt%, trace elements in ppm.

Abbreviations: LOI – loss on ignition, n/a – bellow detection limit, LC – Lower complex, SDC – Struma Diorite complex, COL – Crnook-Osogovo-Lisets complex, w.d. granite – weakly deformed granite. Minerals abbreviated after Whitney and Evans (2010).

References

Whitney, D.L., Evans, B.W., 2010. Abbreviations for names of rock-forming minerals. American Mineralogist 95, 185–187. doi:10.2138/am.2010.3371

Appendix 2-2

LA-ICP-MS instrumentation and operational setting

Appendix 2-2 LA-ICP-MS instrumentation and operational setting

Year of measurement	2010	2013
Laser ablation system		
Make, model & type	Prototype similar to Geolas (Coherent)	Resonetics Resolution 155
Ablation cell & volume	Homemade, rhombic shape, ca. 7 cm3	Laurin Technics 155, constant geometry, aerosol dispersion volume < 1 cm3
Laser wavelength	193 nm	
Pulse width	25 ns	
Fluence [J/cm2]	4	2
Repetition rate [Hz]	10	5
Spot size [µm]	40	30
Sampling mode/Pattern	Single hole drilling	Single hole drilling, 5 cleaning pulses
Carrier gas	100% He	100% He, Ar make-up gas combined inside ablation cell funnel
Ablation duration [s]	50	40
Cell carrier gas flow [l/min]	1,1	0,7
ICP-MS instrument		
Make, model & type	Elan 6100 DRC Q-ICP-MS	Thermo Element XR SF-ICP-MS
Sample introduction	Ablation aerosol only, squid aerosol homogenization device	
RF power [W]	1450	1500
Make-up gas flow	0.8 l/min Ar	0.95 l/min Ar
Detection system	Single detector dual mode SEM, analog	Single detector triple mode SEM, analog, Faraday
Masses measured	202, 204, 206, 207, 208, 232, 235, 238	
Integration time per peak	10 ms (masses 202, 204, 208, 232), 20 ms (masses 235, 238), and 30 ms (masses 206, 207)	12 ms (masses 202, 204), 20 ms (masses 208, 232, 235, 238), and 40 ms (masses 206, 207)
Total integration time per reading [s]	0,14	0,202
IC dead time [ns]	30	8
Data Processing		
Gas blank	40 sec prior to each ablation spot	10 sec prior to each ablation spot
Calibration strategy	GJ-1 used as primary reference material, Plešovice, 91500 & Temora used as secondaries for quality control	
Reference material	91500 (Wiedenbeck et al., 1995) Plešovice (Sláma et al., 2008) GJ1 ^{206}Pb/^{238}U 602.3 ± 1 Ma, ^{207}Pb/^{206}Pb 609.2 ± 0.7 Ma (in-house TIMS, unpublished)	
Data processing software /correction for LIEF	Iolite 2.5 with VizualAge	
Mass discrimination	Mass bias correction for all ratios normalized to primary reference material	
Common-Pb correction, composition and uncertainty	Common-Pb correction not performed	
Uncertainty level and propagation	Ages are given at 2 sigma absolute, propagation is by quadratic addition. Reproducibility of reference material uncertainty is propagated	
Th disequilibrium correction and error propagation	^{206}Pb/^{238}U ages of all samples were corrected using equation of Schärer (1984) or Sakata et al (2013). All errors from ^{206}Pb/^{238}U ratios and ages are propagated.	

Appendix 2-3

Description of samples and results of U–Pb measurements

2-3-1 The Lower Complex

2-3-1.1 Vlajna granitoid (SM02)

Vlajna granitoid is located west of the Vrvi Kobila shear zone (Fig. 2-2). Sample SM02 represents a deformed coarse-grained granodiorite phase from southern part of the Vlajna granitoid. It is characterised by large (230-460μm) mostly yellowish and slightly elongated and acicular, subhedral to euhedral zircons. All grains are rich in inclusions and fractures. Complex internal textures are represented by low luminescence euhedral homogeneous and oscillatory zoned cores with sectored oscillatory overgrowth. A distinctive band of low-luminescent growth is present as a rim concordant to previous crystal faces or as a homogeneous cores. A majority of the grains are affected, to a various extent, by textural deviations including embayments of low-contrast luminescence (e.g. grains o12, o14 and o15 of SM02 in Appendix 2-5), obscured primary textures (e.g. grains o6 and o7 of SM02 in Appendix 2-5) and less frequently convolute zoning (e.g. grains o1 and o3 of SM02 in Appendix 2-5). These features are commonly associated with solid-state recrystallisation (Hoskin and Black, 2000; Corfu et al., 2003; Hoskin and Schaltegger, 2003).

23 measurements on zircon grains yielded age results ranging from 504 to 605 Ma (Appendix 2-4 and Fig. 2-3-1a). The youngest measurement (504±13 Ma; SM02-o1 in Appendix 2-5; Fig. 2-3-1b) was discarded due to suspected influence of detected inclusions, metamict core and fractures on the retentivity of the analysed domain resulting in anomalously young age. Additionally, 3 oldest ages probably representing inheritance were not considered in determining the emplacement age (Fig. 2-3-1b). Remaining 19 analyses are equally distributed within a range of 578-540 Ma. Scatter within this group could be a consequence of intermittent long lasting magmatic activity related to the formation of Vlajna granitoid or partial resetting of ages caused by solid-state

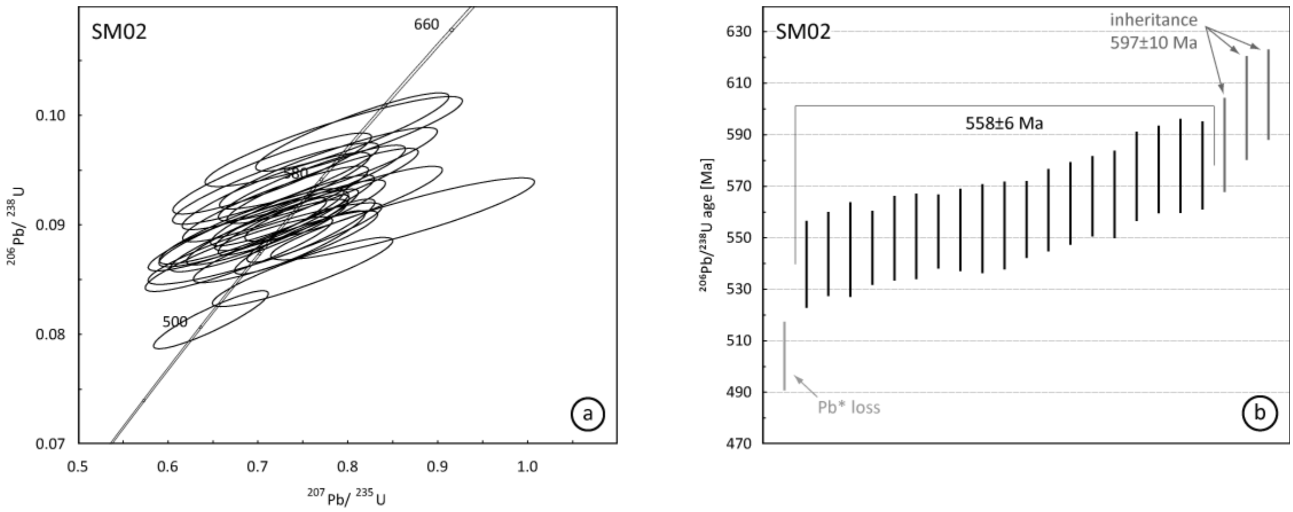

Figure 2-3-1. (a) Concordia diagram and (b) sorted ^{206}Pb/^{238}U age-results for Vlajna granite (SM02). All errors are 2σ. Concordia diagram includes discordant results.

recrystallisation. However, lack of linear decrease in both the ^{232}Th/^{238}U ratio and the obtained age (Appendix 2-4), shows no impact of solid-state recrystallisation on U-Th-Pb system (Hoskin and Schaltegger, 2003; Tichomirowa et al., 2005). Continued scattering of ages in an array without significant clusters is most probably a consequence of systematic radiogenic lead loss possibly caused by the deformation. Thus, the weighted average age of the central group of 558±6 Ma is considered as the emplacement age. Observed low-luminescent rims and cores are probably related to the later stages of the magmatic activity (552±6 Ma).

2-3-1.2 The Golemo Selo locality (SM250-1 and SM250-2)

On a roadside scarp in the vicinity of Golemo Selo village NW of Vranje, an alternation of gneisses and amphibolite is observed. Both seem to be deformed and folded together and therefore their primary contact could not be determined.

2-3-1.2.1 Amphibolite (SM250-1)

The amphibolite sample (SM250-1, Fig. 2-2) has yielded a small amount of rather small subhedral zircon grains (80-160 μm). They are rich in inclusions and annealed fractures. The dominant population is brown and equant, while subordinate group is characterised by transparent and elongate fragments. Most of the grains present a broad rim of oscillatory zoning enclosing rounded cores which are also oscillatory zoned, occasionally metamict and partially recrystallised. Truncation of crystal faces and cavities along fractures indicate possible resorption (e.g. grains o10 and o15 of SM250-1, Appendix 2-5). Additionally, a very thin rim of brightly luminescent growth is observed on the periphery of most of the grains (i.e. grains o4 and o8 of SM250-1, Appendix 2-5).

Only 4 small grains with complex internal structure and high inclusion content (mostly rutile), yielded concordant results (Appendix 2-4 and Fig. 2-3-2a). The 3 youngest zircons have a weighted average age of 462±6 Ma. The fourth concordant measurement on the rounded core of an oscillatory grain yielded an age of 489±14 Ma. Due to distinctive zoning pattern indicative of crystallisation in felsic magma the undisturbed zircons obtained from this amphibolite were interpreted as xenocrysts rather than original crystallisation in a basic magma (Appendix 2-5). Thus the emplacement age of the protolith of Golemo Selo amphibolite is constrained to be at least 462±6 Ma. Resorption indicators and the thin undated growth might represent effects of residence of xenocrysts in basaltic magma of the amphibolite protolith. High luminescence of this overgrowth indicative of low uranium content (Corfu et al., 2003) supports this assumption.

2-3-1.2.2 Gneiss (SM250-2)

The gneiss sample (SM250-2, Fig. 2-2) yielded a heterogeneous group of mostly subhedral to rounded zircon grains, probably of detrital origin (Appendix 2-5). Their size varies between 160 and 300 μm along with their shapes, ranging from more elongated to equant forms. Majority of the grains exhibit abundant inclusions and fractures which are occasionally annealed. Along with their shape, the “pitted” surface of the crystals points to detrital origin. Zircons are mostly transparent

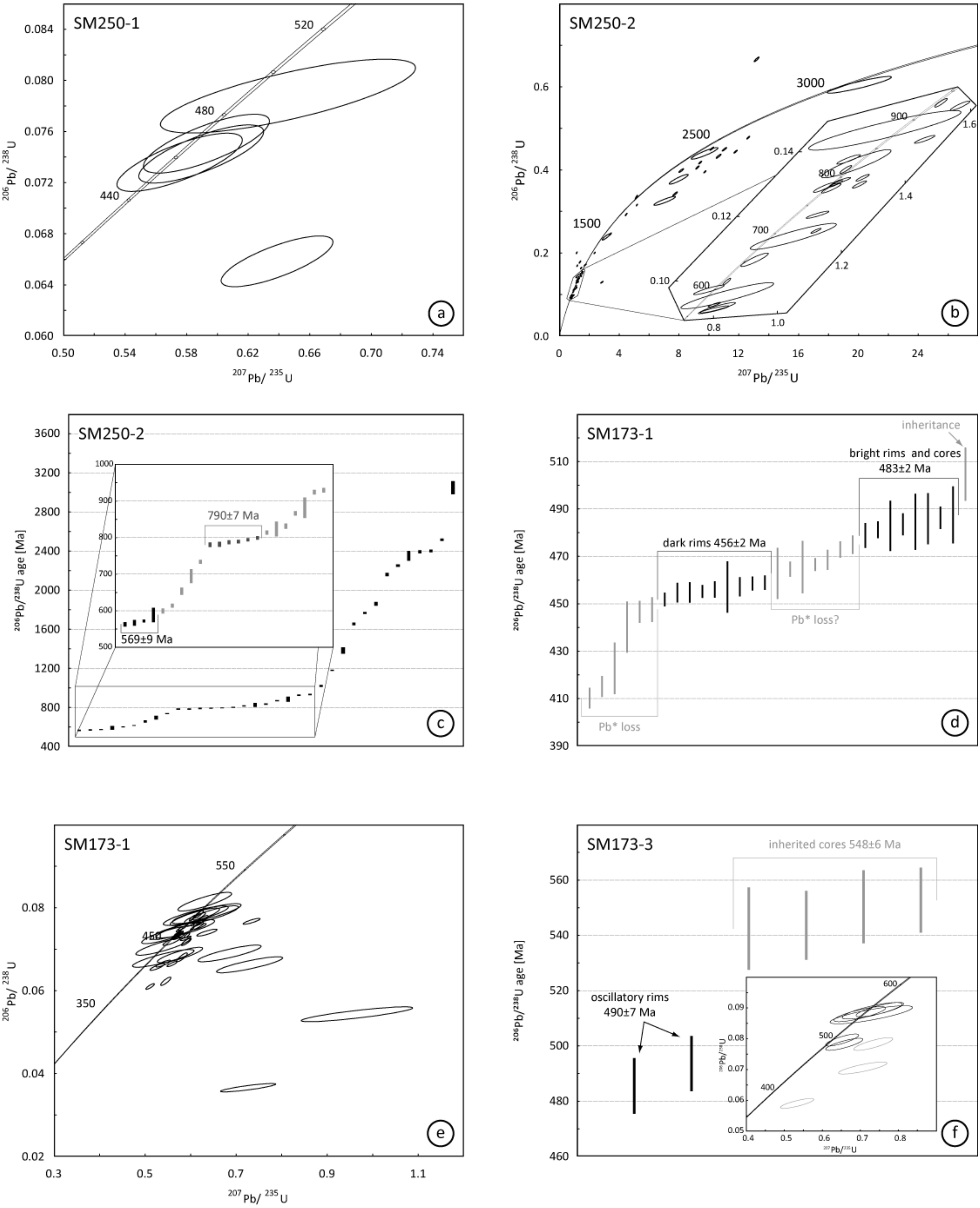

Figure 2-3-2. Concordia diagram for (a) Golemo Selo amphibolite (SM250-1), (b) Golemo Selo para-gneiss (SM250-2), and (e) Vinica amphibolite (SM173-1), and inset in (f) Vinica leucocratic dyke (SM173-3); Sorted ^{206}Pb/^{238}U age-results for (c) Golemo Selo para-gneiss (SM250-2), (d) Vinica amphibolite (SM173-1), and (f) Vinica leucocratic dyke (SM173-3). All errors are 2σ.

unless their colour is altered to yellow or brown due to fractures, inclusions or metamict domains. They commonly display an inherited rounded core with a thin homogeneous rim. Oscillatory and sector zoning is observed in cores as well as in the overgrowth. Occasional homogeneous, banded, diffuse and convolute textures are observed, most probably as a consequence of solid-state recrystallisation.

From the total of 69 analysed grains, 34 had to be discarded due to high discordance or mixed ages (Appendix 2-4). Remaining 35 analyses form a widely scattered array most probably represent a heterogeneous sedimentary sources (Fig. 2-3-2b). The age of the youngest analysed zircon grain in a sedimentary rock must indicate a lower limit for the age of deposition. Hence, the maximum depositional age of the analysed sample is constrained by the cluster of four ages averaging at 569±9 Ma (Fig. 2-3-2c). These four measurements have been taken on sector-zoned or fully recrystallised domains of subhedral grains that have subsequently experienced at least one further stage of zircon growth that could not have been analysed. Another noteworthy group of six results measured at predominantly oscillatory zones is represented by a weighted average of 790±7 Ma, representing a distinctly magmatic source. Remaining 25 results are scattered over a period between 598 and 3049 Ma (Fig. 2-3-2c). The general data scatter of results is interpreted as a result of a reworked sedimentary source material, rather than significant radiogenic lead loss caused by subsequent metamorphic events since no systematic decrease of ^{232}Th/^{238}U ratio with obtained ages could be established (Appendix 2-4).

2-3-1.3 The Vinica locality (SM173-1 and SM173-3)

Samples from concurrently deformed amphibolite (SM173-1) and leucocratic vein (SM173-3) primarily intruded into a two-mica gneiss were taken from a roadside scarp near town of Vinica east of Kočani (Fig. 2-2).

2-3-1.3.1 Amphibolite (SM173-1)

Vinica amphibolite yielded mainly small (100-200µm), stubby, fractured zircons. They are often dark brown or yellow and contain high number of inclusions. Smaller zircon grains (<100 µm) are mostly transparent. Internal textures are commonly represented by a low-luminescent rim enclosing brightly-luminescent cores. Furthermore, a thin brightly luminescent rim is often visible at the outer periphery of the grains.

LA-ICP-MS analysis yielded 31 concordant ages out of 75 measurements (Fig. 2-3-2e). Presence of fractures within the six youngest analysed spots, or their proximity to the periphery of the grains (Appendix 2-5) are considered to have facilitated *Pb loss in grains that manifests as borderline concordant (Fig. 2-3-2d and Appendix 2-4) and anomalously younger ages in comparison to the established age-clusters. A cluster of 9 results with a weighted average age of 456±2 Ma is related to a low-luminescent homogeneous textural domains. A group of 7 slightly older age results (Fig. 2-3-2d) exhibit internal textures inconsistent with the rest of the zircon population. They include diffuse and partially obscured oscillatory zoning, characteristic for solid-state recrystallisation (Appendix 2-5). However, lack of evidence for metamorphism higher than amphibolite facies and high ^{232}Th/^{238}U ratios do not suggest influence of observed recrystallisation on the U-(Th)-Pb system (Appendix 2-4). Thus, the observed scatter is probably related to the radiogenic lead loss along the fractures which were produced during rock deformation. An older age group contains 8 data points with an average age of 483±2 Ma measured at dominantly high-luminescent inherited cores and intermediate bands (Fig. 2-3-2d and Appendix 2-5). A single inherited core of 505±11 Ma is also noted.

2-3-1.3.2 Leucocratic dyke (SM173-3)

Deformed leucocratic dykes from Vinica locality are parallel to the foliation in the host gneiss and amphibolitic schists. Sample SM173-3 yield two distinct zircon groups. The first is represented by large (150-200µm), yellow to brownish, equant, euhedral grains. The second group contains much smaller (100-150µm), highly elongate, transparent, euhedral zircons. Both groups of grains display high number of inclusions. Internal texture is commonly represented by inherited cores enclosed by alternating bands of medium- and low-luminescent oscillatory zoning. Subsequently the earlier features are resorbed to a variable extent. Resulting cavities have been filled with inclusions or a prominent highly luminescent zircon growth which is frequently observed as a relatively narrow rim.

Six zircons from the leucocratic dyke (SM173-3) were successfully analysed (Appendix 2-4 and Fig. 2-3-2f). Hence, only two results from the oscillatory rims define the final magmatic growth at 490±7 Ma (inset in Fig. 2-3-2f). Four ages from the inherited cores average at 548±6 Ma.

Identical zoning patterns and age concordance observed in inherited zircons from the amphibolite (SM173-1) suggests a singular source with the youngest, albeit less populated cluster from the leucocratic sample (SM173-3). Thus we suggest that the population at 548±6 Ma indicates the age of the host rocks which is present as xenocrysts in the leucocratic dykes which were intruded at 483-497 Ma. This younger population has the same age as inheritance in the amphibolite (SM173-1) which was emplaced at 456±2 Ma. Broad homogeneous zoning of the youngest population in an amphibolitic sample indicates growth in a compositionally less evolved magma (Corfu et al., 2003).

2-3-1.4 Lower Complex gneisses (SM184-1 and SM310)

2-3-1.4.1 Sample SM184-1

Sample SM184-1 was taken from strongly deformed two-mica ortho-gneiss with compositional banding in Maleševski Mts. northeast of Ogražden pluton (Fig. 2-2). Recovered zircons are generally large (200-430 µm), subhedral with slightly elongate prisms and well developed pyramids, with occasionally observed acicular fragments or rounded equant grains. Most zircons are yellow, brown and transparent in colour. Convolute zoning (e.g. grain o12 of sample SM184-1, Appendix 2-5), embayments of low and medium luminescent homogeneous areas (e.g. grain o27 of sample SM184-1, Appendix 2-5), partially obscured earlier textures (e.g. grain o14 of sample SM184-1, Appendix 2-5) and large homogeneous or diffuse areas (e.g. grains o19 and o26 of sample SM184-1, Appendix 2-5) suggest solid-state recrystallisation. "Ghost" textures reveal oscillatory and sector zoning as most common initial textures. Additionally, original grains are often preserved as brightly luminescent recrystallised cores enveloped by dark oscillatory overgrowth with low internal contrast (e.g. grain o29 of sample SM184-1, Appendix 2-5).

With the exception of a single result at 425±13 Ma representing radiogenic lead loss on the fractured grain (SM184-1-o30 in Appendix 2-5), six youngest obtained ages averaging at 472±4 Ma are related to the fully recrystallised homogeneous and often highly luminescent cores (inset in Fig. 2-3-3b). Three measurements on dark low-contrast oscillatory zones are also included in this cluster (grains o17b, o18 and o28 of sample SM184-1, Appendix 2-5). Additionally, several metamict inherited cores might have been entirely recrystallised during this event (e.g. grains o19 and o30 of sample SM184-1, Appendix 2-5). Three recrystallised brightly luminescent cores forming minor cluster averaging at 524±8 Ma together with isolated ages at 649±17, 802±22 and 851±24 Ma (Fig. 2-3-3b) are representing various xenocrysts. Another three results, apparently unaffected by

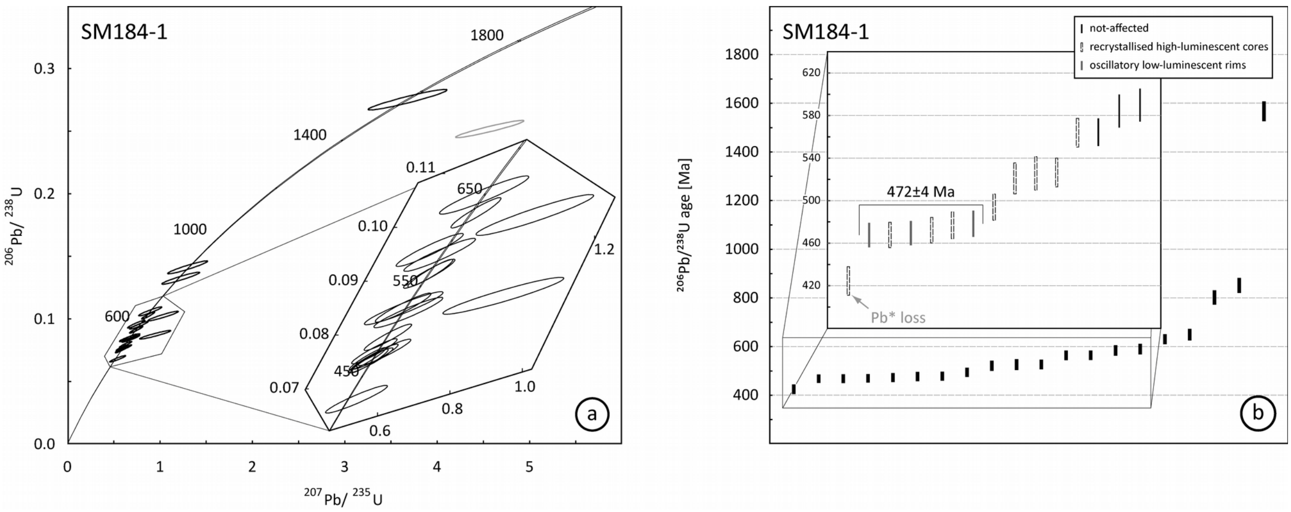

Figure 2-3-3. (a) Concordia diagram and (b) sorted ^{206}Pb/^{238}U age-results for Maleševski Mts. gneiss (SM184-1). All errors are 2σ.

recrystallisation form an array between 564 and 590 Ma (Fig. 2-3-3a). Even earlier inheritance is represented as isolated results at 631±13 and 1567±34 Ma. We suggest that the protolith of the Maleševski Mts. ortho-gneiss was finally emplaced at 472±4 Ma. Observed scatter of age results is not a direct consequence of solid-state recrystallisation due to the lack of systematic decrease in ^{206}Pb/^{238}U age with ^{232}Th/^{238}U ratio (Appendix 2-4), and the presence of inclusions in seemingly recrystallised domains (Appendix 2-5).

2-3-1.4.2 Sample SM310

Additional sample from the Lower Complex was taken from medium-grained micaschists near Sijarinska Banja spa (SM310, Fig. 2-2). These micaschists are a part of the para-metamorphic series reported as stratigraphically higher part of the Lower Complex (Vukanović et al., 1973). The small amount of recovered zircons is represented by rounded grains of small size (120-200µm). They are transparent with few inclusions and fractures. Internal morphology is dominated by oscillatory and sector zoning in the rims, and convolute and banded zones in cores and xenocrysts. Thin overgrowth, discordant to older textures, is occasionally observed on the periphery of the grains. Unfortunately, only 5 age results are within the 95% concordance. Such extremely low statistical population could be used only as a tentative age constraint of the age of the deposition and should not be considered as an argument for serious interpretation (Vermeesch, 2004). The youngest age of 562±6 Ma provides an estimate of the maximum age of deposition of the protolith (Fig. 2-3-4). Remaining measurements yielded crystallisation episodes at 580±4, 613±6, 646±5 and 2800±14 Ma.

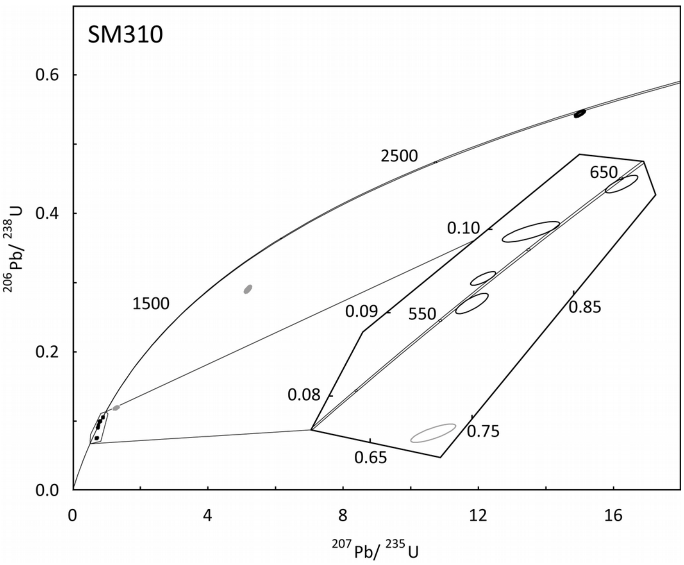

Figure 2-3-4. Concordia diagram for Sijarinska Banja paragneiss (SM310).

2-3-1.5 Bujanovac magmatic complex (SM199-1, SM377-1 and SM377-2)

2-3-1.5.1 Fine-grained Bujanovac granite – central part (SM199-1)

Sample SM199-1 was taken from the central, undeformed parts of the fine-grained Bujanovac granite (Fig. 2-2). Recovered zircons form two major groups. First group comprises large (200-380µm) euhedral to subhedral grains and fragments of elongate to acicular form. Rare stubby grains are smaller in size (100-200µm), subhedral and usually pink, yellow or brown. Zircons predominantly exhibit sectored oscillatory rims, with homogeneous, oscillatory and sector zoned rounded inherited cores.

Acquired ages form two clusters (Fig. 2-3-5b). The younger and less populated (5) of them represents mostly elongated zircons and fragments of acicular grains. Their internal texture is defined by relatively broad oscillatory zoning with well defined sectors. The oldest result in the

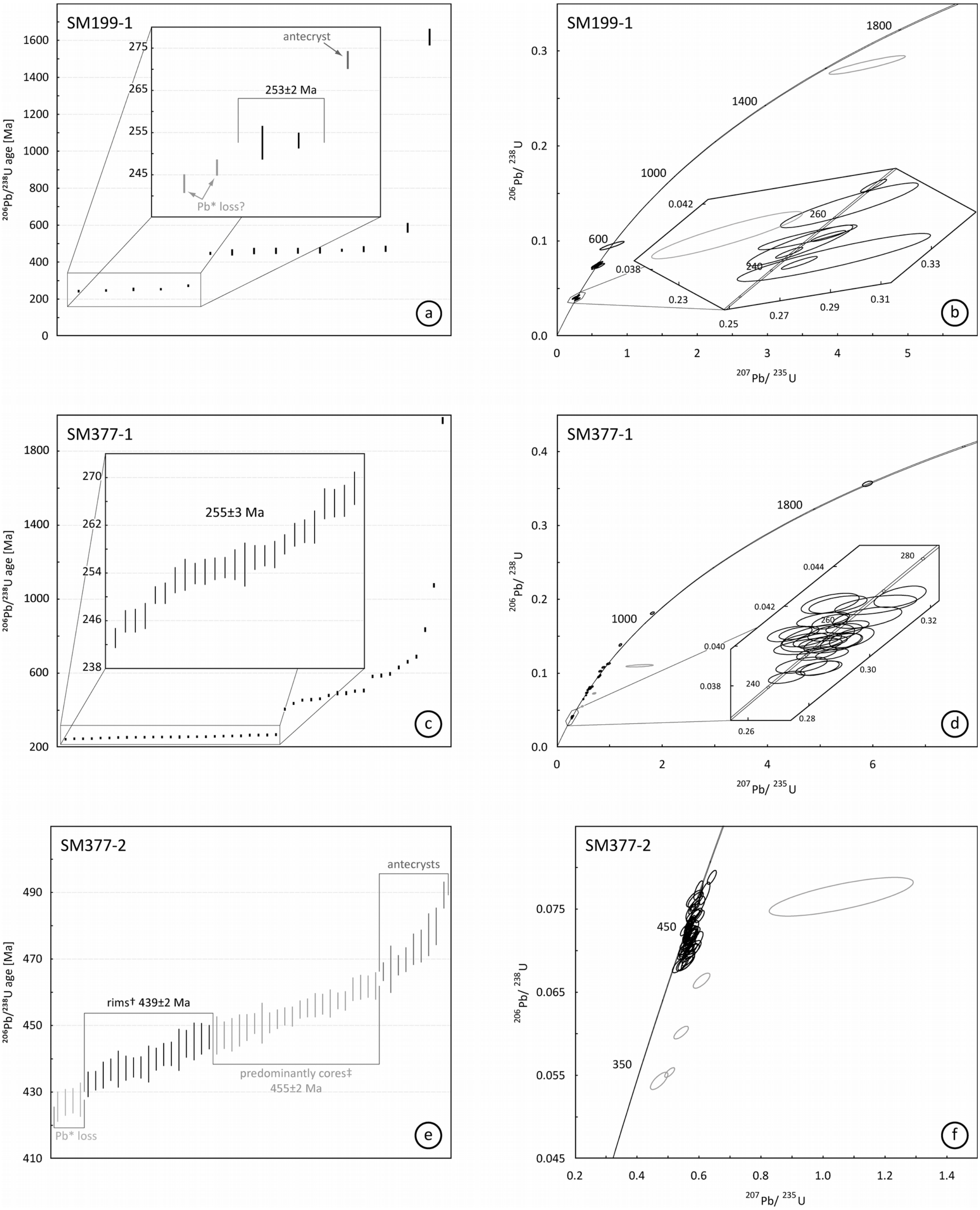

Figure 2-3-5. Sorted ^{206}Pb/^{238}U age-results for (a) Undeformed granite from the central part of the Bujanovac magmatic complex (Borovac locality; SM199-1), (c) Weakly deformed granite from the southeastern part of the Bujanovac magmatic complex (Spančevac locality; SM377-1), and (e) Deformed Qz-monzonite from the southeastern part of the Bujanovac magmatic complex (Spančevac locality; SM377-2); Concordia diagram for (b) Undeformed granite from the central part of the Bujanovac magmatic complex (Borovac locality; SM199-1).

group represents an antecryst and the two youngest ages probably represent an anomalous radiogenic lead loss or a late stage zircon growth (inset in Fig. 2-3-5a). Remaining two ages average at 253±2, and are interpreted as the emplacement age of the fine grained granites in the central area of the Bujanovac pluton. Older and more numerous group of nine results ranging between 447 and 471 Ma obtained from xenocrysts and inherited cores often displaying evidence of recrystallisation. Two inherited cores from late Neoproterozoic and late Palaeoproterozoic have also been defined (Appendix 2-4).

2-3-1.5.2 Fine-grained Bujanovac granite – peripheral part (SM377-1)

Sample SM377-1 was taken from a weakly deformed fine grained mica-bearing phase of the Bujanovac granite intruded into deformed coarse-grained Qz-monzonite along the southeastern periphery of the pluton (Figs. 2-2 and 2-13b). The majority of the separated zircons are transparent and very elongate to acicular, opposed to less abundant equant forms with pronounced pyramids. Their sizes range between 150 and 300 µm. Vast majority of acicular and elongated grains and their fragments show sectored oscillatory zoning (Appendix 2-5).

Equant varieties most often comprise rounded inherited cores with convolute or patchy zoning indicative of recrystallisation. A distinctive low-luminescent oscillatory band is often observed along the periphery of the grains. Occasionally these bands obliterate earlier textures suggesting resorption and new growth (e.g. grains 11 and 17 of sample SM377-1, Appendix 2-5).

An array of 25 youngest ages ranging between 243 and 268 Ma were measured on sectored oscillatory zoning and recrystallised cores of acicular and highly elongated zircons (Fig. 2-3-5d).

Figure 2-3-5 continued. (d) Weakly deformed granite from the southeastern part of the Bujanovac magmatic complex (Spančevac locality; SM377-1), and (f) Deformed Qz-monzonite from the southeastern part of the Bujanovac magmatic complex (Spančevac locality; SM377-2). All errors are 2σ. †with subordinate recrystallised cores; ‡with subordinate recrystallised rims.

Continuous diffusion within this array could be a consequence of the intermittent magmatic activity or a systematic radiogenic lead loss. Textural observations of the youngest measured grains favour the former since they exhibit resorption and precipitation evidence which imply additional pulses of magmatic crystallisation. However, we propose the weighted average of the entire array 255±3 Ma as the best age estimate of this magmatic event. Remaining 19 highly scattered ages were measured on inherited cores or xenocrysts. Notable groups are clustering in Late Ordovician and middle Cambrian. The oldest recorded inheritance are from Stenian and Orosirian periods of the Proterozoic (Appendix 2-4 and Fig. 2-3-5c).

2-3-1.5.3 Deformed coarse-grained Bujanovac Qz monzonite (SM377-2)

Deformed, medium to coarse-grained quartz-monzonite (SM377-2, Fig. 2-2) which was intruded by fine-grained Bujanovac granite was sampled near the southeastern periphery of the magmatic complex (Fig. 11b). Recovered zircons are predominantly large (150-435 μm), transparent, subhedral and elongate. Inclusion rich or fractured grains are yellow or brown in colour. Several equant and rounded grains were also observed. Most of the grains show oscillatory zoning, often with concordant homogeneous cores. However, majority of the grains have suffered solid state recrystallisation evident from “ghosts” of earlier textures, extensive embayments of fully recrystallised medium luminescent areas and convolute zoning. Additionally, very thin brightly luminescent rim is observed on

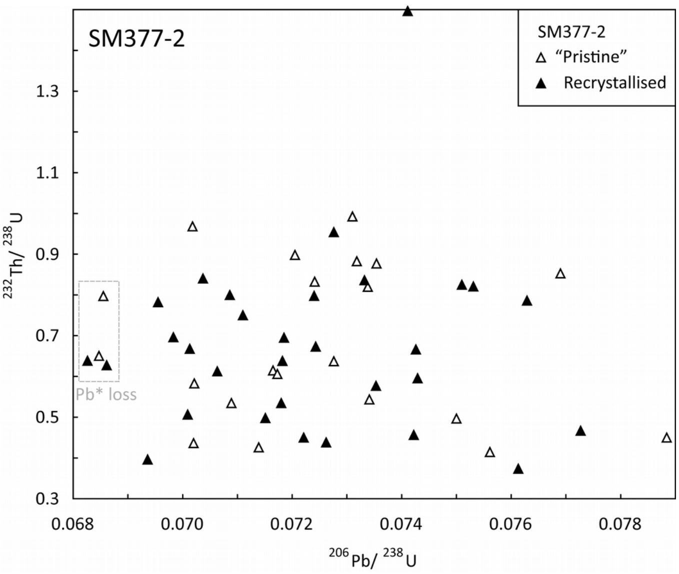

Figure 2-3-6. ^{232}Th/^{238}U versus ^{206}Pb/^{238}U plot for deformed Qz-monzonite from the periphery of the Bujanovac magmatic complex(SM377-2).

periphery of most grains, occasionally forming embayments different from the previous stage of recrystallisation.

The 4 youngest ages were omitted due to presumed extreme radiogenic lead loss along fractures. Remaining ages form a broad array ranging between 430 and 489 Ma with no apparent "plateau" (Fig. 2-3-5f). The broad dissipation of obtained ages may be attributed to the solid state recrystallisation. However, comparison of ^{232}Th/^{238}U ratios with ^{206}Pb/^{238}U ages from areas affected by medium-luminescent recrystallisation and apparently pristine zonation shows that such event did not affect the U-Th-Pb system (Fig. 2-3-6). Hence, the most probable explanation for an extreme diffusion of ages would be systematic radiogenic lead loss caused by the deformational overprint. Younger cluster of 17 ages averaging at 439±2 Ma represents measurements made on pristine oscillatory rims and recrystallised cores and rims (Fig. 2-3-5e). Slightly older group of 22 measurements with weighted average of 455±2 Ma is predominantly related to undisturbed magmatic cores and intermediate bands with additional recrystallised domains. Nine oldest results are interpreted as antecrysts and their recrystallised analogues. We conclude that the weighted average of 439±2 Ma from the group of ages containing pristine rims represents the most probable final emplacement time of the Qz-monzonite.

2-3-1.6 Vrvi Kobila area (SM01 and SM550-1)

2-3-1.6.1 Kukavica granite (SM01)

An intensively deformed part of the Kukavica granites, was sampled for age determination (SM01, Fig. 2-2). Zircons from the Kukavica granite are represented by large (130-320 μm) euhedral to subhedral grains. Colourless elongated to acicular zircons with underdeveloped pyramids are dominant. Subordinate population is represented by pink or yellowish, equant shapes

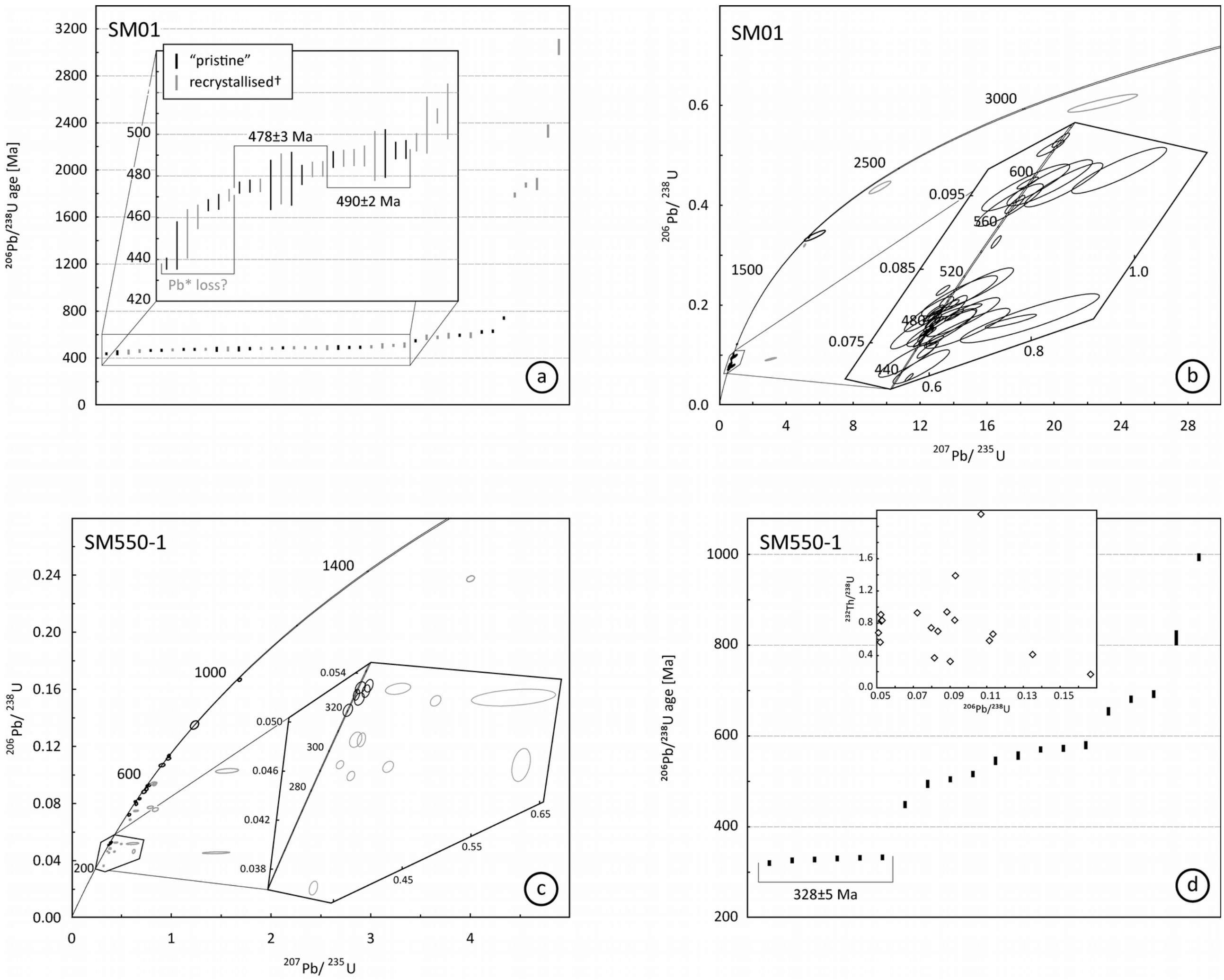

Figure 2-3-7. Sorted ^{206}Pb/^{238}U age-results for (a) Kukavica granite (SM01), and (d) Slatinska Reka granite (SM550-1); Concordia diagram for (b) Kukavica granite (SM01), and (c) Slatinska Reka granite (SM550-1). All errors are 2σ. †partially and fully recrystallised domains.

with prominent pyramids. Internal textures show prominent oscillatory rims enclosing inherited homogeneous or oscillatory and sector zoned cores. Majority of grains are affected by solid state recrystallisation to a various degree leading to partial destruction of previous textures, and convolute or diffuse zoning.

28 age measurements are forming an array between 438 and 511 Ma, followed by scattered inheritance reaching the Mesoarchean era (Appendix 2-4 and Fig. 2-3-7b). Seven youngest results related to rims and recrystallised cores had to be omitted from age interpretation due to presumed radiogenic lead loss resulting from the intensive deformation. Adjacent group of 9 results forms a

singular "plateau" comprising measurements on oscillatory rims, simple grains and partially recrystallised cores (Fig. 2-3-7a). With a weighted average of 478±3 Ma, this group represents probably the youngest magmatic event related to the protolith of the sampled granite. Slightly older possible magmatic event was documented by additional 8 results averaging at 490±2 Ma related to xenocrysts and inherited or partially recrystallised cores.

2-3-1.6.2 Slatinska Reka granite (SM550-1)

North of Kukavica, a group of smaller undeformed granitic bodies are intruded into the gneisses from the footwall of Vrvi Kobila shear zone (Fig. 2-2). They are commonly referred to as Slatinska Reka granites and have previously been related to Kukavica granite or Vlajna granite (Petrović et al., 1973). Sample SM550-1 was taken from the medium grained undeformed Slatinska Reka granites intruded in the gneisses of the Lower Complex (Fig. 2-11a). Extracted zircons are generally euhedral, equant and rarely elongate. They are of variable size (100-300 μm) and hues ranging from brown, yellow to transparent. Three distinctive stages of growth are visible on CL images. The outer low-luminescent rim is homogeneous or oscillatory with low contrast. Homogeneous low-luminescent grains related to this stage of growth are also observed (e.g. grains 2 and 3 of sample SM550-1, Appendix 2-5). These rims are enveloping high-luminescence low-contrast oscillatory zones of variable thickness which are often accompanied by recrystallised older features. The third and innermost crystallisation stage is predominantly low-luminescent oscillatory zoned rim often surrounding rounded cores of various internal textures (e.g. grains 25, 30 and 36 of sample SM550-1, Appendix 2-5). Both older crystallisation stages are affected by extensive solid-state recrystallisation associated with the final homogeneous low-luminescent overgrowth (e.g. grains 9 and 21 of sample SM550-1, Appendix 2-5).

Intrusion of the Slatinska Reka granite is constrained by the average age of 328±5 Ma obtained from six low-luminescence homogeneous grains and low-contrast oscillatory rims (Fig. 2-3-7c). Bright, low contrast oscillatory zone of one single zircon give age of 449±4 Ma. Measurements on eight low-luminescent oscillatory growths give scattered array of Cambrian age (Appendix 2-4 and Fig. 2-3-7d). Additionally, four Cryogenian and a single Tonian rounded core have been measured (600-1000 Ma, Appendix 2-4). Contrary to the expected decrease in $^{232}Th/^{238}U$ ratios due to observed recrystallisation, an opposite trend is observed in inherited cores and “internal rims” (Appendix 2-4 and inset in Fig. 2-3-7d). Thus we conclude that the solid-state recrystallisation had not affected the U-Th-Pb system and that the emplacement of Slatinska Reka granite indeed had occurred at 328±5 Ma as defined by the youngest cluster.

2-3-2 Vlasina Unit

2-3-2.1 Doganica metagranite (SM600-1)

Sample SM600-1 was taken from the northeastern periphery of the deformed Doganica metagranite southeast of Surdulica pluton (Fig. 2-2). A zircon age of ca. 500 Ma was previously reported as time of emplacement (Kräutner and Krstić, 2002). The extracted zircons are subhedral,

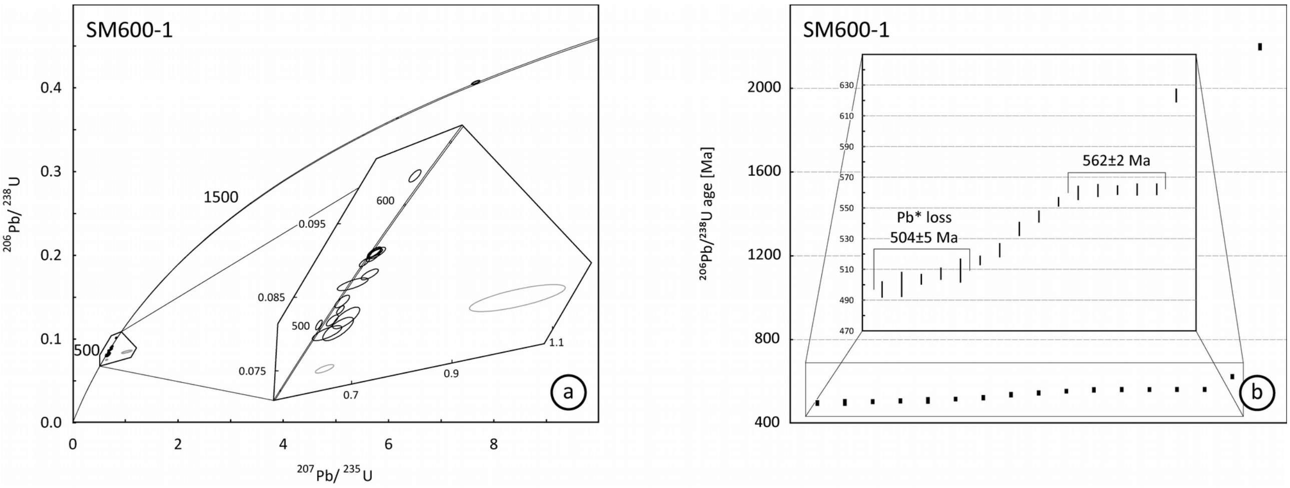

Figure 2-3-8. (a) Concordia diagram and (b) sorted $^{206}Pb/^{238}U$ age-results for Doganica metagranite (SM600-1). All errors are 2σ.

relatively small (100-130 µm), equant and transparent, rarely yellow, pink or brownish. Most of the grains show sector or oscillatory zoning. Patchy zoning and grains composed of several thick homogeneous bands are relatively rare. Annealed fractures are observed in some grains (e.g. grains 3 and 14 of sample SM600-1, Appendix 2-5).

A set of five youngest results with an average age of 504±5 Ma has been measured on homogeneous, banded or sector zoned grains (Fig. 2-3-8b). A trend of decreasing concordance observed for this group together with an array of five decreasing ages (Fig. 2-3-8a) from oscillatory rims were probably caused by radiogenic lead loss that could be related to the subsequent deformation that affected these zircon grains (Appendices 2-4 and 2-5). Unequivocal magmatic crystallisation is defined by the average age of 562±2 obtained from five oscillatory zoned grains obviously unaffected by subsequent metamorphic event(s) (Fig. 2-3-8b). Additionally, an early Ediacaran xenocryst has been dated along with a single rounded grain of Rhyacian age (Appendix 2-4). Majority of the grains are enveloped in a few micrometres thick, porous overgrowth, truncating and often resorbing older textures (e.g. grain 37 of sample SM600-1, Appendix 2-5). The age of the thermal event that have caused the overgrowth could not be determined.

2-3-2.2 Granite from the Božica magmatic complex (SM272-1)

A sample of deformed, medium grained granite was taken from the central parts of the Božica complex (Fig. 2-2). Most of the recovered zircons are represented by transparent subhedral to anhedral, large (135-245 µm), fragments of acicular or elongate grains with underdeveloped pyramids. Darker colouration is caused by the presence of metamict cores, inclusions or fractures. Most of the observed grains contain cores presently displaying homogeneous, diffuse or banded zoning due to intensive recrystallisation. Most commonly “ghosts” of primary oscillatory-sector zoning could be distinguished beyond the recrystallisation overprint (grains 9 and 11 of sample

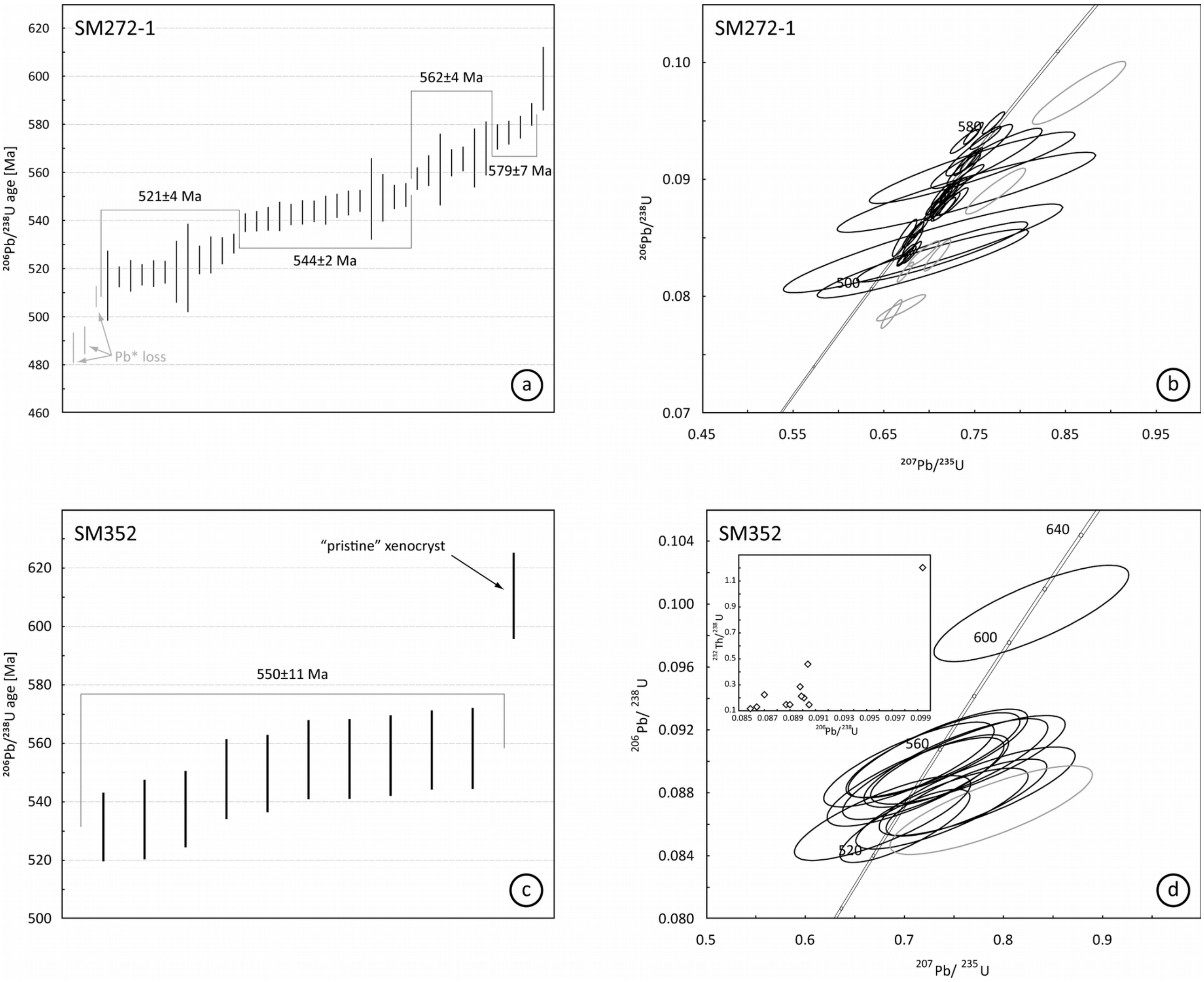

Figure 2-3-9. Sorted $^{206}Pb/^{238}U$ age-results for (a) Granite from the Božica magmatic complex (SM272-1), and (c) Lisina gabbro (SM352); Concordia diagram for (b) Granite from the Božica magmatic complex (SM272-1), and (d) Lisina gabbro (SM352). All errors are 2σ.

SM272-1, Appendix 2-5). Additionally, homogeneous embayments of usually lower luminescence represent a further proof for solid-state recrystallisation (grains 2 and 32 of sample SM272-1, Appendix 2-5).

Results of the radiogenic U–Pb dating reveal a continuous age array spanning the entire Cambrian period (Fig. 2-3-9a). The three youngest results were discarded due to possible influence of measured inclusions. The preceding group of 12 results yielded a weighted mean age of 521±4 Ma. This group is populated by almost equal number of measurements made on cores and rims (5 and 7, respectively). A quiescent period of 9 Ma is observed until the older cluster of 15 ages with a weighted mean of 544±2 Ma. This group contains results from both apparent cores and rims which could have been caused by shallow polishing of the mounted zircons, or a change of melt chemistry causing versatile textures during the same event (grains 19 and 35 of sample SM272-1, Appendix 2-5). Remaining 12 age results most probably represent antecrysts or inheritance of prior magmatic activity at 562±4 and 579±7 Ma. Observed recrystallisation features seem to have no effect on the U-Th-Pb system since no correlation between the ^{232}Th/^{238}U ratio, obtained ages and apparently recrystallised domains could be observed (Appendix 2-4).

However, a single attempt made to reveal the age of recrystallisation by measuring one of the embayments yielded an age belonging to the youngest group (518±5 Ma) and revealed very low ^{232}Th/^{238}U ratio (0.24; SM272-1-21 in Appendices 2-4 and 2-5). Although an isolated result, this occurrence further corroborates the weak effect of recrystallisation, or might imply recrystallisation coeval with the final emplacement, a geologically unlikely scenario. We tentatively propose that the age of final emplacement of the granite from the Božica complex corresponds to weighted mean age of the youngest observed group of results at 521±4 Ma. Alternatively, the wide diffusion of obtained ages could have been caused by partial radiogenic lead loss during subsequent deformational events. This scenario would also explain the presence of both cores and rims within a single age group and a modest decrease in concordance with the "younging" of the ^{206}Pb/^{238}U age (Fig. 2-3-9b).

2-3-2.3 Lisina gabbro (SM352)

Sample SM352 was taken from weakly deformed medium grained gabbro in the valley of Božička river northwest from Bosilegrad (Fig. 2-2). Recovered zircons are small (130-240μm), rich in inclusions and subhedral in shape, predominantly slightly elongated to equant with well developed pyramids. Rare examples of acicular grains with short pyramids are also present. Colours range from pinkish to yellow and transparent. Internal zonation is often represented by broad low contrasting bands with no apparent cores and overgrowth. Minority of grains exhibit oscillatory and sector zoning. Partially obscured oscillatory (e.g. grain 24 of sample SM352, Appendix 2-5) and sector zoning (e.g. grain 20 of sample SM352, Appendix 2-5) and embayments of recrystallised domains along fractures and inclusions (e.g. grain 5 of sample SM352, Appendix 2-5) suggest that the zircons have experienced recrystallisation.

Measurements made on 11 concordant zircons from sample SM352 give an age array from 532 to 558 Ma with a single isolated result at 611±14 Ma (Fig. 2-3-9c). Apart for the older result measured on "pristine" oscillatory zoned grain, all ages were obtained from grains with broad homogeneous bands and fully recrystallised domains of initially oscillatory zoned crystals. Hence, the diffusion of age results is most probably caused by solid-state recrystallisation. This is evident from the systematic decrease of ^{232}Th/^{238}U ratio with ^{206}Pb/^{238}U age (Hoskin and Schaltegger, 2003). Despite the minor disruption caused by recrystallisation, we conclude that the age of emplacement of the Lisina gabbro is best estimated by the weighted average age of 550±11 Ma of the observed array of 10 age results.

2-3-3 Eastern Veles Series

2-3-3.1 Bukovac metagranite (SM315)

Medium grained leucocratic metagranite was sampled below the tectonic contact between the Eastern Veles series and SMM near the Bukovac village, north of Preševo (SM315, Fig. 2-2). Sample yielded large (220-550 µm), brown and yellow, equant to slightly elongate fractured and inclusion rich subhedral zircons. Occasional highly elongate grains are smaller in size (c. 200µm) and transparent. Internal texture of grains shows broad oscillatory zoned growth over rounded and

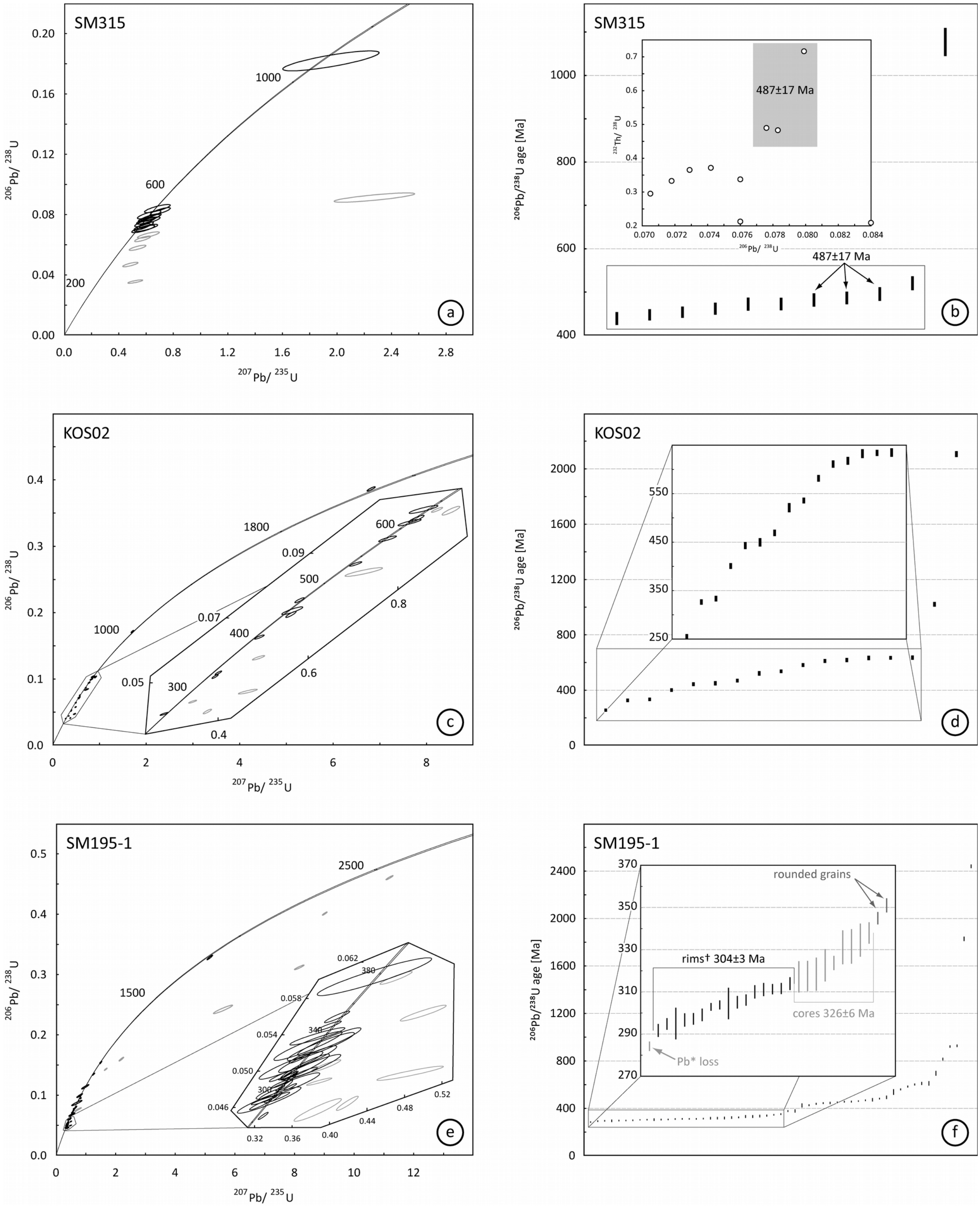

Figure 2-3-10. Concordia diagram for (a) Bukovac ortho-gneiss (SM315), (c) Novo Brdo schist (KOS02), and (d) Granite from the Štip magmatic complex (SM195-1); Sorted $^{206}Pb/^{238}U$ age-results for (b) Bukovac ortho-gneiss (SM315), (d) Novo Brdo schist (KOS02), and (f) Granite from the Štip magmatic complex (SM195-1). All errors are 2σ. †also contains homogeneous and recrystallised cores. Inset in (b) related only to data within the rectangle.

often metamict cores. Convolute zoning and embayments of homogeneous material along fractures, inclusions and within metamict cores were interpreted as evidence of solid state recrystallisation.

Ten age results of measurements from unaffected oscillatory zones and entirely recrystallised areas are loosely clustering between 439 and 495 Ma (Fig. 2-3-10a). Decrease in age and concordance of the results is observed for spots from recrystallised domains (inset in Fig. 2-3-10b). This conclusion is further corroborated by the systematic decrease of ^{232}Th/^{238}U ratios with ^{206}Pb/^{238}U age (inset in Fig. 2-3-10b). Only 3 ages from seemingly intact oscillatory zones are forming the older tier of the array (Fig. 2-3-10b). These three measurements also display ^{232}Th/^{238}U ratios common for unaltered granites (e.g. Xiang et al., 2011) confirming that these age results have not been affected by recrystallisation. Their average age of 487±17 is proposed as the original emplacement time of the granite. Inherited ages are represented by an oscillatory zoned xenocryst at 520±13 Ma and a rounded inherited core at 1077±29 Ma.

2-3-3.2 Novo Brdo schists (KOS02)

Metamorphic rocks near the medieval mining town of Novo Brdo south of Lece volcanic complex, are considered here as a sedimentary cover of the Eastern Veles series (i.e. central Vardar subzone of Dimitrijević, 1997). Their Triassic age was inferred from the fossil spores and pollen recovered from the schists in the area (Pavić et al., 1983). Heterogeneous collection of relatively small (70-170 μm) subhedral zircon grains was obtained from a sample of sericite-quartzitic schist (KOS02 in Fig. 2-2). Indications of recrystallisation (e.g. convolute and “ghost zoning”, grains 3, 11 and 31 in sample KOS02, Appendix 2-5), and annealed fractures (e.g. grain 32 in sample KOS02, 2-Appendix 2-5), occur in the majority of grains. Additionally all grains exhibit up to 10 μm of porous low-luminescent overgrowth, possibly a consequence of hydrothermal activity related to the ore mineralisation (Rubin et al., 1989). Depending on its thickness, this late rim results in grey to black appearance of otherwise clear grains. Beneath the overgrowth, the grains are well rounded, without a common internal texture.

Despite insufficient number of measured grains (N=31) for a comprehensive sedimentary provenance analysis (Vermeesch, 2004), seventeen available age results can be used to tentatively constrain the depositional age of the sedimentary protolith of Novo Brdo schists (Appendix 2-4 and Fig. 2-3-10c). The youngest result of 255±2 Ma represents the maximum depositional age of a sedimentary protolith of Novo Brdo schists. Remaining grains form an array of detrital cores spanning Palaeozoic and Palaeoproterozoic (Appendix 2-4 and Fig. 2-3-10d).

2-3-3.3 Granite from the Štip magmatic complex (SM195-1)

A sample (SM195-1, Fig. 2-2) of undeformed granite from the Štip magmatic complex was taken in the southwestern outskirts of the town of Štip. Majority of the recovered zircons are subhedral, rather small (100-150 μm) and slightly elongate to equant in shape. Lesser population comprises large (200-300μm) and elongate to acicular grains. Entirely homogeneous grains and rounded shaped varieties are present but uncommon. Most of the crystals are transparent, with rare exceptions rich in inclusions and fractures resulting in yellowish hue. Commonly, the zircons exhibit a single, low contrast, oscillatory zoned rim with homogeneous nuclei or inherited cores with various textures. Various indicators for recrystallisation are frequently observed, e.g. convolute zoning (e.g. grain 22 of sample SM195-1, Appendix 2-5), embayments along fractures and inclusions (e.g. grain 28 of sample SM195-1, Appendix 2-5) and partially obscured primary textures (grain 4 of sample SM195-1, Appendix 2-5).

Measurements performed on a total of 86 grains resulted with a highly scattered array of ages, of which 31 were not considered in the age analysis due to mixed zoning and/or discordance (Appendix 2-4 and Fig. 2-3-10e). Furthermore, the youngest result was discarded due to presumed radiogenic lead loss. A cluster of 25 ages is ranging from 292 to 338 Ma (inset in Fig. 2-3-10f) with a younger portion of this group comprising 16 low luminescent and low contrast oscillatory rims and recrystallised homogeneous cores with weighted average age of 304±3 Ma. Indicators of solid-state recrystallisation impartially affecting this group to a various extent were observed (e.g. grains o22, o30, 11, 19 and 24 of sample SM195-1, Appendix 2-5). The older part of this dispersed array averaging at 326±6 Ma is mostly represented by measurements on homogeneous cores and simple grains (Fig. 2-3-10f). Inherited zircon grains yield ages from early Carboniferous to Late Devonian together with six Cadomian results ranging between 538 and 610 Ma. Much older inherited cores and xenocrysts yielded early Neoproterozoic and two Palaeoproterozoic ages (Appendix 2-4 and Fig. 2-3-10f). Lack of reasonably homogeneous age group within the youngest population could be explained by a systematic radiogenic lead loss or the effects of recrystallisation. The latter could not be established due to the lack of correlation between decreasing ^{232}Th/^{238}U ratios and young ^{206}Pb/^{238}U ages (Appendix 2-4). Therefore we tentatively estimate the intrusion of granite of the Štip magmatic complex at 304±3 Ma.

2-3-4 Basement of Struma Unit (including COL complex and SDC)

2-3-4.1 Bosilegrad monzonite (SM236-1)

Bosilegrad monzonite is outcropping beneath the north-eastern part of the Crnook detachment (Fig. 2-2). Sample of deformed medium grained monzonite was taken northwest of Bosilegrad (SM236-1, Fig. 2-2). It yield euhedral to subhedral elongate fractured grains and fragments of zircons in a wide range of sizes. Larger grains (150-200 µm) are more equant with well developed pyramids and often contain more inclusions resulting in brownish or yellowish hue. A number of smaller transparent grains (<100 µm) show highly elongate to acicular with short pyramids. Zircons display a variety of internal textures ranging from oscillatory and sector zoning to patchy and homogeneous grains. Observed convolute zoning, embayments along the fractures and inclusions, and partially erased primary textures indicate that the majority of grains were affected by recrystallisation to various extent (sample SM236-1, Appendix 2-5).

Out of total 39 measurements, 14 had to be discarded due to discordance and/or mixed zoning (Appendix 2-4). Out of the remaining 25 results, additional two younger results had to be discarded due to radiogenic lead loss along fracture or influence of inclusions (Fig. 2-3-11a). Eleven measurements of oscillatory rims and homogeneous grains with a mean age of 522±4 Ma were grouped in the younger part of the array. The array continues with an older cluster of 10

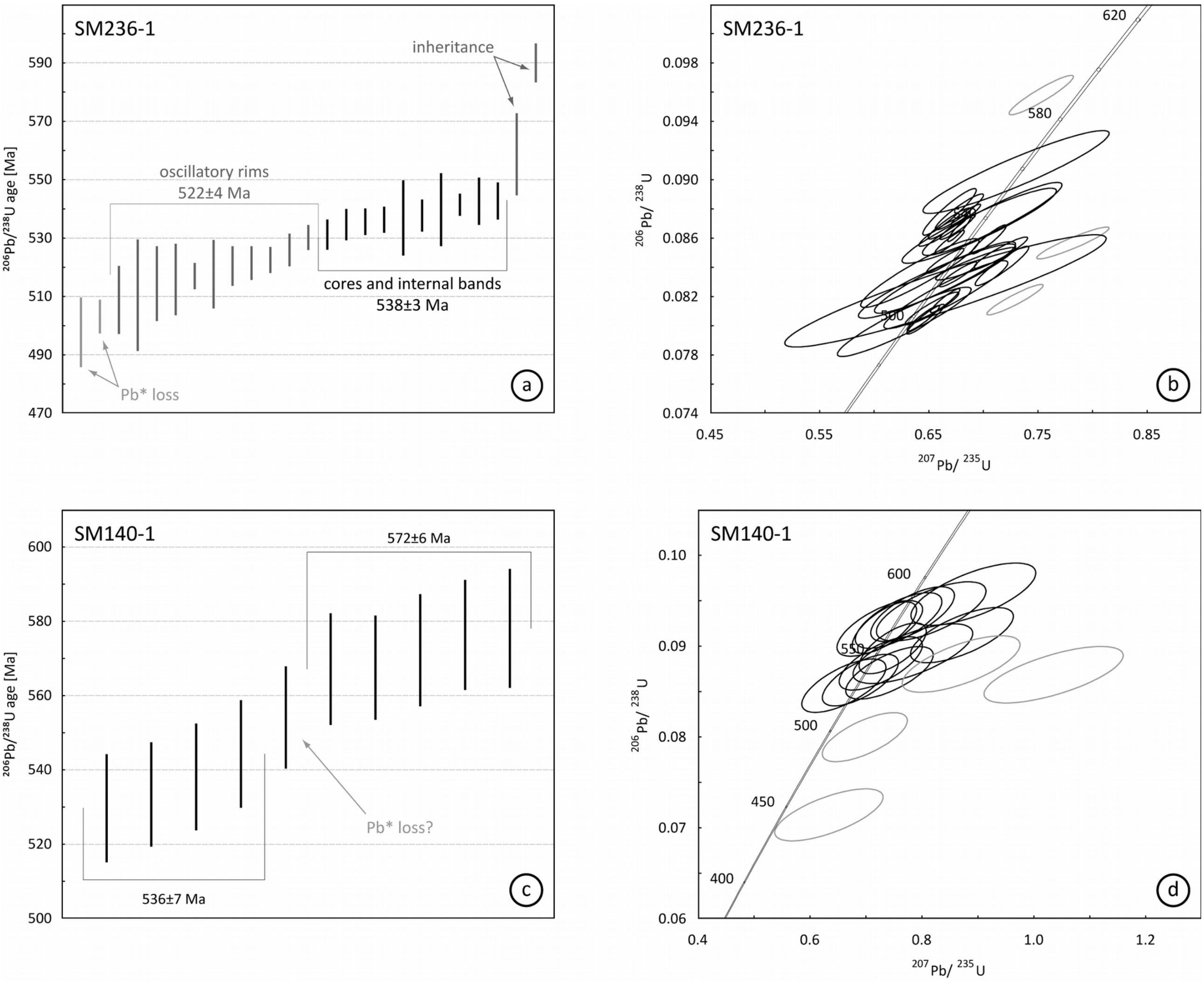

Figure 2-3-11. Sorted $^{206}Pb/^{238}U$ age-results for (a) Bosilegrad monzonite (SM236-1), and (c) Delčevo granite (SM140-1); Concordia diagram for (b) Bosilegrad monzonite (SM236-1), and (d) Delčevo granite (SM140-1). All errors are 2σ.

measurements of cores and internal growth bands averaging at 538±3 Ma. Two Ediacaran ages measured on cores have also been obtained (Appendix 2-4 and Fig. 2-3-11b). Impact of observed recrystallisation was not confirmed due to the lack of evidence for sufficient metamorphic grade and inconclusive relationship between ^{232}Th/^{238}U ratios and ^{206}Pb/^{238}U age (Appendix 2-4), however a systematic radiogenic lead loss is the most likely cause of the large diffusion of the obtained ages. Thus, the emplacement age of Bosilegrad monzonite is assumed to correspond to the weighted average of the youngest magmatic growth at 522±4 Ma.

2-3-4.2 Delčevo granitic complex (SM140-1)

Delčevo granitic complex (i.e. Rakovo granite in the Bulgarian literature) represents one of the largest bodies of the SDC intruded into the Cadomian ophiolites (Frolosh Unit) (Kounov et al., 2012). Delčevo granitic complex encompasses a range of felsic rock types resulting from magmatic differentiation, including coarse-grained biotite granites, medium-grained leucocratic granites, quartz-monzonites, granodiorties and their porphyric and aplitic equivalents (Kovačević et al., 1981; Boev et al., 2002). Formation of this granitic complex was previously estimated as Variscan (Boev et al., 2002). Sample SM140-1 was taken from the coarse grained foliated part of the pluton west of Delčevo (Fig. 2-2). Recovered zircons are mostly euhedral and large (219-450 μm), with elongated prisms and short pyramids. An abundance of inclusions and occasional metamict cores result in yellow and brown hues in otherwise clear grains. Typical internal texture includes oscillatory rims surrounding a slightly rounded cores. Occasional diffuse (e.g. grain 6 of sample SM140-1, Appendix 2-5) and convolute zoning and partially obscured earlier textures (e.g. grain 19 of sample SM140-1, Appendix 2-5) within the inherited cores and rims represent effects of solid-state recrystallisation. Peripheral low-luminescence growth is occasionally observed as a distinctive rim concordant to crystal faces (e.g. grain 11 of sample SM140-1, Appendix 2-5). Abundant annealed fractures were also observed (e.g. grain 13 of sample SM140-1, Appendix 2-5).

Ten concordant U–Pb isotope age determinations resulted in an age array ranging from 530 to 578 Ma (Fig. 2-3-11c and d). Younger cluster is formed by four results averaging at 536±7 Ma representing ages of two oscillatory rims, intermediate growth band of a simple acicular grain and a recrystallised core. The age of a low-luminescent oscillatory rim of 554±13 Ma is representing an antecryst or an error due to radiogenic Pb loss. An older cluster of five ages averaging at 572±6 Ma includes measurement of both rims and cores of xenocrysts. The cause of such scattering of the results might be the protracted intermittent magmatic activity evidenced by variety of rock types comprising Delčevo complex or radiogenic lead loss. The effects of solid-state recrystallisation are not considered due to the absence of correlation between $^{232}Th/^{238}U$ and $^{206}Pb/^{238}U$ ratios (Appendix 2-4). Since the effect of the radiogenic lead loss could not be quantified, we must assume that the emplacement age is defined by the weighted average of the younger group at 536±7 Ma (Fig. 2-3-11c).

References

Boev, B., Lepitkova, S., Petrov, G., 2002. Granitoid formations in the Republic of Macedonia, in: Proceedings of XVII Congress of CBGA. Presented at the XVII Congress of CBGA, VEDA, Bratislava, pp. 1–22.

Corfu, F., Hanchar, J.M., Hoskin, P.W.O., Kinny, P., 2003. Atlas of Zircon Textures. Reviews in Mineralogy and Geochemistry 53, 469–500. doi:10.2113/0530469

Dimitrijević, M.D., 1997. Geology of Yugoslavia. Geological Institute GEMINI, Belgrade.

Hoskin, P. W. O., Black, L. P., 2000. Metamorphic zircon formation by solid-state recrystallization of protolith igneous zircon. Journal of Metamorphic Geology 18, 423–439. doi:10.1046/j.1525-1314.2000.00266.x

Hoskin, P.W.O., Schaltegger, U., 2003. The Composition of Zircon and Igneous and Metamorphic Petrogenesis. Reviews in Mineralogy and Geochemistry 53, 27–62. doi:10.2113/0530027

Kounov, A., Graf, J., von Quadt, A., Bernoulli, D., Burg, J.-P., Seward, D., Ivanov, Z., Fanning, M., 2012. Evidence for a “Cadomian” ophiolite and magmatic-arc complex in SW Bulgaria. Precambrian Research 212–213, 275–295. doi:10.1016/j.precamres.2012.06.003

Kovačević, M., Petkovski, P., Temkova, V., 1981. Tolkuvač za listot Delčevo, Osnovna Geološka Karta 1:100000. Savezni Geološki Zavod, Belgrade.

Kräutner, H.G., Krstić, B., 2002. Alpine and pre-Alpine structural units within the southern Carpathians and eastern Balkanides, in: Proceedings of XVII Congress of CBGA. Presented at the XVII Congress of CBGA, VEDA, Bratislava.

Pavić, A., Menković, L., Košćal, M., 1983. Tumač za list Uroševac, Osnovna Geološka Karta 1:100000. Savezni Geološki Zavod, Belgrade.

Petrović, B., Dimitrijević, M.D., Karamata, S., 1973. Tumač za list Vlasotince, Osnovna Geološka Karta 1:100000. Savezni Geološki Zavod, Belgrade.

Rubin, J., N., Henry, C., D., Price, J., G., 1989. Hydrothermal zircons and zircon overgrowths, Sierra Blanca Peaks, Texas. American Mineralogist 74, 865–869.

Tichomirowa, M., Whitehouse, M.J., Nasdala, L., 2005. Resorption, growth, solid state recrystallisation, and annealing of granulite facies zircon—a case study from the Central Erzgebirge, Bohemian Massif. Lithos 82, 25–50. doi:10.1016/j.lithos.2004.12.005

Vermeesch, P., 2004. How many grains are needed for a provenance study? Earth and Planetary Science Letters 224, 441–451. doi:10.1016/j.epsl.2004.05.037

Vukanović, M., Karajičić, L., Dimitrijević, M.D., Možina, A., Gagić, N., Jevremović, M., 1973. Tumač za list Leskovac, Osnovna Geološka Karta 1:100000. Savezni Geološki Zavod, Belgrade.

Xiang, W., Griffin, W.L., Jie, C., Pinyun, H., Xiang, L., 2011. U and Th Contents and Th/U Ratios of Zircon in Felsic and Mafic Magmatic Rocks: Improved Zircon-Melt Distribution Coefficients. Acta Geologica Sinica - English Edition 85, 164–174. doi:10.1111/j.1755-6724.2011.00387.x

Appendix 2-4

U–Pb LA-ICP-MS results

Spot	Note	Isotopic ratios									Ages [Ma]						Conc.
		^{207}Pb/^{206}Pb	±2σ	^{206}Pb/^{238}U	±2σ	^{207}Pb/^{235}U	±2σ	^{208}Pb/^{232}Th	±2σ	^{232}Th/^{238}U	^{206}Pb/^{238}U	±2σ	^{207}Pb/^{235}U	±2σ	^{208}Pb/^{232}Th	±2σ	[%]
KOS02 Novo Brdo schist																	
KOS02-1		**0,0649**	**0,0015**	**0,04116**	**0,00058**	**0,3761**	**0,0075**	**0,01147**	**0,00033**	**1,38**	**260**	**4**	**324**	**6**	**231**	**7**	**80,3**
KOS02-2		**0,0697**	**0,0021**	**0,0473**	**0,0006**	**0,466**	**0,017**	**0,01232**	**0,00024**	**1,19**	**298**	**4**	**387**	**12**	**247**	**5**	**77**
KOS02-3		**0,0559**	**0,0011**	**0,0442**	**0,00037**	**0,3434**	**0,0071**	**0,01488**	**0,00033**	**0,81**	**279**	**2**	**299**	**5**	**299**	**7**	**93,1**
~~**KOS02-4**~~		~~**0,0644**~~	~~**0,0014**~~	~~**0,06058**~~	~~**0,00075**~~	~~**0,542**~~	~~**0,012**~~	~~**0,02455**~~	~~**0,00063**~~	~~**1,94**~~	~~**379**~~	~~**5**~~	~~**439**~~	~~**8**~~	~~**490**~~	~~**12**~~	~~**86,3**~~
~~**KOS02-5**~~		~~**0,06035**~~	~~**0,00082**~~	~~**0,05368**~~	~~**0,0008**~~	~~**0,4462**~~	~~**0,0065**~~	~~**0,00671**~~	~~**0,00017**~~	~~**0,68**~~	~~**337**~~	~~**5**~~	~~**374**~~	~~**5**~~	~~**135**~~	~~**4**~~	~~**90**~~
KOS02-6	c	0,0647	0,001	0,1031	0,0011	0,918	0,016	0,03376	0,00064	1,21	633	6	661	9	671	12	95,8
KOS02-7	c	0,06255	0,00073	0,10337	0,00062	0,887	0,01	0,03493	0,00035	1,26	634	4	644	6	694	7	98,4
~~**KOS02-8**~~		~~**0,0648**~~	~~**0,0013**~~	~~**0,03667**~~	~~**0,00036**~~	~~**0,3242**~~	~~**0,0066**~~	~~**0,01343**~~	~~**0,00034**~~	~~**0,57**~~	~~**232**~~	~~**2**~~	~~**285**~~	~~**5**~~	~~**270**~~	~~**7**~~	~~**81,5**~~
KOS02-9	ib	0,05645	0,00077	0,0755	0,00063	0,5812	0,0085	0,02597	0,00043	1,08	469	4	465	5	518	9	101
~~**KOS02-10**~~		~~**0,05809**~~	~~**0,00095**~~	~~**0,04446**~~	~~**0,00046**~~	~~**0,3506**~~	~~**0,0069**~~	~~**0,01595**~~	~~**0,00023**~~	~~**1,15**~~	~~**280**~~	~~**3**~~	~~**305**~~	~~**5**~~	~~**320**~~	~~**5**~~	~~**92**~~
KOS02-11ne	c	0,05809	0,00099	0,07111	0,00076	0,562	0,0093	0,02437	0,00048	0,78	443	5	453	6	487	9	97,9
~~KOS02-11sw~~	~~e~~	~~0,05644~~	~~0,00069~~	~~0,07186~~	~~0,00045~~	~~0,5517~~	~~0,0065~~	~~0,02455~~	~~0,00029~~	~~1,02~~	~~447~~	~~3~~	~~446~~	~~4~~	~~490~~	~~6~~	~~100,3~~
KOS02-13	c	0,05583	0,00071	0,05195	0,00048	0,3933	0,0056	0,01765	0,00028	0,51	327	3	337	4	354	6	97
~~**KOS02-14**~~		~~**0,1075**~~	~~**0,0015**~~	~~**0,1263**~~	~~**0,0022**~~	~~**1,848**~~	~~**0,047**~~	~~**0,0256**~~	~~**0,0011**~~	~~**0,6**~~	~~**767**~~	~~**12**~~	~~**1060**~~	~~**17**~~	~~**511**~~	~~**23**~~	~~**72,4**~~
KOS02-16	c	0,07331	0,00094	0,1715	0,0014	1,706	0,023	0,05636	0,00075	0,88	1020	8	1010	9	1108	14	101
KOS02-17	c	0,0574	0,0016	0,07225	0,00097	0,565	0,019	0,02431	0,00097	0,2	450	6	454	12	485	19	99,1
KOS02-18	c	0,0605	0,0012	0,09443	0,00072	0,777	0,016	0,03191	0,00052	1,39	582	4	582	9	635	10	99,9
~~KOS02-19~~	~~r~~	~~0,0592~~	~~0,0017~~	~~0,0833~~	~~0,0014~~	~~0,669~~	~~0,023~~	~~0,02662~~	~~0,00089~~	~~1,03~~	~~516~~	~~9~~	~~519~~	~~14~~	~~531~~	~~18~~	~~99,4~~
KOS02-20	c	0,06115	0,00097	0,10059	0,00091	0,841	0,014	0,0359	0,00055	2,26	618	5	618	8	713	11	99,9
KOS02-21w	r	0,0607	0,0018	0,1035	0,001	0,857	0,026	0,03206	0,00074	1,63	635	6	626	14	638	15	101,4
KOS02-21e	c	0,0607	0,0015	0,09946	0,00081	0,826	0,021	0,03139	0,0005	2,22	611	5	609	12	625	10	100,4
KOS02-22e	r	0,05507	0,00076	0,05308	0,00047	0,4006	0,0059	0,01856	0,0003	0,54	333	3	342	4	372	6	97,5
KOS02-22w	**c**	**0,0618**	**0,0014**	**0,05774**	**0,00056**	**0,49**	**0,011**	**0,02269**	**0,00053**	**0,51**	**362**	**3**	**405**	**8**	**453**	**10**	**89,3**
KOS02-23	ib	0,0506	0,0013	0,04042	0,00036	0,28	0,0072	0,01312	0,0002	2,58	255	2	250	6	263	4	102,1
~~**KOS02-25**~~		~~**0,1775**~~	~~**0,0019**~~	~~**0,236**~~	~~**0,0037**~~	~~**5,75**~~	~~**0,12**~~	~~**0,0578**~~	~~**0,0016**~~	~~**0,48**~~	~~**1365**~~	~~**19**~~	~~**1938**~~	~~**19**~~	~~**1136**~~	~~**30**~~	~~**70,4**~~
~~**KOS02-26**~~		~~**0,2073**~~	~~**0,0024**~~	~~**0,4201**~~	~~**0,0054**~~	~~**12,02**~~	~~**0,18**~~	~~**0,1442**~~	~~**0,0036**~~	~~**0,73**~~	~~**2260**~~	~~**24**~~	~~**2605**~~	~~**14**~~	~~**2721**~~	~~**64**~~	~~**86,8**~~
KOS02-27	c	0,05902	0,00097	0,08668	0,00055	0,706	0,011	0,02904	0,00053	0,44	536	3	542	7	579	10	98,9

Spot	Note	Isotopic ratios									Ages [Ma]						Conc.
		$^{207}Pb/^{206}Pb$	±2σ	$^{206}Pb/^{238}U$	±2σ	$^{207}Pb/^{235}U$	±2σ	$^{208}Pb/^{232}Th$	±2σ	$^{232}Th/^{238}U$	$^{206}Pb/^{238}U$	±2σ	$^{207}Pb/^{235}U$	±2σ	$^{208}Pb/^{232}Th$	±2σ	[%]
KOS02 Novo Brdo schist (continued)																	
~~KOS02-28~~	e	~~0,06244~~	~~0,00064~~	~~0,10608~~	~~0,00067~~	~~0,9107~~	~~0,0093~~	~~0,03255~~	~~0,00035~~	~~0,71~~	~~650~~	~~4~~	~~657~~	~~5~~	~~647~~	~~7~~	~~98,9~~
~~KOS02-29~~		**~~0,0561~~**	**~~0,0012~~**	**~~0,04522~~**	**~~0,00047~~**	**~~0,3498~~**	**~~0,0079~~**	**~~0,01564~~**	**~~0,00029~~**	**~~0,81~~**	**~~285~~**	**~~3~~**	**~~304~~**	**~~6~~**	**~~314~~**	**~~6~~**	**~~93,8~~**
~~KOS02-30~~	e	~~0,1305~~	~~0,0011~~	~~0,3912~~	~~0,0039~~	~~7,089~~	~~0,083~~	~~0,1138~~	~~0,0017~~	~~0,54~~	~~2131~~	~~17~~	~~2122~~	~~10~~	~~2177~~	~~31~~	~~100,4~~
KOS02-31	c	0,128	0,0011	0,3864	0,0026	6,813	0,069	0,1108	0,0017	0,9	2107	12	2086	9	2126	31	101
KOS02-32	c	0,0624	0,0029	0,0842	0,0011	0,724	0,034	0,02746	0,00079	2,72	521	7	547	20	547	15	95,3
KOS02-33	c	0,056	0,001	0,06413	0,00052	0,4919	0,0086	0,02075	0,00046	0,38	401	3	407	6	415	9	98,6
~~KOS02-34~~		**~~0,0586~~**	**~~0,0012~~**	**~~0,04884~~**	**~~0,00057~~**	**~~0,393~~**	**~~0,0081~~**	**~~0,01598~~**	**~~0,00029~~**	**~~1,27~~**	**~~307~~**	**~~4~~**	**~~336~~**	**~~6~~**	**~~321~~**	**~~6~~**	**~~91,4~~**
SM01 Kukavica granite																	
SM01-1c	c	0,05661	0,00065	0,07577	0,00045	0,5861	0,0073	0,02454	0,00029	1,17	471	3	468	5	490	6	100,6
SM01-1e	ib	0,0571	0,0012	0,07782	0,00057	0,607	0,012	0,02513	0,00057	0,93	483	3	481	8	501	11	100,5
SM01-1w	**r**	**0,0727**	**0,0042**	**0,07795**	**0,00076**	**0,76**	**0,041**	**0,0248**	**0,0029**	**0,62**	**484**	**5**	**574**	**24**	**493**	**56**	**84,3**
~~SM01-2e~~	e	~~0,0628~~	~~0,0012~~	~~0,09562~~	~~0,00091~~	~~0,817~~	~~0,017~~	~~0,03597~~	~~0,00054~~	~~1,37~~	~~589~~	~~5~~	~~605~~	~~10~~	~~714~~	~~11~~	~~97,2~~
SM01-2s	r	0,0597	0,0013	0,07523	0,00058	0,611	0,014	0,0304	0,0018	0,19	468	4	483	9	605	34	96,8
SM01-2n	ib	0,064	0,0012	0,12198	0,00091	1,063	0,02	0,03772	0,00062	1,21	742	5	734	10	748	12	101,1
SM01-3	c	0,0605	0,0017	0,10144	0,0009	0,838	0,022	0,03151	0,00048	3,31	623	5	615	12	627	9	101,3
SM01-4c	c	0,05731	0,00099	0,07739	0,00075	0,601	0,01	0,02469	0,00046	0,59	481	5	478	7	493	9	100,5
SM01-4n	ib	0,05846	0,00063	0,0703	0,00043	0,5605	0,0065	0,01307	0,00051	0,54	438	3	452	4	262	10	97
SM01-5s	r	0,0621	0,0032	0,07943	0,00071	0,663	0,033	0,034	0,0048	0,23	493	4	513	18	672	90	96
SM01-5ne	c	0,0606	0,0015	0,07877	0,00064	0,649	0,015	0,02694	0,0008	0,72	489	4	508	10	537	16	96,2
SM01-7	r	0,05686	0,00096	0,07873	0,00063	0,61	0,011	0,02358	0,0007	0,39	489	4	483	7	471	14	101,1
SM01-8	c	0,0562	0,0013	0,07864	0,00062	0,605	0,014	0,02452	0,00093	0,43	488	4	481	9	492	18	101,5
SM01-11e	c	0,11671	0,00098	0,3196	0,0024	5,1	0,048	0,0967	0,0011	0,74	1787	12	1835	8	1866	21	97,4
SM01-11w	ib	0,11682	0,00079	0,3373	0,0024	5,381	0,047	0,09788	0,00083	0,99	1873	12	1881	8	1887	15	99,6
SM01-12		0,0583	0,0014	0,08002	0,00068	0,639	0,016	0,02605	0,00053	0,88	496	4	501	10	520	11	99
SM01-13	c	0,05751	0,00057	0,07655	0,00049	0,6019	0,0064	0,02424	0,00023	1,37	476	3	478	4	484	5	99,4
SM01-14c	c	0,06029	0,00062	0,0887	0,00069	0,7312	0,0081	0,02924	0,00038	0,62	548	4	557	5	583	7	98,4
SM01-14s	r	0,0559	0,001	0,08213	0,00056	0,627	0,011	0,02433	0,00072	0,29	509	3	494	7	486	14	102,9

Spot	Note	Isotopic ratios									Ages [Ma]						Conc.
		$^{207}Pb/^{206}Pb$	±2σ	$^{206}Pb/^{238}U$	±2σ	$^{207}Pb/^{235}U$	±2σ	$^{208}Pb/^{232}Th$	±2σ	$^{232}Th/^{238}U$	$^{206}Pb/^{238}U$	±2σ	$^{207}Pb/^{235}U$	±2σ	$^{208}Pb/^{232}Th$	±2σ	[%]
SM01 Kukavica granite (continued)																	
~~**SM01-16w**~~	~~**c**~~	~~**0,082**~~	~~**0,0019**~~	~~**0,09013**~~	~~**0,00087**~~	~~**1,01**~~	~~**0,025**~~	~~**0,0615**~~	~~**0,0026**~~	~~**0,38**~~	~~**556**~~	~~**5**~~	~~**707**~~	~~**13**~~	~~**1204**~~	~~**50**~~	~~**78,7**~~
SM01-16e	r	0,0586	0,0016	0,07405	0,00091	0,597	0,017	0,0138	0,0011	0,43	460	6	474	11	277	22	97,1
SM01-17	c	0,0576	0,0011	0,07788	0,00056	0,614	0,011	0,02604	0,0007	0,38	483	3	485	7	519	14	99,7
SM01-18	c	0,0598	0,0011	0,0938	0,001	0,768	0,016	0,02946	0,00061	0,44	578	6	577	10	587	12	100,1
SM01-25se	r	0,05695	0,00094	0,07649	0,00047	0,601	0,01	0,0241	0,00065	0,29	475	3	477	6	481	13	99,6
SM01-25c	c	0,0597	0,0013	0,09671	0,00065	0,793	0,017	0,03115	0,0004	2,13	595	4	592	10	620	8	100,5
~~SM01-30~~	~~r~~	~~0,0566~~	~~0,0011~~	~~0,07937~~	~~0,00083~~	~~0,617~~	~~0,012~~	~~0,02483~~	~~0,00053~~	~~0,92~~	~~492~~	~~5~~	~~488~~	~~7~~	~~496~~	~~10~~	~~100,8~~
SM01-32s	r	0,0565	0,0011	0,07934	0,00065	0,612	0,013	0,0282	0,0007	0,27	492	4	487	8	562	14	101,1
SM01-32c	c	0,061	0,001	0,10253	0,00079	0,858	0,014	0,03431	0,00042	1,18	629	5	628	8	682	8	100,2
SM01-39c	r	0,05629	0,00079	0,07638	0,00044	0,5915	0,0084	0,02612	0,00074	0,13	474	3	471	5	521	15	100,7
SM01-39n	c	0,0561	0,0013	0,07892	0,00079	0,61	0,014	0,02731	0,00099	0,38	490	5	483	9	544	19	101,4
SM01-39s	ib	0,05597	0,00075	0,07496	0,00043	0,5781	0,0076	0,02593	0,00043	0,44	466	3	463	5	517	9	100,7
SM01-o1a	**c**	**0,07682**	**0,00778**	**0,07834**	**0,00272**	**0,79726**	**0,11144**	**0,01701**	**0,00246**	**1,05**	**486**	**16**	**595**	**63**	**341**	**49**	**81,7**
SM01-o1b	r	0,05625	0,00282	0,07891	0,00194	0,59967	0,03952	0,02327	0,00398	0,04	490	12	477	25	465	79	102,6
SM01-o2	c	0,05678	0,0036	0,07269	0,00192	0,55726	0,04614	0,02281	0,00344	0,15	452	12	450	30	456	68	100,6
SM01-o3	c	0,16071	0,00584	0,43557	0,01026	9,59953	0,52788	0,11541	0,0144	0,1	2331	46	2397	51	2208	261	97,2
SM01-o4	c	0,06279	0,0033	0,09645	0,00244	0,86356	0,06286	0,02735	0,00348	0,74	594	14	632	34	545	68	**93,9**
SM01-o5	c	0,26981	0,01024	0,60416	0,0147	22,89907	1,69456	0,15245	0,0194	0,69	3047	59	3223	72	2868	340	94,5
SM01-o6	c	0,06004	0,0038	0,08249	0,0022	0,69289	0,0592	0,02361	0,00318	0,79	511	13	535	36	472	63	95,6
~~SM01-o7~~	~~r~~	~~0,05755~~	~~0,00352~~	~~0,07341~~	~~0,00194~~	~~0,56527~~	~~0,04548~~	~~0,02046~~	~~0,0029~~	~~0,42~~	~~457~~	~~12~~	~~455~~	~~30~~	~~409~~	~~57~~	~~100,4~~
SM01-o8	r	0,05915	0,00306	0,09372	0,00236	0,75835	0,05344	0,0263	0,00372	0,34	578	14	573	31	525	73	100,8
SM01-o9a	c	0,12057	0,00562	0,33904	0,00874	5,71352	0,50786	0,09317	0,0134	0,46	1882	42	1933	77	1801	248	97,4
SM01-o9b	**ib**	**0,23112**	**0,01204**	**0,09209**	**0,0026**	**3,07918**	**0,26794**	**0,01716**	**0,00252**	**14,91**	**568**	**15**	**1428**	**67**	**344**	**50**	**39,8**
SM01-o10	**r**	**0,07296**	**0,00404**	**0,09842**	**0,00256**	**0,97256**	**0,07614**	**0,03346**	**0,00518**	**0,52**	**605**	**15**	**690**	**39**	**665**	**101**	**87,7**
SM01-o11	c	0,05884	0,00392	0,07708	0,0021	0,62471	0,05598	0,02018	0,00362	0,18	479	13	493	35	404	72	97,1
SM01-o12	r	0,06094	0,0035	0,07176	0,00188	0,58444	0,04528	0,02257	0,0037	0,46	447	11	467	29	451	73	95,6
SM01-o14	ib	0,06327	0,0037	0,09674	0,00256	0,83635	0,06856	0,02995	0,00552	0,1	595	15	617	38	596	108	96,5

Spot	Note	Isotopic ratios									Ages [Ma]						Conc.
		$^{207}Pb/^{206}Pb$	±2σ	$^{206}Pb/^{238}U$	±2σ	$^{207}Pb/^{235}U$	±2σ	$^{208}Pb/^{232}Th$	±2σ	$^{232}Th/^{238}U$	$^{206}Pb/^{238}U$	±2σ	$^{207}Pb/^{235}U$	±2σ	$^{208}Pb/^{232}Th$	±2σ	[%]
SM01 Kukavica granite (continued)																	
SM01-o15	**c**	**0,06242**	**0,00408**	**0,0785**	**0,00216**	**0,66547**	**0,05956**	**0,02105**	**0,00372**	**0,47**	**487**	**13**	**518**	**36**	**421**	**74**	**94,1**
SM01-o16	c	0,05735	0,00388	0,08139	0,00224	0,6593	0,06098	0,02397	0,00452	0,21	504	13	514	37	479	89	98,1
SM01-o17	ib	0,06002	0,00384	0,09609	0,0026	0,78927	0,07046	0,02736	0,00498	1,05	591	15	591	40	546	98	100,1
SM01-o19	**c**	**0,06178**	**0,00456**	**0,07697**	**0,00222**	**0,67456**	**0,06844**	**0,0216**	**0,00442**	**0,2**	**478**	**13**	**524**	**42**	**432**	**88**	**91,3**
~~SM01-o20~~		~~0,05893~~	~~0,00436~~	~~0,09895~~	~~0,00284~~	~~0,81501~~	~~0,08462~~	~~0,0292~~	~~0,00582~~	~~0,39~~	~~608~~	~~17~~	~~605~~	~~47~~	~~582~~	~~114~~	~~100,5~~
SM01-o21	c	0,06045	0,0033	0,07706	0,00198	0,63533	0,04572	0,02491	0,00314	0,32	479	12	499	28	497	62	95,8
SM01-o22	r	0,06009	0,00238	0,07911	0,0019	0,63395	0,0332	0,03055	0,00378	0,08	491	11	499	21	608	74	98,4
SM01-o23	ib	0,05579	0,00304	0,07658	0,00196	0,57418	0,04082	0,02192	0,0031	0,13	476	12	461	26	438	61	103,3
SM02 Vlajna granite																	
SM02-o1		0,05923	0,00358	0,08134	0,00216	0,64769	0,05214	0,02682	0,00362	0,27	504	13	507	32	535	71	99,4
~~SM02-o2~~	e	~~0,05995~~	~~0,00424~~	~~0,0918~~	~~0,00258~~	~~0,75449~~	~~0,0727~~	~~0,02866~~	~~0,0038~~	~~0,68~~	~~566~~	~~15~~	~~571~~	~~42~~	~~571~~	~~75~~	~~99,2~~
~~SM02-o4a~~	e	~~0,05971~~	~~0,00474~~	~~0,08793~~	~~0,0026~~	~~0,7129~~	~~0,07678~~	~~0,02713~~	~~0,00372~~	~~0,74~~	~~543~~	~~15~~	~~547~~	~~46~~	~~541~~	~~73~~	~~99,4~~
SM02-o4b	r	0,055	0,0049	0,08915	0,00274	0,67721	0,08102	0,02557	0,00378	0,56	551	16	525	49	510	75	104,8
SM02-o5	c	0,0579	0,00538	0,08733	0,00278	0,67885	0,08514	0,02648	0,00396	0,66	540	16	526	51	528	78	102,6
SM02-o3a	**c**	**0,06506**	**0,00522**	**0,0857**	**0,00258**	**0,74969**	**0,08196**	**0,02773**	**0,00418**	**0,53**	**530**	**15**	**568**	**48**	**553**	**82**	**93,3**
SM02-o3b	**r**	**0,06627**	**0,00652**	**0,09055**	**0,00306**	**0,86085**	**0,11988**	**0,02666**	**0,0046**	**0,45**	**559**	**18**	**631**	**65**	**532**	**90**	**88,6**
SM02-o6	c	0,05642	0,0063	0,08829	0,00304	0,70781	0,10626	0,02825	0,00468	0,8	545	18	543	63	563	92	100,4
SM02-o7	c	0,06367	0,00518	0,09193	0,0028	0,79533	0,08974	0,02848	0,0046	0,89	567	16	594	51	568	91	95,4
SM02-o8	c	0,06134	0,0047	0,08956	0,00262	0,71105	0,07396	0,02925	0,00484	0,78	553	16	545	44	583	95	101,4
SM02-o9	r	0,05945	0,0045	0,09088	0,00264	0,74686	0,0776	0,02752	0,00468	0,79	561	16	566	45	549	92	99
SM02-o10	c	0,05925	0,00376	0,09026	0,00246	0,73377	0,06368	0,02978	0,00512	0,82	557	15	559	37	593	100	99,7
SM02-o11	**r**	**0,05718**	**0,00528**	**0,09469**	**0,00302**	**0,71586**	**0,09024**	**0,0295**	**0,0055**	**0,62**	**583**	**18**	**548**	**53**	**588**	**108**	**106,4**
SM02-o12	r	0,06319	0,00354	0,08947	0,00236	0,759	0,05812	0,02938	0,00536	0,35	552	14	573	34	585	105	96,3
SM02-o13	c	0,0589	0,00538	0,09517	0,00304	0,77845	0,09896	0,02766	0,00544	0,63	586	18	585	57	552	107	100,2
SM02-o14	c	0,05736	0,0051	0,08987	0,00282	0,69285	0,08384	0,02938	0,00588	0,62	555	17	535	50	585	115	103,8
SM02-o15	ib	0,05849	0,00472	0,09382	0,00282	0,76001	0,08504	0,02906	0,00592	0,62	578	17	574	49	579	116	100,7
SM02-o16	c	0,05964	0,00488	0,09356	0,0028	0,77185	0,08702	0,02874	0,00374	0,87	577	17	581	50	573	74	99,3

Spot	Note	Isotopic ratios									Ages [Ma]						Conc.
		^{207}Pb/^{206}Pb	±2σ	^{206}Pb/^{238}U	±2σ	^{207}Pb/^{235}U	±2σ	^{208}Pb/^{232}Th	±2σ	^{232}Th/^{238}U	^{206}Pb/^{238}U	±2σ	^{207}Pb/^{235}U	±2σ	^{208}Pb/^{232}Th	±2σ	[%]
SM02 Vlajna granite (continued)																	
SM02-o17	r	0,05984	0,00468	0,09848	0,00292	0,80492	0,08782	0,0287	0,00404	0,47	606	17	600	49	572	79	101
SM02-o18	r	0,05919	0,00516	0,09309	0,00288	0,72003	0,08522	0,02984	0,0043	0,48	574	17	551	50	594	84	104,2
SM02-o19	r	0,06148	0,0036	0,0884	0,00236	0,74646	0,05934	0,02969	0,00394	0,49	546	14	566	35	591	77	96,5
~~SM02-o20~~	e	~~0,06063~~	~~0,00356~~	~~0,09335~~	~~0,00248~~	~~0,77674~~	~~0,0624~~	~~0,03123~~	~~0,00424~~	~~0,45~~	~~575~~	~~15~~	~~584~~	~~36~~	~~622~~	~~83~~	~~98,6~~
SM02-o21	r	0,05849	0,00536	0,08965	0,00284	0,69527	0,08612	0,03084	0,00462	0,55	554	17	536	52	614	91	103,3
SM02-o22	c	0,06046	0,00446	0,09132	0,00264	0,73837	0,0744	0,02979	0,0043	0,72	563	16	562	43	593	84	100,3
SM02-o23	c	0,057	0,00482	0,08903	0,0027	0,70114	0,0805	0,0304	0,00464	0,6	550	16	540	48	605	91	101,9
SM02-o25	c	0,059	0,00568	0,09378	0,00304	0,71978	0,09374	0,03314	0,00526	0,65	578	18	551	55	659	103	105
SM02-o26	r	0,05623	0,00484	0,09191	0,00282	0,7196	0,08438	0,03533	0,00558	0,74	567	17	550	50	702	109	103
SM02-o27	c	0,05815	0,00626	0,09761	0,00336	0,78429	0,11694	0,0321	0,00568	0,7	600	20	588	67	639	111	102,1
SM02-o28	c	0,05931	0,00498	0,08801	0,00268	0,73064	0,08376	0,02983	0,00512	0,89	544	16	557	49	594	101	97,6
SM140-1 Delčevo granite																	
SM140-1-o1	c	0,05988	0,00376	0,08706	0,00236	0,74206	0,06382	0,02668	0,0047	0,48	538	14	564	37	532	92	95,5
SM140-1-o4a	c	0,05774	0,00396	0,08564	0,0024	0,66058	0,06142	0,02604	0,00474	0,62	530	14	515	38	520	93	102,9
SM140-1-o4b	ib	0,06037	0,00424	0,09382	0,00266	0,81658	0,07998	0,03005	0,00576	0,4	578	16	606	45	599	113	95,4
SM140-1-o6	ib	0,0609	0,00344	0,09352	0,00246	0,78336	0,06106	0,02814	0,0054	0,41	576	15	587	35	561	106	98,1
SM140-1-o5	ib	0,05843	0,00366	0,09195	0,0025	0,72469	0,0624	0,02905	0,00582	0,45	567	15	553	37	579	114	102,5
SM140-1-o2a	**c**	**0,06955**	**0,00428**	**0,09121**	**0,00248**	**0,87151**	**0,0751**	**0,03105**	**0,0064**	**0,63**	**563**	**15**	**636**	**41**	**618**	**125**	**88,4**
SM140-1-o2b	**ib**	**0,06502**	**0,0042**	**0,07998**	**0,0022**	**0,69793**	**0,0621**	**0,02417**	**0,00518**	**0,49**	**496**	**13**	**538**	**37**	**483**	**102**	**92,3**
SM140-1-o3	**r**	**0,06163**	**0,00494**	**0,08917**	**0,00268**	**0,78378**	**0,08736**	**0,02687**	**0,00618**	**0,35**	**551**	**16**	**588**	**50**	**536**	**121**	**93,7**
SM140-1-o7	r	0,05895	0,00286	0,08975	0,00228	0,74783	0,04892	0,0275	0,00364	0,03	554	13	567	28	548	72	97,7
SM140-1-o8	r	0,05884	0,0028	0,09203	0,00232	0,73294	0,04692	0,02827	0,00374	0,04	568	14	558	27	564	74	101,7
SM140-1-o9	**c**	**0,06775**	**0,00478**	**0,08803**	**0,00254**	**0,87011**	**0,08598**	**0,03211**	**0,0046**	**0,38**	**544**	**15**	**636**	**47**	**639**	**90**	**85,6**
~~SM140-1-o10~~	e	~~0,05999~~	~~0,00376~~	~~0,08832~~	~~0,00242~~	~~0,71905~~	~~0,06098~~	~~0,02755~~	~~0,00378~~	~~0,39~~	~~546~~	~~14~~	~~550~~	~~36~~	~~549~~	~~75~~	~~99,2~~
~~SM140-1-o14~~	e	~~0,06028~~	~~0,00352~~	~~0,09668~~	~~0,00258~~	~~0,8068~~	~~0,06474~~	~~0,03113~~	~~0,00444~~	~~0,46~~	~~595~~	~~15~~	~~601~~	~~36~~	~~620~~	~~87~~	~~99~~
SM140-1-o12	**c**	**0,0828**	**0,00564**	**0,08685**	**0,00254**	**1,03535**	**0,10152**	**0,03044**	**0,00438**	**0,7**	**537**	**15**	**722**	**51**	**606**	**86**	**74,4**
SM140-1-o11	c	0,05781	0,00354	0,09282	0,0025	0,75831	0,06316	0,02865	0,0042	0,36	572	15	573	36	571	82	99,9

Spot	Note	Isotopic ratios									Ages [Ma]						Conc.
		^{207}Pb/^{206}Pb	±2σ	^{206}Pb/^{238}U	±2σ	^{207}Pb/^{235}U	±2σ	^{208}Pb/^{232}Th	±2σ	^{232}Th/^{238}U	^{206}Pb/^{238}U	±2σ	^{207}Pb/^{235}U	±2σ	^{208}Pb/^{232}Th	±2σ	[%]
SM140-1 Delčevo granite (continued)																	
~~SM140-1-o13~~	**~~ib~~**	**~~0,06204~~**	**~~0,00346~~**	**~~0,08204~~**	**~~0,00216~~**	**~~0,72614~~**	**~~0,05456~~**	**~~0,02296~~**	**~~0,00342~~**	**~~0,76~~**	**~~508~~**	**~~13~~**	**~~554~~**	**~~32~~**	**~~459~~**	**~~68~~**	**~~91,7~~**
~~SM140-1-o15~~	**~~e~~**	**~~0,06233~~**	**~~0,00502~~**	**~~0,09419~~**	**~~0,00286~~**	**~~0,84517~~**	**~~0,09518~~**	**~~0,02872~~**	**~~0,00456~~**	**~~0,45~~**	**~~580~~**	**~~17~~**	**~~622~~**	**~~52~~**	**~~572~~**	**~~90~~**	**~~93,3~~**
SM140-1-o16	ib	0,05791	0,00346	0,08626	0,00232	0,69005	0,05546	0,02496	0,00396	0,37	533	14	533	33	498	78	100,1
~~SM140-1-o17~~	**~~r~~**	**~~0,06338~~**	**~~0,00386~~**	**~~0,09238~~**	**~~0,00252~~**	**~~0,81379~~**	**~~0,06812~~**	**~~0,02918~~**	**~~0,00474~~**	**~~0,58~~**	**~~570~~**	**~~15~~**	**~~605~~**	**~~38~~**	**~~581~~**	**~~93~~**	**~~94,2~~**
SM140-1-o18	ib	0,0591	0,00364	0,0881	0,0024	0,72648	0,0607	0,02629	0,00444	0,3	544	14	555	36	525	88	98,2
~~SM140-1-o19~~	~~e~~	~~0,06219~~	~~0,00344~~	~~0,08448~~	~~0,00222~~	~~0,72293~~	~~0,05396~~	~~0,02586~~	~~0,00432~~	~~0,5~~	~~523~~	~~13~~	~~552~~	~~32~~	~~516~~	~~85~~	~~94,6~~
SM140-1-o20	**c**	**0,06232**	**0,00586**	**0,07143**	**0,00234**	**0,63382**	**0,07904**	**0,01938**	**0,0036**	**0,33**	**445**	**14**	**499**	**49**	**388**	**71**	**89,2**
SM140-1-o21	**ib**	**0,06769**	**0,00496**	**0,09571**	**0,0028**	**0,89189**	**0,09116**	**0,02798**	**0,00512**	**0,92**	**589**	**17**	**647**	**49**	**558**	**101**	**91**
SM173-1 Vinica amphibolite																	
SM173-1-1	c	0,05935	0,00094	0,07259	0,00043	0,5893	0,0095	0,02528	0,00047	0,85	452	3	470	6	505	9	96,2
SM173-1-3	c	0,05682	0,00044	0,07751	0,00054	0,6042	0,0055	0,02531	0,00027	0,87	481	3	480	4	505	5	100,3
~~SM173-1-4~~		~~0,05565~~	~~0,00079~~	~~0,06538~~	~~0,00056~~	~~0,4988~~	~~0,0083~~	~~0,02218~~	~~0,00046~~	~~0,91~~	~~408~~	~~3~~	~~411~~	~~6~~	~~443~~	~~9~~	~~99,5~~
~~SM173-1-5~~		~~0,0577~~	~~0,0012~~	~~0,07586~~	~~0,00077~~	~~0,606~~	~~0,014~~	~~0,02407~~	~~0,00065~~	~~0,91~~	~~471~~	~~5~~	~~481~~	~~9~~	~~481~~	~~13~~	~~98,1~~
SM173-1-6	c	0,0577	0,00075	0,07611	0,00052	0,6012	0,0086	0,02557	0,00045	0,87	473	3	478	5	510	9	99
SM173-1-7	c	0,05658	0,00052	0,07371	0,00043	0,5718	0,0063	0,02533	0,00031	0,79	459	3	459	4	506	6	99,9
SM173-1-8sw	r	0,05643	0,00065	0,07506	0,00039	0,5808	0,0068	0,02569	0,00032	0,76	467	2	465	4	513	6	100,4
SM173-1-8c	c	0,05617	0,00047	0,07473	0,00048	0,5758	0,006	0,02519	0,00023	0,92	465	3	462	4	503	5	100,7
SM173-1-9	c	0,0573	0,001	0,07308	0,00063	0,574	0,011	0,02475	0,00038	0,98	455	4	460	7	494	7	98,9
~~SM173-1-10~~		**~~0,096~~**	**~~0,0025~~**	**~~0,07596~~**	**~~0,0006~~**	**~~0,998~~**	**~~0,027~~**	**~~0,0526~~**	**~~0,0021~~**	**~~0,59~~**	**~~472~~**	**~~4~~**	**~~703~~**	**~~14~~**	**~~1036~~**	**~~41~~**	**~~67,1~~**
~~SM173-1-11c~~		**~~0,062~~**	**~~0,001~~**	**~~0,06371~~**	**~~0,00059~~**	**~~0,544~~**	**~~0,0097~~**	**~~0,01804~~**	**~~0,00081~~**	**~~0,95~~**	**~~398~~**	**~~4~~**	**~~441~~**	**~~6~~**	**~~361~~**	**~~16~~**	**~~90,4~~**
SM173-1-11s	r	0,05698	0,00059	0,0735	0,00061	0,575	0,0071	0,02651	0,0003	0,7	457	4	461	5	529	6	99,2
SM173-1-12	c	0,05923	0,00097	0,07645	0,00059	0,619	0,01	0,0281	0,00045	0,94	475	4	489	6	560	9	97,2
SM173-1-13	c	0,05736	0,00057	0,07837	0,00073	0,6178	0,0081	0,02746	0,00044	0,85	486	4	488	5	547	9	99,7
SM173-1-14se	r	0,0568	0,00053	0,07379	0,00045	0,5757	0,0066	0,02635	0,00027	0,65	459	3	461	4	526	5	99,5
SM173-1-14c	**c**	**0,0624**	**0,0016**	**0,07398**	**0,00068**	**0,636**	**0,018**	**0,0288**	**0,0011**	**0,62**	**460**	**4**	**499**	**11**	**574**	**21**	**92,2**
SM173-1-15	c	0,0596	0,0014	0,07539	0,00064	0,617	0,014	0,02418	0,00054	0,64	469	4	487	9	483	11	96,1
~~SM173-1-16~~		~~0,0575~~	~~0,001~~	~~0,065~~	~~0,0006~~	~~0,5121~~	~~0,0086~~	~~0,02547~~	~~0,00046~~	~~0,62~~	~~406~~	~~4~~	~~420~~	~~6~~	~~508~~	~~9~~	~~96,8~~

Spot	Note	Isotopic ratios									Ages [Ma]						Conc.
		$^{207}Pb/^{206}Pb$	±2σ	$^{206}Pb/^{238}U$	±2σ	$^{207}Pb/^{235}U$	±2σ	$^{208}Pb/^{232}Th$	±2σ	$^{232}Th/^{238}U$	$^{206}Pb/^{238}U$	±2σ	$^{207}Pb/^{235}U$	±2σ	$^{208}Pb/^{232}Th$	±2σ	[%]
SM173-1 Vinica amphibolite (continued)																	
~~SM173-1-17~~		**~~0,05904~~**	**~~0,00085~~**	**~~0,05609~~**	**~~0,00038~~**	**~~0,5091~~**	**~~0,0081~~**	**~~0,02484~~**	**~~0,00054~~**	**~~0,58~~**	**~~352~~**	**~~2~~**	**~~417~~**	**~~5~~**	**~~496~~**	**~~11~~**	**~~84,3~~**
~~SM173-1-18~~		~~0,05749~~	~~0,00083~~	~~0,07612~~	~~0,00058~~	~~0,6008~~	~~0,0099~~	~~0,02578~~	~~0,00045~~	~~0,75~~	~~473~~	~~4~~	~~477~~	~~6~~	~~514~~	~~9~~	~~99,1~~
SM173-1-19	ib	0,0566	0,00048	0,07317	0,0004	0,5695	0,005	0,02517	0,00019	1,19	455	2	458	3	502	4	99,5
SM173-1-20nw	r	0,0586	0,0014	0,06571	0,00067	0,527	0,013	0,02429	0,00065	0,47	410	4	429	9	485	13	95,6
SM173-1-20se	c	0,05651	0,00092	0,07311	0,00066	0,5672	0,0076	0,0243	0,00028	0,84	455	4	456	5	485	6	99,7
SM173-1-21c	**c**	**0,06364**	**0,0009**	**0,06225**	**0,00081**	**0,5455**	**0,0091**	**0,02411**	**0,00026**	**0,95**	**389**	**5**	**442**	**6**	**482**	**5**	**88,1**
SM173-1-21s	**r**	**0,06128**	**0,00082**	**0,061**	**0,00055**	**0,5112**	**0,0076**	**0,02028**	**0,00031**	**1,05**	**382**	**3**	**419**	**5**	**406**	**6**	**91,1**
~~SM173-1-22~~		~~0,05642~~	~~0,00075~~	~~0,07693~~	~~0,00051~~	~~0,5982~~	~~0,0082~~	~~0,02348~~	~~0,00034~~	~~0,71~~	~~478~~	~~3~~	~~476~~	~~5~~	~~469~~	~~7~~	~~100,4~~
SM173-1-23	ib	0,05753	0,00083	0,07789	0,00072	0,619	0,011	0,0233	0,00036	0,79	484	4	489	7	466	7	99
~~SM173-1-24~~		**~~0,1228~~**	**~~0,0011~~**	**~~0,2992~~**	**~~0,0021~~**	**~~5,052~~**	**~~0,048~~**	**~~0,08352~~**	**~~0,00084~~**	**~~0,86~~**	**~~1687~~**	**~~10~~**	**~~1827~~**	**~~8~~**	**~~1621~~**	**~~16~~**	**~~92,3~~**
SM173-1-25c	c	0,0561	0,0017	0,0719	0,00082	0,559	0,016	0,02137	0,00056	0,73	448	5	450	11	427	11	99,5
SM173-1-25se	**r**	**0,06086**	**0,00082**	**0,0664**	**0,0005**	**0,5592**	**0,0088**	**0,02173**	**0,00037**	**0,76**	**414**	**3**	**451**	**6**	**434**	**7**	**92**
~~SM173-1-26~~		~~0,06001~~	~~0,00074~~	~~0,07812~~	~~0,00062~~	~~0,6471~~	~~0,0084~~	~~0,02364~~	~~0,00027~~	~~0,89~~	~~485~~	~~4~~	~~506~~	~~5~~	~~472~~	~~5~~	~~95,8~~
~~SM173-1-27c~~		**~~0,06314~~**	**~~0,00079~~**	**~~0,06099~~**	**~~0,0008~~**	**~~0,5334~~**	**~~0,0084~~**	**~~0,01856~~**	**~~0,00034~~**	**~~0,93~~**	**~~382~~**	**~~5~~**	**~~434~~**	**~~5~~**	**~~372~~**	**~~7~~**	**~~87,9~~**
~~SM173-1-27s~~		~~0,05613~~	~~0,00077~~	~~0,07676~~	~~0,0006~~	~~0,6001~~	~~0,0091~~	~~0,02139~~	~~0,00028~~	~~0,84~~	~~477~~	~~4~~	~~477~~	~~6~~	~~428~~	~~6~~	~~99,9~~
SM173-1-29	**c**	**0,06105**	**0,00073**	**0,06804**	**0,00086**	**0,5813**	**0,0094**	**0,01821**	**0,00028**	**0,84**	**424**	**5**	**465**	**6**	**365**	**6**	**91,2**
~~SM173-1-30c~~		**~~0,0631~~**	**~~0,0016~~**	**~~0,0874~~**	**~~0,0011~~**	**~~0,866~~**	**~~0,024~~**	**~~0,0302~~**	**~~0,001~~**	**~~0,63~~**	**~~540~~**	**~~7~~**	**~~632~~**	**~~13~~**	**~~601~~**	**~~20~~**	**~~85,5~~**
SM173-1-30s	r	0,05792	0,00049	0,0733	0,00051	0,5918	0,0052	0,02042	0,00021	0,84	456	3	472	3	409	4	96,6
~~SM173-1-31c~~		**~~0,0787~~**	**~~0,0013~~**	**~~0,0589~~**	**~~0,001~~**	**~~0,65~~**	**~~0,017~~**	**~~0,022~~**	**~~0,00051~~**	**~~0,7~~**	**~~369~~**	**~~6~~**	**~~508~~**	**~~10~~**	**~~440~~**	**~~10~~**	**~~72,6~~**
~~SM173-1-31n~~		**~~0,0678~~**	**~~0,00079~~**	**~~0,062~~**	**~~0,0013~~**	**~~0,588~~**	**~~0,012~~**	**~~0,02139~~**	**~~0,00038~~**	**~~0,81~~**	**~~388~~**	**~~8~~**	**~~468~~**	**~~8~~**	**~~428~~**	**~~8~~**	**~~82,8~~**
SM173-1-33	**r**	**0,0683**	**0,0014**	**0,0767**	**0,00057**	**0,734**	**0,015**	**0,02515**	**0,00042**	**0,8**	**476**	**3**	**559**	**9**	**502**	**8**	**85,2**
~~SM173-1-34~~		**~~0,0662~~**	**~~0,0026~~**	**~~0,0524~~**	**~~0,00056~~**	**~~0,485~~**	**~~0,019~~**	**~~0,01799~~**	**~~0,00057~~**	**~~0,53~~**	**~~329~~**	**~~4~~**	**~~400~~**	**~~13~~**	**~~360~~**	**~~11~~**	**~~82,3~~**
~~SM173-1-38ne~~		**~~0,06535~~**	**~~0,00098~~**	**~~0,0707~~**	**~~0,0017~~**	**~~0,652~~**	**~~0,019~~**	**~~0,02144~~**	**~~0,00065~~**	**~~0,83~~**	**~~440~~**	**~~11~~**	**~~508~~**	**~~11~~**	**~~429~~**	**~~13~~**	**~~86,6~~**
~~SM173-1-38sw~~		~~0,05838~~	~~0,00074~~	~~0,07331~~	~~0,00061~~	~~0,6031~~	~~0,0083~~	~~0,02167~~	~~0,00037~~	~~0,84~~	~~456~~	~~4~~	~~479~~	~~5~~	~~433~~	~~7~~	~~95,2~~
SM173-1-39c	c	0,0576	0,001	0,07711	0,00082	0,625	0,011	0,02402	0,00054	0,77	479	5	492	7	480	11	97,3
SM173-1-39n	r	0,05819	0,00075	0,07175	0,00071	0,5906	0,0088	0,02244	0,00029	0,74	447	4	471	6	449	6	94,8
~~SM173-1-40c~~		~~0,05761~~	~~0,00098~~	~~0,06641~~	~~0,00055~~	~~0,5404~~	~~0,0097~~	~~0,02125~~	~~0,00039~~	~~0,69~~	~~415~~	~~3~~	~~438~~	~~6~~	~~425~~	~~8~~	~~94,6~~

Spot	Note	Isotopic ratios									Ages [Ma]						Conc.
		^{207}Pb/^{206}Pb	±2σ	^{206}Pb/^{238}U	±2σ	^{207}Pb/^{235}U	±2σ	^{208}Pb/^{232}Th	±2σ	^{232}Th/^{238}U	^{206}Pb/^{238}U	±2σ	^{207}Pb/^{235}U	±2σ	^{208}Pb/^{232}Th	±2σ	[%]
SM173-1 Vinica amphibolite (continued)																	
SM173-1-40s	r	0,0574	0,0014	0,06651	0,00067	0,54	0,013	0,02084	0,0004	0,5	415	4	438	8	417	8	94,8
~~SM173-1-o1~~		~~0,0572~~	~~0,00322~~	~~0,07863~~	~~0,00178~~	~~0,59679~~	~~0,04584~~	~~0,02318~~	~~0,0034~~	~~0,41~~	~~488~~	~~11~~	~~475~~	~~29~~	~~463~~	~~67~~	~~102,7~~
SM173-1-o2a	**c**	**0,07406**	**0,0044**	**0,06897**	**0,00164**	**0,68556**	**0,05656**	**0,02215**	**0,00328**	**0,76**	**430**	**10**	**530**	**34**	**443**	**65**	**81,1**
SM173-1-o2b	r	0,05944	0,0033	0,08144	0,00184	0,63115	0,0481	0,02442	0,0037	0,44	505	11	497	30	488	73	101,6
~~**SM173-1-o3**~~		~~**0,06233**~~	~~**0,00488**~~	~~**0,06778**~~	~~**0,0018**~~	~~**0,55686**~~	~~**0,0588**~~	~~**0,00868**~~	~~**0,00146**~~	~~**0,89**~~	~~**423**~~	~~**11**~~	~~**450**~~	~~**38**~~	~~**175**~~	~~**29**~~	~~**94,1**~~
SM173-1-o4	**r**	**0,06454**	**0,00332**	**0,06858**	**0,00152**	**0,5767**	**0,0406**	**0,02029**	**0,00316**	**0,65**	**428**	**9**	**462**	**26**	**406**	**62**	**92,5**
SM173-1-o6	r	0,05961	0,00322	0,07829	0,00176	0,64562	0,0483	0,0244	0,00392	0,45	486	10	506	30	487	77	96,1
~~SM173-1-o7~~		~~0,06117~~	~~0,00334~~	~~0,07954~~	~~0,0018~~	~~0,64535~~	~~0,04912~~	~~0,02496~~	~~0,00414~~	~~0,44~~	~~493~~	~~11~~	~~506~~	~~30~~	~~498~~	~~82~~	~~97,6~~
SM173-1-o8a	**c**	**0,15329**	**0,00746**	**0,0366**	**0,00082**	**0,72638**	**0,04936**	**0,02009**	**0,00338**	**0,75**	**232**	**5**	**554**	**29**	**402**	**67**	**41,8**
SM173-1-o8b	r	0,05746	0,00298	0,07779	0,00172	0,60917	0,04422	0,02397	0,00418	0,48	483	10	483	28	479	82	100
SM173-1-o9	r	0,05784	0,00348	0,07444	0,00174	0,57032	0,04784	0,02352	0,00442	0,46	463	10	458	31	470	87	101
~~SM173-1-o10~~		~~0,05914~~	~~0,0037~~	~~0,08059~~	~~0,00192~~	~~0,64928~~	~~0,05748~~	~~0,02557~~	~~0,00498~~	~~0,48~~	~~500~~	~~11~~	~~508~~	~~35~~	~~510~~	~~98~~	~~98,4~~
SM173-1-o12	c	0,05888	0,00406	0,07856	0,00196	0,63516	0,06184	0,02465	0,00506	0,38	488	12	499	38	492	100	97,6
~~**SM173-1-o13**~~		~~**0,06201**~~	~~**0,00406**~~	~~**0,07443**~~	~~**0,00182**~~	~~**0,63241**~~	~~**0,05876**~~	~~**0,02404**~~	~~**0,00504**~~	~~**0,42**~~	~~**463**~~	~~**11**~~	~~**498**~~	~~**37**~~	~~**480**~~	~~**99**~~	~~**93**~~
SM173-1-o14	r	0,06002	0,0044	0,06777	0,00174	0,54004	0,05502	0,02064	0,00452	0,45	423	11	438	36	413	90	96,4
SM173-1-o15	r	0,05821	0,0036	0,07489	0,0018	0,5889	0,05218	0,02255	0,005	0,57	466	11	470	33	451	99	99
~~SM173-1-o16~~		~~0,06147~~	~~0,00418~~	~~0,07517~~	~~0,00188~~	~~0,62302~~	~~0,06052~~	~~0,02643~~	~~0,00614~~	~~0,34~~	~~467~~	~~11~~	~~492~~	~~38~~	~~527~~	~~121~~	~~95~~
~~**SM173-1-o17**~~		~~**0,06099**~~	~~**0,00398**~~	~~**0,06743**~~	~~**0,00166**~~	~~**0,55363**~~	~~**0,05178**~~	~~**0,0221**~~	~~**0,00524**~~	~~**0,56**~~	~~**421**~~	~~**10**~~	~~**447**~~	~~**34**~~	~~**442**~~	~~**104**~~	~~**94**~~
SM173-1-o18	r	0,05671	0,00372	0,07807	0,00192	0,61143	0,0582	0,02455	0,00602	0,53	485	12	485	37	490	119	100
SM173-1-o19	**c**	**0,13362**	**0,00934**	**0,0543**	**0,00146**	**0,96538**	**0,09978**	**0,02867**	**0,00728**	**0,71**	**341**	**9**	**686**	**52**	**571**	**143**	**49,7**
SM173-1-o20	c	0,05633	0,0038	0,07067	0,00174	0,53968	0,0487	0,02425	0,00396	0,55	440	10	438	32	484	78	100,5
~~**SM173-1-o21**~~		~~**0,0632**~~	~~**0,003**~~	~~**0,06653**~~	~~**0,00144**~~	~~**0,55756**~~	~~**0,03584**~~	~~**0,02278**~~	~~**0,00358**~~	~~**0,65**~~	~~**415**~~	~~**9**~~	~~**450**~~	~~**23**~~	~~**455**~~	~~**71**~~	~~**92,3**~~
SM173-1-o22	**ib**	**0,08017**	**0,00466**	**0,06623**	**0,00158**	**0,72972**	**0,05918**	**0,0296**	**0,00482**	**0,38**	**413**	**10**	**556**	**35**	**590**	**95**	**74,3**
~~SM173-1-o23~~		~~0,06085~~	~~0,00354~~	~~0,07803~~	~~0,00182~~	~~0,64293~~	~~0,05162~~	~~0,02346~~	~~0,00384~~	~~0,45~~	~~484~~	~~11~~	~~504~~	~~32~~	~~469~~	~~76~~	~~96,1~~
~~SM173-1-o24~~		~~0,05695~~	~~0,00318~~	~~0,07215~~	~~0,00164~~	~~0,57229~~	~~0,04332~~	~~0,02272~~	~~0,00368~~	~~0,61~~	~~449~~	~~10~~	~~460~~	~~28~~	~~454~~	~~73~~	~~97,7~~
SM173-1-o27	c	0,05512	0,00348	0,07348	0,00176	0,55026	0,04698	0,02319	0,00388	0,44	457	11	445	31	464	77	102,7
~~**SM173-1-o28**~~		~~**0,06875**~~	~~**0,00456**~~	~~**0,07457**~~	~~**0,00186**~~	~~**0,70498**~~	~~**0,06546**~~	~~**0,02621**~~	~~**0,0045**~~	~~**0,44**~~	~~**464**~~	~~**11**~~	~~**542**~~	~~**39**~~	~~**523**~~	~~**89**~~	~~**85,6**~~

Spot	Note	Isotopic ratios									Ages [Ma]						Conc.
		^{207}Pb/^{206}Pb	±2σ	^{206}Pb/^{238}U	±2σ	^{207}Pb/^{235}U	±2σ	^{208}Pb/^{232}Th	±2σ	^{232}Th/^{238}U	^{206}Pb/^{238}U	±2σ	^{207}Pb/^{235}U	±2σ	^{208}Pb/^{232}Th	±2σ	[%]
SM173-1 Vinica amphibolite (continued)																	
~~**SM173-1-o29**~~		~~**0,05885**~~	~~**0,0038**~~	~~**0,07046**~~	~~**0,0017**~~	~~**0,58829**~~	~~**0,05206**~~	~~**0,02377**~~	~~**0,00412**~~	~~**0,42**~~	~~**439**~~	~~**10**~~	~~**470**~~	~~**33**~~	~~**475**~~	~~**81**~~	~~**93,4**~~
~~SM173-1-o30~~		~~0,0584~~	~~0,00396~~	~~0,07738~~	~~0,00192~~	~~0,62521~~	~~0,05862~~	~~0,02374~~	~~0,00424~~	~~0,38~~	~~481~~	~~11~~	~~493~~	~~37~~	~~474~~	~~84~~	~~97,4~~
~~**SM173-1-o31**~~		~~**0,06342**~~	~~**0,00408**~~	~~**0,08358**~~	~~**0,00204**~~	~~**0,74666**~~	~~**0,06804**~~	~~**0,02894**~~	~~**0,00512**~~	~~**0,57**~~	~~**517**~~	~~**12**~~	~~**566**~~	~~**40**~~	~~**577**~~	~~**101**~~	~~**91,4**~~
SM173-3 Vinica leucocratic dyke																	
~~**SM173-3-o1**~~		~~**0,0996**~~	~~**0,0039**~~	~~**0,0567**~~	~~**0,0011**~~	~~**0,7635**~~	~~**0,0407**~~	~~**0,016**~~	~~**0,002**~~	~~**0,5345**~~	~~**356**~~	~~**7**~~	~~**576**~~	~~**23**~~	~~**322**~~	~~**40**~~	~~**61,7**~~
SM173-3-o2	r	0,0615	0,0028	0,0782	0,0016	0,6577	0,04	0,0242	0,0031	0,285	486	10	513	25	484	62	94,6
~~SM173-3-o3~~		~~0,0566~~	~~0,0029~~	~~0,0751~~	~~0,0016~~	~~0,5781~~	~~0,0393~~	~~0,0228~~	~~0,0029~~	~~0,5432~~	~~467~~	~~10~~	~~463~~	~~25~~	~~455~~	~~58~~	~~100,8~~
SM173-3-o4	r	0,0596	0,0024	0,0796	0,0016	0,6521	0,0355	0,0247	0,0031	0,4815	494	10	510	22	492	62	96,8
SM173-3-o6	ib	0,0636	0,0031	0,0895	0,0019	0,7512	0,051	0,0293	0,0039	0,3903	553	11	569	30	583	77	97,2
~~SM173-3-o7~~		~~0,0584~~	~~0,0028~~	~~0,0703~~	~~0,0015~~	~~0,556~~	~~0,036~~	~~0,0214~~	~~0,0029~~	~~0,6049~~	~~438~~	~~9~~	~~449~~	~~23~~	~~427~~	~~56~~	~~97,5~~
~~**SM173-3-o8**~~		~~**0,0691**~~	~~**0,0047**~~	~~**0,081**~~	~~**0,002**~~	~~**0,8028**~~	~~**0,0785**~~	~~**0,0239**~~	~~**0,0037**~~	~~**0,3355**~~	~~**502**~~	~~**12**~~	~~**598**~~	~~**44**~~	~~**477**~~	~~**73**~~	~~**83,9**~~
~~**SM173-3-o11**~~		~~**0,066**~~	~~**0,0033**~~	~~**0,0797**~~	~~**0,0017**~~	~~**0,7226**~~	~~**0,0511**~~	~~**0,0288**~~	~~**0,0041**~~	~~**0,4878**~~	~~**494**~~	~~**10**~~	~~**552**~~	~~**30**~~	~~**575**~~	~~**80**~~	~~**89,5**~~
~~SM173-3-o12~~		~~0,0609~~	~~0,0031~~	~~0,1019~~	~~0,0022~~	~~0,8564~~	~~0,0631~~	~~0,0306~~	~~0,0044~~	~~0,5758~~	~~626~~	~~13~~	~~628~~	~~35~~	~~608~~	~~86~~	~~99,6~~
SM173-3-o13		0,0603	0,0052	0,0878	0,0024	0,7287	0,0885	0,0283	0,0048	0,3197	542	14	556	52	564	95	97,6
~~SM173-3-o15~~		~~0,0573~~	~~0,0036~~	~~0,0756~~	~~0,0018~~	~~0,6057~~	~~0,0519~~	~~0,0229~~	~~0,0037~~	~~0,4064~~	~~470~~	~~11~~	~~481~~	~~33~~	~~458~~	~~73~~	~~97,8~~
SM173-3-o19	c	0,0596	0,0033	0,088	0,002	0,6984	0,0555	0,0227	0,0037	0,3392	544	12	538	33	454	74	101,1
~~**SM173-3-o21**~~		~~**0,064**~~	~~**0,0039**~~	~~**0,0786**~~	~~**0,0019**~~	~~**0,6758**~~	~~**0,058**~~	~~**0,0238**~~	~~**0,0041**~~	~~**0,2884**~~	~~**488**~~	~~**11**~~	~~**524**~~	~~**35**~~	~~**475**~~	~~**81**~~	~~**93**~~
SM173-3-o22	**c**	**0,0687**	**0,0033**	**0,059**	**0,0013**	**0,5337**	**0,0358**	**0,0204**	**0,0034**	**0,4236**	**369**	**8**	**434**	**24**	**408**	**68**	**85,1**
~~**SM173-3-o27**~~		~~**0,0634**~~	~~**0,0038**~~	~~**0,0757**~~	~~**0,0018**~~	~~**0,6669**~~	~~**0,056**~~	~~**0,0195**~~	~~**0,0034**~~	~~**0,5058**~~	~~**470**~~	~~**11**~~	~~**519**~~	~~**34**~~	~~**390**~~	~~**68**~~	~~**90,7**~~
~~**SM173-3-o28**~~		~~**0,084**~~	~~**0,0053**~~	~~**0,0762**~~	~~**0,0019**~~	~~**0,928**~~	~~**0,0879**~~	~~**0,0285**~~	~~**0,0052**~~	~~**0,4372**~~	~~**473**~~	~~**12**~~	~~**667**~~	~~**46**~~	~~**568**~~	~~**102**~~	~~**71**~~
SM173-3-o29	c	0,0598	0,0036	0,0891	0,0022	0,731	0,0644	0,026	0,0051	0,1471	550	13	557	38	518	100	98,8
~~SM173-3-o30~~		~~0,0583~~	~~0,0033~~	~~0,0832~~	~~0,002~~	~~0,6559~~	~~0,0529~~	~~0,0241~~	~~0,0045~~	~~0,4509~~	~~515~~	~~12~~	~~512~~	~~32~~	~~480~~	~~90~~	~~100,6~~
SM173-3-o31	**r**	**0,075**	**0,0038**	**0,0705**	**0,0016**	**0,7063**	**0,052**	**0,0261**	**0,005**	**0,574**	**439**	**10**	**543**	**31**	**520**	**99**	**80,9**
~~SM173-3-o32~~		~~0,0612~~	~~0,0038~~	~~0,0721~~	~~0,0018~~	~~0,5959~~	~~0,0536~~	~~0,0251~~	~~0,0051~~	~~0,3892~~	~~449~~	~~11~~	~~475~~	~~34~~	~~501~~	~~100~~	~~94,6~~
SM173-3-o33	**c**	**0,0679**	**0,0029**	**0,0783**	**0,0017**	**0,7339**	**0,0419**	**0,0269**	**0,0029**	**0,312**	**486**	**10**	**559**	**25**	**537**	**57**	**87**
~~SM173-3-o24~~		~~0,059~~	~~0,003~~	~~0,0835~~	~~0,0019~~	~~0,6715~~	~~0,0455~~	~~0,0254~~	~~0,0028~~	~~0,3534~~	~~517~~	~~11~~	~~522~~	~~28~~	~~507~~	~~56~~	~~99,1~~

Spot	Note	Isotopic ratios									Ages [Ma]						Conc.
		^{207}Pb/^{206}Pb	±2σ	^{206}Pb/^{238}U	±2σ	^{207}Pb/^{235}U	±2σ	^{208}Pb/^{232}Th	±2σ	^{232}Th/^{238}U	^{206}Pb/^{238}U	±2σ	^{207}Pb/^{235}U	±2σ	^{208}Pb/^{232}Th	±2σ	[%]
SM184-1 Maleševski Mts. orthogneiss																	
SM184-1-o6	r	0,0616	0,0029	0,1027	0,0023	0,8722	0,0564	0,0323	0,0042	0,2293	631	13	637	31	643	82	99
SM184-1-o7	c	0,0602	0,0046	0,106	0,0029	0,8949	0,1008	0,0294	0,0044	0,4971	649	17	649	54	585	86	100
SM184-1-o10	**ib**	**0,0749**	**0,0073**	**0,0873**	**0,0028**	**0,9479**	**0,1364**	**0,0314**	**0,005**	**0,7163**	**540**	**17**	**677**	**71**	**625**	**98**	**79,7**
SM184-1-o11	**c**	**0,0761**	**0,0065**	**0,1023**	**0,0031**	**1,0349**	**0,1327**	**0,0325**	**0,0051**	**0,9945**	**628**	**18**	**721**	**66**	**647**	**99**	**87**
SM184-1-o12	c	0,0992	0,0052	0,2751	0,0067	3,6793	0,348	0,0772	0,0117	2,27	1567	34	1567	76	1502	220	100
SM184-1-o13	**c**	**0,1352**	**0,0062**	**0,2517**	**0,0056**	**4,5689**	**0,3001**	**0,0778**	**0,0125**	**0,0423**	**1447**	**29**	**1744**	**55**	**1514**	**234**	**83**
SM184-1-o14	ib	0,0589	0,0048	0,0842	0,0023	0,6853	0,0777	0,0336	0,0067	0,1145	521	14	530	47	668	131	98,3
SM184-1-o15	ib	0,0597	0,0044	0,0949	0,0025	0,772	0,0808	0,0275	0,0049	0,3475	584	15	581	46	548	97	100,6
~~SM184-1-o16~~		~~0,0566~~	~~0,0041~~	~~0,0803~~	~~0,0021~~	~~0,6145~~	~~0,062~~	~~0,0254~~	~~0,0051~~	~~0,1105~~	~~498~~	~~13~~	~~486~~	~~39~~	~~506~~	~~102~~	~~102,3~~
SM184-1-o17a	c	0,0654	0,0057	0,1325	0,0039	1,2252	0,166	0,0374	0,0068	1,2759	802	22	812	76	743	133	98,8
SM184-1-o17b	r	0,055	0,003	0,0756	0,0017	0,5725	0,0413	0,0245	0,0039	0,0559	470	10	460	27	490	78	102,2
SM184-1-o18	r	0,0559	0,0031	0,0752	0,0018	0,5773	0,0427	0,0431	0,0115	0,01	468	11	463	27	852	223	101,1
SM184-1-o19a	c	0,0565	0,0037	0,076	0,0019	0,5939	0,0516	0,0217	0,0027	0,4673	472	11	473	33	434	53	99,8
SM184-1-o19b	r	0,055	0,0036	0,0753	0,0019	0,5809	0,0505	0,022	0,003	0,257	468	11	465	32	440	59	100,6
SM184-1-o22	ib	0,0557	0,0038	0,0851	0,0022	0,6709	0,0629	0,0238	0,0032	0,3182	527	13	521	38	475	64	101
~~SM184-1-o23~~		~~0,0552~~	~~0,0039~~	~~0,0892~~	~~0,0023~~	~~0,7205~~	~~0,0722~~	~~0,0274~~	~~0,0038~~	~~0,327~~	~~551~~	~~14~~	~~551~~	~~43~~	~~547~~	~~75~~	~~100~~
SM184-1-o24	c	0,0564	0,0041	0,0958	0,0025	0,7445	0,0757	0,029	0,004	0,4537	590	15	565	44	578	78	104,4
SM184-1-o25	c	0,0577	0,0036	0,0796	0,002	0,6288	0,0535	0,0247	0,0033	0,4357	494	12	495	33	493	66	99,7
SM184-1-o26	c	0,0586	0,0041	0,0768	0,002	0,6197	0,0592	0,0235	0,0032	0,857	477	12	490	37	470	63	97,4
SM184-1-o27	c	0,0591	0,0033	0,0914	0,0022	0,7431	0,0579	0,0277	0,004	0,263	564	13	564	34	553	78	100
SM184-1-o28	c	0,0565	0,0036	0,077	0,0019	0,5913	0,0513	0,0222	0,0034	0,3004	478	11	472	33	444	68	101,4
SM184-1-o29	c	0,0583	0,0028	0,0915	0,0021	0,7461	0,0507	0,0281	0,0042	0,3695	564	12	566	30	559	82	99,7
SM184-1-o30	c	0,0633	0,0062	0,0681	0,0021	0,542	0,0698	0,0264	0,0047	0,3707	425	13	440	46	527	92	96,5
~~SM184-1-o31~~	~~r~~	~~0,0564~~	~~0,0035~~	~~0,0839~~	~~0,0021~~	~~0,6566~~	~~0,0564~~	~~0,0317~~	~~0,0054~~	~~0,1747~~	~~520~~	~~12~~	~~513~~	~~35~~	~~630~~	~~105~~	~~101,4~~
~~SM184-1-o32~~		~~0,0591~~	~~0,0041~~	~~0,0967~~	~~0,0025~~	~~0,7717~~	~~0,0763~~	~~0,0294~~	~~0,0048~~	~~1,653~~	~~595~~	~~15~~	~~581~~	~~44~~	~~585~~	~~95~~	~~102,4~~
SM184-1-o33	ib	0,0537	0,0051	0,085	0,0025	0,6724	0,0888	0,0296	0,0057	0,3141	526	15	522	54	589	111	100,7
SM184-1-o34	c	0,0673	0,0056	0,1412	0,0042	1,2996	0,1755	0,0396	0,0078	0,3733	851	24	846	78	785	151	100,7

Spot	Note	Isotopic ratios									Ages [Ma]						Conc.
		^{207}Pb/^{206}Pb	±2σ	^{206}Pb/^{238}U	±2σ	^{207}Pb/^{235}U	±2σ	^{208}Pb/^{232}Th	±2σ	^{232}Th/^{238}U	^{206}Pb/^{238}U	±2σ	^{207}Pb/^{235}U	±2σ	^{208}Pb/^{232}Th	±2σ	[%]
SM195-1 Granite from the Štip magmatic complex																	
SM195-1-1sw	**c**	**0,0572**	**0,0017**	**0,04885**	**0,00033**	**0,389**	**0,011**	**0,01702**	**0,00034**	**0,88**	**307**	**2**	**333**	**8**	**341**	**7**	**92,4**
SM195-1-1ne	ib	0,05306	0,00083	0,04826	0,00031	0,358	0,0056	0,01575	0,00027	0,35	304	2	310	4	316	5	97,9
SM195-1-2c	**c**	**0,0563**	**0,0022**	**0,05639**	**0,00071**	**0,5**	**0,02**	**0,01928**	**0,0008**	**0,56**	**354**	**4**	**410**	**14**	**386**	**16**	**86,2**
SM195-1-2se	r	0,056	0,0016	0,06026	0,00058	0,471	0,014	0,02251	0,00057	0,64	377	4	391	10	450	11	96,5
SM195-1-3	c	0,052	0,0014	0,05497	0,00044	0,399	0,011	0,01785	0,00079	0,23	345	3	340	8	357	16	101,5
SM195-1-4c	c	0,0553	0,0016	0,0713	0,00068	0,553	0,016	0,02217	0,00061	0,59	444	4	445	11	443	12	99,8
SM195-1-4e	r	0,0561	0,0012	0,07345	0,00081	0,575	0,013	0,02132	0,00095	0,15	457	5	461	8	426	19	99,2
SM195-1-5	c	0,0524	0,0015	0,05597	0,00052	0,408	0,011	0,01695	0,00073	0,3	351	3	346	8	339	15	101,5
~~SM195-1-6~~		~~0,0605~~	~~0,0015~~	~~0,09018~~	~~0,00088~~	~~0,761~~	~~0,019~~	~~0,035~~	~~0,0012~~	~~0,21~~	~~557~~	~~5~~	~~573~~	~~11~~	~~695~~	~~24~~	~~97,1~~
SM195-1-7	**c**	**0,0707**	**0,0045**	**0,04977**	**0,00064**	**0,486**	**0,029**	**0,01948**	**0,00093**	**1,45**	**313**	**4**	**398**	**19**	**390**	**18**	**78,7**
SM195-1-8		0,054	0,0015	0,0499	0,00045	0,374	0,011	0,01642	0,00028	1,66	314	3	322	8	329	6	97,6
SM195-1-9	**c**	**0,16218**	**0,00087**	**0,401**	**0,0022**	**9,015**	**0,063**	**0,1214**	**0,0023**	**0,09**	**2173**	**10**	**2339**	**6**	**2315**	**42**	**92,9**
SM195-1-10n	c	0,07006	0,00089	0,1536	0,0012	1,494	0,021	0,04684	0,00069	0,56	921	7	926	9	925	13	99,4
SM195-1-10s	c	0,0702	0,0012	0,1547	0,0013	1,5	0,026	0,04813	0,00098	0,63	927	7	928	11	950	19	99,9
SM195-1-11wc	c	0,0524	0,001	0,04952	0,00039	0,3579	0,0071	0,01626	0,00019	2,48	312	2	310	5	326	4	100,5
SM195-1-11ne	r	0,05343	0,00059	0,04926	0,00047	0,3595	0,0049	0,01888	0,00043	0,15	310	3	312	4	378	9	99,5
~~SM195-1-12c~~		~~0,0584~~	~~0,0014~~	~~0,07224~~	~~0,00093~~	~~0,583~~	~~0,014~~	~~0,0232~~	~~0,0013~~	~~0,22~~	~~450~~	~~6~~	~~466~~	~~9~~	~~463~~	~~26~~	~~96,4~~
SM195-1-12n	r	0,057	0,0012	0,0733	0,00062	0,571	0,011	0,02481	0,00085	0,22	456	4	459	8	495	17	99,3
SM195-1-12frag		0,0557	0,0011	0,06845	0,00063	0,525	0,011	0,02195	0,00058	0,34	427	4	428	7	439	11	99,6
SM195-1-13	c	0,0522	0,0014	0,05149	0,0005	0,3687	0,0097	0,01659	0,00034	0,56	324	3	318	7	333	7	101,8
SM195-1-14c	c	0,1149	0,0013	0,3282	0,0031	5,158	0,075	0,1	0,0016	0,57	1829	15	1844	12	1926	29	99,2
SM195-1-14s	r	0,0577	0,0013	0,0761	0,0018	0,602	0,019	0,009	0,0011	0,1	472	11	476	12	183	21	99,2
SM195-1-15n	r	0,0525	0,0012	0,04947	0,00036	0,3555	0,008	0,01699	0,00039	0,58	311	2	308	6	340	8	101
SM195-1-15s	c	0,0514	0,0015	0,04944	0,00048	0,348	0,01	0,01614	0,00041	0,61	311	3	302	8	324	8	102,9
SM195-1-17ne	r	0,0521	0,0012	0,04863	0,00039	0,3484	0,0085	0,016	0,00037	0,66	306	2	303	6	321	7	101
~~SM195-1-17c~~		~~0,0534~~	~~0,0012~~	~~0,05495~~	~~0,00058~~	~~0,4032~~	~~0,0092~~	~~0,02176~~	~~0,00059~~	~~0,28~~	~~345~~	~~4~~	~~345~~	~~6~~	~~435~~	~~12~~	~~100,1~~
SM195-1-18nw	r	0,05263	0,00055	0,04812	0,00026	0,3474	0,0039	0,01613	0,00018	0,5	303	2	303	3	324	4	100,1

Spot	Note	Isotopic ratios									Ages [Ma]						Conc.
		^{207}Pb/^{206}Pb	±2σ	^{206}Pb/^{238}U	±2σ	^{207}Pb/^{235}U	±2σ	^{208}Pb/^{232}Th	±2σ	^{232}Th/^{238}U	^{206}Pb/^{238}U	±2σ	^{207}Pb/^{235}U	±2σ	^{208}Pb/^{232}Th	±2σ	[%]
SM195-1 Granite from the Štip magmatic complex (continued)																	
SM195-1-18c	c	0,0606	0,001	0,0992	0,0015	0,823	0,019	0,03414	0,00061	0,59	610	9	609	10	678	12	100,1
SM195-1-19sw	ib	0,0515	0,0017	0,04679	0,0004	0,33	0,011	0,01562	0,00046	0,4	295	3	288	8	313	9	102,3
SM195-1-19c	c	0,0683	0,0018	0,1348	0,0014	1,256	0,032	0,0452	0,0012	0,71	815	8	823	14	893	23	99
SM195-1-20	c	0,0637	0,0015	0,09471	0,00083	0,823	0,018	0,03486	0,00092	0,47	583	5	608	10	692	18	95,9
~~SM195-1-21sw~~		~~0,052~~	~~0,0013~~	~~0,05113~~	~~0,00041~~	~~0,3654~~	~~0,0094~~	~~0,01729~~	~~0,00037~~	~~0,77~~	~~321~~	~~3~~	~~315~~	~~7~~	~~346~~	~~7~~	~~101,9~~
SM195-1-21ne	**r**	**0,0571**	**0,0016**	**0,05058**	**0,00055**	**0,396**	**0,013**	**0,02056**	**0,00088**	**0,4**	**318**	**3**	**338**	**9**	**411**	**17**	**94,2**
SM195-1-22	c	0,0561	0,0014	0,0776	0,00061	0,598	0,016	0,02537	0,00097	0,34	482	4	474	10	506	19	101,7
SM195-1-23	c	0,0554	0,0019	0,0715	0,001	0,542	0,02	0,0229	0,00061	1,22	445	6	437	13	458	12	101,9
SM195-1-24s	c	0,0533	0,0016	0,04711	0,00047	0,344	0,011	0,01705	0,00031	1,97	297	3	300	8	342	6	99
SM195-1-24n	r	0,05326	0,0006	0,04508	0,00032	0,3292	0,0043	0,01732	0,00044	0,09	284	2	289	3	347	9	98,4
SM195-1-25e	**c**	**0,1694**	**0,0023**	**0,3119**	**0,0031**	**8,16**	**0,13**	**0,1055**	**0,0018**	**1,37**	**1750**	**15**	**2247**	**14**	**2026**	**33**	**77,9**
~~**SM195-1-25nw**~~		~~**0,1404**~~	~~**0,0016**~~	~~**0,2009**~~	~~**0,0022**~~	~~**3,867**~~	~~**0,06**~~	~~**0,0536**~~	~~**0,0013**~~	~~**0,57**~~	~~**1180**~~	~~**12**~~	~~**1607**~~	~~**13**~~	~~**1055**~~	~~**25**~~	~~**73,4**~~
SM195-1-26	**r**	**0,0656**	**0,0011**	**0,04646**	**0,00064**	**0,419**	**0,0095**	**0,01439**	**0,00038**	**0,71**	**293**	**4**	**355**	**7**	**289**	**8**	**82,5**
~~SM195-1-27sw~~		~~0,0564~~	~~0,00094~~	~~0,06973~~	~~0,00041~~	~~0,5399~~	~~0,0087~~	~~0,0259~~	~~0,003~~	~~0,02~~	~~435~~	~~3~~	~~438~~	~~6~~	~~514~~	~~60~~	~~99,3~~
SM195-1-27c	c	0,06079	0,0008	0,09777	0,00088	0,817	0,011	0,0314	0,00042	1,66	601	5	606	6	625	8	99,2
~~SM195-1-28e~~		~~0,052~~	~~0,0012~~	~~0,04864~~	~~0,00035~~	~~0,3472~~	~~0,0075~~	~~0,01563~~	~~0,0002~~	~~2,14~~	~~306~~	~~2~~	~~302~~	~~6~~	~~313~~	~~4~~	~~101,4~~
SM195-1-28w	c	0,0515	0,0014	0,04749	0,00045	0,3362	0,0089	0,0158	0,00021	2,97	299	3	293	7	317	4	101,9
SM195-1-29	**c**	**0,1502**	**0,0068**	**0,2422**	**0,0057**	**5,6**	**0,26**	**0,0802**	**0,0033**	**2,32**	**1397**	**30**	**1901**	**42**	**1557**	**62**	**73,5**
SM195-1-30ne	r	0,05609	0,00099	0,07233	0,00056	0,559	0,01	0,02	0,0048	0,01	450	3	450	7	392	94	100,1
SM195-1-30c	c	0,1756	0,0014	0,4605	0,0028	11,188	0,094	0,1291	0,0017	0,46	2441	12	2538	8	2457	30	96,2
~~SM195-1-31~~		~~0,05715~~	~~0,0006~~	~~0,07487~~	~~0,00059~~	~~0,5911~~	~~0,0069~~	~~0,02488~~	~~0,00046~~	~~0,24~~	~~465~~	~~4~~	~~471~~	~~4~~	~~497~~	~~9~~	~~98,8~~
SM195-1-32ne	c	0,0563	0,0011	0,07414	0,00044	0,578	0,012	0,0238	0,00085	0,15	461	3	462	8	475	17	99,7
SM195-1-32sw	ib	0,0568	0,0013	0,07521	0,00058	0,592	0,014	0,02283	0,00055	0,63	467	4	471	9	456	11	99,3
SM195-1-33	c	0,05991	0,0008	0,0907	0,0008	0,7537	0,0099	0,02726	0,0004	0,37	560	5	570	6	544	8	98,2
SM195-1-34	r	0,05246	0,00071	0,04718	0,00041	0,3434	0,005	0,01445	0,00025	0,66	297	3	300	4	290	5	99
SM195-1-35	**c**	**0,0764**	**0,0015**	**0,143**	**0,0015**	**1,668**	**0,037**	**0,04822**	**0,00073**	**1,91**	**861**	**9**	**994**	**14**	**954**	**15**	**86,7**
SM195-1-36	c	0,05257	0,00068	0,04847	0,00044	0,3539	0,0055	0,01437	0,00014	2,03	305	3	307	4	288	3	99,3

Spot	Note	Isotopic ratios									Ages [Ma]						Conc.
		$^{207}Pb/^{206}Pb$	±2σ	$^{206}Pb/^{238}U$	±2σ	$^{207}Pb/^{235}U$	±2σ	$^{208}Pb/^{232}Th$	±2σ	$^{232}Th/^{238}U$	$^{206}Pb/^{238}U$	±2σ	$^{207}Pb/^{235}U$	±2σ	$^{208}Pb/^{232}Th$	±2σ	[%]
SM195-1 Granite from the Štip magmatic complex (continued)																	
~~SM195-1-37~~		~~0,05893~~	~~0,00081~~	~~0,08601~~	~~0,00054~~	~~0,7025~~	~~0,0099~~	~~0,03003~~	~~0,0005~~	~~0,34~~	~~532~~	~~3~~	~~540~~	~~6~~	~~598~~	~~10~~	~~98,6~~
SM195-1-38c	**c**	**0,0983**	**0,0019**	**0,1598**	**0,0025**	**2,192**	**0,062**	**0,0415**	**0,0011**	**0,69**	**955**	**14**	**1176**	**20**	**822**	**22**	**81,2**
SM195-1-38ne	r	0,0579	0,001	0,07033	0,00078	0,5648	0,0098	0,02	0,0012	0,06	438	5	454	6	400	23	96,4
SM195-1-39	**c**	**0,0592**	**0,0024**	**0,074**	**0,0011**	**0,667**	**0,027**	**0,0252**	**0,00056**	**1,68**	**460**	**6**	**515**	**16**	**503**	**11**	**89,4**
SM195-1-40	c	0,0509	0,0014	0,0463	0,00046	0,3257	0,009	0,0085	0,0034	0,01	292	3	286	7	166	69	101,9
SM195-1-41	c	0,052	0,0031	0,05383	0,00078	0,387	0,024	0,01625	0,00068	1,07	338	5	332	17	326	14	101,8
SM195-1-o1	ib	0,0594	0,00238	0,07951	0,00176	0,65388	0,03454	0,02501	0,00294	0,07	493	10	511	21	499	58	96,5
SM195-1-o2	c	0,05388	0,00246	0,05048	0,00114	0,37374	0,02138	0,01589	0,00164	1,52	318	7	322	16	319	32	98,5
SM195-1-o3		0,05389	0,0029	0,05132	0,0012	0,37663	0,02534	0,016	0,00178	0,41	323	7	325	19	321	35	99,4
~~**SM195-1-o4**~~		~~**0,04962**~~	~~**0,00264**~~	~~**0,05183**~~	~~**0,0012**~~	~~**0,3473**~~	~~**0,02296**~~	~~**0,01637**~~	~~**0,00182**~~	~~**0,44**~~	~~**326**~~	~~**7**~~	~~**303**~~	~~**17**~~	~~**328**~~	~~**36**~~	~~**107,6**~~
SM195-1-o5	c	0,06049	0,00406	0,11386	0,00296	0,97839	0,09694	0,0318	0,00416	0,3	695	17	693	50	633	81	100,4
~~SM195-1-o7~~		~~0,06974~~	~~0,0042~~	~~0,14511~~	~~0,0037~~	~~1,36894~~	~~0,131~~	~~0,05077~~	~~0,0058~~	~~0,71~~	~~874~~	~~21~~	~~876~~	~~56~~	~~1001~~	~~111~~	~~99,8~~
~~SM195-1-o10~~		~~0,06091~~	~~0,00424~~	~~0,10264~~	~~0,00272~~	~~0,85319~~	~~0,08514~~	~~0,03042~~	~~0,00462~~	~~0,17~~	~~630~~	~~16~~	~~626~~	~~47~~	~~606~~	~~90~~	~~100,6~~
SM195-1-o8	**c**	**0,0691**	**0,00544**	**0,07656**	**0,00218**	**0,74264**	**0,08148**	**0,02626**	**0,0034**	**0,51**	**476**	**13**	**564**	**47**	**524**	**67**	**84,3**
SM195-1-o11	c	0,05117	0,00318	0,05063	0,00124	0,35889	0,02782	0,01551	0,0019	0,52	318	8	311	21	311	38	102,3
SM195-1-o12	**c**	**0,06196**	**0,00254**	**0,04573**	**0,00102**	**0,38741**	**0,02064**	**0,01641**	**0,00192**	**0,79**	**288**	**6**	**333**	**15**	**329**	**38**	**86,7**
SM195-1-o13	c	0,05207	0,00326	0,05277	0,0013	0,37705	0,02974	0,01599	0,00204	0,44	332	8	325	22	321	41	102
SM195-1-o14	c	0,05757	0,00828	0,08703	0,00348	0,69697	0,13866	0,02682	0,00534	0,35	538	21	537	83	535	105	100,2
~~SM195-1-o16~~		~~0,05736~~	~~0,0029~~	~~0,09043~~	~~0,0021~~	~~0,73556~~	~~0,05098~~	~~0,02781~~	~~0,00352~~	~~0,59~~	~~558~~	~~12~~	~~560~~	~~30~~	~~555~~	~~69~~	~~99,7~~
SM195-1-o18	r	0,05219	0,00346	0,04682	0,00118	0,33557	0,02774	0,01473	0,00214	0,23	295	7	294	21	296	42	100,4
SM195-1-o19	c	0,05235	0,00306	0,05271	0,00126	0,39066	0,02924	0,01566	0,00208	0,59	331	8	335	21	314	42	98,9
~~SM195-1-o20~~		~~0,05485~~	~~0,0032~~	~~0,04462~~	~~0,00108~~	~~0,33909~~	~~0,02506~~	~~0,01466~~	~~0,00198~~	~~0,66~~	~~281~~	~~7~~	~~297~~	~~19~~	~~294~~	~~39~~	~~94,9~~
~~SM195-1-o21~~		~~0,05564~~	~~0,00268~~	~~0,04459~~	~~0,00102~~	~~0,32882~~	~~0,02064~~	~~0,0148~~	~~0,00208~~	~~0,16~~	~~281~~	~~6~~	~~289~~	~~16~~	~~297~~	~~41~~	~~97,4~~
~~SM195-1-o22~~		~~0,05127~~	~~0,00302~~	~~0,04678~~	~~0,00112~~	~~0,33756~~	~~0,02538~~	~~0,01539~~	~~0,00222~~	~~0,33~~	~~295~~	~~7~~	~~295~~	~~19~~	~~309~~	~~44~~	~~99,8~~
SM195-1-o23	c	0,05851	0,00402	0,09931	0,00258	0,79132	0,0768	0,03105	0,00484	0,44	610	15	592	44	618	95	103,1
SM195-1-o24	c	0,05255	0,00608	0,06798	0,00228	0,53022	0,08064	0,02151	0,00378	0,51	424	14	432	54	430	75	98,1
SM195-1-o25	c	0,0531	0,00458	0,06039	0,0017	0,4479	0,04986	0,01863	0,00302	0,72	378	10	376	35	373	60	100,6

Spot	Note	Isotopic ratios									Ages [Ma]						Conc.
		^{207}Pb/^{206}Pb	±2σ	^{206}Pb/^{238}U	±2σ	^{207}Pb/^{235}U	±2σ	^{208}Pb/^{232}Th	±2σ	^{232}Th/^{238}U	^{206}Pb/^{238}U	±2σ	^{207}Pb/^{235}U	±2σ	^{208}Pb/^{232}Th	±2σ	[%]
SM195-1 Granite from the Štip magmatic complex (continued)																	
~~**SM195-1-o26**~~		~~**0,05756**~~	~~**0,00302**~~	~~**0,04275**~~	~~**0,001**~~	~~**0,33295**~~	~~**0,0232**~~	~~**0,01514**~~	~~**0,00242**~~	~~**0,2**~~	~~**270**~~	~~**6**~~	~~**292**~~	~~**18**~~	~~**304**~~	~~**48**~~	~~**92,5**~~
SM195-1-o27	ib	0,05394	0,00276	0,05325	0,00124	0,39973	0,02762	0,01511	0,00244	0,2	335	8	341	20	303	49	98
SM195-1-o28	c	0,05464	0,00274	0,05042	0,00116	0,3801	0,02602	0,01744	0,00286	0,16	317	7	327	19	350	57	96,9
SM195-1-o30	c	0,05306	0,00312	0,04837	0,00118	0,35563	0,02776	0,01454	0,00244	0,67	305	7	309	21	292	48	98,6
~~SM195-1-o31~~		~~0,05523~~	~~0,00414~~	~~0,04831~~	~~0,00128~~	~~0,35209~~	~~0,03392~~	~~0,01574~~	~~0,0028~~	~~0,38~~	~~304~~	~~8~~	~~306~~	~~25~~	~~316~~	~~56~~	~~99,3~~
SM199-1 undeformed Bujanovac granite (central part)																	
SM199-1-1	r	0,0513	0,001	0,04004	0,00027	0,2892	0,0056	0,01288	0,00022	0,68	253	2	258	4	259	4	98,3
~~**SM199-1-22c**~~		~~**0,0633**~~	~~**0,0035**~~	~~**0,0825**~~	~~**0,001**~~	~~**0,728**~~	~~**0,045**~~	~~**0,029**~~	~~**0,0017**~~	~~**0,76**~~	~~**511**~~	~~**6**~~	~~**556**~~	~~**26**~~	~~**578**~~	~~**33**~~	~~**91,9**~~
SM199-1-22ne	r	0,0503	0,0028	0,03996	0,00062	0,281	0,016	0,01488	0,00091	0,41	253	4	250	13	298	18	101
SM199-1-30	r	0,0518	0,0011	0,0384	0,00032	0,2777	0,0058	0,01264	0,00022	0,61	243	2	249	5	254	4	97,8
SM199-1-36	r	0,05642	0,0007	0,07185	0,00054	0,5657	0,0073	0,02282	0,00027	0,89	447	3	455	5	456	5	98,3
SM199-1-37	r	0,05157	0,0008	0,03902	0,00027	0,2737	0,0044	0,01213	0,00016	0,61	247	2	246	4	244	3	100,5
SM199-1-40	r	0,05233	0,00068	0,04312	0,00032	0,3071	0,0042	0,01369	0,00018	0,53	272	2	272	3	275	4	100,2
SM199-1-42	c	0,05704	0,00078	0,07465	0,00052	0,5736	0,0081	0,02281	0,00029	0,89	464	3	460	5	456	6	100,9
SM199-1-o1	r	0,0532	0,00308	0,04192	0,00112	0,2975	0,02232	0,01304	0,00238	0,35	265	7	264	17	262	48	100,2
SM199-1-o2	**r**	**0,0605**	**0,00354**	**0,07394**	**0,00198**	**0,61965**	**0,0486**	**0,02288**	**0,00428**	**0,46**	**460**	**12**	**490**	**30**	**457**	**85**	**93,9**
SM199-1-o5	c	0,05514	0,00356	0,07267	0,002	0,55422	0,04772	0,02212	0,00428	0,48	452	12	448	31	442	85	101
SM199-1-o7	ib	0,05632	0,00362	0,07416	0,00204	0,5512	0,04716	0,02188	0,00434	0,44	461	12	446	31	438	86	103,5
SM199-1-o8	**c**	**0,11357**	**0,00692**	**0,28523**	**0,00802**	**4,42158**	**0,44334**	**0,08888**	**0,0183**	**0,3**	**1618**	**40**	**1716**	**83**	**1721**	**340**	**94,2**
SM199-1-o9	r	0,05588	0,00224	0,07417	0,00184	0,57635	0,02962	0,02321	0,00198	0,46	461	11	462	19	464	39	99,8
SM199-1-o10	ib	0,05557	0,00228	0,07563	0,00188	0,57987	0,03056	0,02278	0,00208	0,23	470	11	464	20	455	41	101,2
SM199-1-o11		**0,04642**	**0,004**	**0,04009**	**0,00118**	**0,2491**	**0,02442**	**0,01244**	**0,00152**	**0,28**	**253**	**7**	**226**	**20**	**250**	**30**	**112,2**
~~**SM199-1-o12a**~~		~~**0,0632**~~	~~**0,00442**~~	~~**0,07621**~~	~~**0,0022**~~	~~**0,68235**~~	~~**0,06316**~~	~~**0,02615**~~	~~**0,00262**~~	~~**0,52**~~	~~**473**~~	~~**13**~~	~~**528**~~	~~**38**~~	~~**522**~~	~~**52**~~	~~**89,6**~~
SM199-1-o12b	ib	0,05701	0,00308	0,07592	0,002	0,60282	0,04212	0,02269	0,00204	0,64	472	12	479	27	453	40	98,5
SM199-1-o13	ib	0,05596	0,00334	0,07451	0,002	0,57027	0,0437	0,02281	0,0022	0,45	463	12	458	28	456	43	101,1
SM199-1-o15	ib	0,05109	0,00268	0,03946	0,00102	0,2779	0,01714	0,01264	0,00122	0,27	250	6	249	14	254	24	100,2
SM199-1-o17	**r**	**0,05384**	**0,00502**	**0,03873**	**0,0012**	**0,29137**	**0,03128**	**0,01219**	**0,00136**	**0,53**	**245**	**7**	**260**	**25**	**245**	**27**	**94,4**

Spot	Note	Isotopic ratios									Ages [Ma]						Conc.
		$^{207}Pb/^{206}Pb$	±2σ	$^{206}Pb/^{238}U$	±2σ	$^{207}Pb/^{235}U$	±2σ	$^{208}Pb/^{232}Th$	±2σ	$^{232}Th/^{238}U$	$^{206}Pb/^{238}U$	±2σ	$^{207}Pb/^{235}U$	±2σ	$^{208}Pb/^{232}Th$	±2σ	[%]
SM199-1 undeformed Bujanovac granite (central part; continued)																	
SM199-1-o18	ib	0,05571	0,00724	0,09511	0,00364	0,78611	0,1399	0,02767	0,00338	0,86	586	21	589	80	552	67	99,4
~~SM199-1-o19~~		~~0,05383~~	~~0,00308~~	~~0,0588~~	~~0,00156~~	~~0,44433~~	~~0,03144~~	~~0,0172~~	~~0,00172~~	~~0,32~~	~~368~~	~~9~~	~~373~~	~~22~~	~~345~~	~~34~~	~~98,7~~
SM236-1 Bosilegrad monzonite																	
SM236-1-2	c	0,0578	0,0013	0,087	0,00087	0,669	0,016	0,026	0,00046	0,57	538	5	519	10	519	9	103,5
SM236-1-3	c	0,0577	0,0019	0,0878	0,0013	0,669	0,02	0,0282	0,0014	0,3	543	8	519	12	563	28	104,6
SM236-1-15	c	0,0587	0,0011	0,08676	0,00069	0,676	0,013	0,0263	0,00063	0,36	536	4	523	8	525	12	102,5
SM236-1-16	c	0,0588	0,0018	0,0958	0,0011	0,753	0,024	0,0275	0,001	0,35	590	6	569	13	548	20	103,7
~~**SM236-1-17**~~		~~**0,0565**~~	~~**0,0021**~~	~~**0,092**~~	~~**0,0011**~~	~~**0,683**~~	~~**0,027**~~	~~**0,0269**~~	~~**0,0011**~~	~~**0,68**~~	~~**567**~~	~~**6**~~	~~**531**~~	~~**15**~~	~~**536**~~	~~**23**~~	~~**106,9**~~
SM236-1-18	r	0,0576	0,0015	0,0878	0,001	0,678	0,018	0,028	0,001	0,46	543	6	525	11	558	20	103,4
~~**SM236-1-19**~~		~~**0,05847**~~	~~**0,00092**~~	~~**0,06274**~~	~~**0,00045**~~	~~**0,5413**~~	~~**0,0085**~~	~~**0,02154**~~	~~**0,00031**~~	~~**0,58**~~	~~**392**~~	~~**3**~~	~~**439**~~	~~**6**~~	~~**431**~~	~~**6**~~	~~**89,4**~~
~~**SM236-1-21**~~		~~**0,065**~~	~~**0,0029**~~	~~**0,0824**~~	~~**0,0014**~~	~~**0,714**~~	~~**0,032**~~	~~**0,0288**~~	~~**0,0013**~~	~~**0,5**~~	~~**511**~~	~~**8**~~	~~**545**~~	~~**19**~~	~~**573**~~	~~**26**~~	~~**93,7**~~
SM236-1-22	c	0,0581	0,00066	0,08664	0,00071	0,678	0,0086	0,0272	0,00039	0,91	536	4	525	5	543	8	102
SM236-1-23	r	0,05793	0,00091	0,08761	0,00058	0,684	0,011	0,02628	0,00058	0,4	541	3	528	7	524	11	102,5
SM236-1-24s	c	0,0566	0,0016	0,08649	0,00085	0,663	0,018	0,02599	0,00092	0,46	535	5	514	11	518	18	104
SM236-1-24n	r	0,05761	0,00093	0,08573	0,00065	0,669	0,011	0,02731	0,00056	0,33	530	4	519	7	545	11	102,1
SM236-1-25	r	0,0573	0,0012	0,08444	0,00069	0,665	0,014	0,0273	0,00068	0,34	523	4	518	9	544	13	100,8
~~SM236-1-26~~		~~0,05895~~	~~0,0007~~	~~0,07451~~	~~0,00056~~	~~0,6067~~	~~0,0076~~	~~0,02497~~	~~0,0003~~	~~0,72~~	~~463~~	~~3~~	~~481~~	~~5~~	~~498~~	~~6~~	~~96,3~~
SM236-1-27	**r**	**0,066**	**0,0024**	**0,08567**	**0,00089**	**0,782**	**0,027**	**0,0331**	**0,0013**	**0,49**	**530**	**5**	**588**	**17**	**657**	**26**	**90,1**
SM236-1-29	r	0,0607	0,0015	0,08501	0,00087	0,716	0,02	0,03116	0,00097	0,34	526	5	546	12	620	19	96,3
~~SM236-1-30~~		~~0,0578~~	~~0,001~~	~~0,08051~~	~~0,00071~~	~~0,645~~	~~0,012~~	~~0,02753~~	~~0,00083~~	~~0,17~~	~~499~~	~~4~~	~~505~~	~~7~~	~~549~~	~~16~~	~~98,9~~
~~SM236-1-31e~~		~~0,058~~	~~0,0013~~	~~0,08045~~	~~0,00083~~	~~0,647~~	~~0,014~~	~~0,02612~~	~~0,00063~~	~~0,44~~	~~499~~	~~5~~	~~506~~	~~9~~	~~521~~	~~12~~	~~98,6~~
SM236-1-31nw	r	0,0593	0,0025	0,08425	0,00091	0,693	0,03	0,0298	0,0014	0,44	521	5	533	18	594	27	97,8
SM236-1-32	c	0,0581	0,0013	0,08352	0,00069	0,677	0,014	0,02935	0,00088	0,4	517	4	524	9	584	17	98,7
SM236-1-33	**r**	**0,0636**	**0,0019**	**0,08179**	**0,00085**	**0,729**	**0,021**	**0,0333**	**0,0013**	**0,25**	**507**	**5**	**554**	**12**	**662**	**26**	**91,5**
~~SM236-1-35~~		~~0,05825~~	~~0,00094~~	~~0,08172~~	~~0,00067~~	~~0,665~~	~~0,011~~	~~0,02695~~	~~0,0005~~	~~0,51~~	~~506~~	~~4~~	~~517~~	~~7~~	~~538~~	~~10~~	~~97,9~~
SM236-1-36		0,0575	0,0017	0,08119	0,00091	0,653	0,02	0,02592	0,00088	0,39	503	5	507	12	517	17	99,2
SM236-1-37	c	0,0587	0,0011	0,08591	0,00081	0,705	0,013	0,03224	0,00086	0,22	531	5	541	8	641	17	98,2

Spot	Note	Isotopic ratios									Ages [Ma]						Conc.
		^{207}Pb/^{206}Pb	±2σ	^{206}Pb/^{238}U	±2σ	^{207}Pb/^{235}U	±2σ	^{208}Pb/^{232}Th	±2σ	^{232}Th/^{238}U	^{206}Pb/^{238}U	±2σ	^{207}Pb/^{235}U	±2σ	^{208}Pb/^{232}Th	±2σ	[%]
SM236-1 Bosilegrad monzonite (continued)																	
SM236-1-38	r	0,0609	0,002	0,0841	0,0011	0,717	0,02	0,0315	0,0014	0,39	520	6	548	12	627	27	95
~~SM236-1-39~~		**~~0,0605~~**	**~~0,0015~~**	**~~0,07387~~**	**~~0,00069~~**	**~~0,69~~**	**~~0,018~~**	**~~0,02802~~**	**~~0,00053~~**	**~~0,84~~**	**~~459~~**	**~~4~~**	**~~531~~**	**~~11~~**	**~~559~~**	**~~10~~**	**~~86,5~~**
SM236-1-o1	c	0,06061	0,00786	0,08239	0,00314	0,66534	0,12028	0,03548	0,0095	0,14	510	19	518	73	705	185	98,6
~~SM236-1-o5~~		~~0,05597~~	~~0,0041~~	~~0,09194~~	~~0,00244~~	~~0,75633~~	~~0,07956~~	~~0,03186~~	~~0,00648~~	~~0,18~~	~~567~~	~~14~~	~~572~~	~~46~~	~~634~~	~~127~~	~~99,1~~
SM236-1-o7	c	0,05869	0,00392	0,09053	0,00232	0,72997	0,06966	0,0294	0,00582	0,37	559	14	557	41	586	114	100,4
SM236-1-o8	c	0,05861	0,00352	0,08685	0,0021	0,69616	0,05774	0,02725	0,00358	0,28	537	13	537	35	543	70	100,1
SM236-1-o9	c	0,06034	0,00322	0,08732	0,00204	0,70809	0,05216	0,0272	0,00336	0,38	540	12	544	31	542	66	99,3
SM236-1-o10	c	0,05827	0,00338	0,08331	0,002	0,66489	0,05276	0,02538	0,00356	0,18	516	12	518	32	507	70	99,7
~~SM236-1-o12~~		**~~0,05897~~**	**~~0,00356~~**	**~~0,05777~~**	**~~0,0014~~**	**~~0,46454~~**	**~~0,03636~~**	**~~0,01736~~**	**~~0,0024~~**	**~~0,24~~**	**~~362~~**	**~~9~~**	**~~387~~**	**~~25~~**	**~~348~~**	**~~48~~**	**~~93,5~~**
SM236-1-o15	c	0,05615	0,00286	0,08361	0,00192	0,64178	0,04424	0,02606	0,00332	0,31	518	11	503	27	520	65	102,8
SM236-1-o17		0,05843	0,0038	0,08306	0,00208	0,65759	0,0588	0,02627	0,0037	0,29	514	12	513	36	524	73	100,3
~~SM236-1-o18~~		~~0,0587~~	~~0,00354~~	~~0,08422~~	~~0,00206~~	~~0,67128~~	~~0,05582~~	~~0,02723~~	~~0,00378~~	~~0,29~~	~~521~~	~~12~~	~~522~~	~~34~~	~~543~~	~~75~~	~~100~~
SM236-1-o20	c	0,05889	0,00344	0,08027	0,00194	0,62756	0,05002	0,02615	0,00356	0,43	498	12	495	31	522	70	100,6
SM236-1-o23	r	0,05956	0,00302	0,08213	0,0019	0,66564	0,04636	0,02845	0,00404	0,18	509	11	518	28	567	79	98,2
~~SM236-1-o27~~		~~0,05655~~	~~0,0031~~	~~0,0886~~	~~0,00208~~	~~0,7116~~	~~0,05408~~	~~0,02712~~	~~0,00378~~	~~0,51~~	~~547~~	~~12~~	~~546~~	~~32~~	~~541~~	~~74~~	~~100,3~~
SM250-1 Golemo Selo amphibolite																	
~~SM250-1-o4~~		~~0,05714~~	~~0,00382~~	~~0,07128~~	~~0,002~~	~~0,55598~~	~~0,04756~~	~~0,0238~~	~~0,00246~~	~~0,37~~	~~444~~	~~12~~	~~449~~	~~31~~	~~476~~	~~49~~	~~98,9~~
~~SM250-1-o3~~		**~~0,05957~~**	**~~0,0026~~**	**~~0,0668~~**	**~~0,00168~~**	**~~0,55427~~**	**~~0,03082~~**	**~~0,01999~~**	**~~0,00172~~**	**~~0,56~~**	**~~417~~**	**~~10~~**	**~~448~~**	**~~20~~**	**~~400~~**	**~~34~~**	**~~93,1~~**
SM250-1-o5	r	0,05699	0,00256	0,07359	0,00186	0,57547	0,03326	0,02246	0,00198	0,44	458	11	462	21	449	39	99,2
SM250-1-o6	r	0,05641	0,00246	0,07505	0,00188	0,59288	0,03342	0,02325	0,00204	0,43	467	11	473	21	465	40	98,7
~~SM250-1-o7~~		**~~0,06028~~**	**~~0,00248~~**	**~~0,06288~~**	**~~0,00156~~**	**~~0,51716~~**	**~~0,02704~~**	**~~0,01618~~**	**~~0,00142~~**	**~~0,47~~**	**~~393~~**	**~~10~~**	**~~423~~**	**~~18~~**	**~~325~~**	**~~28~~**	**~~92,9~~**
SM250-1-o8	**c**	**0,07077**	**0,00254**	**0,06584**	**0,00162**	**0,63875**	**0,02964**	**0,02662**	**0,00224**	**0,34**	**411**	**10**	**502**	**18**	**531**	**44**	**82**
~~SM250-1-o11~~		~~0,05775~~	~~0,00368~~	~~0,08185~~	~~0,00226~~	~~0,64341~~	~~0,05394~~	~~0,02521~~	~~0,0025~~	~~0,46~~	~~507~~	~~13~~	~~504~~	~~33~~	~~503~~	~~49~~	~~100,5~~
~~SM250-1-o12~~		~~0,05615~~	~~0,0025~~	~~0,07111~~	~~0,0018~~	~~0,56264~~	~~0,03214~~	~~0,02137~~	~~0,0019~~	~~0,39~~	~~443~~	~~11~~	~~453~~	~~21~~	~~427~~	~~38~~	~~97,7~~
~~SM250-1-o16~~		~~0,05782~~	~~0,00302~~	~~0,07251~~	~~0,00188~~	~~0,58038~~	~~0,0389~~	~~0,02277~~	~~0,00214~~	~~0,38~~	~~451~~	~~11~~	~~465~~	~~25~~	~~455~~	~~42~~	~~97,1~~
SM250-1-o17	c	0,05732	0,00456	0,07877	0,00236	0,64586	0,06766	0,02704	0,00328	0,28	489	14	506	42	539	65	96,6
SM250-1-o20	r	0,05724	0,0025	0,07424	0,00186	0,58952	0,0331	0,02183	0,00192	0,42	462	11	471	21	436	38	98,1

Spot	Note	Isotopic ratios									Ages [Ma]						Conc.
		$^{207}Pb/^{206}Pb$	±2σ	$^{206}Pb/^{238}U$	±2σ	$^{207}Pb/^{235}U$	±2σ	$^{208}Pb/^{232}Th$	±2σ	$^{232}Th/^{238}U$	$^{206}Pb/^{238}U$	±2σ	$^{207}Pb/^{235}U$	±2σ	$^{208}Pb/^{232}Th$	±2σ	[%]
SM250-1 Golemo Selo amphibolite (continued)																	
~~SM250-1-o23~~		~~0,05867~~	~~0,00282~~	~~0,07072~~	~~0,00182~~	~~0,55595~~	~~0,03422~~	~~0,02272~~	~~0,00206~~	~~0,41~~	~~441~~	~~11~~	~~449~~	~~22~~	~~454~~	~~41~~	~~98,1~~
SM250-2 Golemo Selo paragneiss																	
~~SM250-2-1n~~		~~0,0651~~	~~0,0011~~	~~0,1138~~	~~0,0018~~	~~1,022~~	~~0,022~~	~~0,03861~~	~~0,00067~~	~~0,94~~	~~695~~	~~10~~	~~713~~	~~11~~	~~766~~	~~13~~	~~97,5~~
SM250-2-1c	c	0,0629	0,0022	0,1066	0,0017	0,929	0,035	0,0343	0,0011	0,88	653	10	663	19	682	21	98,5
~~SM250-2-3c~~		~~0,067~~	~~0,0026~~	~~0,1226~~	~~0,0015~~	~~1,136~~	~~0,044~~	~~0,0381~~	~~0,0011~~	~~0,79~~	~~745~~	~~9~~	~~767~~	~~21~~	~~756~~	~~22~~	~~97,2~~
SM250-2-3e	r	0,0657	0,0013	0,1287	0,0012	1,169	0,025	0,03696	0,00092	0,84	780	7	785	12	733	18	99,4
SM250-2-4sw	**r**	**0,1636**	**0,0023**	**0,3423**	**0,0037**	**7,74**	**0,12**	**0,0816**	**0,0022**	**0,89**	**1897**	**18**	**2199**	**14**	**1585**	**41**	**86,3**
SM250-2-4c	**c**	**0,1649**	**0,0013**	**0,4058**	**0,0032**	**9,233**	**0,091**	**0,111**	**0,0013**	**1,4**	**2195**	**15**	**2360**	**9**	**2127**	**24**	**93**
SM250-2-5	c	0,0643	0,0015	0,1289	0,0012	1,145	0,026	0,0371	0,0011	0,46	781	7	772	12	735	22	101,2
SM250-2-6	c	0,11193	0,00065	0,3343	0,004	5,155	0,065	0,1202	0,0097	9,88	1859	19	1843	11	2270	170	100,9
SM250-2-7	**c**	**0,1452**	**0,0023**	**0,1297**	**0,0018**	**2,848**	**0,07**	**0,0877**	**0,0015**	**0,43**	**786**	**10**	**1366**	**18**	**1699**	**28**	**57,5**
SM250-2-8sw	r	0,0659	0,00091	0,13009	0,00082	1,183	0,017	0,03715	0,00045	1,03	788	5	792	8	737	9	99,6
SM250-2-8ne	ib	0,0665	0,0012	0,13102	0,00081	1,201	0,023	0,03735	0,00052	1,55	794	5	799	11	741	10	99,3
SM250-2-9	ib	0,06562	0,00077	0,1345	0,001	1,214	0,015	0,04078	0,00078	0,33	813	6	806	7	808	15	100,9
~~SM250-2-10~~		~~0,07201~~	~~0,00094~~	~~0,1534~~	~~0,0012~~	~~1,52~~	~~0,023~~	~~0,0469~~	~~0,00079~~	~~0,45~~	~~920~~	~~7~~	~~938~~	~~9~~	~~926~~	~~15~~	~~98,1~~
SM250-2-12		0,0592	0,006	0,1138	0,0033	1,05	0,11	0,037	0,0018	2,39	694	19	683	58	733	36	101,6
SM250-2-13	c	0,07083	0,00072	0,1551	0,0011	1,512	0,016	0,048	0,0012	0,14	929	6	935	6	947	23	99,4
SM250-2-14n	ib	0,11082	0,00094	0,2926	0,0024	4,467	0,051	0,08158	0,00091	0,64	1654	12	1724	9	1585	17	96
SM250-2-14c	c	0,1476	0,0016	0,3984	0,0037	8,15	0,13	0,1239	0,0016	1,39	2161	17	2245	15	2361	28	96,3
~~SM250-2-15c~~		**~~0,06565~~**	**~~0,00094~~**	**~~0,09736~~**	**~~0,0009~~**	**~~0,886~~**	**~~0,014~~**	**~~0,03211~~**	**~~0,00051~~**	**~~1,7~~**	**~~599~~**	**~~5~~**	**~~646~~**	**~~7~~**	**~~639~~**	**~~10~~**	**~~92,8~~**
SM250-2-15w	r	0,0582	0,0028	0,0973	0,0012	0,786	0,039	0,0305	0,0011	1,22	598	7	582	22	607	22	102,8
SM250-2-16ne	r	0,06086	0,00069	0,09985	0,00085	0,842	0,01	0,03242	0,00048	0,53	614	5	621	6	645	10	98,8
~~SM250-2-16sw~~		**~~0,0643~~**	**~~0,0011~~**	**~~0,09429~~**	**~~0,00099~~**	**~~0,849~~**	**~~0,017~~**	**~~0,02891~~**	**~~0,00051~~**	**~~1,05~~**	**~~581~~**	**~~6~~**	**~~623~~**	**~~9~~**	**~~576~~**	**~~10~~**	**~~93,2~~**
SM250-2-17sw	r	0,1614	0,0014	0,4511	0,003	10,199	0,099	0,1267	0,0013	1,2	2401	13	2452	9	2411	23	97,9
SM250-2-17c	ib	0,1601	0,0013	0,4177	0,0027	9,42	0,083	0,1174	0,0011	1,42	2250	12	2379	8	2243	19	94,6
SM250-2-18	ib	0,0723	0,0011	0,1542	0,0012	1,572	0,025	0,04554	0,00063	1,15	924	6	958	10	900	12	96,5
~~SM250-2-19ne~~		**~~0,1567~~**	**~~0,00095~~**	**~~0,3987~~**	**~~0,0027~~**	**~~8,849~~**	**~~0,075~~**	**~~0,1147~~**	**~~0,0016~~**	**~~0,15~~**	**~~2163~~**	**~~13~~**	**~~2322~~**	**~~8~~**	**~~2193~~**	**~~29~~**	**~~93,2~~**

Spot	Note	Isotopic ratios									Ages [Ma]						Conc.
		$^{207}Pb/^{206}Pb$	±2σ	$^{206}Pb/^{238}U$	±2σ	$^{207}Pb/^{235}U$	±2σ	$^{208}Pb/^{232}Th$	±2σ	$^{232}Th/^{238}U$	$^{206}Pb/^{238}U$	±2σ	$^{207}Pb/^{235}U$	±2σ	$^{208}Pb/^{232}Th$	±2σ	[%]
SM250-2 Golemo Selo paragneiss (continued)																	
SM250-2-19sw	**c**	**0,1726**	**0,0014**	**0,4329**	**0,0039**	**10,65**	**0,13**	**0,1152**	**0,0014**	**0,51**	**2318**	**17**	**2491**	**11**	**2204**	**25**	**93,1**
SM250-2-20	**r**	**0,0976**	**0,00095**	**0,2457**	**0,0024**	**3,429**	**0,048**	**0,0693**	**0,0015**	**0,1**	**1416**	**13**	**1510**	**11**	**1354**	**28**	**93,8**
~~SM250-2-21e~~		~~0,06525~~	~~0,00065~~	~~0,11685~~	~~0,00082~~	~~1,088~~	~~0,012~~	~~0,03598~~	~~0,00041~~	~~0,91~~	~~712~~	~~5~~	~~747~~	~~6~~	~~715~~	~~8~~	~~95,4~~
SM250-2-21w	ib	0,0651	0,0017	0,12052	0,00091	1,126	0,029	0,03485	0,00078	1,26	734	5	765	14	692	15	95,9
SM250-2-22	c	0,1701	0,0016	0,4497	0,0034	11,04	0,12	0,1142	0,0013	1,32	2393	15	2525	10	2185	23	94,8
SM250-2-23se	c	0,18278	0,00096	0,4776	0,0027	12,63	0,077	0,12112	0,00081	1,04	2516	12	2652	6	2311	15	94,9
~~SM250-2-23nw~~		~~0,18068~~	~~0,00081~~	~~0,5013~~	~~0,0031~~	~~13,133~~	~~0,091~~	~~0,1257~~	~~0,001~~	~~0,91~~	~~2619~~	~~13~~	~~2689~~	~~7~~	~~2392~~	~~18~~	~~97,4~~
~~**SM250-2-24e**~~		~~**0,0603**~~	~~**0,0014**~~	~~**0,08748**~~	~~**0,00077**~~	~~**0,763**~~	~~**0,018**~~	~~**0,02317**~~	~~**0,00061**~~	~~**0,42**~~	~~**541**~~	~~**5**~~	~~**576**~~	~~**10**~~	~~**463**~~	~~**12**~~	~~**93,9**~~
SM250-2-24sw	r	0,0592	0,0012	0,0927	0,00062	0,803	0,016	0,02481	0,00067	0,32	572	4	597	9	495	13	95,7
~~SM250-2-25w~~		~~0,0679~~	~~0,0016~~	~~0,139~~	~~0,0012~~	~~1,379~~	~~0,032~~	~~0,0364~~	~~0,0007~~	~~1,43~~	~~839~~	~~7~~	~~878~~	~~14~~	~~723~~	~~14~~	~~95,5~~
SM250-2-25e	r	0,0696	0,0012	0,1438	0,001	1,461	0,026	0,0419	0,0014	0,19	866	6	913	11	830	27	94,8
SM250-2-26s	r	0,0602	0,0029	0,09117	0,00099	0,801	0,039	0,02422	0,00059	2,11	562	6	590	22	484	12	95,3
SM250-2-26n	c	0,0607	0,0037	0,0918	0,0013	0,814	0,045	0,02374	0,00057	2,82	566	8	598	25	474	11	94,7
SM250-2-27s	c	0,06579	0,00089	0,13194	0,00085	1,267	0,017	0,0346	0,00032	3,1	799	5	830	8	688	6	96,2
SM250-2-27n	**r**	**0,06634**	**0,00073**	**0,11555**	**0,00063**	**1,121**	**0,013**	**0,0304**	**0,00028**	**0,98**	**705**	**4**	**762**	**6**	**605**	**6**	**92,5**
SM250-2-28w	**c**	**0,182**	**0,0011**	**0,4438**	**0,0027**	**11,783**	**0,086**	**0,10784**	**0,00099**	**0,74**	**2367**	**12**	**2586**	**7**	**2070**	**18**	**91,5**
SM250-2-28e	**r**	**0,16898**	**0,00079**	**0,3952**	**0,0021**	**9,728**	**0,061**	**0,1051**	**0,0017**	**0,15**	**2147**	**10**	**2409**	**6**	**2019**	**31**	**89,1**
SM250-2-29	ib	0,06686	0,00097	0,12986	0,00091	1,257	0,018	0,03451	0,00037	1,67	787	5	826	9	686	7	95,2
SM250-2-30	c	0,0818	0,0011	0,2004	0,0014	2,367	0,034	0,05431	0,00066	1,05	1177	7	1231	10	1069	13	95,6
SM250-2-32	r	0,11427	0,00067	0,3153	0,0018	5,181	0,037	0,0807	0,0014	0,11	1766	9	1849	6	1569	27	95,5
~~SM250-2-33~~		~~0,1657~~	~~0,0013~~	~~0,4547~~	~~0,0029~~	~~10,796~~	~~0,098~~	~~0,1149~~	~~0,0011~~	~~1,16~~	~~2416~~	~~13~~	~~2505~~	~~8~~	~~2198~~	~~19~~	~~96,4~~
SM250-2-34	r	0,0671	0,0016	0,1376	0,0012	1,223	0,03	0,0485	0,0011	1,25	831	7	809	14	957	21	102,7
SM250-2-35ne	**r**	**0,0692**	**0,0017**	**0,1638**	**0,0019**	**1,455**	**0,035**	**0,0639**	**0,0022**	**0,62**	**978**	**10**	**910**	**15**	**1251**	**42**	**107,5**
SM250-2-35sw	c	0,0814	0,0028	0,1711	0,0019	1,731	0,058	0,0773	0,0027	0,57	1018	11	1014	21	1504	50	100,4
~~**SM250-2-36**~~		~~**0,0635**~~	~~**0,0017**~~	~~**0,1487**~~	~~**0,0019**~~	~~**1,127**~~	~~**0,034**~~	~~**0,0578**~~	~~**0,0019**~~	~~**0,41**~~	~~**893**~~	~~**10**~~	~~**765**~~	~~**16**~~	~~**1136**~~	~~**37**~~	~~**116,7**~~
SM250-2-37		**0,0679**	**0,0022**	**0,1783**	**0,0022**	**1,382**	**0,044**	**0,0739**	**0,0019**	**0,72**	**1058**	**12**	**878**	**19**	**1440**	**36**	**120,5**
SM250-2-38	**ib**	**0,0656**	**0,0016**	**0,1695**	**0,0015**	**1,2**	**0,027**	**0,0789**	**0,0011**	**1,26**	**1010**	**9**	**799**	**13**	**1534**	**20**	**126,4**

Spot	Note	Isotopic ratios									Ages [Ma]						Conc.
		$^{207}Pb/^{206}Pb$	±2σ	$^{206}Pb/^{238}U$	±2σ	$^{207}Pb/^{235}U$	±2σ	$^{208}Pb/^{232}Th$	±2σ	$^{232}Th/^{238}U$	$^{206}Pb/^{238}U$	±2σ	$^{207}Pb/^{235}U$	±2σ	$^{208}Pb/^{232}Th$	±2σ	[%]
SM250-2 Golemo Selo paragneiss (continued)																	
~~SM250-2-39n~~		**~~0,2324~~**	**~~0,0017~~**	**~~0,7173~~**	**~~0,0059~~**	**~~17,01~~**	**~~0,15~~**	**~~0,3154~~**	**~~0,0032~~**	**~~0,27~~**	**~~3485~~**	**~~22~~**	**~~2935~~**	**~~9~~**	**~~5541~~**	**~~50~~**	**~~118,8~~**
SM250-2-39s	**r**	**0,2087**	**0,0017**	**0,666**	**0,0044**	**13,19**	**0,13**	**0,3216**	**0,0037**	**0,08**	**3290**	**17**	**2693**	**9**	**5634**	**56**	**122,2**
SM250-2-40sw	**r**	**0,0656**	**0,0012**	**0,2003**	**0,0017**	**1,162**	**0,023**	**0,1164**	**0,0023**	**-0,03**	**1177**	**9**	**784**	**11**	**2226**	**42**	**150,1**
~~SM250-2-40ne~~		**~~0,06551~~**	**~~0,00087~~**	**~~0,2105~~**	**~~0,0014~~**	**~~1,114~~**	**~~0,015~~**	**~~0,1326~~**	**~~0,0016~~**	**~~-0,39~~**	**~~1232~~**	**~~8~~**	**~~761~~**	**~~8~~**	**~~2517~~**	**~~28~~**	**~~161,9~~**
SM250-2-o1	r	0,16045	0,0068	0,43979	0,01134	9,7162	0,72482	0,12574	0,01776	0,23	2350	51	2408	69	2394	319	97,6
~~SM250-2-o4~~		**~~0,08035~~**	**~~0,00558~~**	**~~0,08989~~**	**~~0,00268~~**	**~~1,04867~~**	**~~0,10466~~**	**~~0,04172~~**	**~~0,00638~~**	**~~0,38~~**	**~~555~~**	**~~16~~**	**~~728~~**	**~~52~~**	**~~826~~**	**~~124~~**	**~~76,2~~**
SM250-2-o5	**ib**	**0,15214**	**0,00648**	**0,37747**	**0,00958**	**7,98519**	**0,5151**	**0,10668**	**0,0157**	**0,19**	**2064**	**45**	**2229**	**58**	**2049**	**287**	**92,6**
~~SM250-2-o8~~		~~0,06793~~	~~0,00618~~	~~0,12546~~	~~0,00418~~	~~1,2101~~	~~0,16618~~	~~0,0453~~	~~0,00802~~	~~0,4~~	~~762~~	~~24~~	~~805~~	~~76~~	~~895~~	~~155~~	~~94,6~~
SM250-2-o9a	**ib**	**0,15172**	**0,00736**	**0,32541**	**0,00868**	**7,04428**	**0,58522**	**0,11609**	**0,01894**	**0,31**	**1816**	**42**	**2117**	**74**	**2220**	**343**	**85,8**
SM250-2-o9b	r	0,06632	0,00338	0,13627	0,00356	1,24686	0,08868	0,04196	0,00704	0,27	824	20	822	40	831	136	100,2
SM250-2-o11	r	0,09395	0,00456	0,23878	0,0062	3,13319	0,21614	0,07193	0,01272	0,06	1380	32	1441	53	1404	240	95,8
~~SM250-2-o15~~		~~0,05912~~	~~0,00438~~	~~0,0878~~	~~0,00258~~	~~0,69573~~	~~0,06928~~	~~0,02671~~	~~0,00504~~	~~0,33~~	~~543~~	~~15~~	~~536~~	~~41~~	~~533~~	~~99~~	~~101,2~~
~~SM250-2-o17~~		**~~0,06806~~**	**~~0,00758~~**	**~~0,0978~~**	**~~0,00364~~**	**~~0,89563~~**	**~~0,14112~~**	**~~0,04068~~**	**~~0,00904~~**	**~~0,25~~**	**~~602~~**	**~~21~~**	**~~649~~**	**~~76~~**	**~~806~~**	**~~176~~**	**~~92,6~~**
~~SM250-2-o18~~		~~0,05842~~	~~0,00404~~	~~0,09306~~	~~0,00266~~	~~0,73424~~	~~0,06878~~	~~0,02811~~	~~0,0057~~	~~0,19~~	~~574~~	~~16~~	~~559~~	~~40~~	~~560~~	~~112~~	~~102,6~~
SM250-2-o19	c	0,23788	0,01268	0,60477	0,01634	20,0572	1,7491	0,16296	0,03198	0,3	3049	66	3094	84	3051	556	98,5
SM250-2-o21	c	0,06706	0,00638	0,14659	0,005	1,33619	0,1946	0,0461	0,00994	0,54	882	28	862	85	911	192	102,3
SM250-2-o24	c	0,06516	0,00658	0,09549	0,0033	0,84338	0,11846	0,02987	0,0069	0,35	588	19	621	65	595	136	94,7
SM272-1 Granite from the Božica magmatic complex																	
SM272-1-o1	c	0,0618	0,0046	0,0838	0,0021	0,7143	0,0769	0,0234	0,005	0,6168	519	13	547	46	468	99	94,8
SM272-1-o2	c	0,059	0,0057	0,0828	0,0024	0,693	0,095	0,0261	0,0057	0,9178	513	14	535	57	521	113	95,9
SM272-1-o3	c	0,0617	0,0078	0,0841	0,0031	0,6932	0,1256	0,0246	0,0059	0,7487	520	18	535	75	491	115	97,3
SM272-1-o4	c	0,0582	0,0063	0,0889	0,0028	0,741	0,1162	0,0256	0,006	0,7299	549	17	563	68	511	119	97,5
~~SM272-1-o10~~		~~0,0596~~	~~0,005~~	~~0,0832~~	~~0,0023~~	~~0,6896~~	~~0,0836~~	~~0,0241~~	~~0,0056~~	~~0,915~~	~~515~~	~~13~~	~~533~~	~~50~~	~~481~~	~~111~~	~~96,7~~
SM272-1-o21	c	0,0597	0,005	0,091	0,0025	0,7474	0,0925	0,0262	0,0063	0,8307	561	15	567	54	523	123	99
SM272-1-2	r	0,05907	0,00097	0,09356	0,0008	0,762	0,014	0,02909	0,001	0,6008	577	5	576	8	579	20	100,1
SM272-1-3	r	0,0588	0,0012	0,09088	0,0011	0,738	0,015	0,0285	0,0012	0,5456	561	6	561	9	568	24	100
SM272-1-5s	r	0,05899	0,00063	0,09484	0,00077	0,7707	0,01	0,03036	0,00092	0,6873	584	5	580	6	604	18	100,7

Spot	Note	Isotopic ratios									Ages [Ma]						Conc.
		^{207}Pb/^{206}Pb	±2σ	^{206}Pb/^{238}U	±2σ	^{207}Pb/^{235}U	±2σ	^{208}Pb/^{232}Th	±2σ	^{232}Th/^{238}U	^{206}Pb/^{238}U	±2σ	^{207}Pb/^{235}U	±2σ	^{208}Pb/^{232}Th	±2σ	[%]
SM272-1 Granite from the Božica magmatic complex (continued)																	
SM272-1-5n	c	0,05777	0,001	0,09325	0,00084	0,739	0,013	0,02988	0,001	0,7528	575	5	561	8	595	20	102,4
SM272-1-6	r	0,05817	0,00074	0,08526	0,00091	0,6823	0,0096	0,02668	0,001	0,3401	527	5	528	6	532	20	99,9
SM272-1-7se	c	0,05865	0,00063	0,08904	0,00082	0,7219	0,01	0,02827	0,00089	0,4356	550	5	552	6	564	17	99,7
SM272-1-7nw	r	0,06076	0,00058	0,07849	0,001	0,6584	0,0094	0,02399	0,00076	0,3612	487	6	514	6	479	15	94,8
SM272-1-8	r	0,0595	0,0039	0,0918	0,0021	0,763	0,05	0,0337	0,0046	0,2833	566	12	573	28	668	89	98,8
SM272-1-9	ib	0,05835	0,00066	0,08781	0,0007	0,7071	0,0088	0,0266	0,0008	0,5249	543	4	543	5	531	16	100
SM272-1-11		0,06133	0,00094	0,08351	0,0011	0,709	0,012	0,02579	0,00094	0,4545	517	6	544	7	515	18	95,1
~~SM272-1-12~~		~~0,0585~~	~~0,00085~~	~~0,08962~~	~~0,00086~~	~~0,727~~	~~0,011~~	~~0,02709~~	~~0,00097~~	~~0,7018~~	~~553~~	~~5~~	~~555~~	~~7~~	~~540~~	~~19~~	~~99,6~~
SM272-1-13ne	c	0,05812	0,00056	0,08577	0,00066	0,689	0,0077	0,02714	0,00078	0,5724	530	4	532	5	541	15	99,6
SM272-1-13sw	r	0,05923	0,00049	0,08207	0,0007	0,6737	0,0073	0,02593	0,00074	0,6997	508	4	523	4	518	15	97,3
SM272-1-16	ib	0,05888	0,00073	0,08749	0,00079	0,7169	0,01	0,02759	0,00087	0,6901	541	5	549	6	550	17	98,6
SM272-1-17	c	0,05841	0,00054	0,08802	0,00072	0,7113	0,0078	0,02592	0,00073	1,1953	544	4	545	5	517	14	99,7
SM272-1-18	r	0,05866	0,00056	0,08376	0,00076	0,6811	0,0083	0,02659	0,00082	0,4297	519	5	527	5	530	16	98,4
SM272-1-19s	r	0,05983	0,00097	0,09032	0,00077	0,743	0,014	0,02838	0,00099	0,4863	557	5	564	8	565	19	98,8
SM272-1-19c	c	0,05913	0,00085	0,08917	0,00079	0,727	0,012	0,02753	0,00086	0,9078	551	5	555	7	549	17	99,2
SM272-1-20	r	0,0592	0,002	0,0925	0,0018	0,755	0,03	0,0282	0,0016	0,4017	570	11	570	17	562	31	100
SM272-1-21	r	0,0597	0,0011	0,08366	0,00089	0,694	0,014	0,0304	0,0015	0,244	518	5	535	8	605	30	96,8
SM272-1-24	r	0,05885	0,00077	0,08795	0,00081	0,7099	0,011	0,02777	0,00092	0,6284	543	5	544	6	554	18	99,9
SM272-1-25	r	0,0581	0,00079	0,085	0,0013	0,6729	0,011	0,02651	0,001	0,2811	526	8	522	7	529	20	100,7
SM272-1-26	r	0,05897	0,00057	0,08876	0,00072	0,7221	0,0084	0,0275	0,00088	0,2557	548	4	552	5	548	17	99,4
SM272-1-29	r	0,05889	0,0008	0,0917	0,00083	0,7465	0,01	0,02833	0,001	0,4172	566	5	566	6	565	20	99,9
SM272-1-30	c	0,05899	0,00067	0,08841	0,00081	0,7151	0,0086	0,02725	0,00082	0,6124	546	5	548	5	543	16	99,7
SM272-1-31e	r	0,05882	0,00067	0,08343	0,00069	0,675	0,0086	0,02654	0,00081	0,6018	517	4	524	5	529	16	98,7
SM272-1-31w	c	0,0641	0,0026	0,0974	0,0022	0,865	0,042	0,0326	0,0027	0,5084	599	13	632	23	647	53	94,8
SM272-1-32	c	0,05888	0,00071	0,09144	0,00091	0,7408	0,011	0,03048	0,00093	0,7162	564	5	564	6	607	18	100
SM272-1-33	r	0,05924	0,00093	0,08766	0,001	0,718	0,013	0,02728	0,00097	0,538	542	6	549	8	544	19	98,7
SM272-1-34sw	r	0,0617	0,002	0,07902	0,00092	0,669	0,022	0,0242	0,0014	0,6737	490	6	519	14	483	28	94,5

Spot	Note	Isotopic ratios									Ages [Ma]						Conc.
		$^{207}\text{Pb}/^{206}\text{Pb}$	±2σ	$^{206}\text{Pb}/^{238}\text{U}$	±2σ	$^{207}\text{Pb}/^{235}\text{U}$	±2σ	$^{208}\text{Pb}/^{232}\text{Th}$	±2σ	$^{232}\text{Th}/^{238}\text{U}$	$^{206}\text{Pb}/^{238}\text{U}$	±2σ	$^{207}\text{Pb}/^{235}\text{U}$	±2σ	$^{208}\text{Pb}/^{232}\text{Th}$	±2σ	[%]
SM272-1 Granite from the Božica magmatic complex (continued)																	
SM272-1-34ne	r	0,05868	0,00056	0,08357	0,00071	0,6742	0,0078	0,02603	0,00082	0,2602	517	4	523	5	519	16	98,9
SM272-1-35sw	c	0,05883	0,00055	0,08729	0,00067	0,7036	0,0076	0,02713	0,00078	0,561	540	4	541	5	541	15	99,8
SM272-1-35ne	r	0,05901	0,00061	0,08722	0,0006	0,7079	0,0079	0,02705	0,00087	0,3521	539	4	543	5	539	17	99,2
SM272-1-36	c	0,0585	0,00065	0,08462	0,00095	0,6817	0,0092	0,02577	0,00079	0,815	524	6	529	5	514	15	99,1
~~SM272-1-38~~		~~0,0579~~	~~0,0013~~	~~0,0744~~	~~0,0013~~	~~0,604~~	~~0,013~~	~~0,02452~~	~~0,00096~~	~~0,2348~~	~~463~~	~~8~~	~~479~~	~~8~~	~~490~~	~~19~~	~~96,5~~
~~SM272-1-39~~		~~0,05849~~	~~0,00084~~	~~0,08396~~	~~0,00088~~	~~0,6706~~	~~0,011~~	~~0,02713~~	~~0,00087~~	~~0,5437~~	~~520~~	~~5~~	~~522~~	~~6~~	~~541~~	~~17~~	~~99,7~~
SM272-1-40		0,05804	0,00056	0,09394	0,00076	0,7486	0,0088	0,02882	0,00084	0,9034	579	5	568	5	574	17	101,9
SM272-1-41		0,06049	0,00092	0,0881	0,00097	0,727	0,013	0,0284	0,0012	0,2867	544	6	555	8	565	24	98,1
SM272-1-42	r	0,063	0,0016	0,089	0,0016	0,773	0,027	0,03	0,0015	0,3336	550	10	581	15	597	30	94,6
~~SM272-1-43~~		~~0,05848~~	~~0,00072~~	~~0,08524~~	~~0,00078~~	~~0,6867~~	~~0,01~~	~~0,02565~~	~~0,00089~~	~~0,5083~~	~~527~~	~~5~~	~~531~~	~~6~~	~~512~~	~~17~~	~~99,3~~
SM272-1-44	r	0,05873	0,00073	0,08862	0,00082	0,7127	0,0087	0,0273	0,00095	0,541	547	5	546	5	544	19	100,2
SM310 Sijarinska Banja paragneiss																	
~~**SM310-10**~~		~~**0,065**~~	~~**0,0011**~~	~~**0,1125**~~	~~**0,00078**~~	~~**1,148**~~	~~**0,019**~~	~~**0,03435**~~	~~**0,0004**~~	~~**1,3**~~	~~**687**~~	~~**5**~~	~~**775**~~	~~**9**~~	~~**683**~~	~~**8**~~	~~**88,7**~~
SM310-15sw	**c**	**0,0705**	**0,0027**	**0,1191**	**0,0016**	**1,288**	**0,052**	**0,0463**	**0,0018**	**0,35**	**725**	**9**	**835**	**23**	**914**	**35**	**86,9**
SM310-15ne	**r**	**0,0629**	**0,0013**	**0,07555**	**0,0009**	**0,712**	**0,018**	**0,0431**	**0,0027**	**0,04**	**470**	**5**	**545**	**11**	**852**	**52**	**86,2**
SM310-19se	r	0,06229	0,00082	0,10542	0,00086	0,897	0,013	0,04111	0,00077	0,25	646	5	649	7	814	15	99,5
SM310-19nw	c	0,06079	0,00084	0,0911	0,001	0,75	0,013	0,03788	0,00078	0,33	562	6	568	8	751	15	98,9
SM310-20ne	**c**	**0,13201**	**0,0009**	**0,2904**	**0,0036**	**5,185**	**0,065**	**0,0873**	**0,0016**	**0,26**	**1643**	**18**	**1849**	**11**	**1691**	**31**	**88,9**
SM310-20sw	r	0,06011	0,00074	0,09411	0,00067	0,761	0,01	0,03413	0,00047	0,38	580	4	574	6	678	9	100,9
~~**SM310-33sw**~~		~~**0,1456**~~	~~**0,0017**~~	~~**0,1822**~~	~~**0,0022**~~	~~**3,565**~~	~~**0,068**~~	~~**0,1594**~~	~~**0,0039**~~	~~**0,13**~~	~~**1079**~~	~~**12**~~	~~**1539**~~	~~**15**~~	~~**2986**~~	~~**68**~~	~~**70,1**~~
SM310-33ne		0,2065	0,0014	0,544	0,0034	15	0,11	0,179	0,0015	1,23	2800	14	2815	7	3327	26	99,5
SM310-39s	r	0,0608	0,0019	0,0997	0,001	0,808	0,023	0,0369	0,001	0,71	613	6	599	13	732	20	102,3
~~**SM310-39n**~~		~~**0,0586**~~	~~**0,0032**~~	~~**0,104**~~	~~**0,0019**~~	~~**0,814**~~	~~**0,045**~~	~~**0,0371**~~	~~**0,0011**~~	~~**1,23**~~	~~**638**~~	~~**11**~~	~~**596**~~	~~**25**~~	~~**736**~~	~~**22**~~	~~**107,1**~~
SM315 Bukovac metagranite																	
SM315-o10	r	0,0583	0,0045	0,084	0,0022	0,683	0,0767	0,0227	0,0057	0,2089	520	13	529	46	454	113	98,4
SM315-o18	**c**	**0,0599**	**0,0049**	**0,0712**	**0,0019**	**0,5991**	**0,07**	**0,0198**	**0,005**	**0,3955**	**444**	**11**	**477**	**44**	**396**	**99**	**93,1**
SM315-o23a	c	0,0586	0,0036	0,0718	0,0017	0,5717	0,0481	0,0214	0,0032	0,3329	447	10	459	31	429	64	97,4

Spot	Note	Isotopic ratios									Ages [Ma]						Conc.
		^{207}Pb/^{206}Pb	±2σ	^{206}Pb/^{238}U	±2σ	^{207}Pb/^{235}U	±2σ	^{208}Pb/^{232}Th	±2σ	^{232}Th/^{238}U	^{206}Pb/^{238}U	±2σ	^{207}Pb/^{235}U	±2σ	^{208}Pb/^{232}Th	±2σ	[%]
SM315 Bukovac metagranite (continued)																	
SM315-o23b	r	0,0591	0,0036	0,0729	0,0017	0,5935	0,0491	0,0201	0,003	0,3654	453	10	473	31	402	60	95,8
SM315-o1a		0,0571	0,0039	0,076	0,0019	0,5997	0,0563	0,0237	0,0046	0,2128	472	11	477	36	474	90	99
~~SM315-o1b~~		~~0,0601~~	~~0,0035~~	~~0,0762~~	~~0,0018~~	~~0,6309~~	~~0,051~~	~~0,0229~~	~~0,0043~~	~~0,3764~~	~~473~~	~~11~~	~~497~~	~~32~~	~~457~~	~~85~~	~~95,3~~
SM315-o2	**ib**	**0,1783**	**0,0114**	**0,0913**	**0,0025**	**2,2746**	**0,2412**	**0,0697**	**0,0134**	**0,5451**	**563**	**15**	**1204**	**75**	**1361**	**253**	**46,8**
SM315-o3	r	0,0581	0,0039	0,0783	0,0019	0,6365	0,0603	0,0208	0,0041	0,4829	486	12	500	37	417	82	97,2
SM315-o4	**r**	**0,0667**	**0,0044**	**0,058**	**0,0014**	**0,5376**	**0,0495**	**0,0196**	**0,0041**	**0,174**	**363**	**9**	**437**	**33**	**392**	**81**	**83,2**
~~SM315-o5~~		~~0,0593~~	~~0,0042~~	~~0,0826~~	~~0,0021~~	~~0,6843~~	~~0,0682~~	~~0,0236~~	~~0,0049~~	~~0,3488~~	~~511~~	~~12~~	~~529~~	~~41~~	~~471~~	~~97~~	~~96,6~~
SM315-o6	c	0,0612	0,0052	0,0705	0,002	0,5791	0,0683	0,0262	0,0057	0,2951	439	12	464	44	522	113	94,6
SM315-o7	c	0,0738	0,0063	0,1819	0,0054	1,9555	0,2884	0,0529	0,0116	0,6491	1077	29	1100	99	1042	222	97,9
SM315-o8	**c**	**0,0641**	**0,0048**	**0,0665**	**0,0017**	**0,6176**	**0,065**	**0,0234**	**0,0052**	**0,3464**	**415**	**11**	**488**	**41**	**468**	**102**	**85**
SM315-o9	c	0,0585	0,0046	0,0799	0,0022	0,6231	0,0701	0,0214	0,0048	0,7165	495	13	492	44	427	95	100,7
~~SM315-o11a~~		~~0,0563~~	~~0,0027~~	~~0,071~~	~~0,0015~~	~~0,5437~~	~~0,0356~~	~~0,0189~~	~~0,0026~~	~~0,5231~~	~~442~~	~~9~~	~~441~~	~~23~~	~~379~~	~~51~~	~~100,3~~
~~SM315-o11b~~		**~~0,0607~~**	**~~0,003~~**	**~~0,0637~~**	**~~0,0014~~**	**~~0,5296~~**	**~~0,0349~~**	**~~0,017~~**	**~~0,0024~~**	**~~0,3891~~**	**~~398~~**	**~~8~~**	**~~432~~**	**~~23~~**	**~~341~~**	**~~47~~**	**~~92,3~~**
~~SM315-o12~~		**~~0,086~~**	**~~0,0079~~**	**~~0,0753~~**	**~~0,0024~~**	**~~0,9028~~**	**~~0,1233~~**	**~~0,0208~~**	**~~0,0033~~**	**~~0,7046~~**	**~~468~~**	**~~15~~**	**~~653~~**	**~~66~~**	**~~415~~**	**~~66~~**	**~~71,7~~**
SM315-o13	ib	0,0566	0,0036	0,0742	0,0018	0,5777	0,0499	0,0209	0,0032	0,3717	462	11	463	32	417	63	99,7
SM315-o14	**ib**	**0,0656**	**0,004**	**0,0639**	**0,0015**	**0,5746**	**0,0473**	**0,0198**	**0,003**	**0,4048**	**399**	**9**	**461**	**31**	**396**	**60**	**86,6**
~~SM315-o15~~		**~~0,0705~~**	**~~0,004~~**	**~~0,0708~~**	**~~0,0016~~**	**~~0,7041~~**	**~~0,0549~~**	**~~0,0242~~**	**~~0,0037~~**	**~~0,5139~~**	**~~441~~**	**~~10~~**	**~~541~~**	**~~33~~**	**~~483~~**	**~~74~~**	**~~81,5~~**
~~SM315-o16~~		**~~0,0888~~**	**~~0,0062~~**	**~~0,069~~**	**~~0,0018~~**	**~~0,8309~~**	**~~0,0826~~**	**~~0,0294~~**	**~~0,0049~~**	**~~0,4799~~**	**~~430~~**	**~~11~~**	**~~614~~**	**~~46~~**	**~~586~~**	**~~95~~**	**~~70,1~~**
~~SM315-o17~~		~~0,0566~~	~~0,0031~~	~~0,0693~~	~~0,0016~~	~~0,5328~~	~~0,0402~~	~~0,0183~~	~~0,003~~	~~0,5098~~	~~432~~	~~10~~	~~434~~	~~27~~	~~367~~	~~60~~	~~99,5~~
~~SM315-o19~~		~~0,0587~~	~~0,0044~~	~~0,0707~~	~~0,0019~~	~~0,5526~~	~~0,0567~~	~~0,0229~~	~~0,0041~~	~~0,4471~~	~~441~~	~~11~~	~~447~~	~~37~~	~~458~~	~~81~~	~~98,6~~
~~SM315-o20~~		~~0,0588~~	~~0,0031~~	~~0,0708~~	~~0,0016~~	~~0,564~~	~~0,0413~~	~~0,0213~~	~~0,0038~~	~~0,415~~	~~441~~	~~10~~	~~454~~	~~27~~	~~427~~	~~75~~	~~97,1~~
~~SM315-o21a~~		~~0,0562~~	~~0,0033~~	~~0,0785~~	~~0,0018~~	~~0,613~~	~~0,0507~~	~~0,0241~~	~~0,0046~~	~~0,5756~~	~~487~~	~~11~~	~~485~~	~~32~~	~~482~~	~~91~~	~~100,3~~
SM315-o21b	**ib**	**0,0617**	**0,0037**	**0,0823**	**0,0019**	**0,7055**	**0,0589**	**0,0245**	**0,0049**	**0,5347**	**510**	**12**	**542**	**35**	**490**	**96**	**94,1**
~~SM315-o22~~		~~0,0596~~	~~0,0036~~	~~0,0755~~	~~0,0018~~	~~0,6128~~	~~0,0517~~	~~0,0229~~	~~0,0048~~	~~0,2838~~	~~469~~	~~11~~	~~485~~	~~33~~	~~457~~	~~95~~	~~96,6~~
SM315-o24a	**c**	**0,1058**	**0,0063**	**0,0356**	**0,0009**	**0,5211**	**0,0435**	**0,0091**	**0,002**	**0,7915**	**225**	**5**	**426**	**29**	**184**	**40**	**52,9**
SM315-o24b	r	0,0592	0,0044	0,0776	0,002	0,622	0,0643	0,0197	0,0045	0,4896	482	12	491	40	395	90	98,1
SM315-o25a	c	0,0567	0,0042	0,076	0,002	0,6224	0,0654	0,0251	0,006	0,3375	472	12	491	41	501	119	96,1

Spot	Note	Isotopic ratios									Ages [Ma]						Conc.
		^{207}Pb/^{206}Pb	±2σ	^{206}Pb/^{238}U	±2σ	^{207}Pb/^{235}U	±2σ	^{208}Pb/^{232}Th	±2σ	^{232}Th/^{238}U	^{206}Pb/^{238}U	±2σ	^{207}Pb/^{235}U	±2σ	^{208}Pb/^{232}Th	±2σ	[%]
SM315 Bukovac metagranite (continued)																	
SM315-o25b	**ib**	**0,0755**	**0,005**	**0,0469**	**0,0012**	**0,4847**	**0,0451**	**0,0104**	**0,0025**	**0,7088**	**296**	**7**	**401**	**31**	**208**	**51**	**73,6**
~~SM315-o26~~		~~0,0588~~	~~0,0044~~	~~0,0715~~	~~0,0019~~	~~0,5776~~	~~0,0605~~	~~0,0259~~	~~0,0069~~	~~0,1244~~	~~445~~	~~11~~	~~463~~	~~39~~	~~516~~	~~136~~	~~96,1~~
SM352 Lisina gabbro																	
SM352-o2		**0,0615**	**0,0038**	**0,0877**	**0,002**	**0,7626**	**0,0663**	**0,0277**	**0,0044**	**0,1963**	**542**	**12**	**576**	**38**	**552**	**87**	**94,2**
SM352-o5		0,0587	0,0043	0,0901	0,0023	0,7641	0,0802	0,0269	0,0047	0,1994	556	13	576	46	536	92	96,5
SM352-o7		0,0601	0,0033	0,0859	0,0019	0,7005	0,0536	0,0244	0,0041	0,1165	532	11	539	32	487	81	98,6
~~SM352-o8~~		~~0,0559~~	~~0,0047~~	~~0,079~~	~~0,0021~~	~~0,6135~~	~~0,071~~	~~0,022~~	~~0,0037~~	~~0,5194~~	~~490~~	~~13~~	~~486~~	~~45~~	~~440~~	~~73~~	~~100,9~~
~~SM352-o9~~		~~0,0613~~	~~0,0034~~	~~0,0888~~	~~0,002~~	~~0,7511~~	~~0,0593~~	~~0,027~~	~~0,0047~~	~~0,1247~~	~~548~~	~~12~~	~~569~~	~~34~~	~~538~~	~~92~~	~~96,4~~
SM352-o10	r	0,0594	0,0041	0,0904	0,0022	0,7288	0,0717	0,027	0,0046	0,4591	558	13	556	42	539	91	100,4
~~SM352-o11~~		**~~0,0976~~**	**~~0,0075~~**	**~~0,0813~~**	**~~0,0023~~**	**~~1,0848~~**	**~~0,1279~~**	**~~0,0682~~**	**~~0,0127~~**	**~~0,1648~~**	**~~504~~**	**~~14~~**	**~~746~~**	**~~62~~**	**~~1333~~**	**~~241~~**	**~~67,6~~**
SM352-o12		0,0588	0,0041	0,0898	0,0022	0,7046	0,0702	0,0256	0,0048	0,2857	555	13	542	42	510	94	102,4
~~SM352-o13~~		~~0,0562~~	~~0,007~~	~~0,0847~~	~~0,0029~~	~~0,6541~~	~~0,1129~~	~~0,0263~~	~~0,0057~~	~~0,4611~~	~~524~~	~~17~~	~~511~~	~~69~~	~~524~~	~~112~~	~~102,6~~
SM352-o14		**0,062**	**0,0045**	**0,0881**	**0,0023**	**0,7734**	**0,0808**	**0,0293**	**0,0059**	**0,2983**	**544**	**13**	**582**	**46**	**584**	**117**	**93,6**
SM352-o15		0,0631	0,0043	0,087	0,0021	0,7379	0,071	0,0284	0,0059	0,2238	538	13	561	42	566	117	95,8
SM352-o17		0,0602	0,0042	0,0899	0,0023	0,7519	0,0758	0,0291	0,0063	0,2125	555	13	569	44	580	124	97,5
SM352-o18		**0,0696**	**0,0051**	**0,0869**	**0,0023**	**0,7875**	**0,0834**	**0,0363**	**0,0083**	**0,1558**	**537**	**13**	**590**	**47**	**720**	**161**	**91,1**
SM352-o20		0,0579	0,0044	0,0864	0,0022	0,6779	0,0726	0,0279	0,0067	0,1299	534	13	526	44	557	132	101,6
SM352-o21		0,0618	0,0044	0,0905	0,0023	0,7338	0,074	0,03	0,0072	0,1469	558	14	559	43	597	141	99,9
SM352-o22	r	0,0633	0,0043	0,0994	0,0025	0,8281	0,0803	0,0298	0,0071	1,2029	611	14	613	45	594	139	99,7
SM352-o23		0,0601	0,004	0,089	0,0022	0,7214	0,0684	0,0277	0,0069	0,1475	550	13	552	40	551	136	99,7
SM352-o24		0,0602	0,0043	0,0887	0,0023	0,7112	0,0729	0,027	0,0071	0,1475	548	13	545	43	539	140	100,5
SM377-1 weakly deformed Bujanovac granite (southern part)																	
SM377-1-1s	r	0,0514	0,0014	0,04214	0,00042	0,287	0,0078	0,01581	0,00046	0,38	266	3	256	6	317	9	104,1
SM377-1-1n	c	0,0603	0,0015	0,10289	0,00086	0,821	0,021	0,0388	0,0013	0,14	631	5	607	12	769	25	104
SM377-1-2n	r	0,05134	0,00092	0,04066	0,00027	0,2768	0,0054	0,0155	0,00021	0,84	257	2	248	4	311	4	103,7
SM377-1-2s	**c**	**0,107**	**0,014**	**0,1101**	**0,0013**	**1,57**	**0,21**	**0,0352**	**0,0018**	**2,23**	**673**	**8**	**909**	**76**	**699**	**35**	**74,1**
SM377-1-3w	r	0,05261	0,00094	0,04122	0,0003	0,287	0,0049	0,01609	0,00024	0,53	260	2	256	4	323	5	101,7

Spot	Note	Isotopic ratios									Ages [Ma]						Conc.
		$^{207}Pb/^{206}Pb$	±2σ	$^{206}Pb/^{238}U$	±2σ	$^{207}Pb/^{235}U$	±2σ	$^{208}Pb/^{232}Th$	±2σ	$^{232}Th/^{238}U$	$^{206}Pb/^{238}U$	±2σ	$^{207}Pb/^{235}U$	±2σ	$^{208}Pb/^{232}Th$	±2σ	[%]
SM377-1 weakly deformed Bujanovac granite (southern part; continued)																	
SM377-1-3e	c	0,0657	0,001	0,1384	0,0013	1,204	0,02	0,04901	0,0007	0,69	836	8	802	9	967	14	104,3
SM377-1-4	r	0,0512	0,0011	0,04061	0,00032	0,2737	0,006	0,01536	0,00034	0,4	257	2	246	5	308	7	104,4
SM377-1-5ne	r	0,05659	0,0007	0,07723	0,00056	0,5779	0,0067	0,02953	0,00039	0,33	480	3	463	4	588	8	103,6
SM377-1-5sw	c	0,0596	0,0017	0,07935	0,00096	0,629	0,018	0,03196	0,00072	0,54	492	6	495	11	636	14	99,4
SM377-1-6	r	0,0517	0,0014	0,04209	0,00036	0,2896	0,0078	0,0156	0,00033	0,53	266	2	258	6	313	7	103,1
SM377-1-7sw	r	0,05725	0,00091	0,08118	0,00066	0,6187	0,0099	0,03162	0,00045	0,35	503	4	489	6	629	9	103
SM377-1-7ne	ib	0,0575	0,0015	0,0793	0,0012	0,611	0,016	0,0326	0,0011	0,32	492	7	483	10	647	22	101,9
SM377-1-8	c	0,061	0,0015	0,10814	0,00089	0,884	0,023	0,0406	0,00085	0,54	662	5	641	12	804	16	103,3
SM377-1-9	r	0,0513	0,0011	0,04031	0,00028	0,2787	0,0061	0,01493	0,00026	0,54	255	2	249	5	299	5	102,3
~~SM377-1-10~~		~~0,0544~~	~~0,0011~~	~~0,04601~~	~~0,00055~~	~~0,3363~~	~~0,0075~~	~~0,01526~~	~~0,00042~~	~~0,34~~	~~290~~	~~3~~	~~294~~	~~6~~	~~306~~	~~8~~	~~98,6~~
SM377-1-11	r	0,0511	0,0013	0,04133	0,0003	0,2847	0,0071	0,01495	0,00034	0,55	261	2	254	6	300	7	102,8
SM377-1-12	c	0,0738	0,0011	0,1814	0,0013	1,812	0,029	0,06636	0,00097	1,03	1075	7	1048	10	1298	18	102,5
SM377-1-13	r	0,0528	0,0016	0,04143	0,00044	0,2992	0,0093	0,0183	0,0014	0,06	262	3	266	7	367	29	98,6
SM377-1-14	c	0,1215	0,0015	0,3564	0,0029	5,9	0,078	0,1133	0,0013	1,01	1965	14	1960	11	2169	24	100,3
~~SM377-1-15~~		~~0,0575~~	~~0,001~~	~~0,07607~~	~~0,00075~~	~~0,598~~	~~0,011~~	~~0,02485~~	~~0,00041~~	~~1,12~~	~~473~~	~~5~~	~~476~~	~~7~~	~~496~~	~~8~~	~~99,4~~
SM377-1-16	r	0,0517	0,0012	0,04018	0,00027	0,2847	0,0065	0,01412	0,00031	0,6	254	2	254	5	283	6	100
SM377-1-17	r	0,0522	0,0014	0,04015	0,00041	0,288	0,0079	0,01433	0,00028	0,67	254	3	257	6	288	6	98,9
SM377-1-18e	r	0,0561	0,001	0,065	0,00065	0,5013	0,0097	0,02321	0,00099	0,2	406	4	412	7	463	20	98,5
SM377-1-18w	c	0,0627	0,0018	0,1129	0,001	0,978	0,028	0,03799	0,00071	1,4	689	6	688	14	753	14	100,2
SM377-1-19c-nw	c	0,0591	0,0019	0,08165	0,00087	0,663	0,02	0,0276	0,001	0,39	506	5	517	13	551	20	97,9
~~SM377-1-19se~~		~~0,0582~~	~~0,0012~~	~~0,07229~~	~~0,00056~~	~~0,582~~	~~0,012~~	~~0,02618~~	~~0,00074~~	~~0,31~~	~~450~~	~~3~~	~~465~~	~~8~~	~~522~~	~~14~~	~~96,8~~
SM377-1-20	r	0,05653	0,00091	0,07013	0,00049	0,5512	0,0096	0,02372	0,00037	0,7	437	3	445	6	474	7	98,1
SM377-1-21	r	0,05218	0,00088	0,03889	0,0003	0,2836	0,0052	0,01302	0,00017	1,29	246	2	253	4	262	4	97,1
SM377-1-22	**c**	**0,0633**	**0,0024**	**0,07276**	**0,00077**	**0,708**	**0,026**	**0,0304**	**0,0011**	**0,89**	**453**	**5**	**543**	**16**	**605**	**21**	**83,4**
SM377-1-23ne	r	0,05202	0,00078	0,0396	0,00022	0,2876	0,0044	0,0136	0,00019	1,07	250	1	257	4	273	4	97,6
SM377-1-23sw	c	0,05928	0,0008	0,0946	0,00066	0,784	0,011	0,03182	0,0005	0,37	583	4	587	6	633	10	99,2
SM377-1-24w	c	0,0543	0,0012	0,0736	0,0007	0,56	0,013	0,0241	0,0012	0,13	458	4	451	8	480	24	101,4

Spot	Note	Isotopic ratios									Ages [Ma]						Conc.
		$^{207}Pb/^{206}Pb$	±2σ	$^{206}Pb/^{238}U$	±2σ	$^{207}Pb/^{235}U$	±2σ	$^{208}Pb/^{232}Th$	±2σ	$^{232}Th/^{238}U$	$^{206}Pb/^{238}U$	±2σ	$^{207}Pb/^{235}U$	±2σ	$^{208}Pb/^{232}Th$	±2σ	[%]
SM377-1 weakly deformed Bujanovac granite (southern part; continued)																	
~~SM377-1-24c~~		**~~0,0577~~**	**~~0,0011~~**	**~~0,03613~~**	**~~0,00044~~**	**~~0,2905~~**	**~~0,0059~~**	**~~0,01424~~**	**~~0,00041~~**	**~~0,54~~**	**~~229~~**	**~~3~~**	**~~259~~**	**~~5~~**	**~~286~~**	**~~8~~**	**~~88,4~~**
SM377-1-25	r	0,06068	0,00096	0,097	0,00088	0,819	0,013	0,03083	0,00074	0,28	597	5	607	7	614	14	98,3
SM377-1-26	r	0,05119	0,00093	0,03843	0,00025	0,2727	0,0049	0,01251	0,00015	1,28	243	2	245	4	251	3	99,4
SM377-1-28sw	c	0,0504	0,0017	0,03999	0,00034	0,2797	0,0092	0,01356	0,00035	0,69	253	2	249	7	272	7	101,4
SM377-1-28ne	r	0,0519	0,001	0,04096	0,00026	0,2927	0,0058	0,01315	0,00023	0,61	259	2	260	5	264	5	99,4
SM377-1-29	r	0,0505	0,002	0,04041	0,00057	0,2829	0,0099	0,01259	0,00041	0,65	255	4	253	8	253	8	101,1
SM377-1-30	r	0,0508	0,0012	0,0403	0,0003	0,2828	0,0065	0,01336	0,00029	0,58	255	2	252	5	268	6	100,9
SM377-1-31s	r	0,05219	0,00088	0,04022	0,00034	0,2905	0,0055	0,01294	0,00026	0,37	254	2	259	4	260	5	98,3
SM377-1-31n	ib	0,0513	0,0013	0,04069	0,00036	0,2886	0,0073	0,01318	0,0003	0,71	257	2	258	6	265	6	99,8
SM377-1-32	c	0,0605	0,0011	0,09541	0,00099	0,796	0,016	0,03281	0,00065	0,51	587	6	594	9	653	13	99
SM377-1-33n	r	0,0526	0,001	0,04042	0,00041	0,2941	0,006	0,0124	0,00024	0,77	255	3	262	5	249	5	97,6
~~SM377-1-33s~~		**~~0,0589~~**	**~~0,0024~~**	**~~0,04189~~**	**~~0,00045~~**	**~~0,339~~**	**~~0,014~~**	**~~0,01486~~**	**~~0,00052~~**	**~~0,56~~**	**~~265~~**	**~~3~~**	**~~295~~**	**~~10~~**	**~~298~~**	**~~10~~**	**~~89,7~~**
SM377-1-34	r	0,0518	0,001	0,03963	0,00028	0,2826	0,0054	0,01288	0,00021	0,65	251	2	252	4	259	4	99,3
~~SM377-1-35ne~~		~~0,0513~~	~~0,0011~~	~~0,04114~~	~~0,00031~~	~~0,2916~~	~~0,0065~~	~~0,01301~~	~~0,0003~~	~~0,57~~	~~260~~	~~2~~	~~259~~	~~5~~	~~261~~	~~6~~	~~100,2~~
SM377-1-35s	c	0,0513	0,0012	0,03904	0,00033	0,2776	0,0069	0,01248	0,00026	0,89	247	2	248	6	251	5	99,4
SM377-1-36s	r	0,05659	0,00066	0,07305	0,00048	0,5703	0,007	0,02287	0,0003	0,4	455	3	458	5	457	6	99,2
SM377-1-36ne	c	0,05662	0,0008	0,07432	0,00046	0,5802	0,0082	0,02362	0,00028	1,11	462	3	464	5	472	6	99,6
SM377-1-37	**c**	**0,0574**	**0,0021**	**0,05518**	**0,0007**	**0,48**	**0,018**	**0,01913**	**0,00077**	**0,52**	**346**	**4**	**396**	**12**	**383**	**15**	**87,4**
SM377-1-38	r	0,0529	0,0013	0,04248	0,00044	0,31	0,007	0,01262	0,0003	0,59	268	3	274	5	254	6	98
SM377-1-39sw	r	0,0528	0,0011	0,03889	0,00029	0,2833	0,0062	0,01238	0,00021	0,98	246	2	253	5	249	4	97,2
SM377-1-39ne	c	0,0521	0,0019	0,04207	0,0004	0,302	0,011	0,01359	0,00043	0,63	266	3	267	9	273	9	99,5
~~SM377-1-40~~		**~~0,0636~~**	**~~0,0011~~**	**~~0,05385~~**	**~~0,0007~~**	**~~0,4749~~**	**~~0,0099~~**	**~~0,01751~~**	**~~0,00036~~**	**~~0,53~~**	**~~338~~**	**~~4~~**	**~~394~~**	**~~7~~**	**~~351~~**	**~~7~~**	**~~85,8~~**
SM377-2 deformed Bujanovac Qz-monzonite (southern part)																	
SM377-2-1	c	0,05666	0,00075	0,07341	0,00069	0,5774	0,009	0,02173	0,00045	0,54	457	4	463	6	435	9	98,7
SM377-2-2s	c	0,0583	0,0017	0,0718	0,00095	0,578	0,016	0,0215	0,00059	0,53	447	6	464	11	430	12	96,3
SM377-2-2c	c	0,0587	0,001	0,07884	0,00068	0,642	0,012	0,02428	0,00042	0,45	489	4	503	8	485	8	97,3
SM377-2-2n	**r**	**0,0572**	**0,003**	**0,05434**	**0,00085**	**0,472**	**0,023**	**0,0177**	**0,00096**	**0,58**	**341**	**5**	**390**	**16**	**354**	**19**	**87,5**

Spot	Note	Isotopic ratios									Ages [Ma]						Conc.
		^{207}Pb/^{206}Pb	±2σ	^{206}Pb/^{238}U	±2σ	^{207}Pb/^{235}U	±2σ	^{208}Pb/^{232}Th	±2σ	^{232}Th/^{238}U	^{206}Pb/^{238}U	±2σ	^{207}Pb/^{235}U	±2σ	^{208}Pb/^{232}Th	±2σ	[%]
SM377-2 deformed Bujanovac Qz-monzonite (southern part; continued)																	
SM377-2-3	r	0,05637	0,00082	0,07354	0,00042	0,5766	0,0089	0,02198	0,00033	0,88	457	3	462	6	439	7	99,1
~~SM377-2-4sw~~	e	~~0,0575~~	~~0,0012~~	~~0,06986~~	~~0,0005~~	~~0,556~~	~~0,012~~	~~0,02086~~	~~0,0004~~	~~0,97~~	~~435~~	~~3~~	~~449~~	~~8~~	~~417~~	~~8~~	~~97~~
SM377-2-4ne	r	0,0557	0,0019	0,07613	0,00078	0,59	0,02	0,02376	0,00099	0,37	473	5	469	13	474	19	100,8
~~SM377-2-5~~		~~0,05669~~	~~0,00082~~	~~0,06901~~	~~0,00042~~	~~0,5448~~	~~0,0079~~	~~0,02025~~	~~0,00026~~	~~1,09~~	~~430~~	~~3~~	~~441~~	~~5~~	~~405~~	~~5~~	~~97,5~~
SM377-2-6	r	0,0583	0,0011	0,07411	0,00059	0,603	0,012	0,02218	0,00026	1,5	461	4	479	8	443	5	96,3
SM377-2-7	c	0,0562	0,0012	0,07018	0,0006	0,551	0,012	0,02124	0,00038	0,97	437	4	446	8	425	8	98
SM377-2-8	r	0,0564	0,0014	0,07241	0,00052	0,57	0,013	0,02316	0,00044	0,83	451	3	457	9	463	9	98,6
SM377-2-9s	c	0,0565	0,0018	0,07205	0,0008	0,57	0,018	0,02176	0,00057	0,9	449	5	456	12	435	11	98,4
SM377-2-9n	r	0,0569	0,0017	0,07165	0,00076	0,572	0,016	0,02203	0,00064	0,61	446	5	458	11	440	13	97,4
~~SM377-2-10s~~	e	~~0,0561~~	~~0,0012~~	~~0,07372~~	~~0,00056~~	~~0,582~~	~~0,013~~	~~0,0232~~	~~0,00046~~	~~0,66~~	~~459~~	~~3~~	~~465~~	~~9~~	~~464~~	~~9~~	~~98,6~~
~~SM377-2-10n~~		~~0,05576~~	~~0,00099~~	~~0,06947~~	~~0,00053~~	~~0,547~~	~~0,01~~	~~0,0214~~	~~0,00034~~	~~1,03~~	~~433~~	~~3~~	~~443~~	~~7~~	~~428~~	~~7~~	~~97,8~~
SM377-2-11	r	0,0564	0,0013	0,07021	0,00053	0,558	0,013	0,02265	0,00051	0,58	437	3	449	8	453	10	97,4
SM377-2-12ne		0,0558	0,0016	0,07086	0,00055	0,56	0,017	0,02337	0,00052	0,8	441	3	450	11	467	10	98,1
SM377-2-12sw	r	0,0556	0,0014	0,07009	0,00053	0,551	0,014	0,02278	0,00058	0,51	437	3	444	9	455	11	98,3
SM377-2-13n	c	0,0567	0,0014	0,0724	0,001	0,58	0,016	0,02461	0,00068	0,8	451	6	463	10	491	13	97,3
SM377-2-13s	r	0,0564	0,0012	0,07063	0,00055	0,564	0,013	0,02366	0,00055	0,61	440	3	453	8	473	11	97
SM377-2-14	r	0,0563	0,0016	0,06983	0,00065	0,559	0,017	0,02272	0,00053	0,7	435	4	450	11	454	11	96,7
SM377-2-15	ib	0,0567	0,0012	0,07182	0,00068	0,58	0,011	0,02419	0,00053	0,64	447	4	464	7	483	10	96,4
SM377-2-16	c	0,0563	0,0021	0,07185	0,00083	0,577	0,022	0,02399	0,00081	0,69	447	5	460	14	479	16	97,2
SM377-2-17nw	c	0,0567	0,0024	0,06861	0,00085	0,557	0,024	0,02335	0,00093	0,63	428	5	447	16	466	18	95,7
SM377-2-17se	r	0,0564	0,0013	0,0769	0,0011	0,619	0,014	0,02799	0,00065	0,85	477	6	489	9	558	13	97,7
SM377-2-18	r	0,0569	0,001	0,0702	0,00048	0,572	0,011	0,02438	0,00047	0,44	437	3	459	7	487	9	95,3
SM377-2-19	c	0,0572	0,0015	0,06855	0,00064	0,562	0,015	0,02301	0,0005	0,8	427	4	452	10	460	10	94,6
SM377-2-20	r	0,0558	0,0016	0,07139	0,00066	0,572	0,017	0,02392	0,00078	0,43	445	4	458	11	478	15	97,1
SM377-2-21	r	0,0557	0,0014	0,06847	0,00066	0,55	0,014	0,02244	0,00043	0,65	427	4	444	9	449	9	96,1
SM377-2-22e	r	0,0564	0,0016	0,06936	0,00061	0,564	0,017	0,02346	0,00087	0,4	432	4	453	11	468	17	95,4
SM377-2-22w	c	0,0574	0,002	0,0711	0,001	0,588	0,021	0,02451	0,00081	0,75	443	6	468	13	489	16	94,6

Spot	Note	Isotopic ratios									Ages [Ma]						Conc.
		^{207}Pb/^{206}Pb	±2σ	^{206}Pb/^{238}U	±2σ	^{207}Pb/^{235}U	±2σ	^{208}Pb/^{232}Th	±2σ	^{232}Th/^{238}U	^{206}Pb/^{238}U	±2σ	^{207}Pb/^{235}U	±2σ	^{208}Pb/^{232}Th	±2σ	[%]
SM377-2 deformed Bujanovac Qz-monzonite (southern part; continued)																	
SM377-2-23nw	**r**	**0,0575**	**0,0013**	**0,07023**	**0,00054**	**0,58**	**0,012**	**0,02459**	**0,00044**	**0,72**	**438**	**3**	**463**	**8**	**491**	**9**	**94,4**
~~SM377-2-23se~~		~~0,0569~~	~~0,0021~~	~~0,07368~~	~~0,00068~~	~~0,603~~	~~0,023~~	~~0,02482~~	~~0,00081~~	~~0,74~~	~~458~~	~~4~~	~~476~~	~~15~~	~~495~~	~~16~~	~~96,3~~
SM377-2-24sw	c	0,0573	0,0023	0,07013	0,0009	0,578	0,024	0,02307	0,00094	0,67	437	5	462	15	461	19	94,6
SM377-2-24ne	r	0,0561	0,0015	0,07151	0,00091	0,577	0,017	0,0242	0,00077	0,5	445	6	462	11	483	15	96,4
SM377-2-25ne	**r**	**0,0571**	**0,0016**	**0,06906**	**0,00073**	**0,567**	**0,017**	**0,02233**	**0,00043**	**1,35**	**430**	**4**	**456**	**11**	**446**	**9**	**94,4**
SM377-2-25sw	c	0,056	0,0024	0,07037	0,00089	0,563	0,022	0,02242	0,00073	0,84	438	5	452	14	448	14	97
SM377-2-26	**c**	**0,0572**	**0,0015**	**0,05535**	**0,00047**	**0,506**	**0,013**	**0,02116**	**0,00046**	**0,98**	**347**	**3**	**417**	**9**	**423**	**9**	**83,4**
SM377-2-27ne	**r**	**0,0581**	**0,002**	**0,06991**	**0,00074**	**0,577**	**0,02**	**0,02238**	**0,00092**	**0,5**	**436**	**5**	**461**	**13**	**451**	**19**	**94,5**
SM377-2-27sw	c	0,0563	0,0011	0,07276	0,0005	0,567	0,011	0,02297	0,00039	0,95	453	3	455	7	459	8	99,6
SM377-2-28sw	**r**	**0,097**	**0,016**	**0,0765**	**0,0019**	**1,06**	**0,19**	**0,0422**	**0,008**	**0,63**	**475**	**12**	**704**	**86**	**830**	**150**	**67,5**
SM377-2-28ne	c	0,05628	0,00095	0,0731	0,00046	0,5671	0,0095	0,02278	0,00032	0,99	455	3	455	6	455	6	99,9
SM377-2-29nw	r	0,0567	0,0012	0,07531	0,00051	0,588	0,012	0,02357	0,0004	0,82	468	3	468	8	471	8	99,9
SM377-2-29se	ib	0,0565	0,00065	0,07353	0,00048	0,571	0,0071	0,02301	0,00028	0,58	457	3	458	5	460	6	99,8
~~SM377-2-30sw~~		~~0,05684~~	~~0,00069~~	~~0,07438~~	~~0,00046~~	~~0,58~~	~~0,0069~~	~~0,02341~~	~~0,00036~~	~~0,45~~	~~463~~	~~3~~	~~464~~	~~4~~	~~468~~	~~7~~	~~99,7~~
SM377-2-30ne	c	0,05642	0,00084	0,07338	0,00051	0,5695	0,0088	0,02262	0,00039	0,82	456	3	457	6	452	8	99,9
SM377-2-31se	c	0,05662	0,00092	0,07318	0,00047	0,568	0,0092	0,02227	0,00031	0,88	455	3	456	6	445	6	99,8
SM377-2-31nw	r	0,05697	0,00093	0,07276	0,00044	0,5692	0,0099	0,02223	0,00034	0,64	453	3	457	6	444	7	99,1
SM377-2-32sw	c	0,0565	0,0011	0,07332	0,0006	0,572	0,012	0,02267	0,00036	0,84	456	4	458	8	453	7	99,6
~~SM377-2-32ne~~		~~0,0557~~	~~0,0011~~	~~0,07255~~	~~0,00069~~	~~0,555~~	~~0,011~~	~~0,02121~~	~~0,00032~~	~~0,82~~	~~452~~	~~4~~	~~448~~	~~7~~	~~424~~	~~6~~	~~100,8~~
SM377-2-33sw	c	0,05611	0,00085	0,075	0,00047	0,5784	0,009	0,02339	0,00051	0,5	466	3	463	6	467	10	100,7
SM377-2-33ne	r	0,0554	0,001	0,07243	0,00051	0,553	0,01	0,02231	0,00039	0,67	451	3	446	7	446	8	101
SM377-2-34ne	r	0,0569	0,0017	0,07422	0,00061	0,581	0,017	0,02151	0,00067	0,46	462	4	463	11	430	13	99,7
SM377-2-34c	c	0,05595	0,00085	0,07727	0,00093	0,599	0,012	0,02295	0,00052	0,47	480	6	476	7	459	10	100,8
SM377-2-34sw	**c**	**0,0665**	**0,0025**	**0,0664**	**0,00074**	**0,609**	**0,022**	**0,0276**	**0,0012**	**0,46**	**414**	**5**	**481**	**14**	**549**	**23**	**86,2**
SM377-2-35sw	c	0,0563	0,0011	0,07561	0,00062	0,589	0,011	0,02286	0,00049	0,41	470	4	470	7	457	10	100
SM377-2-35ne	ib	0,0573	0,0011	0,07089	0,00058	0,563	0,011	0,02162	0,00045	0,53	442	4	453	7	432	9	97,5
SM377-2-36c	c	0,0554	0,0019	0,07629	0,00082	0,586	0,021	0,02333	0,00067	0,79	474	5	466	13	466	13	101,7

Spot	Note	Isotopic ratios									Ages [Ma]						Conc.
		^{207}Pb/^{206}Pb	±2σ	^{206}Pb/^{238}U	±2σ	^{207}Pb/^{235}U	±2σ	^{208}Pb/^{232}Th	±2σ	^{232}Th/^{238}U	^{206}Pb/^{238}U	±2σ	^{207}Pb/^{235}U	±2σ	^{208}Pb/^{232}Th	±2σ	[%]
SM377-2 deformed Bujanovac Qz-monzonite (southern part; continued)																	
SM377-2-36e	ib	0,05577	0,00098	0,07262	0,00048	0,565	0,01	0,02247	0,00043	0,44	452	3	454	7	449	9	99,6
SM377-2-36sw	r	0,0564	0,0011	0,07173	0,00059	0,563	0,011	0,02298	0,00045	0,61	447	4	453	7	459	9	98,7
SM377-2-37sw	c	0,0566	0,002	0,06826	0,00074	0,538	0,019	0,02092	0,00061	0,64	426	5	435	12	418	12	97,8
SM377-2-37ne	r	0,0563	0,0015	0,06955	0,00047	0,55	0,015	0,02164	0,00042	0,78	433	3	444	10	433	8	97,7
SM377-2-38	r	0,0564	0,0014	0,07426	0,00055	0,587	0,014	0,02415	0,00049	0,67	462	3	468	9	482	10	98,8
SM377-2-39ne	c	0,05603	0,00069	0,07221	0,00066	0,5675	0,0081	0,02267	0,00037	0,45	449	4	456	5	453	7	98,5
SM377-2-39sw	**r**	**0,0572**	**0,0021**	**0,06015**	**0,00062**	**0,543**	**0,019**	**0,02197**	**0,00068**	**0,55**	**377**	**4**	**439**	**13**	**439**	**13**	**85,8**
SM377-2-40s	r	0,0566	0,0015	0,07429	0,00068	0,591	0,016	0,02361	0,00063	0,6	462	4	470	10	472	13	98,3
SM377-2-40n	c	0,0556	0,0022	0,0751	0,0012	0,589	0,025	0,02295	0,00082	0,83	467	7	468	16	459	16	99,8
SM550-1 Slatinska Reka granite																	
SM550-1-1	**r**	**0,0967**	**0,0017**	**0,0465**	**0,0011**	**0,623**	**0,011**	**0,0228**	**0,0005**	**0,67**	**293**	**7**	**491**	**7**	**456**	**10**	**59,7**
SM550-1-2		**0,0572**	**0,0011**	**0,04856**	**0,00051**	**0,3824**	**0,0073**	**0,01578**	**0,00034**	**0,65**	**306**	**3**	**329**	**5**	**317**	**7**	**93**
SM550-1-3		0,05307	0,00082	0,05096	0,00041	0,371	0,0056	0,01488	0,00026	0,68	320	3	321	4	298	5	99,8
SM550-1-4		0,05931	0,00096	0,08337	0,00052	0,683	0,011	0,02587	0,00036	0,7	516	3	528	6	516	7	97,8
SM550-1-5nw	**c**	**0,0864**	**0,0076**	**0,052**	**0,00056**	**0,612**	**0,05**	**0,0244**	**0,0021**	**0,63**	**327**	**3**	**479**	**31**	**487**	**41**	**68,2**
SM550-1-5se	**r**	**0,23**	**0,016**	**0,04558**	**0,00053**	**1,45**	**0,11**	**0,0337**	**0,0021**	**1,25**	**287**	**3**	**889**	**50**	**669**	**41**	**32,3**
SM550-1-6sw	c	0,05448	0,00081	0,05188	0,00041	0,3878	0,0057	0,01583	0,00023	0,56	326	3	333	4	318	5	98,1
SM550-1-6ne	**r**	**0,05993**	**0,0009**	**0,0456**	**0,00031**	**0,3754**	**0,0046**	**0,01423**	**0,00025**	**0,83**	**288**	**2**	**324**	**3**	**286**	**5**	**88,9**
~~**SM550-1-7**~~		~~**0,07249**~~	~~**0,00088**~~	~~**0,05526**~~	~~**0,00067**~~	~~**0,5571**~~	~~**0,0064**~~	~~**0,02418**~~	~~**0,00038**~~	~~**0,49**~~	~~**347**~~	~~**4**~~	~~**449**~~	~~**4**~~	~~**483**~~	~~**7**~~	~~**77,2**~~
~~SM550-1-8~~		~~0,05567~~	~~0,00068~~	~~0,06088~~	~~0,00075~~	~~0,467~~	~~0,0087~~	~~0,021~~	~~0,00035~~	~~0,67~~	~~381~~	~~5~~	~~389~~	~~6~~	~~420~~	~~7~~	~~98~~
SM550-1-9nw	c	0,06022	0,00071	0,09008	0,00098	0,752	0,012	0,02857	0,00084	0,33	557	6	569	7	569	17	97,9
SM550-1-9se	r	0,05509	0,00061	0,05252	0,00042	0,3974	0,0047	0,01495	0,00017	0,83	330	3	340	3	300	3	97,3
SM550-1-10	**c**	**0,062**	**0,0022**	**0,05271**	**0,00037**	**0,444**	**0,015**	**0,01704**	**0,00039**	**1,14**	**331**	**2**	**372**	**10**	**342**	**8**	**89**
SM550-1-11	c	0,06244	0,00066	0,11339	0,00084	0,975	0,011	0,03484	0,00034	0,67	692	5	691	6	692	7	100,2
SM550-1-12	**ib**	**0,12227**	**0,00079**	**0,2374**	**0,0017**	**4,002**	**0,032**	**0,07358**	**0,0006**	**1,52**	**1373**	**9**	**1634**	**7**	**1435**	**11**	**84**
~~SM550-1-13sw~~		~~0,05434~~	~~0,00067~~	~~0,05157~~	~~0,00033~~	~~0,3851~~	~~0,0051~~	~~0,01691~~	~~0,00026~~	~~0,43~~	~~324~~	~~2~~	~~331~~	~~4~~	~~339~~	~~5~~	~~98~~
SM550-1-13ne	**r**	**0,05638**	**0,00063**	**0,04652**	**0,00027**	**0,3596**	**0,0045**	**0,01465**	**0,00017**	**0,66**	**293**	**2**	**312**	**3**	**294**	**3**	**94**

Spot	Note	Isotopic ratios									Ages [Ma]						Conc.
		$^{207}Pb/^{206}Pb$	±2σ	$^{206}Pb/^{238}U$	±2σ	$^{207}Pb/^{235}U$	±2σ	$^{208}Pb/^{232}Th$	±2σ	$^{232}Th/^{238}U$	$^{206}Pb/^{238}U$	±2σ	$^{207}Pb/^{235}U$	±2σ	$^{208}Pb/^{232}Th$	±2σ	[%]
SM550-1 Slatinska Reka granite (continued)																	
SM550-1-14se	**r**	**0,0623**	**0,0018**	**0,07489**	**0,00044**	**0,646**	**0,02**	**0,0271**	**0,0013**	**0,46**	**466**	**3**	**505**	**12**	**540**	**26**	**92,2**
SM550-1-14nw	c	0,06134	0,0009	0,09291	0,00068	0,782	0,011	0,02906	0,00029	1,39	573	4	587	6	579	6	97,7
~~SM550-1-15~~		~~0,05851~~	~~0,00087~~	~~0,06503~~	~~0,00041~~	~~0,5234~~	~~0,0071~~	~~0,02061~~	~~0,0003~~	~~0,66~~	~~406~~	~~3~~	~~427~~	~~5~~	~~412~~	~~6~~	~~95,1~~
SM550-1-16	c	0,0616	0,0017	0,10686	0,00094	0,907	0,024	0,03241	0,0005	2,15	654	6	652	13	646	10	100,4
SM550-1-17	**c**	**0,0647**	**0,0012**	**0,09343**	**0,00077**	**0,83**	**0,015**	**0,03007**	**0,0004**	**1,76**	**576**	**5**	**613**	**8**	**599**	**8**	**93,9**
SM550-1-18w	c	0,0637	0,0017	0,09414	0,00085	0,825	0,025	0,02704	0,00046	2,94	580	5	611	14	539	9	94,9
SM550-1-18e	r	0,05333	0,00048	0,05223	0,00037	0,3835	0,0038	0,01529	0,00021	0,91	328	2	330	3	307	4	99,6
~~SM550-1-19~~		~~0,0573~~	~~0,0012~~	~~0,08521~~	~~0,0009~~	~~0,675~~	~~0,014~~	~~0,02615~~	~~0,00072~~	~~0,42~~	~~527~~	~~5~~	~~523~~	~~8~~	~~522~~	~~14~~	~~100,8~~
~~SM550-1-20~~		~~0,05983~~	~~0,00071~~	~~0,09763~~	~~0,0006~~	~~0,805~~	~~0,011~~	~~0,03164~~	~~0,00062~~	~~0,33~~	~~601~~	~~4~~	~~599~~	~~6~~	~~629~~	~~12~~	~~100,3~~
SM550-1-21	**c**	**0,0808**	**0,0021**	**0,0758**	**0,0011**	**0,84**	**0,024**	**0,0344**	**0,0011**	**0,66**	**471**	**7**	**617**	**13**	**683**	**22**	**76,3**
SM550-1-22	ib	0,05703	0,00089	0,08148	0,0005	0,64	0,01	0,02411	0,00049	0,37	505	3	502	6	482	10	100,7
~~SM550-1-23nw~~		**~~0,06479~~**	**~~0,00085~~**	**~~0,04775~~**	**~~0,0007~~**	**~~0,4251~~**	**~~0,0071~~**	**~~0,0154~~**	**~~0,00026~~**	**~~0,99~~**	**~~301~~**	**~~4~~**	**~~360~~**	**~~5~~**	**~~309~~**	**~~5~~**	**~~83,6~~**
SM550-1-23se	c	0,0599	0,0016	0,08828	0,00097	0,727	0,018	0,02867	0,00074	0,94	545	6	556	11	571	14	98,1
SM550-1-24	c	0,0583	0,0011	0,07211	0,0007	0,578	0,011	0,02322	0,0003	0,93	449	4	463	7	464	6	96,9
~~SM550-1-25sw~~		~~0,05658~~	~~0,00072~~	~~0,07275~~	~~0,00059~~	~~0,567~~	~~0,0076~~	~~0,02317~~	~~0,00036~~	~~0,31~~	~~453~~	~~4~~	~~457~~	~~5~~	~~463~~	~~7~~	~~99,1~~
SM550-1-25ne	**ib**	**0,06206**	**0,00066**	**0,06877**	**0,00041**	**0,5874**	**0,0072**	**0,02324**	**0,0003**	**0,35**	**429**	**3**	**469**	**5**	**464**	**6**	**91,4**
SM550-1-26	c	0,0634	0,0012	0,11144	0,00073	0,972	0,018	0,03471	0,00068	0,59	681	4	688	9	689	13	99
~~SM550-1-27~~		**~~0,0673~~**	**~~0,0015~~**	**~~0,04961~~**	**~~0,00053~~**	**~~0,46~~**	**~~0,011~~**	**~~0,01769~~**	**~~0,00032~~**	**~~0,71~~**	**~~312~~**	**~~3~~**	**~~384~~**	**~~8~~**	**~~354~~**	**~~6~~**	**~~81,4~~**
SM550-1-28	**r**	**0,0676**	**0,0012**	**0,04635**	**0,00037**	**0,4296**	**0,0064**	**0,01447**	**0,00018**	**1,01**	**292**	**2**	**363**	**5**	**291**	**4**	**80,5**
~~SM550-1-29~~		~~0,05687~~	~~0,00056~~	~~0,07456~~	~~0,00056~~	~~0,5822~~	~~0,0062~~	~~0,02424~~	~~0,00029~~	~~0,28~~	~~464~~	~~3~~	~~466~~	~~4~~	~~484~~	~~6~~	~~99,4~~
SM550-1-30sw	c	0,07348	0,00062	0,16663	0,00088	1,686	0,014	0,05471	0,00096	0,17	994	5	1003	6	1076	18	99,1
~~SM550-1-31~~		**~~0,0728~~**	**~~0,001~~**	**~~0,07672~~**	**~~0,00067~~**	**~~0,767~~**	**~~0,012~~**	**~~0,05~~**	**~~0,0012~~**	**~~0,36~~**	**~~477~~**	**~~4~~**	**~~578~~**	**~~7~~**	**~~985~~**	**~~23~~**	**~~82,5~~**
~~SM550-1-32w~~		**~~0,0824~~**	**~~0,0038~~**	**~~0,04534~~**	**~~0,00047~~**	**~~0,511~~**	**~~0,022~~**	**~~0,02121~~**	**~~0,00079~~**	**~~0,75~~**	**~~286~~**	**~~3~~**	**~~418~~**	**~~14~~**	**~~424~~**	**~~16~~**	**~~68,4~~**
SM550-1-32e	ib	0,05939	0,00067	0,07973	0,00085	0,6498	0,0096	0,02536	0,00042	0,74	495	5	508	6	506	8	97,3
SM550-1-33	c	0,05923	0,00053	0,09253	0,00053	0,757	0,0072	0,0293	0,00026	0,84	571	3	572	4	584	5	99,7
~~SM550-1-34~~		~~0,06024~~	~~0,00079~~	~~0,0871~~	~~0,0007~~	~~0,7204~~	~~0,0087~~	~~0,0508~~	~~0,0043~~	~~0,02~~	~~538~~	~~4~~	~~551~~	~~5~~	~~999~~	~~83~~	~~97,8~~
SM550-1-35sw	c	0,0675	0,0028	0,135	0,0024	1,233	0,034	0,0451	0,0023	0,41	816	13	814	14	891	43	100,3

Spot	Note	Isotopic ratios									Ages [Ma]						Conc.
		^{207}Pb/^{206}Pb	±2σ	^{206}Pb/^{238}U	±2σ	^{207}Pb/^{235}U	±2σ	^{208}Pb/^{232}Th	±2σ	^{232}Th/^{238}U	^{206}Pb/^{238}U	±2σ	^{207}Pb/^{235}U	±2σ	^{208}Pb/^{232}Th	±2σ	[%]
SM550-1 Slatinska Reka granite (continued)																	
SM550-1-35ne	**r**	**0,05828**	**0,00058**	**0,04855**	**0,00046**	**0,3907**	**0,0049**	**0,01592**	**0,00018**	**0,89**	**306**	**3**	**335**	**4**	**319**	**4**	**91,3**
~~**SM550-1-36se**~~		~~**0,0581**~~	~~**0,0015**~~	~~**0,0471**~~	~~**0,0025**~~	~~**0,373**~~	~~**0,018**~~	~~**0,01546**~~	~~**0,00038**~~	~~**1,29**~~	~~**296**~~	~~**15**~~	~~**322**~~	~~**14**~~	~~**310**~~	~~**8**~~	~~**91,9**~~
~~**SM550-1-36nw**~~		~~**0,05816**~~	~~**0,00068**~~	~~**0,04938**~~	~~**0,00051**~~	~~**0,398**~~	~~**0,0054**~~	~~**0,01432**~~	~~**0,00025**~~	~~**0,73**~~	~~**311**~~	~~**3**~~	~~**340**~~	~~**4**~~	~~**287**~~	~~**5**~~	~~**91,4**~~
SM550-1-37nw	r	0,0533	0,00074	0,05281	0,00039	0,3892	0,006	0,01753	0,0002	0,84	332	2	334	4	351	4	99,4
SM550-1-37se	**c**	**0,1092**	**0,0063**	**0,1029**	**0,0013**	**1,559**	**0,093**	**0,0887**	**0,0067**	**0,46**	**632**	**8**	**944**	**34**	**1710**	**120**	**66,9**
SM550-1-38	r	0,0552	0,00056	0,05296	0,00042	0,4015	0,005	0,01436	0,0002	0,84	333	3	343	4	288	4	97,1
SM550-1-39ne	**c**	**0,0639**	**0,001**	**0,03646**	**0,00046**	**0,3209**	**0,005**	**0,01259**	**0,00017**	**0,89**	**231**	**3**	**283**	**4**	**253**	**3**	**81,7**
SM550-1-39sw	**c**	**0,0733**	**0,002**	**0,07737**	**0,0007**	**0,789**	**0,024**	**0,02794**	**0,00054**	**1,9**	**480**	**4**	**589**	**14**	**557**	**11**	**81,6**
SM550-1-40	**r**	**0,07006**	**0,00089**	**0,05173**	**0,00035**	**0,4987**	**0,0063**	**0,01877**	**0,00022**	**1,02**	**325**	**2**	**411**	**4**	**376**	**5**	**79,2**
SM600-1 Doganica metagranite																	
~~SM600-1-3~~		~~0,0607~~	0,0017	~~0,09355~~	~~0,00076~~	~~0,78~~	~~0,021~~	~~0,02628~~	~~0,00088~~	~~0,45~~	~~576~~	~~5~~	~~585~~	~~12~~	~~524~~	~~17~~	~~98,5~~
SM600-1-4	r	0,0588	0,0011	0,08443	0,0007	0,681	0,012	0,02758	0,00066	0,5	523	4	527	7	550	13	99,1
~~SM600-1-5~~		~~0,05912~~	~~0,00073~~	~~0,08691~~	~~0,00055~~	~~0,7042~~	~~0,0098~~	~~0,02319~~	~~0,00028~~	~~0,82~~	~~537~~	~~3~~	~~542~~	~~6~~	~~463~~	~~6~~	~~99,1~~
SM600-1-6		0,0588	0,0023	0,08014	0,00083	0,651	0,024	0,02607	0,00066	1,32	497	5	506	15	520	13	98,2
SM600-1-11	ib	0,0597	0,0012	0,09101	0,00065	0,749	0,015	0,03057	0,00055	1,15	561	4	566	9	609	11	99,2
~~SM600-1-12~~	~~r~~	~~0,05961~~	~~0,00093~~	~~0,07188~~	~~0,00055~~	~~0,5887~~	~~0,0091~~	~~0,01947~~	~~0,00031~~	~~1,08~~	~~448~~	~~3~~	~~470~~	~~6~~	~~390~~	~~6~~	~~95,2~~
SM600-1-13	**ib**	**0,0871**	**0,0063**	**0,0849**	**0,0015**	**1,03**	**0,078**	**0,0358**	**0,0018**	**1,11**	**525**	**9**	**706**	**39**	**711**	**35**	**74,4**
~~SM600-1-14~~		~~0,0611~~	~~0,001~~	~~0,07788~~	~~0,00054~~	~~0,656~~	~~0,011~~	~~0,02721~~	~~0,00056~~	~~0,5~~	~~483~~	~~3~~	~~512~~	~~7~~	~~543~~	~~11~~	~~94,5~~
SM600-1-16	r	0,05889	0,00072	0,1015	0,00068	0,8261	0,0098	0,02905	0,00037	0,54	623	4	611	5	579	7	102
SM600-1-17	r	0,0609	0,0011	0,08812	0,0006	0,736	0,014	0,02615	0,0006	0,45	544	4	560	8	522	12	97,3
SM600-1-18		0,1371	0,0011	0,4064	0,0019	7,657	0,062	0,1086	0,0011	1,22	2198	9	2192	7	2083	20	100,3
~~**SM600-1-19**~~		~~**0,1243**~~	~~**0,0011**~~	~~**0,3181**~~	~~**0,003**~~	~~**5,431**~~	~~**0,059**~~	~~**0,0876**~~	~~**0,001**~~	~~**0,87**~~	~~**1780**~~	~~**15**~~	~~**1889**~~	~~**9**~~	~~**1698**~~	~~**19**~~	~~**94,2**~~
~~SM600-1-20~~		~~0,06006~~	~~0,00062~~	~~0,09599~~	~~0,00064~~	~~0,7949~~	~~0,0097~~	~~0,02907~~	~~0,00038~~	~~0,96~~	~~591~~	4	~~593~~	~~6~~	~~579~~	~~8~~	~~99,6~~
SM600-1-21	ib	0,05974	0,00089	0,09103	0,00045	0,748	0,011	0,02722	0,00037	0,52	562	3	566	6	543	7	99,2
SM600-1-22	r	0,05954	0,00097	0,09073	0,00073	0,744	0,012	0,02671	0,00053	0,47	560	4	564	7	533	10	99,3
SM600-1-23	r	0,06	0,0017	0,08678	0,0007	0,702	0,025	0,02661	0,00091	0,48	536	4	538	15	531	18	99,7
~~SM600-1-24~~		~~0,05925~~	~~0,00092~~	~~0,09337~~	~~0,00076~~	~~0,761~~	~~0,012~~	~~0,02746~~	~~0,00063~~	~~0,34~~	~~575~~	~~5~~	~~574~~	~~7~~	~~547~~	~~12~~	~~100,3~~

Spot	Note	Isotopic ratios									Ages [Ma]						Conc.
		^{207}Pb/^{206}Pb	±2σ	^{206}Pb/^{238}U	±2σ	^{207}Pb/^{235}U	±2σ	^{208}Pb/^{232}Th	±2σ	^{232}Th/^{238}U	^{206}Pb/^{238}U	±2σ	^{207}Pb/^{235}U	±2σ	^{208}Pb/^{232}Th	±2σ	[%]
SM600-1 Doganica metagranite (continued)																	
SM600-1-28		0,05669	0,00041	0,08125	0,00053	0,6346	0,0053	0,02332	0,00019	0,47	504	3	499	3	466	4	101
SM600-1-31	**ib**	**0,0621**	**0,0015**	**0,07529**	**0,00047**	**0,646**	**0,015**	**0,0284**	**0,00093**	**0,35**	**468**	**3**	**507**	**10**	**566**	**18**	**92,3**
~~SM600-1-34~~		~~0,05942~~	~~0,00097~~	~~0,09612~~	~~0,00094~~	~~0,788~~	~~0,015~~	~~0,02736~~	~~0,00064~~	~~0,4~~	~~592~~	~~6~~	~~589~~	~~9~~	~~546~~	~~13~~	~~100,4~~
SM600-1-36	ib	0,05961	0,00088	0,0911	0,0006	0,746	0,011	0,02683	0,00065	0,35	562	4	565	6	535	13	99,4
SM600-1-37	r	0,05898	0,0005	0,0833	0,00046	0,6775	0,0062	0,02605	0,00033	0,52	516	3	525	4	520	7	98,2
SM600-1-38		0,0604	0,0019	0,0822	0,0012	0,689	0,022	0,02606	0,00067	1,12	509	7	531	13	520	13	95,9
~~SM600-1-40~~		**~~0,0643~~**	**~~0,0014~~**	**~~0,08902~~**	**~~0,00066~~**	**~~0,786~~**	**~~0,016~~**	**~~0,0317~~**	**~~0,00067~~**	**~~0,52~~**	**~~550~~**	**~~4~~**	**~~588~~**	**~~9~~**	**~~631~~**	**~~13~~**	**~~93,5~~**
SM600-1-43	r	0,05867	0,00069	0,08974	0,00046	0,7252	0,0081	0,02705	0,00031	0,57	554	3	553	5	539	6	100,1
SM600-1-44ne	c	0,05876	0,00085	0,08186	0,00061	0,6615	0,0097	0,02682	0,00034	0,73	507	4	515	6	535	7	98,5
SM600-1-44sw	r	0,05922	0,0008	0,09114	0,00057	0,745	0,011	0,02636	0,00032	0,95	562	3	564	6	526	6	99,6
SM600-1-45	ib	0,0601	0,0022	0,0807	0,0013	0,673	0,025	0,02876	0,00094	0,88	500	8	521	15	573	18	96

Concordance (Conc.) is calculated as 100·((^{206}Pb/^{238}U age)·(^{207}Pb/^{235}U age)$^{-1}$). Values beyond the accepted tolerance (95-105%) are given in bold print. The “mixed results” are stricken-through.

Values in the “Note” column: r – rim, ib – internal growth-band, c – core, empty cell – grain with simple zoning.

See Chapter 2-3 and Appendix 2-3 for details.

Appendix 2-5

Cathodoluminescence images of analysed zircons with $^{206}Pb/^{238}U$ age-results and 2σ errors

Appendix 2-5 Cathodoluminescence images of analysed zircons

Spots that yielded discordant results are designated with a suffix “d.”.

See Appendix 2-3 for details.

KOS02-1 Novo Brdo schist

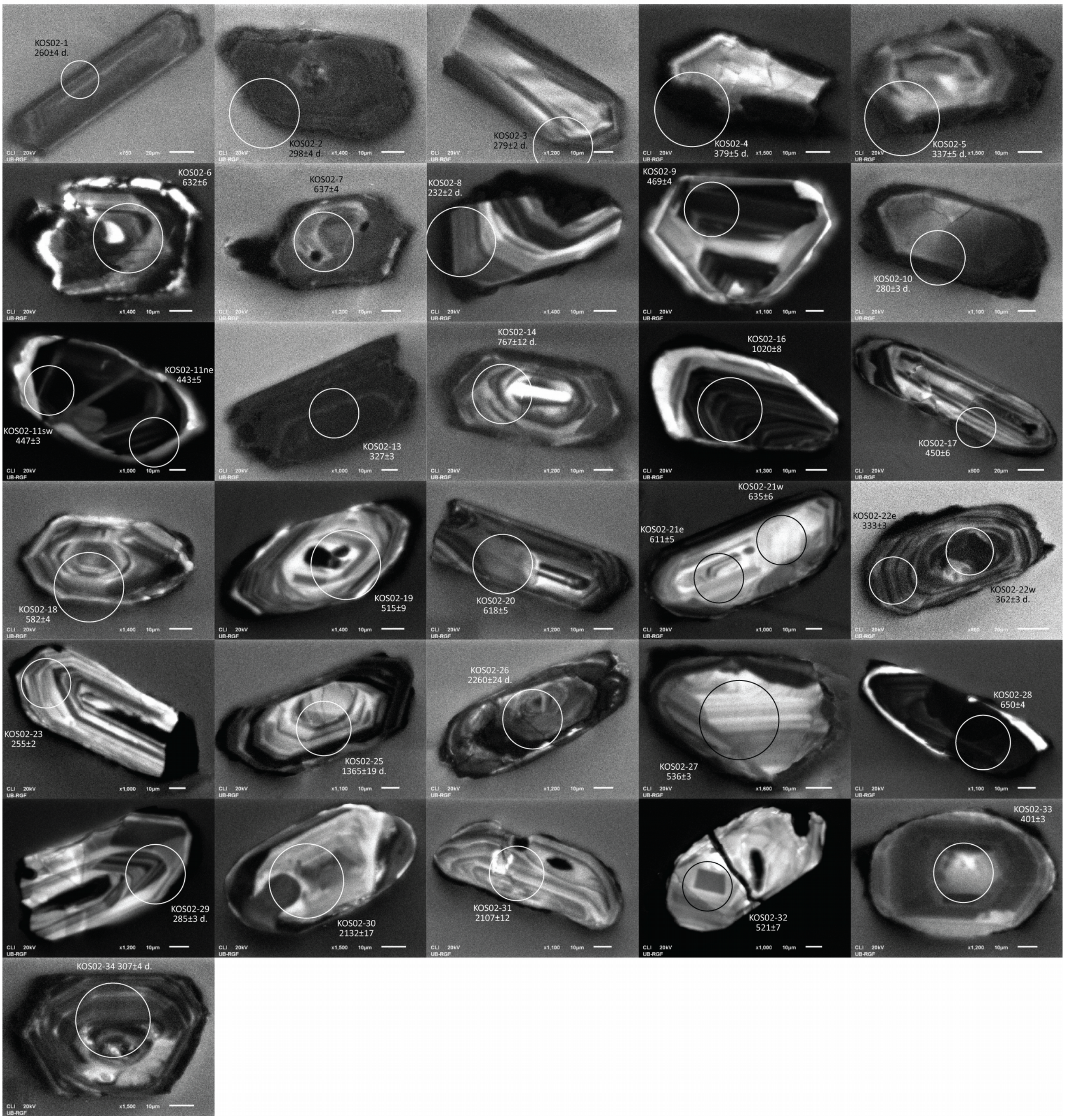

SM01 Kukavica granite

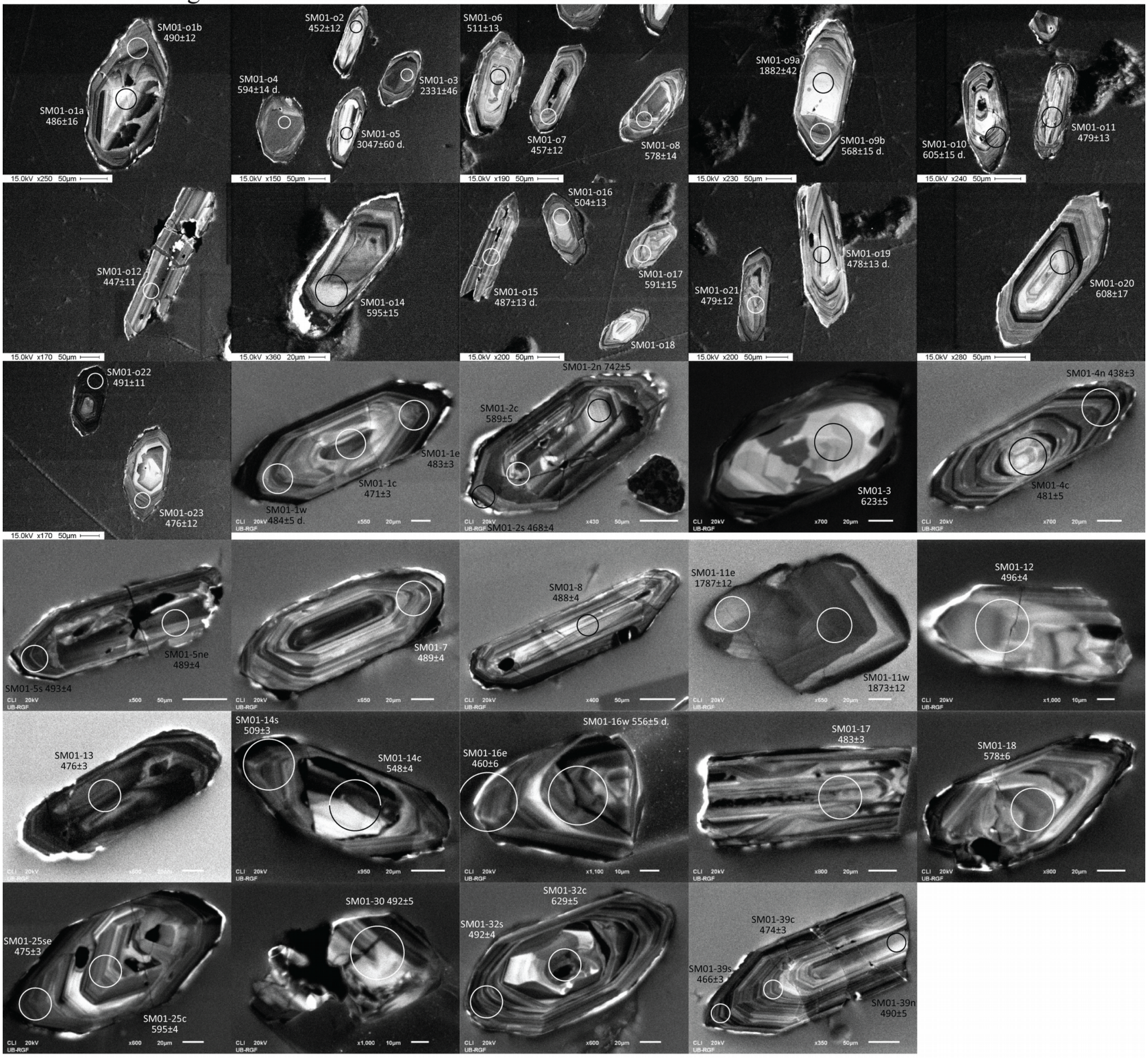

SM02 Vlajna granite

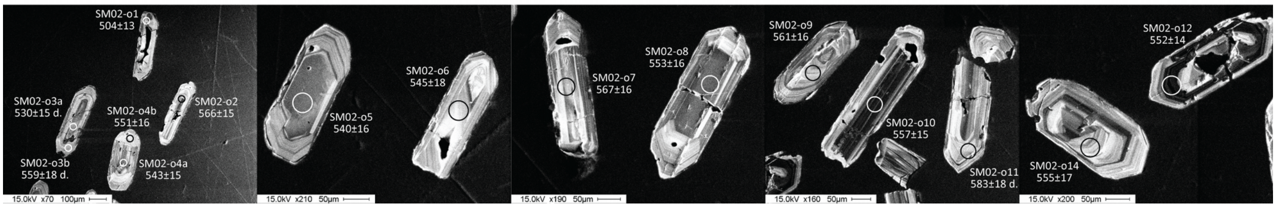

SM02 Vlajna granite (continued)

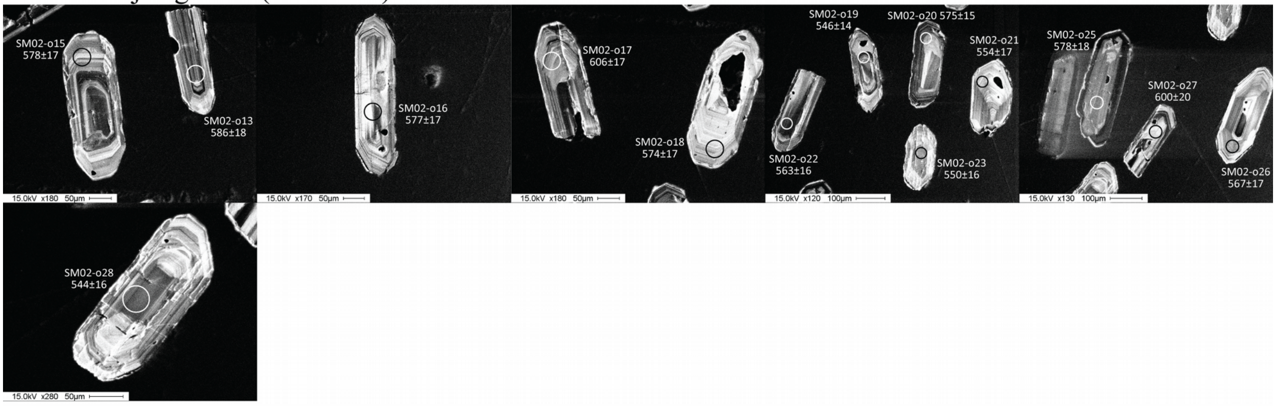

SM140-1 Delčevo granite

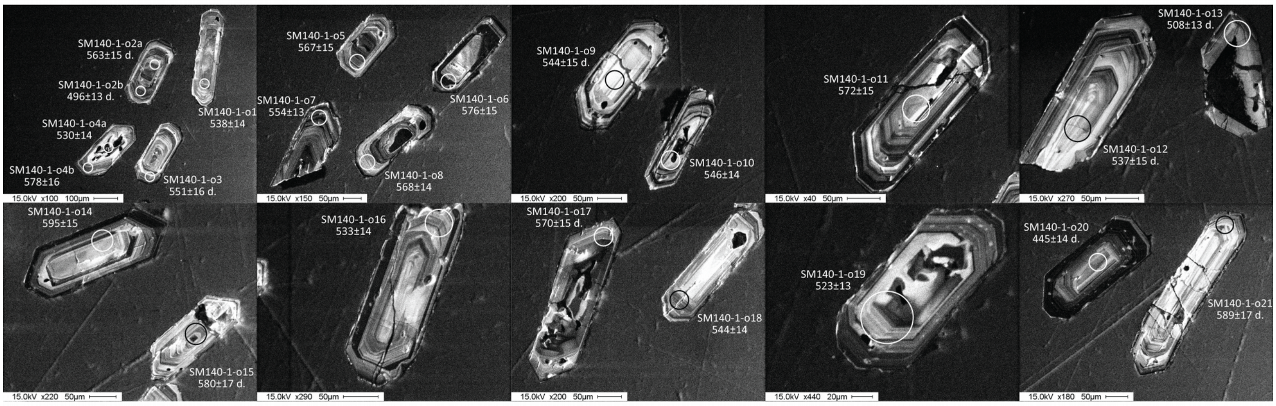

SM173-1 Vinica amphibolite

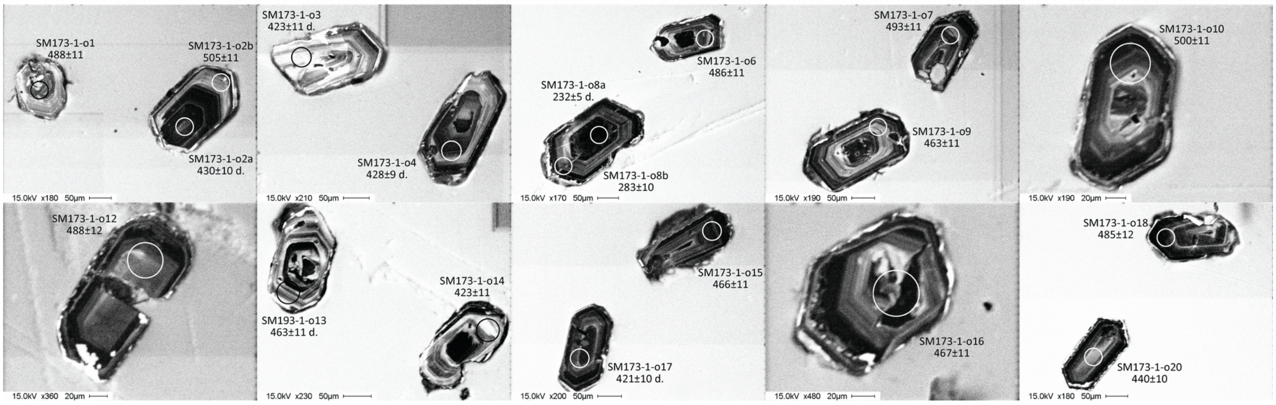

SM173-1 Vinica amphibolite (continued)

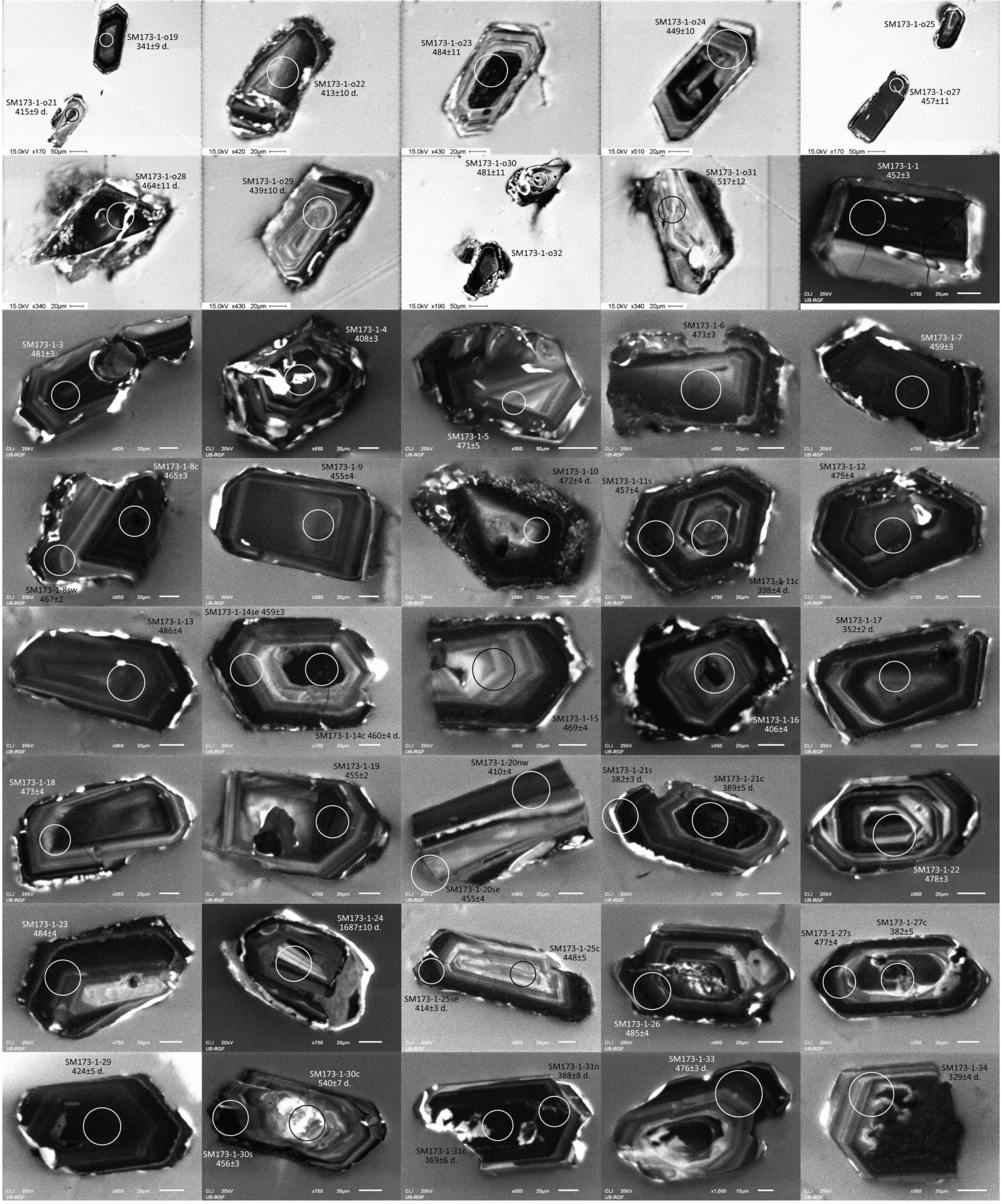

SM173-1 Vinica amphibolite (continued)

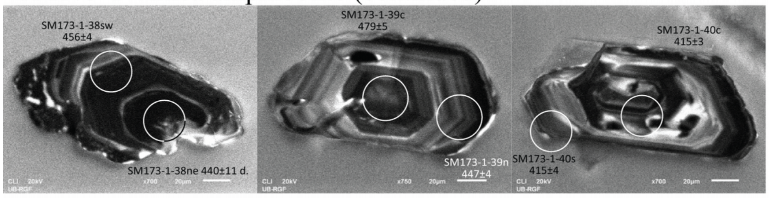

SM173-3 Vinica leucocratic dyke

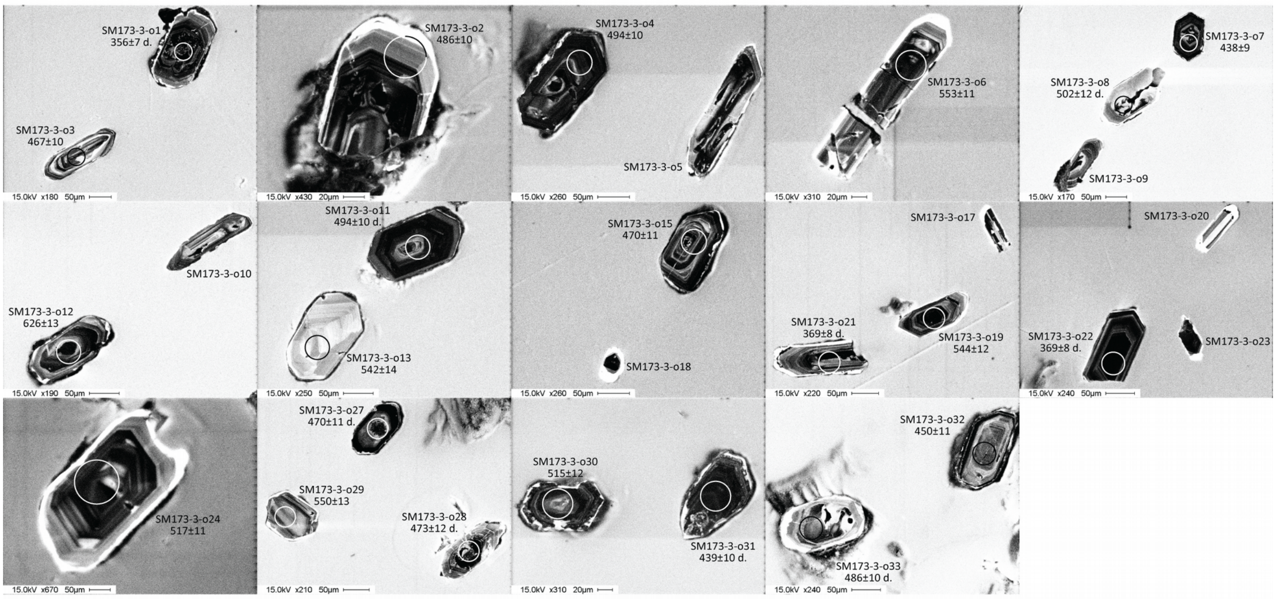

SM184-1 Maleševski Mts. orthogneiss

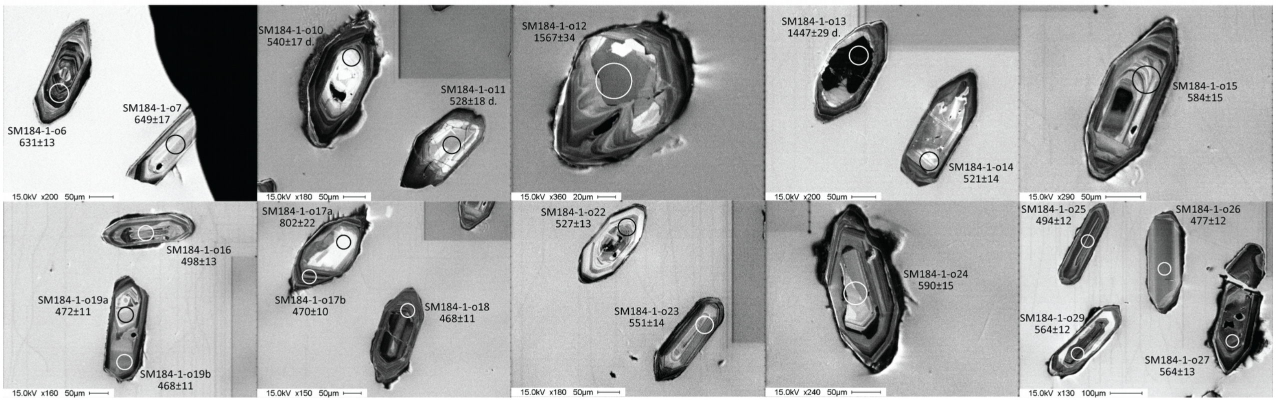

SM184-1 Maleševski Mts. orthogneiss (continued)

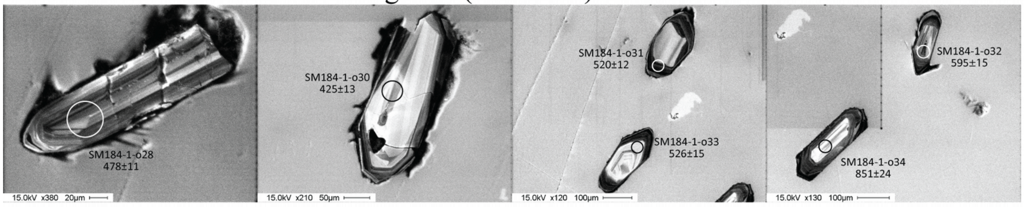

SM195-1 Granite from the Štip magmatic complex

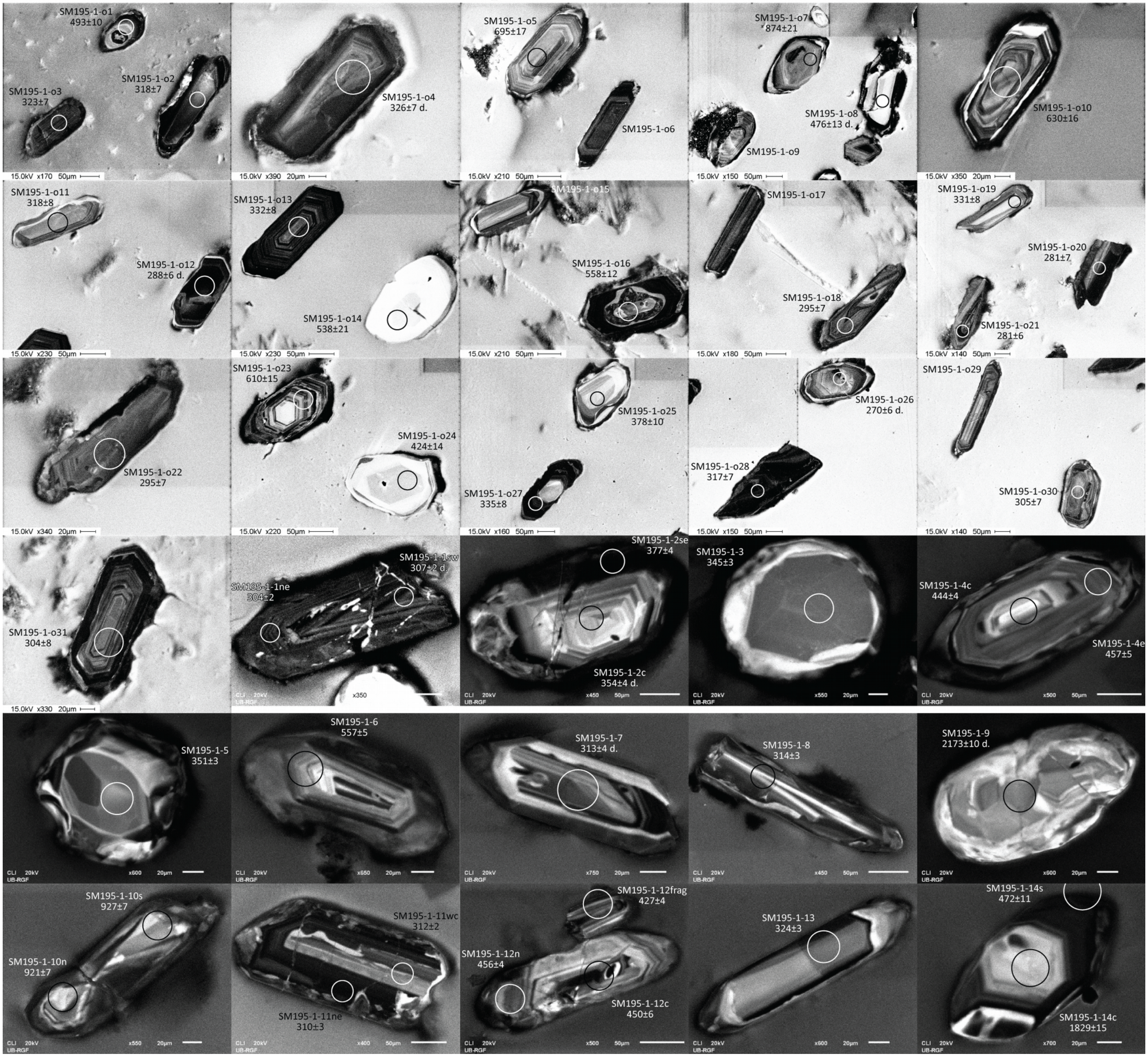

SM195-1 Granite from the Štip magmatic complex (continued)

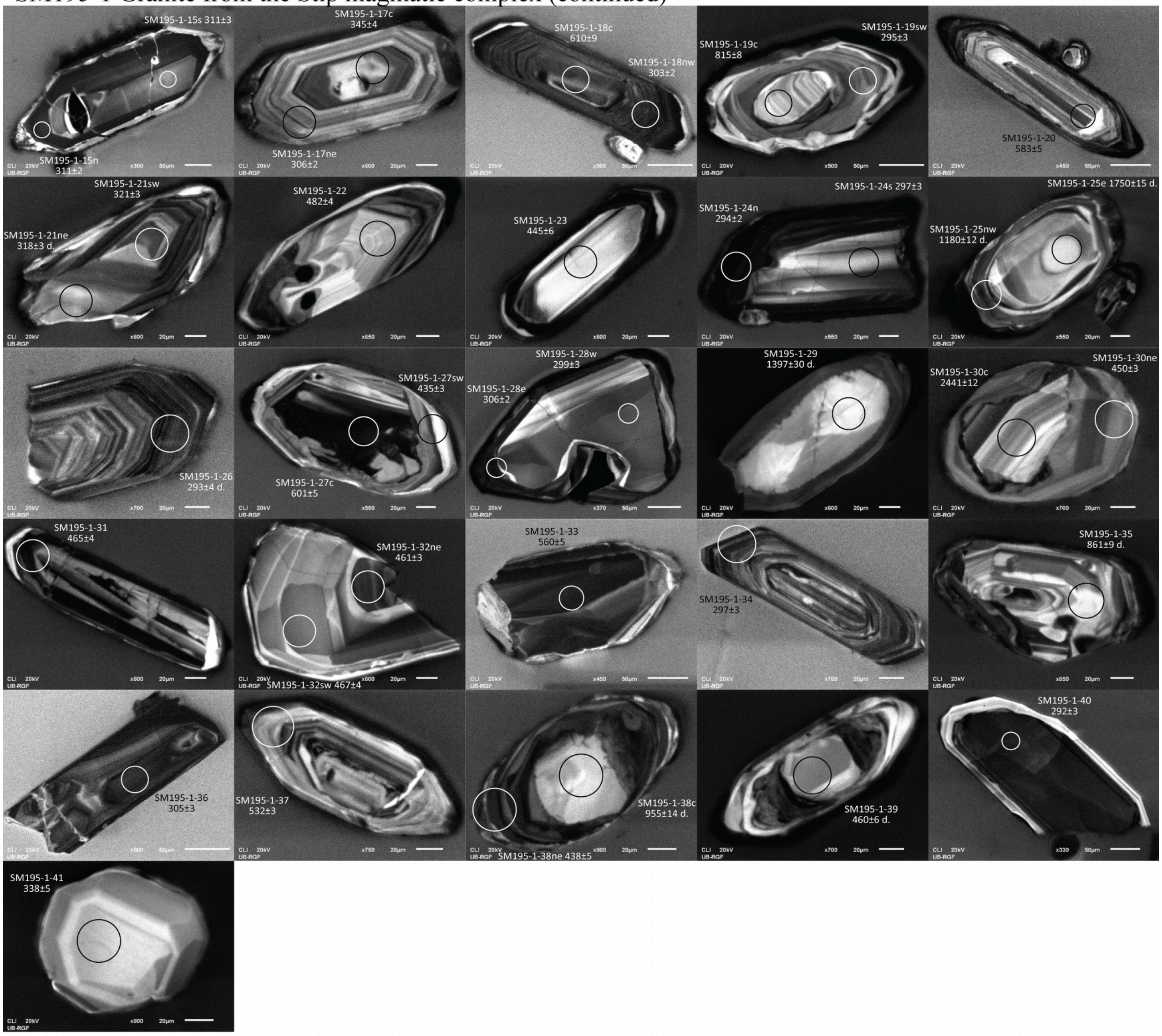

SM199-1 Undeformed Bujanovac granite (central part)

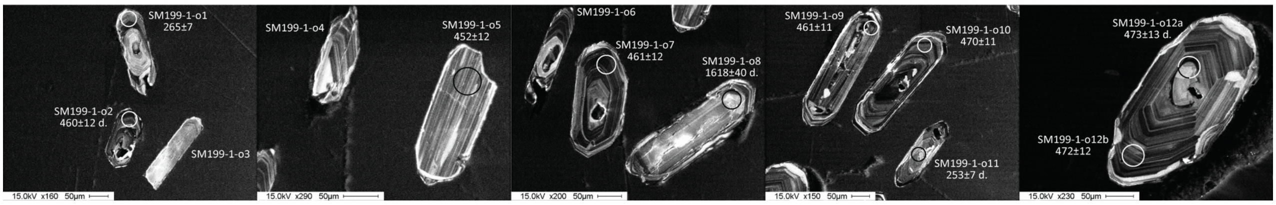

SM199-1 Undeformed Bujanovac granite (central part; continued)

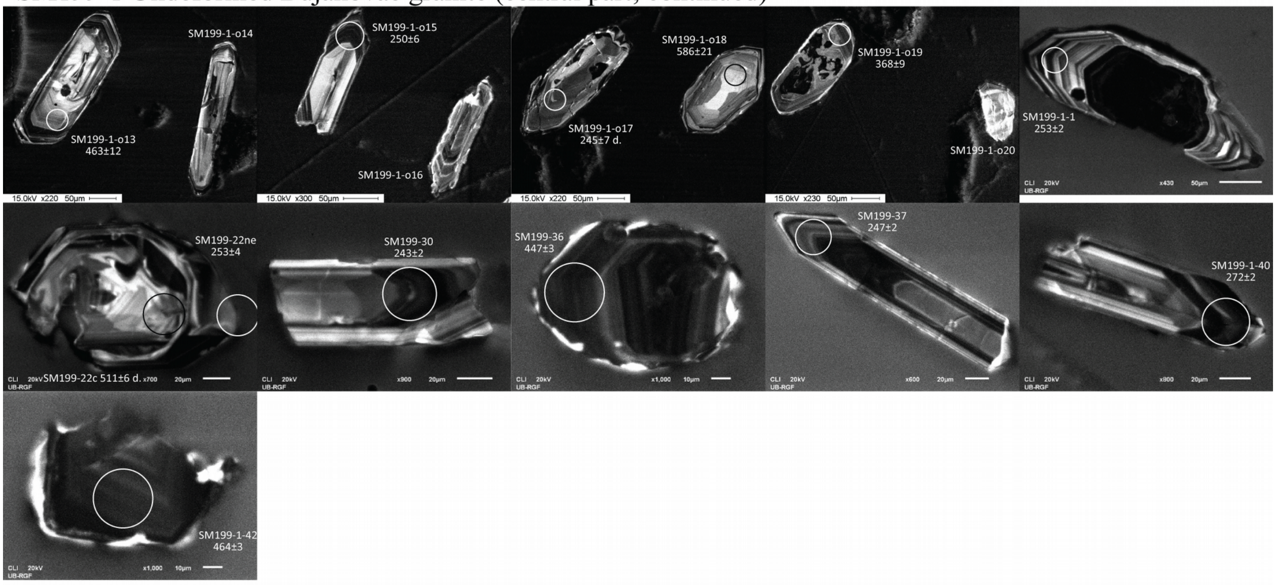

SM236-1 Bosilegrad monzonite

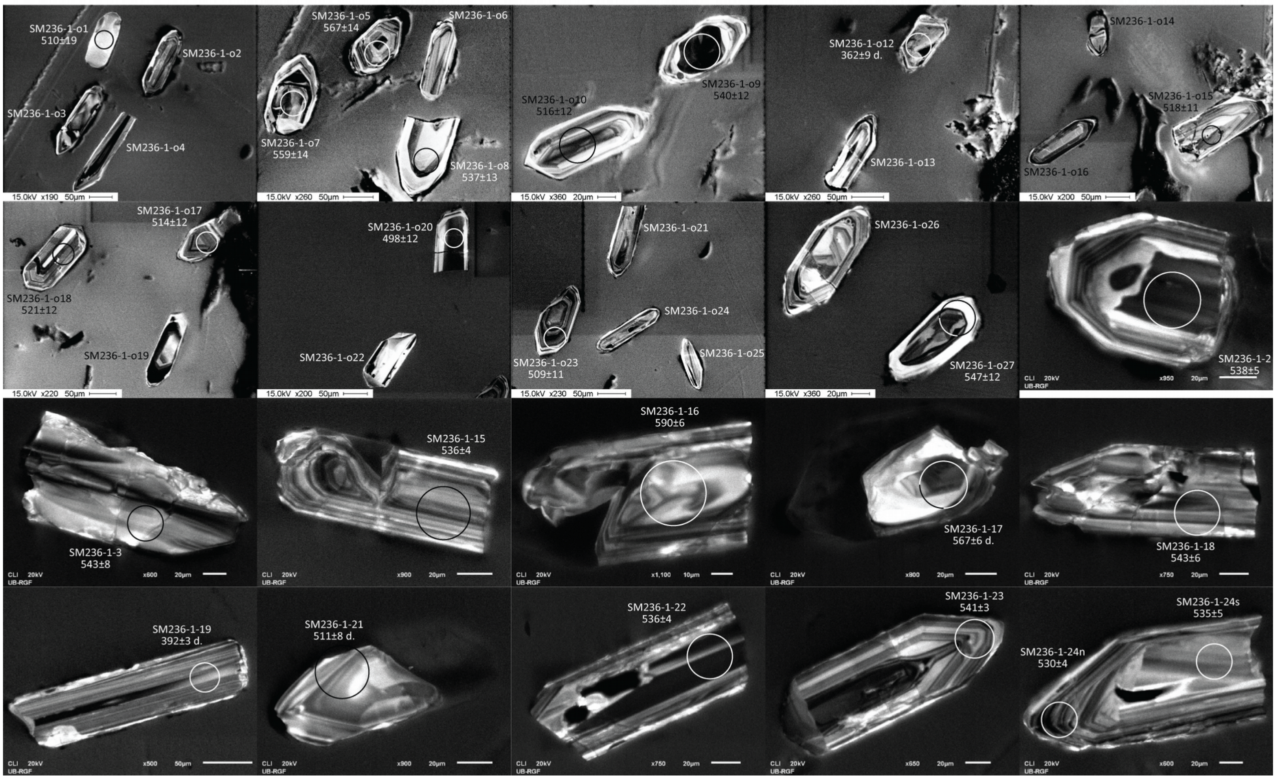

Appendix 2-5 Cathodoluminescence images of analysed zircons

SM236-1 Bosilegrad monzonite (continued)

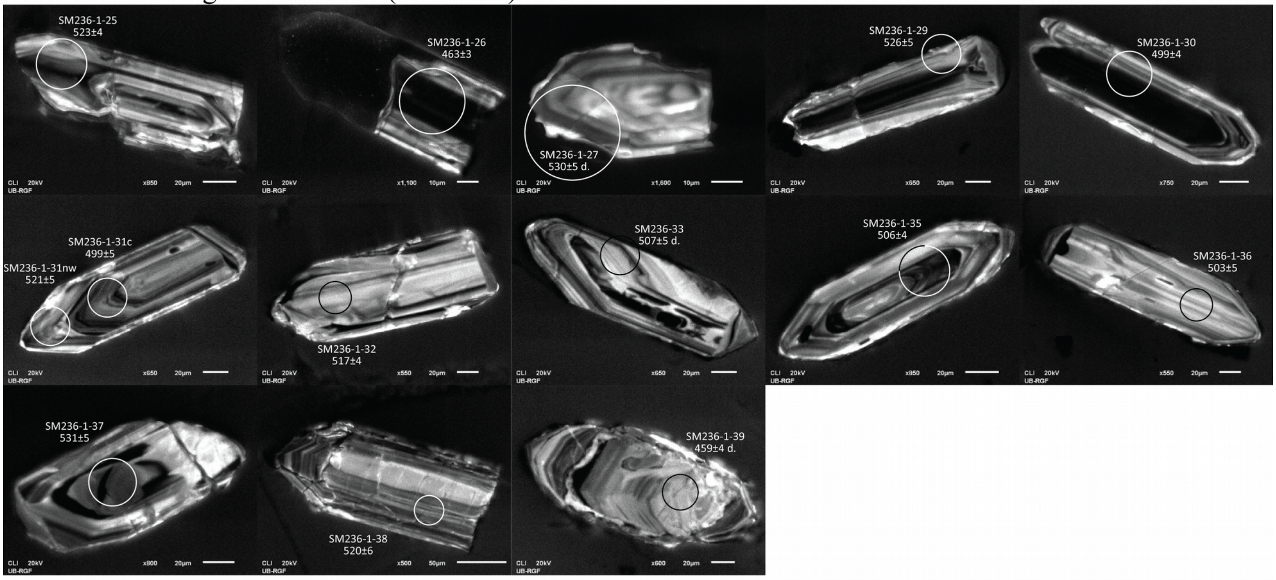

SM250-1 Golemo Selo amphibolite

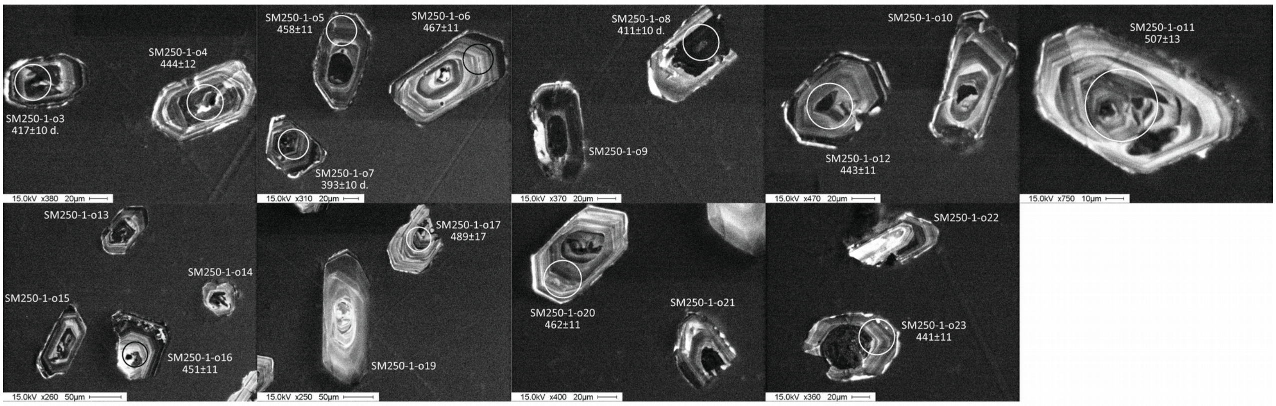

SM250-02 Golemo Selo paragneiss

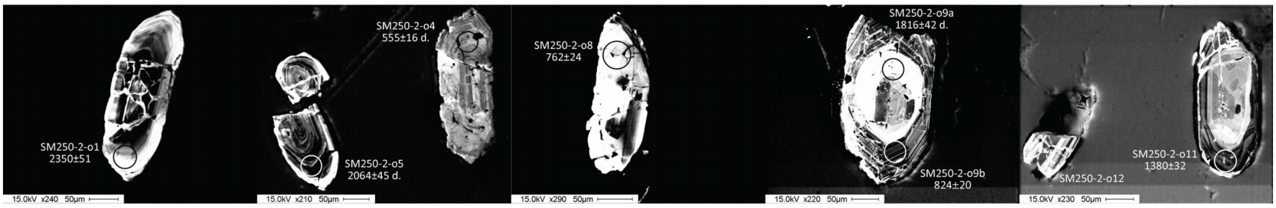

SM250-02 Golemo Selo paragneiss (continued)

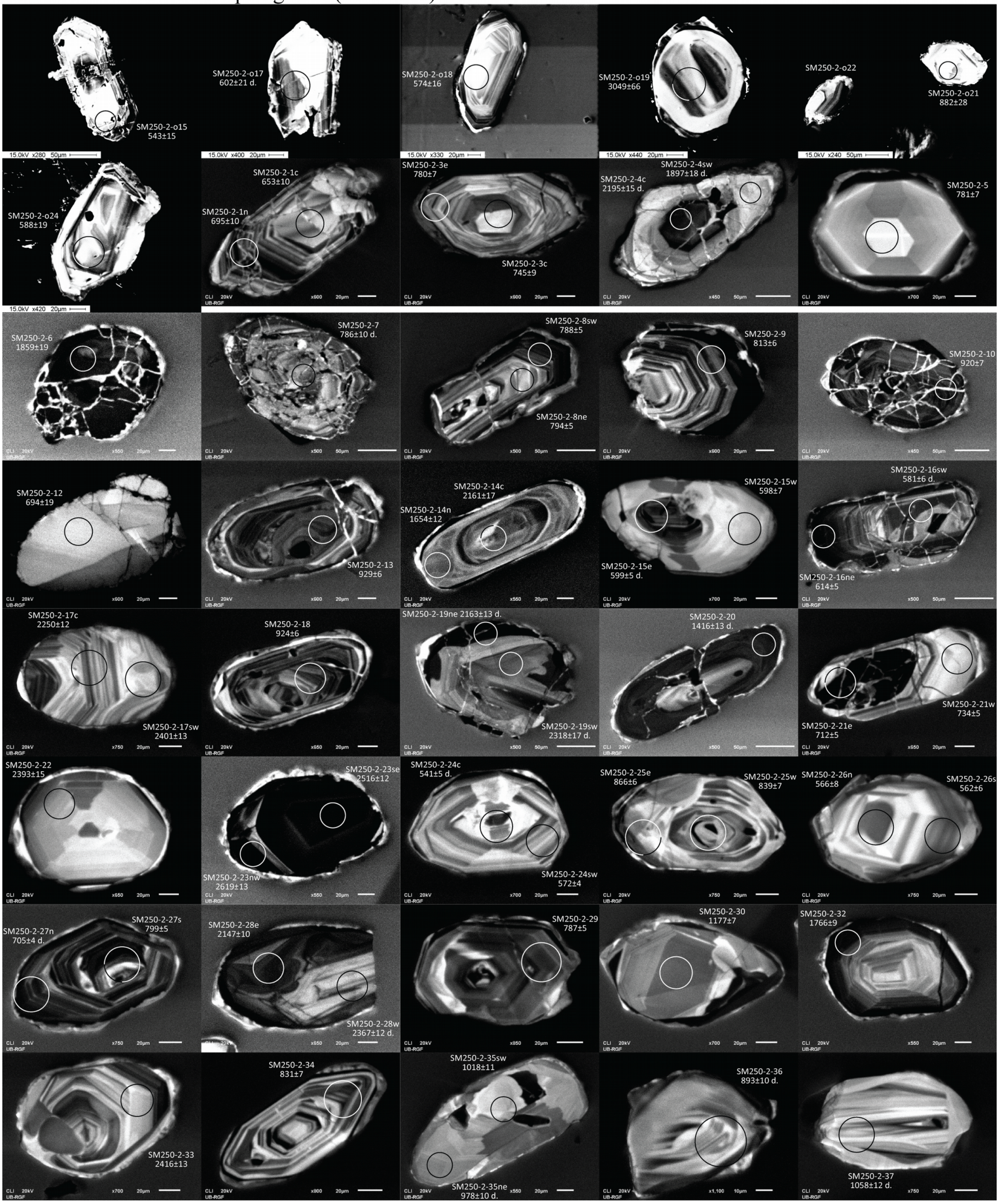

SM250-02 Golemo Selo paragneiss (continued)

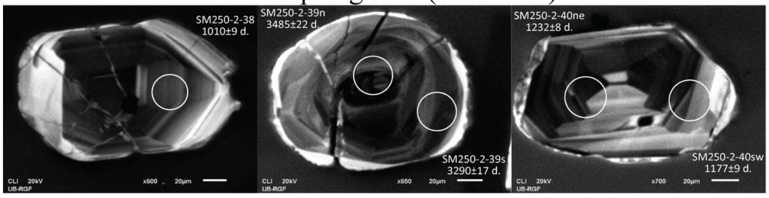

SM272-1 Granite from the Božica magmatic complex

SM272-1 Granite from the Božica magmatic complex (continued)

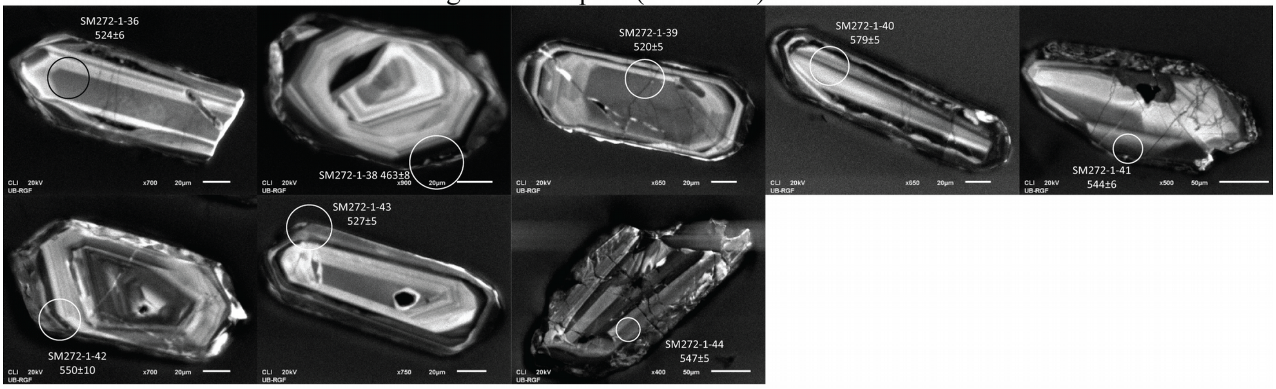

SM310 Sijarinska Banja paragneiss

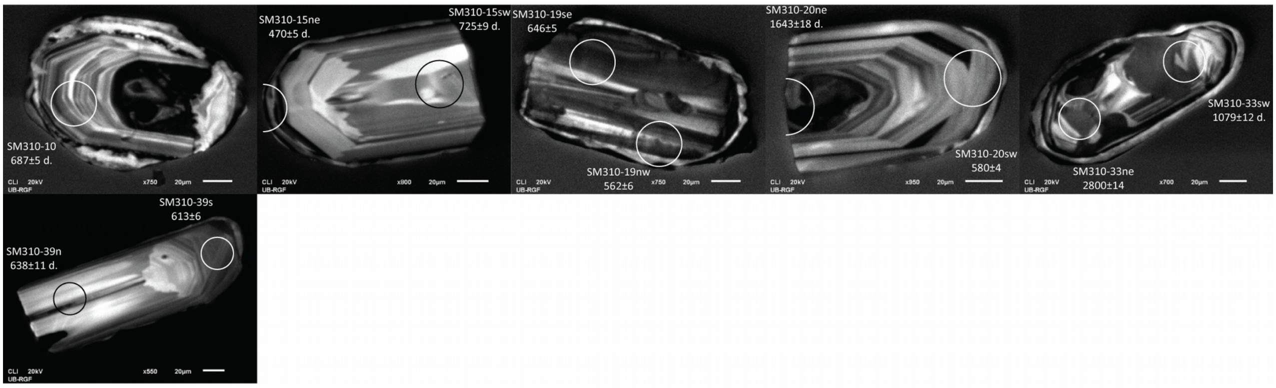

SM315 Bukovac metagranite

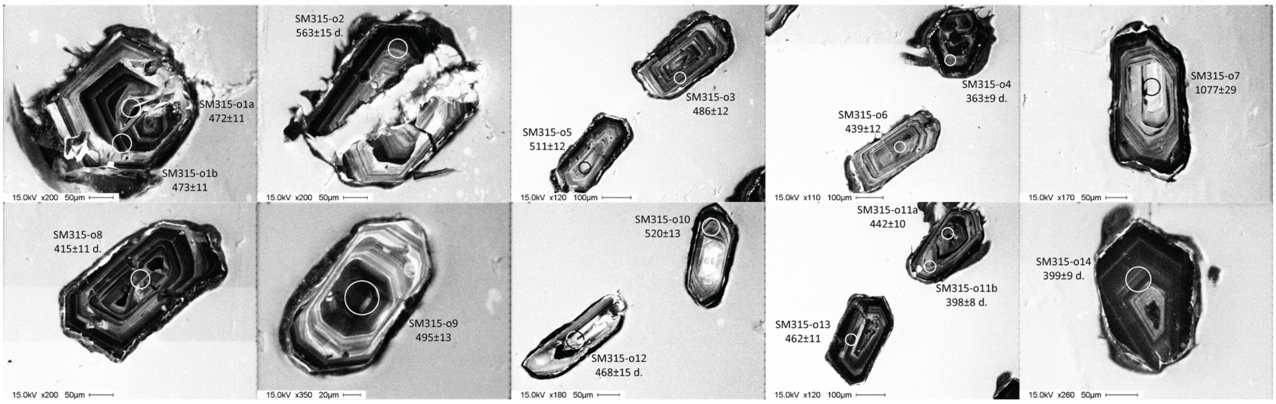

SM315 Bukovac metagranite (continued)

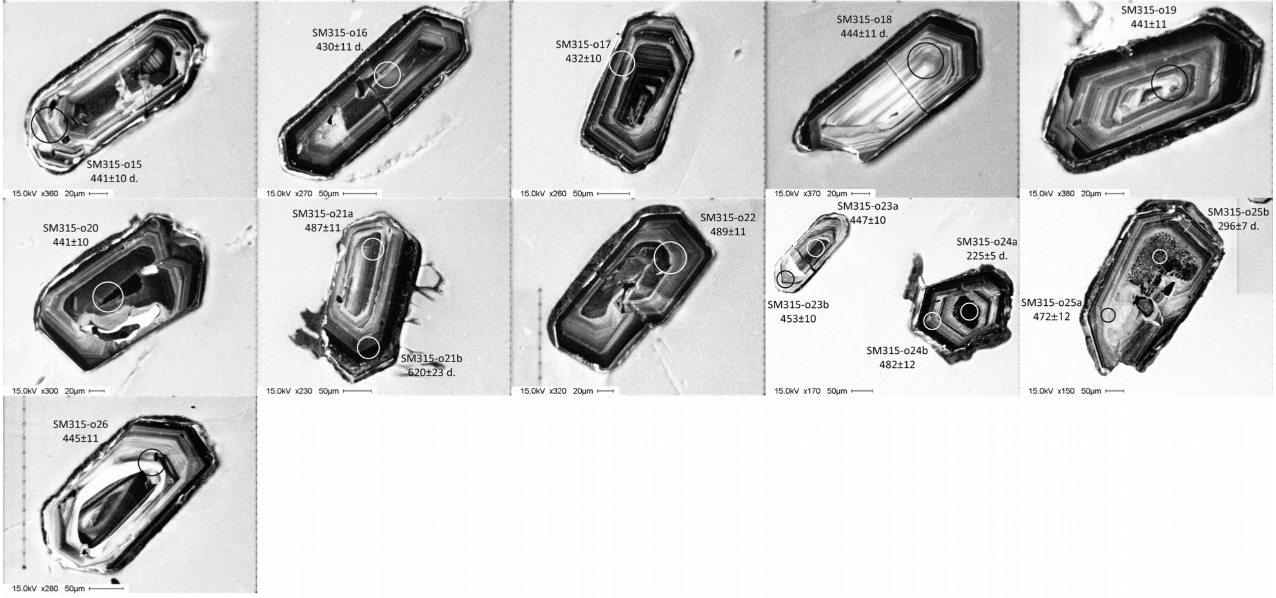

SM352 Lisina gabbro

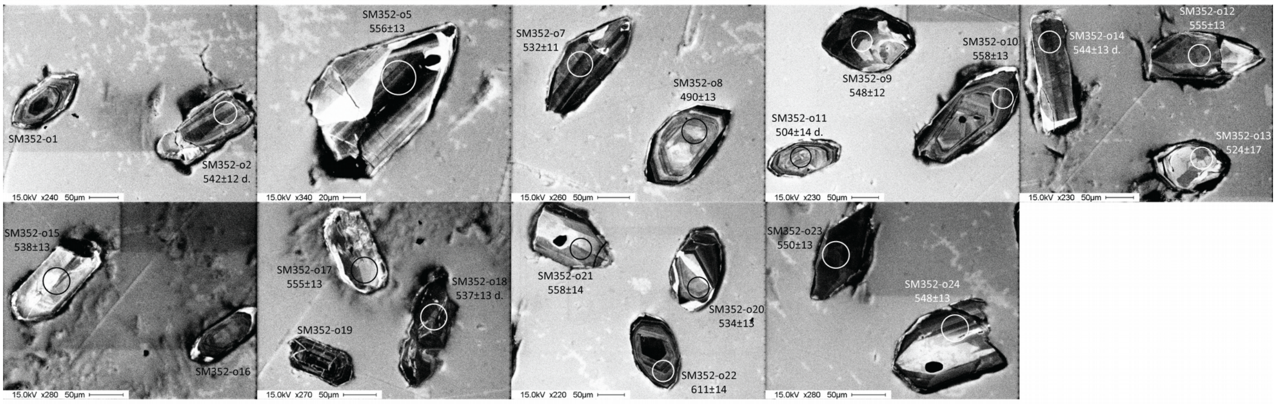

SM377-1 weakly deformed Bujanovac granite (southern part)

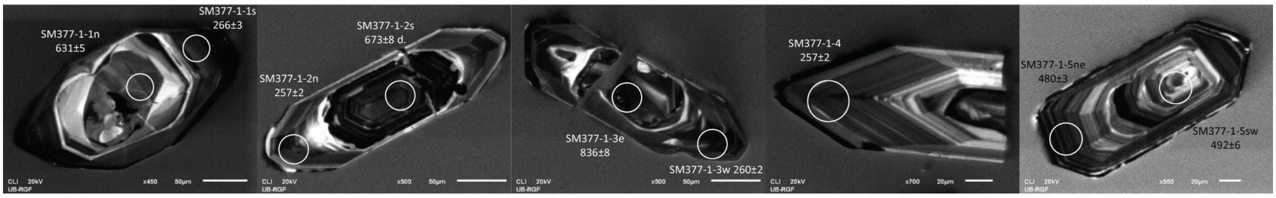

SM377-1 weakly deformed Bujanovac granite (southern part; continued)

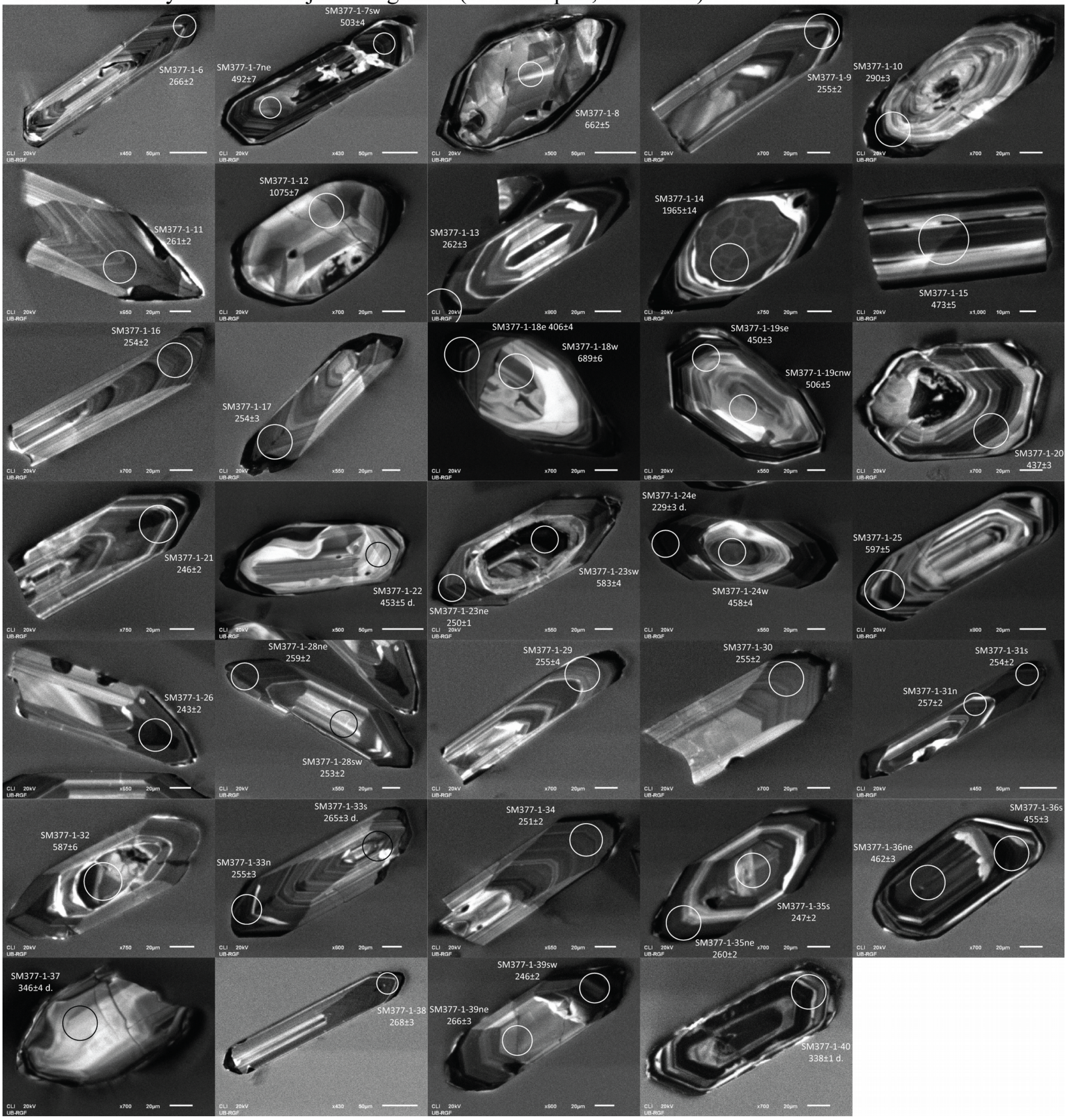

Appendix 2-5 Cathodoluminescence images of analysed zircons

SM377-2 deformed Bujanovac Qz-monzonite (southern part)

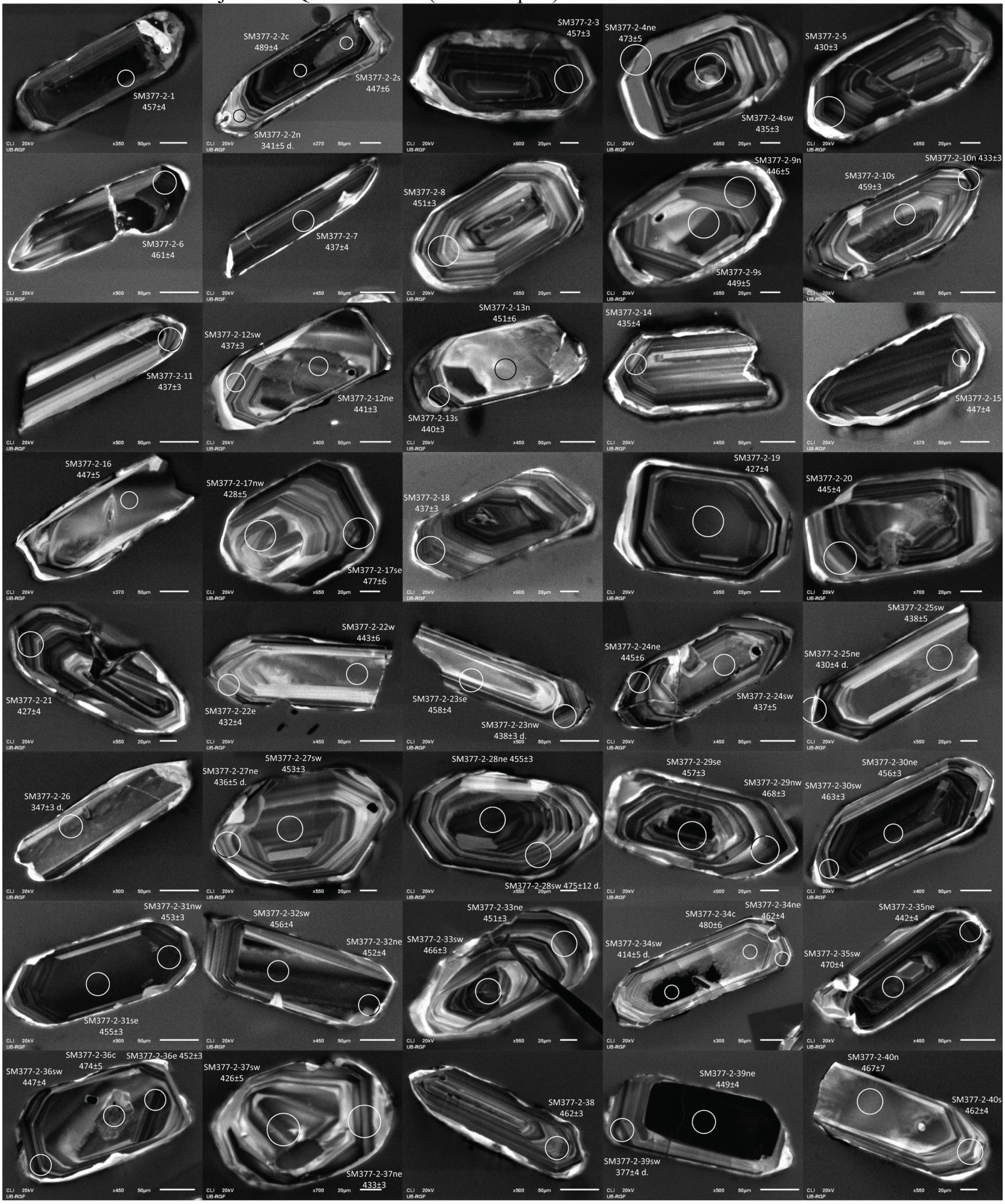

SM550-1 Slatinska Reka granite

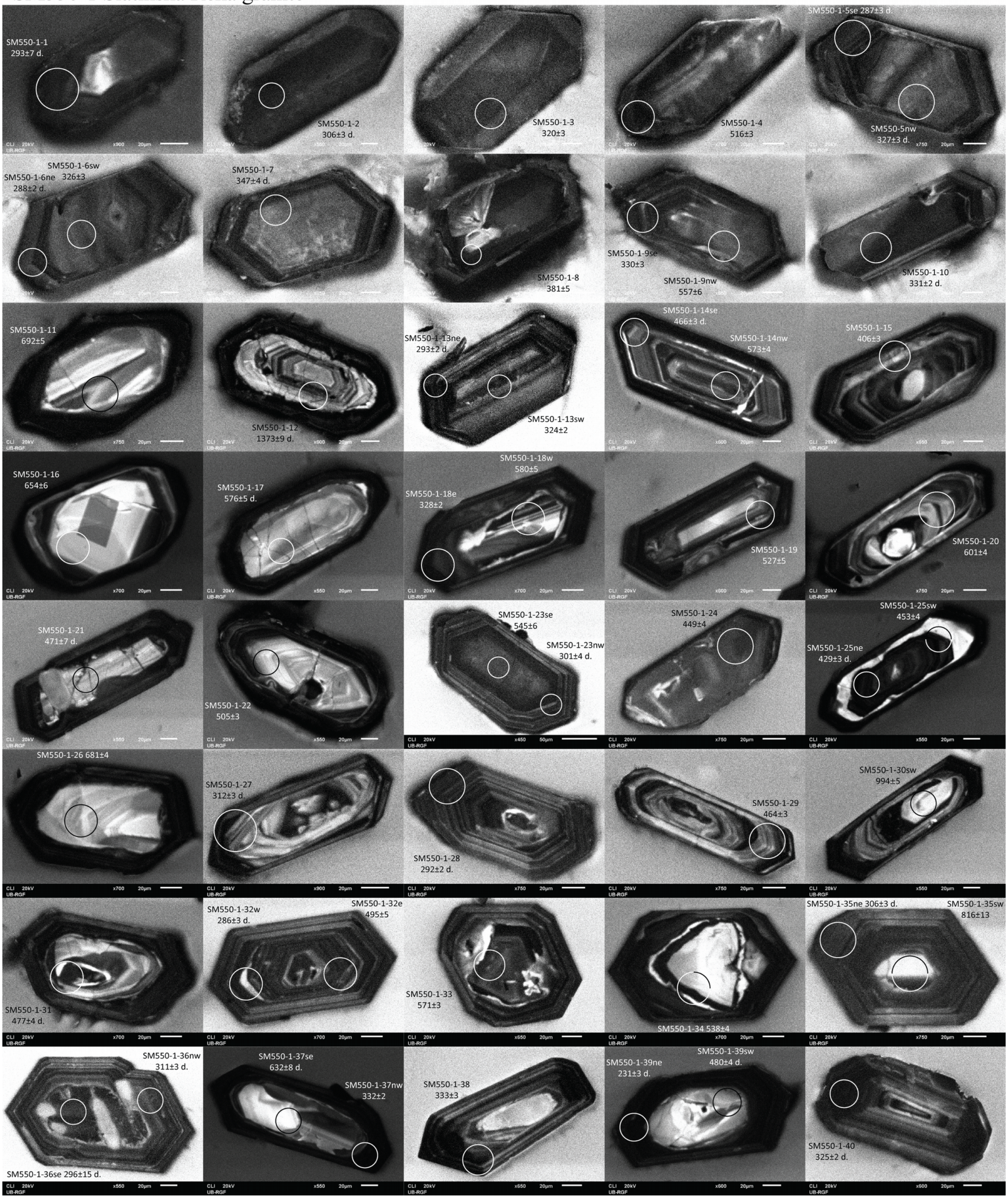

Appendix 2-5 Cathodoluminescence images of analysed zircons

SM600-1 Doganica metagranite

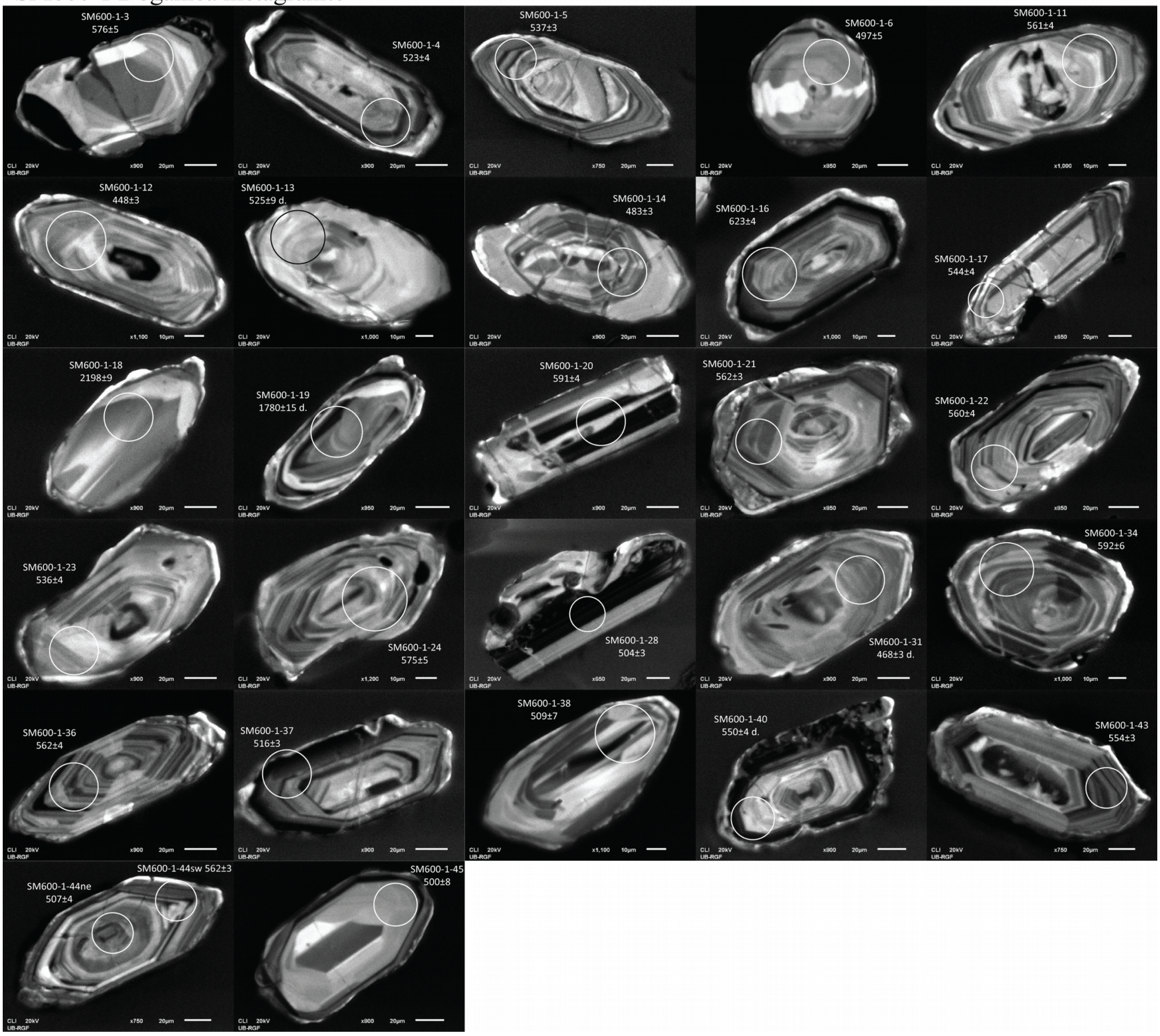

Appendix 2-6

Ternary geochemical discrimination diagram for subalkaline rocks for sample SM502-1 from Vlasina unit

Appendix 2-6. Ternary geochemical discrimination diagram for subalkaline rocks for sample SM502-1 from Vlasina unit (Jensen, 1976).

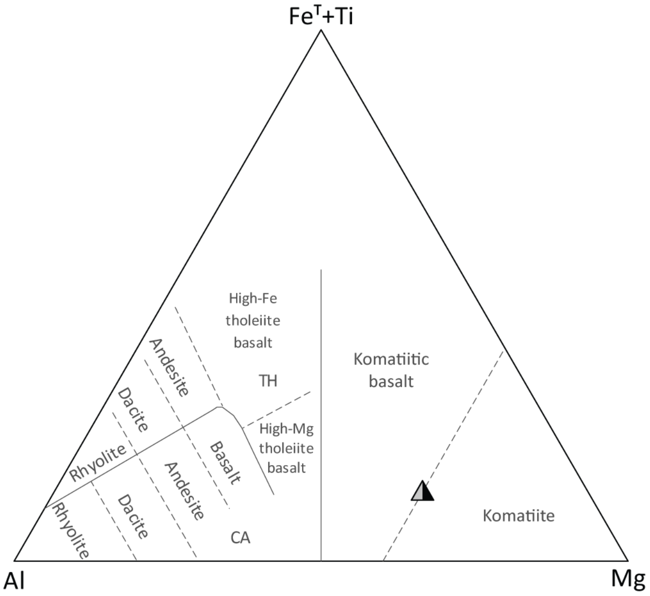

Reference.

Jensen, L.S., 1976. A new cation plot for classifying subalkalic volcanic rocks, Ontario Division of Mines, Miscellaneous papers, 66. Ministry of Natural Resources, Ontario.

Appendix 2-7

LA-MC-ICP-MS Lu-Hf isotope data from zircon spots previously used for U–Pb age determination

Appendix 2-7 LA-MC-ICP-MS Lu-Hf isotope data from zircons

samples	^{176}Yb/^{177}Hf	^{176}Lu/^{177}Hf	^{176}Hf/^{177}Hf	±2σ	^{176}Hf/^{177}Hf$_{(t)}$^{a}	εHf$_{(t)}$^{a}	T$_{DM}$^{b} [Ga]	^{206}Pb/^{238}U [Ma]
KOS02-13	0,1034	0,0024289	0,282522	0,000012	0,282507	-2,21	1,15	326
KOS02-22e	0,0651	0,0016089	0,282395	0,000023	0,282385	-6,38	1,39	333
KOS02-23	0,1116	0,0028672	0,282422	0,000017	0,282408	-7,27	1,38	255
KOS02-32	0,1361	0,003495	0,28249	0,000026	0,282456	0,28	1,17	521
KOS02-33	0,0102	0,0002205	0,282425	0,000008	0,282423	-3,52	1,29	401
KOS02-9	0,1329	0,0029174	0,282452	0,000025	0,282426	-1,91	1,25	469
SM01-14s	0,1451	0,0034599	0,282337	0,000069	0,282304	-5,36	1,47	509
SM01-1e	0,1291	0,0023124	0,282348	0,000009	0,282327	-5,12	1,44	483
SM01-25se	0,1599	0,0038385	0,282359	0,000013	0,282325	-5,37	1,45	475
SM01-2n	0,0632	0,0012415	0,282061	0,000011	0,282044	-9,41	1,88	742
SM01-3	0,0433	0,0091471	0,28237	0,00001	0,282263	-4,28	1,5	623
SM01-32c	0,0598	0,0011256	0,282332	0,00001	0,282319	-2,18	1,39	629
SM01-32s	0,1248	0,0030296	0,282342	0,000013	0,282314	-5,38	1,46	492
SM01-39c	0,0772	0,00149	0,28232	0,000009	0,282307	-6,20	1,48	475
SM01-39n	0,1034	0,0019507	0,282347	0,000011	0,282329	-4,91	1,43	489
SM01-39s	0,1985	0,0043834	0,282391	0,000015	0,282353	-4,41	1,4	466
SM01-5ne	0,1286	0,0030187	0,282384	0,000014	0,282356	-3,95	1,38	489
SM01-7	0,2187	0,0054199	0,282375	0,000024	0,282325	-5,04	1,44	489
SM01-o3	0,0578	0,001418	0,281151	0,000022	0,281088	-7,44	3,03	2331
SM01-o9a	0,0164	0,000415	0,281189	0,000018	0,281174	-14,63	3,06	1882
SM02-o14	0,0443	0,001185	0,282626	0,000019	0,282614	6,63	0,85	555
SM02-o15	0,0458	0,001224	0,282636	0,000021	0,282623	7,47	0,82	578
SM02-o18	0,0364	0,000979	0,282646	0,00002	0,282636	7,83	0,8	574
SM02-o4b	0,0473	0,00133	0,282627	0,00002	0,282613	6,51	0,85	551
SM02-o5	0,0614	0,001584	0,282667	0,000021	0,282651	7,60	0,79	540
SM02-o8	0,0799	0,002027	0,282719	0,000024	0,282698	9,55	0,69	553
SM140-1-o11	0,0616	0,001514	0,282697	0,000018	0,282681	9,38	0,71	572
SM140-1-o16	0,0516	0,001364	0,282675	0,000041	0,282661	7,82	0,77	533
SM140-1-o4b	0,0456	0,001228	0,282682	0,000019	0,282669	9,10	0,73	578
SM140-1-o7	0,0616	0,00163	0,282672	0,000021	0,282655	8,07	0,77	554
SM140-1-o1	0,0806	0,002048	0,282742	0,000021	0,282722	10,07	0,65	538
SM173-1-6	0,1271	0,0019147	0,282567	0,000011	0,28255	2,56	1,01	473

Appendix 2-7 LA-MC-ICP-MS Lu-Hf isotope data from zircons

samples	$^{176}Yb/^{177}Hf$	$^{176}Lu/^{177}Hf$	$^{176}Hf/^{177}Hf$	±2σ	$^{176}Hf/^{177}Hf_{(t)}{}^{a}$	$\varepsilon Hf_{(t)}{}^{a}$	$T_{DM}{}^{b}$ [Ga]	$^{206}Pb/^{238}U$ [Ma]
SM173-1-7	0,1436	0,0024567	0,282578	0,000012	0,282557	2,47	1	458
SM173-1-9	0,1059	0,0016044	0,28257	0,000013	0,282556	2,38	1,01	455
SM173-1-o27	0,0746	0,001638	0,282751	0,000024	0,282736	8,80	0,65	457
SM173-1-o2b	0,0709	0,001696	0,282706	0,000021	0,28269	8,21	0,72	505
SM173-1-o8b	0,0914	0,002205	0,282743	0,000018	0,282723	8,89	0,67	483
SM173-3-o13	0,0844	0,001989	0,282768	0,000032	0,282748	11,10	0,59	542
SM173-3-o2	0,0314	0,000875	0,282673	0,000025	0,282665	6,89	0,78	486
SM173-3-o4	0,0827	0,00186	0,282755	0,000025	0,282738	9,66	0,63	494
SM184-1-o17a	0,0267	0,000631	0,281822	0,000019	0,281812	-16,27	2,3	802
SM184-1-o17b	0,0631	0,001563	0,282493	0,000021	0,282479	-0,02	1,15	470
SM184-1-o19a	0,0217	0,000554	0,282538	0,000024	0,282533	1,93	1,04	472
SM184-1-o19b	0,0662	0,001521	0,282596	0,000027	0,282583	3,59	0,95	468
SM184-1-o26	0,1053	0,002237	0,282766	0,000043	0,282746	9,59	0,62	477
SM195-1-24s	0,1184	0,0024952	0,282513	0,000012	0,282499	-3,13	1,18	297
SM195-1-3	0,0042	0,0000775	0,282397	0,000008	0,282396	-5,70	1,36	345
SM195-1-30c	0,055	0,0012489	0,281339	0,000015	0,281281	1,96	2,62	2441
SM195-1-30ne	0,0474	0,0012682	0,282339	0,000013	0,282328	-5,80	1,45	450
SM195-1-40	0,0176	0,0003311	0,282371	0,000008	0,282369	-7,84	1,44	292
SM195-1-41	0,0068	0,0001292	0,282458	0,000009	0,282457	-3,71	1,25	338
SM195-1-5	0,0045	0,0000758	0,282525	0,000009	0,282525	-1,04	1,11	351
SM195-1-o13	0,0427	0,001132	0,282608	0,00002	0,282601	1,23	0,97	332
SM195-1-o2	0,0442	0,001025	0,282265	0,000121	0,282259	-11,19	1,64	318
SM195-1-o25	0,0443	0,000991	0,282545	0,000015	0,282538	0,04	1,07	378
SM199-1-1	0,0454	0,0099643	0,282969	0,000011	0,282922	10,86	0,37	253
SM199-1-30	0,1166	0,0027708	0,28289	0,000072	0,282877	9,07	0,47	243
SM199-1-36	0,0829	0,0019932	0,282594	0,000011	0,282577	2,95	0,97	447
SM199-1-37	0,1078	0,0023028	0,282869	0,000015	0,282858	8,48	0,5	247
SM199-1-o12b	0,0431	0,001146	0,282513	0,000023	0,282503	0,87	1,1	472
SM199-1-o18	0,0224	0,000541	0,282071	0,000022	0,282065	-12,13	1,9	586
SM199-1-o5	0,0733	0,001863	0,28258	0,000022	0,282564	2,61	0,99	452
SM236-1-32	0,0498	0,0009905	0,282606	0,000012	0,282596	5,17	0,9	517
SM236-1-o1	0,0289	0,000751	0,28258	0,000041	0,282573	4,18	0,95	510

Appendix 2-7 LA-MC-ICP-MS Lu-Hf isotope data from zircons

samples	$^{176}Yb/^{177}Hf$	$^{176}Lu/^{177}Hf$	$^{176}Hf/^{177}Hf$	±2σ	$^{176}Hf/^{177}Hf_{(t)}$ [a]	$\varepsilon Hf_{(t)}$ [a]	T_{DM} [b] [Ga]	$^{206}Pb/^{238}U$ [Ma]
SM236-1-o15	0,0656	0,00166	0,282716	0,000023	0,2827	8,86	0,7	518
SM236-1-o8	0,0146	0,000484	0,282579	0,000021	0,282574	4,82	0,94	537
SM250-1-o20	0,0537	0,001387	0,282691	0,000022	0,282679	6,86	0,76	462
SM250-1-o5	0,1181	0,002836	0,282733	0,000032	0,282709	7,84	0,71	458
SM250-1-o6	0,0739	0,001822	0,282712	0,000023	0,282696	7,59	0,73	467
SM250-2-12	0,0279	0,0006166	0,282263	0,000012	0,282255	-2,99	1,49	694
SM250-2-15w	0,0121	0,0002921	0,28254	0,000007	0,282537	4,85	0,98	598
SM250-2-22	0,02	0,0004556	0,281225	0,000008	0,281204	-1,87	2,79	2393
SM250-2-23se	0,0841	0,0018509	0,281016	0,000009	0,280927	-8,89	3,25	2516
SM250-2-24sw	0,0485	0,00113	0,282497	0,000052	0,282484	2,41	1,1	572
SM250-2-26s	0,0622	0,0013146	0,282473	0,000008	0,282459	1,31	1,15	562
SM250-2-30	0,058	0,001144	0,282179	0	0,282154	4,22	1,48	1177
SM250-2-o1	0,0158	0,000399	0,281522	0,000025	0,281504	7,80	2,24	2350
SM250-2-o19	0,0357	0,000755	0,28078	0,000064	0,280736	-3,33	3,39	3049
SM250-2-o24	0,0492	0,001095	0,282517	0,00007	0,282505	3,50	1,05	588
SM272-1-13ne	0,1069	0,002416	0,282822	0,000021	0,282798	12,62	0,5	530
SM272-1-25	0,0348	0,001164	0,282594	0,000049	0,282582	4,86	0,93	526
SM272-1-3	0,058	0,001479	0,282723	0,000018	0,282708	10,08	0,67	561
SM272-1-35ne	0,0546	0,001451	0,282679	0,000028	0,282664	8,06	0,76	539
SM272-1-35sw	0,082	0,001876	0,282761	0,000016	0,282742	10,82	0,61	540
SM310-20sw	0,0369	0,0009955	0,281905	0,000014	0,281894	-18,30	2,23	580
SM310-39s	0,013	0,0003248	0,282292	0,000016	0,282288	-3,61	1,46	613
SM315-o3	0,069	0,001533	0,282764	0,000019	0,28275	9,94	0,61	486
SM315-o9	0,188	0,004516	0,283035	0,000031	0,282993	18,72	0,13	495
SM352-o12	0,0191	0,00313	0,282443	0,000027	0,282443	0,57	1,18	555
SM352-o20	0,0192	0,000513	0,282393	0,000022	0,282387	-1,85	1,3	534
SM352-o21	0,0161	0,000416	0,28235	0,000023	0,282345	-2,80	1,37	558
SM352-o22	0,0739	0,001844	0,282482	0,000017	0,282461	2,46	1,13	611
SM352-o5	0,029	0,000675	0,282429	0,00003	0,282422	-0,14	1,22	556
SM377-1-12	0,0622	0,001386	0,282028	0,000017	0,282	-3,56	1,82	1075
SM377-1-14	0,004	0,000091	0,281371	0,000013	0,281368	-5,86	2,66	1965
SM377-1-26	0,081	0,0018	0,283012	0,000026	0,283004	13,54	0,22	243

samples	^{176}Yb/^{177}Hf	^{176}Lu/^{177}Hf	^{176}Hf/^{177}Hf	±2σ	^{176}Hf/^{177}Hf$_{(t)}$ [a]	εHf$_{(t)}$ [a]	T$_{DM}$ [b] [Ga]	^{206}Pb/^{238}U [Ma]
SM377-1-31s	0,1192	0,00251	0,283124	0,00002	0,283112	17,63	-0,002	254
SM377-1-4	0,1784	0,003596	0,283186	0,000033	0,283169	19,68	-0,12	257
SM377-1-8	0,0333	0,000735	0,28258	0,000017	0,282571	7,47	0,89	662
SM377-2-1	0,0628	0,00157	0,282589	0,000021	0,282575	3,09	0,97	457
SM377-2-29nw	0,0475	0,001235	0,282493	0,000037	0,282482	0,03	1,14	468
SM377-2-35ne	0,0355	0,00087	0,282558	0,000018	0,282551	1,88	1,02	442
SM377-2-7	0,0779	0,001561	0,282634	0,000026	0,282621	4,27	0,89	437
SM550-1-16	0,0359	0,000693	0,282104	0,000026	0,282095	-9,52	1,81	654
SM550-1-18e	0,0761	0,00218	0,282497	0,000035	0,282484	-2,98	1,2	328
SM550-1-18w	0,0285	0,000552	0,28192	0,000024	0,281914	-17,58	2,19	580
SM550-1-3	0,0002	0,00141	0,282654	0,000014	0,282646	2,58	0,89	320
SM550-1-9nw	0,078	0,001669	0,28266	0,000018	0,282642	7,68	0,79	557
SM550-1-9se	0,102	0,002905	0,282658	0,000023	0,28264	2,59	0,89	330
SM600-1-16	0,0482	0,001543	0,282494	0,000022	0,282476	3,28	1,09	623
SM600-1-18	0,0307	0,000746	0,281528	0,000019	0,281497	4,05	2,31	2198
SM600-1-36	0,0468	0,001513	0,282543	0,000033	0,282527	3,70	1,02	562

[a] ^{176}Hf/^{177}Hf$_{(t)}$ and εHf$_{(t)}$ were calculated using the measured ^{176}Hf/^{177}Hf ratio for each spot, apparent ^{206}Pb/^{238}U ages determined by LA-ICP-MS measurements, and average values of ^{176}Lu/^{177}Hf and ^{176}Hf/^{177}Hf in chondrites of 0.0332 and 0.282772 (Blichert-Toft and Albarède, 1997), respectively. Lu decay constant of 1,865E-11 was used (Scherer et al., 2001).

[b] Two stage depleted mantle model age was calculated using measured ^{176}Lu/^{177}Hf for each spot, an average value of ^{176}Lu/^{177}Hf for the continental crust 0.0113 (after Linnemann et al., 2014), and depleted mantle (DM) ^{176}Lu/^{177}Hf and ^{176}Hf/^{177}Hf of 0.0384 and 0.283165, respectively (Chauvel et al., 2008).

References

Blichert-Toft, J., Albarède, F., 1997. The Lu-Hf isotope geochemistry of chondrites and the evolution of the mantle-crust system. Earth and Planetary Science Letters 148, 243–258. doi:10.1016/S0012-821X(97)00040-X

Chauvel, C., Lewin, E., Carpentier, M., Arndt, N.T., Marini, J.-C., 2008. Role of recycled oceanic basalt and sediment in generating the Hf–Nd mantle array. Nature Geosci 1, 64–67. doi:10.1038/ngeo.2007.51

Linnemann, U., Gerdes, A., Drost, K., Buschmann, B., 2007. The continuum between Cadomian orogenesis and opening of the Rheic Ocean: Constraints from LA-ICP-MS U-Pb zircon dating and analysis of plate-tectonic setting (Saxo-Thuringian zone, northeastern Bohemian Massif, Germany). Geological Society of America Special Papers 423, 61–96. doi:10.1130/2007.2423(03)

Scherer, E., Münker, C., Mezger, K., 2001. Calibration of the Lutetium-Hafnium Clock. Science 293, 683–687.

Chapter 3

Evidence of Variscan and Alpine tectonics in the structural and thermochronological record of the central Serbo-Macedonian Massif (southeastern Serbia)

Milorad D. Antić[1], Alexandre Kounov[1], Branislav Trivić[2], Richard Spikings[3], Andreas Wetzel[1]

[1]Institute for Geology and Palaeontology, University of Basel, 4056 Basel, Switzerland;

[2]Faculty of Mining and Geology, University of Belgrade, 11000 Belgrade, Serbia

[3]Section des Sciences de la Terre et de l'Environnement, Université de Genève, 1205 Genève, Switzerland

This chapter has been published in: International Journal of Earth Sciences. doi:10.1007/s00531-016-1380-6

Abstract

The Serbo-Macedonian Massif (SMM) represents a composite crystalline belt within the Eastern European Alpine orogen, outcropping from the Pannonian basin in the north to the Aegean Sea in the south. The central parts of this massif (southeastern Serbia) consist of the medium to high-grade Lower Complex and the low-grade Vlasina Unit. Outcrop- and micro-scale ductile structures in this area document three major stages of ductile deformation. The earliest stage D_1 is related to isoclinal folding, commonly preserved as up to decimetre-scale quartz-feldspar rootless fold hinges. D_2 is associated with general southeastward tectonic transport and refolding of earlier structures into recumbent metre- to kilometre-scale tight to isoclinal folds. Stages D_1 and D_2 could not be temporally separated, and probably took place in close sequence. The age of these two ductile deformation stages was constrained to the Variscan orogeny based on indirect geological evidence (i.e. ca. 408-ca. 328). During this period the SMM was involved in a transpressional amalgamation of the western and eastern parts of the Galatian super-terrane and subsequent collision with Laurussia. Outcrop-scale evidence of the final stage D_3 is limited to spaced and crenulation cleavage, which are probably related to formation of the large-scale open upright folds as reported previously.

$^{40}Ar/^{39}Ar$ thermochronology was applied on hornblende, muscovite and biotite samples in order to constrain the age of tectonothermal events and activity along major shear zones. These $^{40}Ar/^{39}Ar$ data reveal three major cooling episodes affecting the central SMM. Cooling below greenschist facies conditions in the western part of the Vlasina Unit took place in a post-orogenic setting (extensional or transtensional) in the early Permian (284±1 Ma). The age of activity along the top-to-the-west shear zone formed within the orthogneiss in the Božica area of the Vlasina Unit was constrained to Middle Triassic (246±1 Ma). This age coincides with widespread extension related to the opening of the Mesozoic Tethys. The greenschist facies retrogression in the Lower

Complex probably occurred in the Early Jurassic (195±1 Ma) and it was related to the thermal processes in the overriding plate above the subducting slab of the Mesozoic Tethys Ocean.

3.1 Introduction

Crystalline terranes within the Eastern Mediterranean Alpine orogen (e.g. Tisza, Pelagonia, Rhodope, Serbo-Macedonian Massif) commonly display a high degree of structural complexity resulting from the interplay between inherited structures and variable amount of Alpine deformational overprint (e.g. Dimitrijević 1972; Stampfli et al. 2002; Neubauer 2002; von Raumer et al. 2003; Burg 2012; von Raumer et al. 2013). These basement units usually represent segments of the North-Gondwanan margin that drifted along multiple branching oceanic domains, and subsequently accreted to the Eurasian margin during the Variscan orogeny (e.g. Neubauer 2002; Karamata 2006; Stampfli et al. 2013). A similar evolution took place again during the Alpine orogeny with polyphase opening of the Mesozoic Tethys and its consequent closure involving collision of multiple crustal segments (e.g. Robertson et al. 1991; Ricou 1994; Schmid et al. 2008; Stampfli and Hochard 2009). Therefore, to reveal the tectonic evolution of these intra-Alpine crystalline units, their complex structural patterns need to be studied in detail together with determination of age of their protoliths and timing of metamorphism.

The crystalline Serbo-Macedonian Massif (SMM; Dimitrijević 1957) is lodged between the Dinaride and the Carpatho-Balkanide chains of the Alpine orogen (Fig. 3-1). Paucity of structural, geo- and thermochronological data has led to a number of contrasting tectonic interpretations and structural subdivisions within the SMM (Popović 1991; Popović 1995; Ricou et al. 1998; Grubić et al. 1999; Kräutner and Krstić 2002; Grubić et al. 2005; Zagorchev and Milovanović 2006). A similar degree of uncertainty also plagued the neighbouring Rhodope metamorphic complex, until its tectonic evolution was re-evaluated using combined detailed structural and geochronological studies (e.g. Burg et al. 1995; Mukasa et al. 2003; Peytcheva et al. 2004; Liati 2005; Bosse et al. 2009; Bonev et al. 2010; Turpaud and Reischmann 2010; Jahn-Awe et al. 2010; Himmerkus et al. 2011; Jahn-Awe et al. 2012; Froitzheim et al. 2014; Bonev et al. 2015; Georgiev et al. 2016). Detailed reconstructions of the tectonic evolution of areas surrounding the SMM (i.e. Southern Carpathians, Internal Dinarides) have also been recently produced based on reliable data-sets (Dallmeyer et al. 1998; Matenco and Schmid 1999; Fügenschuh and Schmid 2005; Schmid et al. 2008; Ustaszewski et al. 2009; Zelic et al. 2010; Stojadinovic et al. 2013; Toljić et al. 2013). Furthermore, recent detailed studies in the southern part of the SMM (i.e. Vertiskos Unit in Greece) have provided valuable constraints on the magmatic and deformation events that affected this unit (e.g. Himmerkus et al., 2009a, 2009b; Meinhold et al., 2010; Kydonakis et al., 2014, 2015). Due to its particular position between the two divergent belts of the Alpine orogen, unravelling of thermal and deformation history of the SMM becomes essential for correct reconstruction of the evolution of tectonic units in southeastern Europe. The central parts of the SMM (southeastern Serbia) were chosen for this study due to relative scarcity of reliable data and relatively good condition of rock exposures. This study provides new

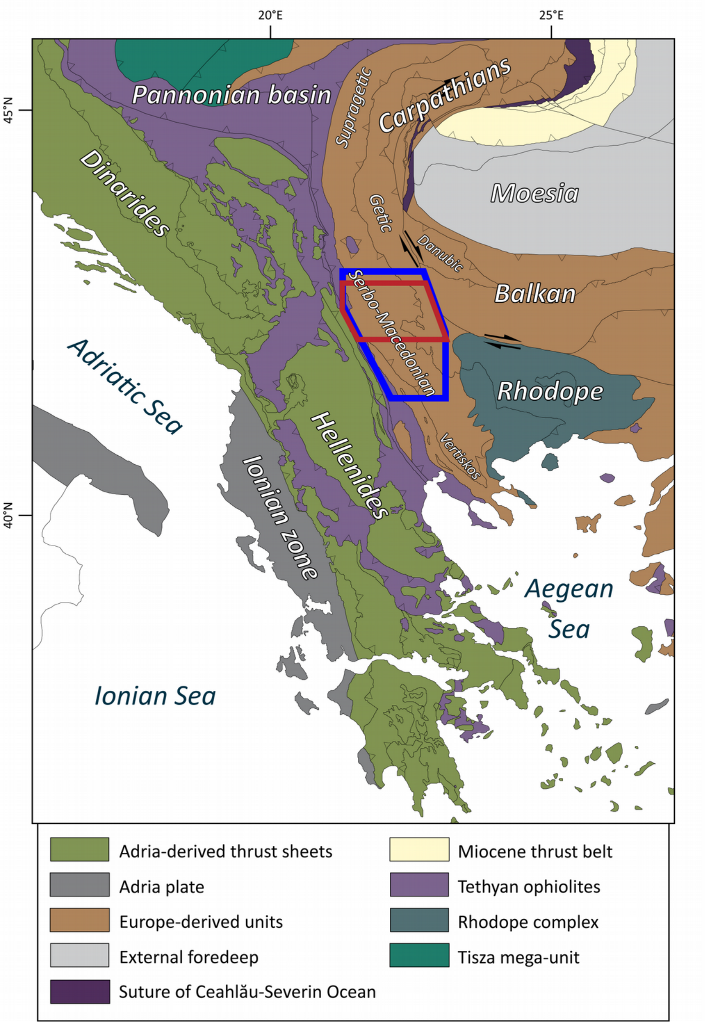

Figure 3-1. Tectonic map of the Balkan Peninsula (modified after Schmid et al. 2008; van Hinsbergen and Schmid 2012). Blue polygon outlines the area of the map in Figure 3-2, and the red polygon in Figure 3-3.

detailed structural data and ^{40}Ar/^{39}Ar thermochronology results from the central SMM, which were used to unravel its long and complex deformation history since the Palaeozoic.

3.2 Geological setting

The SMM represents a crystalline belt outcropping from the Pannonian basin in the north to the Aegean Sea in the south (Fig. 3-1). It should be noted that although our study concerns both Variscan and Alpine tectonics in the SMM, the names of the tectonic units discussed below only refer to the later (i.e. Alpine) tectonics so that results presented here could be correlated with the previously published tectonic frameworks of southeastern Europe. The Supragetic nappe sequence of the South Carpathians is considered to be the continuation of the SMM east and northeast of the Pannonian basin (Săndulescu 1984; Dimitrijević 1997; Schmid et al. 2008). As originally proposed by Dimitrijević (1957), the SMM in Serbia comprises a structurally lower (the Lower Complex) and upper unit (Vlasina Unit). These are commonly distinguished by their metamorphic grade, i.e. the Lower Complex underwent medium to lower amphibolite facies metamorphism, whereas the Vlasina Unit was metamorphosed at greenschist facies conditions. In Bulgaria, the continuations of the Lower Complex and the Vlasina Unit are referred to as the Ograzhden Unit (Dimitrijević 1967; Zagorchev 1984; Dabovski et al. 2002), and Morava Unit (e.g. Zagorchev 1985; Zagortchev 1993), respectively. The SMM can be followed farther southwards into Greece, where the Vertiskos unit is usually correlated with rocks of the Lower Complex (Kockel et al. 1971; Burg et al. 1995; Himmerkus et al. 2006; Himmerkus et al. 2009a). However, only the central parts of the SMM (southeastern Serbia) were investigated during this study.

3.2.1 Lower Complex

The Lower Complex consists mainly of gneisses, micaschists, quartzites, amphibolites and occasionally marbles and migmatites (Dimitrijević 1963). These rocks represent a Cadomian (Late Neoproterozoic–earliest Cambrian) volcano-sedimentary complex developed along the active margin of north Gondwana, which was subsequently intruded by igneous rocks during several magmatic pulses (Chapters 2 and 4). Although medium- to lower-amphibolite facies metamorphism is characteristic for the Lower Complex (Dimitrijević 1967; Milovanović 1990; Cvetković 1992; Milovanović 1992), relicts of eclogite facies rocks are also reported as isolated occurrences throughout this unit (Balogh et al. 1994; Iancu et al. 1998; Korikovsky et al. 2003; Zidarov et al. 2003a; Macheva et al. 2005; Nenova and Zidarov 2008; Ivanova and Zidarov 2011; Kydonakis et al. 2015b). The timing of high-pressure (HP) metamorphism, deduced from overprinting relationships and whole-rock Rb/Sr data, was reported to be of pre-Cadomian or Cadomian age (ca. 750-550 Ma), with an amphibolite facies overprint and locally migmatisation occurring in the Variscan (Dimitrijević 1967; Balogh et al. 1994; Zagorchev and Milovanović 2006; Nenova and Zidarov 2008; Peytcheva et al. 2009a; Chapter 2). Additionally, U-Pb dating of titanite and several K/Ar analyses have yielded Early Cretaceous ages (Milovanović 1990; Balogh et al. 1994; Zidarov et al. 2003b).

3.2.2 Vlasina Unit

The Vlasina Unit represents a Cadomian volcano-sedimentary sequence, which, although similar to the protoliths of the Lower Complex, is generally dominated by ocean-floor sediments (Pantić et al. 1967; Petrović 1969), intruded by late Cadomian igneous rocks (Chapter 2), covered by a Lower Ordovician to Lower Carboniferous sedimentary sequence (post-Cambrian in Fig. 3-2;

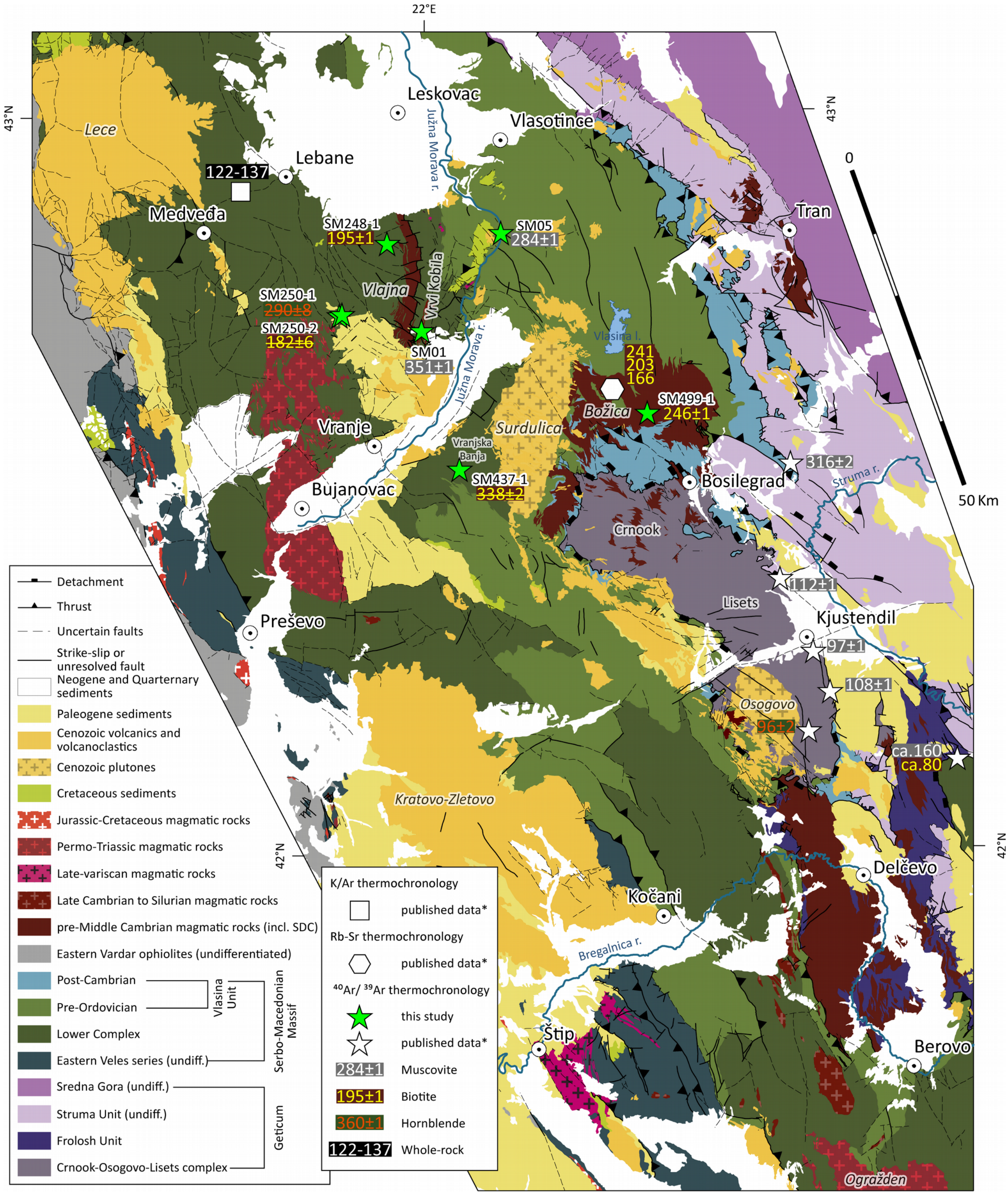

Figure 3-2. Tectonic map of the study area with the sampling locations and results of ^{40}Ar/^{39}Ar thermochronology (after Basic geological maps of SFR Yugoslavia 1:100 0000 and Geological maps of Bulgaria 1:100 000 and 1:50 000). Labels in a regular type represent toponyms, whereas labels in an italic type represent igneous complexes. (*) Literature data from Babović et al. (1977), Milovanović (1990), Kounov (2002), Kounov et al. (2010). Striken-through dates are related to the ^{40}Ar/^{39}Ar analyses with no reliable plateau dates. See text for details.

Pavlović 1962; Babović et al. 1977; Kräutner and Krstić 2002), and finally intruded by late Palaeogene magmatic rocks (Chapter 4). The pre-Ordovician Vlasina (Chapter 2) is typically represented by various schists, phyllites and quartzites (Dimitrijević 1967). Peak metamorphic conditions of 450-500 °C at 3 to 5 kbar (0.3-0.5 GPa) were reported in the pre-Ordovician Vlasina (Milovanović et al. 1988; Vasković 2002). However, relicts of metamorphic assemblages indicative of conditions exceeding greenschist facies have been reported in the vicinity of the Božica magmatic complex and Vranjska Banja area (Fig. 3-2; Petrović 1969; Vujanović et al. 1974; Babović et al. 1977; Pavlović 1977; Vasković 1998; Vasković et al. 2003).

Post-Cambrian Vlasina (Chapter 2) comprises Ordovician schists, phyllites, calcschists, argillites, quartzite and marbles, Silurian graptolitic schists, Middle Devonian carbonates and argillites, and Upper Devonian to Lower Carboniferous turbidites with spilites (Pavlović 1962; Petrović et al. 1973; Spassov 1973; Babović et al. 1977; Pavlović 1977; Zagorčev and Bončeva 1988; Banjac 2004; Lakova 2009). These rocks are considered to have experienced very low-grade metamorphism with only occasional occurrences of greenschist-facies assemblages (Petrović et al. 1973; Spassov 1973; Babović et al. 1977; Graf 2001; Krstić et al. 2002).

The tectonic contact of the Lower Complex with the Vlasina Unit is reported as the Vrvi Kobila shear zone (Fig. 3-2). It was previously considered as a pre-Mesozoic west-vergent thrust juxtaposing the Vlasina Unit over the Lower Complex (Vukanović et al. 1973; Krstić and Karamata 1992), or, alternatively, as a post-Late Cretaceous dextral shear zone (Kräutner and Krstić 2002). Additionally, several reports suggest that these units originally had a stratigraphic contact, which was later tectonically reworked (Petrović and Karamata 1965; Petrović 1969; Dimitrijević 1997).

3.2.3 Eastern Veles series

Southwest of Bujanovac (Fig. 3-2), the Lower Complex overlies the eastern part of the Veles series. This contact was previously considered as a strike-slip fault (Malešević et al. 1980; Vukanović et al. 1982), an east-vergent thrust (Krstić and Karamata 1992), or a westward thrust reactivated as dextral strike slip in the Neogene (Kräutner and Krstić 2002). It has been recently interpreted as a ductile shear zone (Stefan M. Schmid, personal communication, September 2014), along which no significant vertical movement occurred since the Late Cretaceous (Chapter 4). Jurassic ophiolites of the Eastern Vardar oceanic domain together with the Upper Cretaceous flysch (Vukanović et al. 1977; Pavić et al. 1983; Karamata and Krstić 1996) divide the Veles series into eastern and western part. The Eastern Veles series (EVS) is largely composed of a lower Palaeozoic sedimentary sequence and Early Ordovician meta-granites (Pavlović 1977; Chapter 2), with minor Triassic sedimentary cover (Pavić et al. 1983). These rocks underwent amphibolite facies metamorphism, followed by a post-Triassic intensive retrogression in greenschist facies (Dimitrijević 1997). In contrast Devonian to Triassic greenschist-facies meta-sedimentary rocks constitute the majority of the Western Veles series (Pavić et al. 1983; Grubić and Ercegovac 2002). The Veles series is considered to be a part of the Circum-Rhodope belt (Zagorchev and Milovanović 2006; Schmid et al. 2008), or the "internal Vardar zone" (Dimitrijević and Drakulić 1958; Robertson et al. 2009). This study only addresses the lower-Palaeozoic-dominated EVS, which was recently attributed to the Palaeozoic Galatian supra-terrane together with the SMM (Chapter 2).

3.2.4 Struma Unit and Crnook-Osogovo-Lisets Complex

During the late Early Cretaceous, the Vlasina Unit was thrust to the east onto the Struma and other Getic units along a system of east- to northeast-vergent thrusts (Petković 1930; Mihailescu et al. 1967; Petrović 1969; Zagorchev and Ruseva 1982; Lilov and Zagorchev 1993; Kounov et al. 2010). The Struma Unit consists of a basement represented by variably deformed continent- and ocean-derived rocks of Ediacaran to early Cambrian age (Kounov et al. 2012), and a transgressive

Permian to Lower Cretaceous sedimentary cover (Zagorchev 1981).

The Crnook-Osogovo-Lisets (COL) complex in southeastern part of the study area represents an extensional dome exhumed from below Struma and Vlasina units during middle Eocene to Oligocene (Kounov et al. 2004; Chapter 4). It consists of micaschists, gneisses, amphibolites and quartzites (Dimitrova 1964; Dimitrijević 1972; Babović et al. 1977). Magmatic rocks of the COL complex and the basement of Struma Unit are derived from the same calc-alkaline magma source associated with a magmatic-arc complex formed during the Ediacaran to early Cambrian (Kounov et al. 2012; Chapter 2). These rocks have experienced lower-amphibolite facies metamorphism during an early Late Cretaceous compressional event (Kounov et al. 2010).

3.2.5 Sedimentary cover and brittle tectonics

The oldest undeformed and non-metamorphosed rocks in the study area are the Santonian to Lower Maastrichtian sedimentary rocks (86–70 Ma, Fig. 3-2). These relatively shallow Late Cretaceous basins were filled with predominantly terrigenous clastic deposits with subordinate marls and limestones (Petrović et al. 1973). Palaeogene sedimentary rocks in the area are represented by middle Eocene carbonate continental deposits (Petrović et al. 1973; Vukanović et al. 1973; Anđelković and Anđelković 1995), upper Eocene turbidites (Vukanović et al. 1977; Dimitrijević and Dimitrijević 1987), and Oligocene marine to lacustrine sedimentary rocks (Vukanović et al. 1973; Vukanović et al. 1977) deposited in extensional basins that were coeval with the exhumation of the COL core complex. Palaeogene sedimentary rocks are often intercalated with various pyroclastic rocks or intruded by small dacitic or andesitic bodies that also intrude the basement. The most prominent igneous complexes in the study area are the Surdulica granodiorite (Chapter 4), and the Lece andesitic complex (Karamata et al. 1992).

Neogene sedimentary rocks in the area are represented by middle Miocene clastic deposits and fresh-water marls, which were continually deposited during the Pliocene (Vukanović et al. 1973; Vukanović et al. 1977). These rocks are intercalated with dacitic and andesitic volcanoclastic rocks (Vukanović et al. 1977).

Apart from the Early Cretaceous compression discussed above, brittle deformation in central SMM also includes Late Cretaceous normal faulting, Eocene-Oligocene extension (Chapter 4), and dextral strike-slip and oblique faulting during Miocene to recent wrench tectonics (Petrović 1969; Marović et al. 2007; Burchfiel et al. 2008; Kounov et al. 2011; Tranos and Lacombe 2014; Mladenović et al. 2014).

3.3 Structural data

No coherent ductile fabric could be followed throughout the entire study area (i.e. central SMM), as abrupt changes in orientation of structural elements occur even within relatively small areas (Fig. 3-3). These changes are considered to result from a much younger brittle tectonic overprint. The structural observations were hampered further by generally poor exposure and highly weathered state of rocks in the study area. Despite these difficulties, three major stages of ductile deformation affecting the entire study area were identified based on overprinting relationships and internal geometries of the resulting structures (i.e. style of deformation).

3.3.1 Lower Complex

Due to complex structural patterns, the deformation in the Lower Complex will be described in five separate domains that display some degree of structural homogeneity (Fig. 3-4).

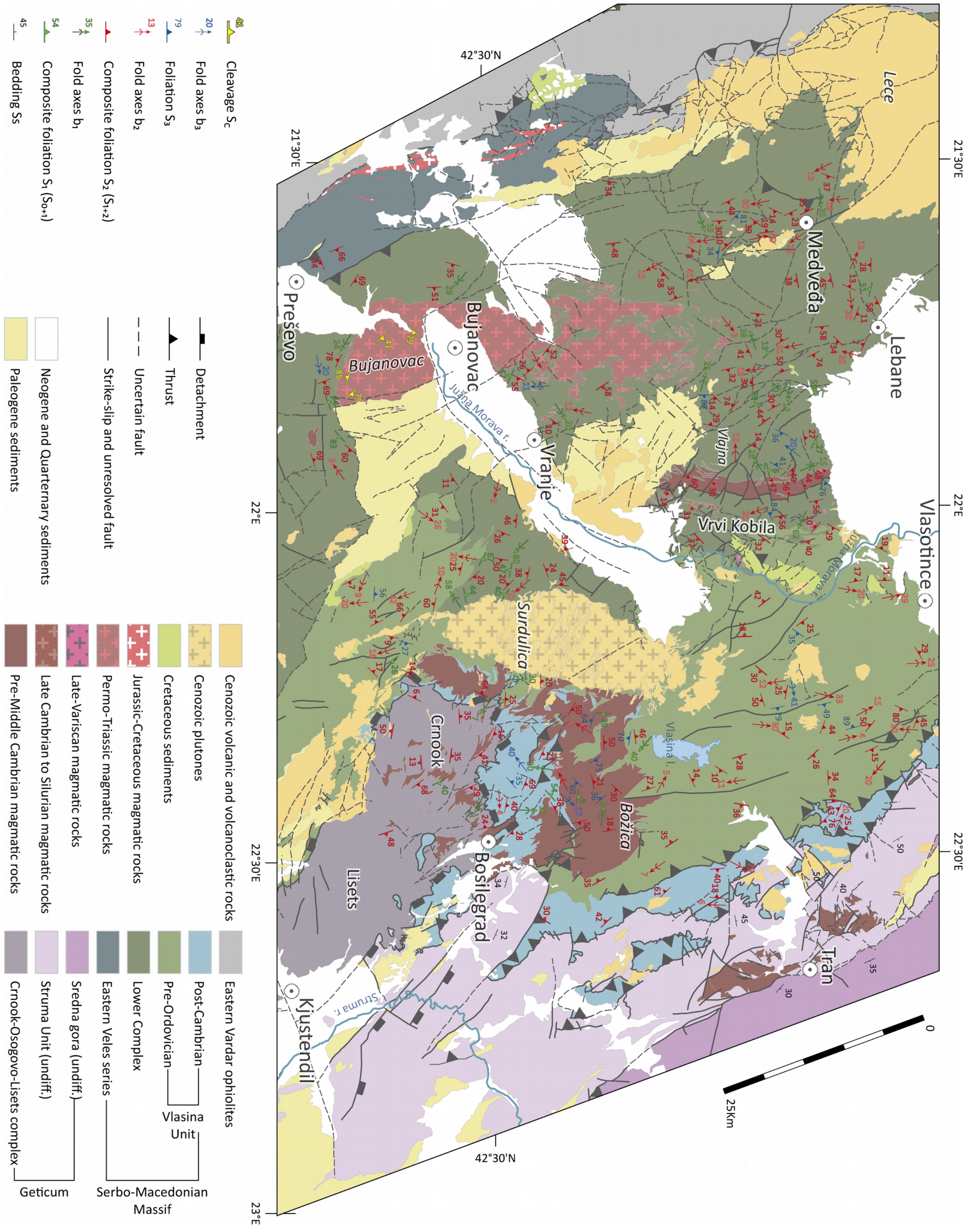
Cleavage S_c
Fold axes b_3
Foliation S_3
Fold axes b_2
Composite foliation S_2 (S_{1+2})
Fold axes b_1
Composite foliation S_1 (S_{0+1})
Bedding Ss
Detachment
Thrust
Uncertain fault
Strike-slip and unresolved fault
Neogene and Quarternary sediments
Paleogene sediments
Cenozoic volcanic and volcanoclastic rocks
Cenozoic plutones
Cretaceous sediments
Jurassic-Cretaceous magmatic rocks
Permo-Triassic magmatic rocks
Late-Variscan magmatic rocks
Late Cambrian to Silurian magmatic rocks
Pre-Middle Cambrian magmatic rocks
Eastern Vardar ophiolites
Post-Cambrian
Pre-Ordovician
Vlasina Unit
Lower Complex
Eastern Veles series
Serbo-Macedonian Massif
Sredna gora (undiff.)
Struma Unit (undiff.)
Crnook-Osogovo-Lisets complex
Geticum
42°30'N
21°30'E
22°E
22°30'E
23°E
0
25Km
Lece
Medveđa
Lebane
Vlasotince
Vlajna
Vrvi Kobila
Bujanovac
Preševo
Vranje
Južna Morava r.
Surdulica
Vlasina
Božica
Crnook
Bosilegrad
Lisets
Trn
Kjustendil
Struma r.

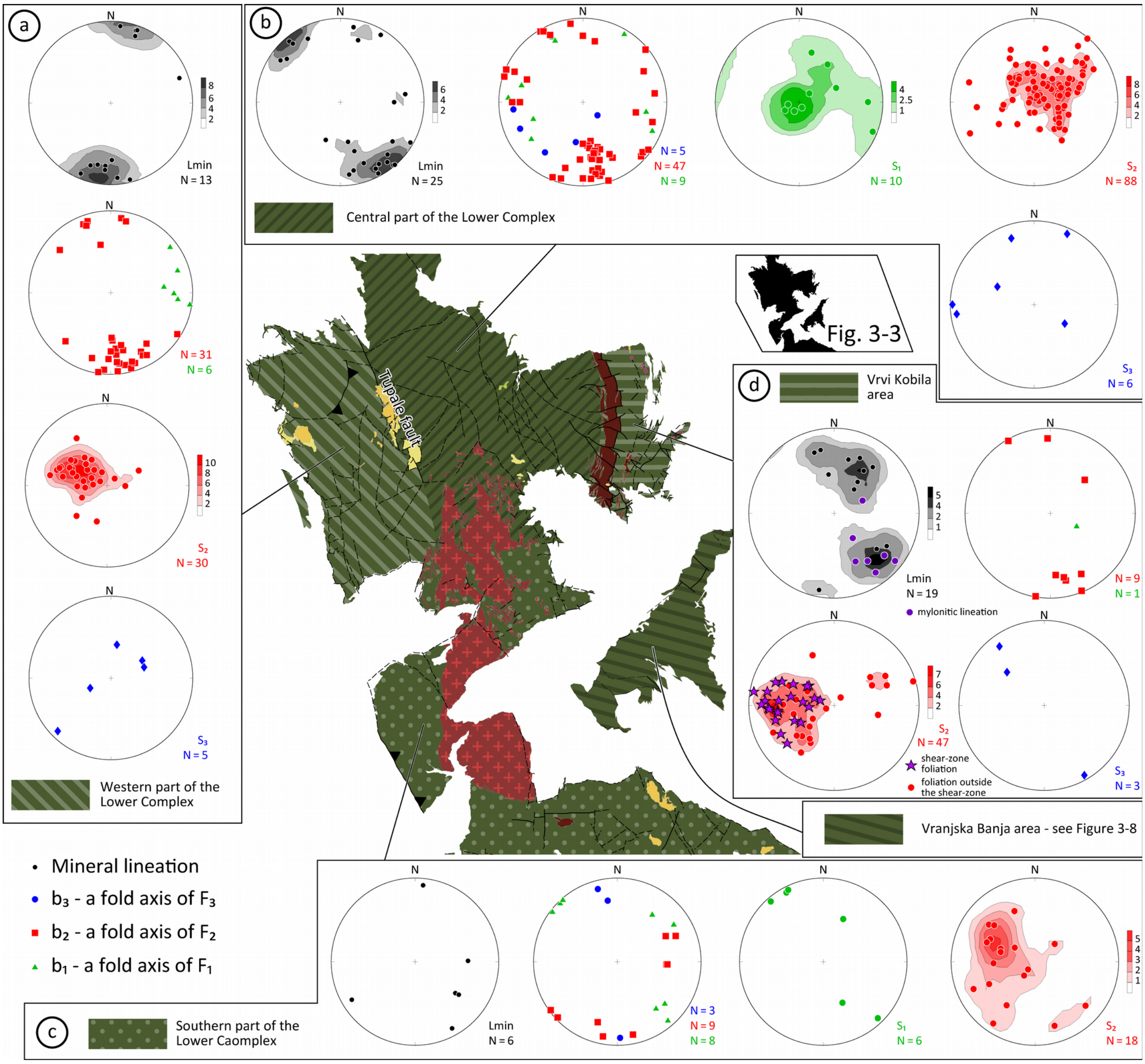

Figure 3-4. Lower hemisphere equal-area plots of structural elements from (a) western part of the Lower Complex, (b) central part of the Lower Complex, (c) southern part of the Lower Complex, and (d) Vrvi Kobila area. For structural data in Vranjska Banja area please see Figure 3-8. Inset shows the relative scale and position in Figure 3-3.

3.3.1.1 Western part of the Lower Complex

The area west of the brittle Tupale fault is characterised by a predominantly east dipping main foliation S_2, which represents the axial-plane cleavage of overturned to recumbent metre- to kilometre-scale isoclinal F_2 folds (Fig. 3-4a). Fold axes b_2 are shallowly plunging in the north to

---

Figure 3-3 (opposite page). Tectonic map of the study area with structural elements (after Basic geological maps of SFR Yugoslavia 1:100 0000 and Geological maps of Bulgaria 1:100 000 and 1:50 000). Labels in regular type represent toponyms, whereas labels in italic type represent igneous complexes.

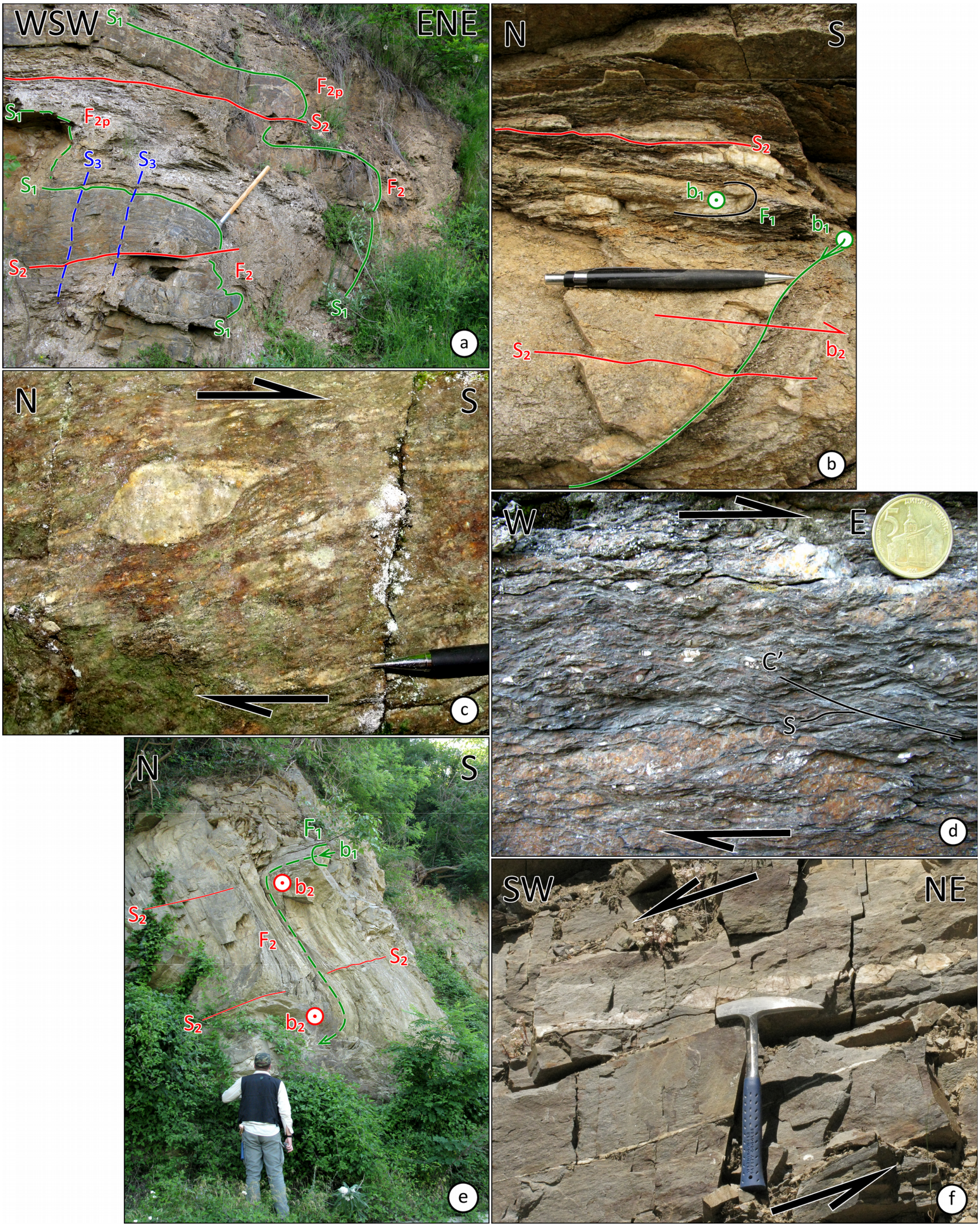

Figure 3-5. (a) Folded alternation of gneiss, schists and amphibolite in the western part of the Lower Complex (21°38'16.153"E, 42°45'8.295"N). Earlier foliation S_1 preserved in the competent amphibolites is folded into metre-scale isoclinal folds F_2 and parasitic folds F_{2p}. Minor transposition of limbs of F_2 folds along the axial-plane cleavage S_2 can also be observed. Late cleavage S_3 nearly perpendicular to the composite foliation S_1/S_2 is weakly developed. Length of hammer ca. 60 cm.

northwest–south to southeast direction (Figs. 3-4a and 3-5a), and are generally perpendicular to subhorizontal fold axes b_1 of earlier folds F_1 (Fig. 3-4a). Refolding of decimetre-scale isoclinal F_1 folds (i.e. folded quartz-feldspar bands with fold axis b_1 perpendicular to the plane of image in Fig. 3-5b), by isoclinal folds F_2 at high to almost right angles (parallel to the plane of image in Fig. 3-5b) has been observed at several outcrops. Therefore, an earlier foliation (S_i) is presumed to be initially folded into F_1 and subsequently refolded into F_2 folds. Away from the hinges of F_2 folds the supposed initial foliation S_i and foliation S_1 formed during D_1 were completely transposed during D_2 such that the main fabric represents a $S_i/S_1/S_2$ composite foliation, which is designated as S_2 for convenience. Apart from the rare outcrops where the relationships between folds F_1 and F_2 could be directly observed, the early folds F_1 are usually found as rootless fold hinges in the microlithons bound by foliation S_2. A clear distinction between fold structures related to deformation stages D_1 and D_2 is only possible in areas where their respective fold axes intersect at high angles.

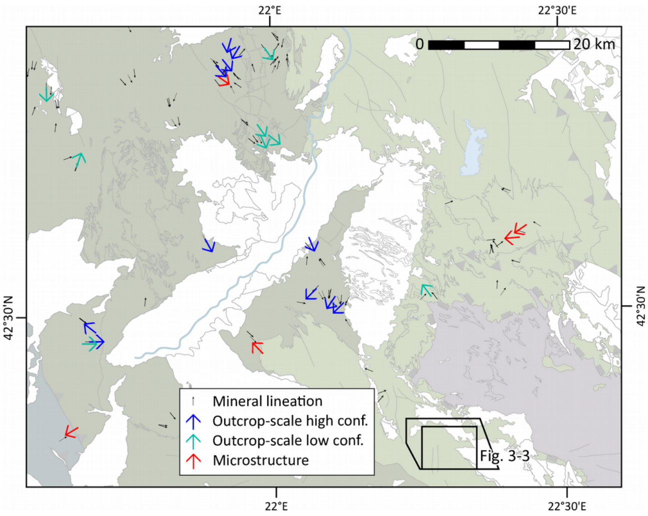

Figure 3-6. Simplified tectonic map of the study area with arrows representing local directions of tectonic transport. See text for details.

A younger spaced cleavage S_3 is usually perpendicular or at a high angle to S_2, and generally strikes northwest-southeast (Fig. 3-4a).

A subhorizontal stretching lineation defined by biotite and elongated quartz-feldspar

---

Figure 3-5 continued. (b) Micaschists in the western part of the Lower Complex (21°37'47.381"E, 42°45'8.195"N). Older isoclinal folds F_1 with fold axes b_1 perpendicular to the plane of image, are refolded by isoclinal fold F_2 with fold axis parallel to the plane of image. Length of pencil 143 mm. (c) Polycrystalline sigmoid indicating top-to-the-southwest shear sense, west of the Vrvi Kobila shear zone (Fig. 3-3; 21°55'25.176"E, 42°49'19.199"N). Length of metal tip on a pencil 21 mm. (d) C' shear bands indicating top-to-the-east sense of shear in micaschists of the southern Lower Complex (21°53'27.018"E, 42°34'46.569"N). Coin diameter 24 mm. (e) Isoclinal folds F_1 from Vranjska Banja area refolded by asymmetric fold F_2 with axes b_2 perpendicular to the axis b_1 (22°4'38.741"E, 42°30'33.75"N). S_2 represents an axial plane-cleavage of folds F_2. (f) Layer-parallel train of asymmetric tapered boudins from Vranjska Banja area indicating top-to-the-southwest sense of shear (22°7'7.324"E, 42°29'57.556"N). Length of hammer 330 mm.

aggregates trends north to northeast–south to southwest (Fig. 3-4a). Polycrystalline sigmoids and δ-type aggregates observed in XZ planes at two locations indicate a top-to-the-north to northeast and a top-to-the-south sense of shear (Fig. 3-6).

3.3.1.2 Central part of the Lower Complex

A relatively large area in the central part of the Lower Complex is characterised by predominantly shallow dipping penetrative foliation with a preferred dip direction in the southwestern quadrant (S_2; Fig. 3-4b). This fabric is predominantly formed by flattened quartz-feldspar aggregates and biotite. The earlier foliation S_1 is preserved only at the hinges of large scale (Dm to km) isoclinal recumbent folds F_2. In these hinge zones S_1 is often folded into metre-size parasitic F_2 folds whereas S_2 represents the axial plane cleavage. As the foliation S_1 was observed only at hinges of folds F_2, its statistical distribution (Fig. 3-4b) reflects the geometry of limbs of large recumbent folds F_2. The subhorizontal maximum of S_1 is related to the shallow inclination of one of the limbs, whereas the generally steeply inclined foliations are measured along the other limb of F_2 folds. Occasionally observed steep inclination of the composite foliation (S_2) is probably caused by rotation during a later brittle deformation rather than representing a feature intrinsic to the D_2 style of deformation in the area. Axes b_1 of centimetre-scale rootless fold hinges F_1 are commonly perpendicular or at a high angle to b_2 (Fig. 3-4b), although several exceptions were also noted.

The stretching lineation observed on the main foliation S_2, represented by preferential growth of biotite and elongate ribbons of quartz, plunges gently in northwest-southeast direction (L_{min} in Fig. 3-4b). The fold axes b_2 of large recumbent folds F_2 generally exhibit a shallow to moderate plunge in virtually all directions, with a maximum towards the south to southeast (Fig. 3-4b). The apparent parallelism between stretching lineation and maximum of b_2 fold axes suggests that both structures are related to the same deformation stage (D_2). Later rotation of blocks in the brittle regime has caused further dispersion in the orientation of b_2 fold axes.

Crenulation cleavage S_3 intersects foliation S_2 at high angles and is generally sub-vertical to steep with apparently no preferred orientation (Fig. 3-4b). The orientation of b_3 axes are determined by calculating the intersection of foliation S_2 folded into large open folds in outcrop scale, or by scarce intersection lineation between S_2 and crenulation cleavage S_3. These axes are generally plunging in the southwestern quadrant (Fig. 3-4b).

Kinematic indicators such as shear bands, polycrystalline sigmoids and asymmetric clasts on outcrops, as well as biotite fish in thin sections were observed in the XZ plane, and indicate generally top-to-the-south to southeast sense of shear. Additionally, a number of σ-type mantled clasts and sigmoids in the same area show top-to-the-southwest sense of shear (Fig. 3-5c).

Low-grade retrogression of amphibolite-grade assemblage in this area is suggested by evidence of dynamic recrystallization of quartz by bulging (BLG) and late muscovite and sericite growth at the boundaries of feldspar grains.

3.3.1.3 Southern part of the Lower Complex

Penetrative foliation S_2 in an area surrounding the Bujanovac magmatic complex (Figs. 3-3 and 3-4c) is generally dipping towards the east to southeast at moderate angles (Fig. 3-4c). It is commonly defined by biotite, muscovite and flattened quartz-feldspar aggregates. Variation in orientation of S_2 is observed, but no apparent structural pattern could be established (Fig. 3-4c). The subhorizontal to shallow fold axes b_2 of tight to isoclinal folds F_2 are plunging towards the southwest and the northeast (Fig. 3-4c). Subvertical older foliation S_1 was observed only in the broad planar hinges of decametre-scale recumbent F_2 folds (Fig. 3-4c). Fold axes b_1 of small-scale rootless fold hinges F_1 are usually perpendicular to b_2 (Fig. 3-4c), with the exception of a single locality where the observed b_1 and b_2 are sub-parallel. Rarely observed stretching lineation defined by biotite and elongated quartz-feldspar aggregates is generally shallow to moderately plunging towards the southeast (Fig. 3-4c).

Cleavage S_3 related to large-scale open folds F_3 was observed at several locations, whereas north-south directed subhorizontal plunge of fold axes b_3 was inferred from intersection lineation or calculated from the orientations of the limbs of gently folded S_2 (Fig. 3-4c).

C' shear bands observed in gneiss north of Vranje show top-to-the-southeast direction of tectonic transport (Figs. 3-5d and 3-6). C' shear bands, δ-type mantled clasts and polycrystalline sigmoids observed in the western periphery of the Permo-Triassic pluton within the Bujanovac magmatic complex show top-to-the-E sense of shear, although a top-to-the-northwest shearing was also observed.

3.3.1.4 Vrvi Kobila area

Previous studies in the Vrvi Kobila area describe a 3 km thick zone of intensive deformation, composed of phyllonites and mylonites (Vrvi Kobila fault zone, Petrović et al. 1973), along which the Vlasina Unit has been thrust onto the Lower Complex (Dimitrijević 1963; Vukanović et al. 1973; Krstić and Karamata 1992; Kräutner and Krstić 2002). Our studies in the area suggest the existence of a major ductile east-dipping shear zone with top-to-the-east to southeast sense of tectonic transport (Fig. 3-6). However, our observations also show that the hanging wall of the Vrvi Kobila shear zone is predominantly composed of two-mica gneiss and mica schists, which deviates from the typical lithological description of low-grade Vlasina Unit. Therefore this shear zone does not separate the Lower Complex from the Vlasina Unit, as previously reported, and it is entirely developed within the former (Fig. 3-7). Presence of high-grade metamorphic rocks in the hanging wall was previously explained by the “granitisation effect”

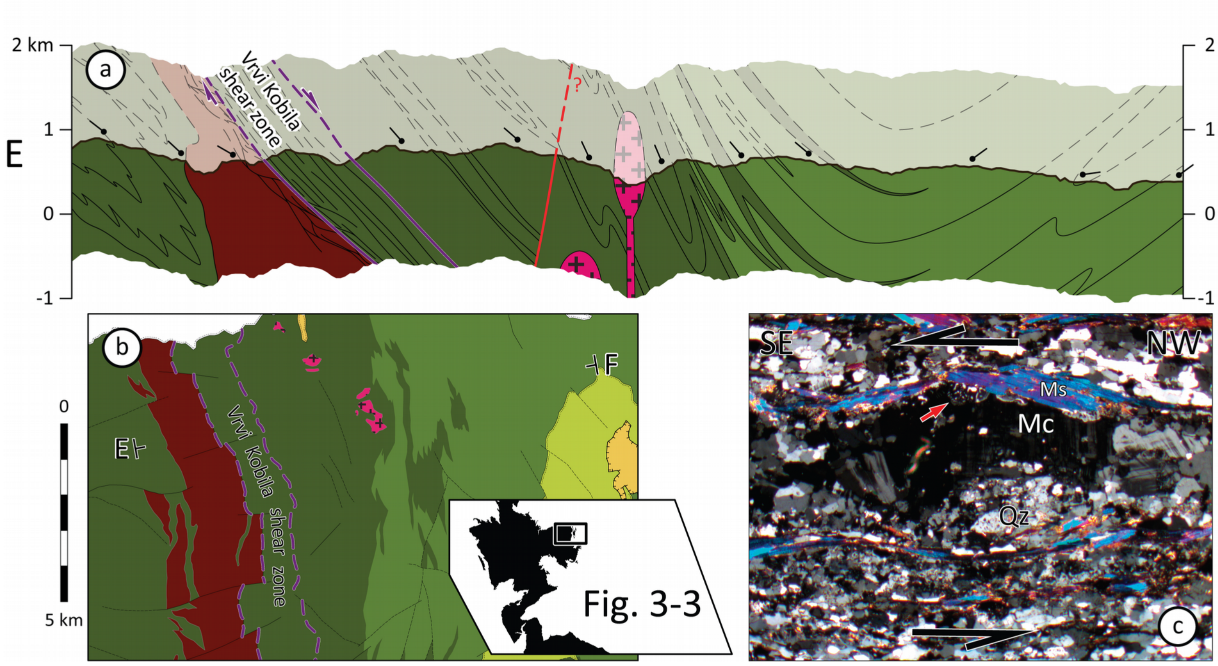

Figure 3-7. (a) Cross-section EF through the Vrvi Kobila area. (b) Detail of the map in Figure 3-2 with a trace of the cross-section EF. Location of the map relative to Figure 3-3 and the Lower Complex (black silhouette) is indicated by a black rectangle in the inset. (c) Thin section of a mylonite within the Vrvi Kobila shear zone (SM01; 21°59'15.981"E, 42°42'27.645"N). Red arrow points to an asymmetric myrmekite. Large black half-arrows indicate sense of shear. Crossed nicols. Width of image 5.9 mm.

on the schists of Vlasina Unit in the hanging wall, exerted by the intrusion of Vlajna granite in the footwall (Petrović 1969; Vujanović et al. 1974). Our studies show that the emplacement of Vlajna granite (Chapter 2) predates the activity along the Vrvi Kobila shear zone, as a large part of this granite is deformed and transformed into coarse-grained gneiss that is observed within the zone and its hanging wall (Fig. 3-7a). Therefore, the extent of the Vlajna magmatic complex present on maps (Figs. 3-2 and 3-3) and previous reports corresponds only to the weakly- or undeformed part of the complex.

Foliation S_2 in the Vrvi Kobila area is moderately to steeply dipping towards the east (Fig. 3-4d). Variations in the orientation of S_2 are probably caused by the younger brittle deformation. The foliation S_2 is defined mostly by flattened quartz-feldspar aggregates and syn-deformation growth of muscovite and biotite. Several F_2 folds with axes b_2 generally parallel to the strike of the shear zone have been observed within low-strain domains in the area (Fig. 3-4d), as well as anastomosing shear zones in the Vlajna magmatic complex. Scarce subvertical to steep solution cleavage S_3 is striking northeast-southwest (Fig. 3-4d).

The stretching lineation represented by quartz-feldspar ribbons, muscovite and biotite forms an array with two maximums, one towards the southeast, and the other to the northeast (Fig. 3-4d). The lineations showing a maximum towards the southeast together with outcrop-scale sigmoids and asymmetrically stretched boudins which indicate top-to-the-southeast sense of shear, were mainly observed along the Vrvi Kobila shear zone (Figs. 3-4d and 3-6). This southeastward shearing and the general southeast-northwest orientation of fold axes b_2 are considered to be related to deformation stage D_2. The lineations oriented differently than the southeastern maximum could represent earlier structures not fully reworked during D_2 that were preserved away from the Vrvi Kobila shear zone (Fig. 3-6).

3.3.1.5 Vranjska Banja area

Metamorphic rocks of Vranjska Banja area, located between the Surdulica granodiorite and the Južna Morava River (Fig. 3-2), were traditionally attributed to Vlasina Unit although they show evidence of higher metamorphic grade than the greenschist facies typical for the Vlasina Unit (Babović et al. 1977). Mineral assemblages in Vranjska Banja area showing the peak metamorphic conditions of 530-585°C at 5.2-6.1 kbar (0.52-0.61 GPa; i.e. the boundary conditions between greenschist and amphibolite facies), are overprinting low-grade assemblages formed at 350-450°C and 3.5 kbar (Vasković 1998; Vasković et al. 2003). As the division of central SMM into the Lower Complex and Vlasina Unit is generally based on the metamorphic grade, we designate the metamorphic rocks in Vranjska Banja area as a part of the Lower Complex (Figs. 3-2 and 3-3).

Structural fabric of Vranjska Banja area was mostly examined along a Banjska river valley east of Vranje (Figs. 3-3 and 3-8). Foliation S_2 in this area, predominantly defined by biotite,

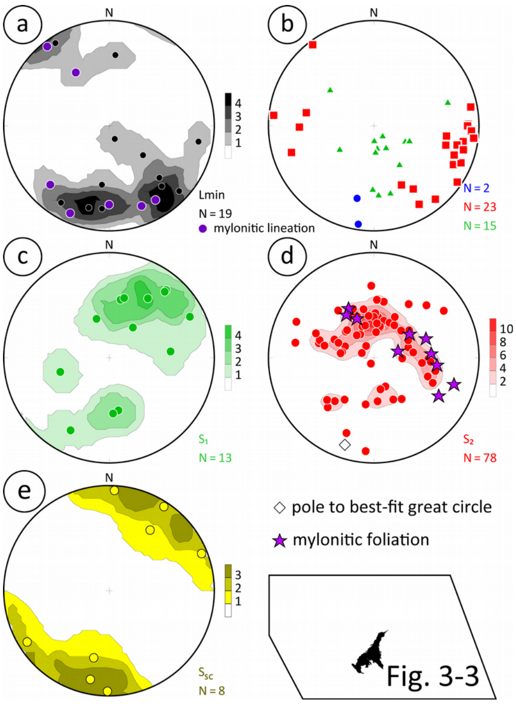

Figure 3-8. Lower hemisphere equal-area plots of (a) mineral lineation, (b) fold axes, (c) poles to foliation related to D$_1$, (d) poles to foliation related to D$_2$ and (e) poles to spaced cleavage in Vranjska Banja area. See text for details. Symbol legend is given in Figure 3-4. Relative scale and position in reference to Figure 3-3 is given in the inset.

clinozoisite and flattened quartz-feldspar aggregates, dips shallowly to moderately towards the south, with small populations dipping towards the southeast and southwest (Fig. 3-8d). Metre-scale asymmetric parasitic folds F$_2$ were observed in the limbs of presumed kilometre scale recumbent folds (Figs. 3-8b and 3-5e), with shallowly plunging, east to southeast – west to southwest trending axes b$_2$. The earlier foliation S$_1$ was observed in the hinge areas of parasitic folds F$_2$, and it steeply dips towards the northeast and southwest (Fig. 3-8c). The rootless hinges of small folds F$_1$ are characterised by steep fold axes b$_1$ plunging towards south to southeast (Fig. 3-8b). Two axes b$_3$ of large folds F$_3$ were recognised based on the intersections of crenulation cleavage with foliation S$_2$, and their shallow plunge towards south to southwest coincides with the π-axis of S$_2$ (Fig. 3-8b). The stretching lineation represented by preferential growth of biotite and muscovite observed on the main foliation S$_2$ plunges mainly towards the southeast and southwest with considerable scatter (Lmin in Fig. 3-8a). The northwest-southeast strike of steep to sub-vertical spaced cleavage S$_{SC}$ is nearly perpendicular to the trend of b$_3$ and therefore could not be related to D$_3$ but possibly represents much younger processes (Fig. 3-8e).

Two distinct zones of localised shear strain composed of highly deformed mylonitic to ultramylonitic rocks were observed in this area (Fig. 3-8d). Kinematic indicators such as foliation-parallel asymmetric drawn boudins (Fig. 3-5f; drawn- to shearband-boudin transition of Goscombe et al. 2004) and C' shear bands suggest top-to-the-southwest sense of shear (Fig. 3-6).

3.3.2 Vlasina Unit

Due to structural complexity encountered in the Vlasina Unit, its deformation pattern will be presented in three domains showing relative structural homogeneity (Fig. 3-9).

3.3.2.1 Southern part of Vlasina Unit

Penetrative foliation S_2 in the southern part of Vlasina Unit is sub-horizontal to shallow dipping towards the southeast, with southwestward moderate to steep dip in a narrow area proximal to a belt of Eocene volcanic rocks south of Surdulica pluton (Figs. 3-3 and 3-9a). The foliation S_2 often represents the axial-plane cleavage of tight to isoclinal recumbent folds F_2 (Fig. 3-10a). Due to their presumed kilometre-scale size, these folds F_2 are discernible only in hinge areas or by their decimetre- to metre-scale parasitic folds (Fig. 3-10a). Axes b_2 of these folds are plunging at low angles generally towards the south and southeast, and towards the northeast in the western periphery of this area (Figs. 3-3 and 3-9a). Earlier folds F_1 are occasionally observed as isoclinally folded quartz-feldspar bands, refolded by F_2 (Fig. 3-10a). Due to small number of measurements, significance of mineral lineation and occurrences of late cleavage S_3 could not be critically evaluated in this area (Fig. 3-9a).

3.3.2.2 Northern part of Vlasina Unit

Ductile structures in the northern part of the Vlasina Unit were examined in the schists of the pre-Ordovician Vlasina as well in the post-Cambrian metasediments (Fig. 3-9b). Penetrative subhorizontal to shallow foliation S_2 is predominantly dipping towards the northwest with minor population dipping at moderate angles towards the northeast (Fig. 3-9b). The variation of the

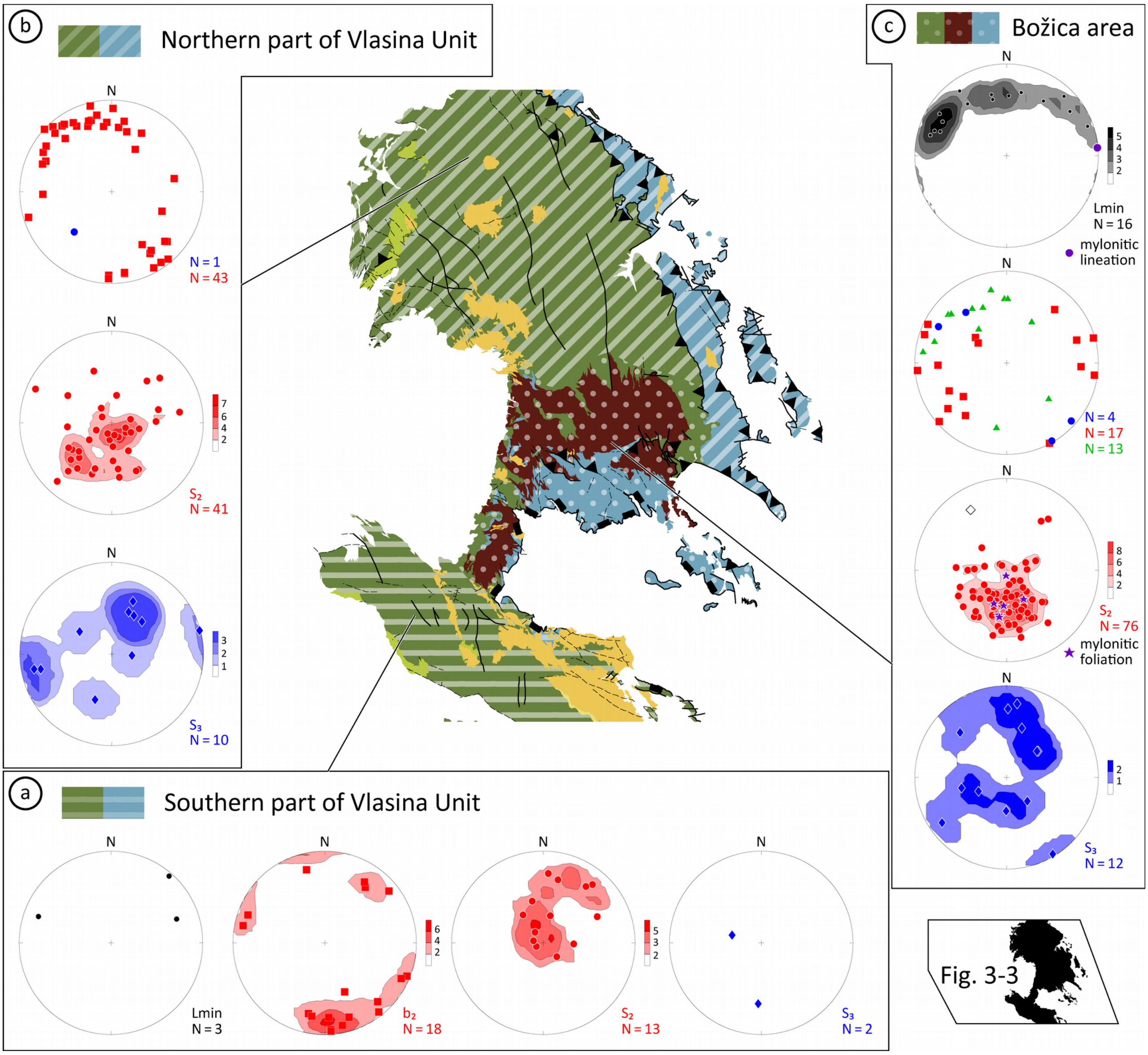

Figure 3-9. Lower hemisphere equal-area plots of structural elements from the (a) southern part of Vlasina Unit, (b) northern part of Vlasina unit, and (c) Božica area. Symbol legend is given in Figure 3-4. Inset shows the relative scale and position in Figure 3-3.

orientation of S_2 is assigned to subsequent brittle deformation, including Cretaceous east-northeastward thrusting, especially prominent in the eastern part of this area. The foliation S_2 generally represents axial-plane cleavage of recumbent decimetre- to decametre-scale tight to isoclinal folds F_2 (Fig. 3-10b and c). Foliation S_2 is defined by muscovite and chlorite. Fold axes b_2 are predominantly sub-horizontally to shallowly plunging in north to northwest – south to southeast direction (Fig. 3-9b). An initial foliation S_i is defined by quartz-feldspar bands that were isoclinally

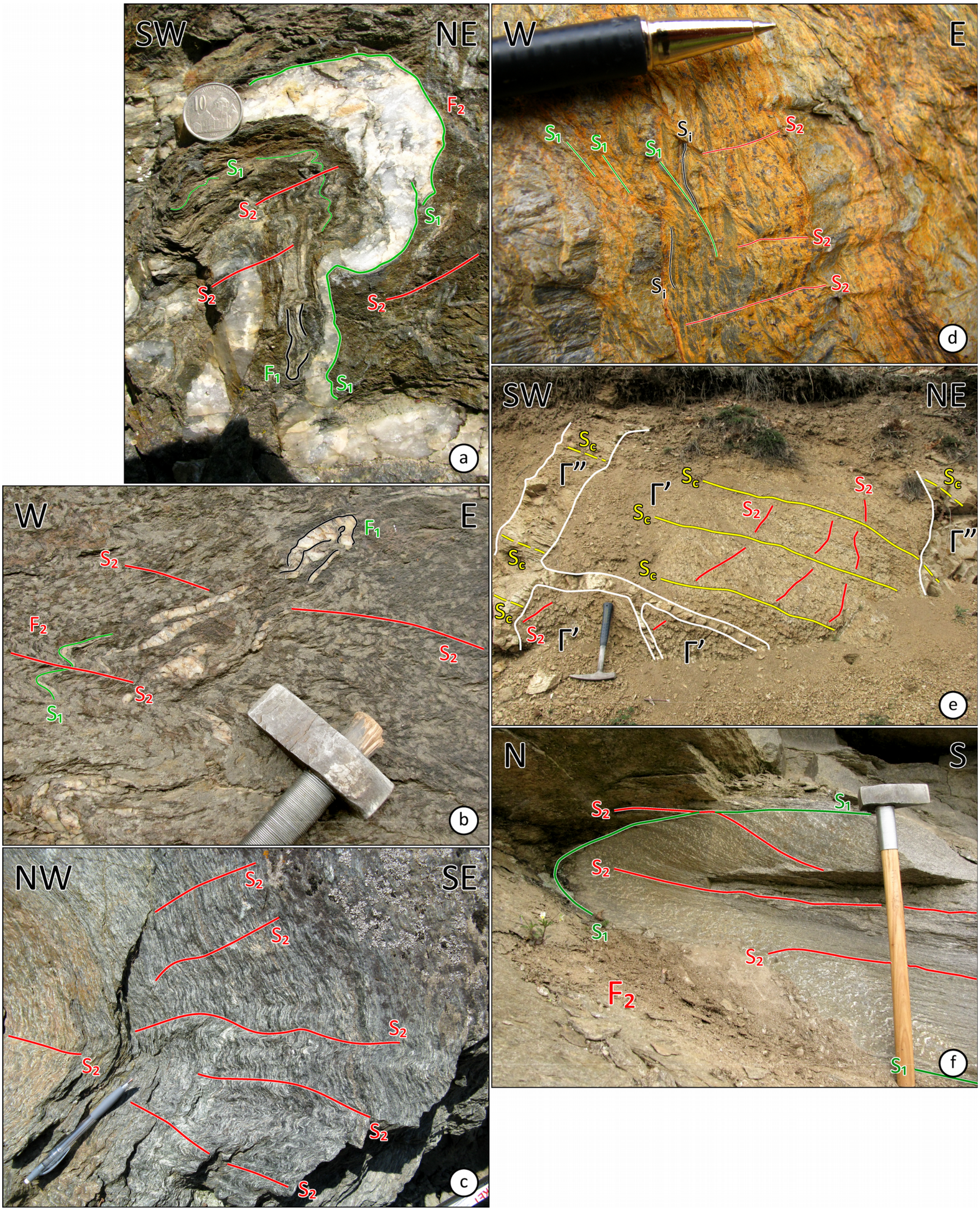

Figure 3-10 opposite page.(a) Isoclinal fold F_1 refolded by later isoclinal fold F_2 with axial-plane cleavage S_2 in chlorite-muscovite schists in the southern part of the Vlasina Unit (22°5'52.149"E, 42°22'5.121"N). Diameter of coin 26 mm. (b) Quartz-feldspar bands folded into isoclinal folds F_1 represented by rootless hinges in a matrix of chlorite-muscovite schists in the northern part of Vlasina unit (22°4'57.756"E, 42°53'43.306"N). Size of the head of hammer 136 mm.

folded into centimetre-scale folds F_1 (Fig. 3-10b) and subsequently refolded into large recumbent folds F_2. This initial foliation (S_i) is better observed in the thrust-sheets composed of low- to very-low-grade lower Palaeozoic meta-sediments (Fig. 3-3). In the upper Silurian to Lower Devonian argillites the foliation S_i is defined by sericite-rich bands folded in centimetre-scale chevron folds F_1, of which only limbs have remained due to strong reworking by the axial-plane cleavage S_1, whereas the late S_2 represents a crenulation cleavage developed at a high angle to S_1 (Fig. 3-10d).

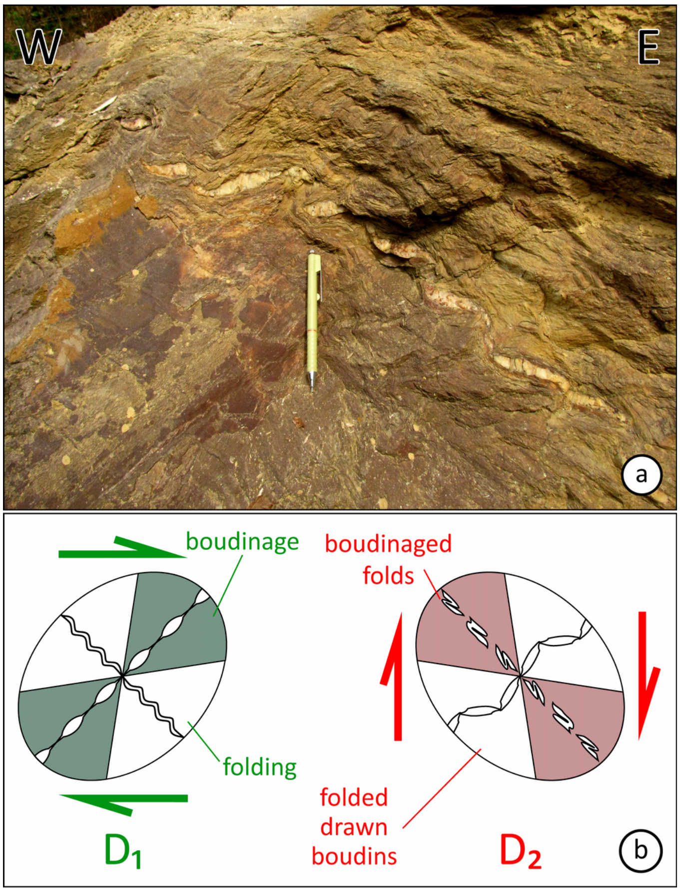

Figure 3-11. (a) Folded train of drawn boudins within the Ordovician meta-argillites in the northern part of Vlasina Unit (22°25'47.903"E, 42°51'49.239"N). Size of pencil 13.5 mm. (b) Evolution of structures through deformation stages D_1 and D_2. Shaded areas of strain ellipsoids represent extensional quadrants, whereas blank areas represent compressional quadrants.

The difference in orientation of strain axes during the deformation stages D_1 and D_2 resulted in the formation of folded drawn boudin trains in Ordovician meta-argillites (Fig. 3-11). The boudin trains were initially formed in the extensional domain of D_1 strain ellipsoid and were subsequently folded by simple shearing during D_2 (Fig. 3-11b).

Spaced and crenulation cleavage S_3 was distinguished only where it intersects composite

---

Figure 3-10 continued. (c) Fanning axial-plane cleavage S_2 in the chlorite schists in the northern part of Vlasina Unit (22°18'15.775"E, 42°48'21.52"N). Size of pen 152 mm. (d) Initial foliation S_i folded in centimetre-scale chevron folds F_1 preserved only as limbs due to strong reworking by the axial-plane cleavage S_1, with superimposed crenulation cleavage S_2 in upper Silurian to Lower Devonian argillites of the northern part of Vlasina unit (22°32'33.657"E, 42°45'9.631"N). Size of metal tip of a pen 17 mm. (e) Spaced cleavage S_c is observed in the Early Silurian coarse-grained Qz-monzonite (Γ') and Permo-Triassic fine-grained granites (Γ”), whereas the foliation S_2 can be seen only in the former (21°49'51.156"E, 42°21'30.213"N). Hammer length 330 mm. (f) Refraction of S_2 in the folded granodiorite in the western part of the Lower Complex (21°37'48.583"E, 42°45'9.15"N). Length of hammer ca. 60 cm.

foliation at high angles in medium- to low-grade rocks, generally in areas close to Južna Morava river (Fig. 3-3). Maximum of S_3 is dipping towards the northeast at a moderate angle, but a significant population of subvertical cleavage striking north to northeast-south to southwest is also observed (Fig. 3-9b). A single axis b_3 moderately plunging towards the southwest of a large open fold F_3 was measured in an area away from the thrust-front (Fig. 3-9b).

3.3.2.3 Božica area

Božica area comprises the Božica magmatic complex and the post-Cambrian meta-sedimentary succession (Lisina series of Dimitrijević 1963; Babović et al. 1977), south of the magmatic complex (Figs. 3-3 and 3-9c). In this area foliation S_2 is generally dipping at moderate to low angles towards the north (Fig. 3-9). Fold-axes b_2 of decimetre-scale asymmetric parasitic folds F_2 are trending east to southeast–west to northwest (Figs. 3-9c and 3-12a). Foliation S_2 represents an axial-plane cleavage of folds F_2 (Fig. 3-12a). Earlier centimetre-scale isoclinal folds F_1 are preserved as rootless fold hinges, refolded by F_2 at various intersection angles (Figs. 3-9c and 3-12a).

Late crenulation (Fig. 3-12b) or spaced cleavage S_3 is usually distinguished by high intersection angles with S_2 and it is moderately to steeply dipping with no preferential direction (Fig. 3-9c). Subhorizontal to shallow fold axes b_3 trending north to northwest – south to southeast are inferred from intersection lineation of S_3 on S_2 and crenulation lineation (Fig. 3-9c). The mineral lineation statistically forms a girdle with approximate orientation 000/30 having a single maximum at 304/20 (Fig. 3-9c). Although neatly aligned in the spherical projection, these lineations are anisotropically distributed throughout the Božica area.

Presence of mylonite, ultramylonite and discrete anastomosing shear zones developed in the southern part of Božica magmatic complex indicate that these rocks have experienced considerable

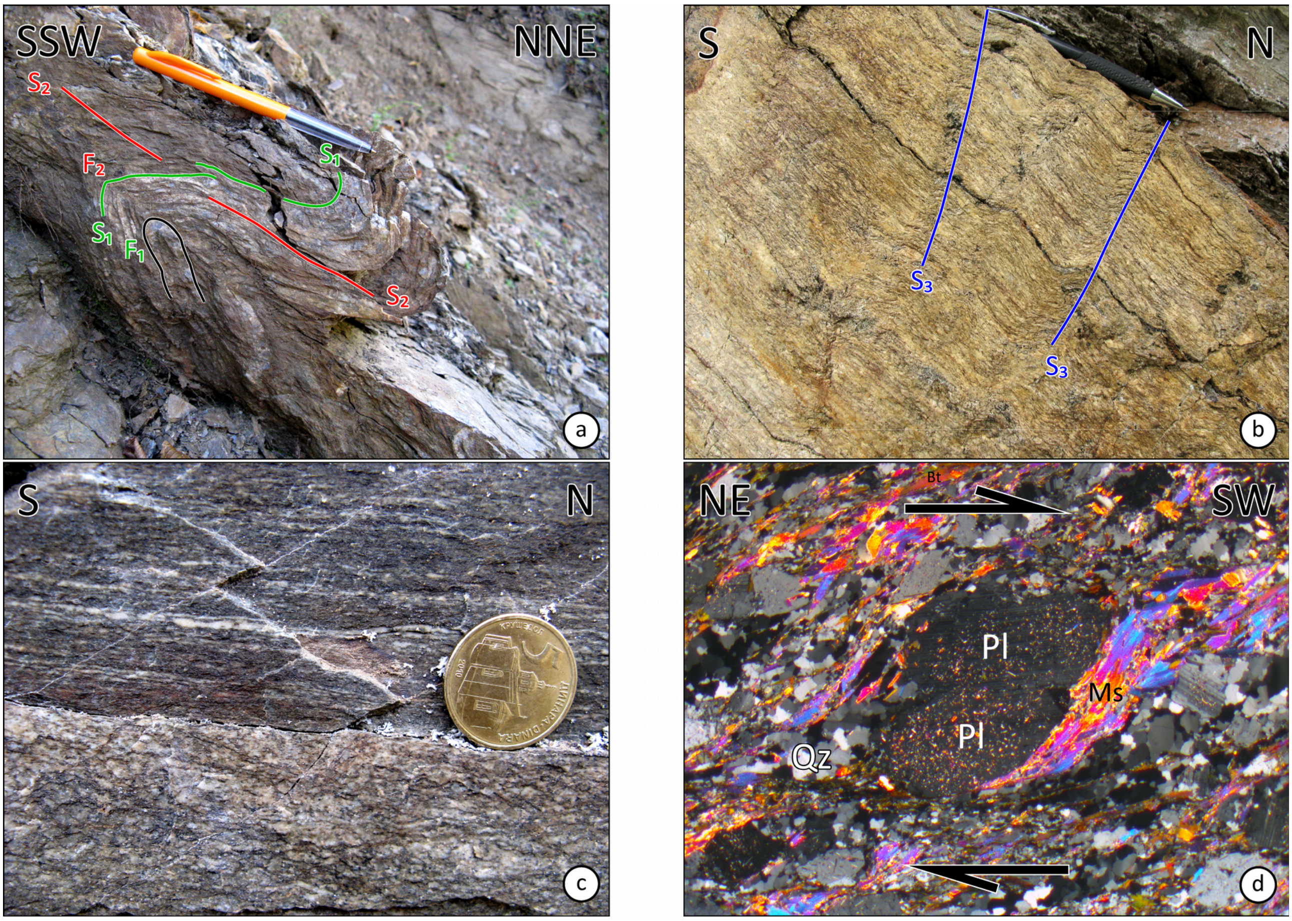

Figure 3-12. Structural features in the Božica area: (a) Rootless hinges of folds F_1 in the hinge of isoclinal fold F_2 in Ordovician sericite-chlorite schists (22°23'8.132"E, 42°33'6.694"N). Minor transposition of S_1 along axial-plane cleavage S_2 can also be observed. Size of pen 145 mm. (b) Crenulation cleavage S_3 in the mylonites formed in the Božica magmatic complex (22°23'40.552"E, 42°35'28.461"N). Length of pencil 143 mm. (c) Ultramylonites within the Božica magmatic complex (22°23'40.552"E, 42°35'28.461"N). Diameter of the coin 24 mm. (d) A σ-type K-feldspar mantled porphyroblasts indicating top-to-the-southwest sense of shear (SM272-1; 22°24'50.956"E, 42°35'42.182"N). Crossed nicols. Width of image 5.9 mm.

amount of shear strain (Fig. 3-12c). Foliation is defined by syn-deformation muscovite, biotite and clinozoisite. Kinematic indicators such as δ- and σ-type mantled clasts of feldspar (Fig. 3-12d) indicate top-to-the-west to southwest sense of shear (Fig. 3-6).

3.3.3 Eastern Veles series

Structural data from the EVS was collected only along a single transect across the contact with the Lower Complex, north of Preševo (Figs. 3-2 and 3-3). Although the contact itself could not be directly observed, it was established that the penetrative foliation in the EVS is steeply dipping towards east to northeast (Fig. 3-13a) being parallel to the orientation of S_2 in the Lower Complex near the contact (Fig. 3-4). Structural concordance between these penetrative fabrics suggests a ductile character of the contact. The foliation in gneisses of the EVS is defined by flattened quartz-feldspar aggregates, biotite and muscovite. Asymmetric K-feldspar grains (sheared boudin trains, sigmoids and δ-like clasts) in late Cambrian leucocratic orthogneiss (Chapter 2) indicate top-to-the-southwest sense of shear (Figs. 3-6 and 3-13b). Replacement of K-feldspar by muscovite and sericite is widespread (Fig. 3-13b). Quartz grains show sweeping undulose extinction and deformation lamellae as well as evidence of dynamic recrystallisation predominantly by grain boundary migration (GBM) with less prominent evidence of sub-grain rotation (SGR; Fig. 3-13b).

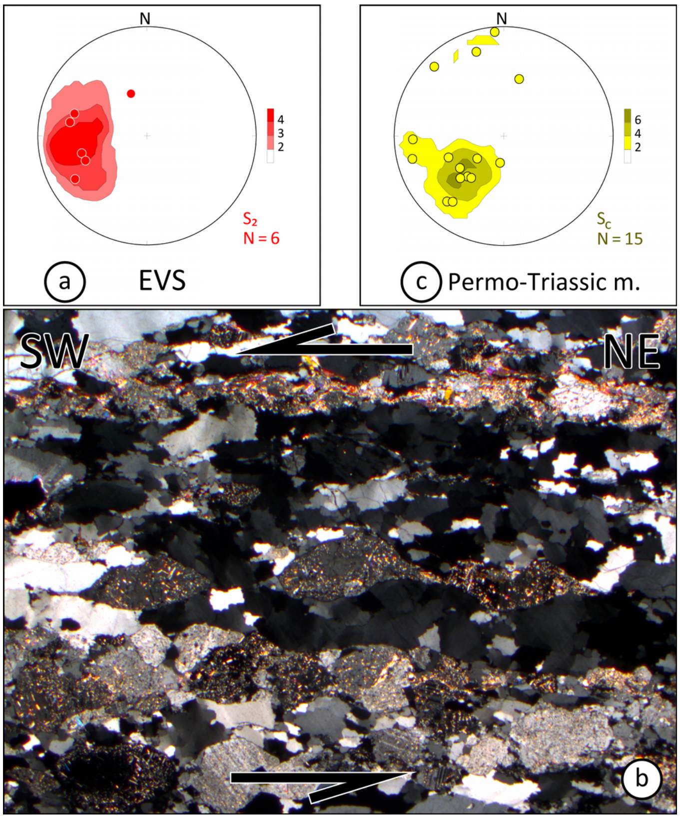

Figure 3-13. Lower hemisphere equal-area plot of (a) the measured foliation S_2 in the EVS. (b) Asymmetric K-feldspar grains indicating top-to-the-southwest sense of shear in leucocratic orthogneiss in the EVS (SM315; 21°38'37.896"E, 42°20'43.603"N). Crossed nicols. Width of the image 5.9 mm. (c) Lower hemisphere equal-area plot of spaced cleavage S_c in Permo-Triassic magmatic rocks (i.e. fine-grained Bujanovac granite)

3.3.4 Permo-Triassic Bujanovac pluton

The Bujanovac magmatic complex encompasses two distinct generations of igneous rocks, (i) a coarse-grained quartz-monzonite emplaced in early Silurian intruded by (ii) a fine-grained granite in late Permian to Early Triassic (Chapter 2). The early Silurian monzonite is strongly deformed and transformed into gneiss with a penetrative regional foliation S_2. Field observations revealed a weakly developed cleavage S_C in both the younger and the older magmatic rocks (Fig. 3-10e). Occasionally this late cleavage S_C in the old quartz-monzonite intersects the older foliation S_2 at low angles, resulting in a structure similar to pencil cleavage (Fig. 3-10e). Late cleavage S_C predominantly dips at moderate angles towards the northeast (Fig. 3-13c). Macroscopic S-C fabric observed in central parts of the younger fine-grained granite shows a general top-to-the-north shear direction. Additionally, a number of anastomosing shear zones separating low-strain domains were observed in the younger granite.

3.4 ^{40}Ar/^{39}Ar thermochronology

An overview of the ^{40}Ar/^{39}Ar thermochronology method is given in Appendix 3-1 together with a detailed description of the analysed material and complete ^{40}Ar/^{39}Ar data. A brief overview of critical sample information is given in Table 3-1, while relevant ^{40}Ar/^{39}Ar date spectra, K/Ca diagrams and isotope correlation plots are shown in Figure 3-14. Additionally, the ^{40}Ar/^{39}Ar dates are presented in Figure 3-2 along with previously published K/Ar, Rb/Sr and ^{40}Ar/^{39}Ar dates. Plateau date is defined by at least three contiguous heating steps with indistinguishable dates spanning more than 50% of the ^{39}Ar released (Dalrymple and Lanphere 1974). The ^{40}Ar/^{39}Ar date is considered robust only if the plateau age overlaps with the inverse isochron date. When these conditions are not met, the weighted mean date is used, which is defined by at least three contiguous heating steps that yield dates that differ by less than 5%, and span at least 50% of ^{39}Ar released. Mineral names are abbreviated according to Whitney and Evans (2010).

Newly-formed muscovite (i.e. without inherited domains) that defines a mylonitic foliation within the Vrvi Kobila shear zone yielded an early Carboniferous plateau date (351±1 Ma; SM01; Table 3-1 and Figs. 3-2, 3-7c and 3-14). Thermal history of the Vlasina Unit was examined by

Table 3-1 Overview of the results of $^{40}Ar/^{39}Ar$ thermochronology

Sample name	Locality	Rock type	Tectonic unit	Sampling location [DMS]		Elevation [m asl]	Mineral phase	$^{40}Ar/^{39}Ar$ date [Ma]	±2σ [Ma]	$^{39}Ar_k$[1] [%]	Inverse isochron date [Ma]	±2σ [Ma]	MSWD[2]
				Longitude	Latitude								
SM01	Kukavica	Mylonite	Lower complex	22°0'50.825"E	42°41'39.368"N	738	Ms	351 (P)	1	59,87	352	2	n/a
SM05	Predejane	Chl-schist	Vlasina unit	22°5'9.39"E	42°48'45.797"N	309	Ms	284 (P)	1	46	285	1	0,49
SM248-1	Vlajna	Bt-gneiss	Lower complex	21°56'45.673"E	42°48'12.532"N	599	Bt	195 (P)	1	58,35	195	3	2,58
SM250-1	Golemo Selo	Amphibolite	Lower complex	21°50'38.126"E	42°43'54.05"N	485	Hbl	290 (W)	8	54,69	234	28	36,58
SM250-2	Golemo Selo	Bt-gneiss	Lower complex	21°50'38.126"E	42°43'54.05"N	485	Bt	179 (W)	1	96,81	185	3	9,56
SM437-1	Vranjska Banja	Mylonite	Lower complex	21°53'58.876"E	42°27'45.765"N	483	Bt	338 (W)	2	78,57	345	12	2,81
SM499-1	Božica	Mylonite	Vlasina unit	22°24'2.255"E	42°35'38.648"N	1112	Bt	246 (P)	1	56,48	247	1	0,58

[1] Percentage of ^{39}Ar released during steps used in data calculation.

[2] Mean square of weighted deviates of the inverse isochron linear regression.

Weighted mean dates (W) are tentative and their interpretation requires caution. See text for details.

Mass discrimination factor = 0,983±0,051.

Abbreviations:

Mineral abbreviated according to Whitney and Evans (2010): Ms – muscovite; Bt – biotite; Hbl – hornblende.

EVS – Eastern Veles series.

P – Plateau, i.e. > 3 contiguous heating steps that span > 50% ^{39}Ar released (the date is the weighted mean date of the plateau).

W – Weighted mean date of > 3 contiguous heating steps that yield distinguishable dates that differ by less than 5%, and span > 50% ^{39}Ar released.

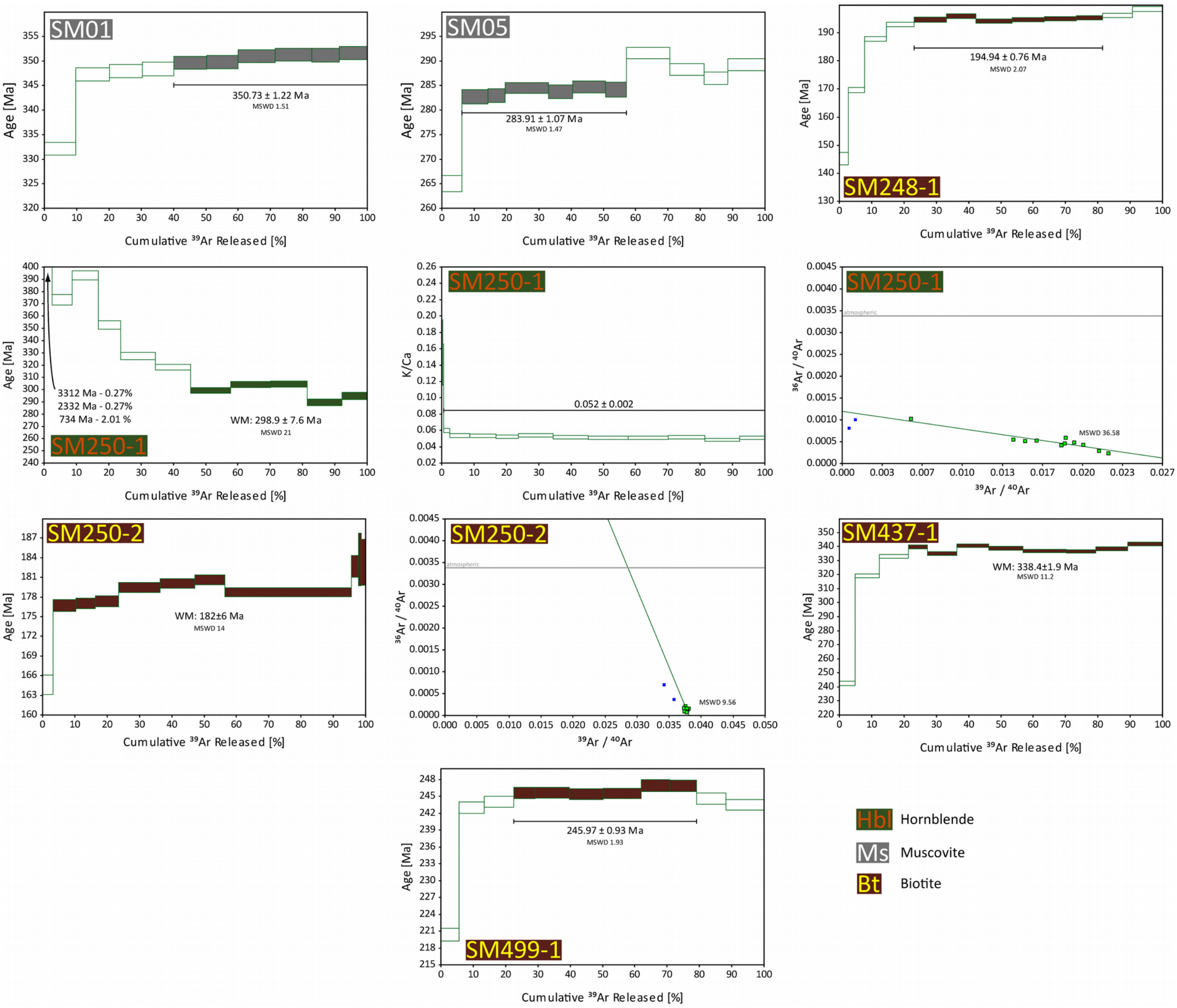

Figure 3-14. Relevant ^{40}Ar/^{39}Ar date spectra, K/Ca yield diagrams and isotope correlation plots for samples from the central SMM. All uncertainties are ±2σ. Plateau dates are defined according to Dalrymple and Lanphere (1974). WM – weighted mean date. See Appendix 3-1 for further details.

analysing undeformed muscovite from chlorite-schists, which showed a lower Permian plateau date (284±1 Ma; SM05; Table 3-1 and Figs. 3-2 and 3-14). An aliquot of syn-tectonic biotite from a mylonite formed under higher-greenschist facies conditions, sampled within a shear zone with a top-to-the-west sense of shear formed in the Božica magmatic complex yielded a Middle Triassic plateau date (246±1 Ma; SM499-1; Table 3-1 and Figs. 3-2 and 3-14). Thermal evolution of a Lower Complex gneiss that experienced retrogression was investigated by analysis of biotite grains that are forming the foliation in these rocks and have not been affected by retrogression. These biotites showed Lower Jurassic plateau date (195±1 Ma; SM248-1; Table 3-1 and Figs. 3-2 and 3-14). Two remaining biotite samples (SM437-1 and SM250-2) and a hornblende concentrate (SM250-1) yielded more ambiguous results reported only as weighted mean dates (338±2, 182±6 and 290±8 Ma, respectively). These results are interpreted only by consideration of additional geological observations (Table 3-1 and Figs. 3-2 and 3-14).

3.5 Discussion

The results of structural analysis and $^{40}Ar/^{39}Ar$ thermochronology revealed a sequence of major tectonothermal events that affected the central SMM. The individual stages of deformational and thermal evolution are discussed below in chronological order.

3.5.1 Variscan Orogeny

3.5.1.1 First deformation stage D_1

Evidence of deformation stage D_1 is generally scarce, as the resulting structures have been strongly overprinted during the subsequent deformation stage D_2. Structures formed during D_1 were documented in both the Lower Complex (e.g. Fig. 3-5b) and the Vlasina Unit (e.g. Figs. 3-5f and 3-12a). The most common structural elements preserved from this stage are centimetre-scale rootless hinges of folds F_1 in the microlithons bound by foliation S_2, with fold-axes b_1 usually at high angles to axes b_2 of younger folds F_2. Rarely, refolded decimetre-scale folds F_1 could be observed in the hinge areas of larger folds F_2 (Fig. 3-5e). As an exception, structures related to D_1 were better preserved in the low-grade metasediments of the post-Cambrian Vlasina, located in the Cretaceous thrust-sheets in the northeastern part of the study area (Fig. 3-3). These structures include folds F_1

and drawn boudin trains showing only minor deformational overprint related to D_2 (Figs. 3-10d and 3-11a, respectively).

The strong overprint during D_2 in most of the study area and the subsequent brittle deformation do not allow reconstruction of either the general orientation of main stress axes, nor the direction of tectonic transport during D_1. Likewise, none of the observed stretching lineations could be unequivocally attributed to D_1. At locations where the stretching lineations were considered as related to D_1 due to their misalignment to the perceived general trend (e.g. Vrvi Kobila area), their original orientation was not preserved due to reworking during D_2 as shown by the complete transposition of S_1. However, the intersection angles between fold axes b_1 and b_2, ranging within 90° (Figs. 3-4, 3-8b and 3-9) could be interpreted as a consequence of the initial orientation of b_1, or exclusively a result of varying intensity of the later deformational overprint(s).

Based on the similarities in structural style, the deformation stage D_1 corresponds to the "phase I" from the detailed structural study of the Vlasina Unit by Petrović, (1969). The youngest rocks containing the effects of D_1 are the upper Silurian to Lower Devonian metasediments (Marinova et al. 2010) in the thrust-sheets of post-Cambrian Vlasina (Fig. 3-10d), thus constraining a maximum age of D_1 to the lower Emsian (ca. 408±3 Ma; Cohen et al. 2013). Minimum age constraints on D_1 could not be clearly defined, but it certainly predates the onset of the deformation stage D_2, which is discussed below.

3.5.1.2 Second deformation stage D_2

Penetrative foliation S_2 shows predominantly subhorizontal to shallow dip since it formed as an axial-plane cleavage to the kilometre-scale recumbent folds F_2 (Figs. 3-4, 3-8b, 3-9 and 3-13a). These large folds could be detected only by the asymmetric parasitic folds at decimetre- to metre-scales (e.g. Figs. 3-5e, 3-8b, 3-10a and c). Foliation S_2 in the hinge areas of these folds is observed as axial-plane cleavage (Fig. 3-10f), whereas in the limbs the older foliation(s) are completely transposed.

Although its orientation generally varies in individual domains presented above, the fold axes b_2 of recumbent isoclinal folds F_2 most often shows similar orientation to that of the stretching lineation, which is assumed to be formed during D_2 (Figs. 3-4a and b). This parallelism is commonly reported in domains deformed by recumbent folds (Bastida et al. 2014 and references therein) and it could result from a progressive deformation during D_2 (sensu Tobisch and Paterson 1988), implying a relatively constant orientation of the regional stress field in a geologically short period of time producing various sets of structures with similar orientation, sense of movement, style and prevailing metamorphic conditions. It is possible that during the early stages of D_2 the isoclinal folds F_2 were initiated, whereas these folds were amplified into recumbent and less cylindrical forms in the later stage of the same deformation stage. A progressive non-coaxial deformation would cause an amplification of folds while increasing the curvature of hinge-lines leading to the reorientation of fold axes b_2, and eventually to transposition of older structures along S_2 during the late D_2. The suggested partial reorientation of fold axes b_2 could explain the observed dispersion in their orientation (e.g. Figs. 3-4, 3-8b and 3-9). Alternatively, the parallelism of linear elements (i.e. fold axes b_2 and stretching lineation) to the direction of tectonic transport could be explained by the laterally constricted thrusting (Fossen 1993; Passchier et al. 1997; Fernández et al. 2007). In this case, the western part of the Lower Complex seems to be affected the most based on the uniformity of linear structures it displays (Fig. 3-4a). This might be a consequence of the lowermost position in the crust it held during the Variscan orogeny and thus the least rheological competence. The effects of this mode of deformation (i.e. parallelism between the stretching lineation and the fold axes b_2) are less evident in the remaining areas of the central SMM, which were presumably at relatively shallower depths during D_2. Additionally, local variations in geometry of all structural elements formed during D_2 were probably disturbed further during the subsequent events involving magmatic intrusions and block rotations in the brittle regime.

The majority of the observed kinematic indicators in central SMM suggest southeastward direction of tectonic transport (Fig. 3-6). This transport direction is most probably related to the last high-strain event in the area – D_2, together with the corresponding mineral lineation trending northwest-southeast (Figs. 3-4, 3-8a and 3-9c). Several exceptions are observed in the western domain of the Lower Complex and the Vranjska banja area (Figs. 3-4a and 3-8a). In the western part of the Lower Complex (i.e. west of Tupale fault; Fig. 3-4a), stretching lineation Lmin and fold axes b_2 trend generally north–south. The misalignment of these structures with the prevailing northwest-southeast trend could be caused by a local difference in D_2 strain field or represents mineral lineation from an early D_2 that were incompletely rotated during progressive deformation. Similar south to southwestward plunge of stretching lineation together with southwestward sense of shear was observed in the Vranjska Banja area. Furthermore, the observed scatter in the orientation of stretching lineation and shear sense indicators could be a result of block rotation in the brittle regime during the Alpine orogeny, which had considerably reshaped this area (Chapter 4). Additionally, the rheological contrast between adjacent domains could have caused the observed opposite senses of shear (Burg 1987). The stretching lineations and shear sense indicators were rarely observed in the Vlasina Unit, except for the deformation in Božica area, which will be discussed below.

The metamorphic grade and strain intensity within the central SMM are observed to decrease eastwards (in present coordinates; i.e. from the Lower Complex to the metasediments in the post-Cambrian Vlasina). A probable cause for this trend could be the structural level of these units within the Variscan orogen. The amphibolite-grade Lower Complex was in a mid-crustal position, whereas the pre-Ordovician Vlasina with mineral assemblages indicating greenschist facies peak-conditions was located within the upper crust, below the anchimetamorphosed rocks of the post-Cambrian Vlasina. Vranjska Banja and Božica areas with transitional metamorphic grade between amphibolite and greenschists facies, probably held intermediate crustal positions. Abrupt changes in metamorphic grade observed across brittle thrusts in the eastern part of the study area could be explained by telescoping during the Cretaceous compression.

The general southeastward tectonic transport during D_2 cannot explain the increase of the metamorphic grade from east to west observed in the studied area. This metamorphic pattern must be related to a general westward thrusting and thickening of the crust. Therefore we suggest that the westward sense of tectonic transport was most probably related to stage D_1, when the peak metamorphic conditions were attained in the central SMM.

The minimum age of deformation stage D_2 is constrained by the undeformed Slatinska Reka granite, which intruded the Lower Complex gneisses in the Vrvi Kobila region at 328±5 Ma (U-Pb zircon age; Chapter 2). At the contact with these granites the hinge of F_2 open fold with well developed axial-plane cleavage S_2 were observed together with rootless hinge of fold F_1 generated during the earlier deformation stage D_1 (Fig. 3-15). These observations clearly show that the granite intrusion postdates both D_1 and D_2 deformation stages.

Based on style of deformation, the structures generated during progressive deformation of D_2 are comparable to those of “phases II and III” previously established as syn-metamorphic folding stages in the Vlasina Unit (Petrović 1969).

Indirect constraints on the age of both deformation stages D_1 and D_2 presented above suggest that they have taken place during the Variscan orogeny (i.e. between 408 and 328 Ma, lower age limit is discussed further below). At this time, the central SMM was involved in a series of tectonic events related to amalgamation of eastern and western parts of the Galatian super-terrane and its final collision with Laurasia (Stampfli et al. 2013; Chapter 2). Variscan age of the peak

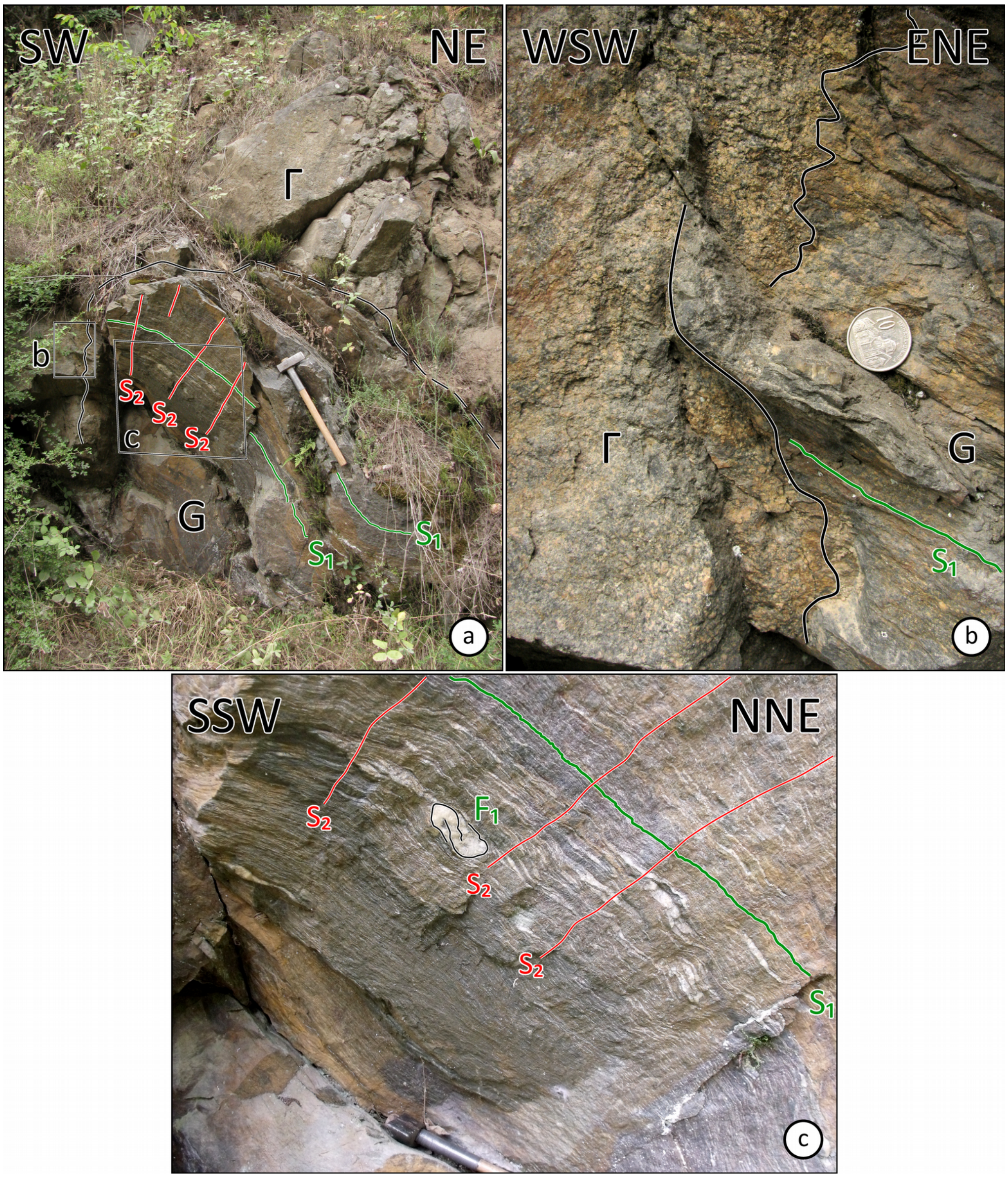

Figure 3-15. (a) Intrusive contact of Slatinska Reka granite (Γ) and Lower Complex gneiss (G) in the Slatinska Reka Valley (22°1'30.716"E, 42°50'53.365"N). Trace of the contact plane is indicated by black line. S_1 –foliation formed during D_1 and folded into isoclinal folds F_2; S_2 – axial-plane cleavage related to folds F_2 during D_2. Length of hammer ca. 60 cm. (b) Detail from (a). Diameter of the coin 26 mm. (c) Detail from (a) showing the quartzitic rootless hinge of fold F_1 and axial plane cleavage S_2 of fold F_2. Hammer head length 134 mm.

metamorphism and high-strain deformation has been reported for a number of crystalline units in the Carpatho-Balkanid orogen (Dimitrijević 1958; Dallmeyer et al. 1998; Ilic et al. 2005; Carrigan et al. 2005; Karamata 2006). North-south oriented compression (in present orientation) related to the Variscan orogeny was previously reported for the crystalline basement of the Getic tectonic zone in Romania (Plissart et al. 2012). Farther east in the Central Stara Planina Unit of the Balkan belt, Gerdjikov et al. (2010a; 2010b) reported an early Carboniferous (336–315 Ma) km-scale transpressional ductile shear zone trending east-west that juxtaposes higher-grade over lower-grade Variscan metamorphic rocks. The remnants of the Variscan orogen in the Balkan belt represent a direct prolongation of the Variscan metamorphic rocks from the Getic zone and the SMM that have experienced clockwise rotation and dextral strike slip tectonics during the Alpine orogeny (e.g. Csontos and Vörös 2004; Fügenschuh and Schmid 2005).

The evidence of pre-Variscan deformation and HP metamorphism proposed previously (Dimitrijević 1959; Petrović 1969; Milovanović 1989; Balogh et al. 1994; Karamata and Krstić 1996; Zagorchev and Milovanović 2006) was not observed during this study.

High occurrence of mylonites observed in the Vrvi Kobila area together with anastomosing shear zones in the competent magmatic rocks of the Vlajna magmatic complex (Figs. 3-2 and 3-7) constitute an important shear zone characterised by southeastward direction of tectonic transport. Evidence of dynamically recrystallised quartz by GBM and SGR (Stipp et al. 2002), along with asymmetric myrmekite (Fig. 3-7c; Simpson and Wintsch 1989) indicate that this shear zone was active during high-grade conditions. Folding within this area was observed only in isolated low-strain zones and in the periphery of the shear zone (Figs. 3-7a and 3-15). Observations made during this study show that this shear zone does not separate the Lower Complex from the Vlasina Unit as previously reported, but it is entirely formed within the former (discussed above). Discrete contact between these two units was not directly observed in the study area. However, the proximity of amphibolite-facies gneisses of Lower Complex and greenschist-facies rocks of Vlasina Unit in the hanging wall of the Vrvi Kobila shear zone, and relative structural concordance of foliation S_2 in both rock types suggest that some telescoping must have occurred prior to the end of stage D_2 (Figs. 3-7a and b). It must be noted that apart from difference in metamorphic grade, the metamorphic rocks of Lower Complex and Vlasina Unit also had different protoliths. Therefore the speculative structure that had telescoped the metamorphic sequence, also had juxtaposed two contrasting protolith lithologies.

An early Carboniferous $^{40}Ar/^{39}Ar$ plateau date of muscovite from the Vrvi Kobila area (SM01: 351±1 Ma) is interpreted as the minimum age of activity along this shear zone which most probably took place during deformation stage D_2 (Figs. 3-2, 3-14 and 3-16). A similar Rb-Sr date of 349 Ma was reported for muscovite from the leucocratic vein in the Lower Complex, north of the research area (i.e. north of Lece volcanic complex in Fig. 3-2; Deleon 1969). Nevertheless, the possibility that the Vrvi Kobila shear zone is related to a post-D_2 late orogenic extension cannot be entirely ruled out. This shear zone was previously considered as a continuation of the Gabrov Dol detachment in Bulgaria, which was reported as a Cretaceous extensional boundary between the Bulgarian equivalent of Lower Complex (i.e. Ograzhden unit) and Vlasina Unit (i.e. low-grade ophiolitic rocks of Struma unit; Zagorchev 1984; Bonev et al. 1995; Ricou et al. 1998). Later, the Cretaceous age of this complex structure was rejected and it was related to the Variscan orogeny (Kounov et al. 2010; Gerdjikov et al. 2013; Chapters 2 and 4). However, Vrvi Kobila and Gabrov Dol shear zones do not share the same tectonic position nor the same metamorphic grade of the deformation, as the Gabrov Dol zone was formed under green-schist facies conditions and it unequivocally separates high-grade from lower grade metamorphic rocks (Bonev et al. 1995; Gerdjikov et al. 2013).

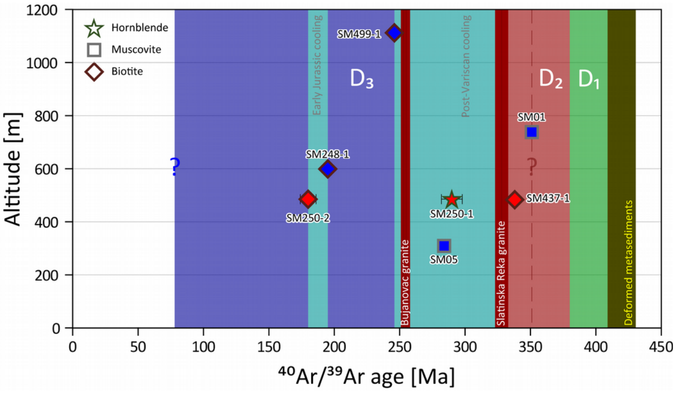

Figure 3-16. Altitude vs. $^{40}Ar/^{39}Ar$ dates of samples from this study. Symbols with blue fill represent plateau dates whereas those with red fill represent weighted mean dates. Inferred durations of major deformation stages are given as blue, red and green fields, whereas durations of thermal events are shown as fields in light blue colour. Vertical bars indicate indirect geological time constraints on duration of the deformation stages (in case of magmatic ages the width of the bar represents 2σ uncertainty). See text for details.

Biotite from a mylonitic zone in the Vranjska Banja area with a top-to-the-southwest sense of shear (Figs. 3-3 and 3-8d) yielded a disturbed pattern with an average

^{40}Ar/^{39}Ar date of 338±2 Ma (SM437-1; Figs. 3-2 and 3-14). The older muscovite ^{40}Ar/^{39}Ar plateau date in Vrvi Kobila compared to the biotite date in Vranjska Banja could be related to different closure temperatures of the two mineral phases (Appendix 3-1), which record regional cooling during the early Carboniferous. Although the ^{40}Ar/^{39}Ar data from the latter sample does not satisfy the criteria for a plateau date, it makes considerable geological sense that these two shear zones were both active during the deformation stage D_2.

3.5.2 Post-Variscan cooling

3.5.2.1 Early Permian cooling

An early Permian ^{40}Ar/^{39}Ar date of muscovite from the chlorite-schists of Vlasina Unit south of Vlasotince (SM05; 284±1 Ma; Table 3-1 and Figs. 3-2 and 3-14) is interpreted as the time of cooling below the greenschist-facies conditions to which this area was exposed during the Variscan orogeny (Karamata and Krstić 1996; Graf 2001). Similar dates were obtained from a majority of the high temperature heating steps in a disturbed ^{40}Ar/^{39}Ar date spectrum yielded by hornblende from the amphibolites in the Lower Complex west to southwest of the Vlajna magmatic complex (weighted mean date of 290±8 Ma; SM250-1; Table 3-1 and Figs. 3-2 and 3-14). The elevated dates of higher temperature steps are almost certainly a result of excess ^{40}Ar. Late Carboniferous to early Permian ^{40}Ar/^{39}Ar dates of detrital white mica have been previously reported as a prominent population in the Mesozoic sedimentary rocks of the Dinarides of western Serbia (332-281 Ma; Ilic et al. 2005) and Struma Unit east of the study area (Fig. 3-2; Kounov 2002), confirming the regional extent of this cooling event. Similar long-lasting cooling and exhumation following the Variscan orogeny is already known in the Supragetic, Getic and Danubian basement units of the South Carpathians (330-300 Ma; Fig. 3-2; Zagorchev 1980; Dallmeyer et al. 1998; Kounov 2002).

Additionally, this time period corresponds to extensional tectonics reported throughout Europe resulting in the opening of fault-bound Stephanian-Permian sedimentary basins (Protić 1966; Maslarević and Krstić 1999; Yanev et al. 2001; McCann et al. 2006). Dallmeyer et al. (1998) report Early Permian dextral strike-slip tectonics in Variscan units of the Romanian South Carpathians. Therefore, the Early Permian cooling in Vlasina Unit could have also taken place in a transtensional setting rather than a purely extensional one. Retention of older ^{40}Ar/^{39}Ar dates (samples SM01 and SM437-1; Table 3-1 and Fig. 3-2) in central parts of the study area shows that this region had already cooled below ca. 310 °C (closure temperature of biotite; Harrison et al. 1985) during the early Carboniferous and was not affected by the Early Permian extension and/or transtension. This area must have been juxtaposed to the vicinity of sample SM05 during strike-slip or compressional Alpine tectonics. Alternatively, it is possible that the entire central SMM had cooled down to temperatures below ca. 310 °C in the Carboniferous and only certain areas were reheated to temperatures above ca. 405 °C (closure temperature of muscovite; Harrison et al. 2009) during the early Permian rifting. In either case the extent of unaffected and affected areas could not be exactly determined due to low spatial resolution of thermochronological data. Deformational structures related to this tectonothermal stage in the study area were not recognised and the dated minerals belong to structures formed during Variscan tectonics.

3.5.2.2 Westward shear in Božica area

A relatively wide shear zone with top-to-the-west sense of shear formed within the Božica magmatic complex was recognised, although its exact regional extent and significance could not be evaluated. Mylonitic foliation is formed by clinozoisite and biotite with topotactic chlorite, suggesting that the shear zone was active under greenschist facies conditions. A biotite from this mylonite yielded an ^{40}Ar/^{39}Ar plateau date of 246±1 Ma (SM499-1), representing a minimum time-constraint for activity along the shear zone (Table 3-1 and Figs. 3-2, 3-14 and 3-16). It must be noted that relicts of high grade deformation (augen-gneiss) have been observed in the Božica area, and its peak metamorphic conditions are somewhat higher (transitional high-greenschist to low-amphibolite facies) than in the majority of Vlasina Unit. Unfortunately, boundaries and exact relationship of the rocks in Božica area with the schists of Vlasina Unit could not be directly observed. A vast scatter in orientation of mineral lineation observed in this area potentially represents effects of incomplete reworking of previous structures by the westward shearing event (Fig. 3-9c). Middle Triassic shearing in the Božica area closely postdates widespread extension along the European margin (ca. 250 Ma; De Wet et al. 1989; Himmerkus et al. 2009b; Peytcheva et al. 2009b), that eventually led to the opening of the Mesozoic Tethys west of the SMM (Robertson et al. 1991; Karamata and Krstić 1996; Pe-Piper 1998; Stampfli et al. 2002; Burg 2012). In western part of the central SMM, this extensional event is manifested by the Permo-Triassic granitic intrusion in the Bujanovac magmatic complex (Chapter 2). Therefore, this regional extensional event was most probably responsible for the formation of the shear zone in Božica area, whereas the evolution of this area since the end of Variscan orogeny until the Middle Triassic remains unresolved.

3.5.3 Third deformation stage D3

Detailed structural investigations completed during the geological mapping of the central SMM in the 1970's provide evidence of kilometre-scale open folds in both the Lower Complex and the Vlasina Unit (Petrović 1969; Petrović et al. 1973; Vukanović et al. 1973; Babović et al. 1977; Vukanović et al. 1977). Statistical analysis of the structural data obtained during this study did not provide clear evidence of such a pattern, probably due to the relatively restricted number of observation points (e.g. Figs. 3-4, 3-9, and 3-13a). However, foliation S_2 in western and central parts of the Lower complex (Figs. 3-4a and b) possibly indicates orientation of limbs of a large-scale fold F_3. Additionally, scarce spaced and crenulation cleavage, sub-perpendicular or at a high-angle to the earlier foliation S_2 (Fig. 3-12b), provides outcrop-scale evidence for a third deformation stage (D_3). Crenulation cleavage formed in the Early Triassic syn-metamorphic mylonites in the Božica magmatic complex (biotite $^{40}Ar/^{39}Ar$ plateau date 246±1 Ma; SM499-1; Table 3-1 and Fig. 3-14) provides a maximum age constraint on D_3 (Fig. 3-16). Minimum age constraint is given by zircon fission-track age from the orthogneiss of the Božica magmatic complex suggesting temperatures below 250 °C in the Late Cretaceous (Chapter 4).

3.5.4 Deformation in the Permo-Triassic Bujanovac pluton

The predominantly northeastward dipping spaced cleavage and S-C fabric formed in the Permo-Triassic Bujanovac granite (U-Pb zircon ages of 255±3 and 253±2 Ma; Chapter 2) is clear evidence for Mesozoic ductile deformation (Figs. 3-10e and 3-13b). Due to a relatively small number of observations, these structures could not be clearly attributed to any of the deformation stages discussed above. The structural evidence for this deformation was not recognised farther away from the Bujanovac magmatic complex, probably due to generally low strain exerted during this event or the very low angle between the new cleavage S_c (Fig. 3-13c) and the older penetrative foliation S_2 (Fig. 3-4c). Likewise, the area affected by this deformation could not be clearly determined. Deformation of much higher intensity than that observed in Bujanovac granite has been reported in the Arnea granite in Greece (Kydonakis et al. 2015a). This granite is of similar age as Bujanovac (De Wet et al. 1989; Himmerkus et al. 2009b) and its deformation is reported to be related to Early Cretaceous southwestward thrusting.

3.5.5 Jurassic cooling

Evidence of retrogression of the mineral assemblages in the Lower Complex and the EVS is provided by the commonly observed replacement of K-feldspar by muscovite and sericite. No ductile deformation accompanied this retrogression. The Early Jurassic $^{40}Ar/^{39}Ar$ plateau date of biotite from gneiss west of the Vlajna magmatic complex in central parts of the Lower Complex (SM248-1; 195±1 Ma; Table 3-1; Figs. 3-2 and 3-14) suggests that some local reheating to temperatures above ca. 310 °C (closure temperature of biotite; Appendix 3-1) took place in Early Jurassic. During this local thermal event, which could explain the evidence of retrogression observed in the Lower Complex gneisses (protolith U-Pb zircon age of 569±9 Ma; Chapter 2), no ductile deformation occurred as the dated biotite forms foliation S_2 that was related to Variscan orogeny and shows no signs of subsequent recrystallisation. In this case the $^{40}Ar/^{39}Ar$ plateau date of 195±1 Ma represents cooling below temperatures that caused retrogression, thus setting a minimum age constraint on the low-grade overprint (Fig. 3-16). Although exhibiting a disturbed step-date spectrum, the Early Jurassic mean $^{40}Ar/^{39}Ar$ date of biotite from a Lower Complex gneiss west to southwest of Vlajna magmatic complex (182±6 Ma; SM250-2; Table 3-1; Figs. 3-2 and 3-14) highlights the regional importance of this thermal event. The low-grade overprint in Lower Complex of central SMM is probably contemporaneous to the greenschist metamorphism and deformation of Triassic sedimentary cover in northwestern corner of the EVS (Novo Brdo schists; Pavić et al. 1983; Chapter 2). In this case the Triassic age of sedimentary protoliths of Novo Brdo schists represents the maximum age constraint on the retrogression observed in the Lower Complex.

Previous Rb-Sr dating of biotite in Božica orthogneiss yielded dates of 166, 203 and 241 Ma (uncertainties not reported; Babović et al. 1977), which are interpreted as partial resetting of an original Permo-Triassic cooling age by the Jurassic low-grade event. Younger K-Ar cooling dates were previously reported for the whole-rock samples from the western part of the Lower Complex

(137-122 Ma; Milovanović 1990) and mica from the same unit north of the study area (151 to 127 Ma; Balogh et al. 1994).

West of SMM (in present coordinates) the Early to Middle Jurassic intra-oceanic subduction of the Triassic Vardar ocean (Kostopoulos et al. 2001; Brown and Robertson 2003; Zachariadis 2007) led to opening of a supra-subduction-zone basin in Middle Jurassic (Channell and Kozur 1997; Božović et al. 2013). The effects of thermal convection in the mantle wedge on the overriding continental crust along with penetration of the dehydration fluids from the subducted slab of Vardar might have caused the initial thermal event, locally resetting the argon isotopic system of mica in gneisses of the Lower Complex. Alternatively, this thermal event could be related to shoulder extension and exhumation during the rifting stage of Ceahlău-Severin Ocean, which had completely opened in Middle Jurassic (Dallmeyer et al. 1998; Iancu et al. 2005). However given the lack of evidence of Ceahlău-Severin Ocean south of Kula Unit in northwestern Bulgaria, the subduction of Vardar represents a more probable cause for the Jurassic thermal event in central SMM. General Early Jurassic hiatus in sedimentary sequences of Supragetic and Getic units in Serbia and Bulgaria may represent a further evidence for the regional exhumation and cooling at that time (e.g. Anđelković 1967; Tchoumatchenco 2006).

Although they share similar pre-Variscan evolution (Chapter 2), the Vertiskos unit in northern Greece and the Ograzhden Unit in southwestern Bulgaria and eastern Macedonia, which are traditionally considered as parts of SMM, show somewhat different Alpine evolution compared to the central SMM. After Variscan metamorphism (e.g. Zidarov et al. 2004; Peytcheva et al. 2005; Zidarov et al. 2007; Kounov et al. 2012), the rocks of Ograzhden Unit southeast of Kjustendil were brought to shallower crustal levels during Late Jurassic (muscovite $^{40}Ar/^{39}Ar$ mean date of ca. 160 Ma; Fig. 3-2; Kounov et al. 2010). The rocks of Vertiskos Unit were also initially metamorphosed during Variscan orogeny (Borsi et al. 1965; Kockel et al. 1977), whereas they have suffered local

HP metamorphism during Early Jurassic (Reischmann and Kostopoulos 2001; Kydonakis et al. 2015b) followed by Barrovian metamorphism and intensive ductile deformation during Cretaceous, which almost completely reworked the older fabric (Dixon and Dimitriadis 1984; De Wet et al. 1989; Burg et al. 1995; Kilias et al. 1997; Kilias et al. 1999; Kostopoulos et al. 2001; Kydonakis et al. 2015a).

3.6 Conclusions

Structural investigation provided evidence of at least three major stages of ductile deformation in the central SMM. Despite different peak metamorphic conditions in the Lower Complex and the Vlasina Unit, both units experienced a common deformational evolution. $^{40}Ar/^{39}Ar$ data helped refine the established deformational evolution and asses the regional importance of the determined tectonic events.

- The earliest stage of deformation D_1 in the central SMM is related to isoclinal folding, commonly preserved as decimetre-scale quartz-feldspar rootless fold hinges.
- The second deformation stage D_2 is associated with general southeastward direction of tectonic transport and refolding of older structures into recumbent metre- to kilometre-scale tight to isoclinal folds.
- Deformation stages D_1 and D_2 could not be temporally separated and probably have taken place in close sequence. Based on the stratigraphic age of the youngest affected sediments, and the intrusion ages of the oldest undeformed magmatic rocks, the age of these two ductile deformation stages is constrained to Variscan orogeny (i.e. ca. 408-ca. 328). During this time the SMM was involved in a transpressional amalgamation of the western and eastern parts of the Galatian super-terrane and subsequent collision with Laurussia, which could account for the changes in direction of strain axes during D_1 and D_2.

- A trend of diminishing strain and metamorphic grade from amphibolite facies in the Lower Complex, across greenschist facies in the pre-Ordovician Vlasina to anchimetamorphism in the post-Cambrian Vlasina suggests different crustal positions of the constituents of central SMM during Variscan orogeny.
- Cooling below greenschist facies conditions in western part of Vlasina Unit has taken place in a post-orogenic setting (extensional or transtensional) in early Permian (284±1 Ma).
- The age of activity along top-to-the-west shear zone formed within orthogneiss in Božica area of Vlasina Unit was constrained to Middle Triassic (246±1 Ma). This age coincides with widespread extension related to the opening of the Mesozoic Tethys.
- Rare outcrop-scale evidence of the final stage of ductile deformation D_3 is limited to spaced and crenulation cleavage. These structures are probably related to the large-scale folding reported by earlier studies. The maximum age of this event is constrained by crenulation of the Middle Triassic mylonitic foliation in Božica area.
- Anastomosing shear zones, S-C fabric and spaced cleavage developed in the Permo-Triassic Bujanovac granite provide evidence of an additional post-Triassic ductile deformation event. Additional data is needed to constrain the area affected by this deformation and its exact timing.
- A greenschist facies retrogression in the Lower Complex had probably occurred in Early Jurassic and it is probably related to thermal processes in the overriding plate above subducting slab of the Mesozoic Tethys Ocean.

References

Anđelković M (1967) Strukturno facijalne zone središnje i istočne Srbije.

Anđelković M, Anđelković J (1995) Značaj Ilirske faze za geološki razvoj Moravida. Ann Géol Penins Balk 59:1–11.

Babović M, Roglić Č, Avramović V, Marić S (1977) Tumač za list Trgovište sa Radomirom. Savezni Geološki Zavod, Belgrade

Balogh K, Svingor É, Cvetković V (1994) Ages and intensities of metamorphic processes in the Batočina area, Serbo-Macedonian massif. Acta Mineralogica-Petrographica XXXV:81–94.

Banjac N (2004) Stratigrafija Srbije i Crne Gore. Rudarsko-geološki fakultet, Belgrade

Bastida F, Aller J, Fernández FJ, et al (2014) Recumbent folds: Key structural elements in orogenic belts. Earth-Sci Rev 135:162–183. doi: 10.1016/j.earscirev.2014.05.002

Bonev K, Ivanov Z, Ricou L-E (1995) Dénudation tectonique au toit du noyau métamorphique Rhodopien-macédonien: La faille normale ductile de Gabrov Dol (Bulgarie). Bull Soc Géol France 166:47–55.

Bonev N, Marchev P, Moritz R, Collings D (2015) Jurassic subduction zone tectonics of the Rhodope Massif in the Thrace region (NE Greece) as revealed by new U–Pb and ^{40}Ar/^{39}Ar geochronology of the Evros ophiolite and high-grade basement rocks. Gondwana Research 27:760–775. doi: 10.1016/j.gr.2014.08.008

Bonev N, Marchev P, Ovtcharova M, et al (2010) U-Pb LA-ICP/MS zircon geochronology of metamorphic basement and Oligocene volcanic rocks from the SE Rhodopes: inferences for the geological history of the Eastern Rhodope crystalline basement. Bulgarian Geological Society, Sofia, pp 115–116

Borsi S, Ferrara G, Mercier J (1965) Détermination de l’âge des séries métamorphiques du Massif Serbo-Macédonien au Nord-Est de Thessalonique (Grèce) par les méthodes Rb/Sr et K/Ar. Annales Société Géologique du Nord 84:223–225.

Bosse V, Boulvais P, Gautier P, et al (2009) Fluid-induced disturbance of the monazite Th–Pb chronometer: In situ dating and element mapping in pegmatites from the Rhodope (Greece, Bulgaria). Chem Geol 261:286–302. doi: 10.1016/j.chemgeo.2008.10.025

Božović M, Prelević D, Romer RL, et al (2013) The Demir Kapija Ophiolite, Macedonia (FYROM): a Snapshot of Subduction Initiation within a Back-arc. J Petrol 54:1427–1453. doi: 10.1093/petrology/egt017

Brown SAM, Robertson AHF (2003) Sedimentary geology as a key to understanding the tectonic evolution of the Mesozoic–Early Tertiary Paikon Massif, Vardar suture zone, N Greece. Sediment Geol 160:179–212. doi: 10.1016/S0037-0738(02)00376-7

Burchfiel BC, Nakov R, Dumurdžanov N, et al (2008) Evolution and dynamics of the Cenozoic tectonics of the South Balkan extensional system. Geosphere 4:919–938. doi: 10.1130/GES00169.1

Burg J-P (2012) Rhodope: From Mesozoic convergence to Cenozoic extension. Review of petro-structural data in the geochronological frame.

Burg J-P (1987) Regional shear variation in relation to diapirism and folding. J Struct Geol 9:925–934. doi: 10.1016/0191-8141(87)90002-2

Burg J-P, Godfriaux I, Ricou L-E (1995) Extension of the Mesozoic Rhodope thrust units in the Vertiskos-Kerdilion Massifs (Northern Greece). C R Acad Sci Paris 320:889–896.

Carrigan CW, Mukasa SB, Haydoutov I, Kolcheva K (2005) Age of Variscan magmatism from the Balkan sector of the orogen, central Bulgaria. Lithos 82:125–147. doi: 10.1016/j.lithos.2004.12.010

Channell JET, Kozur HW (1997) How many oceans? Meliata, Vardar and Pindos oceans in Mesozoic Alpine paleogeography. Geology 25:183–186. doi: 10.1130/0091-7613(1997)025<0183:HMOMVA>2.3.CO;2

Cohen KM, Finney SC, Gibbard PL, Fan J (2013) The ICS International Chronostratigraphic Chart. Episodes 36:199–204.

Csontos L, Vörös A (2004) Mesozoic plate tectonic reconstruction of the Carpathian region. Palaeogeogr Palaeocl 210:1–56. doi: 10.1016/j.palaeo.2004.02.033

Cvetković V (1992) Petrology of the metamorphic rocks from the northern parts of the Serbo-macedonian massif in the Batočina area. Magistar thesis, Faculty of Mining and Geology

Dabovski C, Boyanov I, Khrischev K, et al (2002) Structure and Alpine evolution of Bulgaria. Geologica Balcanica 32:9–15.

Dallmeyer RD, Neubauer F, Fritz H, Mocanu V (1998) Variscan vs. Alpine tectonothermal evolution of the Southern Carpathian orogen: constraints from ^{40}Ar/^{39}Ar ages. Tectonophysics 290:111–135. doi: 10.1016/S0040-1951(98)00006-7

Dalrymple GB, Lanphere MA (1974) ^{40}Ar/^{39}Ar age spectra of some undisturbed terrestrial samples. Geochim Cosmochim Ac 38:715–738. doi: 10.1016/0016-7037(74)90146-X

Deleon G (1969) Pregled rezultata određivanja apsolutne geološke starosti granitoidnih stena u Jugoslaviji. Radovi Instituta za geološko-rudarska istraživanja i ispitivanja nuklearnih i drugih mineralnih sirovina 6:165–180.

De Wet AP, Miller JA, Bickle MJ, Chapman HJ (1989) Geology and geochronology of the Arnea, Sithonia and Ouranopolis intrusions, Chalkidiki peninsula, northern Greece. Tectonophysics 161:65–79. doi: 10.1016/0040-1951(89)90303-X

Dimitrijević MD (1972) Variscijski metamorfizam u aksijalnom delu Balkanskog poluostrva (mogućnosti nove genetske interpretacije). Zapisnici SGD za 1971. godinu:115–124.

Dimitrijević MD (1957) Struktura kristalastih terena između Slišana i Preševa. Referati, predavanja, diskusije. Savez geoloških društava Jugoslavije, Sarajevo,

Dimitrijević MD (1997) Geology of Yugoslavia. Geological Institute GEMINI, Belgrade

Dimitrijević MD (1967) Some Problems of Crystalline Schists in the Serbo-Macedonian Massif. Reports. Serbian Geological Society, Belgrade, pp 59–67

Dimitrijević MD (1963) Sur l'âge du métamorphisme et des plissements dans la masse Serbo-macédonienne. Bulletin. Instytut Geologiczny, Warszawa, pp 339–347

Dimitrijević MD (1958) Geološki sastav i struktura bujanovačkog granitskog masiva.

Dimitrijević MD (1959) Osnovne karakteristike stuba Srpsko-makedonske mase. Abstracts. Belgrade,

Dimitrijević MD, Drakulić N (1958) Kristalasti škriljci Jablanice.

Dimitrijević MN, Dimitrijević MD (1987) The Turbiditic Basins of Serbia. Serbian Academy of Science and Arts, Belgrade

Dimitrova E (1964) Petrologie des kristallinen Sockels des Osogovo Gebirges. Bulgarian Academy of Sciences Bulletin of the Geological Institute 13:99–110.

Dixon JE, Dimitriadis S (1984) Metamorphosed ophiolitic rocks from the Serbo-Macedonian Massif, near Lake Volvi, North-east Greece. Geol Soc SP 17:603–618. doi: 10.1144/GSL.SP.1984.017.01.47

Fernández FJ, Aller J, Bastida F (2007) Kinematics of a kilometric recumbent fold: The Courel syncline (Iberian massif, NW Spain). J Struct Geol 29:1650–1664. doi: 10.1016/j.jsg.2007.05.009

Fossen H (1993) Linear fabrics in the Bergsdalen Nappes, southwest Norway: implications for deformation history and fold development. Norsk Geol Tidsskr 73:95–108.

Froitzheim N, Jahn-Awe S, Frei D, et al (2014) Age and composition of meta-ophiolite from the Rhodope Middle Allochthon (Satovcha, Bulgaria): A test for the maximum-allochthony hypothesis of the Hellenides. Tectonics 33:2014TC003526. doi: 10.1002/2014TC003526

Fügenschuh B, Schmid SM (2005) Age and significance of core complex formation in a very curved orogen: Evidence from fission track studies in the South Carpathians (Romania). Tectonophysics 404:33–53. doi: 10.1016/j.tecto.2005.03.019

Georgiev N, Froitzheim N, Cherneva Z, et al (2016) Structure and U–Pb zircon geochronology of an Alpine nappe stack telescoped by extensional detachment faulting (Kulidzhik area, Eastern Rhodopes, Bulgaria). Int J Earth Sci (Geol Rundsch) 1–28. doi: 10.1007/s00531-016-1293-4

Gerdjikov I, Lazarova A, Balkanska E, et al (2010a) A New Model For the Pre-Permian Basement of the Central Stara Planina Mountain. Comptes Rendus de l'Académie bulgare des Sciences 63:1169–1176.

Gerdjikov I, Lazarova A, Kounov A, Vangelov D (2013) High-grade metamorphic complexes in Bulgaria. Annual of the University of Mining and Geology "St Ivan Rilski" 56:47–52.

Gerdjikov I, Ruffet G, Lazarova A, et al (2010b) ^{40}Ar/^{39}Ar geochronologic constraints of a Variscan transpression in Central Stara Planina Mountain. Proceedings. Bulgarian Geological Society, Sofia, pp 109–110

Goscombe BD, Passchier CW, Hand M (2004) Boudinage classification: end-member boudin types and modified boudin structures. J Struct Geol 26:739–763. doi: 10.1016/j.jsg.2003.08.015

Graf J (2001) Alpine tectonics in Western Bulgaria: Cretaceous compression of the Kraishte region and Cenozoic exhumation of the crystalline Osogovo–Lisets Complex. PhD, ETH Zürich

Grubić A, Đoković I, Marović M, Branković M (1999) Srpsko-Makedonska masa ne postoji. Vesnik 49:1–14.

Grubić A, Đoković I, Marović M, Branković M (2005) Problem tektonskog položaja kristalina Srpsko-Makedonske mase. Zapisnici SGD za 1998, 1999, 2000, 2001, 2002 i 2003. godinu:35–39.

Grubić A, Ercegovac M (2002) Age of the Veles "Schistes Lustres" Formation from the Vardar Ocean. Proceedings of XVII Congress of CBGA. VEDA, Bratislava, pp 66–68

Harrison TM, Célérier J, Aikman AB, et al (2009) Diffusion of ^{40}Ar in muscovite. Geochim Cosmochim Ac 73:1039–1051. doi: 10.1016/j.gca.2008.09.038

Harrison TM, Duncan I, McDougall I (1985) Diffusion of ^{40}Ar in biotite: Temperature, pressure and compositional effects. Geochim Cosmochim Ac 49:2461–2468. doi: 10.1016/0016-7037(85)90246-7

Himmerkus F, Reischmann T, Kostopoulos D (2009b) Triassic rift-related meta-granites in the Internal Hellenides, Greece. Geol Mag 146:252. doi: 10.1017/S001675680800592X

Himmerkus F, Reischmann T, Kostopoulos D (2009a) Serbo-Macedonian revisited: A Silurian basement terrane from northern Gondwana in the Internal Hellenides, Greece. Tectonophysics 473:20–35. doi: 10.1016/j.tecto.2008.10.016

Himmerkus F, Reischmann T, Kostopoulos D (2006) Late Proterozoic and Silurian basement units within the Serbo-Macedonian Massif, northern Greece: the significance of terrane accretion in the Hellenides. Geol Soc SP 260:35–50. doi: 10.1144/GSL.SP.2006.260.01.03

Himmerkus F, Zachariadis P, Reischmann T, Kostopoulos D (2011) The basement of the Mount Athos peninsula, northern Greece: insights from geochemistry and zircon ages. Int J Earth Sci (Geol Rundsch) 101:1467–1485. doi: 10.1007/s00531-011-0644-4

Iancu V, Berza T, Seghedi A, et al (2005) Alpine polyphase tectono-metamorphic evolution of the South Carpathians: A new overview. Tectonophysics 410:337–365. doi: 10.1016/j.tecto.2004.12.038

Iancu V, Màruntiu M, Johan V, Ledru P (1998) High-grade metamorphic rocks in the pre-Alpine nappe stack of the Getic-Supragetic basement (Median Dacides, South Carpathians, Romania). Miner Petrol 63:173–198. doi: 10.1007/BF01164150

Ilic A, Neubauer F, Handler R (2005) Late Paleozoic–Mesozoic tectonics of the Dinarides revisited: Implications from ^{40}Ar/^{39}Ar dating of detrital white micas. Geology 33:233–236. doi:

10.1130/G20979.1

Ivanova P, Zidarov N (2011) Metamorphic evolution of spinel clinopyroxenites with clinopyroxene megacrysts from Ograzhden Mountain, SW Bulgaria. Proceedings. Bulgarian Geological Society, Sofia, pp 61–62

Jahn-Awe S, Froitzheim N, Nagel TJ, et al (2010) Structural and geochronological evidence for Paleogene thrusting in the western Rhodopes, SW Bulgaria: Elements for a new tectonic model of the Rhodope Metamorphic Province. Tectonics 29:TC3008. doi: 10.1029/2009TC002558

Jahn-Awe S, Pleuger J, Frei D, et al (2012) Time constraints for low-angle shear zones in the Central Rhodopes (Bulgaria) and their significance for the exhumation of high-pressure rocks. Int J Earth Sci (Geol Rundsch) 101:1971–2004. doi: 10.1007/s00531-012-0764-5

Karamata S (2006) The geological development of the Balkan Peninsula related to the approach, collision and compression of Gondwanan and Eurasian units. Geol Soc SP 260:155–178. doi: 10.1144/GSL.SP.2006.260.01.07

Karamata S, Krstić B (1996) Terranes of Serbia and Neighbouring Areas. In: Knežević-Đorđević V, Krstić B (eds) Terranes of Serbia. Faculty of Mining and Geology, University of Belgrade, Belgrade, pp 25–40

Karamata S, Stojanov R, Serafimovski T, et al (1992) Tertiary magmatism in the Dinarides of the Vardar zone and the Serbo–Macedonian Massif. Geologica Macedonica 6:127–186.

Kilias A, Falalakis G, Mountrakis D (1999) Cretaceous–Tertiary structures and kinematics of the Serbomacedonian metamorphic rocks and their relation to the exhumation of the Hellenic hinterland (Macedonia, Greece). Int J Earth Sci (Geol Rundsch) 88:513–531. doi: 10.1007/s005310050282

Kilias A, Falalakis G, Mountrakis D (1997) Alpine tectonometamorphic history of the Serbomacedonian metamorphic rocks: implication for the tertiary unroofing of the Serbomacedonian-Rhodope metamorphic complexes (Makedonia, Greece). Ορυκτός Πλούτος 105:32–50. doi: RefwID:14314

Kockel F, Mollat H, Walther HW (1971) Geologie der Serbo-Mazedonischen Massivs und seines mesozoischen Rahmens (Nordgriechenland). Geologisches Jahrbuch 89:529–551.

Kockel F, Mollat H, Walther HW (1977) Erläuterungen zur Geologischen Karte der Chalkidiki und angrenzender Gebiete 1:100000 (Nord-Griechenland). Bundesanstalt für Geowissenschaften und Rohstoffe, Hannover

Korikovsky S, Karamata S, Milovanović D (2003) Retrograted kyanite eclogites and eclogittized gabbro-norites of the Serbo-macedonian unit, Central Serbia, reaction textures and geothermobarometry. Zbornik abstraktov. Bratislava, pp 13–14

Kostopoulos D, Reischmann T, Sklavounos S (2001) Palaeozoic and Early Mesozoic magmatism and metamorphism in the Serbo-Macedonian massif, Central Macedonia, Northern Greece. Abstracts. Cambridge Publications, Strasbourg, p 318

Kounov A (2002) Thermotectonic evolution of Kraishte, western Bulgaria. PhD, ETH Zürich

Kounov A, Burg J-P, Bernoulli D, et al (2011) Paleostress analysis of Cenozoic faulting in the Kraishte area, SW Bulgaria. J Struct Geol 33:859–874. doi: 10.1016/j.jsg.2011.03.006

Kounov A, Graf J, von Quadt A, et al (2012) Evidence for a "Cadomian" ophiolite and magmatic-arc complex in SW Bulgaria. Precambrian Res 212–213:275–295. doi: 10.1016/j.precamres.2012.06.003

Kounov A, Seward D, Bernoulli D, et al (2004) Thermotectonic evolution of an extensional dome: the Cenozoic Osogovo-Lisets core complex (Kraishte zone, western Bulgaria). Int J Earth Sci (Geol Rundsch) 93:1008–1024. doi: 10.1007/s00531-004-0435-2

Kounov A, Seward D, Burg J-P, et al (2010) Geochronological and structural constraints on the Cretaceous thermotectonic evolution of the Kraishte zone, western Bulgaria. Tectonics 29:TC2002. doi: 10.1029/2009TC002509

Kräutner HG, Krstić B (2002) Alpine and pre-Alpine structural units within the southern Carpathians and eastern Balkanides. Proceedings of XVII Congress of CBGA. VEDA, Bratislava,

Krstić B, Maslarević L, Ercegovac M, Đajić S (2002) Devonian of the Serbian Carpatho-Balkanides. Proceedings of XVII Congress of CBGA. VEDA, Bratislava,

Krstić N, Karamata S (1992) Terani u Karpato-Balkanidima istočne Srbije. Zapisnici SGD jubilarna knjiga (1891-1991):57–69.

Kydonakis K, Brun J-P, Sokoutis D, Gueydan F (2015a) Kinematics of Cretaceous subduction and exhumation in the western Rhodope (Chalkidiki block). Tectonophysics 665:218–235. doi: 10.1016/j.tecto.2015.09.034

Kydonakis K, Gallagher K, Brun J-P, et al (2014) Upper Cretaceous exhumation of the western Rhodope Metamorphic Province (Chalkidiki Peninsula, northern Greece). Tectonics 33:2014TC003572. doi: 10.1002/2014TC003572

Kydonakis K, Moulas E, Chatzitheodoridis E, et al (2015b) First-report on Mesozoic eclogite-facies metamorphism preceding Barrovian overprint from the western Rhodope (Chalkidiki, northern Greece). Lithos 220–223:147–163. doi: 10.1016/j.lithos.2015.02.007

Lakova I (2009) Acritarch evidence on Silurian age of the low-grade metamorphic Palaeozoic rocks in the Kraishte area (Morava Unit). Review of the Bulgarian Geological Society 70:23–30.

Liati A (2005) Identification of repeated Alpine (ultra) high-pressure metamorphic events by U–Pb SHRIMP geochronology and REE geochemistry of zircon: the Rhodope zone of Northern Greece. Contrib Mineral Petrol 150:608–630. doi: 10.1007/s00410-005-0038-3

Lilov P, Zagorchev IS (1993) K-Ar data for the deformation and low-grade metamorphism in Permian and Triassic red beds in SW Bulgaria. Geologica Balcanica 23:46.

Macheva L, Titorenkova R, Zidarov N (2005) Kyanite-staurolite-garnet orthoschists. Central Laboratory of Mineralogy and Crystallography “Acad. Ivan Kostov,” Sofia

Malešević M, Vukanović M, Obradinović Z, et al (1980) Tumač za list Kuršumlija. Savezni Geološki Zavod, Belgrade

Marinova R, Grozdev V, Ivanova D, et al (2010) List Tsarvena Jabuka, Vlasotince, Tran-North and Tran-South. Ministry of Environment and Water, Bulgarian National Geological Survey, Sofia

Marović M, Toljić M, Rundić L, Milivojević J (2007) Neoalpine Tectonics of Serbia. Serbian Geological Society, Belgrade

Maslarević L, Krstić B (1999) Permian Continental Redbeds of the Serbian South-Carpathian and Balkan (Stara Planina) Mountains. Abstracts. Brescia, pp 92–64

Matenco L, Schmid S (1999) Exhumation of the Danubian nappes system (South Carpathians) during the Early Tertiary: inferences from kinematic and paleostress analysis at the Getic/Danubian nappes contact. Tectonophysics 314:401–422. doi: 10.1016/S0040-1951(99)00221-8

McCann T, Pascal C, Timmerman MJ, et al (2006) Post-Variscan (end Carboniferous-Early Permian) basin evolution in Western and Central Europe. Geo Soc Mem 32:355–388. doi: 10.1144/GSL.MEM.2006.032.01.22

Meinhold G, Kostopoulos D, Frei D, et al (2010) U–Pb LA-SF-ICP-MS zircon geochronology of the Serbo-Macedonian Massif, Greece: palaeotectonic constraints for Gondwana-derived terranes in the Eastern Mediterranean. Int J Earth Sci (Geol Rundsch) 99:813–832. doi:

10.1007/s00531-009-0425-5

Mihailescu N, Dimitrijević MD, Dimitrijević MN (1967) Les fossiles dans le flysch. Reports. Serbian Geological Society, Belgrade, pp 371–378

Milovanović D (1990) Petrologija gnajseva Srpsko-makedonske mase u području između Tulara i Lebana. Proceedings of the XII Congress of the Geologists of Yugoslavia. Prosveta, Ohrid, pp 310–321

Milovanović D (1992) Amfibolske stene u području između Medveđe i Lebana. Ann Géol Penins Balk 56:253–268.

Milovanović D (1989) Metamorphism of the Serbo-Macedonian massif. Proceedings. Washington, pp 439–441

Milovanović D, Milovanović M, Oberhänsli R (1988) Petrology of green-rocks of the Vlasina complex in the Manastiriška river area (Vlasotince). Vesnik 44:101–128.

Mladenović A, Trivić B, Antić M, et al (2014) The recent fault kinematics in the westernmost part of the Getic nappe system (Eastern Serbia): Evidence from fault slip and focal mechanism data. Geologica Carpathica 65:147–161. doi: 10.2478/geoca-2014-0010

Mukasa SB, Haydoutov I, Carrigan CW, Kolcheva K (2003) Thermobarometry and ^{40}Ar/^{39}Ar ages of eclogitic and gneissic rocks in the Sredna Gora and Rhodope terranes of Bulgaria. Journal of the Czech Geological Society 48:94–95.

Nenova P, Zidarov N (2008) Eclogites from Maleshevska Mountain, SW Bulgaria. Central Laboratory of Mineralogy and Crystallography “Acad. Ivan Kostov,” Sofia

Neubauer F (2002) Evolution of late Neoproterozoic to early Paleozoic tectonic elements in Central and Southeast European Alpine mountain belts: review and synthesis. Tectonophysics 352:87–103. doi: 10.1016/S0040-1951(02)00190-7

Pantić N, Dimitrijević MD, Hercegovac M (1967) Mikroflioristički podaci o starosti Vlasinskog kompleksa.

Passchier CW, den Brok SWI, van Gool J a. M, et al (1997) A laterally constricted shear zone system — the Nordre Strømfjord steep belt, Nagssugtoqidian Orogen, W. Greenland. Terra Nova 9:199–202. doi: 10.1111/j.1365-3121.1997.tb00012.x

Pavić A, Menković L, Košćal M (1983) Tumač za list Uroševac. Savezni Geološki Zavod, Belgrade

Pavlović P (1962) O nekim ordovicijskim inartikulatnim brahiopodima u metamorfnim stenama kod Bosiljgrada (Jugoistočna Srbija) i o značaju ovog nalaska. Ann Géol Penins Balk 39:99–112.

Pavlović P (1977) O “Gornjem (Vlasinskom) kompleksu” i podeli metamorfnih stena Srpsko-Makedonskog metamorfnog terena. Zapisnici SGD za 1975. i 1976. godinu:123–132.

Pe-Piper G (1998) The nature of Triassic extension-related magmatism in Greece; evidence from Nd and Pb isotope geochemistry. Geol Mag 135:331–348.

Petković V (1930) O tektonskom sklopu istočne Srbije. Glas Srpske kraljevske akademije 140:151–188.

Petrović B, Dimitrijević MD, Karamata S (1973) Tumač za list Vlasotince. Savezni Geološki Zavod, Belgrade

Petrović B S (1969) The Structure of the Vlasina Crystalline Complex in the Broad Area of Crna Trava. Rudarsko-geološki fakultet, Belgrade

Petrović B S, Karamata S (1965) Metaklastiti - baza gornjeg kompleksa kristalastih škriljaca SMM. Proceedings. Zagreb,

Peytcheva I, von Quadt A, Ovtcharova M, et al (2004) Metagranitoids from the eastern part of the Central Rhodopean Dome (Bulgaria): U–Pb, Rb–Sr and ^{40}Ar/^{39}Ar timing of emplacement and exhumation and isotope-geochemical features. Miner Petrol 82:1–31. doi:

10.1007/s00710-004-0039-3

Peytcheva I, von Quadt A, Sarov S, et al (2009a) U-Pb LA-ICP/MS zircon geochronology of metamorphic basement and Oligocene volcanic rocks from the SE Rhodopes: inferences for the geological history of the Eastern Rhodope crystalline basement. Bulgarian Geological Society, Sofia, pp 17–18

Peytcheva I, von Quadt A, Tarassov M, et al (2009b) Timing of Igralishte pluton in Ograzhden Mountain, SW Bulgaria: implications for the tectono-magmatic evolution of the region. Geologica Balcanica 38:5–14.

Peytcheva I, von Quadt A, Titorenkova R, et al (2005) Skrut Granitoids from Belassitsa Mountain, SW Bulgaria: Constraints from isotope geochronological and geochemical zircon data. Proceedings. Bulgarian Geological Society, Sofia, pp 205–208

Plissart G, Diot H, Monnier C, et al (2012) Relationship between a syntectonic granitic intrusion and a shear zone in the Southern Carpathian-Balkan area (Almăj Mountains, Romania): Implications for late Variscan kinematics and Cherbelezu granitoid emplacement. J Struct Geol 39:83–102. doi: 10.1016/j.jsg.2012.03.004

Popović R (1991) Srpsko-Makedonska masa ili Pelagonsko-Rodopski i Moravski masiv. Radovi Geoinstituta 25:7–20.

Popović R (1995) Srpsko-Makedonska masa: da ili ne? Zapisnici SGD za 1990. i 1991. godinu:59–61.

Protić M (1966) Permski crveni peščari istočne Srbije - sredine njihovog stvaranja. Referati. Ohrid,

Reischmann T, Kostopoulos D (2001) Geochronology and P-T Constraints on the Exhumation History of an UHP Eclogite from Northern Greece. Abstracts. Eos Trans. AGU, San Francisco, p 0987

Ricou L-E (1994) Tethys reconstructed : plates, continental fragments and their Boundaries since 260 Ma from Central America to South-eastern Asia. Geodin Acta 7:169–218. doi: 10.1080/09853111.1994.11105266

Ricou L-E, Burg J-P, Godfriaux I, Ivanov Z (1998) Rhodope and Vardar: the metamorphic and the olistostromic paired belts related to the Cretaceous subduction under Europe. Geodin Acta 11:285–309. doi: 10.1016/S0985-3111(99)80018-7

Robertson AHF, Clift PD, Degnan PJ, Jones G (1991) Palaeogeographic and palaeotectonic evolution of the Eastern Mediterranean Neotethys. Palaeogeogr Palaeocl 87:289–343. doi: 10.1016/0031-0182(91)90140-M

Robertson A, Karamata S, Šarić K (2009) Overview of ophiolites and related units in the Late Palaeozoic–Early Cenozoic magmatic and tectonic development of Tethys in the northern part of the Balkan region. Lithos 108:1–36. doi: 10.1016/j.lithos.2008.09.007

Săndulescu M (1984) Geotectonica Romaniei. Editura Tehnică, Bucharest

Schmid SM, Bernoulli D, Fügenschuh B, et al (2008) The Alpine-Carpathian-Dinaridic orogenic system: correlation and evolution of tectonic units. Swiss Journal of Geosciences 101:139–183. doi: 10.1007/s00015-008-1247-3

Simpson C, Wintsch RP (1989) Evidence for deformation-induced K-feldspar replacement by myrmekite. J Metamorph Geol 7:261–275. doi: 10.1111/j.1525-1314.1989.tb00588.x

Spassov C (1973) Stratigraphie des Devons in Sudwest-Bulgarien. Bulletin of the Geological Institute 22:5–38.

Stampfli GM, Hochard C (2009) Plate tectonics of the Alpine realm. Geol Soc SP 327:89–111. doi: 10.1144/SP327.6

Stampfli GM, Hochard C, Vérard C, et al (2013) The formation of Pangea. Tectonophysics 593:1–19. doi: 10.1016/j.tecto.2013.02.037

Stampfli GM, von Raumer JF, Borel GD (2002) Paleozoic evolution of pre-Variscan terranes: From Gondwana to the Variscan collision. Geol S Am S 364:263–280. doi: 10.1130/0-8137-2364-7.263

Stipp M, Stünitz H, Heilbronner R, Schmid SM (2002) The eastern Tonale fault zone: a "natural laboratory" for crystal plastic deformation of quartz over a temperature range from 250 to 700 °C. J Struct Geol 24:1861–1884. doi: 10.1016/S0191-8141(02)00035-4

Stojadinovic U, Matenco L, Andriessen PAM, et al (2013) The balance between orogenic building and subsequent extension during the Tertiary evolution of the NE Dinarides: Constraints from low-temperature thermochronology. Global Planet Change 103:19–38. doi: 10.1016/j.gloplacha.2012.08.004

Tchoumatchenco P (2006) Jurassic tectonics of Bulgaria and the adjacent areas. Review of the Bulgarian Geological Society 67:86–103.

Tobisch OT, Paterson SR (1988) Analysis and interpretation of composite foliations in areas of progressive deformation. J Struct Geol 10:745–754. doi: 10.1016/0191-8141(88)90081-8

Toljić M, Matenco L, Ducea MN, et al (2013) The evolution of a key segment in the Europe–Adria collision: The Fruška Gora of northern Serbia. Global Planet Change 103:39–62. doi: 10.1016/j.gloplacha.2012.10.009

Tranos MD, Lacombe O (2014) Late Cenozoic faulting in SW Bulgaria: Fault geometry, kinematics and driving stress regimes. Implications for late orogenic processes in the Hellenic hinterland. Journal of Geodynamics 74:32–55. doi: 10.1016/j.jog.2013.12.001

Turpaud P, Reischmann T (2010) Characterisation of igneous terranes by zircon dating: implications for UHP occurrences and suture identification in the Central Rhodope, northern Greece. Int J Earth Sci (Geol Rundsch) 99:567–591. doi: 10.1007/s00531-008-0409-x

Ustaszewski K, Schmid SM, Lugović B, et al (2009) Late Cretaceous intra-oceanic magmatism in the internal Dinarides (northern Bosnia and Herzegovina): Implications for the collision of the Adriatic and European plates. Lithos 108:106–125. doi: http://dx.doi.org/10.1016/j.lithos.2008.09.010

van Hinsbergen DJJ, Schmid SM (2012) Map view restoration of Aegean–West Anatolian accretion and extension since the Eocene. Tectonics 31:TC5005. doi: 10.1029/2012TC003132

Vasković N (2002) Petrology and P-T condition of white mica-chlorite schists from Vlasina series - Surdulica, SE Serbia. Ann Géol Penins Balk 199–220. doi: 10.2298/GABP0264199V

Vasković N (1998) P-T condition of the mica schists from the Vranjska Banja Series. Proceedings of the XIII Congress of the Geologists of Yugoslavia. Herceg Novi, pp 41–59

Vasković N, Matović V, Srećković-Batoćanin D (2003) Petrology of Garnet-amphibolite with White Mica from Vranjska Banja Series (Serbian-Macedonian Massif, SE Serbia). Studia Universitatis Babeş-Bolyai 128–133.

von Raumer JF, Bussy F, Schaltegger U, et al (2013) Pre-Mesozoic Alpine basements—Their place in the European Paleozoic framework. Geol Soc Am Bull 125:89–108. doi: 10.1130/B30654.1

von Raumer JF, Stampfli GM, Bussy F (2003) Gondwana-derived microcontinents — the constituents of the Variscan and Alpine collisional orogens. Tectonophysics 365:7–22. doi: 10.1016/S0040-1951(03)00015-5

Vujanović V, Cvetić S, Teofilović M (1974) Poreklo gnajseva Srbije i Makedonije. Zapisnici SGD za 1973. godinu:266–270.

Vukanović M, Dimitrijević MD, Dimitrijević M, et al (1977) Tumač za list Vranje. Savezni Geološki Zavod, Belgrade

Vukanović M, Dimitrijević M, Dimitrijević MD, et al (1982) Tumač za list Podujevo. Savezni

Geološki Zavod, Belgrade

Vukanović M, Karajičić L, Dimitrijević MD, et al (1973) Tumač za list Leskovac. Savezni Geološki Zavod, Belgrade

Whitney DL, Evans BW (2010) Abbreviations for names of rock-forming minerals. Am Mineral 95:185–187. doi: 10.2138/am.2010.3371

Yanev S, Popa M, Seghedi A, Oaie G (2001) Overview of the continental Permian deposits of Bulgaria and Romania. Natura Bresciana 25:269–279.

Zachariadis P (2007) Ophiolites of the eastern Vardar Zone, N. Greece. Johannes Gutenberg Universität

Zagorčev IS, Bončeva I (1988) Indications of Devonian basic volcanism in Southwest Bulgaria. Geologica Balcanica 18:55–63.

Zagorchev IS (1984) Pre-Alpine structure of South-west Bulgaria. In: Zagorchev IS, Mankov S, Bozkov I (eds) Problems of the geology of Southwestern Bulgaria. Tehnika, Sofia, pp 9–20

Zagorchev IS (1985) Deformation during the first stage of the Alpine Orogeny in the Skrino-Poletintsi faulted zone; IV Shipochan Anticline. Review of the Bulgarian Geological Society 46:287–298.

Zagorchev IS (1981) Early Alpine deformations in the red beds within the Poletinci-Skrino fault zone. 2. Structure and deformations in the northern parts of the Vlahina block. Geologica Balcanica 11:101–126.

Zagorchev IS (1980) Early Alpine deformations in the red beds within the Poletinci-Skrino fault zone. 1. Litostratigraphic features in light of structural studies. Geologica Balcanica 10:37–60.

Zagorchev IS, Milovanović D (2006) Deformations and Metamorphism in the Eastern Parts of the Serbo-Macedonian Massif. Proceedings. Serbian Geological Society, Belgrade, pp 670–673

Zagorchev IS, Ruseva M (1982) Nappe structure of the southern parts of Osogovo Mts and the Pijanec region (SW Bulgaria). Geologica Balcanica 12:35–57.

Zagortchev IS (1993) Alpine evolution of the pre-Alpine amphibolite-facies basement in South Bulgaria. Mitteilungen der Österreichischen Geologischen Gesellschaft 86:9–21.

Zelic M, Levi N, Malasoma A, et al (2010) Alpine tectono-metamorphic history of the continental units from Vardar zone: the Kopaonik Metamorphic Complex (Dinaric-Hellenic belt, Serbia). Geol J 45:59–77. doi: 10.1002/gj.1169

Zidarov N, Peytcheva I, von Quadt A, et al (2003a) Mineral-petrological, geochemical and isotope studies of geological units in Serbo-Macedonian Massif, SW Bulgaria. Central Laboratory of Mineralogy and Crystallography “Acad. Ivan Kostov,” Sofia

Zidarov N, Peytcheva I, von Quadt A, et al (2003b) Timing and Magma Sources of Metagranites from the Serbo-Macedonian Massif (Ograzhden and Maleshavska Mountains, SW Bulgaria): Constraints from UPb and Hf-Zircon and Sr Whole Rock Isotope Studies. Proceedings. Bulgarian Geological Society, Sofia, pp 89–91

Zidarov N, Peytcheva I, von Quadt A, et al (2004) Timing and Magma Sources of Igralishte Pluton (SW Bulgaria): Preliminary Isotope-Geochronological and Geochemical Data. Proceedings. Bulgarian Geological Society, Sofia,

Zidarov N, Tarassova E, Peytcheva I, et al (2007) Petrology, geochemistry and age dating of Skrut granitoids – new evidence for Early Triassic magmatism in Belasitsa Mountain (SW Bulgaria). Geologica Balcanica 36:17–29.

Appendix to
Chapter 3: Evidence of Variscan and Alpine tectonics in the structural and thermochronological record of the central Serbo-Macedonian Massif (southeastern Serbia)

Milorad D. Antić[1], Alexandre Kounov[1], Branislav Trivić[2], Richard Spikings[3], Andreas Wetzel[1]

[1]Institute for Geology and Palaeontology, University of Basel, 4056 Basel, Switzerland;

[2]Faculty of Mining and Geology, University of Belgrade, 11000 Belgrade, Serbia

[3]Section des Sciences de la Terre et de l'Environnement, Université de Genève, 1205 Genève, Switzerland

Appendix 3-1 : $^{40}Ar/^{39}Ar$ thermochronology

3-1.1 Analytical method

Seven whole-rock samples were mechanically fragmented (jaw crusher, milling) and sieved through a 450 μm sieve. A light-minerals concentrate was obtained by gravity separation (Wilfley table), and further processed by magnetic susceptibility separation (i.e. the Frantz isodynamic separator). Aliquots of ca. 5 mg of the desired mineral phase (unaltered muscovite, biotite or hornblende) were than hand-picked from the concentrate of appropriate magnetic susceptibility. The samples were irradiated for 15 hours at Oregon State University, TRIGA, CLICIT, ^{39}Ar/^{37}Ar 6.73E-4, ^{36}Ar/^{37}Ar 2.64E-4, ^{40}Ar/^{39}Ar 1.01E-3, ^{38}Ar/^{39}Ar 1.138E-2. Fish Canyon Tuff sanidine was used as a fluence monitor with an age of 28.02 ±0.16 Ma (1σ internal uncertainty; Renne et al., 1998), and dates were calculated using the ^{40}K decay constant from Steiger and Jäger (1977). The samples were step-heated (0.5-8 W) with an IR-CO2 laser for 30 seconds, with a 5 minutes cleaning period, using a ST101 and AP10 getter in a UHV stainless steel extraction line. Data were collected with an Argus V mass spectrometer at the University of Geneva, Switzerland. Multi collection was performed with a 1E11Ω Faraday (^{40}Ar) and 1E12Ω Faradays (^{39}Ar, ^{38}Ar, ^{37}Ar, and ^{36}Ar). A mass discrimination factor of 0.983±0.051 was used. The data is presented in Tables 3-1 and 3-1-1. The results were corrected for baselines, blanks, interfering nucleogenic reactions and the decay of ^{37}Ar and ^{39}Ar. The analytical procedure is identical to that described in Villagómez and Spikings (2013). All uncertainties are ±2σ, unless explicitly stated otherwise. Plateaus are defined according to Dalrymple and Lanphere, (1974). The bulk values of closure temperatures (T_c) of analysed mineral phases, estimated using experimentally derived diffusion parameters, range between ca. 545-511 °C for hornblende (McDougall and Harrison, 1999 and references therein), ca. 405 °C for muscovite (at 5 kbar; Harrison et al., 2009), and ca. 310 °C for biotite (Harrison et al., 1985) at moderate cooling rates (ca. 10 °C·Ma^{-1}).

3-1.2 Sample description results and interpretation

A summary of the results of $^{40}Ar/^{39}Ar$ thermochronology is presented in Table 3-1, and the $^{40}Ar/^{39}Ar$ date spectra are shown in Figure A1. Complete data sets and additional plots are provided in Table 3-1-1.

3-1.2.1 Mylonite from the Vrvi Kobila area (SM01)

Sample SM01 was taken from a mylonite within the Vrvi Kobila shear zone (Fig. 3-2). Foliation S_2 is defined by flattened quartz-feldspar (often as microcline) aggregates, and newly-formed muscovite and biotite (i.e. no apparent inherited domains were observed in the mica; Fig. 3-7c). An aliquot of muscovite grains between 300 and 250 μm in size were hand-picked for $^{40}Ar/^{39}Ar$ analysis. The first heating step yielded a date of 332±1 Ma, with subsequent steps giving much older dates that gradually increase with each heating step until reaching a relatively stable plateau beginning at ca. 40% of released ^{39}Ar with a date of 351±1 Ma (Table 3-1 and Fig. 3-1-1).

3-1.2.2 Chlorite-schist from the Vlasina Unit (SM05)

Sample of chlorite-schists SM05 was taken in the northern part of Vlasina Unit (Fig. 3-2). Foliation S_2 is defined by chlorite, muscovite and elongated quartz grains. A majority of the quartz grains show a sweeping undulose extinction and occasional evidence of dynamic recrystallisation by SGR and less frequently BLG.

An aliquot of muscovite grains between 200 and 160 μm in size, were hand-picked for $^{40}Ar/^{39}Ar$ analysis. After the initial heating step with a date of 265 Ma, a sequence of six heating steps yielding 46% of released ^{39}Ar, forms a plateau with a date of 284±1 Ma (Fig. 3-1-1).

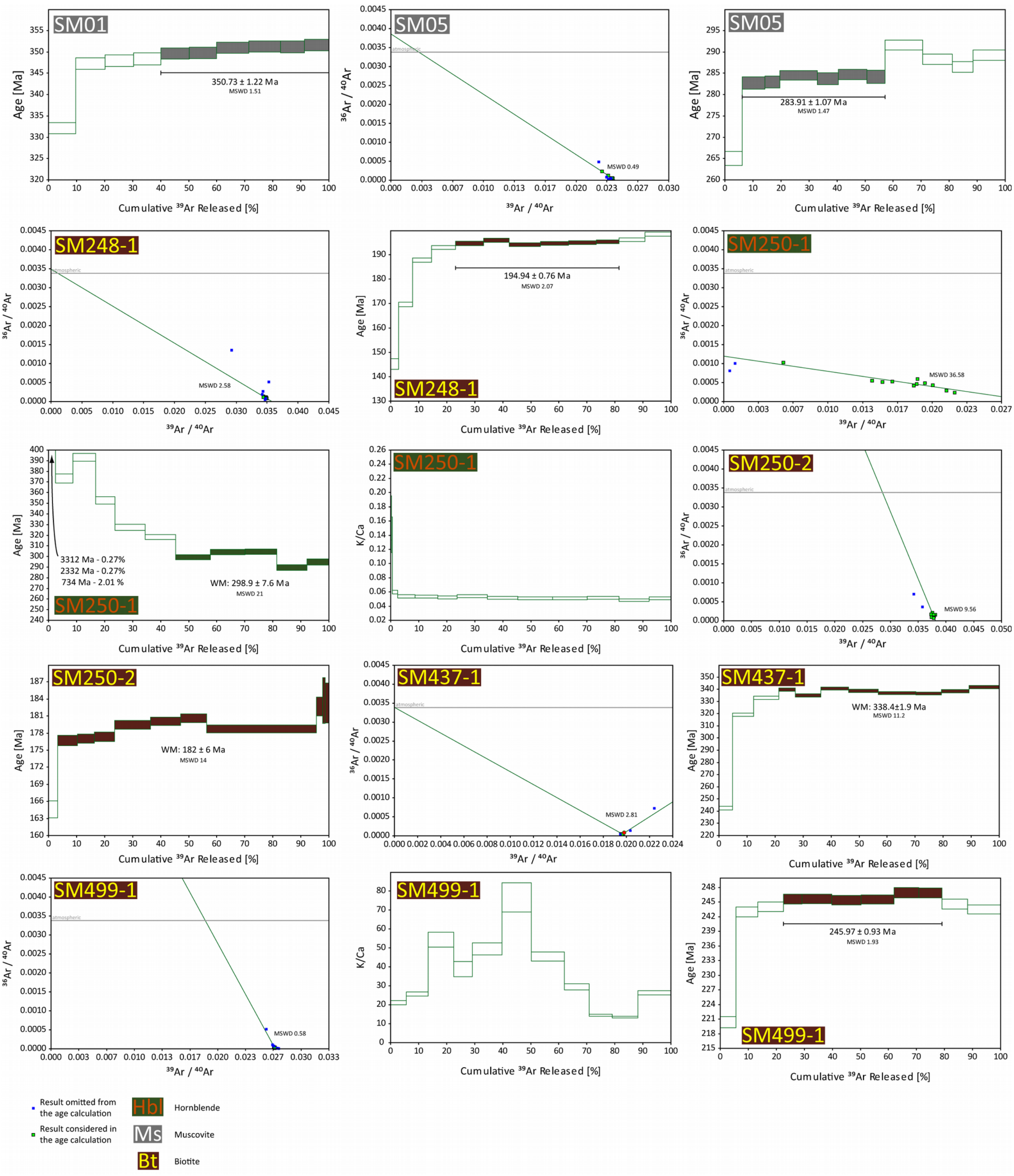

Figure 3-1-1. $^{40}Ar/^{39}Ar$ date spectra, K/Ca yield diagrams and isotope correlation plots for samples from the central SMM. All uncertainties are ±2σ. Plateau dates are defined according to Dalrymple and Lanphere (1974). WM – weighted mean date, MSWD – mean square weighted deviation. See text for details.

Subsequent four steps show a disturbed pattern with dates varying between 292 and 286 Ma (Table 3-1-1). Plateau date of 284±1 Ma was interpreted as the time of cooling of muscovite below the closure temperature (ca. 405 °C at a moderate cooling rate of ca. 10 °C·Ma^{-1}).

3-1.2.3 Biotite-gneiss from the Lower Complex (SM248-1)

Biotite bearing gneiss SM248-1 was taken from the Lower Complex west of the Vrvi Kobila shear zone (Fig. 3-2 and 3-7). This sample is predominantly composed of K-feldspar (mostly microcline), quartz, plagioclase, biotite, muscovite, and accessory zircon, garnet and rutile. The foliation S_2 is mostly defined by biotite and flattened quartz-feldspar aggregates. Late replacement of feldspar by undeformed muscovite and sericite was observed.

A biotite concentrate was hand-picked from the fraction coarser than 160 µm. The first four heating steps yielding a total of ca. 23% of released ^{39}Ar show an increasing date-spectrum ranging from 193 to 145 Ma (Fig. 3-1-1). The following six contiguous heating steps during which ca. 58% of ^{39}Ar was released, form a plateau with a date of 195±1 Ma (Table 3-1). The final two heating steps yield older dates of ca. 196 and ca. 199 Ma respectively, and do not form a plateau. The plateau date of 195±1 Ma was interpreted as a cooling age of biotite, probably related to the retrogression observed in these rocks.

3-1.2.4 Amphibolite from Golemo Selo (SM250-1)

An amphibolite folded together with biotite gneiss (SM250-2) by F_2 folds near the village of Golemo Selo, in the Lower Complex west of Vrvi Kobila shear zone (Fig. 3-2) is predominantly composed of hornblende and plagioclase-rich bands (ca. 65% An).

Hornblende yields a highly disturbed date spectrum, with step-dates ranging between 3312 and 295 Ma. The first three heating steps, during which a total of 2.55% of cumulative ^{39}Ar was released, yield dates older than 734 Ma (Fig. 3-1-1). The remaining heating steps gave dates between 393 and 290 Ma in an irregular pattern. The overall disturbed shape of the pattern is probably caused by excess ^{40}Ar that is released at higher temperatures, and the K/Ca ratios reveal a hornblende with generally homogeneous composition with respect to these elements (Fig. 3-1-1). Apart from minor variation in the first two steps, the pattern of K/Ca ratio shows no correlation with the date spectrum, thus excluding possibility of ^{39}Ar recoil (Fig. 3-1-1). A weighted mean date of 299±8 Ma was determined for the final five heat-steps showing the least disturbance (4.98% variation in date; Table 3-1). Unfortunately, this date could not be compared with an inverse isochron due to the high scattering of step-heating data (MSWD=36.58; Fig. 3-1-1). Although a statistically robust cooling age could not be determined, a potential geological explanation of the weighted average date is discussed in main text.

3-1.2.5 Biotite-gneiss from Golemo Selo (SM250-2)

Sample SM250-2 was collected from biotite-gneiss folded together with amphibolite (SM250-1), near the village of Golemo Selo in the Lower Complex west of Vrvi Kobila (Fig. 3-2). The penetrative foliation S_2 is primarily defined by biotite and quartz aggregates.

^{40}Ar/^{39}Ar analysis of large (>500 μm) biotite minerals resulted in step-dates varying between 184 Ma and 165 Ma in a relatively gentle staircase pattern (Fig. 3-1-1). Although without an adequate plateau and questionable resolution (39% of ^{39}Ar has been released during the eighth heating step), the obtained dates differ within 3.89%, excluding the initial heating step that yielded 165 Ma. A mean date of 182±6 Ma was obtained from ten heating steps releasing ca. 97% of cumulative ^{39}Ar. However, this result could not be evaluated further as the high scatter of results of step-heating do not define an inverse isochron (MSWD= 9.56; Fig. 3-1-1). Although the disturbances of the date-spectra impeded determination of an unequivocal cooling age, geological significance of the mean date (182±6 Ma) is discussed in the main text.

3-1.2.6 Mylonite from Vranjska Banja area (SM437-1)

Sample SM437-1 was collected from a mylonite in the Vranjska Banja area (Fig. 3-2). Foliation is defined by biotite and clinozoisite together with flattened quartz-feldspar microlithons. An aliquot of biotite grains between 250 and 160 µm in size, yielded ^{40}Ar/^{39}Ar step-dates between 242 and 342 Ma (Fig. 3-1-1). Apart from the three initial heating steps that yield a steep staircase pattern from 242 to 333 Ma and yield a total of ca. 24% of ^{39}Ar released, dates of the remaining steps only vary from each other by 1.97% and give a weighted average date of 338±2 Ma (Table 3-1 and Fig. 3-1-1).

3-1.2.7 Mylonite from the Božica area (SM499-1)

Sample SM499-1 was taken from a mylonite formed in the southern periphery of the Božica magmatic complex (Fig. 3-2). Penetrative foliation is primarily defined by flattened sericite-quartz aggregates, as well as syn-tectonic biotite and clinozoisite. Top-to-the-west sense of shear was determined based on mica fish and domino-fragmented grains of biotite, as well as quartzitic sigmoids.

An aliquot of biotite grains between 250 and 160 µm in size were analysed, yielding ^{40}Ar/^{39}Ar step-dates ranging between 247 and 220 Ma (Fig. 3-1-1). Apart from the anomalously young initial heating step of 220 Ma, the central six steps form a plateau with a date of 246±1 Ma. This cooling age probably represents a minimum time constraint on the syn-tectonic metamorphism in the analysed rock, and therefore activity along the shear zone in the southern part of the Božica

Table 3-1-1 Results of ^{40}Ar/^{39}Ar thermochronology

Heating step	**^{40}Ar/^{39}Ar**	**±1σ**	**^{37}Ar/^{39}Ar**	**±1σ**	**^{36}Ar/^{39}Ar**	**±1σ**	**^{40}Ar*/^{39}Ar$_k$**	**±1σ**	**^{40}Ar [mol]**	**^{40}Ar* [%]**	**^{39}Ar$_k$ [%]**	**Date [Ma]**	**±2σ [Ma]**	**K/Ca**	**±2σ**
SM01 muscovite, J=0.0041493±0.0000125					Plateau Age 350.73±1.22 Ma										
1	50,85029	,10256	,00000	,00166	,00723	,00015	48,71306	,10729	2,065E-14	95,80	9,67	332,11	1,34	n/a	n/a
2	51,52104	,10388	,00000	,00093	,00124	,00009	51,15502	,10684	2,288E-14	99,29	10,58	347,26	1,32	n/a	n/a
3	51,42681	,10345	,00000	,00186	,00055	,00011	51,26320	,10837	2,194E-14	99,68	10,16	347,92	1,34	n/a	n/a
4	51,56955	,10375	,00000	,00129	,00080	,00015	51,33223	,11223	2,106E-14	99,54	9,72	348,35	1,39	n/a	n/a
5	**51,69162**	**,10505**	**,00000**	**,00159**	**,00052**	**,00010**	**51,53836**	**,10888**	**2,191E-14**	**99,70**	**10,09**	**349,62**	**1,34**	**n/a**	**n/a**
6	**51,76376**	**,10526**	**,00000**	**,00149**	**,00068**	**,00011**	**51,56088**	**,10963**	**2,097E-14**	**99,61**	**9,65**	**349,76**	**1,35**	**n/a**	**n/a**
7	**51,75656**	**,10442**	**,00000**	**,00130**	**,00000**	**,00010**	**51,75555**	**,10441**	**2,500E-14**	**100,00**	**11,50**	**350,96**	**1,29**	**n/a**	**n/a**
8	**51,80123**	**,10483**	**,00000**	**,00179**	**,00000**	**,00013**	**51,80022**	**,10482**	**2,464E-14**	**100,00**	**11,33**	**351,24**	**1,29**	**n/a**	**n/a**
9	**51,88959**	**,10616**	**,00000**	**,00167**	**,00033**	**,00013**	**51,79187**	**,11294**	**1,862E-14**	**99,81**	**8,55**	**351,18**	**1,39**	**n/a**	**n/a**
10	**51,86245**	**,10581**	**,00000**	**,00144**	**,00001**	**,00011**	**51,85869**	**,11063**	**1,906E-14**	**99,99**	**8,75**	**351,60**	**1,36**	**n/a**	**n/a**
SM05 muscovite, J=0.0041453±0.0000125					Plateau Age 283.91±1.07 Ma										
1	44,53192	,09572	,00000	,00219	,02150	,00033	38,178777	,12702	9,088E-15	85,73	5,52	265,06	1,64	n/a	n/a
2	**43,83626**	**,09137**	**,00000**	**,00188**	**,00984**	**,00026**	**40,927564**	**,11511**	**1,183E-14**	**93,36**	**7,30**	**282,72**	**1,47**	**n/a**	**n/a**
3	**42,52971**	**,09213**	**,00000**	**,00293**	**,00530**	**,00023**	**40,962506**	**,11252**	**7,626E-15**	**96,32**	**4,85**	**282,94**	**1,44**	**n/a**	**n/a**
4	**41,94061**	**,08442**	**,00000**	**,00111**	**,00247**	**,00009**	**41,208337**	**,08730**	**1,866E-14**	**98,25**	**12,04**	**284,51**	**1,12**	**n/a**	**n/a**
5	**41,80627**	**,08597**	**,00000**	**,00282**	**,00244**	**,00022**	**41,085238**	**,10723**	**1,047E-14**	**98,28**	**6,78**	**283,73**	**1,37**	**n/a**	**n/a**
6	**41,73297**	**,08461**	**,00000**	**,00160**	**,00168**	**,00016**	**41,234217**	**,09572**	**1,417E-14**	**98,80**	**9,19**	**284,68**	**1,22**	**n/a**	**n/a**
7	**41,84337**	**,08825**	**,00000**	**,00333**	**,00232**	**,00028**	**41,155351**	**,11919**	**9,035E-15**	**98,36**	**5,84**	**284,17**	**1,52**	**n/a**	**n/a**
8	42,55575	,08586	,00000	,00121	,00081	,00011	42,314927	,09164	1,908E-14	99,43	12,13	291,57	1,17	n/a	n/a
9	42,22256	,08589	,00000	,00149	,00144	,00012	41,794652	,09178	1,484E-14	98,99	9,51	288,25	1,17	n/a	n/a
10	42,04239	,08701	,00000	,00166	,00177	,00015	41,518409	,09680	1,040E-14	98,75	6,69	286,49	1,24	n/a	n/a
11	42,91824	,08751	,00000	,00118	,00330	,00014	41,941941	,09475	1,642E-14	97,73	10,35	289,19	1,21	n/a	n/a
SM248-1 biotite, J=0.0040887±0.0000125					Plateau Age 194.94±0.76 Ma										
1	34,15384	,07241	,00682	,00076	,04617	,00054	20,509223	,16296	6,084E-15	60,05	2,85	145,27	2,22	63,09	14,08
2	28,35069	,05729	,00212	,00059	,01435	,00016	24,108030	,06764	8,857E-15	85,03	5,00	169,60	0,91	202,55	111,85
3	29,08257	,05848	,00105	,00036	,00761	,00010	26,832031	,06192	1,233E-14	92,26	6,78	187,80	0,82	407,73	274,52
4	29,18555	,05877	,00061	,00032	,00534	,00008	27,607794	,06075	1,541E-14	94,59	8,45	192,95	0,81	703,16	738,94

Table 3-1-1 continued

Heating step	$^{40}Ar/^{39}Ar$	±1σ	$^{37}Ar/^{39}Ar$	±1σ	$^{36}Ar/^{39}Ar$	±1σ	$^{40}Ar^{*}/^{39}Ar_k$	±1σ	^{40}Ar [mol]	$^{40}Ar^{*}$ [%]	$^{39}Ar_k$ [%]	Date [Ma]	±2σ [Ma]	K/Ca	±2σ
SM248-1 biotite, continued															
5	**29,01521**	**,05849**	**,00000**	**,00028**	**,00389**	**,00012**	**27,864108**	**,06649**	**1,833E-14**	**96,03**	**10,11**	**194,65**	**0,88**	**703,16**	**738,94**
6	**29,02345**	**,05837**	**,00000**	**,00030**	**,00329**	**,00010**	**28,051038**	**,06394**	**1,634E-14**	**96,65**	**9,01**	**195,88**	**0,85**	**703,16**	**738,94**
7	**28,70585**	**,05772**	**,00000**	**,00017**	**,00307**	**,00008**	**27,797780**	**,06066**	**2,021E-14**	**96,84**	**11,26**	**194,21**	**0,80**	**703,16**	**738,94**
8	**28,65927**	**,05751**	**,00000**	**,00027**	**,00270**	**,00007**	**27,860768**	**,06002**	**1,802E-14**	**97,21**	**10,06**	**194,62**	**0,79**	**703,16**	**738,94**
9	**28,57279**	**,05739**	**,00000**	**,00034**	**,00221**	**,00008**	**27,918123**	**,06053**	**1,765E-14**	**97,71**	**9,89**	**195,00**	**0,80**	**703,16**	**738,94**
10	**28,65051**	**,05781**	**,00009**	**,00027**	**,00232**	**,00006**	**27,965212**	**,05882**	**1,438E-14**	**97,61**	**8,03**	**195,32**	**0,78**	**4691,83**	**27561,18**
11	28,72251	,05775	,00093	,00027	,00214	,00006	28,089189	,05918	1,664E-14	97,79	9,27	196,14	0,78	464,74	273,02
12	28,83959	,05821	,00155	,00029	,00130	,00010	28,453208	,06466	1,675E-14	98,66	9,29	198,54	0,85	277,04	104,48
SM250-1 hornblende, J=0.0041372±0.0000125							~~Weighted mean age 298.9±7.6 Ma~~								
1	1274,190663	73,41153	1667,56953	95,57575	2,61181	,24551	1,33950	,07948	3,472E-15	76,28	,27	3312,34	174,73	0,16	0,03
2	638,677536	43,30101	903,88527	60,11037	3,05317	,27672	,90273	,06579	1,851E-15	70,51	,27	2332,00	177,46	0,14	0,03
3	121,313082	1,50990	173,33390	1,65674	7,18549	,15820	,17992	,00365	2,680E-15	69,65	2,01	733,77	15,01	0,06	0,00
4	55,581625	,35322	65,13882	,23779	7,95440	,15900	,03545	,00098	3,060E-15	84,87	6,10	373,40	4,29	0,05	0,00
5	58,844818	,30505	69,74170	,19506	7,98694	,15855	,04005	,00087	4,367E-15	83,92	8,13	393,09	3,66	0,05	0,00
6	52,194072	,29560	61,37087	,18940	8,15118	,16230	,03417	,00084	3,301E-15	84,58	6,98	352,72	3,63	0,05	0,00
7	48,103731	,22889	54,46520	,14678	7,93878	,15750	,02449	,00063	4,525E-15	87,85	10,78	327,44	2,85	0,05	0,00
8	46,646326	,19111	53,66656	,13641	8,30667	,16599	,02683	,00050	4,459E-15	86,43	10,78	318,35	2,39	0,05	0,00
9	**43,622169**	**,18095**	**49,50915**	**,12041**	**8,38143**	**,16731**	**,02296**	**,00049**	**4,762E-15**	**87,61**	**12,48**	**299,32**	**2,29**	**0,05**	**0,00**
10	**44,379235**	**,20921**	**53,40187**	**,13976**	**8,40166**	**,16790**	**,03360**	**,00058**	**5,093E-15**	**82,63**	**12,37**	**304,11**	**2,64**	**0,05**	**0,00**
11	**44,430341**	**,20747**	**51,41502**	**,12422**	**8,23816**	**,16453**	**,02664**	**,00060**	**4,463E-15**	**85,94**	**11,26**	**304,43**	**2,62**	**0,05**	**0,00**
12	**42,083649**	**,22104**	**44,82769**	**,09948**	**8,83419**	**,17637**	**,01246**	**,00067**	**3,744E-15**	**93,32**	**10,83**	**289,57**	**2,81**	**0,05**	**0,00**
13	**42,900593**	**,23370**	**46,50754**	**,12690**	**8,36955**	**,16770**	**,01523**	**,00068**	**2,776E-15**	**91,72**	**7,75**	**294,76**	**2,96**	**0,05**	**0,00**
SM250-2 biotite, J=0.0041204±0.0000125							~~Weighted mean age 178.9±1.2 Ma~~								
1	29,19342	,06222	,00000	,00130	,02034	,00033	23,180987	,10918	5,286E-15	79,40	3,19	164,58	1,48	n/a	n/a
2	**27,90342**	**,05648**	**,00000**	**,00064**	**,00990**	**,00015**	**24,977954**	**,06731**	**1,118E-14**	**89,52**	**7,06**	**176,73**	**0,91**	**n/a**	**n/a**
3	**26,61888**	**,05394**	**,00000**	**,00065**	**,00540**	**,00011**	**25,020774**	**,05993**	**9,124E-15**	**94,00**	**6,04**	**177,02**	**0,81**	**n/a**	**n/a**
4	**26,21687**	**,05293**	**,00000**	**,00065**	**,00389**	**,00012**	**25,067286**	**,06241**	**1,077E-14**	**95,62**	**7,23**	**177,33**	**0,84**	**n/a**	**n/a**

Table 3-1-1 continued

Heating step	$^{40}Ar/^{39}Ar$	±1σ	$^{37}Ar/^{39}Ar$	±1σ	$^{36}Ar/^{39}Ar$	±1σ	$^{40}Ar^{*}/^{39}Ar_{k}$	±1σ	^{40}Ar [mol]	$^{40}Ar^{*}$ [%]	$^{39}Ar_{k}$ [%]	Date [Ma]	±2σ [Ma]	K/Ca	±2σ
SM250-2 biotite, continued															
5	26,52557	,05321	,00000	,00042	,00385	,00009	25,386394	,05717	1,942E-14	95,71	12,90	179,48	0,77	n/a	n/a
6	26,75510	,05373	,00000	,00058	,00432	,00007	25,476342	,05505	1,627E-14	95,22	10,71	180,08	0,74	n/a	n/a
7	26,39708	,05308	,00000	,00044	,00285	,00008	25,553915	,05715	1,383E-14	96,81	9,23	180,61	0,77	n/a	n/a
8	26,43464	,05294	,00000	,00016	,00392	,00004	25,274605	,05199	5,895E-14	95,61	39,28	178,73	0,70	n/a	n/a
9	26,55857	,05597	,00000	,00241	,00235	,00037	25,862811	,12188	3,296E-15	97,38	2,19	182,68	1,64	n/a	n/a
10	26,71475	,07101	,01531	,00852	,00236	,00098	26,018971	,29800	1,300E-15	97,39	,86	183,73	4,00	n/a	n/a
11	26,45506	,05725	,00323	,00500	,00169	,00086	25,955340	,25969	1,999E-15	98,11	1,33	183,30	3,49	n/a	n/a
SM437-1 biotite, J=0.0040981±0.0000125					Weighted mean age 338.4±1.9 Ma										
1	44,58129	,09506	,01333	,00086	,03207	,00034	35,103573	,12370	8,923E-15	78,74	4,83	242,48	1,60	n/a	n/a
2	49,07771	,09986	,00528	,00054	,00632	,00017	47,208411	,10821	1,544E-14	96,19	7,60	319,07	1,34	n/a	n/a
3	50,39352	,10293	,00034	,00052	,00321	,00014	49,445198	,10893	1,878E-14	98,12	9,00	332,87	1,34	n/a	n/a
4	51,16690	,10749	,00193	,00122	,00210	,00017	50,546359	,11762	1,231E-14	98,79	5,81	339,63	1,44	n/a	n/a
5	50,61788	,10346	,00000	,00073	,00282	,00015	49,784469	,11088	1,902E-14	98,35	9,07	334,96	1,36	n/a	n/a
6	51,28312	,10476	,00000	,00051	,00196	,00008	50,702658	,10629	2,123E-14	98,87	10,00	340,59	1,30	n/a	n/a
7	51,04962	,10273	,00000	,00000	,00227	,00014	50,377547	,10918	2,245E-14	98,68	10,62	338,60	1,34	n/a	n/a
8	50,74428	,10197	,00000	,00000	,00218	,00009	50,097906	,10402	2,813E-14	98,73	13,38	336,88	1,28	n/a	n/a
9	50,74246	,10322	,00000	,00000	,00240	,00013	50,032341	,10828	1,910E-14	98,60	9,09	336,48	1,33	n/a	n/a
10	50,87641	,10338	,00197	,00043	,00187	,00011	50,324104	,10732	2,083E-14	98,91	9,89	338,27	1,32	n/a	n/a
11	51,25926	,10352	,00234	,00054	,00131	,00010	50,871819	,10658	2,276E-14	99,24	10,72	341,62	1,30	n/a	n/a
SM499-1 biotite, J=0.0039525±0.0000125					Plateau Age 245.97±0.93 Ma										
1	38,69200	,07903	,02037	,00053	,01970	,00021	32,872904	,09021	1,067E-14	84,96	5,58	220,38	1,14	21,11	1,09
2	37,60454	,07707	,01683	,00036	,00381	,00010	36,480219	,07996	1,453E-14	97,01	7,81	243,00	1,00	25,55	1,09
3	37,36827	,07596	,00791	,00029	,00242	,00007	36,651670	,07746	1,697E-14	98,08	9,18	244,07	0,96	54,36	4,00
4	37,36508	,07635	,01108	,00056	,00159	,00011	36,896208	,08213	1,209E-14	98,74	6,54	245,59	1,02	38,80	3,95
5	37,28082	,07540	,00869	,00027	,00126	,00009	36,908169	,07951	1,967E-14	99,00	10,67	245,67	0,99	49,47	3,11
6	37,19686	,07502	,00561	,00028	,00110	,00008	36,870084	,07768	1,910E-14	99,12	10,38	245,43	0,97	76,69	7,75
7	37,18435	,07489	,00947	,00025	,00102	,00007	36,883571	,07679	2,170E-14	99,19	11,80	245,51	0,96	45,42	2,41

Table 3-1-1 continued

Heating step	^{40}Ar/^{39}Ar	±1σ	^{37}Ar/^{39}Ar	±1σ	^{36}Ar/^{39}Ar	±1σ	^{40}Ar*/^{39}Ar$_k$	±1σ	^{40}Ar [mol]	^{40}Ar* [%]	^{39}Ar$_k$ [%]	Date [Ma]	±2σ [Ma]	K/Ca	±2σ
SM499-1 biotite, conitnued															
8	**37,20496**	**,07507**	**,01461**	**,00039**	**,00033**	**,00013**	**37,109044**	**,08452**	**1,622E-14**	**99,74**	**8,82**	**246,92**	**1,05**	**29,43**	**1,55**
9	**37,22211**	**,07516**	**,02972**	**,00052**	**,00040**	**,00011**	**37,106665**	**,08184**	**1,523E-14**	**99,69**	**8,27**	**246,90**	**1,02**	**14,47**	**0,51**
10	36,84912	,07525	,03183	,00051	,00038	,00012	36,739309	,08239	1,683E-14	99,70	9,23	244,61	1,03	13,51	0,44
11	36,57213	,07350	,01635	,00034	,00006	,00007	36,555721	,07618	2,119E-14	99,95	11,71	243,47	0,95	26,29	1,09

Mass discrimination 0.983±0.051.

Data are corrected for blanks, interfering nucleogenic reactions and decay of ^{37}Ar and ^{39}Ar.

Irradiated for 15 hours at Oregon State University, TRIGA, CLICIT, ^{39}Ar/^{37}Ar 6,73E-4, ^{36}Ar/^{37}Ar 2,64E-4, ^{40}Ar/^{39}Ar 1,01E-3, ^{38}Ar/^{39}Ar 1,138E-2.

Steps highlighted with bold text are included in the calculation of the weighted mean date or the plateau date.

Low-confidence date values are stricken-through .

Samples heated with a IR-CO2 laser for 30 seconds, with 5 minutes cleaning with a ST101 and AP10 getter in a stainless steel extraction line.

Data collected with an Argus mass spectrometer. Multi collection with 1E11Ω Faraday (^{40}Ar) and 1E12Ω Faradays (^{39}Ar. ^{38}Ar. ^{37}Ar. ^{36}Ar).

Procedure identical to that described in Villagomez and Spikings (2013).

^{40}Ar* – radiogenic argon isotope

^{39}Ar$_K$ – Potassium derived isotope of argon

K/Ca ratio is not available for samples with Ca content below the limits of detection.

magmatic complex (Table 3-1).

References

Dalrymple, G.B., Lanphere, M.A., 1974. ^{40}Ar/^{39}Ar age spectra of some undisturbed terrestrial samples. Geochimica et Cosmochimica Acta 38, 715–738.

Harrison, T.M., Célérier, J., Aikman, A.B., Hermann, J., Heizler, M.T., 2009. Diffusion of ^{40}Ar in muscovite. Geochimica et Cosmochimica Acta 73, 1039–1051.

Harrison, T.M., Duncan, I., McDougall, I., 1985. Diffusion of ^{40}Ar in biotite: Temperature, pressure and compositional effects. Geochimica et Cosmochimica Acta 49, 2461–2468.

McDougall, I., Harrison, T.M., 1999. Geochronology and Thermochronology by the ^{40}Ar/^{39}Ar Method, 2nd ed. Oxford University Press, Oxford.

Renne, P.R., Swisher, C.C., Deino, A.L., Karner, D.B., Owens, T.L., DePaolo, D.J., 1998. Intercalibration of standards, absolute ages and uncertainties in ^{40}Ar/^{39}Ar dating. Chemical Geology 145, 117–152.

Steiger, R.H., Jäger, E., 1977. Subcommission on geochronology: Convention on the use of decay constants in geo- and cosmochronology. Earth and Planetary Science Letters 36, 359–362.

Villagómez, D., Spikings, R., 2013. Thermochronology and tectonics of the Central and Western Cordilleras of Colombia: Early Cretaceous–Tertiary evolution of the Northern Andes. Lithos 160–161, 228–249.

Chapter 4

Alpine thermal events in the central Serbo-Macedonian Massif (southeastern Serbia)

Milorad D. Antić[1], Alexandre Kounov[1], Branislav Trivić[2], Andreas Wetzel[1], Irena Peytcheva[3,4], Albrecht von Quadt[3]

[1]Institute for Geology and Palaeontology, University of Basel, 4056 Basel, Switzerland;
[2]Faculty of Mining and Geology, University of Belgrade, 11000 Belgrade, Serbia
[3]Institute of Geochemistry and Petrology, ETH-Zürich, 8092 Zürich, Switzerland
[4]Geological Institute, Bulgarian Academy of Sciences, 1113 Sofia, Bulgaria

This chapter has been published in: International Journal of Earth Sciences 105, 1485–1505.

doi:10.1007/s00531-015-1266-z

Abstract

The Serbo-Macedonian Massif (SMM) represents a crystalline belt situated between the two diverging branches of the Eastern Mediterranean Alpine orogenic system, the northeast-vergent Carpatho-Balkanides and the southwest-vergent Dinarides and the Hellenides.

We have applied fission-track (FT) analysis on apatites and zircons, coupled with structural field observations in order to reveal the low-temperature evolution of the SMM. Additionally, the age and geochemistry of the Palaeogene igneous rocks (i.e. Surdulica granodiorite and dacitic volcanic rocks) were determined by the LA-ICPMS U–Pb geochronology of zircons and geochemical analysis of main and trace elements in whole-rock samples.

Three major cooling stages have been distinguished from the late Early Cretaceous to the Oligocene. The first stage represents rapid cooling through the partial annealing zones of zircon and apatite (300–60 °C) during the late Early to early Late Cretaceous (ca. 110–ca. 90 Ma). It is related to a post-orogenic extension following the regional nappe-stacking event in the Early Cretaceous. Middle to late Eocene (ca. 48–ca. 39 Ma) cooling is related to the formation of the Crnook-Osogovo-Lisets extensional dome and its exhumation along low angle normal faults. The third event is related to regional cooling following the late Eocene magmatic pulse. During this pulse the areas surrounding the Surdulica granodiorite (36±1 Ma) and the slightly younger volcanic bodies (ca. 35 Ma) have reached temperatures higher than the apatite closure temperature (120 °C) but lower than ca. 250 °C. The geochemistry of the igneous samples reveals late- to post-orogenic tectonic setting during magma generation.

4.1 Introduction

Geological studies conducted along the Eastern Mediterranean Alpine orogen during the last few decades brought significant advances in understanding of the tectonic evolution of a number of crystalline terrains (e.g. Tisza, Rhodope, Serbo-Macedonian) previously considered as ancient microcontinents ("Zwischengebirge" of Kober 1952) trapped within the Alpine orogenic belt (e.g. Bonev et al. 1995; Burg et al. 1996; Schmid et al. 2008; Burg 2012; Kydonakis et al. 2014). Challenges arising in the study of these "intra-Alpine" basement units stem from the varying degrees of inherited tectonic complexity and equally convoluted effects of Alpine deformational overprint. In the case of the Serbo-Macedonian Massif (SMM; Dimitrijević 1957), lodged between the diverging Dinaride–Hellenide, and the Carpatho-Balkanide chains of the Alpine orogen (Fig. 4-1), these difficulties are supplemented by the lack of a relevant sedimentary record and reliable geochronological data. The paucity of appropriate constraints on ages of the deformational events affecting the SMM, led to a number of highly divergent subdivision schemes and tectonic interpretations (Popović 1991; Popović 1995; Ricou et al. 1998; Grubić et al. 1999; Kräutner and Krstić 2002; Grubić et al. 2005; Zagorchev and Milovanović 2006). The major stage of metamorphism affecting the SMM was previously reported as Precambrian (Balogh et al. 1994; Zagorchev and Milovanović 2006; Nenova and Zidarov 2008), Mesozoic (Milovanović 1990; Balogh et al. 1994; Zidarov et al. 2003; Himmerkus et al. 2009),

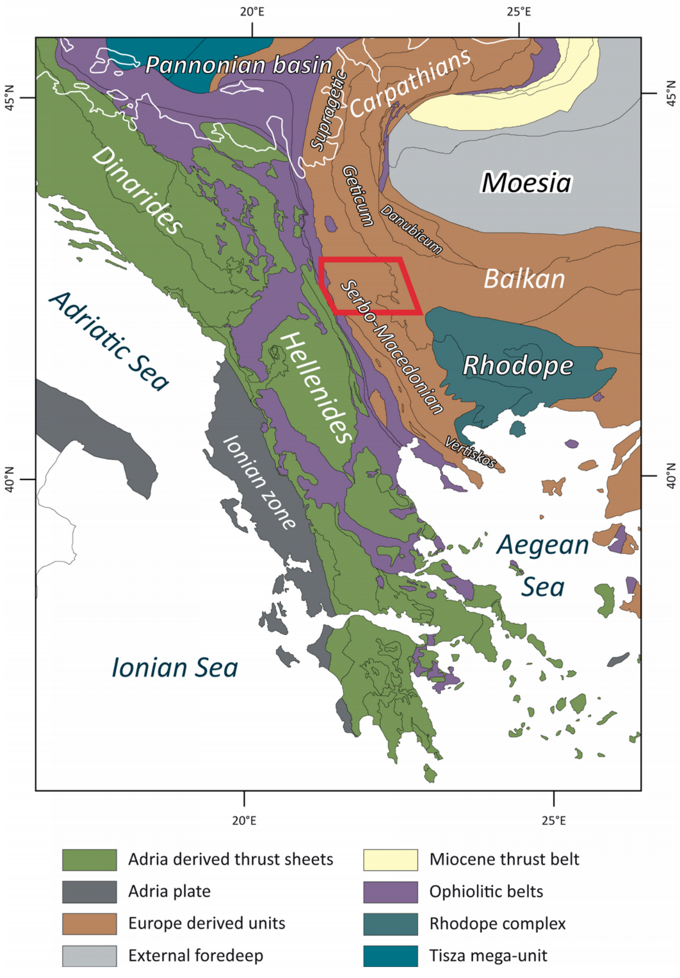

Figure 4-1. Tectonic sketch of the Balkan Peninsula (Schmid et al. 2008; van Hinsbergen and Schmid 2012) with the position of the study area (red polygon). White line delineates the extent of the Pannonian basin.

or Cenozoic in age (Ricou et al. 1998). Similar uncertainties have marked the interpretations of the mode and age of activities along the major tectonic structures in the region, e.g. the western contact of the SMM with the Jurassic ophiolites of the Eastern Vardar zone (Krstić and Karamata 1992; Robertson and Karamata 1994), was previously reported as an east-vergent thrust (Schmid et al. 2008), strike-slip fault (Krstić and Karamata 1992), west-vergent thrust (Vukanović et al. 1977), and a west-vergent thrust reactivated as a Miocene dextral strike-slip fault (Kräutner and Krstić 2002).

Although the southernmost extent of the SMM in Greece and Bulgaria was under continual geo- and thermochronological investigation that inevitably yielded a significant number of valid results (Kilias et al. 1997; Himmerkus et al. 2006; Zidarov et al. 2007; Nenova and Zidarov 2008; Zagorchev 2008; Himmerkus et al. 2009; Meinhold et al. 2010; Zagorchev et al. 2011; Kydonakis et al. 2014), the central part remained beyond the focus of such studies. Therefore the tectonic evolution of the central part of the SMM, within the framework of the Eastern-Mediterranean Alpine orogen, remains unresolved. In order to resolve this problem we have applied fission-track analysis on apatite and zircon crystals, coupled with U–Pb LA-ICPMS geochronology on zircon. The low-temperature FT method is used to constrain the time of the tectonic activity along the major structures, as well as to investigate the thermal evolution of the main constituents of the SMM in the range of 300 to 60 °C. U–Pb dating is used to obtain the emplacement age of Palaeogene igneous rocks, while the results of the FT analysis contribute in resolving the influence of this magmatism on the regional thermal gradient.

4.2 Geological setting

The Serbo-Macedonian Massif represents a crystalline belt located between the Pannonian basin in the north and the Aegean Sea in the south (Fig. 4-1). The Supragetic nappe sequence of the South

Carpathians is considered to be the continuation of the SMM east to northeast of the Pannonian basin (Săndulescu 1984; Dimitrijević 1997; Schmid et al. 2008). As originally proposed by Dimitrijević (1957), the SMM in Serbia comprises a structurally lower (the Lower Complex) and an upper unit (Vlasina Unit; Fig. 4-2). They are commonly differentiated on the basis of their metamorphic grade, with the Lower Complex metamorphosed at medium to lower amphibolite facies, whereas mineral assemblages in Vlasina Unit point to peak metamorphic conditions corresponding to greenschist facies. The continuation of the Lower Complex and Vlasina Unit in Bulgaria are referred to as the Ograzhden Unit (Dimitrijević 1967; Zagorchev 1984a; Dabovski et al. 2002), and Morava Unit (Zagorchev 1985; Zagortchev 1993), respectively.

The Lower Complex is composed mainly of gneisses, micaschists, quartzites, amphibolites and occasional marbles and migmatites (Dimitrijević 1963). These rocks represent a Cadomian (Late Neoproterozoic–earliest Cambrian) volcano-sedimentary complex developed along the active margin of North Gondwana, which was later intruded by igneous rocks during several magmatic pulses (Chapter 2). The high-strain deformation and metamorphism occurred between the early Silurian and the late Carboniferous (Chapter 2).

The Vlasina Unit represents a Cadomian volcano-sedimentary sequence, similar to the Lower Complex, but dominated by ocean-floor sediments (Pantić et al. 1967; Petrović 1969). These rocks were intruded by late Cadomian igneous rocks, and covered by Lower Ordovician to Lower Carboniferous sedimentary sequence (post-Cambrian in Fig. 4-2; Pavlović 1962; Babović et al. 1977; Kräutner and Krstić 2002). Pre-Ordovician and post-Cambrian constituents of the Vlasina Unit share a similar deformation style and metamorphic grade (Petrović 1969; Pavlović 1977; Milovanović et al. 1988; Vasković 1998; Vasković 2002). The pre-Ordovician Vlasina is typically represented by various schists, phyllites and quartzites (Dimitrijević 1967). Relicts of higher grade metamorphism in retrograde rocks have been reported mostly in the vicinity of the Božica

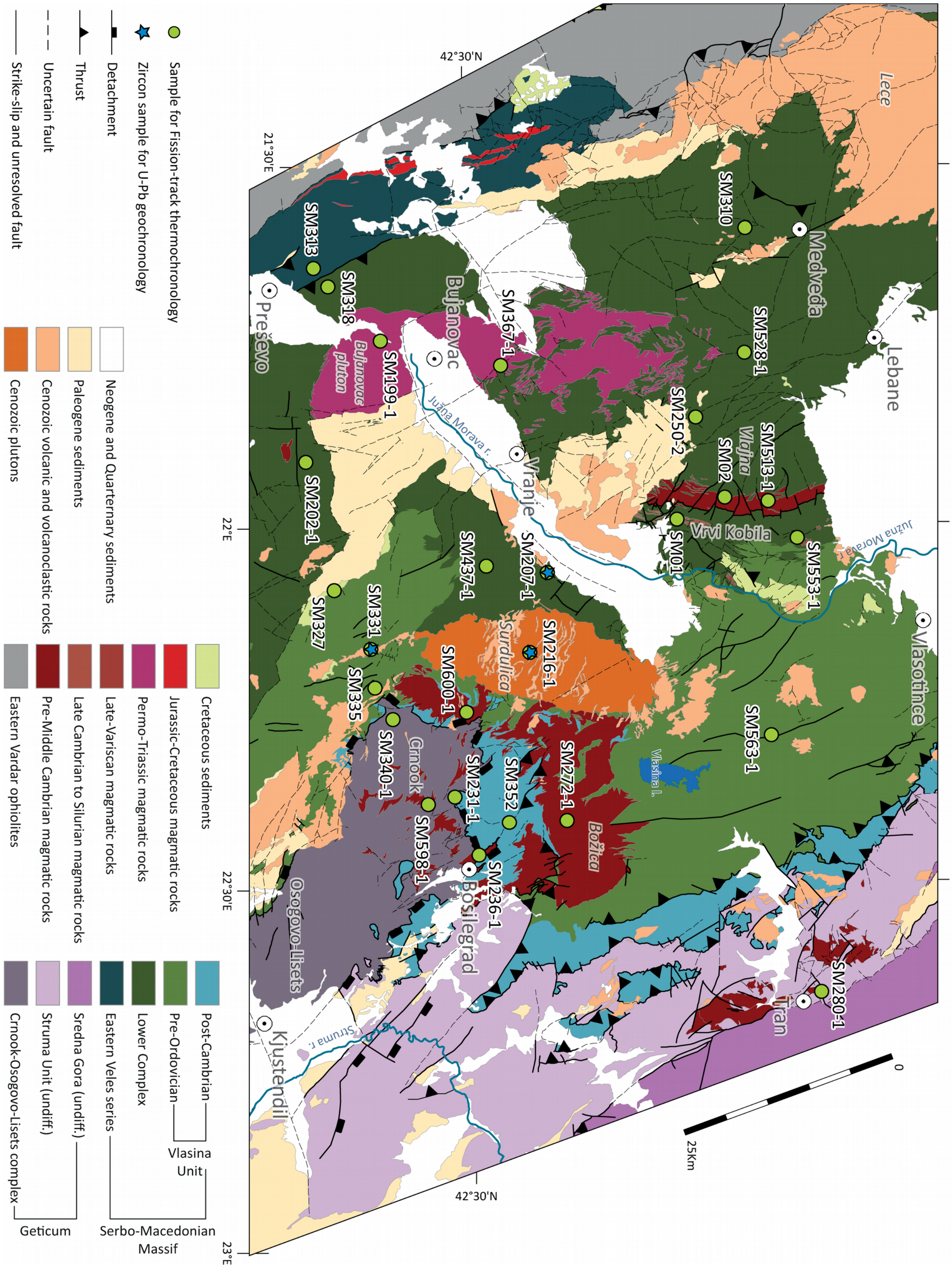
Sample for Fission-track thermochronology
Zircon sample for U-Pb geochronology
Detachment
Thrust
Uncertain fault
Strike-slip and unresolved fault
Neogene and Quarternary sediments
Paleogene sediments
Cenozoic volcanic and volcanoclastic rocks
Cenozoic plutons
Cretaceous sediments
Jurassic-Cretaceous magmatic rocks
Permo-Triassic magmatic rocks
Late-Variscan magmatic rocks
Late Cambrian to Silurian magmatic rocks
Pre-Middle Cambrian magmatic rocks
Eastern Vardar ophiolites
Post-Cambrian
Pre-Ordovician
Vlasina Unit
Lower Complex
Eastern Veles series
Serbo-Macedonian Massif
Sredna Gora (undiff.)
Struma Unit (undiff.)
Crnook-Osogovo-Lisets complex
Geticum
42°30'N
42°30'N
21°30'E
22°E
22°30'E
23°E
0
25Km
Lece
Medveđa
Lebane
Vlasotince
Bujanovac
Bujanovac pluton
Preševo
Vranje
Južna Morava r.
Vrvi Kobila
Vlajna
Surdulica
Vlasina l.
Božica
Crnook
Bosilegrad
Osogovo-Lisets
Kjustendil
Struma r.
Tran
SM310
SM528-1
SM250-2
SM513-1
SM02
SM01
SM553-1
SM313
SM318
SM367-1
SM199-1
SM202-1
SM327
SM437-1
SM207-1
SM331
SM335
SM600-1
SM216-1
SM563-1
SM340-1
SM231-1
SM352
SM272-1
SM598-1
SM236-1
SM280-1

magmatic complex and Surdulica pluton (Petrović 1969; Babović et al. 1977; Pavlović 1977; Vasković 1998; Vasković et al. 2003). The Post-Cambrian Vlasina is composed of Ordovician schists, phyllites, calcschists, quartzite and marbles, Silurian graptolitic schists, Middle Devonian carbonates and Upper Devonian to Lower Carboniferous turbidites with spilites (Pavlović 1962; Petrović et al. 1973; Spassov 1973; Babović et al. 1977; Pavlović 1977; Zagorčev and Bončeva 1988; Banjac 2004; Lakova 2009).

An inlier, structurally beneath the Vlasina Unit, located southwest of Bosilegrad and southeast of Surdulica pluton is distinguished as the Crnook dome (Fig. 4-2; Dimitrijević 1972; Babović et al. 1977). The contact of the amphibolitic grade mica schists, gneisses and amphibolites of the Crnook dome with the overlying schists of the post-Cambrian Vlasina was previously reported as transgressive or gradual (Pavlović 1962; Pavlović 1962; Babović et al. 1977).

The contact between the Lower Complex and Vlasina Unit is reported as the Vrvi Kobila shear zone (Fig. 4-2). It was considered as a pre-Mesozoic west-vergent thrust of Vlasina over the Lower Complex (Vukanović et al. 1973; Krstić and Karamata 1992), or post-Late Cretaceous dextral shear zone (Kräutner and Krstić 2002). Dimitrijević (1997) suggests that the contact between the two units was initially stratigraphic and that it was later tectonically reworked.

South of the early Oligocene Lece volcanic complex (Fig. 4-2), the Lower Complex overlies the eastern part of the Veles series along a contact previously interpreted as a west-vergent brittle thrust (Vukanović et al. 1977), or a ductile shear zone (Stefan M. Schmid, personal communication, September 2014). The Jurassic ophiolites of Eastern Vardar together with the Upper Cretaceous flysch of the Sava Zone (Vukanović et al. 1977; Pavić et al. 1983; Karamata and Krstić 1996), divide the Veles series into eastern and western parts (Fig. 4-2). The Eastern Veles series (EVS) is composed largely of a Lower Palaeozoic sedimentary sequence and Early

---

Figure 4-2. Tectonic map of the study area with the position of the analysed samples (after Basic geological maps of SFR Yugoslavia 1:100 0000 and Geological maps of Bulgaria 1:100 000 and 1:50 000).

Ordovician meta-granites (Pavlović 1977; Chapter 2), with a minor extent of Triassic sedimentary cover (Pavić et al. 1983). These rocks underwent amphibolitic facies metamorphism prior to a post-Triassic intensive retrogression to greenschist facies (Dimitrijević 1997). In contrast, greenschist facies Devonian to Triassic meta-sediments constitute the majority of the Western Veles series (Pavić et al. 1983; Grubić and Ercegovac 2002). The Veles series was traditionally considered as part of the Circum-Rhodope belt (Zagorchev and Milovanović 2006; Schmid et al. 2008), or ”Internal Vardar zone” (Dimitrijević and Drakulić 1958; Robertson et al. 2009). This study involves only the lower-Palaeozoic-dominated EVS, that was recently attributed to the Palaeozoic Galatian supra-terrane together with the SMM (Chapter 2).

During the late Early Cretaceous, the Vlasina Unit was thrust to the east onto the Struma Unit along a system of east- to northeast-vergent thrusts (Petković 1930; Mihailescu et al. 1967; Petrović 1969; Zagorchev and Ruseva 1982; Zagorchev 1984b; Lilov and Zagorchev 1993; Kounov et al. 2010). The Struma Unit consists of basement represented by variably deformed Ediacaran to early Cambrian continent- and ocean-derived rocks (Kounov et al. 2012), unconformably overlain by a Permian to Lower Cretaceous sedimentary cover (Zagorchev 1981). The Osogovo-Lisets complex, situated southeast of the study area, represents an extensional dome exhumed from below the Struma Unit during the middle Eocene to the Oligocene (Kounov et al. 2004). It consists of micaschists, gneisses, amphibolites and quartzites (Dimitrova 1964). The magmatic rocks of the Osogovo-Lisets complex and the basement of Struma Unit were derived from the same calc-alkaline magma source associated with the magmatic-arc complex formed during the Ediacaran to early Cambrian times (Kounov et al. 2012). These rocks have experienced lower amphibolite facies metamorphism during the early Late Cretaceous compressional event (Kounov et al. 2010).

The oldest undeformed and non-metamorphosed rocks in the study area are the Upper Cretaceous sediments (Santonian to Lower Maastrichtian; 86–70 Ma, Fig. 4-2). Deposition in a relatively shallow basin began with terrigenous sediments, followed by clastic limestones, marls and marly limestones, ending with micritic and biogenic limestones, and finally conglomerates (Petrović et al. 1973).

Sedimentation in the Palaeogene began with terrigenous to carbonate continental deposits of middle Eocene age (Petrović et al. 1973; Vukanović et al. 1973; Anđelković and Anđelković 1995), followed by turbidites of the Upper Eocene (Vukanović et al. 1977; Dimitrijević and Dimitrijević 1987), and marine to limnic sediments in the Oligocene (Vukanović et al. 1973; Vukanović et al. 1977). They are often intercalated with various volcaniclastic rocks or intruded by small dacitic or andesitic bodies and dykes that also intrude the basement. The largest magmatic body in the area is the Surdulica granodiorite (Fig. 4-2), previously reported to be emplaced at 30–25 Ma (Rb-Sr ages of biotite; Deleon 1969), or 34–28 Ma (K-Ar ages of micas and whole-rock samples; Simić 1997). The most prominent occurrence of Oligocene volcanism is the Lece andesitic complex (Vukanović et al. 1973), with a formation age of 32-28 Ma determined by K-Ar method (analysed material not reported; Karamata et al. 1992).

The Neogene sediments in the area are represented by middle Miocene to Pliocene clastic deposits and fresh-water marls (Vukanović et al. 1973; Vukanović et al. 1977). These sediments are intercalated with dacitic and andesitic volcanoclastic rocks (Vukanović et al. 1977).

4.3 Analytical methods

Fission-track analysis and U–Pb age determinations were conducted according to the procedures described in Appendix 4-1. Results of the FT analyses and sampling locations are presented in Table 4-1 and Figure 4-3. All ages are central ages (Galbraith and Laslett 1993). Radial plots with single grain FT ages and the results of thermal modelling are provided in Appendix 4-2, while the detailed sample descriptions and results of the U–Pb geochronology are presented in Appendix 4-3. All errors are reported as 2σ unless stated otherwise. Mineral names are abbreviated after Whitney and Evans (2010).

4.4 Results

4.4.1 Fission-track analysis

4.4.1.1 The Lower Complex

The zircon FT (ZFT) ages from the Lower Complex are exclusively Cretaceous, ranging between 109±16 and 73±13 Ma (Table 4-1 and Fig. 4-3). Similarly, a vast majority of the apatite FT (AFT) ages from the Lower Complex are Late Cretaceous (97±21–73±13 Ma, Table 4-1 and Fig. 4-3). Exceptions are the two Cenozoic apatite FT ages from Sijarinska Banja paragneiss (59±15 Ma, SM310) and Vranjska Banja mylonite (39±10 Ma, SM437-1, Figs. 4-2 and 4-3). Relatively short mean track lengths of 13.7–11.0 µm with standard deviations (SD) between 2.2 and 0.9 µm were obtained from the apatites of the Lower Complex. The results of thermal modelling reveal rapid cooling through zircon and apatite partial annealing zones (PAZ) during the late Early- to early Late Cretaceous (ca. 110 - ca. 90 Ma), followed by gradual cooling, except for sample SM01 that shows reheating to temperatures up to ca. 80 °C between 35 and 25 Ma (Fig. 4-4a). Thermal models based on relatively low number of fission-track lengths (e.g. N=28 horizontal confined fission-track lengths from sample SM528-1; Appendix 4-2) show time-temperature paths similar to models based on high number of track-lengths (e.g. N=101 horizontal confined fission-track length from sample SM199-1; Appendix 4-2). Therefore, we consider that the former could be treated as reliable

---

Figure 4-3. (opposite page) Tectonic map of the study area with the results of the fission-track (FT) analysis and U–Pb geochronology. Numbers on green fields indicate the apatite FT ages, yellow numbers on red fields represent the zircon FT ages, yellow numbers on black correspond to $^{206}Pb/^{238}U$ zircon ages. For legend see Fig. 4-2. Cross-sections corresponding to traces AB, CD, EF and GH in Figure 4-7.

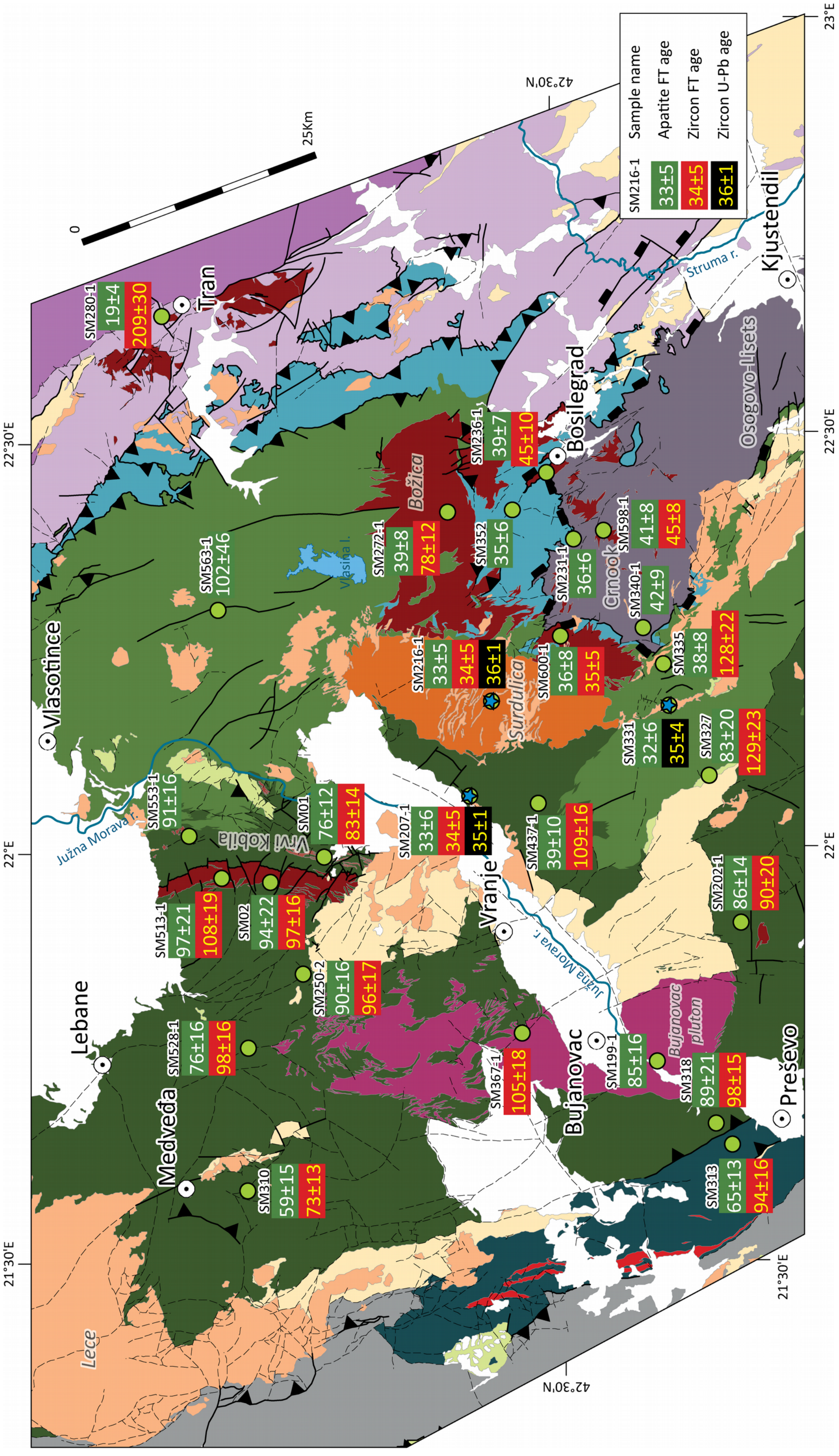
SM216-1 Sample name
33±5 Apatite FT age
34±5 Zircon FT age
36±1 Zircon U-Pb age
0
25Km
21°30'E
22°E
22°30'E
23°E
42°30'N
Vlasotince
Lebane
Medveđa
Tran
Vranje
Bujanovac
Preševo
Bosilegrad
Kjustendil
Lece
Vlasina l.
Južna Morava r.
Struma r.
Vrvi Kobila
Božica
Surdulica
Crnook
Osogovo-Lisets
Bujanovac pluton
SM280-1 19±4 209±30
SM563-1 102±46
SM272-1 39±8 78±12
SM236-1 39±7 45±10
SM352 35±6
SM231-1 36±6
SM598-1 41±8 45±8
SM340-1 42±9
SM216-1 33±5 34±5 36±1
SM600-1 36±8 35±5
SM335 38±8 128±22
SM331 32±6 35±4
SM327 83±20 129±23
SM553-1 91±16
SM01 76±12 83±14
SM207-1 33±6 34±5 35±1
SM437-1 39±10 109±16
SM202-1 86±14 90±20
SM513-1 97±21 108±19
SM02 94±22 97±16
SM250-2 90±16 96±17
SM528-1 76±16 98±16
SM367-1 105±18
SM199-1 85±16
SM318 89±21 98±15
SM310 59±15 73±13
SM313 65±13 94±16

Table 4-1. Results of the fission-track analysis

	Sample name	Min.	x* y*	Alt. [m]	Rock type	Location	Num. gr.	ρ_d(Nd) [·10^6 cm-^{2}]	ρ_s(Ns) [·10^6 cm^{-2}]	ρ_i(Ni) [·10^6 cm^{-2}]	P(χ^2) [%]	U. conc. [ppm]	Central age ±2σ [Ma]	MTL [µm]	±1σ [µm]	SD (N) [µm]	Dpar [µm]
	Lower Complex																
1	**SM01**	Ap	7581020	738	Mylonite	Ovča Strana	37	1,3084 (8213)	1,7852 (1862)	49,917 (5206)	95	45 ± 10	**76,3 ± 11,6**	11,02	0,16	1,64 (101)	1,23
		Zr	4729839				11	0,4201 (2407)	11,882 (906)	4,5422 (346)	36	343 ± 103	**82,6 ± 14**				
2	**SM02**	Ap	7579581	1296	Granite	Kukavica	19	1,2525 (8213)	0,4317 (177)	0,934 (382)	100	10 ± 3	**94,2 ± 21,6**	n/a	n/a	n/a (0)	1,49
		Zr	4735334				19	0,4075 (2407)	6,9719 (1127)	2,2085 (357)	100	172 ± 43	**96,6 ± 16**				
3	**SM199-1**	Ap	7561075	429	Granite	Borovac	21	1,4293 (8213)	1,0954 (402)	2,9946 (1099)	99	26 ± 7	**85,2 ± 15,6**	13,05	0,14	1,37 (101)	1,17
			4697110														
4	**SM202-1**	Ap	7574539	534	Gneiss	Prohor Pčinjski	20	1,4758 (8213)	2,4773 (763)	6,9448 (2139)	100	53 ± 15	**85,8 ± 14**	12,09	0,17	1,75 (101)	1,26
		Zr	4688527				7	0,4129 (2407)	13,2892 (381)	4,572 (131)	100	355 ± 85	**90,2 ± 20,8**				
5	**SM250-2**	Ap	7569098	485	Ms-Bt gneiss	Golemo Selo	20	1,2618 (8213)	1,6451 (686)	3,7506 (1564)	99	35 ± 6	**90,1 ± 15,2**	11,99	n/a	n/a (1)	1,5
		Zr	4732307				20	0,3967 (2407)	10,7746 (861)	3,3538 (268)	100	271 ± 60	**95,7 ± 17,2**				
6	**SM528-1**	Ap	7562085	477	Granite	Šumanska Reka	23	1,4424 (7998)	1,0439 (238)	3,2224 (734)	100	28 ± 15	**76,2 ± 15,6**	12,12	0,42	2,22 (28)	1,41
		Zr	4738543				20	0,4594 (2821)	10,8773 (982)	3,8214 (345)	100	262 ± 42	**98,2 ± 16,4**				
7	**SM513-1**	Ap	7579303	964	Granite	Brobinjak	20	1,4586 (7998)	0,7525 (225)	1,8429 (551)	100	15 ± 10	**96,9 ± 20,6**	12,25	0,74	1,66 (5)	1,15
		Zr	4740640				13	0,4633 (2821)	16,375 (889)	5,2809 (286)	100	362 ± 40	**107,8 ± 18,8**				
8	**SM553-1**	Ap	7583439	476	Gneiss	Slatinska Reka	20	1,41 (7998)	1,5824 (413)	3,9847 (1040)	95	34 ± 23	**91,2 ± 16,6**	13,47	0,62	0,88 (2)	1,65
			4744329														
9	**SM318**	Ap	7553970	652	Gneiss	Bukovac	21	1,3452 (7998)	0,7301 (165)	1,8009 (407)	100	16 ± 7	**88,8 ± 20,6**	13,18	n/a	n/a (1)	1,24
		Zr	4690418				20	0,4868 (2821)	13,1412 (1491)	4,8828 (554)	100	335 ± 70	**98,4 ± 14,6**				
10	**SM310**	Ap	7548389	416	Bt gneiss	Sijarinska Banja	20	1,1231 (6652)	7,091 (117)	2,2182 (366)	99	23 ± 8	**58,6 ± 15**	13,65	0,21	1,08 (26)	1,25
		Zr	4738347				18	0.4946 (2821)	8,6594 (655)	4,392 (332)	96	286 ± 123	**73,4 ± 12,8**				
11	**SM367-1**		7564110	672	Gneiss	Vrtogoš											
		Zr	4710641				20	0,4711 (2821)	8,4684 (904)	2,8571 (305)	99	198 ± 65	**104,8 ± 18**				
12	**SM437-1**	Ap	7586720	483	Mylonite	Vranjska Banja	20	0,9306 (6652)	0,444 (103)	1,7219 (399)	45	20 ± 12	**39,2 ± 10,2**	n/a	n/a	n/a (0)	1,47
		Zr	4709077				20	0,4672 (2821)	15,159 (1535)	4,8983 (496)	37	324 ± 100	**108,5 ± 16,4**				

Table 4-1. continued

	Sample name	Min.	x* y*	Alt. [m]	Rock type	Location	Num. gr.	ρ_d(Nd) [$\cdot 10^6$ cm-^{2}]	ρ_s(Ns) [$\cdot 10^6$ cm^{-2}]	ρ_i(Ni) [$\cdot 10^6$ cm^{-2}]	P(χ^2) [%]	U. conc. [ppm]	Central age ±2σ [Ma]	MTL [µm]	±1σ [µm]	SD (N) [µm]	Dpar [µm]
Vlasina Unit (undifferentiated)																	
13	**SM272-1**	Ap	7615854	1075	Gneiss	Božica	20	1,2805 (8213)	0,5767 (248)	3,0767 (1323)	65	27 ± 12	**39,3 ± 7,8**	14,5	0,68	0,96 (2)	1,34
		Zr	4718033				21	0,435 (2407)	10,1772 (1074)	4,1058 (433)	92	309 ± 102	**77,6 ± 12,4**				
14	**SM352**	Ap	7615948	352	Gabbro	Donja Lisina	20	1,3921 (8213)	0,7524 (635)	4,8863 (4124)	88	42 ± 11	**35,1 ± 5,8**	13,44	0,13	1,3 (101)	1,29
			4711742														
15	**SM563-1**	Ap	7605886	1073	Ms schist	Crna Trava	9	1,3938 (7998)	0,4571 (32)	1,0156 (71)	100	8 ± 2	**102,1 ± 45,8**	12,54	n/a	n/a (1)	1,4
			4741362														
16	**SM600-1**	Ap	7604563	1091	Gneiss	Gornja Ljubata	20	1,3614 (7998)	0,8596 (245)	5,3298 (1519)	62	45 ± 19	**35,9 ± 7,2**	14,21	0,13	1,1 (70)	1,43
		Zr	4706769				20	0,4555 (2821)	6,6654 (679)	6,5083 (663)	100	519 ± 192	**35,2 ± 5,4**				
17	**SM335**	Ap	7601503	947	Gneiss	Radovnica	20	1,0268 (6652)	0,5864 (173)	2,5763 (760)	94	30 ± 11	**38,2 ± 8,4**	n/a	n/a	n/a (0)	1,23
		Zr	4697381				20	0,479 (2821)	11,6301 (1128)	3,2581 (316)	100	221 ± 60	**128,1 ± 21,6**				
Eastern Veles series																	
18	**SM313**	Ap	7553564	588	Gneiss	Bukovac	20	1,1039 (6652)	1,2029 (249)	3,3188 (687)	98	35 ± 20	**65,3 ± 13,4**	13,01	0,23	1,37 (36)	1,25
		Zr	4689510				20	0,4907 (2821)	5,2803 (829)	2,0764 (326)	96	136 ± 46	**93,7 ± 16**				
Crnook dome																	
19	**SM231-1**	Ap	7612988	943	Gabbro	Donja Ljubata	32	1,2339 (8213)	0,7835 (1140)	4,4119 (6419)	35	45 ± 15	**35,8 ± 5,6**	12,76	0,36	2,05 (32)	1,94
			4705575														
20	**SM236-1**	Ap	7618183	875	Granite	Bosilegrad	20	1,4851 (8213)	1,6497 (518)	10,1592 (3190)	100	82 ± 18	**39,4 ± 6,6**	12,33	0,18	1,76 (101)	1,4
		Zr	4710189				8	0,4021 (2407)	7,2131 (264)	4,9036 (179)	99	387 ± 101	**44,6 ± 10**				
21	**SM598-1**	Ap	7613884	1080	Gneiss	Crnoštica	20	1,3776 (7998)	0,8826 (263)	4,9027 (1461)	93	41 ± 9	**40,5 ± 7,8**	14,68	0,16	1,04 (44)	1,37
		Zr	4702724				20	0,4496 (2821)	6,9527 (598)	5,2087 (448)	100	371 ± 104	**45,2 ± 7,6**				
22	**SM340-1**	Ap	7603673	1020	Pegmatite	Crven Grad	20	1,0076 (6652)	0,6182 (170)	2,4327 (669)	100	28 ± 10	**41,9 ± 9,4**	n/a	n/a	n/a (0)	1,35
			4698527														
Palaeogene magmatics																	
24	**SM207-1**	Ap	7587130	541	Dacite	Korbevac	40	1,3363 (8213)	0,2714 (368)	1,7842 (2419)	94	16 ± 4	**33,2 ± 6**	14,59	0,69	1,38 (4)	2,05
		Zr	4716163				20	0,4219 (2407)	9,4416 (766)	8,8993 (722)	100	667 ± 207	**33,8 ± 5,2**				

Table 4-1. continued

	Sample name	Min.	x* y*	Alt. [m]	Rock type	Location	Num. gr.	ρ_d(Nd) [$\cdot10^6$ cm-^{2}]	ρ_s(Ns) [$\cdot10^6$ cm^{-2}]	ρ_i(Ni) [$\cdot10^6$ cm^{-2}]	P(χ^2) [%]	U. conc. [ppm]	Central age ±2σ [Ma]	MTL [μm]	±1σ [μm]	SD (N) [μm]	Dpar [μm]
	Palaeogene magmatics (continued)																
25	**SM216-1**	Ap	7596862	1235	Granodiorite	Kriva Feja	20	1,395 (7905)	0,5023 (548)	3,5087 (3828)	59	29 ± 7	**32,7 ± 5,4**	13,65	0,2	1,45 (52)	1,29
		Zr	4714069				21	0,4273 (2407)	12,5186 (1176)	11,9438 (1122)	99	897 ± 179	**33,8 ± 4,8**				
26	**SM331**	Ap	7596166	856	Dacite	Stajevac	20	1,3549 (8213)	0,2948 (326)	2,0723 (2292)	100	18 ± 3	**31,5 ± 5,8**	13,67	n/a	n/a (1)	2,14
			4696054														
	Cretaceous sandstone																
27	**SM327**	Ap	7596166	856	Sandstone	Trgovište	21	1,0557 (6652)	0,497 (165)	1,0258 (340)	99	12 ± 5	**83,3 ± 19,8**	14,6	0,48	1,79 (14)	2,56
		Zr	4696054				20	0,4829 (2821)	11,8439 (932)	3,3295 (262)	92	261 ± 78	**128,7 ± 23**				
	Struma Unit (undifferentiated)																
28	**SM280-1**	Ap	7635240	913	Gabbrodiorite	Tran	20	1,1809 (6652)	0,6676 (231)	6,8382 (2366)	92	68 ± 14	**18,9 ± 3,8**	14,74	0,26	1,53 (36)	1,67
		Zr	4746277				21	0,5044 (2821)	16,6582 (2957)	2,997 (532)	100	194 ± 45	**208,7 ± 30,2**				

*Coordinates in Gauß-Krüger system used in SFR-Yugoslavian Basic Geological 1:100 000 maps.

All ages are central ages (Galbraith, 1981). $\lambda D = 1.55125 \times 10^{-10}$. A geometry factor of 0.5 was used.

The ζ values of 327.97±22.81 yr·cm² for CN5/apatite and 151.3±7.85 for yr·cm² CN1/zircon were used (analyst Milorad Antić).

P(χ^2) is the probability of obtaining χ^2 values for ν degrees of freedom where ν is the number of crystals -1.

The ρ_d, ρ_s and ρ_i values represent the standard, sample spontaneous and induced track densities, respectively, while N_d, N_s and N_i represent the number of corresponding measurements.

The Dpar value represents the diameter of etch pits.

Abbreviations: MTL – mean track length; SD – standard deviation.

sources of information, especially in cases with relatively simple thermal histories (Rahn and Seward 2000).

4.4.1.2 Vlasina Unit

Only three zircon samples from the Vlasina Unit were successfully analysed, yielding Cretaceous (128±22 and 78±12 Ma), and late Eocene (35±5 Ma), ages (Table 4-1 and Fig. 4-3). Five samples from the Vlasina Unit yielded apatites in sufficient quantity and quality for FT analysis. Four of these samples yielded late Eocene AFT ages (39±8–35±6 Ma) with relatively long mean track lengths (14.5–13.4 µm) and standard deviations between 1.3 and 1.0 µm (Table 4-1 and Fig. 4-3). A single Cretaceous apatite age of 102±46 Ma in Vlasina Unit was obtained from only 9 apatite grains recovered from the Crna Trava muscovite-schist (SM563-1, Figs. 4-2 and 4-3). Thermal models of samples from the Vlasina Unit reveal rapid cooling in late Eocene to early Oligocene (ca. 42 to ca. 30 Ma; Fig. 4-4b).

4.4.1.3 Crnook dome

Analysis of two zircon samples from the Crnook dome yielded middle Eocene ages (45±8 and 45±10 Ma). Apatite ages from the Crnook dome range within middle to late Eocene (42±9–36±6 Ma; Table 4-1 and Fig. 4-3). Relatively short track lengths were measured in the two younger apatite samples (12.8±2.0 µm and 12.3±1.8 µm for SM231-1 and SM236-1 respectively, Table 4-1), while substantially longer tracks (14.7±1.04 µm) were measured in sample SM598-1 with an age of 41±8 Ma (Table 4-1). Results of thermal modelling of samples from the Crnook dome reveal rapid cooling through apatite and zircon PAZ during the early Eocene (ca. 48 to ca. 42 Ma; Fig. 4-4c).

4.4.1.4 Eastern Veles series

An orthogneiss from the footwall of a ductile shear zone north of Preševo (SM313; Fig. 4-2) yielded a zircon age of 94±16 Ma and an apatite age of 65±13 Ma, with track lengths of 13.0 ± 0.2 µm (Table 4-1 and Fig. 4-3). Thermal model based on 36 horizontal confined fission-track lengths shows relatively slow cooling during the Late Cretaceous and Paleocene, followed by rapid cooling during late Eocene (sample SM313; Appendix 4-2).

4.4.1.5 Struma Unit

A single sample was taken from the gabbro-diorite near Tran (SM280-1, Fig. 4-2). Zircons yielded a Late Triassic central age of 209±30 Ma, and apatites an early Miocene age of 19±4 Ma (Table 4-1 and Fig. 4-3) with track lengths of 14.7±0.3 µm. Thermal model based on 36 horizontal confined fission-track lengths from sample SM280-1 shows very rapid cooling in the lower Miocene (Appendix 4-2).

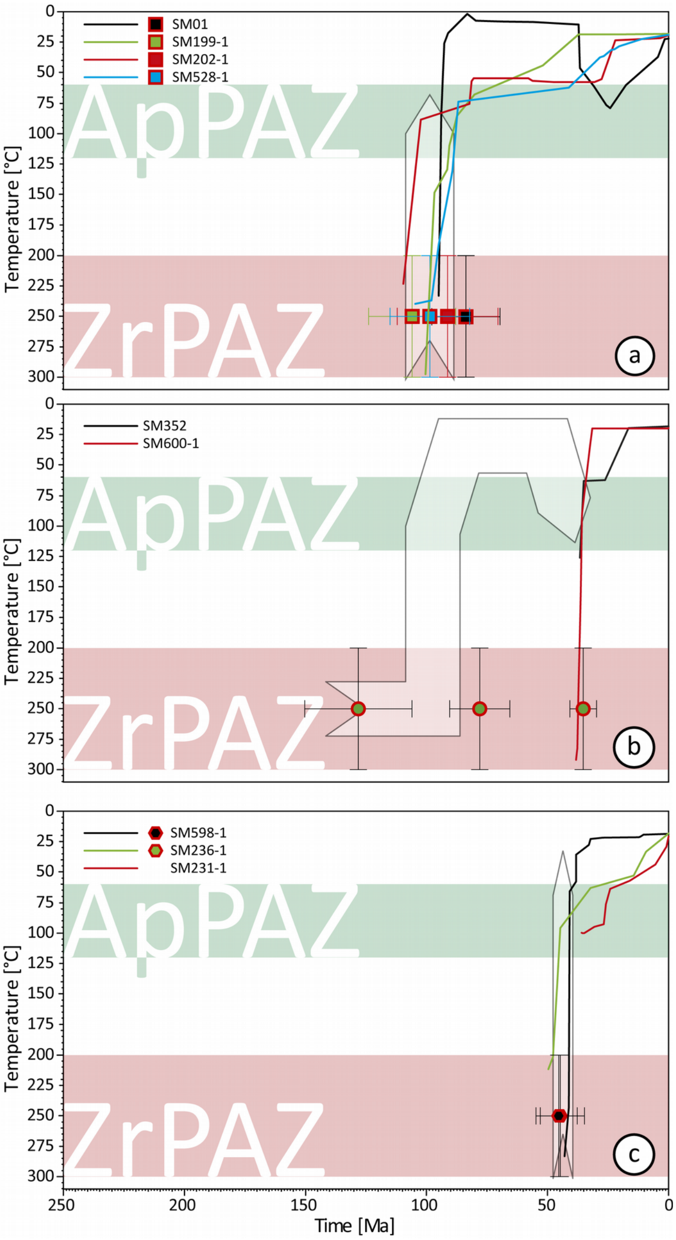

Figure 4-4. Thermal modelling results of samples from (a) the Lower Complex (arrow corresponds to a major cooling event); (b) the Vlasina Unit (arrow indicates suggested thermal path prior to complete resetting of the apatite AFT system); (c) the Crnook dome (arrow corresponds to a major cooling event). Areas designated as ApPAZ and ZrPAZ correspond to partial annealing zones of apatite and zircon, respectively. Thick coloured lines represent the best fit time-temperature paths obtained by the modelling. For detailed modelling results of individual samples see Appendix 4-2.

4.4.1.6 Upper Cretaceous sandstone

A single sedimentary sample was taken from the Upper Cretaceous sandstone (ca. 89–ca. 80 Ma; Babović et al. 1977) outcropping in the south of the study area (SM327; Fig. 4-2). Zircons yielded age of 129±23 Ma (Table 4-1 and Fig. 4-3) and the apatite age is 83±20 Ma, with relatively long track lengths (14.6±0.48 μm). This apatite age overlaps the stratigraphic age of the sampled sandstone, while the zircon FT age is older. The distribution of single grain FT ages of both apatites and zircons is independent of approximate U content and Dpar (Appendix 4-2), and both passed the $P\chi^2$ test (>5%; Table 4-1). Hence both ages separately represent single detrital populations (Table 4-1).

4.4.1.7 Palaeogene magmatic rocks

A single sample of a Palaeogene pluton (SM216-1; Surdulica granodiorite), and two samples of volcanic rocks (SM207-1 and SM331) were analysed. Two zircon samples yielded identical ages of 34±5 Ma (Table 4-1 and Fig. 4-3). All apatite ages are within the range of 33±6 to 32±6 Ma (Table 4-1 and Fig. 4-3) all with relatively long track lengths (13.7 and 14.6 μm). A thermal model based on 52 horizontal confined fission-track lengths from sample SM216-1 shows a very rapid cooling during late Eocene, followed by a period of relatively slower cooling (Appendix 4-2).

4.4.2 Results of U–Pb geochronology

Three samples of Palaeogene igneous rocks were analysed (Fig. 4-2), in order to test the previously reported emplacement ages of the Surdulica granodiorite (30–25 Ma; Deleon 1969; Simić 1997) and the felsic volcanic bodies of 39–22 Ma (Simić 1997). A zircon age of 36±1 Ma was determined by LA-ICPMS analyses for the Surdulica granodiorite (SM216-1; Fig. 4-5a), and 35±1 and 35±4 Ma for volcanic samples (SM207-1 and SM331 respectively; Fig. 4-5b and c; Appendix 4-3).

4.5 Discussion

4.5.1 Early Cretaceous “Austrian” compression

The east- to northeastward thrusting of the Vlasina Unit onto the Struma Unit (Petković 1930; Petrović 1969; Zagorchev and Ruseva 1982; Zagorchev 1984b) was related to the Early Cretaceous tectonic phase reported throughout the Carpatho-Balkan region of southeastern Europe (locally referred to as “Austrian” compression; Fig. 4-6b). The sedimentation within the Niš-Troyan foreland basin (Nachev 1974; Fig. 4-6a) had ended by the Valangian (140-134 Ma; age of the oldest sediments involved in the thrusting) marking the maximum age of the onset of thrusting in the area (e.g. Kounov et al. 2010). In the South Carpathians of Serbia and Romania, and the Balkanides in Bulgaria, Cretaceous sedimentation lasted until the Aptian (125-112 Ma; e.g. Gocev 1982; Banjac 2004; Iancu et al. 2005), suggesting a gradual northward temporal propagation of the onset of thrusting. Thermochronological data associated with the Early Cretaceous tectonic event in the Carpatho-Balkan orogen is generally within the range of 139-112 Ma (Lilov and Zagorchev 1993; Iancu et al. 2005; Kounov et al. 2010). This compressional event was probably caused by the ongoing subduction of the Mesozoic Tethys beneath the European margin (e.g. Schmid et al. 2008; Robertson et al. 2009; Ferrière et al. 2012), or more precisely by the possible collision of an Early-Middle Jurassic intra-oceanic arc (Kostopoulos et al. 2001; Brown and Robertson 2003; Zachariadis 2007; Šarić et al. 2009) with this margin (Fig. 4-6b).

The gneiss of the pre-Ordovician Vlasina in the south of the study area and Upper Cretaceous sandstones from a nearby basin have almost identical ZFT ages (respectively 128±22

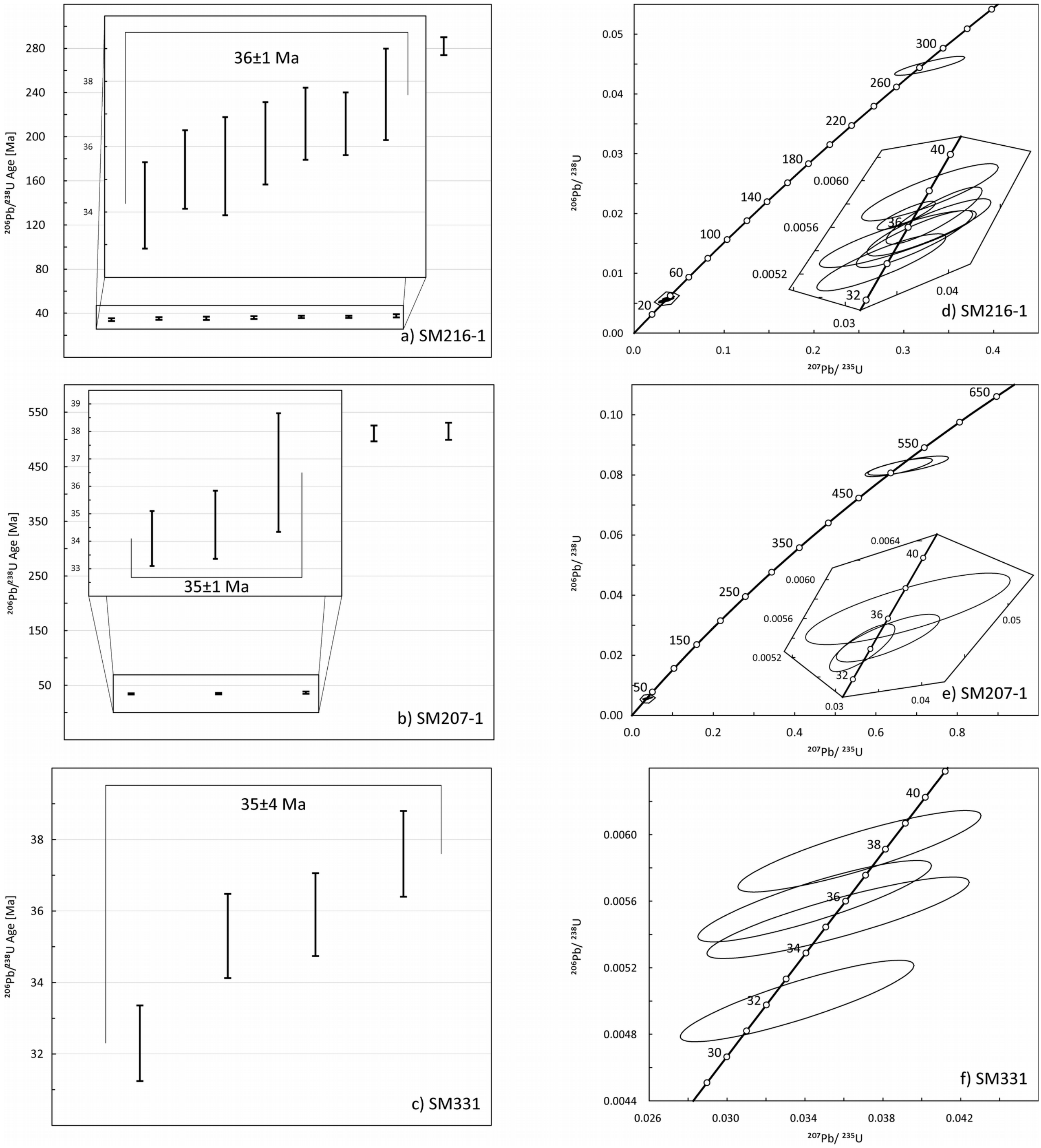

Figure 4-5. Sorted $^{206}Pb/^{238}U$ age-results for (a) Surdulica granodiorite (SM216-1), (b) Korbevac dacite (SM207-1), and (c) Stajevac dacite (SM331). Concordia diagrams for (d) Surdulica granodiorite (SM216-1), (e) Korbevac dacite (SM207-1), and (f) Stajevac dacite (SM331). Note that only concordant results were plotted. All errors are 2σ.

Ma, SM335 and 129±23 Ma, SM 327; Figs. 4-3, 4-7 and 4-8c) suggesting that the gneiss was the source area of the sandstones. This implies that the gneiss was outcropping during the Late Cretaceous. Possibly this gneiss was a part of the highest structural level of the nappe edifice at

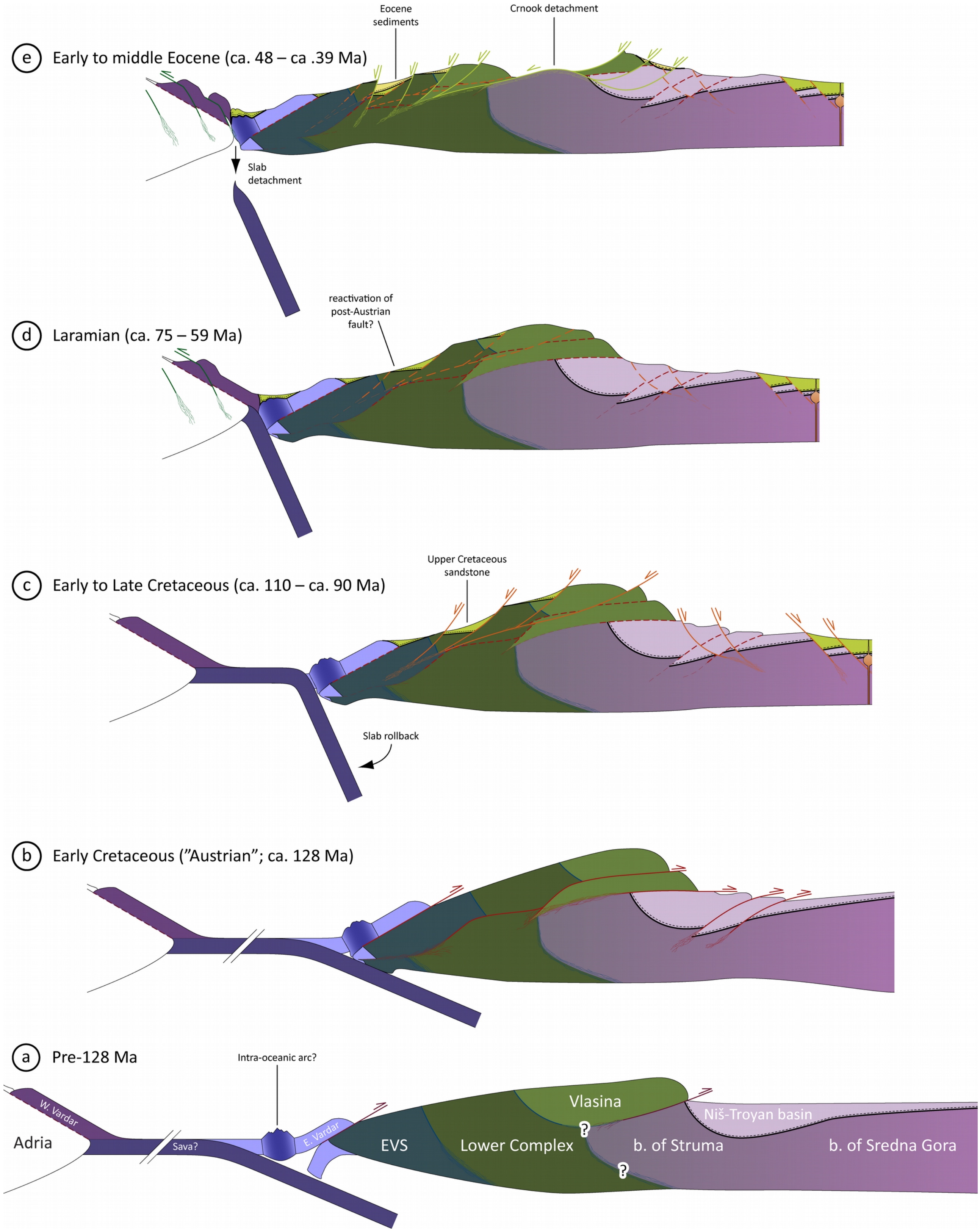

Figure 4-6. Unscaled sketch of the tectonic evolution of the SMM since the pre-Early Cretaceous until the early Miocene. Depicted time periods are related to obtained geo- and thermochronological results in this study and do not constrain the duration of presented tectonic and magmatic activities. In cross-section (a) the abbreviation "b." stands for "basement".

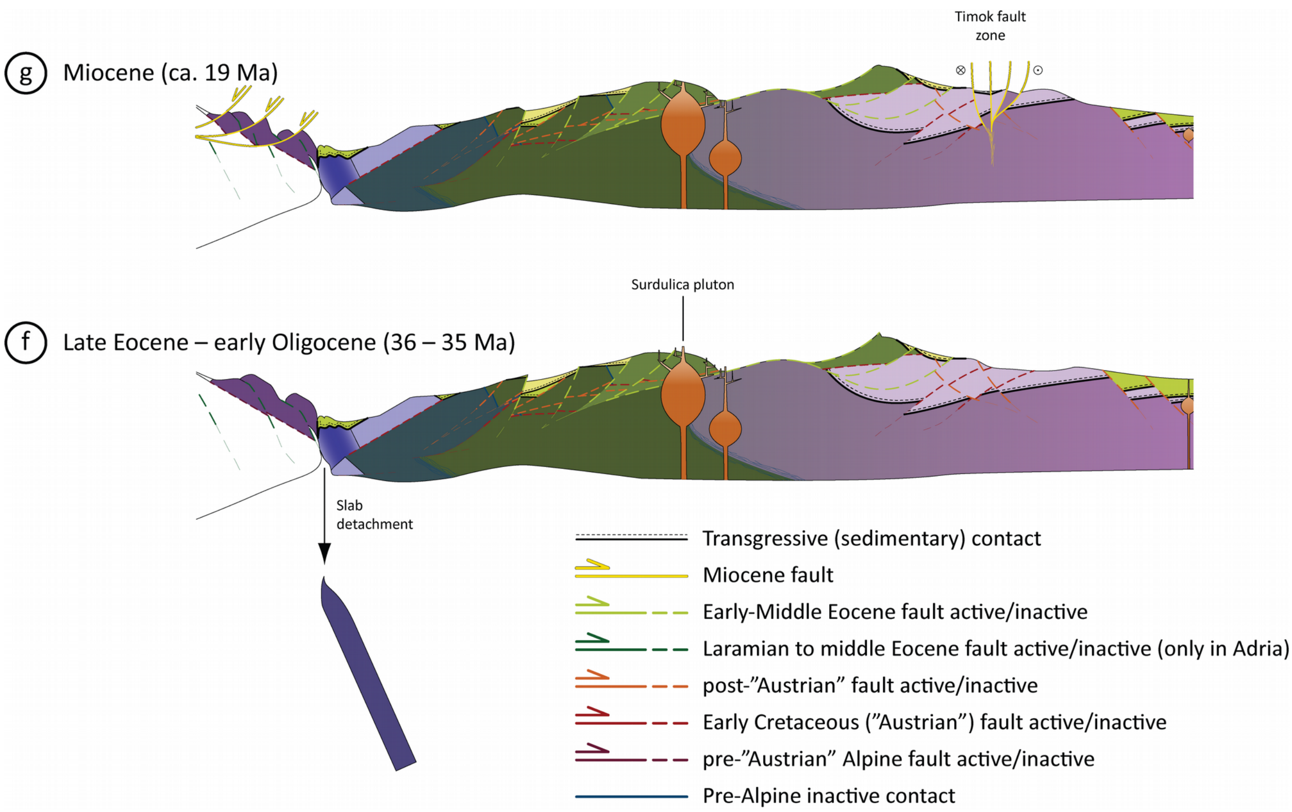

Figure 4-6 continued.

temperatures lower than 250 °C during the eastward thrusting of the Vlasina Unit (Fig. 4-6a).

A single ZFT age of 209±30 Ma was determined for the early Cambrian Tran gabbrodiorites (Dyulgerov et al. 2006), of the Struma Unit (SM280-1 in Table 4-1, Figs. 4-3 and 4-7). The upper Permian continental sediments deposited nearby (e.g. Protić 1966; Yanev et al. 2001), indicate that the Tran gabbrodiorite was already at the surface or near it at this time. Hence, the Late Triassic ZFT age does not represent the cooling age of these rocks and it is most probably a result of a later thermal overprint. Further evidence of partial resetting is the relatively wide spectrum of post-Variscan single grain ages (242—196 Ma) obtained from this sample (SM280-1; Appendix 4-2). These single-zircon FT ages reflect the reduction of age from initial cooling in the late Permian, towards the later thermal event that caused the partial resetting (residence within the PAZ, but below the closure temperature). Therefore, that younger thermal event cannot precede the youngest single-zircon age resulting from the partial resetting. Hence, the Early Jurassic single-zircon FT age

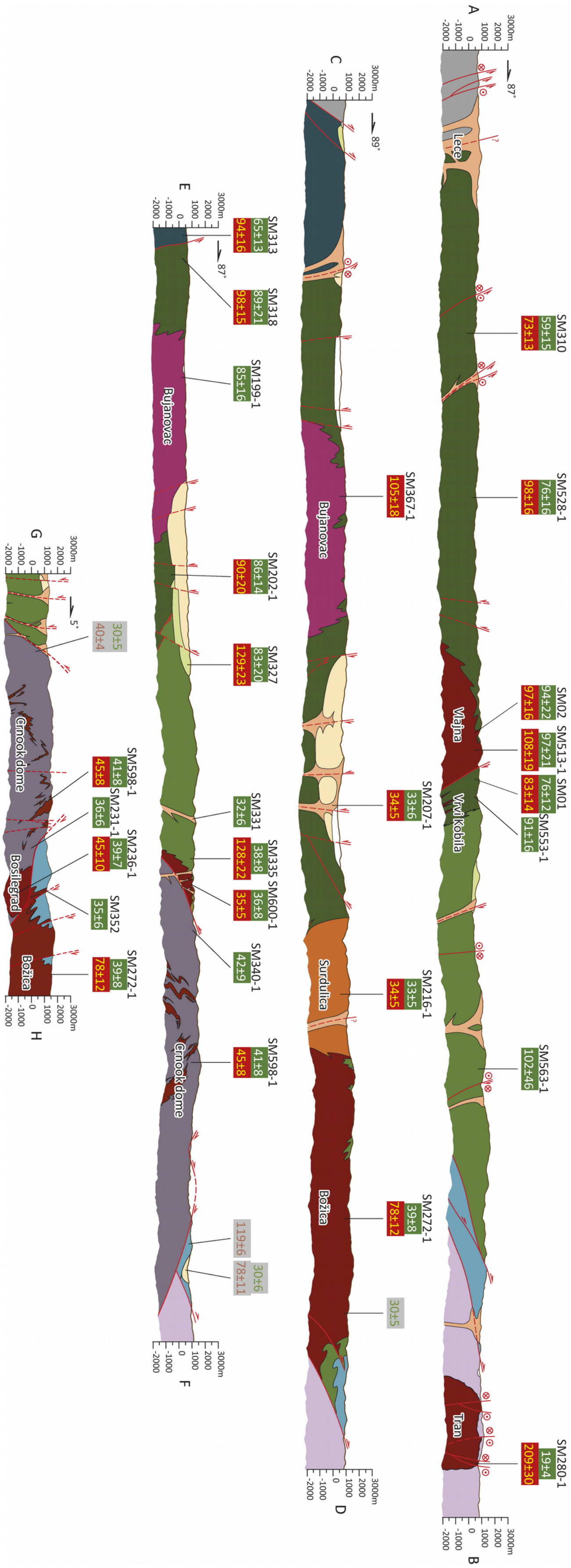

Figure 4-7. Cross-sections AB, CD, EF, GH corresponding to traces in Figure 4-3. Numbers on green fields indicate apatite FT ages, yellow numbers on red fields represent the zircon FT ages, and numbers on grey correspond to previously published apatite and zircon FT data (Kounov et al. 2004; Kounov et al. 2010). For legend see Figure 4-2.

(196±45 Ma; Appendix 4-2) sets the maximum age of the overprinting thermal event. This thermal effect could be related to the Early Cretaceous thrusting of Vlasina onto the Struma Unit (Mihailescu et al. 1967; Petrović 1969; Zagorchev and Ruseva 1982; Lilov and Zagorchev 1993; Kounov et al. 2010), possibly raising the temperature in the footwall to more than 200 °C (i.e. within the range of zircon PAZ; Fig. 4-8a). Such a thermal overprint was already proposed for a group of samples with similar ZFT ages in the Struma Unit of southwestern Bulgaria (Kounov et al. 2010). Additionally, Palaeogene magmatism reported in the Tran area (Peytcheva et al. 2012) might have also affected the ZFT system. However, the first scenario is more probable as the Cenozoic magmatism in this area is represented by sub-volcanic dykes which are concentrated in an area at a considerable distance to the sampling location (ca. 10 km). Therefore, during the Cretaceous compression the Tran area must have been buried underneath the nappe, although its

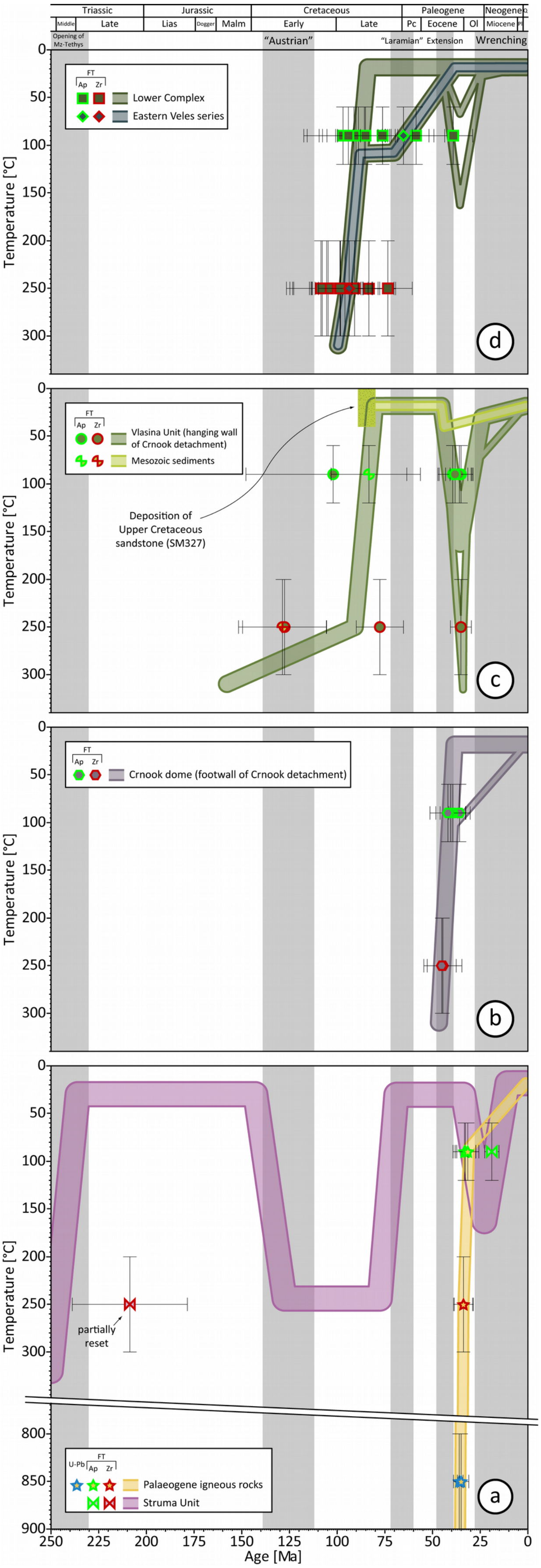

Figure 4-8. Time vs. temperature plot with generalised time-temperature paths of the main tectonic units in the study area. Gray fields represent major tectonic phases affecting the analysed rocks (see text). Abbreviations: Pc – Palaeocene, Ol – Oligocene, Pl – Pliocene, Q – Quaternary.

thickness was insufficient to cause temperatures higher than the effective closure for ZFT system in the footwall (250±50 °C; Tagami 2005).

4.5.2 Late Early to Late Cretaceous cooling event

Samples from the Lower Complex and the Vlasina Unit show predominantly late Early to Late Cretaceous ZFT ages (109±16–73±13 Ma, Figs. 4-3 and 4-7). Most of the apatites from the Lower Complex yielded ages in a similar range, i.e. between 97±21 and 76±12 Ma (Figs. 4-3 and 4-7). Nearly coeval AFT and ZFT ages suggest rapid cooling, which is confirmed by the results of the thermal modelling (Fig. 4-4a and Appendix 4-2). All models based on samples from the Lower Complex show rapid cooling between ca. 110 and ca. 90 Ma through zircon and apatite PAZ (Figs. 4-4a and 4-8d). However, several samples from the Lower Complex have experienced cooling only to temperatures within the apatite PAZ (e.g. SM199-1 and SM528-1; Fig. 4-4a). Thermal models for samples from the Vlasina Unit do not provide information regarding this event due to complete resetting of the apatite FT system during the Cenozoic (Fig. 4-4b). Most of these samples were collected in the southeastern part of the study area which was affected by the Cenozoic thermal overprint, while the samples from the rest of the Vlasina Unit have not yielded mineral concentrates of sufficient quantity and/or quality for a meaningful FT analysis (e.g. SM563-1; Table 4-1 and Fig. 4-2). However, based on the similarity of zircon cooling ages from the Vlasina Unit and the Lower Complex, it is evident that the Vlasina Unit experienced the same late Early- to Late Cretaceous exhumation-related rapid cooling (white arrow in Fig. 4-4b; Fig. 4-8c).

Additional proof of rapid exhumation of the central SMM in the late Early to Late Cretaceous is the concurrence between the FT age of detrital apatites from a sandstone sample (83±20 Ma; SM327; Fig. 4-3) and its Upper Cretaceous stratigraphic age (ca. 89–ca. 80 Ma; Babović et al. 1977). The similarity of these ages suggests rapid denudation in the source area (Figs.

4-9 and 4-8c). However, the exhumation might not have been the only cause of the rapid cooling, as the additional drop in temperature could be attributed to the thermal relaxation following the Early Cretaceous (Austrian) crustal thickening.

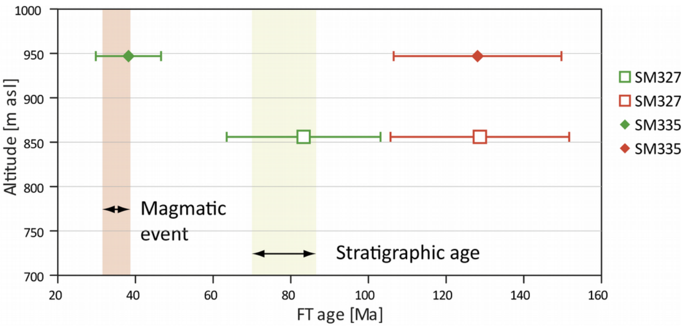

Figure 4-9. Zircon and apatite FT ages vs. altitude plot for the Radovnica gneiss (SM335) and Senonian sandstone southwest of Surdulica pluton (SM327; Fig. 4-3). Zircon FT ages are given in red, apatite FT ages in green. Open symbols are assigned to the detrital sample, and the filled symbols to the suggested source area.

The preponderance of late Early- to Late Cretaceous apatite and zircon FT ages was used to limit the age of activity along several major structures in the study area. The Vrvi Kobila shear zone outcropping in the northern part of the study area (Fig. 4-2), is regarded as an exemplary tectonic contact between the Vlasina Unit in the hanging wall, and the Lower Complex in the footwall position (Dimitrijević 1963; Vukanović et al. 1973; Krstić and Karamata 1992; Kräutner and Krstić 2002). The samples from both the hanging wall and the footwall of this structure show similar late Early- to Late Cretaceous zircon and apatite FT ages, excluding any possibility of significant vertical movement along the Vrvi Kobila shear zone during and since that time (Figs. 4-3 and 4-7). Generally, a regional exhumation causes the samples from the structurally lower position in a homogeneous block, to cool below the closure temperature of the FT system later than those situated structurally higher, resulting in the younger FT ages of the former. Therefore, slightly younger ages of samples from the hanging wall (SM553-1 and SM01, centre of cross-section AB in Fig. 4-7), are most probably a consequence of their lower altitudes compared to those of samples from the footwall (SM02 and SM513-1; Fig. 4-10).

Similar results were obtained across the contact of the Lower Complex with the Eastern Veles series north of Preševo (Fig. 4-3). Zircons from both sides of the west-vergent shear zone yielded similar cooling ages (98±15 and 94±16 Ma, Figs. 4-3 and 4-7), again excluding any significant differential movement along this structure since the Late Cretaceous (Fig. 4-8d).

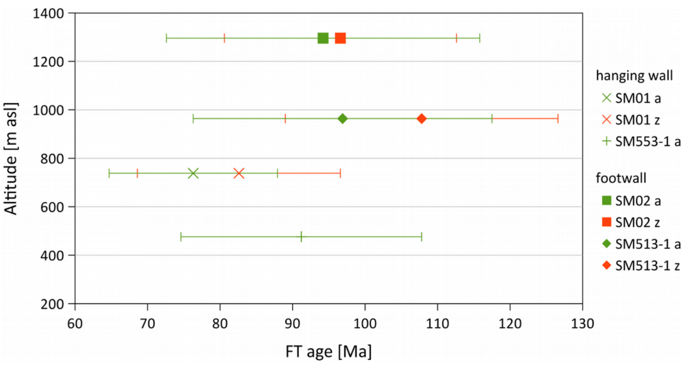

Figure 4-10. Zircon and apatite central FT age vs. altitude plot of samples from the Vrvi Kobila area. Zircon FT ages are given in red, apatite FT ages in green. Suffixes a and z to sample names designate apatite and zircon ages, respectively.

No major tectonic structures or deformation that could be unequivocally related to this stage of rapid cooling have been reported previously, nor have been recognised during our study. Also, the preserved Upper Cretaceous sediments do not give any further information on the tectonic evolution of the SMM during this period, mostly due to their limited extent. This cooling event could be tentatively associated with a tectonically induced denudation during an extensional event (Fig. 4-6c) caused by the gravitational collapse following the “Austrian” nappe-stacking (Schmid et al. 2008), or the westward rollback of the Eastern-Vardar slab (von Quadt et al. 2005; Kolb et al. 2013). Coeval extension was also documented in southwestern Bulgaria (Kounov et al. 2010), as well as along the Carpatho-Balkan orogen northeast of the study area accompanied by “Banatitic” calc-alkaline magmatism (Karamata et al. 1997; Berza et al. 1998; Banješević et al. 2002; von Quadt et al. 2005; Zimmerman et al. 2008; Kolb et al. 2013; Reiser 2015), exhumation of core complexes (Bojar et al. 1998), and formation of Gosau-type (Willingshofer et al. 1999; Ljubović-Obradović et al. 2011), and back-arc basins (Nachev 1978).

4.5.3 Late Cretaceous – early Palaeocene “Laramian” compression

Results of the thermal modelling of samples from the Lower Complex that remained within the apatite PAZ at the end of the late Early- to Late Cretaceous rapid exhumation, show relatively gradual cooling after ca. 75 Ma (SM199 and SM528; Fig. 4-4a). Similar slow cooling through the apatite PAZ may also be suggested for samples from the western part of the study area showing Late Cretaceous to early Palaeocene AFT ages (e.g. 65±13 Ma of SM313, 59±15 Ma of SM310; Figs. 4-3 and 4-7). Although statistically not entirely reliable due to relatively small number of confined fission-tracks (N=36), the thermal model of sample SM313 and the large spread of single grain AFT ages in the neighbouring sample SM318 (Appendix 4-2), could also be related to this slow cooling. Since the Late Cretaceous and early Palaeocene activity could not be recognised along any distinct structures in the study area, this gradual cooling might only be related to erosional denudation. However, minor reactivation of earlier structures in the westernmost parts of the SMM could not be completely excluded (Fig. 4-6d). General compressional tectonics during Maastrichtian to Danian time often referred to as the "Laramian" phase are reported in the Romanian South and East Carpathians (Bojar et al. 1998; Berza et al. 1998; Fügenschuh and Schmid 2005; Iancu et al. 2005; Schmid et al. 2008) and Sredna Gora Unit in central Bulgaria (Rieser et al. 2008). In the Serbian part of the Carpatho-Balkan orogen north of the study area, this compressional event resulted in folding and reverse faulting of Cretaceous sediments (Antonijević et al. 1970; Veselinović et al. 1970; Anđelković and Nikolić 1974). The Laramian phase is associated with the final closure of the Mesozoic Tethys and docking of Dinarides (Adria in Fig. 4-6) to the Eurasian margin (e.g. Karamata 2006; Schmid et al. 2008; Robertson et al. 2009; Kolb et al. 2013). The results of low-temperature thermochronology in the internal Hellenides were interpreted as a proof of Upper Cretaceous exhumation of the Vertiskos Unit (i.e. the continuation of SMM in Greece; Kydonakis et al. 2014).

4.5.4 Early to middle Eocene extension

AFT and ZFT ages from the Crnook dome generally suggest a middle Eocene cooling event (45±8–39±7 Ma, Figs. 4-3 and 4-7), with the exception of apatites from the Donja Ljubata gabbro which were fully reset during the late Eocene (36±6 Ma, SM231-1). Rapid cooling of rocks in the Crnook dome during the early to middle Eocene is confirmed by the thermal models (ca. 48–ca. 39 Ma, Figs. 4-4c and 4-8b). Our field observations at two locations show that the contact between the Crnook dome and Vlasina Unit represents a low-angle shear zone. North of Bosilegrad (Fig. 4-2) this shear zone separates the Ordovician schists of the post-Cambrian Vlasina in the hanging wall, from the early Cambrian Bosilegrad monzonite of the Crnook dome in the footwall. Vergence of folds in the footwall suggests normal slip along the fault plane (Figs. 4-3 and 4-11a). South to southeast of the Surdulica pluton a ca. 10 – ca. 20 cm thick fault gouge horizon marks the contact between the muscovite-gneiss of pre-Ordovician Vlasina in the hanging wall (Fig. 4-11b), and the brecciated biotite-gneiss of the Crnook dome in the footwall (Fig. 4-11c). This structure is referred to as the Crnook detachment, along which the Crnook dome was rapidly exhumed during the early to middle Eocene. The majority of zircons in the hanging wall represented by Vlasina Unit, show Cretaceous cooling ages (Figs. 4-3 and 4-7). Similar structures, lithologies and FT age pattern were reported in the Osogovo-Lisets complex in southwestern Bulgaria by Kounov et al. (2004). Thus, it becomes evident that the Crnook dome and Osogovo-Lisets complex represent a single unit with a common mode and age of exhumation, for which we now use the term the Crnook-Osogovo-Lisets extensional core complex (COL; Figs. 4-2 and 4-3).

This extensional phase is also associated with the formation of sedimentary basins in the hanging wall of the Crnook detachment (Figs. 4-3 and 4-7), containing upper Eocene turbidites (Petrović et al. 1973; Vukanović et al. 1977; Dimitrijević and Dimitrijević 1987; Anđelković and Anđelković 1995). These sediments filled the half-graben structure formed by rotation of blocks along listric faults in the hanging wall of the detachment (Fig. 4-6e). The activity along the Crnook detachment must have ceased prior to the late Eocene pulse of volcanism as undeformed dacitic bodies intrude the western extent of this structure (Figs. 4-3 and 4-7).

Extension in the SMM is coeval with the extension reported from the southern Balkan Peninsula (e.g. Gautier and Brun 1994; Jolivet et al. 1998; Burchfiel et al. 2000; Burchfiel et al. 2008; Burg 2012; Jolivet et al. 2013). Most notably, the exhumation of COL complex coincides with the early stages of extension and core complex formation in the Rhodope complex (e.g. Burg et al. 1996; Ricou et al. 1998; Bonev 2006; Brun and Sokoutis 2007; Jahn-Awe et al. 2012; Kounov et al. 2015). The extension in the Balkan Peninsula probably began in the middle to late Eocene (Burchfiel et al. 2000; Kounov et al. 2004; Brun and Sokoutis 2007) and was related to east- to northeastward (in present orientation) subduction that migrated from the Vardar

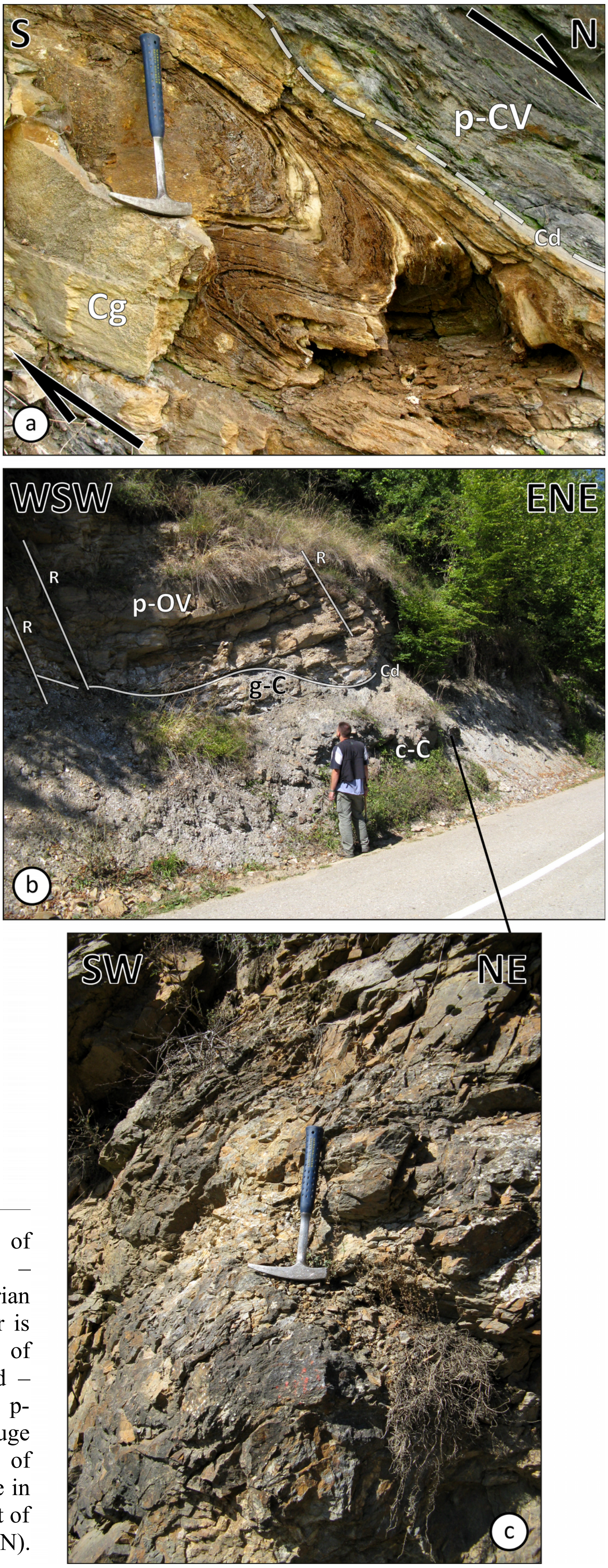

Figure 4-11. (a) Crnook detachment northwest of Bosilegrad (22°25'53.052"E, 42°31'51.549"N). Cd – Crnook detachment, p-CV – schists of the Post-Cambrian Vlasina, Cg – Crnook dome gneiss. Length of hammer is 363 mm; (b) Crnook detachment south to southeast of Surdulica pluton (22°14'2.172"E, 42°24'48.144"N). Cd – Crnook detachment, R – younger generation of faults, p-OV – Ms-gneiss of pre-Ordovician Vlasina, g-C – gouge horizon, c-C – cataclastically deformed Bt-gneiss of Crnook dome; (c) Cataclastic Bt-gneiss of Crnook dome in the footwall of the Crnook detachment south to southeast of Surdulica pluton (22°14'13.592"E, 42°24'59.136"N). Length of hammer is 363 mm.

zone in latest Mesozoic – early Cenozoic time, westward to its present position in the Hellenic trench. Southward migration of extensional faulting and basin formation, as well as periods of magmatic activity were related to progressive rollback of the subducted slab (Jolivet et al. 2003; Brun and Faccenna 2008; Forster and Lister 2009).

4.5.5 Late Eocene igneous activity

Previously reported relationship of volcanic rocks and the Surdulica pluton they intrude (e.g. Vasković and Tasić 1997; Simić 1997), was confirmed by results of U-Pb analyses obtained during this study, suggesting that the emplacement of the Surdulica granodiorite at 36±1 Ma, closely preceded the dacitic volcanism in the area (ca. 35 Ma; Figs. 4-3 and 4-5). Results of geochemical analysis of three samples from the central part of the Surdulica pluton (Appendix 4-3) are in accordance with a late- to post-collisional setting reported in previous studies (e.g. Vasković and Tasić 1997; Simić 1997). However, some variation in geochemical signature might be expected as Surdulica granodiorite was reported as a composite magmatic body (Vasković and Tasić 1997). Both the zircon and apatite FT ages from the Palaeogene igneous suites (34±5–32±6 Ma) overlap within analytical errors with the crystallisation ages of zircons from the same samples (Fig. 4-12), suggesting that these rocks were cooled within several million years after their emplacement and have not experienced any significant thermal overprint since (Fig. 4-8a). Nearly identical thermal history is evident from thermal modelling of sample SM280-1 (Appendix 4-2).

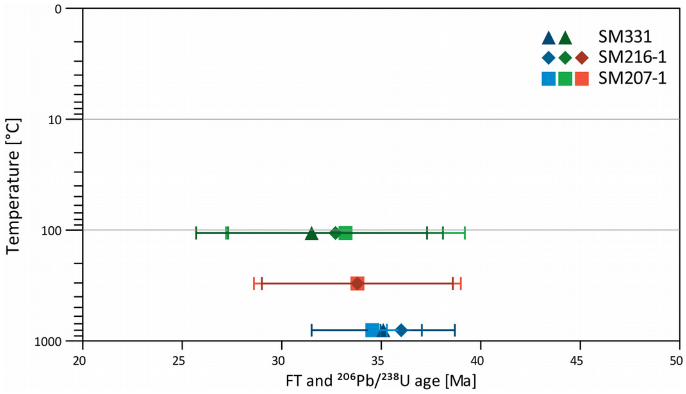

Figure 4-12. Zircon and apatite FT, and $^{206}Pb/^{238}U$ age vs. the “closure” temperatures of the corresponding methods for Palaeogene magmatic rocks. LA-ICP-MS U–Pb ages are given in blue, zircon FT ages in red, and apatite FT ages in green.

A number of samples from the host

rocks of the Palaeogene igneous bodies have been fully reset during this period of igneous activity. These samples are commonly situated in the vicinity of the Surdulica granodioritic pluton (Fig. 4-3), and the area surrounding and within the Crnook dome. The latter region is characterised by a high occurrence of small volcanic bodies, dykes and related hydrothermal ore mineralisations (e.g. Simić 1992; Simić 1996; Stanić et al. 1996; Stajević 1997). Thermal models of samples from the Vlasina Unit (Fig. 4-4b), and Crnook dome (SM231-1; Fig. 4-4c), suggest that the basement rocks had experienced relatively fast cooling after this thermal event. A less intensive thermal overprint in the late Eocene to early Oligocene was also revealed by the results of thermal modelling of apatites from several samples (e.g. SM01; Fig. 4-4a, and SM327; Fig. 4-8c and Appendix 4-2), that show reheating to conditions within the apatite PAZ most probably due to overall increase in thermal gradient during the pulses of magmatic and volcanic activity in their vicinity (Fig. 4-2).

Most of the samples from the affected areas reveal late Eocene AFT ages, while the zircons predominantly retain Cretaceous cooling ages (SM272-1, SM335, SM437-1, and SM272-1; Table 4-1 and Figs. 4-3 and 4-7), suggesting that these rocks reached temperatures higher than 120 °C, but lower than ca. 250 °C necessary to reset the zircon FT system (Appendix 4-1). Such a prominent thermal effect could have been caused by the voluminous Surdulica granodiorite emplaced at a relatively shallow depth (5-10 Km; Vasković and Tasić 1997) and a large number of smaller sub-volcanic bodies and dykes. The palaeothermal gradient is expected to be already elevated prior to this magmatic episode, due to attenuation of continental crust during the early to middle Eocene extension. Elevated thermal gradients during the late Eocene to early Oligocene have also been reported in the region southeast of the study area (Kounov et al. 2004).

The only late Eocene ZFT age (35±5 Ma; SM600-1) from the host-rock of the Palaeogene igneous bodies was determined for the Ediacaran Doganica metagranite (Chapter 2). This sample was taken ca. 1130 m away from the nearest outcrop of a late Eocene dacitic body, in an area with high occurrence of dykes and ore mineralisation (e.g. Stajević 1997; Fig. 4-2). Temperatures exceeding the ZFT closure temperature (250±50 °C; after Tagami 2005) at this location were most probably caused by the elevated thermal gradient during the emplacement of the nearby dacitic bodies and dykes. Late-magmatic hydrothermal flow evident from widespread ore mineralisation (Stajević 1997) could be indicative of prolonged period with high thermal gradient. Similar thermal resetting caused by the Palaeogene igneous activity was reported also for the Rb–Sr system in biotite of Early Triassic Igralishte granite in the Ograzhden block of southwestern Bulgaria (36±1 Ma; Zidarov et al. 2004; Peytcheva et al. 2009).

Prominent late- to post-collisional magmatism and similar Palaeogene ages are observed in a continuous belt along the Balkan Peninsula, stretching from southern Romania to eastern Greece (Harkovska et al. 1989; Marchev et al. 1998; Burchfiel et al. 2000; Perugini et al. 2004; Cvetković et al. 2004b; Cvetković et al. 2004a; Dumurdžanov et al. 2005; Marchev et al. 2005; Soldatos et al. 2008; Burchfiel et al. 2008; Grozdev 2011; Schefer et al. 2011; Peychev et al. 2012). Crustal delamination was proposed as a major cause for this regional event (Burg 2012; Marchev et al. 2013), as well as slab detachment (Fig. 4-6f; Perugini et al. 2004; Schefer et al. 2011).

4.5.6 Miocene cooling

A sample of the Tran gabbrodiorites from the Struma Unit yielded early Miocene AFT age (19±4 Ma; SM280-1 in Table 4-1, and Figs. 4-3 and 4-7). The relatively fast cooling of this sample through the partial annealing zone of apatite (120-60 °C; Appendix 4-2) was most probably related to activity along normal and/or strike-slip faults (e.g. Timok fault zone in Fig. 4-6g) in a transtensional setting (Kounov et al. 2011). Similar structures and mode of basin formation were also reported north of the study area (cf. Đoković and Marović 1989). The transtensional setting responsible for the early Miocene exhumation in Struma Unit is related to the wrenching of the

Carpatho-Balkanid orogen around the Moesian indenter since the late Oligocene, facilitating escape tectonics along the dextral strike-slip Timok fault zone (Burchfiel 1980; Bojar et al. 1998; Kräutner and Krstić 2002; Fügenschuh and Schmid 2005; Marović et al. 2007; Kounov et al. 2011).

4.6 Conclusions

The new results of thermo- and geochronological analyses reveal three main cooling stages along the central parts of the Serbo-Macedonian Massif:

- The late Early- to early Late Cretaceous rapid cooling (ca. 110–ca. 90 Ma), affected the SMM. This event was most probably related to the post-collisional extension following the Early Cretaceous compressional phase that affected the Carpatho-Balkanid orogen in southeastern Europe. Additionally, similar Late Cretaceous ages from both sides of the contacts between the Eastern Veles series and the Lower Complex, and the Lower Complex and the Vlasina Unit (Vrvi Kobila shear zone) exclude any possibility of major vertical displacement along these structures since that time.
- Early to middle Eocene rapid cooling (ca. 48–ca. 39 Ma) of rocks from the Crnook dome was most probably related to the crustal extension associated with the formation of the core complex exhumed along the system of low-angle detachments (i.e. Crnook detachment). Based on similarities in lithology, structures, age and mode of the exhumation, the Crnook dome is considered to be a continuation of the Osogovo-Lisets core complex (now termed the Crnook-Osogovo-Lisets complex).
- Relatively rapid late Eocene post-magmatic cooling (34–32 Ma), followed the emplacement of the Surdulica granodiorite (36±1 Ma) and subsequent hydrothermal and volcanic activity in the study area (ca. 35 Ma). The igneous activity was associated with late- to post-orogenic tectonic setting.

References

Anđelković M, Anđelković J (1995) Značaj Ilirske faze za geološki razvoj Moravida. Ann Géol Penins Balk 59:1–11.

Anđelković M, Nikolić P (1974) Veliki šarijaž u tektonskoj građi Istočne Srbije. Zapisnici SGD za 1973. g.

Antonijević I, Veselinović M, Đorđević M, et al (1970) Tumač za list Žagubica. Savezni Geološki Zavod, Belgrade

Babović M, Roglić Č, Avramović V, Marić S (1977) Tumač za list Trgovište sa Radomirom. Savezni Geološki Zavod, Belgrade

Balogh K, Svingor É, Cvetković V (1994) Ages and intensities of metamorphic processes in the Batočina area, Serbo-Macedonian massif. Acta Mineralogica-Petrographica XXXV:81–94.

Banjac N (2004) Stratigrafija Srbije i Crne Gore. Rudarsko-geološki fakultet, Belgrade

Banješević M, Cvetković V, Koželj D, et al (2002) The Timok magmatic complex and Ridanj-Krepoljin zone: geodynamical evolution. In: Jelenković R, Koželj D (eds)Copper Institute Bor, Bor Lake, pp 199–202

Berza T, Constantinescu E, Vlad Sl (1998) Upper Cretaceous Magmatic Series and Associated Mineralisation in the Carpathian – Balkan Orogen. Resour Geol 48:291–306. doi: 10.1111/j.1751-3928.1998.tb00026.x

Bojar A-V, Neubauer F, Fritz H (1998) Cretaceous to Cenozoic thermal evolution of the southwestern South Carpathians: evidence from fission-track thermochronology. Tectonophysics 297:229–249. doi: 10.1016/S0040-1951(98)00170-X

Bonev K, Ivanov Z, Ricou L-E (1995) Dénudation tectonique au toit du noyau métamorphique Rhodopien-macédonien: La faille normale ductile de Gabrov Dol (Bulgarie). Bull Soc Géol France 166:47–55.

Bonev N (2006) Cenozoic tectonic evolution of the eastern Rhodope massif (Bulgaria): Basement structure and kinematics of syn- to postcollisional extensional deformation. Geol Soc Am S 409:211–235. doi: 10.1130/2006.2409(12)

Brown SAM, Robertson AHF (2003) Sedimentary geology as a key to understanding the tectonic evolution of the Mesozoic–Early Tertiary Paikon Massif, Vardar suture zone, N Greece. Sediment Geol 160:179–212. doi: 10.1016/S0037-0738(02)00376-7

Brun J-P, Faccenna C (2008) Exhumation of high-pressure rocks driven by slab rollback. Earth Planet Sc Lett 272:1–7. doi: 10.1016/j.epsl.2008.02.038

Brun J-P, Sokoutis D (2007) Kinematics of the Southern Rhodope Core Complex (North Greece). Int J Earth Sci (Geol Rundsch) 96:1079–1099. doi: 10.1007/s00531-007-0174-2

Burchfiel BC (1980) Eastern European Alpine system and the Carpathian orocline as an example of collision tectonics. Tectonophysics 63:31–61. doi: 10.1016/0040-1951(80)90106-7

Burchfiel BC, King RW, Nakov R, et al (2008) Patterns of Cenozoic Extensional Tectonism in the South Balkan Extensional System. In: Husebye ES (ed) Earthquake Monitoring and Seismic Hazard Mitigation in Balkan Countries. Springer Netherlands, pp 3–18

Burchfiel CB, Nakov R, Tzankov T, Royden LH (2000) Cenozoic Extension in Bulgaria and Northern Greece: the Northern Part of the Aegean Extensional Regime. Geol Soc SP 173:325–352. doi: 10.1144/GSL.SP.2000.173.01.16

Burg J-P (2012) Rhodope: From Mesozoic convergence to Cenozoic extension. Review of petro-structural data in the geochronological frame. J Virtual Explor 42

Burg J-P, Ricou L-E, Ivano Z, et al (1996) Syn-metamorphic nappe complex in the Rhodope

Massif. Structure and kinematics. Terra Nova 8:6–15. doi: 10.1111/j.1365-3121.1996.tb00720.x

Cvetković V, Downes H, Prelević D, et al (2004a) Characteristics of the lithospheric mantle beneath East Serbia inferred from ultramafic xenoliths in Palaeogene basanites. Contrib Mineral Petrol 148:335–357. doi: 10.1007/s00410-004-0607-x

Cvetković V, Prelević D, Downes H, et al (2004b) Origin and geodynamic significance of Tertiary postcollisional basaltic magmatism in Serbia (central Balkan Peninsula). Lithos 73:161–186. doi: 10.1016/j.lithos.2003.12.004

Dabovski C, Boyanov I, Khrischev K, et al (2002) Structure and Alpine evolution of Bulgaria. Geologica Balcanica 32:9–15.

Deleon G (1969) Pregled rezultata određivanja apsolutne geološke starosti granitoidnih stena u Jugoslaviji. Radovi Instituta za geološko-rudarska istraživanja i ispitivanja nuklearnih i drugih mineralnih sirovina 6:165–180.

Dimitrijević MD (1957) Struktura kristalastih terena između Slišana i Preševa. Referati, predavanja, diskusije. Savez geoloških društava Jugoslavije, Sarajevo,

Dimitrijević MD (1997) Geology of Yugoslavia. Geological Institute GEMINI, Belgrade

Dimitrijević MD (1967) Some Problems of Crystalline Schists in the Serbo-Macedonian Massif. Reports. Serbian Geological Society, Belgrade, pp 59–67

Dimitrijević MD (1963) Sur l'âge du métamorphisme et des plissements dans la masse Serbo-macédonienne. Bulletin. Instytut Geologiczny, Warszawa, pp 339–347

Dimitrijević MD (1972) Variscijski metamorfizam u aksijalnom delu Balkanskog poluostrva (mogućnosti nove genetske interpretacije). Zapisnici SGD za 1971. godinu:115–124.

Dimitrijević MD, Drakulić N (1958) Kristalasti škriljci Jablanice. Zbornik radova RGF 6

Dimitrijević MN, Dimitrijević MD (1987) The Turbiditic Basins of Serbia. Serbian Academy of Science and Arts, Belgrade

Dimitrova E (1964) Petrologie des kristallinen Sockels des Osogovo Gebirges. Bulgarian Academy of Sciences Bulletin of the Geological Institute 13:99–110.

Đoković I, Marović M (1989) Sklop Niškog neogenog basena. Ann Géol Penins Balk 58:199–205.

Dumurdžanov N, Serafimovski T, Burchfiel BC (2005) Cenozoic tectonics of Macedonia and its relation to the South Balkan extensional regime. Geosphere 1:1–22. doi: 10.1130/GES00006.1

Dyulgerov M, Peytcheva I, von Quadt A, Nedyalkov R (2006) Source and age heterogeneities between the rocks of Lutzkan pluton. Proceedings. Bulgarian Geological Society, Sofia, pp 117–180

Ferrière J, Chanier F, Ditbanjong P (2012) The Hellenic ophiolites: eastward or westward obduction of the Maliac Ocean, a discussion. Int J Earth Sci (Geol Rundsch) 101:1559–1580. doi: 10.1007/s00531-012-0797-9

Forster M, Lister G (2009) Core-complex-related extension of the Aegean lithosphere initiated at the Eocene-Oligocene transition. J Geophys Res-Sol Ea 114:B02401. doi: 10.1029/2007JB005382

Fügenschuh B, Schmid SM (2005) Age and significance of core complex formation in a very curved orogen: Evidence from fission track studies in the South Carpathians (Romania). Tectonophysics 404:33–53. doi: 10.1016/j.tecto.2005.03.019

Galbraith RF (1981) On statistical models for fission track counts. J Int Ass Math Geol 13:471–478. doi: 10.1007/BF01034498

Galbraith RF, Laslett GM (1993) Statistical models for mixed fission track ages. Nucl Tracks Rad Meas 21:459–470. doi: 10.1016/1359-0189(93)90185-C

Gautier P, Brun J-P (1994) Crustal-scale geometry and kinematics of late-orogenic extension in the central Aegean (Cyclades and Ewia Island). Tectonophysics 238:399–424. doi: 10.1016/0040-1951(94)90066-3

Gocev PM (1982) On the problem of Alpine zoning, vergence and other features of nappes in Bulgaria and eastern part of the Balkan peninsula. In: Mahel M (ed) Alpine structural elements: Carpathian-Balkan-Caucasus-Pamir Orogene Zone. VEDA, Bratislava, pp 75–93

Grozdev V (2011) U-Pb zircon dating and zircon population analyses of the of the Paleogene. Proceedings. Bulgarian Geological Society, Sofia,

Grubić A, Đoković I, Marović M, Branković M (1999) Srpsko-Makedonska masa ne postoji. Vesnik 49:1–14.

Grubić A, Đoković I, Marović M, Branković M (2005) Problem tektonskog položaja kristalina Srpsko-Makedonske mase. Zapisnici SGD za 1998, 1999, 2000, 2001, 2002 i 2003. godinu:35–39.

Grubić A, Ercegovac M (2002) Age of the Veles "Schistes Lustres" Formation from the Vardar Ocean. Proceedings of XVII Congress of CBGA. VEDA, Bratislava, pp 66–68

Harkovska A, Yanev Y, Marchev P (1989) General features of the Paleogene orogenic magmatism in Bulgaria. Geologica Balcanica 19:37–72.

Himmerkus F, Reischmann T, Kostopoulos D (2009) Serbo-Macedonian revisited: A Silurian basement terrane from northern Gondwana in the Internal Hellenides, Greece. Tectonophysics 473:20–35. doi: 10.1016/j.tecto.2008.10.016

Himmerkus F, Reischmann T, Kostopoulos D (2006) Late Proterozoic and Silurian basement units within the Serbo-Macedonian Massif, northern Greece: the significance of terrane accretion in the Hellenides. Geol Soc SP 260:35–50. doi: 10.1144/GSL.SP.2006.260.01.03

Iancu V, Berza T, Seghedi A, et al (2005) Alpine polyphase tectono-metamorphic evolution of the South Carpathians: A new overview. Tectonophysics 410:337–365. doi: 10.1016/j.tecto.2004.12.038

Jahn-Awe S, Pleuger J, Frei D, et al (2012) Time constraints for low-angle shear zones in the Central Rhodopes (Bulgaria) and their significance for the exhumation of high-pressure rocks. Int J Earth Sci (Geol Rundsch) 101:1971–2004. doi: 10.1007/s00531-012-0764-5

Jolivet L, Faccenna C, Goffé B, et al (1998) Midcrustal shear zones in postorogenic extension: Example from the northern Tyrrhenian Sea. J Geophys Res-Sol Ea 103:12123–12160. doi: 10.1029/97JB03616

Jolivet L, Faccenna C, Goffé B, et al (2003) Subduction tectonics and exhumation of high-pressure metamorphic rocks in the Mediterranean orogens. Am J Sci 303:353–409. doi: 10.2475/ajs.303.5.353

Jolivet L, Faccenna C, Huet B, et al (2013) Aegean tectonics: Strain localisation, slab tearing and trench retreat. Tectonophysics 597–598:1–33. doi: 10.1016/j.tecto.2012.06.011

Karamata S (2006) The geological development of the Balkan Peninsula related to the approach, collision and compression of Gondwanan and Eurasian units. Geol Soc SP 260:155–178. doi: 10.1144/GSL.SP.2006.260.01.07

Karamata S, Knežević V, Pécskay Z, Đorđević M (1997) Magmatism and metallogeny of the Ridanj-Krepoljin belt (eastern Serbia) and their correlation with northern and eastern analogues. Miner Deposita 32:452–458. doi: 10.1007/s001260050114

Karamata S, Krstić B (1996) Terranes of Serbia and Neighbouring Areas. In: Knežević-Đorđević V, Krstić B (eds) Terranes of Serbia. Faculty of Mining and Geology, University of Belgrade, Belgrade, pp 25–40

Karamata S, Stojanov R, Serafimovski T, et al (1992) Tertiary magmatism in the Dinarides of the Vardar zone and the Serbo–Macedonian Massif. Geologica Macedonica 6:127–186.

Kilias A, Falalakis G, Mountrakis D (1997) Alpine tectonometamorphic history of the Serbomacedonian metamorphic rocks: implication for the tertiary unroofing of the Serbomacedonian-Rhodope metamorphic complexes (Makedonia, Greece). Ορυκτός Πλούτος 105:32–50. doi: RefwID:14314

Kober L (1952) Leitlinen der Tektonik Jugoslawiens. Naučna knjiga, Beograd

Kolb M, von Quadt A, Peytcheva I, et al (2013) Adakite-like and Normal Arc Magmas: Distinct Fractionation Paths in the East Serbian Segment of the Balkan–Carpathian Arc. J Petrol 54:421–451. doi: 10.1093/petrology/egs072

Kostopoulos D, Reischmann T, Sklavounos S (2001) Palaeozoic and Early Mesozoic magmatism and metamorphism in the Serbo-Macedonian massif, Central Macedonia, Northern Greece. Abstracts. Cambridge Publications, Strasbourg, p 318

Kounov A, Burg J-P, Bernoulli D, et al (2011) Paleostress analysis of Cenozoic faulting in the Kraishte area, SW Bulgaria. J Struct Geol 33:859–874. doi: 10.1016/j.jsg.2011.03.006

Kounov A, Graf J, von Quadt A, et al (2012) Evidence for a "Cadomian" ophiolite and magmatic-arc complex in SW Bulgaria. Precambrian Res 212–213:275–295. doi: 10.1016/j.precamres.2012.06.003

Kounov A, Seward D, Bernoulli D, et al (2004) Thermotectonic evolution of an extensional dome: the Cenozoic Osogovo-Lisets core complex (Kraishte zone, western Bulgaria). Int J Earth Sci (Geol Rundsch) 93:1008–1024. doi: 10.1007/s00531-004-0435-2

Kounov A, Seward D, Burg J-P, et al (2010) Geochronological and structural constraints on the Cretaceous thermotectonic evolution of the Kraishte zone, western Bulgaria. Tectonics 29:TC2002. doi: 10.1029/2009TC002509

Kounov A, Wüthrich E, Seward D, et al (2015) Low-temperature constraints on the Cenozoic thermal evolution of the Southern Rhodope Core Complex (Northern Greece). Int J Earth Sci (Geol Rundsch) 104:1–16. doi: 10.1007/s00531-015-1158-2

Kräutner HG, Krstić B (2002) Alpine and pre-Alpine structural units within the southern Carpathians and eastern Balkanides. Proceedings of XVII Congress of CBGA. VEDA, Bratislava,

Krstić N, Karamata S (1992) Terani u Karpato-Balkanidima istočne Srbije. Zapisnici SGD jubilarna knjiga (1891-1991):57–69.

Kydonakis K, Gallagher K, Brun J-P, et al (2014) Upper Cretaceous exhumation of the western Rhodope Metamorphic Province (Chalkidiki Peninsula, northern Greece). Tectonics 33:2014TC003572. doi: 10.1002/2014TC003572

Lakova I (2009) Acritarch evidence on Silurian age of the low-grade metamorphic Palaeozoic rocks in the Kraishte area (Morava Unit). Review of the Bulgarian Geological Society 70:23–30.

Lilov P, Zagorchev IS (1993) K-Ar data for the deformation and low-grade metamorphism in Permian and Triassic red beds in SW Bulgaria. Geologica Balcanica 23:46.

Ljubović-Obradović D, Carević I, Mirković M, Protić N (2011) Upper Cretaceous volcanoclastic-sedimentary formations in the Timok eruptive area (Eastern Serbia): New biostratigraphic data from planktonic foraminifera. Geol Carpath 62:435–446.

Marchev P, Georgiev S, Raicheva R, et al (2013) Adakitic magmatism in post-collisional setting: An example from the Early–Middle Eocene Magmatic Belt in Southern Bulgaria and Northern Greece. Lithos 180–181:159–180. doi: 10.1016/j.lithos.2013.08.024

Marchev P, Kaiser-Rohrmeier M, Heinrich C, et al (2005) Hydrothermal ore deposits related to post-orogenic extensional magmatism and core complex formation: The Rhodope Massif of Bulgaria and Greece. Ore Geol Rev 27:53–89. doi: 10.1016/j.oregeorev.2005.07.027

Marchev P, Rogers G, Conrey R, et al (1998) Paleogene orogenic and alkaline basic magmas in the

Rhodope zone: Relationships, nature of magma sources, and role of crustal contamination. Acta Vulcanologica 10:217–232.

Marović M, Toljić M, Rundić L, Milivojević J (2007) Neoalpine Tectonics of Serbia. Serbian Geological Society, Belgrade

Meinhold G, Kostopoulos D, Frei D, et al (2010) U–Pb LA-SF-ICP-MS zircon geochronology of the Serbo-Macedonian Massif, Greece: palaeotectonic constraints for Gondwana-derived terranes in the Eastern Mediterranean. Int J Earth Sci (Geol Rundsch) 99:813–832. doi: 10.1007/s00531-009-0425-5

Mihailescu N, Dimitrijević MD, Dimitrijević MN (1967) Les fossiles dans le flysch. Reports. Serbian Geological Society, Belgrade, pp 371–378

Milovanović D (1990) Petrologija gnajseva Srpsko-makedonske mase u području između Tulara i Lebana. Proceedings of the XII Congress of the Geologists of Yugoslavia. Prosveta, Ohrid, pp 310–321

Milovanović D, Milovanović M, Oberhänsli R (1988) Petrology of green-rocks of the Vlasina complex in the Manastiriška river area (Vlasotince). Vesnik 44:101–128.

Nachev IK (1974) The Tithonian flysch in Bulgaria. Bulgarian Academy of Sciences Bulletin of the Geological Institute 23:191–204.

Nachev IK (1978) On the Upper Cretaceous basin model in the Srednogorie zone. Comptes Rendus de l'Académie bulgare des Sciences 31:213–216.

Nenova P, Zidarov N (2008) Eclogites from Maleshevska Mountain, SW Bulgaria. Central Laboratory of Mineralogy and Crystallography "Acad. Ivan Kostov," Sofia

Pantić N, Dimitrijević MD, Hercegovac M (1967) Mikrofloristički podaci o starosti Vlasinskog kompleksa. Zapisnici SGD za 1966. g

Pavić A, Menković L, Koščal M (1983) Tumač za list Uroševac. Savezni Geološki Zavod, Belgrade

Pavlović P (1962) O nekim ordovicijskim inartikulatnim brahiopodima u metamorfnim stenama kod Bosiljgrada (Jugoistočna Srbija) i o značaju ovog nalaska. Ann Géol Penins Balk 39:99–112.

Pavlović P (1977) O "Gornjem (Vlasinskom) kompleksu" i podeli metamorfnih stena Srpsko-Makedonskog metamorfnog terena. Zapisnici SGD za 1975. i 1976. godinu:123–132.

Perugini D, Poli G, Christofides G, et al (2004) Mantle-derived and crustal melts dichotomy in northern Greece: spatiotemporal and geodynamic implications. Geol J 39:63–80. doi: 10.1002/gj.944

Petković V (1930) O tektonskom sklopu istočne Srbije. Glas Srpske kraljevske akademije 140:151–188.

Petrović B, Dimitrijević MD, Karamata S (1973) Tumač za list Vlasotince. Savezni Geološki Zavod, Belgrade

Petrović B S (1969) The Structure of the Vlasina Crystalline Complex in the Broad Area of Crna Trava. Rudarsko-geološki fakultet, Belgrade

Peychev K, Kiselinov H, Georgiev S, et al (2012) The Vlahina-Maleshevo detachment fault in Southwest Bulgaria - combined structural and zircon LA-ICPMS U-Pb study. Proceedings. Bulgarian Geological Society, Sofia, p 114

Peytcheva I, von Quadt A, Marchev P, et al (2012) Age and isotope-geochemical characteristics of the Tertiary magmatism in Kraishte region, W. Bulgaria. Abstracts Book. Dokuz Eylül University, Izmir, p 73

Peytcheva I, von Quadt A, Tarassov M, et al (2009) Timing of Igralishte pluton in Ograzhden Mountain, SW Bulgaria: implications for the tectono-magmatic evolution of the region. Geologica Balcanica 38:5–14.

Popović R (1991) Srpsko-Makedonska masa ili Pelagonsko-Rodopski i Moravski masiv. Radovi

Geoinstituta 25:7–20.
Popović R (1995) Srpsko-Makedonska masa: da ili ne? Zapisnici SGD za 1990. i 1991. godinu:59–61.

Protić M (1966) Permski crveni peščari istočne Srbije - sredine njihovog stvaranja. Referati. Ohrid,
Rahn M, Seward D (2000) How many track lengths do we need? Ontrack 20:12–15.
Reiser MK (2015) The tectonometamorphic evolution of the Apuseni Mountains during the Cretaceous. PhD, University of Innsbruck
Ricou L-E, Burg J-P, Godfriaux I, Ivanov Z (1998) Rhodope and Vardar: the metamorphic and the olistostromic paired belts related to the Cretaceous subduction under Europe. Geodin Acta 11:285–309. doi: 10.1016/S0985-3111(99)80018-7
Rieser AB, Neubauer F, Handler R, et al (2008) New 40Ar/39Ar age constraints on the timing of magmatic events in the Panagyurishte region, Bulgaria. Swiss J Geosci 101:107–123. doi: 10.1007/s00015-007-1243-z
Robertson AHF, Karamata S (1994) The role of subduction-accretion processes in the tectonic evolution of the Mesozoic Tethys in Serbia. Tectonophysics 234:73–94. doi: 10.1016/0040-1951(94)90205-4
Robertson A, Karamata S, Šarić K (2009) Overview of ophiolites and related units in the Late Palaeozoic–Early Cenozoic magmatic and tectonic development of Tethys in the northern part of the Balkan region. Lithos 108:1–36. doi: 10.1016/j.lithos.2008.09.007
Săndulescu M (1984) Geotectonica Romaniei. Editura Tehnică, Bucharest
Šarić K, Cvetković V, Romer RL, et al (2009) Granitoids associated with East Vardar ophiolites (Serbia, F.Y.R. of Macedonia and northern Greece): Origin, evolution and geodynamic significance inferred from major and trace element data and Sr–Nd–Pb isotopes. Lithos 108:131–150. doi: 10.1016/j.lithos.2008.06.001
Schefer S, Cvetković V, Fügenschuh B, et al (2011) Cenozoic granitoids in the Dinarides of southern Serbia: age of intrusion, isotope geochemistry, exhumation history and significance for the geodynamic evolution of the Balkan Peninsula. Int J Earth Sci (Geol Rundsch) 100:1181–1206. doi: 10.1007/s00531-010-0599-x
Schmid SM, Bernoulli D, Fügenschuh B, et al (2008) The Alpine-Carpathian-Dinaridic orogenic system: correlation and evolution of tectonic units. Swiss Journal of Geosciences 101:139–183. doi: 10.1007/s00015-008-1247-3
Simić M (1997) Geohronološka starost tercijarnih granitoida Surdulice (JI Srbija). Ann Géol Penins Balk 61:63–82.
Simić M (1992) Geološka istraživanja Cu-Mo pojava na Krivoj Feji. Radovi Geoinstituta 27:131–147.
Simić M (1996) Metalogenetske karakteristike Mo-mineralizacija u Ćurkovici - Surdulički eruptivni masiv. Radovi Geoinstituta 33:35–43.
Soldatos T, Koroneos A, Kamenov BK, et al (2008) New U-Pb and Ar-Ar mineral ages for the Barutin-Buynovo-Elatia-Skaloti-Paranesti batholith (Bulgaria and Greece): Refinement of its debatable age. Geochemistry, Mineralogy and Petrology 46:85–102.

Spassov C (1973) Stratigraphie des Devons in Sudwest-Bulgarien. Bulletin of the Geological Institute 22:5–38.
Stajević B (1997) Strukture rudnih polja Blagodat i Karamanica prema podacima daljinske detekcije. Ann Géol Penins Balk 61:419–433.
Stanić N, Pavlović R, Marković M (1996) Rupturni sklop i tercijarni vulkanizam Vranjskog basena. Radovi Geoinstituta 32:189–197.

Tagami T (2005) Zircon Fission-Track Thermochronology and Applications to Fault Studies. Rev Mineral Geochem 58:95–122. doi: 10.2138/rmg.2005.58.4

van Hinsbergen DJJ, Schmid SM (2012) Map view restoration of Aegean–West Anatolian accretion and extension since the Eocene. Tectonics 31:TC5005. doi: 10.1029/2012TC003132

Vasković N (1998) P-T condition of the mica schists from the Vranjska Banja Series. Proceedings of the XIII Congress of the Geologists of Yugoslavia. Herceg Novi, pp 41–59

Vasković N (2002) Petrology and P-T condition of white mica-chlorite schists from Vlasina series - Surdulica, SE Serbia. Ann Géol Penins Balk 199–220. doi: 10.2298/GABP0264199V

Vasković N, Matović V, Srećković-Batoćanin D (2003) Petrology of Garnet-amphibolite with White Mica from Vranjska Banja Series (Serbian-Macedonian Massif, SE Serbia). Studia Universitatis Babeş-Bolyai 128–133.

Vasković N, Tasić Z (1997) Geologija granodioritskog masiva Surdulice. Savezno ministarstvo za privredu SRJ, Belgrade

Veselinović M, Antonijević I, Milošaković V, et al (1970) Tumač za list Boljevac. Savezni Geološki Zavod, Belgrade

von Quadt A, Moritz R, Peytcheva I, Heinrich CA (2005) Geochronology and geodynamics of Late Cretaceous magmatism and Cu–Au mineralization in the Panagyurishte region of the Apuseni–Banat–Timok–Srednogorie belt, Bulgaria. Ore Geol Rev 27:95–126. doi: 10.1016/j.oregeorev.2005.07.024

Vukanović M, Dimitrijević MD, Dimitrijević M, et al (1977) Tumač za list Vranje. Savezni Geološki Zavod, Belgrade

Vukanović M, Karajičić L, Dimitrijević MD, et al (1973) Tumač za list Leskovac. Savezni Geološki Zavod, Belgrade

Whitney DL, Evans BW (2010) Abbreviations for names of rock-forming minerals. Am Mineral 95:185–187. doi: 10.2138/am.2010.3371

Willingshofer E, Neubauer F, Cloetingh S (1999) The significance of Gosau-type basins for the late cretaceous tectonic history of the Alpine-Carpathian belt. Phys Chem Earth Pt A 24:687–695. doi: 10.1016/S1464-1895(99)00100-3

Yanev S, Popa M, Seghedi A, Oaie G (2001) Overview of the continental Permian deposits of Bulgaria and Romania. Natura Bresciana 25:269–279.

Zachariadis P (2007) Ophiolites of the eastern Vardar Zone, N. Greece. Johannes Gutenberg Universität

Zagorčev IS, Bončeva I (1988) Indications of Devonian basic volcanism in Southwest Bulgaria. Geologica Balcanica 18:55–63.

Zagorchev IS (2008) Amphibolite-facies metamorphic complexes in Bulgaria and Precambrian geodynamics: controversies and “state of the art.” Geologica Balcanica 37:33–46.

Zagorchev IS (1984a) Pre-Alpine structure of South-west Bulgaria. In: Zagorchev IS, Mankov S, Bozkov I (eds) Problems of the geology of Southwestern Bulgaria. Tehnika, Sofia, pp 9–20

Zagorchev IS (1985) Deformation during the first stage of the Alpine Orogeny in the Skrino-Poletintsi faulted zone; IV Shipochan Anticline. Review of the Bulgarian Geological Society 46:287–298.

Zagorchev IS (1984b) The role of overthrusts in the Alpine structure of Krajistides. Geologica Balcanica 14:37–64.

Zagorchev IS (1981) Early Alpine deformations in the red beds within the Poletinci-Skrino fault zone. 2. Structure and deformations in the northern parts of the Vlahina block. Geologica Balcanica 11:101–126.

Zagorchev IS, Balica C, Balintoni I, et al (2011) New Isotopic Data on the Metamorphic Rocks in

SW Bulgaria. Proceedings of the 3rd International Symposium on the Geology of the Black Sea Region. GeoEcoMar, Bucharest, pp 223–225

Zagorchev IS, Milovanović D (2006) Deformations and Metamorphism in the Eastern Parts of the Serbo-Macedonian Massif. Proceedings. Serbian Geological Society, Belgrade, pp 670–673

Zagorchev IS, Ruseva M (1982) Nappe structure of the southern parts of Osogovo Mts and the Pijanec region (SW Bulgaria). Geologica Balcanica 12:35–57.

Zagortchev IS (1993) Alpine evolution of the pre-Alpine amphibolite-facies basement in South Bulgaria. Mitteilungen der Österreichischen Geologischen Gesellschaft 86:9–21.

Zidarov N, Peytcheva I, von Quadt A, et al (2003) Mineral-petrological, geochemical and isotope studies of geological units in Serbo-Macedonian Massif, SW Bulgaria. Central Laboratory of Mineralogy and Crystallography “Acad. Ivan Kostov,” Sofia

Zidarov N, Peytcheva I, von Quadt A, et al (2007) Distinction of crustal terranes in Ograzhden and Belassitsa Mountains, Serbo-Macedonian Massif (SW Bulgaria), based on U-Pb conventional and LA-ICP-MS dating of zircons. Central Laboratory of Mineralogy and Crystallography “Acad. Ivan Kostov,” Sofia

Zidarov N, Peytcheva I, von Quadt A, et al (2004) Timing and Magma Sources of Igralishte Pluton (SW Bulgaria): Preliminary Isotope-Geochronological and Geochemical Data. Proceedings. Bulgarian Geological Society, Sofia,

Zimmerman A, Stein HJ, Hannah JL, et al (2008) Tectonic configuration of the Apuseni–Banat—Timok–Srednogorie belt, Balkans-South Carpathians, constrained by high precision Re–Os molybdenite ages. Miner Deposita 43:1–21. doi: 10.1007/s00126-007-0149-z

Appendices to

Chapter 4: Alpine thermal events in the central Serbo-Macedonian Massif (southeastern Serbia)

Milorad D. Antić[1], Alexandre Kounov[1], Branislav Trivić[2], Andreas Wetzel[1], Irena Peytcheva[3,4], Albrecht von Quadt[3]

[1]Institute for Geology and Palaeontology, Basel University, 4056 Basel, Switzerland;

[2]Faculty of Mining and Geology, University of Belgrade, 11000 Belgrade, Serbia

[3]Institute of Geochemistry and Petrology, ETH-Zürich, 8092 Zürich, Switzerland

[4]Geological Institute, Bulgarian Academy of Sciences, 1113 Sofia, Bulgaria

Contents

2-1 Analytical methods

2-2 FT radial plots for all fission-track age determinations and results of the thermal modelling

2-3 U–Pb and geochemistry sample descriptions and results

2-4 Operational parameters of instruments used for measuring of the isotopic ratios

Appendix 4-1

Analytical methods

4-1.1 Fission-track thermochronology

Whole rock samples were mechanically fragmented (jaw crusher, milling) and sieved through a 450μm sieve. A heavy minerals concentrates were obtained by gravity separation (Wilfley table). Apatite and zircon fractions were recovered by conventional heavy liquid (methylene iodide 3.3 g·cm^{-3}, and methylene iodide + acetone solution 3.1 g·cm^{-3}), and magnetic susceptibility (Frantz isodynamic separator) separation methods. Apatite grains were mounted in epoxy resin, polished and etched with 5.5 M HNO_3 at 21 °C for 20 s. Zircon grains were mounted in teflon®, polished and etched in an eutectic mixture of KOH and NaOH at 220 °C for 6 to 42 h. Irradiation was performed at the Oregon State University Radiation Centre, OR, USA. Teflon tubes containing zircon mounts and CN1 dosimeter glass were irradiated by a total integrated flux of 1E15 n·cm^{-2}, while the tubes with apatite mounts and CN5 dosimeter glass were subjected to flux of 1E16 n·cm^{-2}. Microscopic analysis was completed at Basel University using an optical microscope with a Kinetek computer-driven stage (Dumitru 1993). Fission tracks in apatite were counted and horizontal confined track-lengths were measured on 1250x magnification. Estimates of the compositional influence on the fission-track annealing in apatites were obtained by measuring the etch-pit diameters (Dpar; Carlson et al. 1999) on the same magnification. Fission tracks in zircons were counted at 1600× magnification (dry objective). Fission-track ages were calculated with the TrackKey software (v4.2g; Dunkl 2002), using the ζ approach (Hurford and Green 1983) with ζ values of 327,97 ± 22,81 yr·cm^2 for apatites (CN5 standard glass) and 151,3 ± 7,85 yr·cm^2 for zircons (CN1 standard glass; Table 1; analyst: M. Antić). Reported age results correspond to the central ages of Galbraith and Laslett, (1993) with a 2σ uncertainty (Table 1 and Fig. 4). The chi-square test ($P\chi^2<5\%$) was applied to the single grain fission-track ages from the sediment samples in order to determine the possibility of presence of multiple populations (e.g. Galbraith 1981; Brandon et al. 1998; Garver et al. 2000; Stewart and Brandon 2004). Detailed results of the FT analysis are presented in Appendix 4-2. Radial plots were produced using the RadialPlotter application (v6.1; Vermeesch 2009).

The temperatures at which fission tracks in apatite and zircon partially anneal (i.e. partial resetting) are not sharply defined. The temperature range within which partial track annealing occurs is known as the partial annealing zone (PAZ). The effective closure of the system lies within this PAZ and depends on overall cooling rate and kinetic properties of the host mineral. The specific partial annealing zone for apatite lies between 60 and 120 °C (Green and Duddy 1989; Corrigan 1993), with a mean effective closure temperature of 110±10 °C (Gleadow and Duddy 1981).

Unfortunately, our knowledge of zircon annealing is less advanced and a wide-range of temperature intervals has been published for the partial annealing zone of zircon. Yamada et al. (1995) suggested temperature limits of ca. 390–ca. 170 °C, whereas Tagami and Dumitru (1996) and Tagami et al. (1998) suggested temperature limits of ca. 310–ca. 230 °C. Recently, in his overview on the zircon fission-track dating method, Tagami (2005) reported temperature ranges for the closure temperature between 300 and 200 °C. Accordingly, we use a value of 250±50 °C for the mean effective closure temperature and the 200–300 °C temperature interval for the partial annealing zone.

Fission tracks in apatite form continuously through time, with an initial mean length of ca. 16.3 μm (Gleadow et al. 1986). Upon heating, tracks gradually anneal and shorten to a length that depends on the integrated effect of the thermal overprint (duration and temperature). For example, tracks become completely annealed at a temperature of 110–120 °C for a period of 105–106 years (Gleadow and Duddy 1981). Annealing characteristics make it possible to generate time-temperature paths by inverse modelling (e.g. Gallagher and Sambridge 1994; Ketcham 2005). Low-temperature thermal histories for our samples were modelled using the software HeFTy (v1.7.4.55;

Ketcham 2005). Fission-track age, track-length distribution and etch-pit diameters (Dpar), in combination with user-defined time-temperature (t-T) boxes (dark blue square outlines in Appendix 4-2) served as our input parameters. An inverse Monte Carlo algorithm with a multi-kinetic annealing model (Ketcham et al. 2007) was used to generate time-temperature paths. The algorithm generated a large number of time-temperature paths, which were tested against the input data, that is, the t-T paths are forced to pass through user-defined time-temperature boxes. The fit between measured and modelled data was evaluated statistically and quantified by the so-called "goodness of fit" value (GOF). A "good" result corresponds to GOF values >0.5, whereas a value between 0.5 and 0.05 is considered to reflect an “acceptable” fit between modelled and measured data. Envelopes surrounding all “acceptable” and “good” paths are represented by green and purple fields, respectively (Appendix 4-2).

4-1.2 U–Pb zircon geochronology

Zircon grains were hand picked from the zircon mineral concentrates produced during the sample preparation for the FT analyses. The polished mounts were photographed, and SEM cathodoluminescence (CL) and backscatter electron images were made in order to analyse the internal structures of the grains prior to the LA-ICP-MS analysis. Instrument parameters used during the course of this study are detailed in Appendix 4-4. Data acquisition was performed at Dept. of Earth Science, ETH Zürich in 2010 using an Elan 6100 ICP-MS (PerkinElmer, Norwalk, CT, USA) coupled to an 193 nm ArF-Excimer laser ablation system similar to a Geolas system (Coherent, USA). The laser was operated at 10 Hz, spot size was 40 micrometer and a fluence of 4.0 J·cm^{-2} was used. All experiments were performed using helium as carrier gas. The carrier gas was mixed with argon as make-up gas before entering the ICP (Appendix 4-4).

Appendix 4-3 contains detailed descriptions of the samples and the obtained U–Pb ages, as well as a comprehensive table with results of the U, Th and Pb isotopic measurements, and the CL images of analysed zircon grains. Weighted average plots were produced using the program Isoplot (v3.71.09.05.23nx; Ludwig 2012). Unless explicitly stated, uncertainties in the calculated weighted mean ages are reported at 95 % confidence limit. Results referred to as concordant are within 95-105 % tolerance defined by $100\cdot((^{206}Pb/^{238}U \text{ age})\cdot(^{207}Pb/^{235}U \text{ age})^{-1})$. Weighted average plots do not include discordant measurements. Since annealing and chemical leaching were not performed on the zircon grains, the results obtained on partially metamict domains display younger ages probably due to partial radiogenic lead loss, despite the high concordance. In cases where collection of age results are forming a continuous array lacking “plateau” or evident clustering of specific textures or growth domains, the weighted average of the array is reported as the most correct result. Discordant measurements and results from spots located in the “mixed zones” within the zircon grain (e.g. on the interface of core and rim), were omitted from the interpretation and the plots.

4-1.3 Geochemical analysis

Major elements analyses on whole-rock samples were performed using the X-ray fluorescence (XRF) method, whereas the trace element and REE measurements were carried out with the Laser Ablation Inductively Coupled Plasma-Mass Spectrometry (LA-ICPMS) at ETH-Zürich. All diagrams representing results of geochemical analyses were plotted using GCDkit software (v2.3; Janoušek et al. 2006). The results of the chemical analyses are presented in Appendix 4-3.

References

Brandon MT, Roden-Tice MK, Garver JI (1998) Late Cenozoic exhumation of the Cascadia accretionary wedge in the Olympic Mountains, northwest Washington State. Geol Soc Am Bull 110:985–1009. doi: 10.1130/0016-7606(1998)110<0985:LCEOTC>2.3.CO;2

Carlson WD, Donelick RA, Ketcham RA (1999) Variability of apatite fission-track annealing kinetics; I, Experimental results. Am Mineral 84:1213–1223.

Corrigan JD (1993) Apatite fission-track analysis of Oligocene strata in South Texas, U.S.A.: Testing annealing models. Chem Geol 104:227–249. doi: 10.1016/0009-2541(93)90153-A

Dumitru TA (1993) A new computer-automated microscope stage system for fission-track analysis. Nucl Tracks Rad Meas 21:575–580. doi: 10.1016/1359-0189(93)90198-I

Dunkl I (2002) Trackkey: a Windows program for calculation and graphical presentation of fission track data. Comput Geosci 28:3–12. doi: 10.1016/S0098-3004(01)00024-3

Galbraith RF (1981) On statistical models for fission track counts. J Int Ass Math Geol 13:471–478. doi: 10.1007/BF01034498

Galbraith RF, Laslett GM (1993) Statistical models for mixed fission track ages. Nucl Tracks Rad Meas 21:459–470. doi: 10.1016/1359-0189(93)90185-C

Gallagher K, Sambridge M (1994) Genetic algorithms: A powerful tool for large-scale nonlinear optimization problems. Comput Geosci 20:1229–1236. doi: 10.1016/0098-3004(94)90072-8

Garver JI, Soloviev AV, Bullen ME, Brandon MT (2000) Towards a more complete record of magmatism and exhumation in continental arcs using detrital fission track thermochronometry. Phys Chem Earth 25:565–570.

Gleadow AJW, Duddy IR (1981) A natural long-term track annealing experiment for apatite. Nuclear Tracks 5:169–174. doi: 10.1016/0191-278X(81)90039-1

Gleadow AJW, Duddy IR, Green PF, Lovering JF (1986) Confined fission track lengths in apatite: a diagnostic tool for thermal history analysis. Contrib Mineral Petrol 94:405–415. doi: 10.1007/BF00376334

Green P., Duddy I r. (1989) Some Comments on Paleotemperature Estimation from Apatite Fission Track Analysis. J Petrol Geol 12:111–114. doi: 10.1111/j.1747-5457.1989.tb00224.x

Hurford AJ, Green PF (1983) The zeta age calibration of fission-track dating. Chem Geol 41:285–317. doi: 10.1016/S0009-2541(83)80026-6

Janoušek V, Farrow CM, Erban V (2006) Interpretation of Whole-rock Geochemical Data in Igneous Geochemistry: Introducing Geochemical Data Toolkit (GCDkit). J Petrol 47:1255–1259. doi: 10.1093/petrology/egl013

Ketcham RA (2005) Forward and Inverse Modeling of Low-Temperature Thermochronometry Data. Rev Mineral Geochem 58:275–314. doi: 10.2138/rmg.2005.58.11

Ketcham RA, Carter A, Donelick RA, et al (2007) Improved modeling of fission-track annealing in apatite. Am Mineral 92:799–810. doi: 10.2138/am.2007.2281

Ludwig KR (2012) Isoplot 3.75: A Geochronological Toolkit for Microsoft Excel. Berkeley Geochronological Center, Berkeley

Stewart RJ, Brandon MT (2004) Detrital-zircon fission-track ages for the “Hoh Formation”: Implications for late Cenozoic evolution of the Cascadia subduction wedge. Geol Soc Am Bull 116:60–75. doi: 10.1130/B22101.1

Tagami T (2005) Zircon Fission-Track Thermochronology and Applications to Fault Studies. Rev Mineral Geochem 58:95–122. doi: 10.2138/rmg.2005.58.4

Tagami T, Dumitru TA (1996) Provenance and thermal history of the Franciscan accretionary complex: Constraints from zircon fission track thermochronology. J Geophys Res-Sol Ea

101:11353–11364. doi: 10.1029/96JB00407

Tagami T, Galbraith RF, Yamada R, Laslett GM (1998) Revised Annealing Kinetics of Fission Tracks in Zircon and Geological Implications. In: Haute P van den, Corte F de (eds) Advances in Fission-Track Geochronology. Springer Netherlands, pp 99–112

Vermeesch P (2009) RadialPlotter: A Java application for fission track, luminescence and other radial plots. Radiat Meas 44:409–410. doi: 10.1016/j.radmeas.2009.05.003

Yamada R, Tagami T, Nishimura S, Ito H (1995) Annealing kinetics of fission tracks in zircon: an experimental study. Chem Geol 122:249–258. doi: 10.1016/0009-2541(95)00006-8

Appendix 4-2

FT radial plots for all fission-track age determinations and results of the thermal modelling

Appendix 4-2 FT radial plots and thermal models

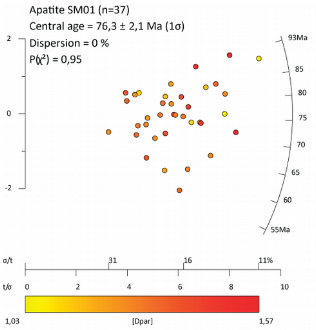

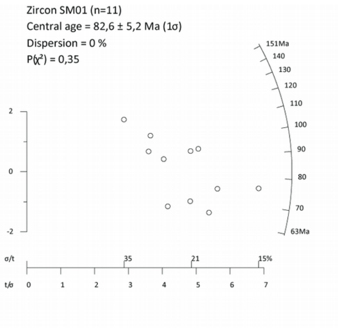

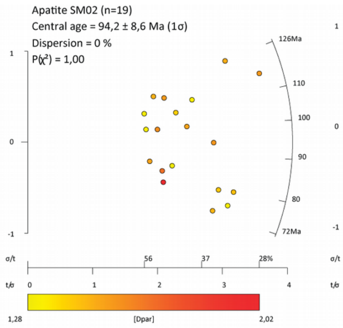

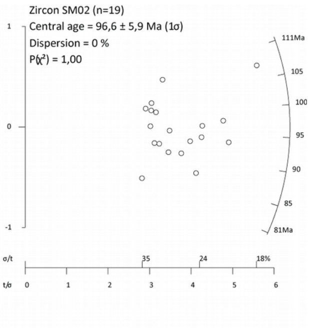

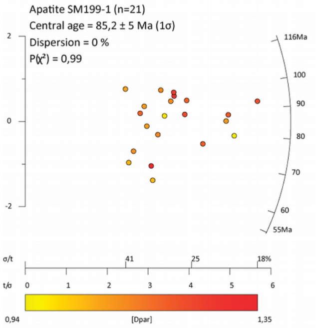

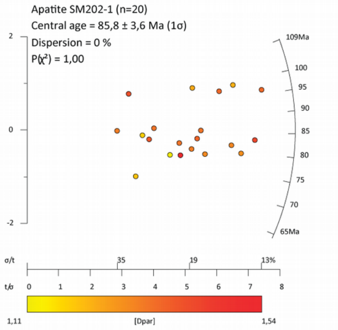

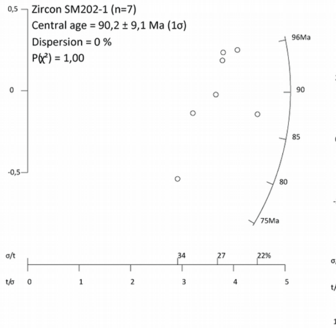

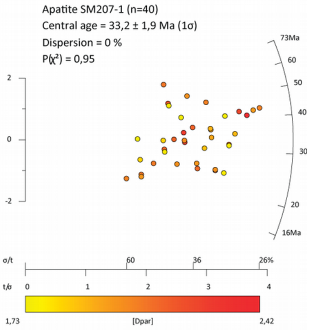

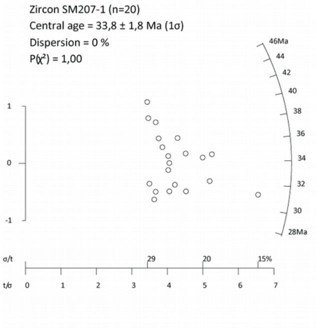

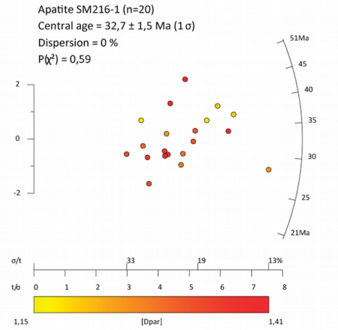

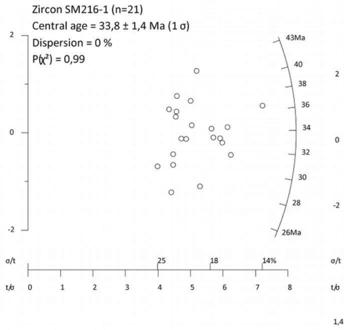

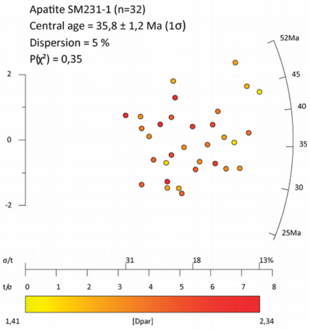

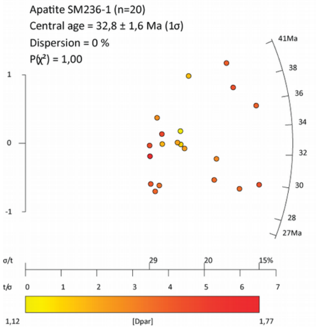

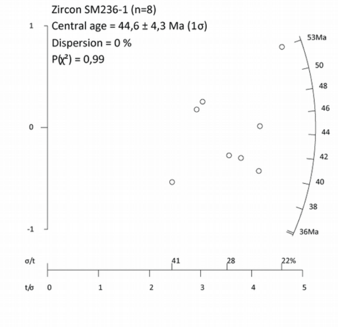

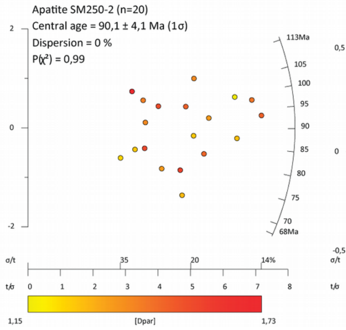

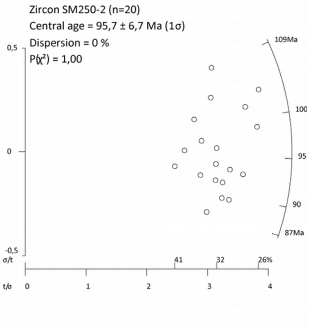

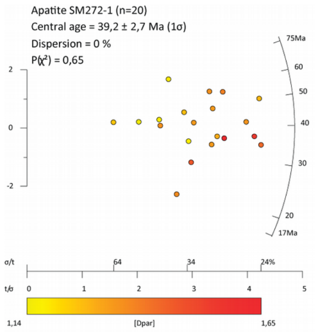
Apatite SM272-1 (n=20)
Central age = 39,2 ± 2,7 Ma (1σ)
Dispersion = 0 %
P(χ^2) = 0,65

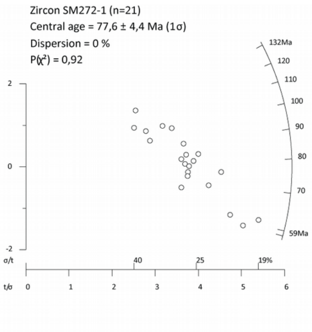
Zircon SM272-1 (n=21)
Central age = 77,6 ± 4,4 Ma (1σ)
Dispersion = 0 %
P(χ^2) = 0,92

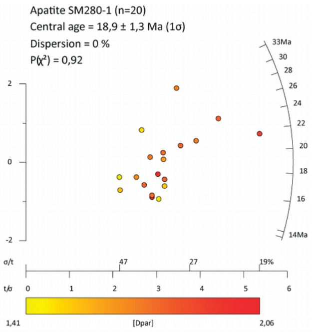
Apatite SM280-1 (n=20)
Central age = 18,9 ± 1,3 Ma (1σ)
Dispersion = 0 %
P(χ^2) = 0,92

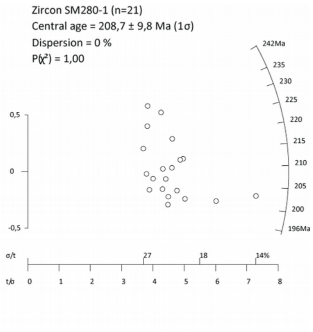
Zircon SM280-1 (n=21)
Central age = 208,7 ± 9,8 Ma (1σ)
Dispersion = 0 %
P(χ^2) = 1,00

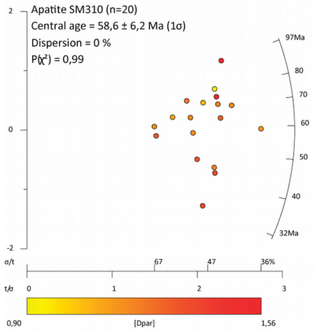
Apatite SM310 (n=20)
Central age = 58,6 ± 6,2 Ma (1σ)
Dispersion = 0 %
P(χ^2) = 0,99

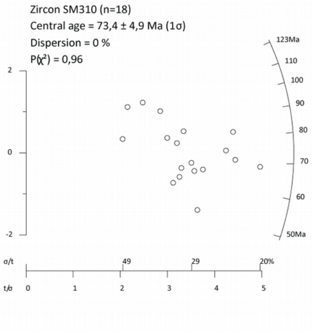
Zircon SM310 (n=18)
Central age = 73,4 ± 4,9 Ma (1σ)
Dispersion = 0 %
P(χ^2) = 0,96

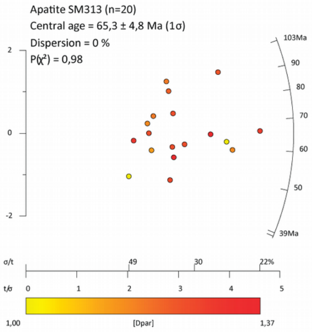
Apatite SM313 (n=20)
Central age = 65,3 ± 4,8 Ma (1σ)
Dispersion = 0 %
P(χ^2) = 0,98

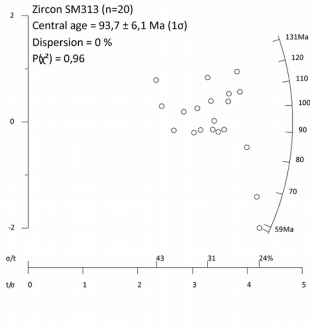
Zircon SM313 (n=20)
Central age = 93,7 ± 6,1 Ma (1σ)
Dispersion = 0 %
P(χ^2) = 0,96

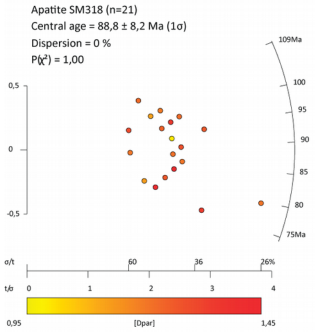
Apatite SM318 (n=21)
Central age = 88,8 ± 8,2 Ma (1σ)
Dispersion = 0 %
P(χ^2) = 1,00

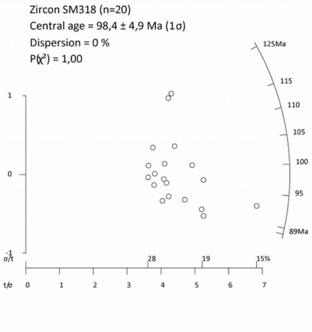
Zircon SM318 (n=20)
Central age = 98,4 ± 4,9 Ma (1σ)
Dispersion = 0 %
P(χ^2) = 1,00

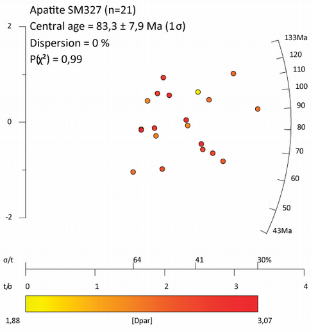
Apatite SM327 (n=21)
Central age = 83,3 ± 7,9 Ma (1σ)
Dispersion = 0 %
P(χ^2) = 0,99

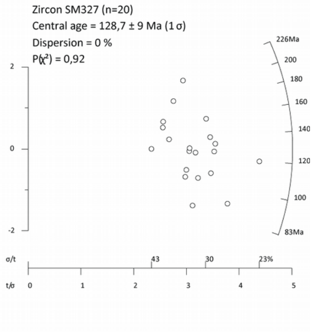
Zircon SM327 (n=20)
Central age = 128,7 ± 9 Ma (1σ)
Dispersion = 0 %
P(χ^2) = 0,92

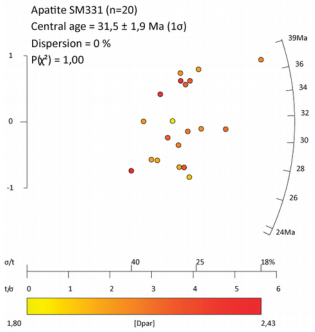
Apatite SM331 (n=20)
Central age = 31,5 ± 1,9 Ma (1σ)
Dispersion = 0 %
P(χ^2) = 1,00

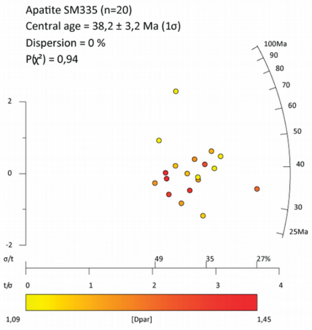
Apatite SM335 (n=20)
Central age = 38,2 ± 3,2 Ma (1σ)
Dispersion = 0 %
P(χ^2) = 0,94

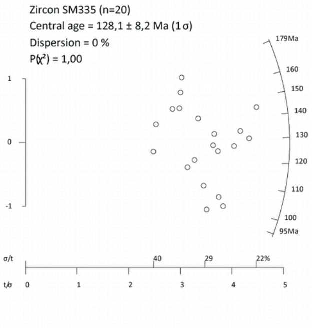
Zircon SM335 (n=20)
Central age = 128,1 ± 8,2 Ma (1σ)
Dispersion = 0 %
P(χ^2) = 1,00

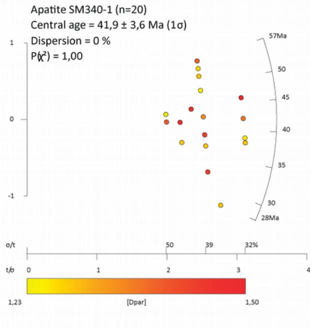
Apatite SM340-1 (n=20)
Central age = 41,9 ± 3,6 Ma (1σ)
Dispersion = 0 %
P(χ^2) = 1,00

Appendix 4-2 FT radial plots and thermal models

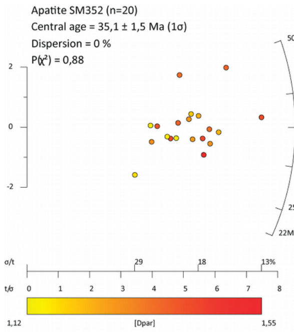

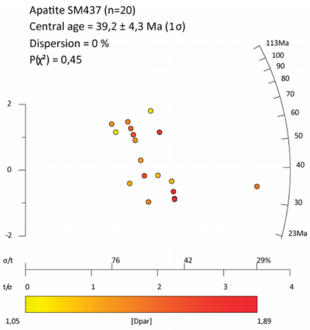

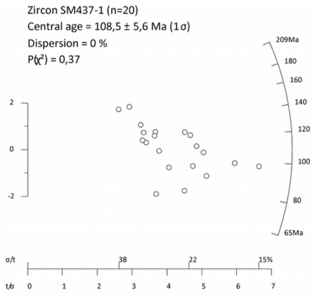

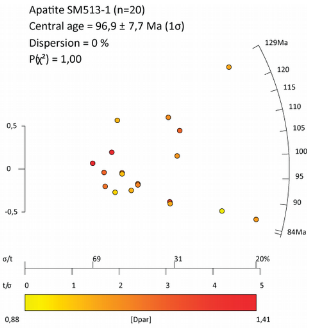

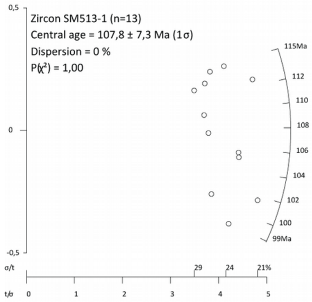

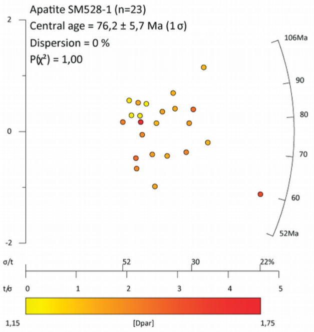

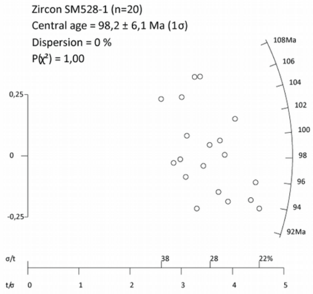

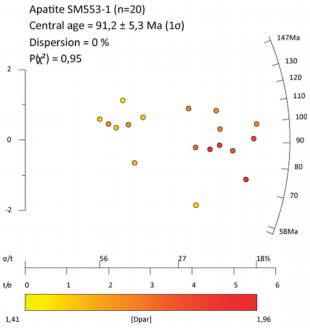

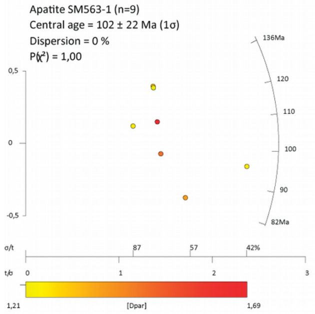

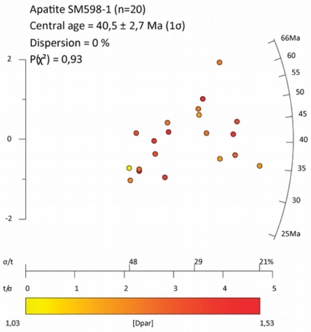

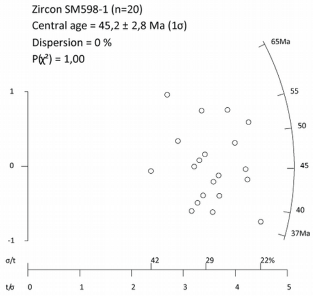

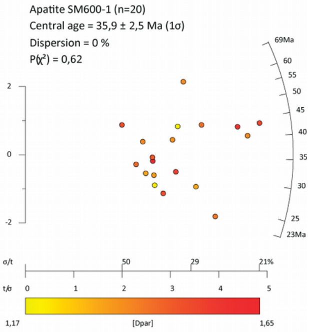

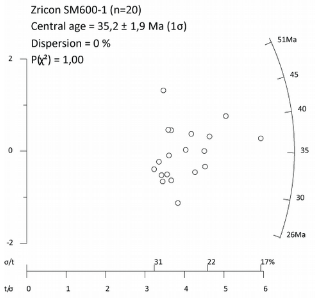

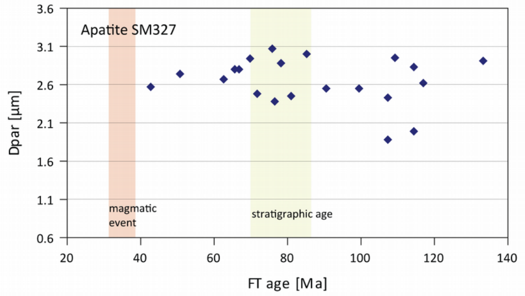

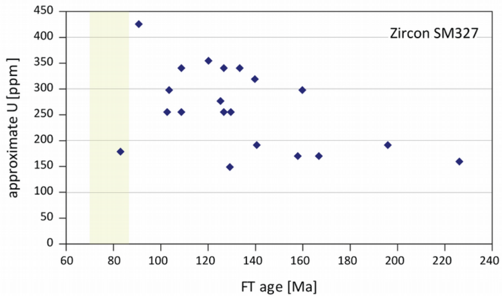

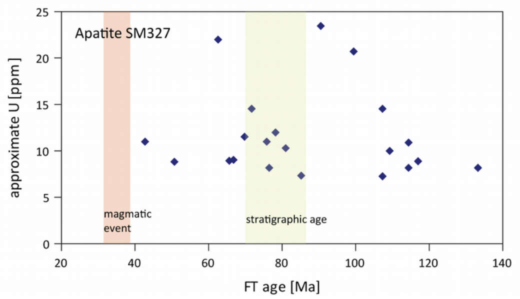

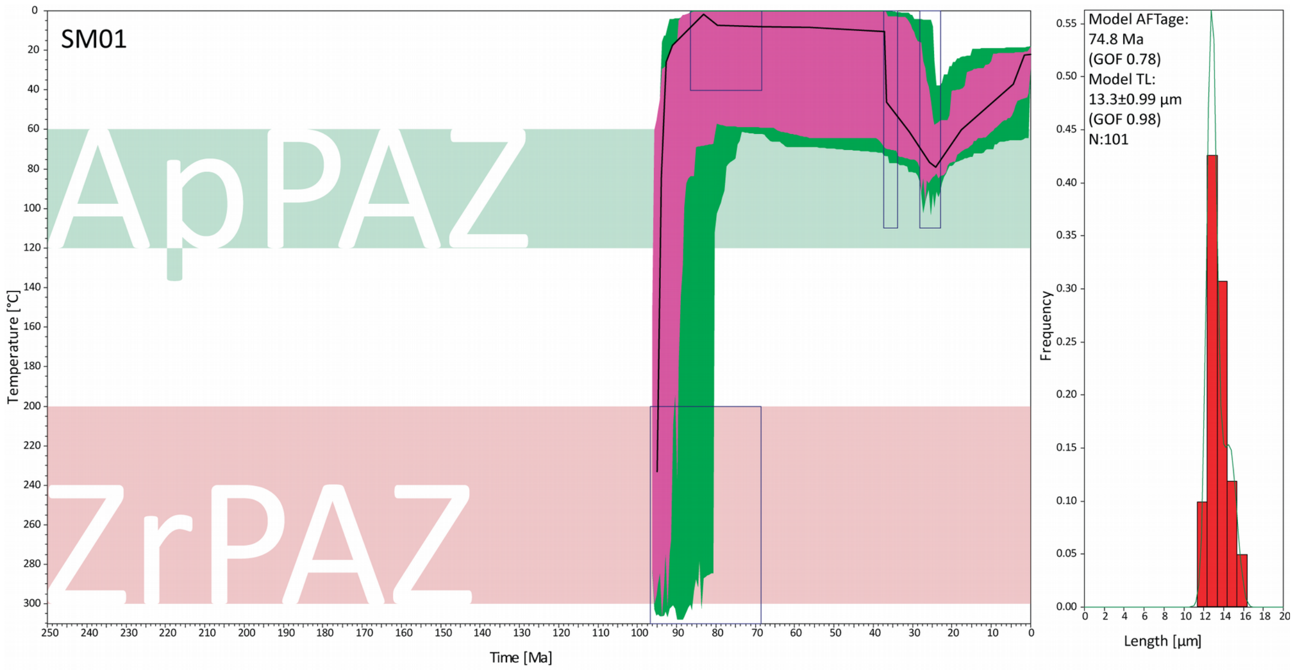
SM01
ApPAZ
ZrPAZ
Temperature [°C]
0
20
40
60
80
100
120
140
160
180
200
220
240
260
280
300
Time [Ma]
250 240 230 220 210 200 190 180 170 160 150 140 130 120 110 100 90 80 70 60 50 40 30 20 10 0
Model AFTage:
74.8 Ma
(GOF 0.78)
Model TL:
13.3±0.99 µm
(GOF 0.98)
N:101
Frequency
0.00 0.05 0.10 0.15 0.20 0.25 0.30 0.35 0.40 0.45 0.50 0.55
Length [µm]
0 2 4 6 8 10 12 14 16 18 20

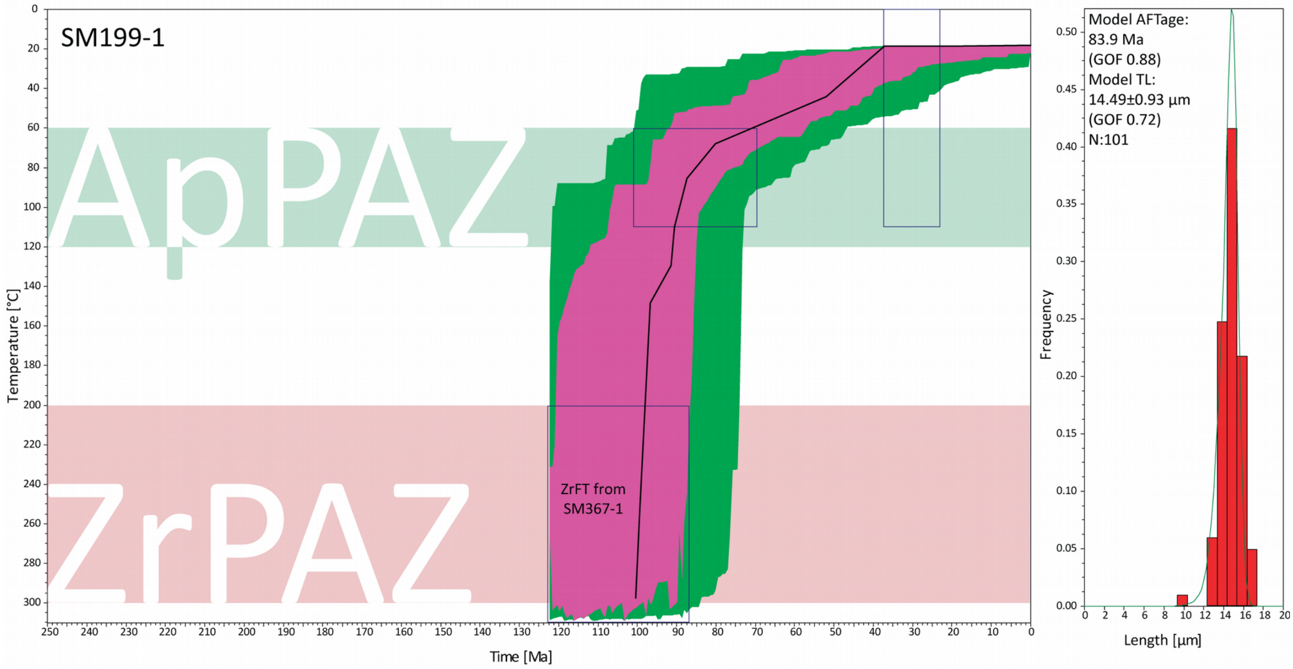
SM199-1
ApPAZ
ZrPAZ
ZrFT from
SM367-1
Temperature [°C]
0
20
40
60
80
100
120
140
160
180
200
220
240
260
280
300
Time [Ma]
250 240 230 220 210 200 190 180 170 160 150 140 130 120 110 100 90 80 70 60 50 40 30 20 10 0
Model AFTage:
83.9 Ma
(GOF 0.88)
Model TL:
14.49±0.93 µm
(GOF 0.72)
N:101
Frequency
0.00 0.05 0.10 0.15 0.20 0.25 0.30 0.35 0.40 0.45 0.50
Length [µm]
0 2 4 6 8 10 12 14 16 18 20

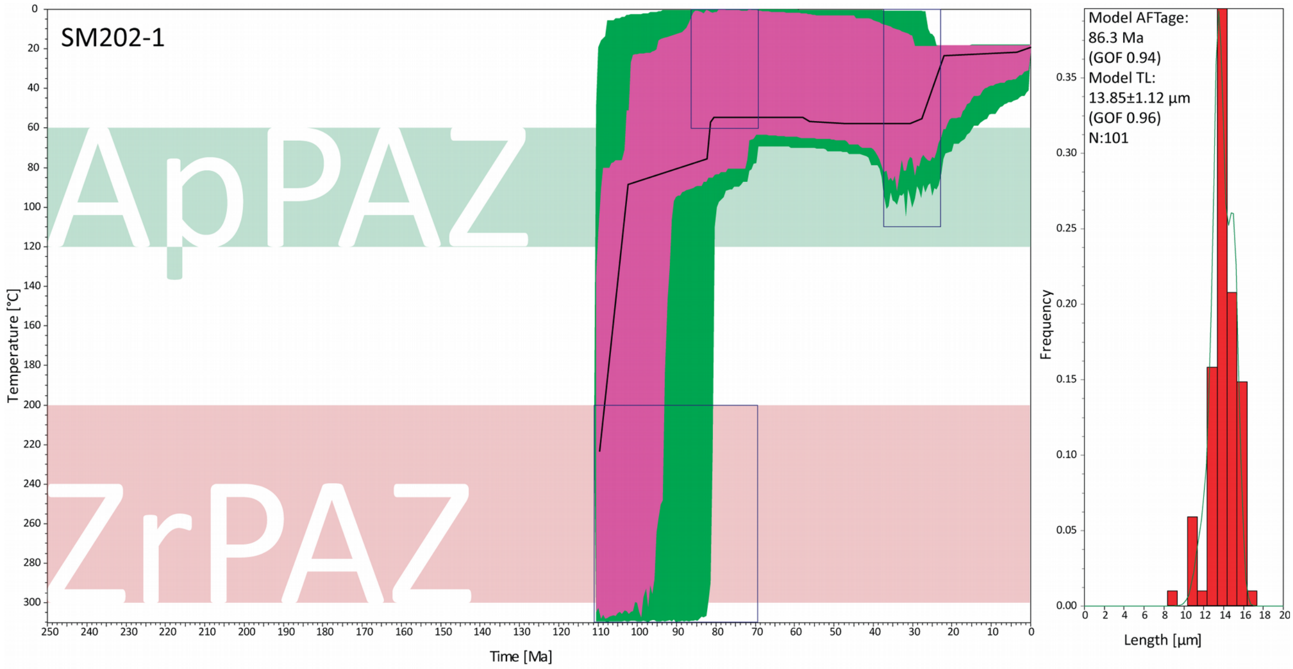
SM202-1
ApPAZ
ZrPAZ
Temperature [°C]
Time [Ma]
Model AFTage:
86.3 Ma
(GOF 0.94)
Model TL:
13.85±1.12 µm
(GOF 0.96)
N:101
Frequency
Length [µm]

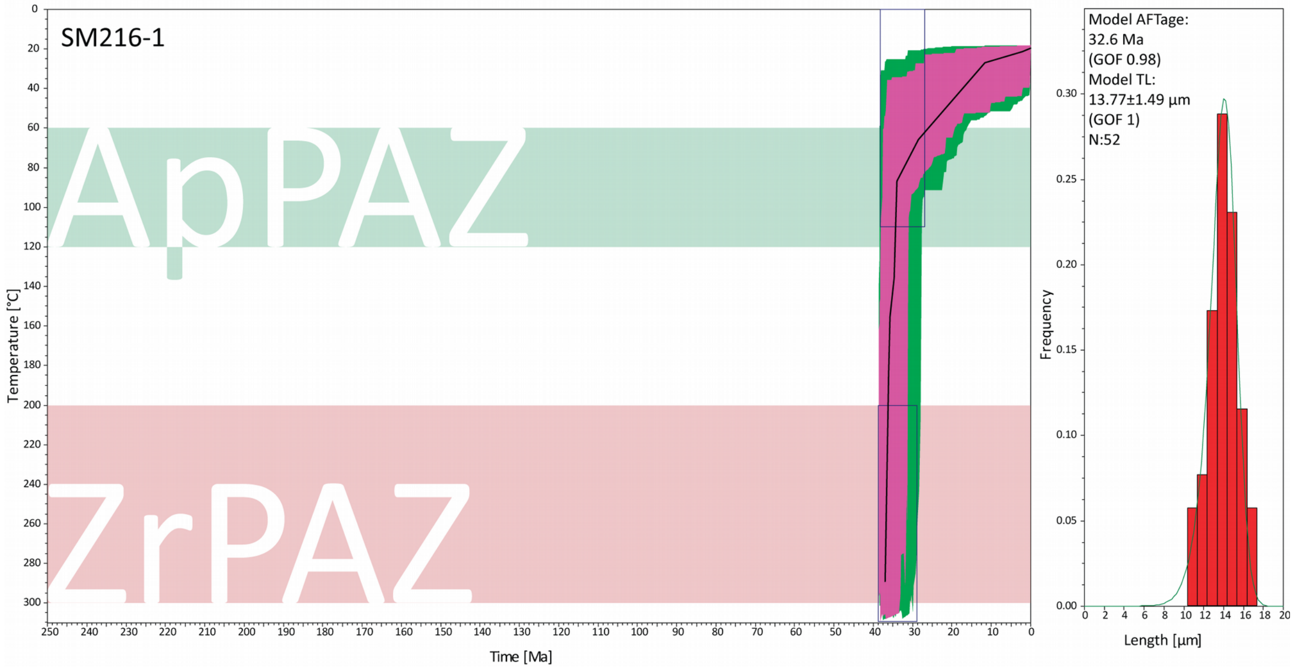
SM216-1
ApPAZ
ZrPAZ
Temperature [°C]
Time [Ma]
Model AFTage:
32.6 Ma
(GOF 0.98)
Model TL:
13.77±1.49 µm
(GOF 1)
N:52
Frequency
Length [µm]

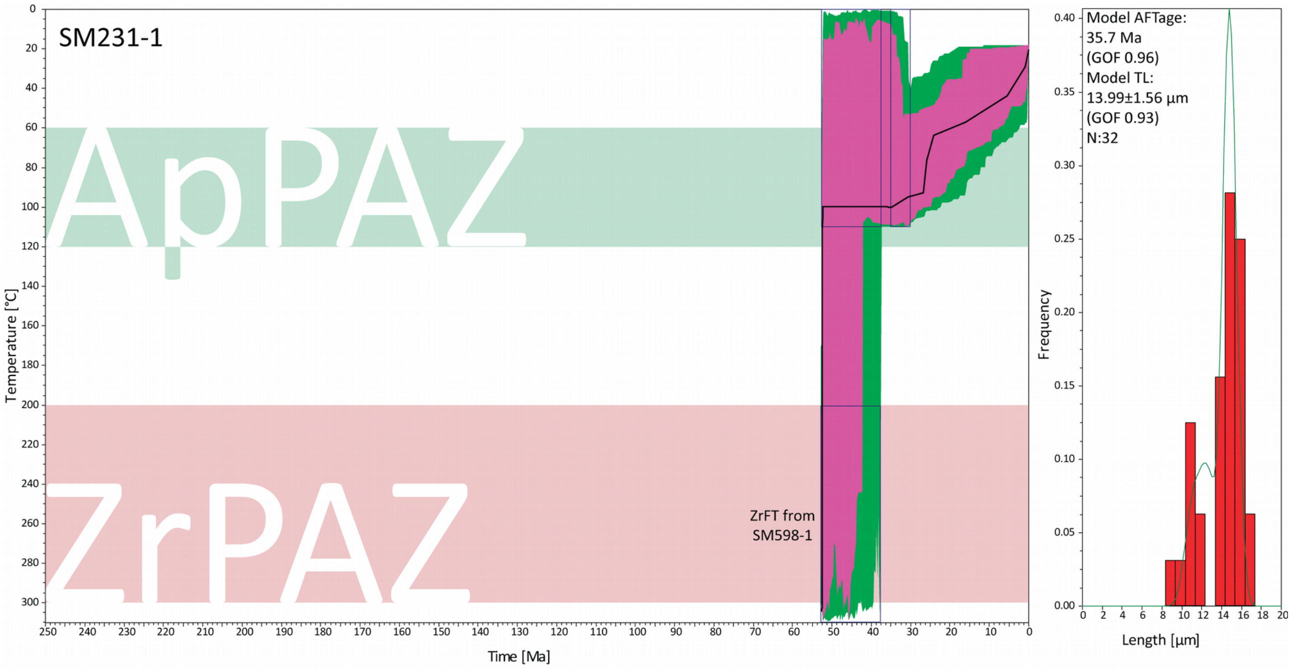
SM231-1
ApPAZ
ZrPAZ
ZrFT from SM598-1
Temperature [°C]
Time [Ma]
Model AFTage:
35.7 Ma
(GOF 0.96)
Model TL:
13.99±1.56 µm
(GOF 0.93)
N:32
Frequency
Length [µm]

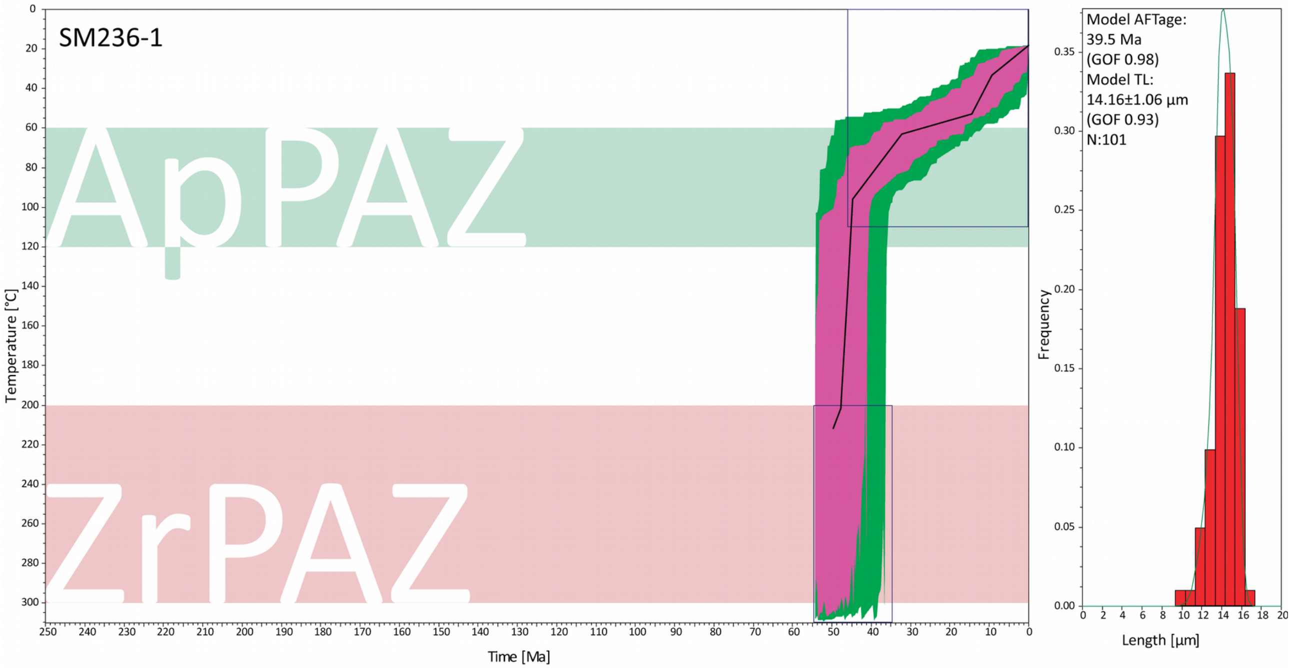
SM236-1
ApPAZ
ZrPAZ
Temperature [°C]
Time [Ma]
Model AFTage:
39.5 Ma
(GOF 0.98)
Model TL:
14.16±1.06 µm
(GOF 0.93)
N:101
Frequency
Length [µm]

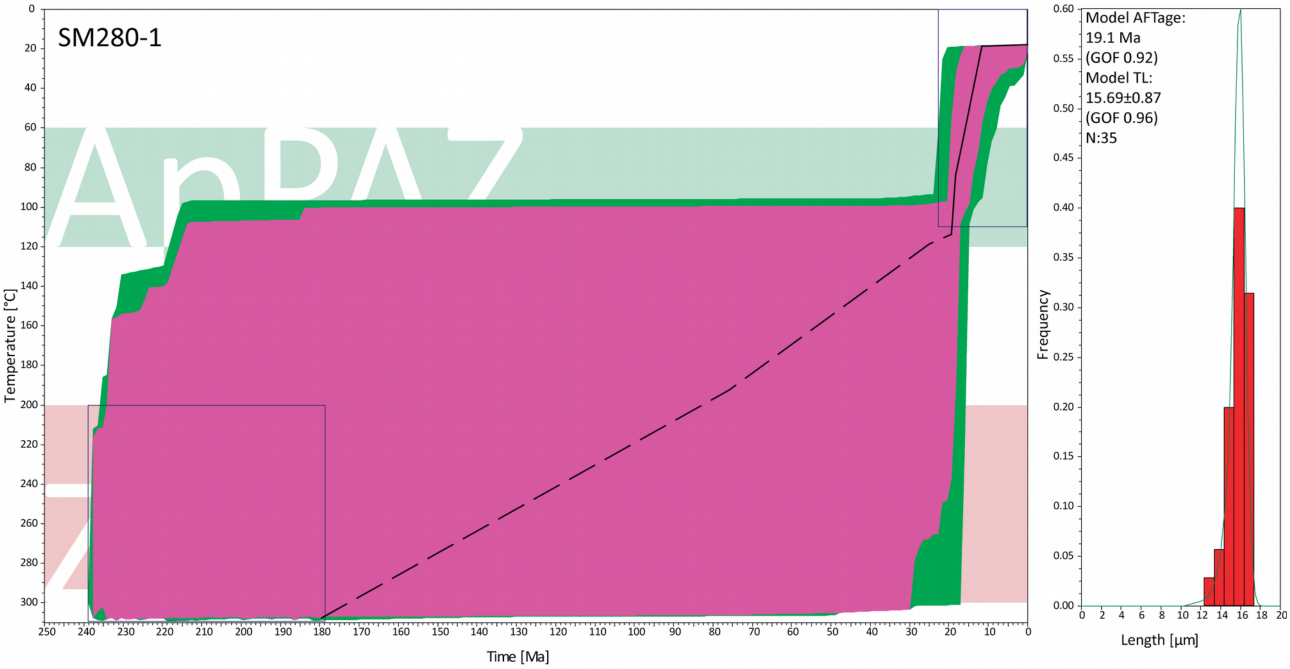
SM280-1
ApPAZ
ZrPAZ
Temperature [°C]
0
20
40
60
80
100
120
140
160
180
200
220
240
260
280
300
Time [Ma]
250
240
230
220
210
200
190
180
170
160
150
140
130
120
110
100
90
80
70
60
50
40
30
20
10
0
Model AFTage:
19.1 Ma
(GOF 0.92)
Model TL:
15.69±0.87
(GOF 0.96)
N:35
Frequency
0.00
0.05
0.10
0.15
0.20
0.25
0.30
0.35
0.40
0.45
0.50
0.55
0.60
Length [µm]
0
2
4
6
8
10
12
14
16
18
20

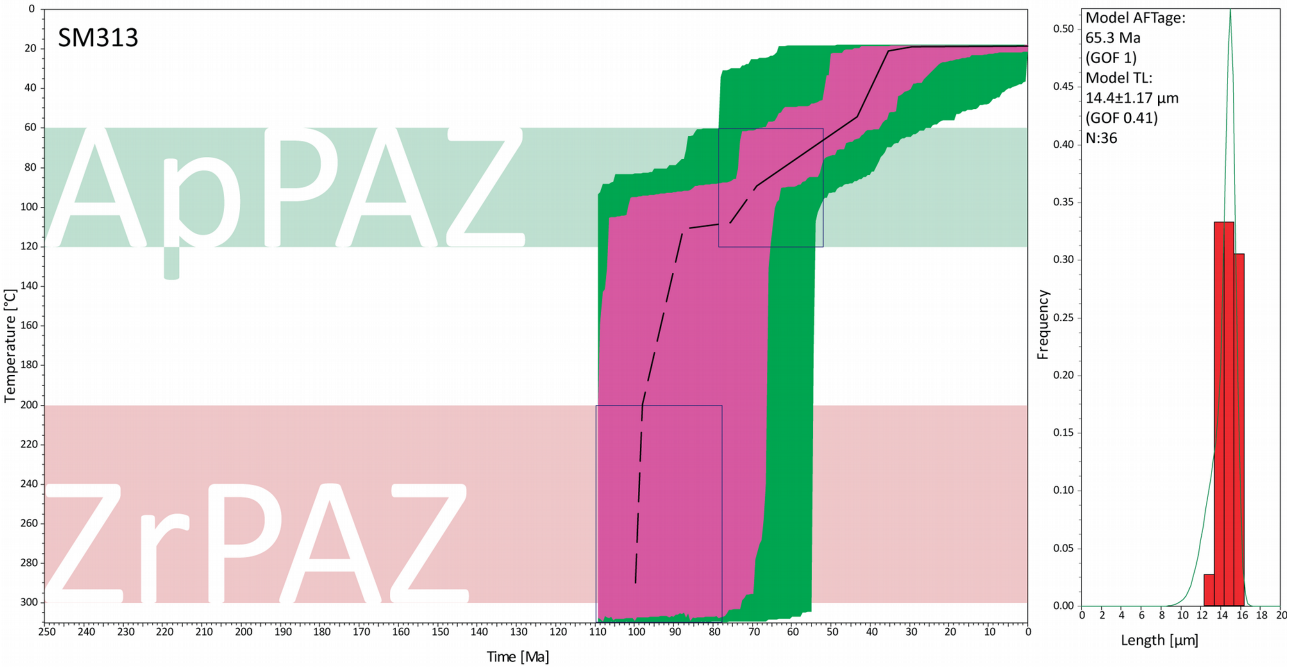
SM313
ApPAZ
ZrPAZ
Temperature [°C]
0
20
40
60
80
100
120
140
160
180
200
220
240
260
280
300
Time [Ma]
250
240
230
220
210
200
190
180
170
160
150
140
130
120
110
100
90
80
70
60
50
40
30
20
10
0
Model AFTage:
65.3 Ma
(GOF 1)
Model TL:
14.4±1.17 µm
(GOF 0.41)
N:36
Frequency
0.00
0.05
0.10
0.15
0.20
0.25
0.30
0.35
0.40
0.45
0.50
Length [µm]
0
2
4
6
8
10
12
14
16
18
20

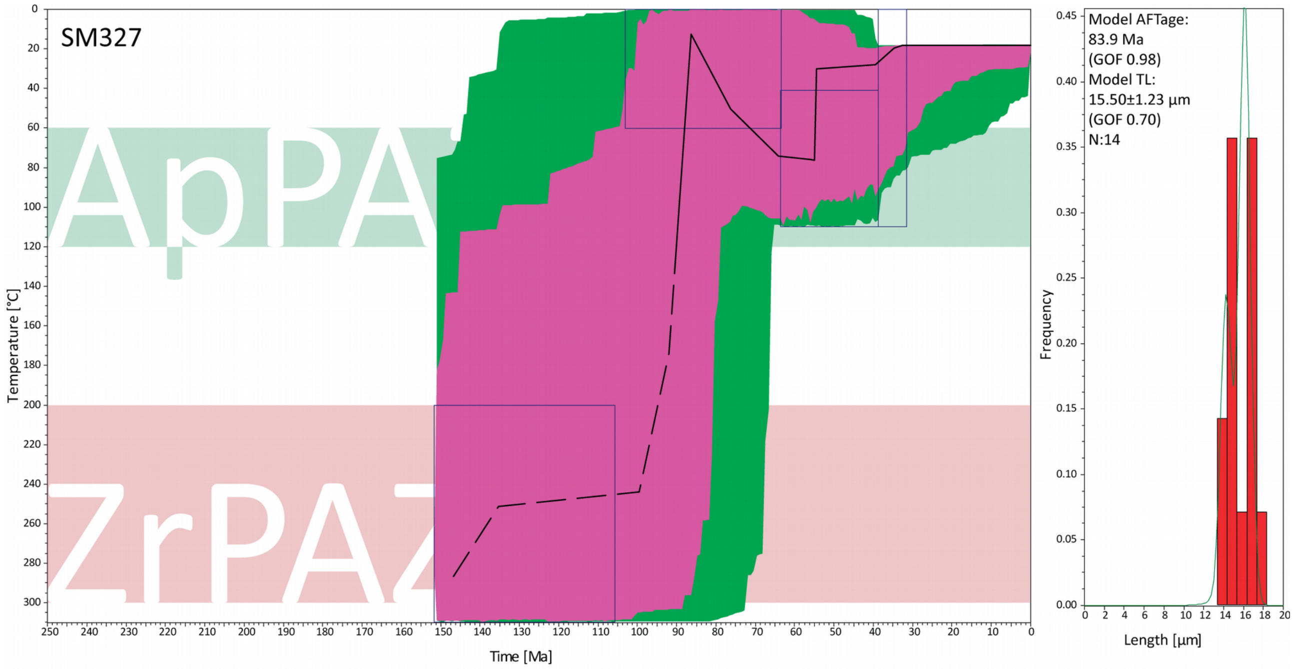
SM327
ApPAZ
ZrPAZ
Temperature [°C]
0
20
40
60
80
100
120
140
160
180
200
220
240
260
280
300
250
240
230
220
210
200
190
180
170
160
150
140
130
120
110
100
90
80
70
60
50
40
30
20
10
0
Time [Ma]
Model AFTage:
83.9 Ma
(GOF 0.98)
Model TL:
15.50±1.23 µm
(GOF 0.70)
N:14
Frequency
0.00
0.05
0.10
0.15
0.20
0.25
0.30
0.35
0.40
0.45
0
2
4
6
8
10
12
14
16
18
20
Length [µm]

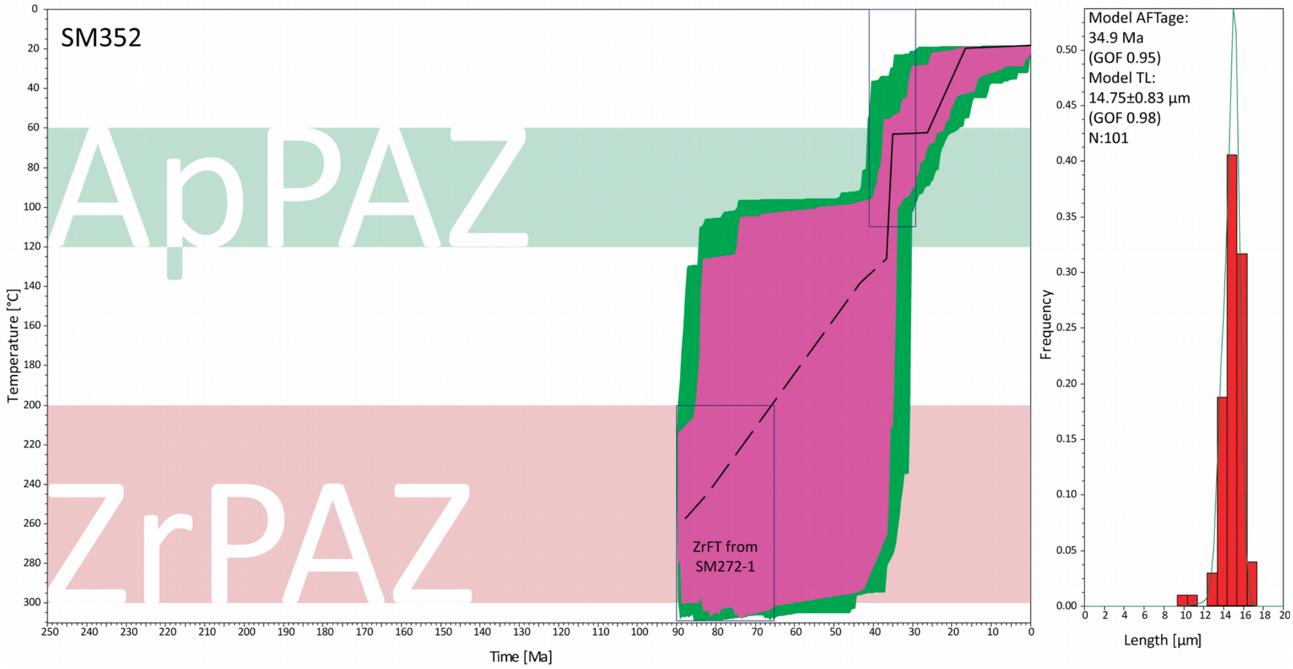
SM352
ApPAZ
ZrPAZ
ZrFT from
SM272-1
Temperature [°C]
0
20
40
60
80
100
120
140
160
180
200
220
240
260
280
300
250
240
230
220
210
200
190
180
170
160
150
140
130
120
110
100
90
80
70
60
50
40
30
20
10
0
Time [Ma]
Model AFTage:
34.9 Ma
(GOF 0.95)
Model TL:
14.75±0.83 µm
(GOF 0.98)
N:101
Frequency
0.00
0.05
0.10
0.15
0.20
0.25
0.30
0.35
0.40
0.45
0.50
0
2
4
6
8
10
12
14
16
18
20
Length [µm]

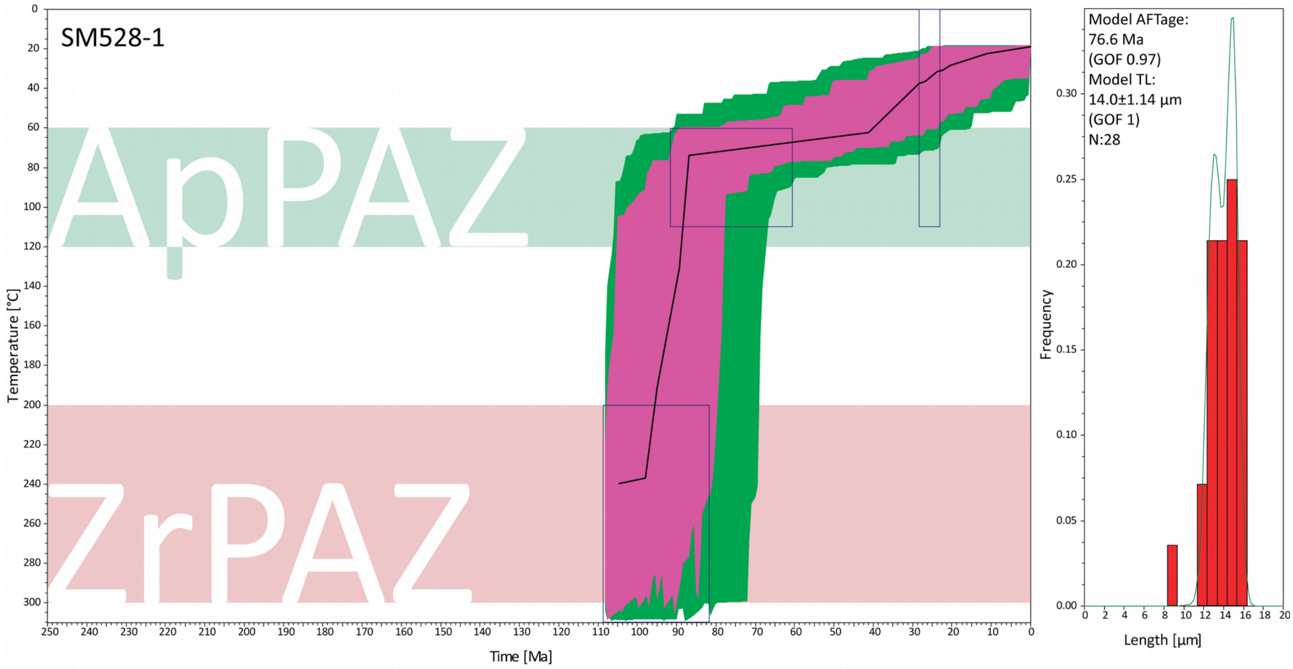
SM528-1
ApPAZ
ZrPAZ
Temperature [°C]
Time [Ma]
0
20
40
60
80
100
120
140
160
180
200
220
240
260
280
300
250
240
230
220
210
200
190
180
170
160
150
140
130
120
110
100
90
80
70
60
50
40
30
20
10
0
Model AFTage:
76.6 Ma
(GOF 0.97)
Model TL:
14.0±1.14 μm
(GOF 1)
N:28
Frequency
Length [μm]
0.00
0.05
0.10
0.15
0.20
0.25
0.30
0
2
4
6
8
10
12
14
16
18
20

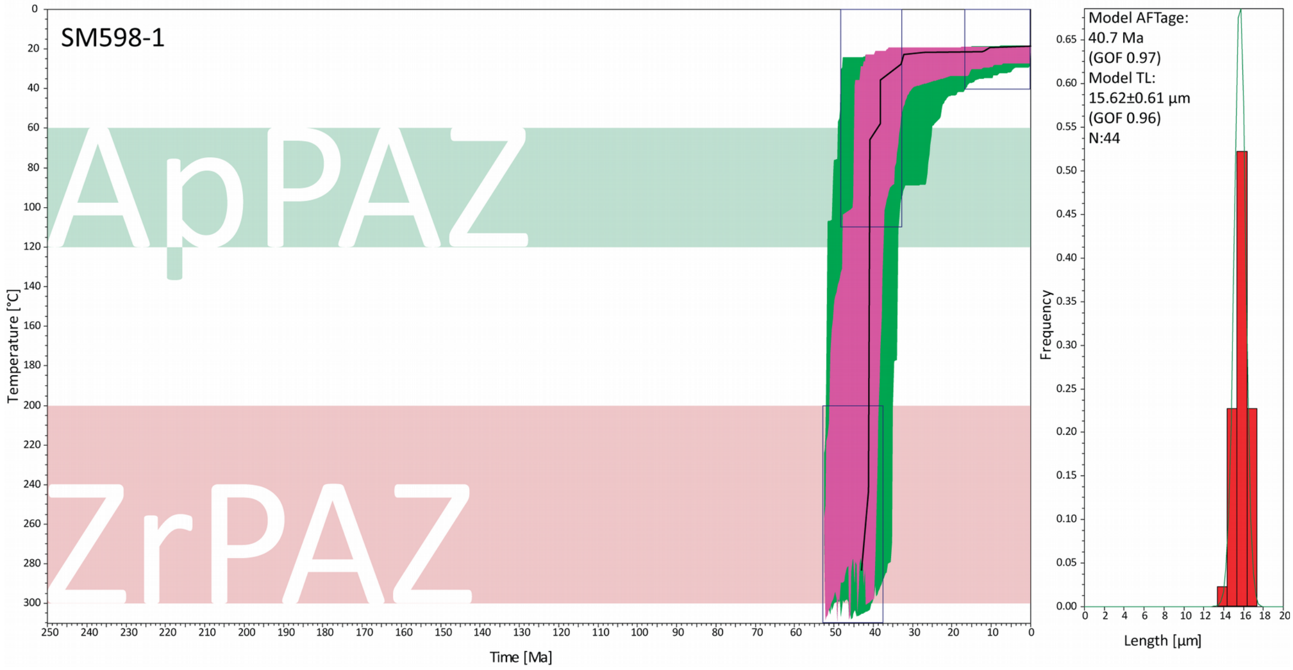
SM598-1
ApPAZ
ZrPAZ
Temperature [°C]
Time [Ma]
0
20
40
60
80
100
120
140
160
180
200
220
240
260
280
300
250
240
230
220
210
200
190
180
170
160
150
140
130
120
110
100
90
80
70
60
50
40
30
20
10
0
Model AFTage:
40.7 Ma
(GOF 0.97)
Model TL:
15.62±0.61 μm
(GOF 0.96)
N:44
Frequency
Length [μm]
0.00
0.05
0.10
0.15
0.20
0.25
0.30
0.35
0.40
0.45
0.50
0.55
0.60
0.65
0
2
4
6
8
10
12
14
16
18
20

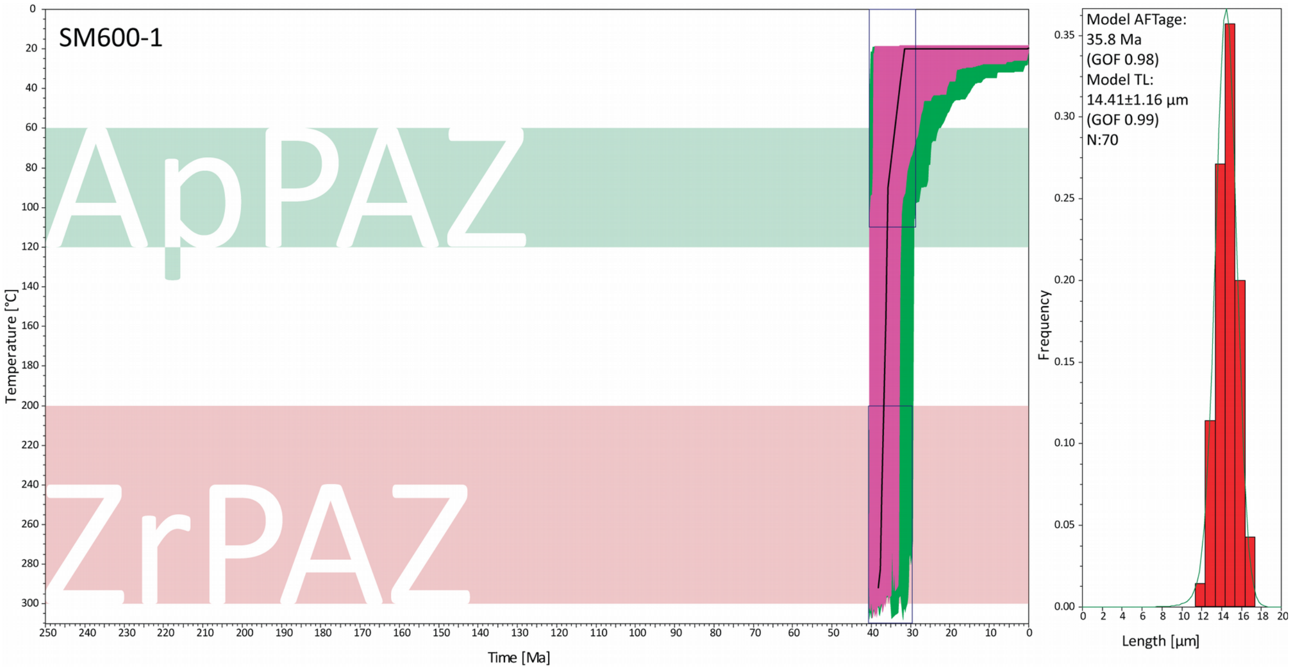

Complete tabulated data is available on request.
For more details see Appendix 4-1.

Appendix 4-3

U–Pb and geochemistry sample descriptions and results

4-3.1 Geochemistry

The chemistry of the Paleogene igneous rocks was analysed on a sample of Surdulica granodioritic pluton, and Korbevac and Stajevac dacites (SM207-1 and SM331, respectively; Fig. 4-3). Analytical results are presented in Table 4-3-1.

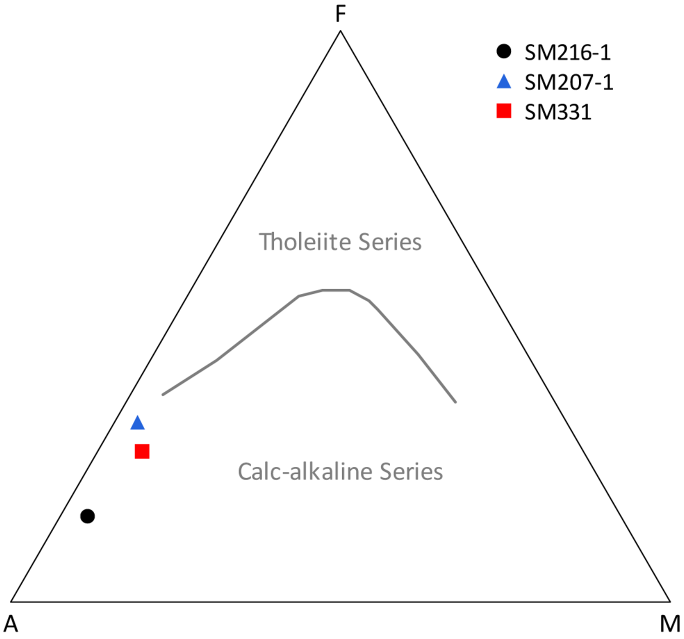

Figure 4-3-1. AFM plot of Irvine and Baragar (1971) with samples from Paleogene igneous rocks.

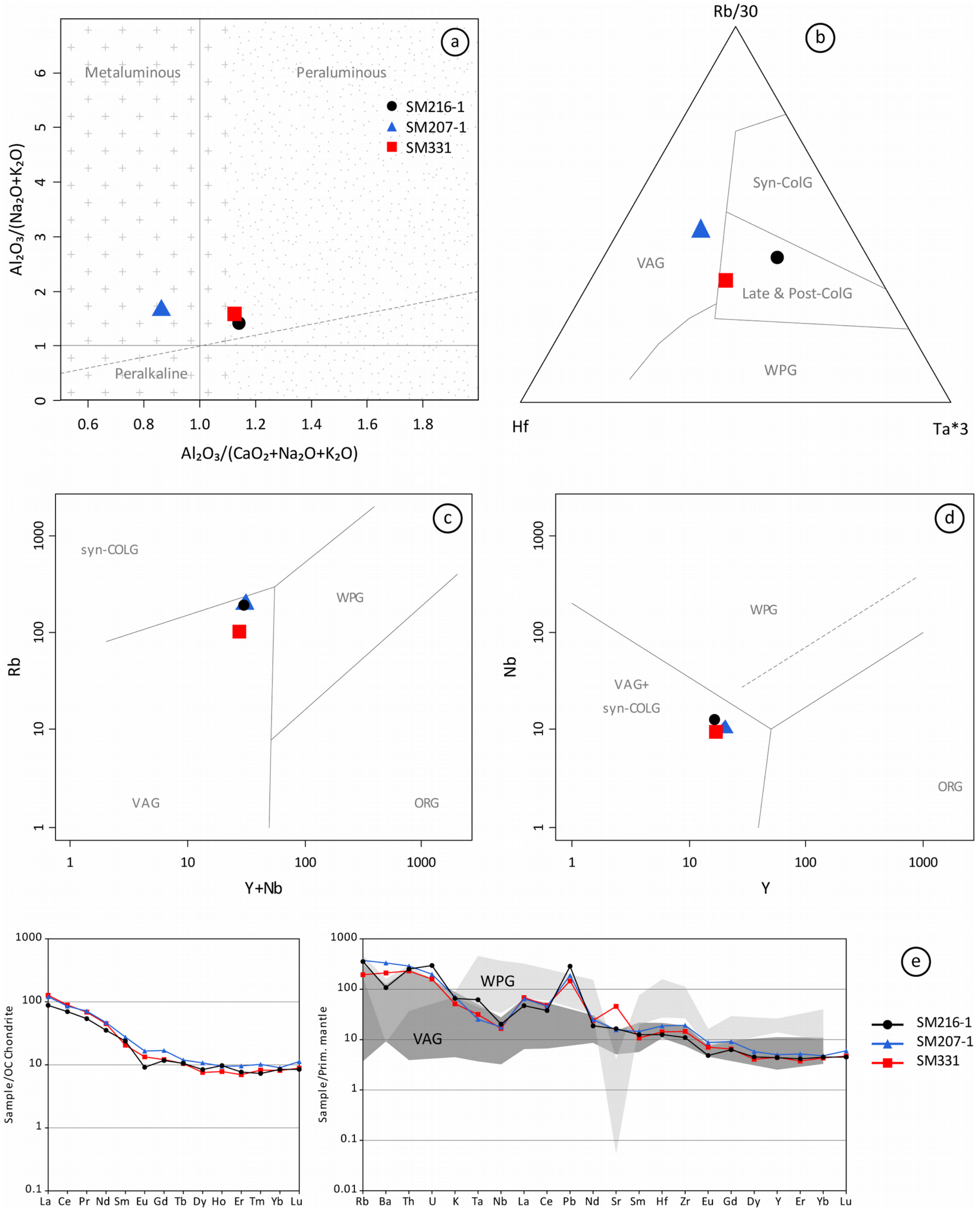

Figure 4-3-2. (a) A/CNK vs. A/NK classification plot (Shand 1943) for granitic samples; area stippled with dots is related to S-type granites; area stippled with plus symbols denominates I-type granites. (b) Ternary geotectonic discrimination diagram for granites (Harris et al. 1986); (c) and (d) Tectonomagmatic discrimination diagrams for granites (Pearce et al. 1984). Abbreviations: Syn-COLG – syn-collisional granites, WPG – within-plate granites, ORG – ocean ridge granites,VAG – volcanic arc granites; (e) Trace element pattern plots normalised for chondritic (Nakamura 1974), and primitive mantle concentrations (Hofmann 1988). Shaded areas WPG and VAG represent envelope concentrations of within-plate and volcanic-arc granites, respectively (Pearce et al. 1984)

sample	SM207-1	SM216-1	SM331
location	Korbevac	Kriva Feja	Stajevac
rock type	dacite	granodiorite	dacite
SiO_2	63,678	71,697	68,703
TiO_2	0,416	0,187	0,262
Al_2O_3	14,611	14,827	15,845
Fe_2O_3 total	3,629	1,607	3,168
MnO	0,072	0,048	0,058
MgO	0,367	0,417	0,722
CaO	4,505	1,342	2,237
Na_2O	2,439	3,717	3,994
K_2O	4,394	4,081	3,193
P_2O_5	0,287	0,086	0,136
LOI	5,017	0,940	1,047
Total	99,416	98,949	99,367
Ba	2012,908	650,571	1276,120
Rb	199,387	189,855	103,997
Sr	284,783	300,046	833,686
Zr	187,294	106,684	141,115
Nb	10,939	12,526	10,288
Ni	n/a	n/a	2,305
Co	6,551	2,098	3,681
Zn	39,427	28,111	22,334
Cr	23,797	26,747	n/a
La	39,701	28,992	41,908
Ce	73,993	60,504	77,173
Pr	7,979	6,062	7,690
Nd	29,557	22,305	28,408
Sm	5,598	4,840	4,168
Eu	1,275	0,704	1,029
Gd	4,671	3,236	3,343
Tb	0,559	0,496	0,492
Dy	3,684	2,886	2,595
Ho	0,665	0,681	0,548
Er	2,160	1,730	1,568
Tm	0,305	0,219	0,247
Yb	1,979	1,860	1,795
Lu	0,382	0,287	0,300
Y	19,807	17,269	17,537
Cs	6,250	5,339	2,795
Ta	0,888	2,173	1,107
Hf	4,994	3,372	3,810
Be	5,388	7,419	3,614
Sc	8,303	3,375	4,324
V	67,431	21,004	47,879
Cu	1,326	1,766	n/a
Ga	16,741	18,472	16,289
As	1,689	n/a	1,358
Mo	1,192	2,017	0,573
Sn	n/a	2,118	1,849
Sb	n/a	n/a	n/a
W	2,657	1,778	1,243
Tl	1,603	0,976	0,249
Pb	32,902	50,055	25,643
Bi	n/a	0,470	0,163
Th	23,482	20,493	18,764
U	4,030	6,003	3,226

Table 4-3-1. Results of main and trace elements measurements: Major element oxides in wt%, trace elements in ppm. Abbreviations: LOI – loss on ignition, n/a – bellow detection limit

4-3.2 U–Pb geochronology

4-3.2.1 Surdulica granodiorite SM216-1

Sample was taken from a roadside outcrop of undeformed, coarse-grained granodiorite close to the approximate centre of the Surdulica pluton (Fig. 4-2). The majority of the zircons are elongate and transparent, with subordinate dark yellow and stubby grains. The zircon grains typically contain inherited cores with disturbed internal texture, overgrown by oscillatory zoning (i.e. SM216-1-21a and SM216-1-21b in Fig. 4-3-3).

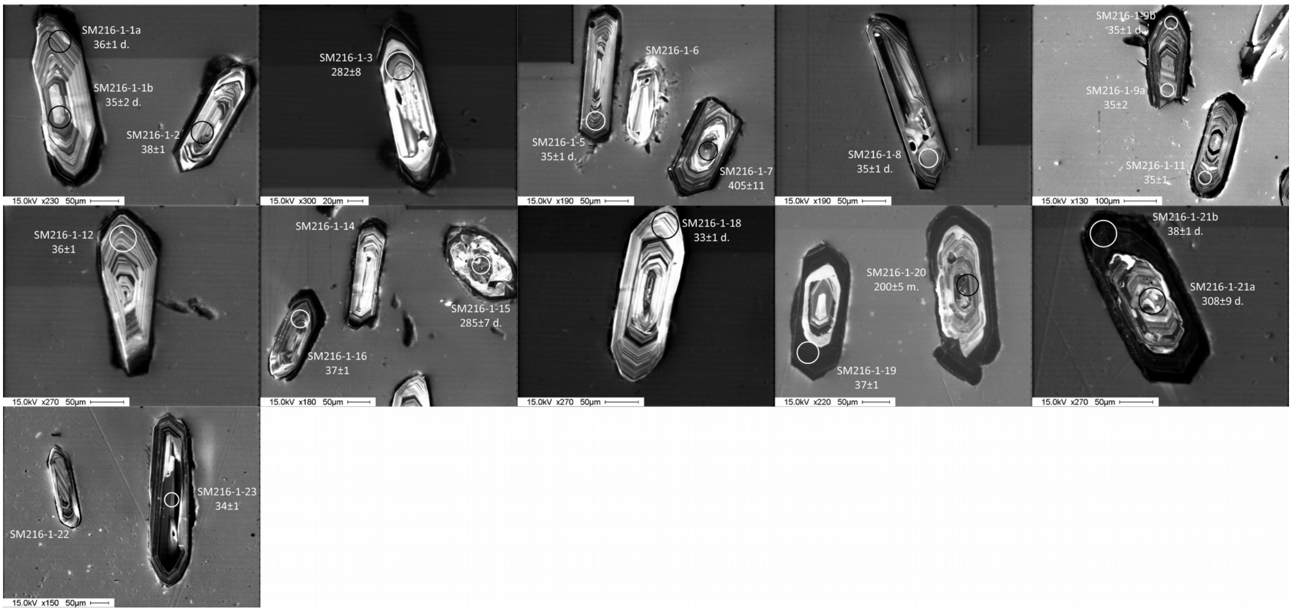

Figure 4-3-3. Cathodoluminescence images of the analysed zircons of Surdulica granodiorite (SM216-1) with $^{206}Pb/^{238}U$ age-results in Ma with 2σ errors. Suffix "d." to age results designates spots with discordant results, while suffix "m" denotes spots measured on "mixed zones", see Appendix A for details.

Eight of initial nineteen measurements yielded concordant results (Table 4-3-2). Weighted average of seven age results belonging to the youngest group, define the emplacement of Surdulica granodiorite at 36±1 Ma (Fig. 4-5a). A single inherited core gave an early Permian age of 282±8 Ma.

4-3.2.2 Korbevac dacite SM207-1

Dacitic sample was taken near Korbevac west of the Surdulica granodioritic pluton (Fig. 4-2). Recovered zircons are predominantly euhedral, elongate to acicular and transparent. More equant variety with pink hue resulting from higher inclusion content are also present. Occasional dark opaque fragments of inherited metamict cores are observed. Inherited cores are frequent and show a variety of textures often disrupted by solid state recrystallisation (e.g. SM207-1-6 in Fig. 4-3-4; Hoskin and Schaltegger 2003), or resorption (e.g. SM207-1-18 in Fig. 4-3-4; Corfu et al. 2003). The rim predominantly shows magmatic oscillatory zoning (e.g. SM207-1-14 in Fig. 4-3-4).

Only 5 of initial 28 measured spots gave concordant results (Table 4-3-2). Two inherited cores yielded an early Cambrian age (526–512 Ma), while the three spots from the youngest oscillatory growth yielded weighted average age of 35±1 Ma (Fig. 4-5b). This age is considered as the emplacement age of the dacite.

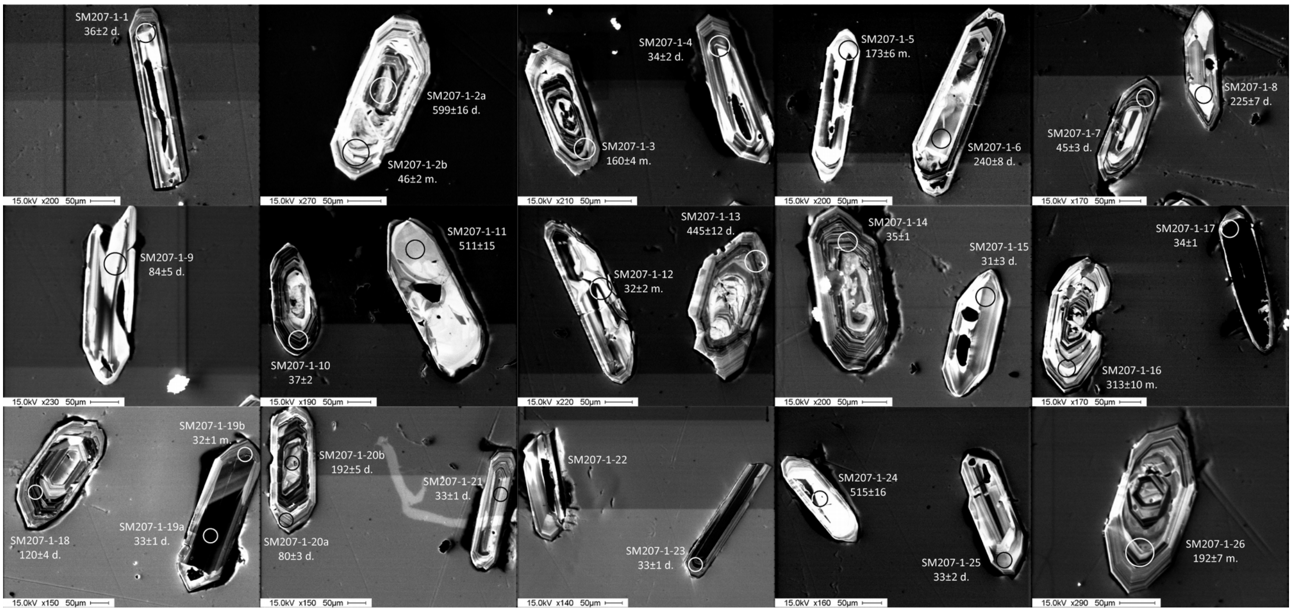

Figure 4-3-4. Cathodoluminescence images of the analysed zircons from Korbevac dacite (SM207-1) with ^{206}Pb/^{238}U age-results in Ma with 2σ errors. Suffix “d.” to age results designates spots with discordant results, while suffix “m” denotes spots measured on “mixed zones”, see Appendix A for details.

4-3.2.3 Stajevac dacite SM331

A second dacitic sample was taken from a porphyric dyke exposed in the Stajevac village south of Surdulica pluton (Fig. 4-2). Majority of the zircon grains are transparent and elongate, rarely yellow and rich in inclusions or dark due to inherited metamict cores. Simple grains with oscillatory zoning are dominant (e.g. SM331-16 in Fig. 4-3-5), although core-and-rim varieties were also commonly observed (SM311-9 in Fig. 4-3-5).

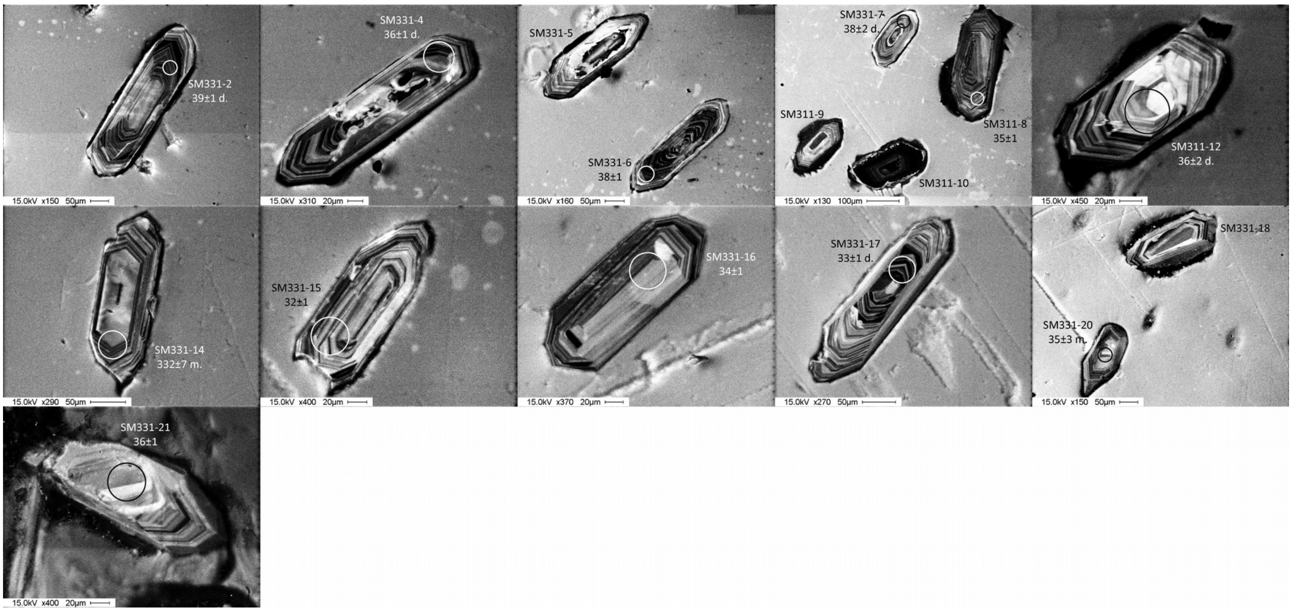

Figure 4-3-5. Cathodoluminescence image of the analysed zircons from Stajevac dacite (SM331) with ^{206}Pb/^{238}U age-results in Ma with 2σ errors. Suffix "d." to age results designates spots with discordant results, while suffix "m" denotes spots measured on "mixed zones", see Appendix A for details.

Four of originally twelve measured spots show concordant ages (Table 4-3-2). Although slightly scattered, these four results yielded a weighted average age of 35±4 Ma (Fig. 4-5c), which corresponds to the emplacement of the Stajevac porphyric dacite.

Table 4-3-2 U–Pb LA-ICP-MS results

		Isotopic ratios									Ages [Ma]						Conc.
Spot	Note	^{207}Pb/^{206}Pb	±2σ	^{206}Pb/^{238}U	±2σ	^{207}Pb/^{235}U	±2σ	^{208}Pb/^{232}Th	±2σ	^{232}Th/^{238}U	^{206}Pb/^{238}U	±2σ	^{207}Pb/^{235}U	±2σ	^{208}Pb/^{232}Th	±2σ	[%]
SM207-1 Korbevac dacite																	
SM207-1-1	**c**	**0,1033**	**0,0143**	**0,0055**	**0,0003**	**0,0782**	**0,0111**	**0,0026**	**0,0004**	**0,71**	**35,5**	**1,68**	**76,4**	**10,4**	**51,8**	**8,38**	**46,47**
SM207-1-2a	**c**	**0,0814**	**0,005**	**0,0973**	**0,0028**	**1,1264**	**0,1019**	**0,039**	**0,0053**	**0,25**	**598,7**	**16,26**	**766**	**48,64**	**773,4**	**103,4**	**78,16**
~~**SM207-1-2b**~~		~~**0,0591**~~	~~**0,012**~~	~~**0,0071**~~	~~**0,0004**~~	~~**0,0592**~~	~~**0,0123**~~	~~**0,0023**~~	~~**0,0008**~~	~~**0,19**~~	~~**45,7**~~	~~**2,4**~~	~~**58,3**~~	~~**11,74**~~	~~**46,2**~~	~~**15,18**~~	~~**78,39**~~
~~**SM207-1-3**~~		~~**0,0566**~~	~~**0,0034**~~	~~**0,0251**~~	~~**0,0007**~~	~~**0,1943**~~	~~**0,0139**~~	~~**0,0093**~~	~~**0,0012**~~	~~**0,29**~~	~~**160**~~	~~**4,26**~~	~~**180,3**~~	~~**11,82**~~	~~**187,3**~~	~~**24,42**~~	~~**88,74**~~
SM207-1-4	**r**	**0,1247**	**0,0175**	**0,0052**	**0,0003**	**0,0915**	**0,0131**	**0,0019**	**0,0003**	**1,84**	**33,5**	**1,7**	**88,9**	**12,22**	**38,4**	**5,72**	**37,68**
~~SM207-1-5~~		~~0,0497~~	~~0,0058~~	~~0,0273~~	~~0,0009~~	~~0,1822~~	~~0,0237~~	~~0,0133~~	~~0,0018~~	~~0,86~~	~~173,4~~	~~5,92~~	~~170~~	~~20,4~~	~~267,9~~	~~36,42~~	~~102~~
SM207-1-6	**c**	**0,0667**	**0,0067**	**0,038**	**0,0013**	**0,3612**	**0,0434**	**0,0138**	**0,0021**	**0,57**	**240,2**	**8,04**	**313,1**	**32,38**	**277,5**	**41,28**	**76,72**
SM207-1-7	**lb**	**0,2623**	**0,0319**	**0,007**	**0,0004**	**0,2435**	**0,0314**	**0,0055**	**0,0009**	**0,86**	**44,9**	**2,6**	**221,2**	**25,6**	**110,7**	**18,14**	**20,3**
SM207-1-8	**c**	**0,055**	**0,0045**	**0,0356**	**0,0011**	**0,2691**	**0,0261**	**0,011**	**0,0017**	**0,41**	**225,3**	**6,62**	**242**	**20,88**	**221,5**	**33,34**	**93,1**
SM207-1-9	**c**	**0,5857**	**0,0598**	**0,013**	**0,0008**	**1,0546**	**0,1345**	**0,0225**	**0,0036**	**0,7**	**83,5**	**5,2**	**731,2**	**66,48**	**449,9**	**70,9**	**11,42**
SM207-1-10	r	0,0523	0,0131	0,0057	0,0003	0,0384	0,0097	0,0016	0,0004	0,62	36,5	2,16	38,2	9,5	31,7	7,98	95,55
SM207-1-11	c	0,0585	0,0045	0,0825	0,0025	0,656	0,0676	0,0267	0,0044	0,35	511	14,6	512,2	41,44	531,9	86,38	99,77
~~**SM207-1-12**~~		~~**0,0602**~~	~~**0,0137**~~	~~**0,005**~~	~~**0,0003**~~	~~**0,0406**~~	~~**0,0094**~~	~~**0,0019**~~	~~**0,0005**~~	~~**0,5**~~	~~**31,9**~~	~~**1,84**~~	~~**40,4**~~	~~**9,12**~~	~~**37,4**~~	~~**9,14**~~	~~**78,96**~~
SM207-1-13	**r**	**0,0597**	**0,0038**	**0,0715**	**0,002**	**0,5944**	**0,0502**	**0,0217**	**0,0036**	**0,34**	**445,1**	**11,94**	**473,7**	**31,94**	**434,4**	**71,14**	**93,96**
SM207-1-14	r	0,0491	0,0063	0,0054	0,0002	0,0361	0,0049	0,0017	0,0003	0,54	34,6	1,24	36	4,8	33,7	6,36	96,11
SM207-1-15	**c**	**0,0591**	**0,0209**	**0,0049**	**0,0004**	**0,0404**	**0,0143**	**0,0013**	**0,0003**	**1,61**	**31,2**	**2,62**	**40,2**	**13,98**	**27**	**6,78**	**77,61**
~~SM207-1-16~~		~~0,0518~~	~~0,0048~~	~~0,0497~~	~~0,0016~~	~~0,3742~~	~~0,0433~~	~~0,0151~~	~~0,0028~~	~~0,6~~	~~312,9~~	~~9,64~~	~~322,8~~	~~32~~	~~302,5~~	~~55,08~~	~~96,93~~
SM207-1-17		0,0477	0,0039	0,0053	0,0002	0,0331	0,0031	0,0012	0,0002	3,94	34,1	1	33,1	3,04	23,4	4,16	103
SM207-1-18		**0,0619**	**0,0051**	**0,0189**	**0,0006**	**0,1579**	**0,0157**	**0,0097**	**0,002**	**0,16**	**120,4**	**3,66**	**148,8**	**13,74**	**195,9**	**39,18**	**80,91**
SM207-1-19a		**0,0617**	**0,0092**	**0,0051**	**0,0002**	**0,0425**	**0,0067**	**0,0015**	**0,0003**	**1,63**	**33,1**	**1,4**	**42,2**	**6,48**	**31**	**6,22**	**78,44**
~~**SM207-1-19b**~~		~~**0,0521**~~	~~**0,008**~~	~~**0,005**~~	~~**0,0002**~~	~~**0,035**~~	~~**0,0055**~~	~~**0,0015**~~	~~**0,0002**~~	~~**1,37**~~	~~**32,4**~~	~~**1,32**~~	~~**35**~~	~~**5,36**~~	~~**30,2**~~	~~**4,02**~~	~~**92,57**~~
SM207-1-20a	**r**	**0,0669**	**0,0069**	**0,0125**	**0,0004**	**0,1116**	**0,0123**	**0,0032**	**0,0005**	**0,47**	**79,9**	**2,74**	**107,4**	**11,24**	**65,3**	**9,92**	**74,39**
SM207-1-20b	**c**	**0,0588**	**0,0042**	**0,0302**	**0,0009**	**0,2393**	**0,0199**	**0,0092**	**0,0011**	**1,07**	**191,8**	**5,42**	**217,8**	**16,28**	**184,6**	**21,6**	**88,06**
SM207-1-21		**0,0503**	**0,0054**	**0,0051**	**0,0002**	**0,0349**	**0,0039**	**0,0015**	**0,0002**	**0,65**	**32,9**	**1,08**	**34,8**	**3,84**	**30,8**	**4,2**	**94,54**
SM207-1-23		**0,067**	**0,0063**	**0,0052**	**0,0002**	**0,0464**	**0,0046**	**0,0016**	**0,0002**	**2,1**	**33,2**	**1,08**	**46,1**	**4,44**	**32,8**	**4,02**	**72,02**
SM207-1-24	c	0,0577	0,0052	0,0831	0,0026	0,6793	0,081	0,0261	0,0038	0,41	514,8	15,66	526,4	48,96	521,1	74,46	97,8
SM207-1-25	**r**	**0,06**	**0,0156**	**0,0051**	**0,0003**	**0,0424**	**0,0111**	**0,0019**	**0,0005**	**0,47**	**32,6**	**2,1**	**42,2**	**10,84**	**38,7**	**9,76**	**77,25**
~~**SM207-1-26**~~		~~**0,0543**~~	~~**0,0066**~~	~~**0,0302**~~	~~**0,0011**~~	~~**0,2238**~~	~~**0,0307**~~	~~**0,0035**~~	~~**0,0015**~~	~~**0,1**~~	~~**191,8**~~	~~**6,84**~~	~~**205,1**~~	~~**25,5**~~	~~**70,7**~~	~~**29,42**~~	~~**93,52**~~

Table 4-3-2 continued

		Isotopic ratios									Ages [Ma]						Conc.
Spot	Note	^{207}Pb/^{206}Pb	±2σ	^{206}Pb/^{238}U	±2σ	^{207}Pb/^{235}U	±2σ	^{208}Pb/^{232}Th	±2σ	^{232}Th/^{238}U	^{206}Pb/^{238}U	±2σ	^{207}Pb/^{235}U	±2σ	^{208}Pb/^{232}Th	±2σ	[%]
SM216-1 Kriva Feja granodiorite																	
SM216-1-1a	**r**	**0,0535**	**0,0058**	**0,0056**	**0,0002**	**0,0409**	**0,0047**	**0,0018**	**0,0003**	**0,21**	**36,2**	**1,22**	**40,7**	**4,56**	**36,7**	**6,9**	**88,94**
SM216-1-1b	**c**	**0,0409**	**0,0079**	**0,0054**	**0,0002**	**0,0308**	**0,0061**	**0,0014**	**0,0003**	**0,42**	**34,5**	**1,52**	**30,8**	**5,96**	**28,8**	**6,24**	**112**
SM216-1-2		0,0489	0,0067	0,0059	0,0002	0,0382	0,0054	0,002	0,0005	0,16	37,6	1,4	38	5,28	40,5	9,62	98,95
SM216-1-3	c	0,0546	0,0043	0,0447	0,0013	0,3288	0,0319	0,0137	0,0022	0,41	282	8,18	288,6	24,4	275,5	44,5	97,71
SM216-1-5	**r**	**0,0506**	**0,0061**	**0,0055**	**0,0002**	**0,0389**	**0,0049**	**0,0015**	**0,0003**	**0,28**	**35,2**	**1,24**	**38,7**	**4,8**	**29,8**	**6,2**	**90,96**
SM216-1-7	**c**	**0,0577**	**0,004**	**0,0648**	**0,0018**	**0,5304**	**0,0476**	**0,021**	**0,0036**	**0,23**	**404,8**	**11,12**	**432,1**	**31,58**	**419,6**	**71,86**	**93,68**
SM216-1-8	**c**	**0,0447**	**0,0058**	**0,0055**	**0,0002**	**0,0332**	**0,0045**	**0,0018**	**0,0004**	**0,39**	**35,1**	**1,24**	**33,1**	**4,46**	**36,4**	**7,16**	**106**
SM216-1-9a	c	0,0465	0,0079	0,0055	0,0002	0,0351	0,0062	0,002	0,0005	0,27	35,4	1,5	35	6,04	40	9,66	101
SM216-1-9b	**r**	**0,0423**	**0,0055**	**0,0054**	**0,0002**	**0,0319**	**0,0044**	**0,0017**	**0,0004**	**0,3**	**35**	**1,24**	**31,9**	**4,36**	**33,3**	**7,22**	**110**
SM216-1-11	r	0,0474	0,0056	0,0055	0,0002	0,0367	0,0046	0,0016	0,0004	0,31	35,3	1,2	36,6	4,54	32,7	7,08	96,45
SM216-1-12	r	0,0486	0,0058	0,0056	0,0002	0,0381	0,0049	0,0017	0,0004	0,3	36,1	1,26	37,9	4,82	34,6	7,74	95,25
SM216-1-16	r	0,0491	0,0041	0,0057	0,0002	0,0386	0,0038	0,0017	0,0004	0,19	36,7	1,1	38,5	3,7	34,3	7,42	95,32
SM216-1-15	**c**	**0,078**	**0,0039**	**0,0452**	**0,0012**	**0,4867**	**0,0315**	**0,0188**	**0,0023**	**0,33**	**285,1**	**7,34**	**402,7**	**21,5**	**375,8**	**46,52**	**70,8**
SM216-1-18	**r**	**0,05**	**0,0052**	**0,0052**	**0,0002**	**0,0359**	**0,0039**	**0,0015**	**0,0002**	**0,33**	**33,2**	**1,08**	**35,9**	**3,82**	**29,8**	**4,84**	**92,48**
SM216-1-19	r	0,0468	0,0027	0,0057	0,0001	0,0359	0,0023	0,0018	0,0003	0,13	36,7	0,96	35,8	2,3	35,6	5,04	103
~~SM216-1-20~~		**~~0,0624~~**	**~~0,004~~**	**~~0,0315~~**	**~~0,0009~~**	**~~0,271~~**	**~~0,021~~**	**~~0,0103~~**	**~~0,0013~~**	**~~0,93~~**	**~~199,8~~**	**~~5,48~~**	**~~243,5~~**	**~~16,78~~**	**~~207,7~~**	**~~26,62~~**	**~~82,05~~**
SM216-1-21a	**c**	**0,0616**	**0,0044**	**0,049**	**0,0014**	**0,421**	**0,0376**	**0,0239**	**0,0039**	**0,11**	**308,3**	**8,7**	**356,7**	**26,88**	**476,4**	**76,68**	**86,43**
SM216-1-21b	**r**	**0,0572**	**0,0034**	**0,0059**	**0,0002**	**0,0455**	**0,0031**	**0,0027**	**0,0004**	**0,11**	**38,1**	**1,02**	**45,1**	**3,02**	**54,1**	**8,14**	**84,48**
SM216-1-23	c	0,0464	0,0069	0,0053	0,0002	0,0335	0,0051	0,0016	0,0003	0,76	34,2	1,32	33,5	5,02	32,8	5,42	102
SM331 Stajevac dacite																	
SM331-2	**r**	**0,051**	**0,0064**	**0,0061**	**0,0002**	**0,0426**	**0,0056**	**0,0021**	**0,0005**	**0,2459**	**38,9**	**1,2**	**42,3**	**5,42**	**42,9**	**9,48**	**91,96**
SM331-4	**r**	**0,0495**	**0,0091**	**0,0055**	**0,0002**	**0,038**	**0,0072**	**0,0016**	**0,0004**	**0,3293**	**35,5**	**1,44**	**37,9**	**7,02**	**32,1**	**8,62**	**93,67**
SM331-6	r	0,0466	0,0061	0,0059	0,0002	0,0368	0,0051	0,0017	0,0004	0,2083	37,6	1,2	36,7	4,98	33,7	8,46	102
SM331-7	**r**	**0,0543**	**0,0091**	**0,006**	**0,0002**	**0,045**	**0,0078**	**0,0015**	**0,0004**	**0,3864**	**38,2**	**1,5**	**44,7**	**7,58**	**29,6**	**8,02**	**85,46**
SM331-8	r	0,0471	0,007	0,0055	0,0002	0,0357	0,0055	0,0018	0,0004	0,4073	35,3	1,18	35,6	5,38	35,4	7,6	99,16
SM331-12		**0,0349**	**0,016**	**0,0055**	**0,0004**	**0,0258**	**0,0119**	**0,0014**	**0,0005**	**0,6498**	**35,6**	**2,46**	**25,8**	**11,76**	**28,9**	**9,86**	**138**
~~SM331-14~~		**~~0,0598~~**	**~~0,0032~~**	**~~0,0528~~**	**~~0,0011~~**	**~~0,4261~~**	**~~0,0311~~**	**~~0,008~~**	**~~0,0015~~**	**~~0,3116~~**	**~~331,8~~**	**~~6,9~~**	**~~360,4~~**	**~~22,12~~**	**~~160,3~~**	**~~29,48~~**	**~~92,06~~**
SM331-15		0,0483	0,0067	0,005	0,0002	0,0336	0,0049	0,0017	0,0004	0,3898	32,3	1,06	33,6	4,82	34,3	7,42	96,13

		Isotopic ratios									Ages [Ma]						Conc.
Spot	Note	^{207}Pb/^{206}Pb	±2σ	^{206}Pb/^{238}U	±2σ	^{207}Pb/^{235}U	±2σ	^{208}Pb/^{232}Th	±2σ	^{232}Th/^{238}U	^{206}Pb/^{238}U	±2σ	^{207}Pb/^{235}U	±2σ	^{208}Pb/^{232}Th	±2σ	[%]
SM331 Stajevac dacite (continued)																	
SM331-16		**0,043**	**0,0065**	**0,0053**	**0,0002**	**0,032**	**0,0051**	**0,0015**	**0,0003**	**0,5601**	**33,7**	**1,12**	**32**	**5,02**	**29,4**	**6,32**	**105**
SM331-17	**ib**	**0,0514**	**0,006**	**0,0051**	**0,0002**	**0,0359**	**0,0045**	**0,0016**	**0,0003**	**0,3673**	**32,7**	**1**	**35,8**	**4,44**	**31,3**	**6,84**	**91,34**
~~**SM331-20**~~		~~**0,0712**~~	~~**0,0316**~~	~~**0,0055**~~	~~**0,0005**~~	~~**0,0523**~~	~~**0,0235**~~	~~**0,0018**~~	~~**0,0008**~~	~~**0,5947**~~	~~**35**~~	~~**3,18**~~	~~**51,7**~~	~~**22,64**~~	~~**35,9**~~	~~**15,7**~~	~~**67,7**~~
SM331-21		0,0455	0,006	0,0056	0,0002	0,0345	0,0049	0,0018	0,0004	0,5658	35,9	1,16	34,4	4,86	36,7	8,2	104

Note:

Concordance (Conc.) is calculated as 100·((^{206}Pb/^{238}U age)·(^{207}Pb/^{235}U age)$^{-1}$)

Values beyond the accepted tolerance (95—105%) are given in bold print

The “mixed results” are stricken-through

Explanation of values in the “Note” column:

r – rim

ib – internal growth-band

c – core

empty cell – grain with simple zoning

References

Corfu F, Hanchar JM, Hoskin PWO, Kinny P (2003) Atlas of Zircon Textures. Rev Mineral Geochem 53:469–500. doi: 10.2113/0530469

Hoskin PWO, Schaltegger U (2003) The Composition of Zircon and Igneous and Metamorphic Petrogenesis. Rev Mineral Geochem 53:27–62. doi: 10.2113/0530027

Appendix 4-4

Operational parameters of instruments used for measuring of the isotopic ratios

Table 4-4-1. Operational parameters of instruments used for measuring of the isotopic ratios.

Laser ablation system	
Make, model & type	Prototype similar to Geolas (Coherent)
Ablation cell & volume	Homemade, rhombic shape, ca. 7 cm^3
Laser wavelength	193 nm
Pulse width	25 ns
Fluence [J/cm2]	4
Repetition rate [Hz]	10
Spot size [μm]	40
Sampling mode/Pattern	Single hole drilling
Carrier gas	100% He
Ablation duration [s]	50
Cell carrier gas flow [l/min]	1,1
ICP-MS Instrument	
Make, model & type	Elan 6100 DRC Q-ICP-MS
Sample introduction	Ablation aerosol only, squid aerosol homogenization device
RF power [W]	1450
Make-up gas flow	0.8 $l \cdot min^{-1}$ Ar
Detection system	Single detector dual mode SEM, analog
Masses measured	202, 204, 206, 207, 208, 232, 235, 238
Integration time per peak	10 ms (masses 202, 204, 208, 232), 20 ms (masses 235, 238), and 30 ms (masses 206, 207)
Total integration time per reading [s]	0,14
IC dead time [ns]	30
Data Processing	
Gas blank	40 sec prior to each ablation spot
Calibration strategy	GJ-1 used as primary reference material, Plešovice, 91500 & Temora used as secondaries for quality control
Reference material	91500 (Wiedenbeck et al., 1995), Plešovice (Sláma et al., 2008), GJ1 $^{206}Pb/^{238}U$ 602.3 ± 1 Ma, $^{207}Pb/^{206}Pb$ 609.2 ± 0.7 Ma (in-house TIMS, unpublished)
Data processing software/correction for LIEF	Iolite 2.5 with VizualAge
Mass discrimination	Mass bias correction for all ratios normalized to primary reference material
Common-Pb correction, composition and uncertainty	Common-Pb correction not performed
Uncertainty level and propagation	Ages are given at 2σ absolute, propagation is by quadratic addition. Reproducibility of reference material uncertainty is propagated
Th disequilibrium correction and error propagation	$^{206}Pb/^{238}U$ ages of all samples were corrected using equation of Schärer (1984) or Sakata et al (2013). All errors from $^{206}Pb/^{238}U$ ratios and ages are propagated

Chapter 5

Summary

5 Summary

The central parts of the crystalline Serbo-Macedonian Massif (SMM) have a long and complex geological history which can be summarised in four main episodes: (i) Formation of the protoliths took place in a North-Gondwanan magmatic arc from late Neoproterozoic until the earliest Silurian, (ii) since Early Devonian until late Carboniferous the central SMM was subjected to high-strain ductile deformation associated with the assembly of the Galatian super-terrane and subsequent collision with Laurussia, (iii) from late Permian until the Late Cretaceous the SMM was affected by processes related to the evolution of the Mesozoic Tethys Ocean, and (iiii) since the early Late Cretaceous the central SMM was exhumed to shallow crustal position and deformed in brittle regime. The results presented in the individual chapters are outlined below as synoptic conclusions. Furthermore, new questions arising from the conclusion of this study are given together with suggested prospects for future research.

5.1 Main results

The geochemical analysis, Hf isotope measurements, and U–Pb LA-ICP-MS zircon dating of igneous and sedimentary rocks from the central SMM and the basement of the adjacent units, presented in Chapter 2 have allowed the following conclusions to be made:

- During the Cadomian orogenic cycle the Lower Complex of the central SMM represented a part of the continental magmatic-arc developed along the northern margin of Gondwana. The Lower Complex could be correlated with the Lotru and Pirgadikia units of the Carpathians and the Internal Hellenides, respectively. Based on inherited and detrital zircon data, its late Neoproterozoic position in the eastern part of the northern margin of Gondwana is tentatively proposed (i.e. northeast of Saharan metacraton and southwest of South-China craton).

- The volcano-sedimentary pre-Ordovician Vlasina Unit most probably represented a part of the late Neoproterozoic accretionary wedge dominated by ocean-floor sediments. During this time the Lower Complex was most probably a more internal part of the same volcano-sedimentary succession or a fore-arc basin.

- The magmatic-arc activity in the study area was detected in the Ediacaran to the mid-Cambrian in the Lower Complex, Vlasina Unit and the basement of Struma Unit. These units together with the Eastern Veles series, experienced renewal of arc-related magmatism in the late Cambrian to Early Ordovician, whereas mafic magmatism associated with rifting occurred in the Lower Complex during Middle to Late Ordovician. Minor pulse of within-plate felsic magmatism in the Lower Complex took place in the early Silurian.

- The age of the high-strain deformation and peak metamorphism in the SMM was constrained to the Variscan orogeny by the presence of highly deformed early Silurian meta-granites (Bujanovac Qz monzonite) in the Lower Complex, and undeformed late Carboniferous granites (Slatinska Reka granites) intruding gneisses of the same unit.

- The Variscan collisional tectonics led to the differential burial of constituents of the SMM (i.e. Lower Complex, Vlasina Unit, basement of Struma Unit, and Eastern Veles series), resulting in different metamorphic grades of these domains with a common late Neoproterozoic–early Palaeozoic history. Subsequently, this complex Variscan framework was severely disrupted during the Alpine events.

- During Permian-Triassic the entire SMM experienced widespread crustal extension and emplacement of within-plate granites, most probably related to the rifting of the Mesozoic

Neotethys.

The structural investigations presented in Chapter 3 led to recognition of at least three major stages of ductile deformation in the central SMM. Despite the different peak metamorphic conditions in the Lower Complex and Vlasina Unit, both units show a common deformational evolution. Results of the $^{40}Ar/^{39}Ar$ thermochronological analyses helped to refine the established deformational evolution and asses the regional importance of determined tectonic events.

- The earliest stage of deformation D_1 in the central SMM is related to isoclinal folding, commonly preserved as quartz-feldspar rootless fold hinges up to decimetre-scale.

- The second deformation stage D_2 is associated with general southeastward tectonic transport and refolding of older structures into recumbent metre- to kilometre-scale tight to isoclinal folds.

- The deformation stages D_1 and D_2 could not be temporally separated, and probably took place in close sequence. Based on the stratigraphic age of the youngest affected sediments, and the intrusion ages of the oldest undeformed magmatic rocks, the age of these two ductile deformation stages was constrained to the Variscan orogeny (i.e. ca. 408-ca. 328). During this time the SMM was involved in a transpressional amalgamation of the western and eastern parts of the Galatian super-terrane and subsequent collision with Laurussia, which could account for the changes in direction of strain axes during D_1 and D_2.

- A trend of diminishing strain and metamorphic grade from amphibolite facies in the Lower Complex, across the greenschist facies in the pre-Ordovician Vlasina to anchimetamorphism in thesedimentary rocks of post-Cambrian Vlasina, suggests different crustal positions of the central SMM during the Variscan orogeny.

- Cooling below the greenschist facies conditions in the western part of the Vlasina Unit has taken place in a post-orogenic setting (extensional or transtensional) in the early Permian (284±1 Ma).

- The age of activity along the top-to-the-west shear zone formed within the ortho-gneiss in the Božica area of the Vlasina Unit was constrained to Middle Triassic (246±1 Ma). This age coincides with widespread extension related to the opening of the Mesozoic Tethys.
- Rare outcrop-scale evidence of the final stage of ductile deformation D_3 is limited to the formation of spaced and crenulation cleavage. These structures are probably related to the large-scale folding reported by earlier studies. The maximum age of this event is constrained by the crenulation of the Middle Triassic mylonitic foliation in the Božica area.
- Anastomosing shear zones, S-C fabric and spaced cleavage developed in the Permo-Triassic Bujanovac granite provide evidence of an additional post-Triassic ductile deformational event. Additional data is needed to constrain the area affected by this deformation and its exact timing.
- The greenschist facies retrogression in the Lower Complex probably occurred in the Early Jurassic and it is probably related to the thermal processes in the overriding plate above the subducting slab of the Mesozoic Tethys Ocean.

The new results of thermo- and geochronological analyses reveal three main cooling stages along the central parts of the SMM since the Cretaceous (see Chapter 4 for details):

- The late Early- to early Late Cretaceous rapid cooling (ca. 110–ca. 90 Ma), affected the SMM. This event was most probably related to the post-collisional extension following the “Austrian” compressional phase that affected the entire Carpatho-Balkanid orogen. Additionally, similar Late Cretaceous fission-track ages from both sides of the contacts between the Eastern Veles series and the Lower complex, and the latter and the Vlasina unit (Vrvi Kobila shear zone) exclude any possibility of major vertical displacement along these structures since this time.
- Early to middle Eocene rapid cooling (ca. 48–ca. 39 Ma) of rocks from the Crnook dome was most probably related to the crustal extension associated with the formation of the core complex

exhumed along the system of low-angle detachments (i.e. Crnook detachment). Based on similarities in lithology, structures, age and mode of the exhumation, the Crnook dome is considered as a continuation of the Osogovo-Lisets core complex (i.e. Crnook-Osogovo-Lisets complex).

- Relatively rapid late Eocene post-magmatic cooling (34–32 Ma), followed the emplacement of the Surdulica granodiorite (36±1 Ma) and subsequent hydrothermal and volcanic activity in the study area (ca. 35 Ma). The igneous activity was associated with late- to post-orogenic tectonic setting.

5.2 Future research perspectives

New scientific conclusions inevitably lead to further questions. This is also true for the results of the present study. Hence, a number of new topics based on these advances are outlined below.

The presence of early Cadomian (694-580 Ma) xenocrysts, inherited cores and detrital zircons suggests the existence of a hypothetical basement of the magmatic and sedimentary rocks of the central SMM. Although such rocks were not observed during this study, they were reported in the Struma Unit, Pelagonian zone, İstanbul zone and Sakarya zone. Therefore, localised studies concentrating on geochronological record in para- and orthogneisses from the central SMM could potentially prove the presence of such continental basement.

Due to deep-oceanic provenance of sedimentary rocks, and mafic and ultramafic character of igneous rocks in the Vlasina Unit, samples from this unit did not yield a sufficient zircon material for credible geochronological analysis. Hence, the age of volcano-sedimentary sequence in pre-Ordovician Vlasina was constrained only by indirect evidence (intrusions of Cadomian granites and earlier palaeontological record). A detailed geochronological study dedicated to this issue, and also including methods appropriate for these rock-types (i.e. Sm-Nd analysis on garnets), could provide direct evidence for the timing of formation of the pre-Ordovician Vlasina.

The presence of migmatites west of Bujanovac magmatic complex was previously considered to be related to the intrusion of fine-grained Bujanovac granites, revealed here to be of Permo-Triassic age. Alternatively, these rocks could be related to the partial in situ melting of rocks under high- or in case of fluid-saturated rocks medium-grade metamorphic conditions. Only a careful petrological and geochronological investigation of these rocks would give a definite solution of this problem.

Although the geochemistry and petrology of the rocks from the central SMM were well documented prior to this study, a careful mapping of the spatial distribution of particular metamorphic assemblages could supplement the knowledge of the exact peak conditions and extents of different metamorphic facies within the central SMM, as well as the scope of early Alpine retrogression in the Lower Complex and the hypothetical high-pressure event.

Due to the regional approach of this study and the generally poor outcrop conditions, the brittle deformation in the central SMM could not be studied in satisfactory detail. More localised mapping investigations would certainly yield valuable results which would supplement the thermochronological data presented in this study.

Acknowledgements

PhD projects in most people evoke images of hard work, stress and absence of social life. Although true, they also provide space for personal growth of the candidate through joys of new experiences, overcoming challenges and applying acquired knowledge. The people named below made it possible for me to experience the positive sides of this PhD project more often than the negatives.

First of all, I am most grateful for having Alexandre Kounov as my ~~supervisor~~advisor and mentor. Beside providing me with the unique opportunity to study (in my opinion) the most interesting rocks that Serbia has to offer, he had patiently guided me through every slope and curve of this journey, from field- and lab work to interpretation and presentation of results. I consider myself extremely lucky to have such a considerate teacher and a friend. Enormous help was also provided by Andreas Wetzel who believed in the success of this project and selflessly supported its continuation.

The expertise of Irena Peytcheva and Albrecth von Quadt (ETH Zürich) was indispensable for geochemical and geochronological analyses and interpretation of their results. The help of Daniela Gallhofer, Melanie Moll, Markus Wälle and Lydia Zehnder is also gratefully acknowledged. Branislav Trivić, Ana Mladenović and Dragana Petrović (University of Belgrade) provided much needed assistance and (often comic) relief during field work, structural studies, conferences, workshops and literature-hunts. Discussions on geology of southwestern Bulgaria with Neven Georgiev and Ianko Gerdjikov (Sofia University "St. Kliment Ohridski") are greatly appreciated. Additionally, Ianko's considerable knowledge on Variscan orogenic processes had vastly improved Chapter 2. The help of Todor Serafimovski and Goran Tasev (Štip University

"Goce Delčev") were crucial for accomplishing our work in eastern Macedonia. Richard Spikings (University of Geneva) is thanked for help with ^{40}Ar/^{39}Ar analyses and interpretation of their results.

I would also like to thank all professors and staff at University of Basel for their support, most notably Leander Frantz for help with petrology, Willy Tschudin for sample preparation and Mme Joelle Glanzmann for tackling huge amount of paperwork on my behalf. I am very grateful for support and friendship of colleagues and friends Matěj Peč, Anja Thust, Sina Marti, Achim Reisdorf, Adrian Roth, Lukas Egli and Rüdiger Kilian, who made me feel welcome in Basel. The biggest thanks go to my office-mate Nicola Kern who had translated the abstract to German and with whom I enjoyed many discussions, gigs and table-top skirmishes. Necessary levels of distraction were provided by the film-night/probenraum crew: Giorgio, Tobias, Baptiste, Ilaria, June, Doriana, Slađa, Neda, and Ben. May the Great Rabbit bless you for all the evenings I can't forget and can't remember. \/ My long-term friends are thanked for their regular (but ultimately insufficient) visits, road-trips and sticking with me through thick and thin. You know who you are.

I would also like to thank my family, especially those incidentally residing in Switzerland, with whom I shared some great moments. And probably the biggest thanks go to Jelena whose love and support gave me comfort which nothing else could provide.

This study was made possible by the financial support of the Swiss National Science Foundation through grants NEW1532 and NUW1518, and a very welcome grant from the Freiwillige Akademische Gesellschaft Basel.

A total of 217176 fission tracks were counted during this project.

Curriculum Vitae

Milorad Dušan Antić

Personal Details

Date of birth:	29th of November 1982
Place of birth:	Belgrade (SFR Yugoslavia)
Marital status:	Married
Citizenship:	Serbian

Address:

Vladetina 21a
11120 Belgrade
Serbia

Tel: +381 66 95 77 88 6
Email: antatj@gmail.com

Education

2010-2015	PhD in Earth Sciences at University of Basel: *“Origin and tectonic evolution of the central Serbo-Macedonian Massif”* *Supervisors: P.D. Dr. A. Kounov and Prof. Dr. A. Wetzel*
April 2010.	Diploma in Geology at University of Belgrade: *“Structural and Tectonic Characteristics of the Gornjak – Suva Planina Zone at the Broader Space of the Gornjak gorge”* *Mentor: Prof. Dr. Branislav Trivić*
2001-2010	Studies in Geology at University of Belgrade
1997-2001	Electro-technical vocational School “Nikola Tesla”, Belgrade

Refereed publications

Antić, M., Kounov, A., Trivić, B., Spikings, R., Wetzel, A. 2016. Evidence of Variscan and Alpine tectonics in the structural and thermochronological record of the central Serbo-Macedonian Massif (southeastern Serbia). International Journal of Earth Sciences. DOI:10.1007/s00531-016-1380-6

Antić, M., Kounov, A., Trivić, B., Wetzel, A., Peytcheva, I., von Quadt, A., 2015a. Alpine thermal events in the central Serbo-Macedonian Massif (southeastern Serbia). International Journal of Earth Sciences. 105, 5, 1485-1505. DOI: 10.1007/s00531-015-1266-z

Antić, M., Peytcheva, I., von Quadt, A., Kounov, A., Trivić, B., Serafimovski, T., Tasev, G., Gerdjikov, I., Wetzel, A., 2015b. Pre-Alpine evolution of a segment of the North-Gondwanan margin: Geochronological and geochemical evidence from the central Serbo-Macedonian Massif. Gondwana Research. 36. 523-544. DOI: 10.1016/j.gr.2015.07.020

Mladenović, A., Trivić, B., **Antić, M.**, Cvetković, V., Pavlović, R., Radovanović, S., Fügenschuh, B., 2014. The recent fault kinematics in the westernmost part of the Getic nappe system (Eastern Serbia): Evidence from fault slip and focal mechanism data. Geologica Carpathica 65, 147–161. DOI: 10.2478/geoca-2014-0010

Chapter 5

Summary

5 Summary

The central parts of the crystalline Serbo-Macedonian Massif (SMM) have a long and complex geological history which can be summarised in four main episodes: (i) Formation of the protoliths took place in a North-Gondwanan magmatic arc from late Neoproterozoic until the earliest Silurian, (ii) since Early Devonian until late Carboniferous the central SMM was subjected to high-strain ductile deformation associated with the assembly of the Galatian super-terrane and subsequent collision with Laurussia, (iii) from late Permian until the Late Cretaceous the SMM was affected by processes related to the evolution of the Mesozoic Tethys Ocean, and (iiii) since the early Late Cretaceous the central SMM was exhumed to shallow crustal position and deformed in brittle regime. The results presented in the individual chapters are outlined below as synoptic conclusions. Furthermore, new questions arising from the conclusion of this study are given together with suggested prospects for future research.

5.1 Main results

The geochemical analysis, Hf isotope measurements, and U–Pb LA-ICP-MS zircon dating of igneous and sedimentary rocks from the central SMM and the basement of the adjacent units, presented in Chapter 2 have allowed the following conclusions to be made:

- During the Cadomian orogenic cycle the Lower Complex of the central SMM represented a part of the continental magmatic-arc developed along the northern margin of Gondwana. The Lower Complex could be correlated with the Lotru and Pirgadikia units of the Carpathians and the Internal Hellenides, respectively. Based on inherited and detrital zircon data, its late Neoproterozoic position in the eastern part of the northern margin of Gondwana is tentatively proposed (i.e. northeast of Saharan metacraton and southwest of South-China craton).

- The volcano-sedimentary pre-Ordovician Vlasina Unit most probably represented a part of the late Neoproterozoic accretionary wedge dominated by ocean-floor sediments. During this time the Lower Complex was most probably a more internal part of the same volcano-sedimentary succession or a fore-arc basin.

- The magmatic-arc activity in the study area was detected in the Ediacaran to the mid-Cambrian in the Lower Complex, Vlasina Unit and the basement of Struma Unit. These units together with the Eastern Veles series, experienced renewal of arc-related magmatism in the late Cambrian to Early Ordovician, whereas mafic magmatism associated with rifting occurred in the Lower Complex during Middle to Late Ordovician. Minor pulse of within-plate felsic magmatism in the Lower Complex took place in the early Silurian.

- The age of the high-strain deformation and peak metamorphism in the SMM was constrained to the Variscan orogeny by the presence of highly deformed early Silurian meta-granites (Bujanovac Qz monzonite) in the Lower Complex, and undeformed late Carboniferous granites (Slatinska Reka granites) intruding gneisses of the same unit.

- The Variscan collisional tectonics led to the differential burial of constituents of the SMM (i.e. Lower Complex, Vlasina Unit, basement of Struma Unit, and Eastern Veles series), resulting in different metamorphic grades of these domains with a common late Neoproterozoic–early Palaeozoic history. Subsequently, this complex Variscan framework was severely disrupted during the Alpine events.

- During Permian-Triassic the entire SMM experienced widespread crustal extension and emplacement of within-plate granites, most probably related to the rifting of the Mesozoic

Neotethys.

The structural investigations presented in Chapter 3 led to recognition of at least three major stages of ductile deformation in the central SMM. Despite the different peak metamorphic conditions in the Lower Complex and Vlasina Unit, both units show a common deformational evolution. Results of the $^{40}Ar/^{39}Ar$ thermochronological analyses helped to refine the established deformational evolution and asses the regional importance of determined tectonic events.

- The earliest stage of deformation D_1 in the central SMM is related to isoclinal folding, commonly preserved as quartz-feldspar rootless fold hinges up to decimetre-scale.

- The second deformation stage D_2 is associated with general southeastward tectonic transport and refolding of older structures into recumbent metre- to kilometre-scale tight to isoclinal folds.

- The deformation stages D_1 and D_2 could not be temporally separated, and probably took place in close sequence. Based on the stratigraphic age of the youngest affected sediments, and the intrusion ages of the oldest undeformed magmatic rocks, the age of these two ductile deformation stages was constrained to the Variscan orogeny (i.e. ca. 408-ca. 328). During this time the SMM was involved in a transpressional amalgamation of the western and eastern parts of the Galatian super-terrane and subsequent collision with Laurussia, which could account for the changes in direction of strain axes during D_1 and D_2.

- A trend of diminishing strain and metamorphic grade from amphibolite facies in the Lower Complex, across the greenschist facies in the pre-Ordovician Vlasina to anchimetamorphism in thesedimentary rocks of post-Cambrian Vlasina, suggests different crustal positions of the central SMM during the Variscan orogeny.

- Cooling below the greenschist facies conditions in the western part of the Vlasina Unit has taken place in a post-orogenic setting (extensional or transtensional) in the early Permian (284±1 Ma).

- The age of activity along the top-to-the-west shear zone formed within the ortho-gneiss in the Božica area of the Vlasina Unit was constrained to Middle Triassic (246±1 Ma). This age coincides with widespread extension related to the opening of the Mesozoic Tethys.

- Rare outcrop-scale evidence of the final stage of ductile deformation D_3 is limited to the formation of spaced and crenulation cleavage. These structures are probably related to the large-scale folding reported by earlier studies. The maximum age of this event is constrained by the crenulation of the Middle Triassic mylonitic foliation in the Božica area.

- Anastomosing shear zones, S-C fabric and spaced cleavage developed in the Permo-Triassic Bujanovac granite provide evidence of an additional post-Triassic ductile deformational event. Additional data is needed to constrain the area affected by this deformation and its exact timing.

- The greenschist facies retrogression in the Lower Complex probably occurred in the Early Jurassic and it is probably related to the thermal processes in the overriding plate above the subducting slab of the Mesozoic Tethys Ocean.

The new results of thermo- and geochronological analyses reveal three main cooling stages along the central parts of the SMM since the Cretaceous (see Chapter 4 for details):

- The late Early- to early Late Cretaceous rapid cooling (ca. 110–ca. 90 Ma), affected the SMM. This event was most probably related to the post-collisional extension following the "Austrian" compressional phase that affected the entire Carpatho-Balkanid orogen. Additionally, similar Late Cretaceous fission-track ages from both sides of the contacts between the Eastern Veles series and the Lower complex, and the latter and the Vlasina unit (Vrvi Kobila shear zone) exclude any possibility of major vertical displacement along these structures since this time.

- Early to middle Eocene rapid cooling (ca. 48–ca. 39 Ma) of rocks from the Crnook dome was most probably related to the crustal extension associated with the formation of the core complex exhumed along the system of low-angle detachments (i.e. Crnook detachment). Based on similarities in lithology, structures, age and mode of the exhumation, the Crnook dome is considered as a continuation of the Osogovo-Lisets core complex (i.e. Crnook-Osogovo-Lisets complex).

- Relatively rapid late Eocene post-magmatic cooling (34–32 Ma), followed the emplacement of the Surdulica granodiorite (36±1 Ma) and subsequent hydrothermal and volcanic activity in the study area (ca. 35 Ma). The igneous activity was associated with late- to post-orogenic tectonic setting.

5.2 Future research perspectives

New scientific conclusions inevitably lead to further questions. This is also true for the results of the present study. Hence, a number of new topics based on these advances are outlined below.

The presence of early Cadomian (694-580 Ma) xenocrysts, inherited cores and detrital zircons suggests the existence of a hypothetical basement of the magmatic and sedimentary rocks of the central SMM. Although such rocks were not observed during this study, they were reported in the Struma Unit, Pelagonian zone, İstanbul zone and Sakarya zone. Therefore, localised studies concentrating on geochronological record in para- and orthogneisses from the central SMM could potentially prove the presence of such continental basement.

Due to deep-oceanic provenance of sedimentary rocks, and mafic and ultramafic character of igneous rocks in the Vlasina Unit, samples from this unit did not yield a sufficient zircon material for credible geochronological analysis. Hence, the age of volcano-sedimentary sequence in pre-Ordovician Vlasina was constrained only by indirect evidence (intrusions of Cadomian granites and earlier palaeontological record). A detailed geochronological study dedicated to this issue, and also including methods appropriate for these rock-types (i.e. Sm-Nd analysis on garnets), could provide direct evidence for the timing of formation of the pre-Ordovician Vlasina.

The presence of migmatites west of Bujanovac magmatic complex was previously considered to be related to the intrusion of fine-grained Bujanovac granites, revealed here to be of Permo-Triassic age. Alternatively, these rocks could be related to the partial in situ melting of rocks under high- or in case of fluid-saturated rocks medium-grade metamorphic conditions. Only a careful petrological and geochronological investigation of these rocks would give a definite solution of this problem.

Although the geochemistry and petrology of the rocks from the central SMM were well documented prior to this study, a careful mapping of the spatial distribution of particular metamorphic assemblages could supplement the knowledge of the exact peak conditions and extents of different metamorphic facies within the central SMM, as well as the scope of early Alpine retrogression in the Lower Complex and the hypothetical high-pressure event.

Due to the regional approach of this study and the generally poor outcrop conditions, the brittle deformation in the central SMM could not be studied in satisfactory detail. More localised mapping investigations would certainly yield valuable results which would supplement the thermochronological data presented in this study.

Acknowledgements

PhD projects in most people evoke images of hard work, stress and absence of social life. Although true, they also provide space for personal growth of the candidate through joys of new experiences, overcoming challenges and applying acquired knowledge. The people named below made it possible for me to experience the positive sides of this PhD project more often than the negatives.

First of all, I am most grateful for having Alexandre Kounov as my ~~supervisor~~advisor and mentor. Beside providing me with the unique opportunity to study (in my opinion) the most interesting rocks that Serbia has to offer, he had patiently guided me through every slope and curve of this journey, from field- and lab work to interpretation and presentation of results. I consider myself extremely lucky to have such a considerate teacher and a friend. Enormous help was also provided by Andreas Wetzel who believed in the success of this project and selflessly supported its continuation.

The expertise of Irena Peytcheva and Albrecth von Quadt (ETH Zürich) was indispensable for geochemical and geochronological analyses and interpretation of their results. The help of Daniela Gallhofer, Melanie Moll, Markus Wälle and Lydia Zehnder is also gratefully acknowledged. Branislav Trivić, Ana Mladenović and Dragana Petrović (University of Belgrade) provided much needed assistance and (often comic) relief during field work, structural studies, conferences, workshops and literature-hunts. Discussions on geology of southwestern Bulgaria with Neven Georgiev and Ianko Gerdjikov (Sofia University "St. Kliment Ohridski") are greatly appreciated. Additionally, Ianko's considerable knowledge on Variscan orogenic processes had vastly improved Chapter 2. The help of Todor Serafimovski and Goran Tasev (Štip University

"Goce Delčev") were crucial for accomplishing our work in eastern Macedonia. Richard Spikings (University of Geneva) is thanked for help with ^{40}Ar/^{39}Ar analyses and interpretation of their results.

I would also like to thank all professors and staff at University of Basel for their support, most notably Leander Frantz for help with petrology, Willy Tschudin for sample preparation and Mme Joelle Glanzmann for tackling huge amount of paperwork on my behalf. I am very grateful for support and friendship of colleagues and friends Matěj Peč, Anja Thust, Sina Marti, Achim Reisdorf, Adrian Roth, Lukas Egli and Rüdiger Kilian, who made me feel welcome in Basel. The biggest thanks go to my office-mate Nicola Kern who had translated the abstract to German and with whom I enjoyed many discussions, gigs and table-top skirmishes. Necessary levels of distraction were provided by the film-night/probenraum crew: Giorgio, Tobias, Baptiste, Ilaria, June, Doriana, Slađa, Neda, and Ben. May the Great Rabbit bless you for all the evenings I can't forget and can't remember. \/ My long-term friends are thanked for their regular (but ultimately insufficient) visits, road-trips and sticking with me through thick and thin. You know who you are.

I would also like to thank my family, especially those incidentally residing in Switzerland, with whom I shared some great moments. And probably the biggest thanks go to Jelena whose love and support gave me comfort which nothing else could provide.

This study was made possible by the financial support of the Swiss National Science Foundation through grants NEW1532 and NUW1518, and a very welcome grant from the Freiwillige Akademische Gesellschaft Basel.

A total of 217176 fission tracks were counted during this project.

Curriculum Vitae

Milorad Dušan Antić

Personal Details

Date of birth:	29th of November 1982
Place of birth:	Belgrade (SFR Yugoslavia)
Marital status:	Married
Citizenship:	Serbian

Address:

Vladetina 21a
11120 Belgrade
Serbia

Tel: +381 66 95 77 88 6
Email: antatj@gmail.com

Education

2010-2015	PhD in Earth Sciences at University of Basel: *“Origin and tectonic evolution of the central Serbo-Macedonian Massif”* *Supervisors: PD Dr. A. Kounov and Prof. Dr. A. Wetzel*
April 2010.	Diploma in Geology at University of Belgrade: *“Structural and Tectonic Characteristics of the Gornjak – Suva Planina Zone at the Broader Space of the Gornjak gorge”* *Mentor: Prof. Dr. Branislav Trivić*
2001-2010	Studies in Geology at University of Belgrade
1997-2001	Electro-technical vocational School “Nikola Tesla”, Belgrade

Refereed publications

Antić, M., Kounov, A., Trivić, B., Spikings, R., Wetzel, A. 2016. Evidence of Variscan and Alpine tectonics in the structural and thermochronological record of the central Serbo-Macedonian Massif (southeastern Serbia). International Journal of Earth Sciences. DOI:10.1007/s00531-016-1380-6

Antić, M., Kounov, A., Trivić, B., Wetzel, A., Peytcheva, I., von Quadt, A., 2015a. Alpine thermal events in the central Serbo-Macedonian Massif (southeastern Serbia). International Journal of Earth Sciences. 105, 5, 1485-1505. DOI: 10.1007/s00531-015-1266-z

Antić, M., Peytcheva, I., von Quadt, A., Kounov, A., Trivić, B., Serafimovski, T., Tasev, G., Gerdjikov, I., Wetzel, A., 2015b. Pre-Alpine evolution of a segment of the North-Gondwanan margin: Geochronological and geochemical evidence from the central Serbo-Macedonian Massif. Gondwana Research. 36. 523-544. DOI: 10.1016/j.gr.2015.07.020

Mladenović, A., Trivić, B., **Antić, M.**, Cvetković, V., Pavlović, R., Radovanović, S., Fügenschuh, B., 2014. The recent fault kinematics in the westernmost part of the Getic nappe system (Eastern Serbia): Evidence from fault slip and focal mechanism data. Geologica Carpathica 65, 147–161. DOI: 10.2478/geoca-2014-0010